

Journal of Advanced Transportation

Intelligent Transportation Systems for Smart Cities 2021

Lead Guest Editor: Sang-Bing Tsai

Guest Editors: Xiaolong Xu and Yuan Yuan





Intelligent Transportation Systems for Smart Cities 2021

Journal of Advanced Transportation

Intelligent Transportation Systems for Smart Cities 2021

Lead Guest Editor: Sang-Bing Tsai





Guest Editors: Xiaolong Xu and Yuan Yuan



Copyright © 2023 Hindawi Limited. All rights reserved.





























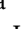
This is a special issue published in "Journal of Advanced Transportation." All articles are open access articles distributed under the Creative Commons Attribution License, which permits unrestricted use, distribution, and reproduction in any medium, provided the original work is properly cited.


Associate Editors








Juan C. Cano , Spain
Steven I. Chien , USA
Antonio Comi , Italy
Zhi-Chun Li, China
Jinjun Tang , China

Academic Editors

Kun An, China
Shriniwas Arkatkar, India
José M. Armingol , Spain
Socrates Basbas , Greece
Francesco Bella , Italy
Abdelaziz Bensrhair, France
María Calderon, Spain
Tiziana Campisi , Italy
Giulio E. Cantarella , Italy
Maria Castro , Spain
Mei Chen , USA
Pierluigi Coppola , Italy
Maria Vittoria Corazza , Italy
Luca D'Acierno , Italy
Andrea D'Ariano, Italy
Stefano De Luca , Italy
Rocío De Oña , Spain
Luigi Dell'Olio , Spain
Cédric Demonceaux , France
Sunder Lall Dhingra, India
Roberta Di Pace, Italy
Dilum Dissanayake, United Kingdom
Jing Dong , USA
Yuchuan Du , China
Juan-Antonio Escareno, France
Domokos Esztergár-Kiss , Hungary
Saber Fallah , United Kingdom
Gianfranco Fancello, Italy
Zhixiang Fang , China
Francesco Galante , Italy
Yuan Gao , China
Laura Garach, Spain
Indrajit Ghosh , India
Ren-Yong Guo , China


Yanyong Guo , China
Jérôme Ha#rri, France
Hocine Imine, France
Umar Iqbal , Canada
Rui Jiang , China
Peter J. Jin, USA
Sheng Jin , China
Lina Kattan, Canada
Mehdi Keyvan-Ekbatani , New Zealand
Victor L. Knoop , The Netherlands
Michela Le Pira , Italy
Jaeyoung Lee , USA
Seungjae Lee, Republic of Korea
Ruimin Li , China
Zhenning Li , China
Christian Liebchen, Germany
Tao Liu, China
Chung-Cheng Lu , Taiwan
Tom Hao Luan, China
Filomena Mauriello , Italy
Luis Miranda-Moreno, Canada
Rakesh Mishra, United Kingdom
Tomio Miwa , Japan
Andrea Monteriù , Italy
Sara Moridpour , Australia
Giuseppe Musolino , Italy
Jose E. Naranjo , Spain
Mehdi Nourinejad , Canada
Eneko Osaba , Spain
Eleonora Papadimitriou, The Netherlands
Dongjoo Park , Republic of Korea
Luca Pugi , Italy
Alessandro Severino, Italy
Nirajan Shiwakoti , Australia
Michele D. Simoni, Sweden
Ziqi Song , USA
Amanda Stathopoulos , USA
Lijun Sun , Canada
Richard S. Tay , Australia
Daxin Tian , China
Alejandro Tirachini, Chile
Long Truong , Australia
Avinash Unnikrishnan , USA



Pascal Vasseur , France
Nagendra R Velaga, India
Antonino Vitetta , Italy
S. Travis Waller, Australia
Jianbin Xin, China
Hongtai Yang , China
Zhihong Yao , China
Vincent F. Yu , Taiwan
Jacek Zak , Poland
Jing Zhao, China
Ming Zhong , China
Yajie Zou , China


Contents

Intelligent Transportation Systems for Smart Cities 2021

Sang-Bing Tsai , Xiaolong Xu, and Yuan Yuan


Editorial (1 page), Article ID 9896512, Volume 2023 (2023)

Analysis of Fuel Tank Collision Structure Based on Defense Point Method

Wenguang Liu , Haijiang Liu, Lin Jiang, and Shanshan Bi

Research Article (7 pages), Article ID 8445650, Volume 2022 (2022)

Refined Judgment of Urban Traffic State Based on Machine Learning and Edge Computing

Lijuan Liu 



Research Article (9 pages), Article ID 7593772, Volume 2022 (2022)

Outdoor Clothing Design for Traffic Safety Based on Big Data and Artificial Intelligence

Ya Zhou  and Yun Shi


Research Article (13 pages), Article ID 8697421, Volume 2022 (2022)

A New Approach to Regional Traffic Estimation for Intelligent Transport Systems

Minghe Yu , Jianhua Feng, Tianmiao Zhang, and Tiancheng Zhang 


Research Article (9 pages), Article ID 8588911, Volume 2022 (2022)

Research on the Development Model of Rural Tourism Based on Multiobjective Planning and Intelligent Optimization Algorithm

Lu Yang and Xiaoying Dong 


Research Article (12 pages), Article ID 6219438, Volume 2022 (2022)

Coordinated Development of Urban Intelligent Transportation Data System and Supply Chain Management

Qian Chen 




Research Article (11 pages), Article ID 6308728, Volume 2022 (2022)

Evaluation Method of Ecological Tourism Carrying Capacity of Popular Scenic Spots Based on Set Pair Analysis Method

Xiangrong Yan 

Research Article (11 pages), Article ID 9715248, Volume 2022 (2022)

The Shared Transportation Industry in China: Examining the Influence of Regional Environmental Factors on New Venture Formation

Yan Zhou, Sangmoon Park , Justin Zuopeng Zhang , and Xin Rong 


Research Article (13 pages), Article ID 6462381, Volume 2022 (2022)

Finite-Element Analysis of Vertical Displacement of Laminated Rubber Bearing under Earthquake Action for Disaster Resilience of the Smart City

Denglian Yang  and Yanli Liu 

Research Article (23 pages), Article ID 7574272, Volume 2022 (2022)

Mathematical Model and Algorithm of Multi-Index Transportation Problem in the Background of Artificial Intelligence

Junfang Cao 

Research Article (11 pages), Article ID 3664105, Volume 2022 (2022)

Urban Traffic State Estimation with Online Car-Hailing Data: A Dynamic Tensor-Based Bayesian Probabilistic Decomposition Approach

Wenqi Lu , Ziwei Yi , Dongyu Luo , Yikang Rui , Bin Ran , Jianqing Wu, and Tao Li

Research Article (16 pages), Article ID 1793060, Volume 2022 (2022)

Seismic Analysis of Reticulated Shell Structure Based on Sensor Network for Smart Transportation Seismic Isolation Bearings

Jun Peng  and Yufei Li


Research Article (13 pages), Article ID 5985542, Volume 2022 (2022)

Data Transmission Control of Vehicle Ad Hoc Network in Intelligent Transportation Systems for Smart Cities

Zhenhua Li  and Guicai Yu 


Research Article (8 pages), Article ID 8680880, Volume 2022 (2022)

Multidimensional Dynamics and Forecast Models of Network Public Opinions Based on the Fusion of Smart Transportation and Big Data

Guojun Sheng and Yi Guan 



Research Article (12 pages), Article ID 3184938, Volume 2022 (2022)

Optimization of Traffic Congestion Management in Smart Cities under Bidirectional Long and Short-Term Memory Model

Yujia Zhai, Yan Wan, and Xiaoxiao Wang 

Research Article (8 pages), Article ID 3305400, Volume 2022 (2022)

Identification of Working Trucks and Critical Path Nodes for Construction Waste Transportation Based on Electric Waybills: A Case Study of Shenzhen, China

Jun Bi , Qiuyue Sai , Fujun Wang, and Yakun Chen


Research Article (13 pages), Article ID 7647121, Volume 2022 (2022)

Rural Road Network Planning Based on 5G and Traffic Big Data

Minqing Zhu, Zi Wang , Hongjun Cui , and Sheng Yao

Research Article (9 pages), Article ID 1991757, Volume 2022 (2022)

Rotary Kiln Thermal Simulation Model and Smart Supply Chain Logistics Transportation Monitoring Management

Zesheng Liu 

Research Article (13 pages), Article ID 2116280, Volume 2022 (2022)

Contents

Power Allocation for 5G Mobile Multiuser Cooperative Networks
Fagen Yin  and Wencai Du 
Research Article (7 pages), Article ID 3882100, Volume 2021 (2021)

Editorial

Intelligent Transportation Systems for Smart Cities 2021

Sang-Bing Tsai ,¹ **Xiaolong Xu**,² and **Yuan Yuan**³

¹Regional Green Economy Development Research Center, School of Business, Wuyi University, Wuyishan 354300, China

²Nanjing University of Information Science and Technology, Nanjing, China

³Michigan State University, East Lansing, MI, USA

Correspondence should be addressed to Sang-Bing Tsai; sangbing@hotmail.com

Received 2 August 2022; Accepted 2 August 2022; Published 22 June 2023

Copyright © 2023 Sang-Bing Tsai et al. This is an open access article distributed under the Creative Commons Attribution License, which permits unrestricted use, distribution, and reproduction in any medium, provided the original work is properly cited.

The developing objectives of Intelligent Transport Infrastructure contain four aspects. The first is to enhance Intelligent Design of City from the perspective of city planning. The second is to provide intelligent applications of information decisions with the prospect that it can offer correct and clear information for decision makers to make Smart Decision. The third is to use sufficient information and guidance control technology to maximize the efficiency of the existing network. The final aspect is that dynamic information combined with tax mechanism is utilized to make customers do the smartest decision and have some changes in their behaviors.

Intelligent Transport is supposed to combine EV, Smart Grid, Green Building, Green Transportation, and other applications of intelligent life all together in order to process integrated test and practical deployment. Simultaneously, the demand for social mobility of the elderly should also be

combined with infrastructure, vehicle design, social welfare, and other departments for planning and design, so that the promotion of smart transportation can be specifically upgraded to the plan of smart cities.

This Special Issue mainly focuses on recent advances in intelligent and smart transportation systems for smart cities. This Special Issue has collected some good articles. It had great repercussions and success. We thank all authors for their participation.

Conflicts of Interest

The guest editors declare no conflicts of interest.

Sang-Bing Tsai
Xiaolong Xu
Yuan Yuan

Research Article

Analysis of Fuel Tank Collision Structure Based on Defense Point Method

Wenguang Liu ^{1,2}, Haijiang Liu,² Lin Jiang,³ and Shanshan Bi¹

¹School of Automotive and Traffic Engineering, Jiangsu University, 301 Xuefu Road, Zhenjiang, Jiangsu, China

²Tongji University, Shanghai, China

³YAPP Automotive Systems Co., Ltd., Yangzhou, China

Correspondence should be addressed to Wenguang Liu; liuwg@ujs.edu.cn

Received 6 April 2022; Revised 17 May 2022; Accepted 21 June 2022; Published 10 August 2022

Academic Editor: Sang-Bing Tsai

Copyright © 2022 Wenguang Liu et al. This is an open access article distributed under the Creative Commons Attribution License, which permits unrestricted use, distribution, and reproduction in any medium, provided the original work is properly cited.

Aiming at the impact process of a fuel tank, which is a transient energy conversion process, the material absorbs energy through deformation to analyze the mechanical properties of the fuel tank during the impact process. The defense node method is adopted to simulate the dynamic response of the fuel tank during impact. The results show that it can accurately evaluate the safety of the container.

1. Introduction

The automobile fuel tank is the important component of the automobile fuel supply system. The country has strict requirements for its safety and environmental protection. To make full use of the limited automotive chassis space and adapt to various vehicle types, the shape of the automobile fuel tank is varied. The classical mechanic's method cannot analyze and answer the fuel tank of various schemes at the same time, and there can be no measured data at the beginning of the design. Therefore, it is significant to check the strength and stiffness of the fuel tank effectively and quickly and find out the weak links of the fuel tank to provide a reference for the design and modification of the automobile fuel tank. At the same time, to shorten the development cycle, improve the quality of development, adapt to the rapid growth of the market requirements, and enhance the competitiveness of the product market have important practical significance. However, the fuel tank manufacturer still stays at the stage of trial and error in the design of fuel tank structure, mainly relying on the experience of designers, and hardly calculates and optimizes the shape of reinforcing ribs, the thickness of the tank wall, the aperture of the wave-proof plate, and so on, which results in the

unreasonable distribution of the material of the tank. The general design process is to manually make fuel tank product samples at first and then to find out the problems by testing and modifying them. From design to the factory, a product needs a long design cycle. Particularly for the fuel tank, it has a large volume, complex structure, and many related inspection indicators, which leads to an increase in production costs.

The fuel tank impact test is a simulated impact test of the product. The purpose of this test is to verify the product is qualified in all aspects of the product when it is subjected to external force shock or external force under normal operating conditions.

Because collision action is a complex process, it is affected by many factors, such as the constraints of the collision body, the relative speed of contact, the geometry and duration of the contact surface, local plastic deformation, and so on [1–3]. Aiming at the collision model of the system, Stronge et al. analyzed the energy change during the oblique collision and the velocity relationship before and after the collision and established the dynamic model of viscous/sliding friction contact [4]. The CEL method is used to simulate the dynamic response of liquid storage vessel in the process of drop collision and the space motion state of liquid

at different times. By comparing with the results of previous literature, the dynamic response and space state in the process of drop collision are discussed in four cases, namely, different drop angle, drop height, vessel thickness, and liquid storage capacity, and the impact of factors on the vessel is also discussed [5]. The composite structure is vulnerable to all kinds of low-energy impact during the process of production and application, which will make invisible visual damage in the laminates and degenerate the mechanical properties of the composite. Composite laminate is closely related to structural safety and life expectancy. So, it is significant to evaluate the low-energy impact resistance and damage prediction of composite structures.

In a variety of collision detection algorithms, the oriented bounding box algorithm had widely used. By using the characteristics of the triangle surrounded by the rectangle in the leaf node and the value calculated in the rectangle-rectangle intersection test phase, the new algorithm contains a better triangle-triangle intersection algorithm in the oriented bounding box. The two triangles are converted into the same coordinate system and then test the two triangles., but this step could be omitted by using the coordinates of the bounding boxes to replace the coordinates of the triangles. This method reduces a lot of redundant coordinate transformation operations compared to the original algorithm [6]. Chai and Wu established a single-degree-of-freedom collision vibration model and studied the effects of parameters, such as collision clearance, damping, stiffness, and excitation frequency, on the bifurcation and chaos phenomena of the system motion using nonlinear dynamic analysis and numerical simulation [7]. Fan et al. use the penalty stiffness method in the contact algorithm, by adjusting the penalty stiffness value reasonably, controlling the penetration distance effectively, and avoiding the ill-conditioned stiffness matrix, which makes the calculation result approach the true value [8]. Collision detection is a hot topic in computer graphics, augmented reality, human-computer interaction, and other fields. In recent years, real-time simulation of large-scale complex scenes has attracted many scholars' attention, especially the emergence of cloud computing and big data technology, which puts forward higher requirements for real-time scene simulation, which also brings unprecedented opportunities and challenges to researchers. As the geometric complexity of the virtual environment increases, the computational complexity of collision detection greatly improved, and the interaction of complex scenes consumes a lot of computer resources. Therefore, the fast collision detection problem has become a bottleneck in the virtual environment. How to design an efficient collision detection algorithm to meet the requirements of real time and accuracy has become a current problem to be solved. Qu had put forward a multiple date parallel collision algorithm based on optimization operator. The search space is confined in a nonuniform local minimum area to reduce the colony search time [9]. Chen et al., based on the local search algorithm of surface, characterized the contact sheet by the coordinates of the center of the face and the length of the feature, carried out presearch to quickly eliminate potential contact pairs that would not occur

contact, eliminated the blind area of contact search, and had good robustness and calculation accuracy [10]. Li et al. propose an improved collision detection algorithm based on deformable objects, which is difficult to solve the real-time and fidelity problems of deformable objects. To improve the efficiency of collision detection, an improved particle selection method and the idea of a multiswarm particle optimization algorithm are used to construct a multiline group on the multiline composed of the control point cluster and the center point of the Snake model [11]. Due to the short action time of external transient load and the difficulty of experiment control, the measured data are limited, and the continuous results in space and time are not obtained. Wang simulated and analyzed the drop of metal cylinder structure under empty shell condition by ANSYS/LS-DYNA software and studied the strain distribution law of metal thin-walled cylinder structure under different drop conditions (different height and different fall angle). The variation of stress and impact duration, impact force, and peak overload (impact acceleration) are discussed [12]. An algorithm for simulating friction contact between soil and rigid or flexible structure in the SPH frame is proposed [13]. The calculation domain divides into several subdomains, and the contact force is used as a bridge to establish the connection between the subdomains to finally realize the global solution. When the SPH discretizes governing equations of soil motion in each subdomain, the inherent boundary defects of SPH are corrected. It makes the SPH particles near the contact boundary have accurate acceleration, which ensures the accuracy of contact detection. It is assumed that the soil SPH particles are allowed to invade the structure locally. According to the allowable residual invasion amount and the principle of momentum, normal and tangential contact forces of the contact surface are corrected by the slip condition so that they do not exceed the limit friction. Compared with the existing methods that usually use "particle-particle" contact or ignore friction slip in SPH, the method has higher calculation efficiency and accuracy. It is suitable for the simulation of the interaction between geotechnical materials and rigid or deformable structures. The accuracy and stability of this method verifies in many examples. The calculation shows that the SPH is based on a contact algorithm. The results are in good agreement with the theoretical solution or the finite element solution. The algorithm is effective and can be used to expand the calculation ability and application scope of the SPH. Considering the fluid-structure interaction effects in the analysis of liquid storage container dropping [14], CEL method simulates the inertia effect of fluid and the lateral hydraulic pressure to the container, and the fluid-structure interaction effects on the deformation and dynamic response of the container during the process of dropping are considered. The numerical result shows that the method can provide a more accurate evaluation of vessel safety and structural design. Therefore, the CEL mentioned in the paper also provides a reference design evaluation method for the same structure. Considering particularity and uncertainty of drop impact crashworthiness design, the dynamic response of drop impact and impact crashworthiness robust design has been made. Drop

impact crashworthiness robust design optimize is based on crashworthiness evaluation for virtual drop test [15]. This work enriches the design theory and method for dynamic design. Precision electronic products mobile hard disk and liquid-solid coupled fluid-filled containers are chosen as two samples to investigate the capability of dynamic drop impact, crashworthiness design, optimism of structural parameters, and design of crashworthiness.

The collision of the fuel tank is a transient energy conversion process in which the material absorbs energy through deformation. However, the structure of the fuel tank is sophisticated, which will lead to long calculation time and difficulty to ensure accuracy in collision operation. Aimed at the structural characteristics of the fuel tank, this paper adopts a defense node algorithm that avoids solving simultaneous equations and ensures constraints and accurately calculates contact force.

2. Kinetic Analysis of Tank Collision

2.1. Collision Mechanical of Materials. For the collision body made of the fuel tank, the maximum shear stress σ_τ is related to the surface pressure. The following simple formula expresses their relationship [16].

$$\sigma_\tau = \left[(1 + \nu)(s \cot^{-1} s^{-1}) + \frac{3}{2(1 + s^2)} \right] q_0(t). \quad (1)$$

Among them, ν is the velocity at contact.

The maximum value of σ_τ occurs at $s \approx 2/(1 + \nu)\pi$ and $q_0(t)$ is the maximum surface pressure at given time t . For materials with low shear strength, collision will cause shear failure near the surface. The maximum value occurs at $0.5 t_0$, and then its duration occurs at t_0 . The equivalent plastic strain criterion is used for the failure of fuel tank structural materials. When the equivalent plastic strain of the element reaches the threshold, the material is destroyed, and the corresponding part is deleted.

2.2. Fluid-Solid Coupling Analysis. The dynamic characteristics of liquids are affected by the geometrial parameter, filling height, internal structure distribution, frequency, and amplitude of load excitation. At the same time, the physical properties of liquids, such as density, compressibility, and viscosity, also have different effects on the dynamic performance.

The basic principle of the continuum equation is the conservation of mass. The mass δm contained in the Lagrangian infinitesimal fluid unit δV is as follows [17]:

$$\delta V = \rho \delta m. \quad (2)$$

In the formula, m is mass and ρ is density.

For the mass conservation is satisfied in the Lagrangian fluid unit, the mass does not change with time; that is to say, the following equation is satisfied.

$$\frac{d\delta m}{dt} = \delta V \frac{d\rho}{dt} + \rho \frac{d\delta V}{dt}. \quad (3)$$

The fluid is a uniform, nonviscous, and incompressible theoretical fluid, ignoring the fluid-solid momentum transfer and the local pressure-density linear relationship [18]. The coupling equation is

$$\begin{bmatrix} M_s & 0 \\ A^T & M_f \end{bmatrix} \{ \ddot{u} \ \ddot{p} \} + \begin{bmatrix} K_s & -A \\ A^T & K_f \end{bmatrix} \begin{Bmatrix} u \\ p \end{Bmatrix} = \begin{Bmatrix} F_s \\ F_f \end{Bmatrix}. \quad (4)$$

Here, M_s and K_s are the mass matrix and stiffness matrix of the structure; M_f and K_f are the mass matrix and stiffness matrix of the fluid, respectively; A is a fluid-solid coupling matrix; F_s and F_f are structural loads and acoustic loads, respectively; u is the structural node displacement vector; and p is the fluid node pressure vector.

On the coupling interface Γ , the displacement and load balance conditions the following formula:

$$\begin{aligned} d^s \cdot e^s + d^f \cdot e^f &= 0, \\ \sigma^s \cdot e^s + \sigma^f \cdot e^f &= 0. \end{aligned} \quad (5)$$

Here, d^s and d^f are the displacement vectors of the solid domain and fluid domain interfaces, respectively. σ^s and σ^f are the stress vectors at the interface of the solid domain and the fluid domain, respectively. e^s and e^f are the unit displacement base vectors of the solid domain and the fluid domain interface, respectively.

3. Contact Analysis

3.1. Research on Contact Problems during Collision Contact.

The collision process of the fuel tank has nonlinear characteristics. When the collision height is short and the impact energy is small, the elastic force $F(x)$ of the cushioning material has a linear relationship with the deformation x . That is to say, simplifying the buffer material becomes a single-degree-of-freedom spring-mass system with a constant stiffness coefficient in the process of drop impact.

The dynamic impact process is a series of dynamic processes varying with time. Subjected to shock excitation, the system will produce a corresponding shock response. It proves theoretically that the maximum value is related to the duration of shock τ and the inherent period T_n of the system itself after shock excitation. When $T_n < \tau$, the maximum shock response of the system may be twice the peak value of the shock wave, while when $T_n > \tau$, the shock response will be weakened. The impact process is a transient energy conversion process, and the buffer material absorbs energy through deformation.

3.1.1. Kinematic Constraints. The contact and collision structure of the fuel tank is shown in Figure 1. When two contacts are in contact, two points x_2^t and x_1^t coincide at the contact interface. Point x_2^t is the orthogonal projection of point x_1^t on boundary Γ^1 of contact 1 on boundary Γ^2 . According to kinematic constraints, the formula is as follows [19].

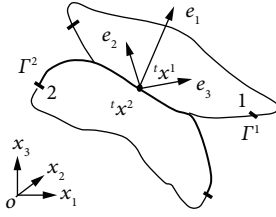


FIGURE 1: Contact-impact interface model.

$$(x_1^t - x_2^t) \bullet e_1 \geq 0. \quad (6)$$

Among them, e_1 is the usual unit vector.

3.1.2. Dynamic Constraints. The contact force on the unit contact surface is pressure, and its pressure value p_e should be satisfied.

$$p_e > 0. \quad (7)$$

The tangential friction p_{et} on the contact surface is the resultant force of the tangential contact forces in the other two directions.

$$p_{et} = \sqrt{p_{et2}^2 + p_{et3}^2}. \quad (8)$$

Among them, p_{et2} and p_{et3} are the tangential friction forces of unit tangent vectors e_2 and e_3 , respectively.

If the Coulomb friction model is adopted, when the maximum static friction force is less than the maximum static friction force, the points on the two contact surfaces are relatively static; that is, the relative tangential velocity A of the points on the two contact faces is

$$v_t^t = (v_1^t - v_2^t) - [(v_1^t - v_2^t) \cdot e_1] e_1 = 0. \quad (9)$$

Among them, v_1^t and v_2^t are the tangential relative speeds of points x_1^t and x_2^t , respectively.

When it is equal to the sliding friction, point x_1^t and point x_2^t are relatively slipped:

$$v_t^t \bullet [p_{1,c}^t - p_{1,c}^t \cdot e_1] e_1 \leq 0. \quad (10)$$

Because the collision time is short and the tangential force is relatively small relative to the normal force, the influence of the tangential force during the collision is ignored.

3.2. Contact Force Algorithm for Contact Collision. Through the analysis of the contact interface, the contact point is found out, and then the contact force is calculated by using the motion law of the object. The value of the contact force contact constraints is limited. The contact point is not allowed to penetrate the contact boundary, and the contact force cannot be tensile.

The usual methods to calculate the contact force are the penalty function method and the Lagrange multiplier method. These two methods are quite different in the explicit algorithms and the implicit algorithms. Lagrange multiplier method involves solving the simultaneous equations of unknown contact

forces, which cannot be directly used in the explicit algorithm; in contrast, it does not solve any simultaneous equations. Therefore, in the explicit algorithm, the penalty function method is often used to calculate the contact force.

The penalty function method has the disadvantages of introducing artificial error and affecting the stability of the explicit algorithm. To make the error introduced by penalty function method small enough, choose reasonable penalty parameters, effectively control the stability of it, and select appropriate penalty parameters is the most significant problem of using penalty function method to calculate contact force. Another one is the calculation of contact penetration. To avoid the error caused by the penalty function method and the influence on the stability of the solution, some particular algorithms are used to solve the contact force by the Lagrange multiplier method, which avoid solution of the simultaneous equations.

For implicit algorithm, whether the penalty function method or Lagrange multiplier method is used, it involves the establishment of contact stiffness matrix, and different iterative algorithms have different requirements for contact stiffness matrix. In the implicit algorithm, a new contact point may not only affect the number of zero elements in the coefficient matrix of the algebraic equation but also affect the bandwidth of the coefficient matrix. When using the Lagrange multiplier method, the total number of unknowns increases, which leads to the change of dimension of the coefficient matrix. So, these will affect the memory allocation and management in the process of solving and also affect the calculation workload. In the implicit algorithm, if the penalty function method is used to calculate the contact force, the penalty parameter should not be too large; otherwise, the coefficient matrix may become ill-conditioned and hinder the solution.

The contact algorithm accomplishes the interaction between colliding structures or components. Within each time step of the solution, check whether the slave node penetrates the main surface. If it penetrates, the force is applied in a direction perpendicular to the main surface by a penalty function to prevent further penetration of the slave node, if not worn. Pass through and then proceed. In the penalty function method, it is difficult to select the penalty parameter value, and it is difficult to obtain the ideal calculation result by experience. To ensure accuracy, the defense node method is used to calculate the contact force. That is, the Lagrange multiplier method is used to satisfy the constraints accurately, and the algorithm of solving simultaneous equations is avoided. The defense node is calculated by adding a virtual contact point to each contact pair.

Assuming the mass of the defense node is M , the motion equation of the defense node and the contact point can be written as follows [20].

$$\begin{aligned} M_1 a_1 &= F_1 + f_1, \\ M_2 a_2 &= F_2 + f_2. \end{aligned} \quad (11)$$

Among them, subscripts 1 and 2 represent, respectively, from the contact point and the defense node. F and f are normal force and contact force, respectively.

The Lagrange multiplier method is used to calculate the contact force to satisfy the constraints. The motion equation is obtained by using the central difference method from the contact point and the defense node.

$$\begin{aligned} M_1 \frac{[\tau v_1 - ({}^t s_1 - {}^\tau s_1)/\Delta t]}{\Delta t} &= {}^\tau F_1 + {}^\tau f_1, \\ M_2 \frac{[\tau v_2 - ({}^t s_2 - {}^\tau s_2)/\Delta t]}{\Delta t} &= {}^\tau F_2 + {}^\tau f_2. \end{aligned} \quad (12)$$

Among them, ${}^\tau s$, ${}^\tau v$ are the displacement and velocity after contact; ${}^t s$, ${}^t v$ are the displacement and velocity before contact.

According to the same magnitude of the defense point force and the force from the contact point, the normal distance is 0, and the defense node force is 0.

$${}^\tau f_1 = M_1 M_2 \frac{({}^\tau F_2/M_2 - {}^\tau F_1/M_1 + {}^l v_2/\Delta t - {}^l v_1/\Delta t - {}^\tau g/\Delta t)}{(M_1 + M_2)}. \quad (13)$$

Among them, ${}^\tau g$ is the total gap between the defensive point and the contact point.

The contact search algorithm plays a significant role in reducing calculation time and improving calculation accuracy. Any contact level has its contact domain, which can be defined as an extension domain. If a slave falls into an extension domain of the main block, the two may contact to form a test pair. If a slave falls into the contact area of it (edge, point), the two contact and shape a contact pair [21].

Contact search includes precontact search and post-contact search. The precontact search is usually divided into two steps, namely, global search and local search, for the slave points that are not in contact state in the previous calculation. The global search roughly determines the slave points that may be contacted and the main blocks that may be contacted with the slave points processed, which is to find out all the test pairs. Local search accurately locates the target of the slave point, calculates the penetration of the slave point relative to its target point, and judges the contact state of the slave point, to find out all contact pairs from the test pair.

Through the contact search algorithm, all the slave points in contact state and their corresponding main blocks (edges, points) in the mechanical system are determined, and the homologous contact force algorithm is used to calculate the contact force. Use the explicit calculation of the central differential and use the contact algorithm to solve the problem. Then, the acceleration of the nodes is used to calculate other physical quantities.

3.3. Stress Failure Criteria. The surface pressure is caused by collision, the failure form is caused by three-dimensional internal stress, and the time sequence of various failure forms. Therefore, appropriate failure criteria can be adopted for the three-dimensional stress state caused by a collision at

each point in the collision object. For composite materials, there are three common criteria:

Cai-Hill Tsai-Hill Strength Theory

$$\frac{\sigma_L^2}{F_L^2} - \frac{\sigma_L \sigma_T}{F_L^2} + \frac{\sigma_T^2}{F_T^2} + \frac{\tau_{LT}^2}{F_{LT}^2} = 1. \quad (14)$$

Hoffman Failure Criterion

$$\frac{\sigma_L^2 - \sigma_L \sigma_T}{F_{Lt} F_{Lc}} + \frac{\sigma_L^2}{F_L^2} - \frac{F_{Lc} - F_{Lt}}{F_{Lt} F_{Lc}} \sigma_L + \frac{F_{Tc} - F_{Tt}}{F_T F_{Tt}} \sigma_T + \frac{\tau_{LT}^2}{F_{LT}^2} = 1. \quad (15)$$

Tsai-Wu Tensor Theory

$$\begin{aligned} \frac{\sigma_1^2}{F_{Lt} F_{Lc}} - \frac{\sigma_1 \sigma_2}{\sqrt{F_{Lt} F_{Lc} F_T F_{Tt}}} + \frac{\sigma_2^2}{F_{Lt} F_{Lc}} + \frac{\sigma_6^2}{\tau^2} \\ + \frac{F_{Lc} - F_{Lt}}{F_{Lt} F_{Lc}} \sigma_1 + \frac{F_{Tc} - F_{Tt}}{F_T F_{Tt}} \sigma_2 = 1. \end{aligned} \quad (16)$$

For the plane stress-strain state, the improved maximum stress failure criterion is used to judge the failure of the matrix material.

3.4. Analysis of Simulation Results. The fuel tank used in this calculation is shown in Figure 2. According to the requirements of the enterprise, use 348 kg slider impact the fuel tank at the height of 2.04 m, and the fuel tank is filled with liquid. For the convenience of analysis, it is considered that the baffle and the slider are rigid parts, and two points of their collision are taken as test data, respectively. The stress simulation results are shown in the figure.

After the tank collides, the displacement deformation in different directions can be obtained. Since the collision mainly occurs in a different direction, the major deformation is shown in Figure 3.

- (a) Before the collision
- (b) Displacement diagram in the x -direction after the collision
- (c) Displacement diagram in the y -direction after the collision
- (d) Displacement diagram in the z -direction after the collision

In terms of displacement, the front end with relatively large deformation is taken. As the fuel tank is a curved part, it is convenient to fix the sensor. The sensor is placed on the plane of the fuel tank in the front section. After measuring its position, the collision and simulation experiments are carried out (Figure 4). In the process of impact test, the major deformation is in the x -axis direction, so this test also mainly considers the impact on the x -axis, and the simulation results are consistent with the experimental results, meeting our impact requirements.

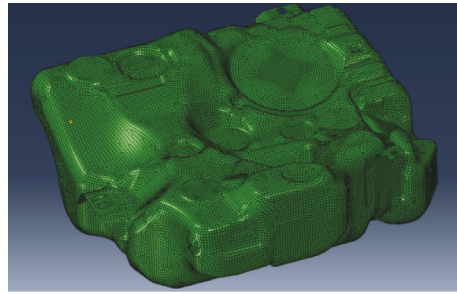


FIGURE 2: Fuel tank structure diagram.

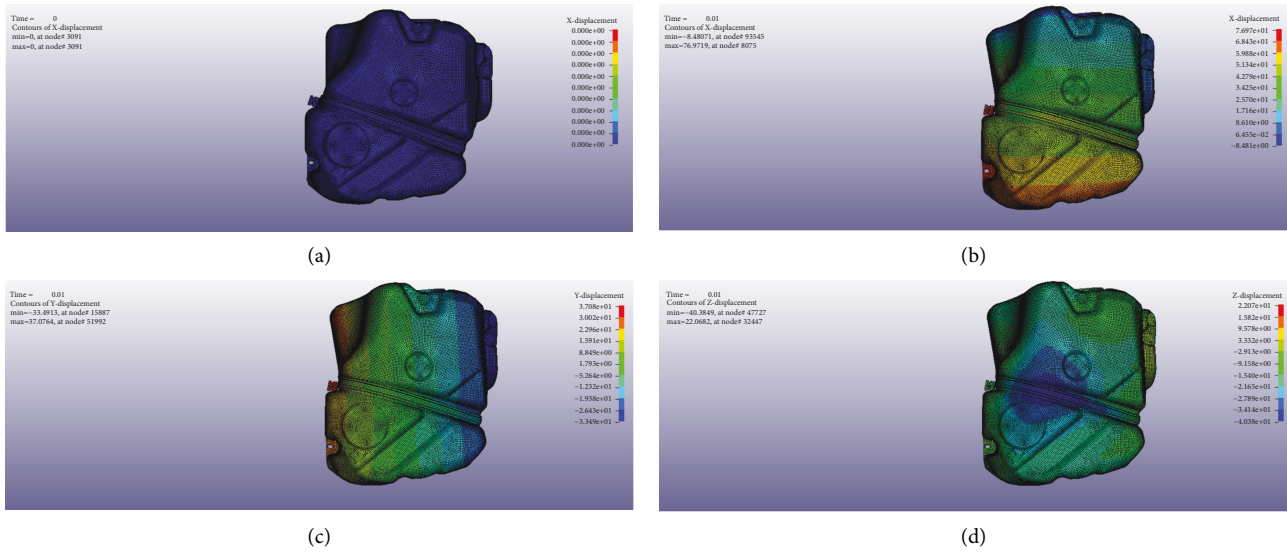


FIGURE 3: Displacement diagram of the fuel tank. (a) Before the collision. (b) Displacement diagram in the x -direction after the collision. (c) Displacement diagram in the y -direction after the collision. (d) Displacement diagram in the z -direction after the collision.

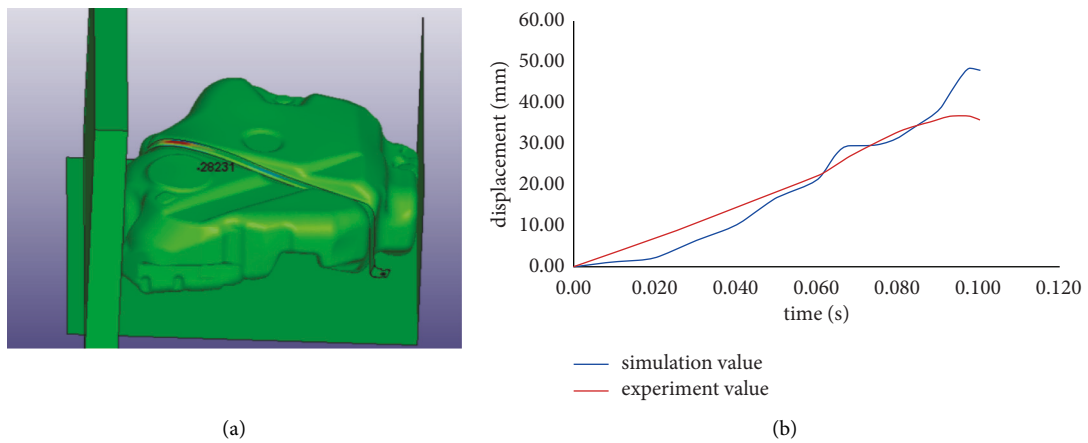


FIGURE 4: Fuel tank configuration and stress-strain diagram. (a) Test point. (b) X displacement of test point.

4. Conclusion

In this paper, the structure of the fuel tank is analyzed, and the mechanical analysis of the collision body made of the fuel tank is carried out. In the collision operation, the problems such as long calculation time and difficulty to guarantee accuracy are caused. The collision impact process of the fuel tank is analyzed, and the deformation process of the fuel tank is simulated and analyzed by the defense node algorithm. This study has important practical significance for the actual collision process of the fuel tank.

Data Availability

The data that support the findings of this study are available from the corresponding author upon reasonable request.

Conflicts of Interest

The authors declare that there are no conflicts of interest regarding the publication of this paper. The paper was presented as a preprint in Research Square (https://assets.researchsquare.com/files/rs-71519/v1_stamped.pdf).

Authors' Contributions

Wenguang Liu analyzed and supervised the study. Haijiang Liu analyzed the study. Lin Jiang analyzed the study. Shanshan Bi analyzed the study.

Acknowledgments

This work was supported in part by a grant from the Jiangsu Provincial Six Talent Projects Funding (JXQC-009).

References

- [1] Y. Gao, Z. Ge, W. Zhai, and S. Tan, "The finite element modelling and dynamic characteristics analysis about one kind of armoured vehicles' fuel tanks," *Materials Science & Engineering Conference Series*, vol. 301, 2018.
- [2] S. J. Magdum, A. Das, V. Shetty, R. Sivakumar, and G. Sakthivel, "DOE study of 'the effect of various parameters on fuel tank sloshing using multiphase CFD'," *International Journal of Ambient Energy*, vol. 42, pp. 1–10, 2018.
- [3] M. Martin, M. Zmindak, and P. Pastorek, "Dynamic analysis of fuel tank," *Procedia Engineering*, vol. 136, pp. 45–49, 2016.
- [4] W. J. Stronge, R. James, and B. Ravani, "Oblique impact with friction and tangential compliance," *Philosophical Transactions of the Royal Society of London, Series A: Mathematical, Physical and Engineering Sciences*, vol. 359, no. 1789, pp. 2447–2465, 2001.
- [5] L. H. Zhang, *Finite Element Simulation on Dropping Impact of Liquid Storage Container*, Dalian University of Technology, Liaoning, China, 2014.
- [6] C. Liu, X. Jiang, and H. Shi, "Mended collision detection algorithm based on oriented bounding box," *Computer Technology and Development*, vol. 28, no. 6, pp. 49–54, 2018.
- [7] L. Chai and X.-M. Wu, "Evolution of bifurcation and chaos in mechanical vibro-impact system with parameters," *Journal of Xiamen University*, vol. 53, no. 4, pp. 508–513, 2014.
- [8] J. Fan, M. Wu, and J. Hu, "Dynamic analysis of vehicle-bridge interaction based on interfacial contact algorithm," *China Journal of Highway and Transport*, vol. 30, no. 4, pp. 52–58, 2017.
- [9] H. Qu, W. Zhao, and A. Qin, "A fast collision detection algorithm based on optimization operator," *Journal of Jilin University (Engineering and Technology Edition)*, vol. 47, no. 5, pp. 1598–1603, 2017.
- [10] C. Chen, M. Liu, and X. Chen, "A contact-impact algorithm based on the segment-to-segment local searching method," *Chinese Journal of Computational Mechanics*, no. 1, pp. 105–110, 2018.
- [11] Z. Li, Y. Jin, and Z. Qin, "Collision detection algorithm of deformable object-based on Snake model optimization," *Journal of System Simulation*, no. 1, pp. 62–68, 2018.
- [12] B. Wang, *Metal Thin-Walled Tube Structure Drop experiment and Simulation*, Beijing Institute of Technology, Beijing, China, 2015.
- [13] J. Wang, H. Wu, and C. Gu, "Simulation of friction contact in smooth particle hydrodynamics (SPH)," *China Science: Technology Science*, vol. 56, no. 11, pp. 1208–1218, 2013.
- [14] J. Nie, H. Zhang, and H. Li, "Dropping accident analysis of liquid storage container using finite element method," *Nuclear Power Engineering*, vol. 34, no. 3, pp. 145–147, 2013.
- [15] S. Yang, *Drop Impact Dynamics and Crashworthiness Robust Design for Manufactured Products*, China University of Mining and technology, Haidian, China, 2009.
- [16] Z. Zhang, *A Study on Impact of Composite Material CNG cylinder*, North China University Technology, Beijing, China, 2006.
- [17] L. Fu, *Dynamic Analysis of Liquid Sloshing and Sloshing Suppression Design for a Tank*, Nanjing University of Aeronautics and Astronautics, Nanjing, China, 2010.
- [18] G. Fu, J. Liang, and H. Luo, "Fluid-structure coupling modal analysis of auto oiltank," *Automotive Technology*, no. 2, pp. 25–28, 2016.
- [19] Z. Yang, Z. Zhong, and G. Li, "Review on contact algorithms calculating the contact-impact interface in mechanical system with explicit FEM," *Journal of Mechanical Engineering*, vol. 47, no. 13, pp. 44–58, 2011.
- [20] H. Hong and G. Li, "Analysis of sheet metal forming based on defence node algorithm," *Computer Simulation*, vol. 28, no. 8, pp. 320–322, 2011.
- [21] W. Liu, H. Liu, L. Jiang, and S. Bi, *Analysis of Fuel Tank Collision Structure Based on Defense point Method*, 2020.

Research Article

Refined Judgment of Urban Traffic State Based on Machine Learning and Edge Computing

Lijuan Liu 

School of Artificial Intelligence, Neijiang Normal University, Neijiang, Sichuan 641112, China

Correspondence should be addressed to Lijuan Liu; liulijuan@njtc.edu.cn

Received 25 November 2021; Revised 10 February 2022; Accepted 23 June 2022; Published 15 July 2022

Academic Editor: Sang-Bing Tsai

Copyright © 2022 Lijuan Liu. This is an open access article distributed under the Creative Commons Attribution License, which permits unrestricted use, distribution, and reproduction in any medium, provided the original work is properly cited.

Machine learning is a discipline that covers probability theory, statistics, approximate theoretical knowledge, and complex algorithm knowledge. It is committed to real-time simulation of human learning methods, which can effectively improve learning efficiency. The main function of this calculation method is to use a relatively open platform to integrate the Internet, computers, memory, and other terminal applications through integrated technical means. For providing short-distance services and applications, we should start from the edge of the program to create a faster network. Service response covers the basic needs of real-time processing industry, intelligent applications, and security and privacy protection. This paper aims to study the recognition of urban traffic conditions and refine the recognition through the improvement of edge computing algorithms. This paper proposes a method to calculate traffic flow parameters, preprocess the traffic flow data, delete irrelevant features, use flow theory to delete wrong data, and change the data in time according to actual needs, carrying out refined discrimination and analysis of urban traffic status. The experimental results in this paper show that the use of edge computing to fine-tune the state of urban traffic can divert traffic, greatly reduce traffic congestion, and increase traffic safety by 13%. Among them, the efficiency of road network time and space resources has also increased by 23%.

1. Introduction

At present, the economy is developing rapidly and the demand for road traffic is also increasing. However, the increase in traffic accidents and traffic congestion has seriously affected the effectiveness of social operations and has also posed a huge threat to social development and the safety of people's lives and property. According to the analysis of relevant experts, the number of vehicles in the future will still maintain strong growth potential, environmental pollution will be serious, and congestion, parking difficulties, and road safety problems will become increasingly obvious. Traffic congestion leads to reduced vehicle speeds, longer travel times, increased emissions, and increased travel costs. These problems immediately become one of the bottlenecks restricting urban development. At present, there are also many compact new energy vehicles, but the penetration rate is not high, and they will also cause pollution and congestion.

In Intelligent Transportation Systems (ITS), urban traffic flow prediction and traffic state recognition functions are very important. Urban traffic congestion assessment and real-time traffic flow prediction can also provide a basis for the design of driving routes. The use of a series of detection methods to monitor road status parameters, understand the overall operating status of the current road, and take effective measures to improve road operation efficiency has become a measure of traffic optimization widely adopted by governments of various countries.

Chen et al. mentioned in their article that there are many ways to classify data. They first introduced the concept of deep learning to hyperspectral data classification. First, they verified the eligibility of stacked autoencoders by following classification based on classical spectrum information. However, most of them do not extract deep features in layers [1]. Taleb et al. proposed a new calculation method in his research, which can effectively reduce the waiting time of users. In addition, they also introduced the MEC survey and

focused on the basic key support technology [2]. The probability modeling dependence proposed by Werner et al. is essential for many applications in risk assessment and decision-making under uncertainty. Ignoring the dependence between multiple uncertainties may distort the model output and hinder the correct understanding of the overall risk. Whenever there is a lack of relevant data to quantify and model the dependence between uncertain variables, expert judgment may be sought to assess the joint distribution. However, due to too many unstable factors in the evaluation, the results are inaccurate [3]. The Japan Railway Institute of Technology has carried out research on sound source analysis and prediction methods to improve the operating efficiency of the Shinkansen and optimize the aerodynamic performance in order to reduce aerodynamic noise.

The innovation of this paper is as follows: (1) By dividing the four traffic conditions to characterize the running state of the vehicle on the road and using the VISSIM traffic simulation software to create a simulation environment, this indicates that the vehicle tail length algorithm and the traffic density algorithm can identify the road traffic condition. VISSIM software can simulate the evacuation of pedestrians in large gatherings, and so on. In addition, VISSIM advanced applications can also carry out dynamic traffic allocation to the road network. (2) Obtain urban bayonet passing data through data acquisition technology, select and calculate traffic flow parameters based on existing research, identify and process wrong data, and repair missing data.

2. The Method of Judging Traffic State Based on Edge Computing

2.1. Data Acquisition and Processing Methods of Edge Computing

2.1.1. Data Acquisition. In the context of the widespread application of big data technology, in order to complete data analysis through algorithms, such as machine learning and artificial intelligence, we need to use various types of equipment for data collection [4]. Therefore, the system needs to use the edge device itself or related sensors to collect the data required by the system according to the algorithm and actual application environment [5].

2.1.2. Data Processing. Errors and other issues appeared [6]. Therefore, in order to minimize the deviation in the original data and ensure the consistency of the data, it is necessary to correct the collected data in order to obtain more accurate data. The data collected in the experiment may have missing values, repeated values, and so on, and data preprocessing is required before use. Common processes are removing unique attributes, dealing with missing values, attribute coding, data standardization and regularization, feature selection, and principal component analysis. The processed data samples are still unusable, and these data need to be distinguished. Therefore, we need to perform feature extraction on naked data to extract statistical features that can well characterize specific behaviors [7].

2.2. Calculation of Traffic Flow Parameters. According to the specific field conditions of the passing record of the intelligent transportation system, four parameters of traffic flow, speed, travel time, and traffic density are selected to describe the road traffic operation state [8].

2.2.1. Traffic Flow. For a certain road section, the actual number of vehicles passing in a unit time period is the concept of traffic volume. Traffic volume is a dynamic variable, and its value changes with time and space. Therefore, it is usually necessary to observe whether its value exceeds its specific threshold range when using traffic volume to determine congestion [9]. However, for the same traffic volume, there may be completely opposite traffic conditions. Therefore, the traffic volume cannot be used as a single discrimination parameter and should be combined with other parameters for joint judgment. In addition, in practical applications, we usually use toroidal coil detectors to collect traffic volume. Try to place a coil in each lane to avoid missed detection. However, the use of toroidal coils usually cannot distinguish between large and small traffic flows. Vehicles can therefore be combined with video capture equipment to determine the distribution of vehicles and improve data accuracy through fusion processing [10]. The traffic flow value ranges from 0 to 10, divided into five levels. Among them, 0–2, 2–4, 4–6, 6–8, and 8–10 correspond to the five levels of “unblocked,” “basically unblocked,” “slightly congested,” “moderately congested,” and “severely congested”; the higher the value, the more serious the traffic congestion.

Traffic flow refers to the number of vehicles passing a unit in a specific direction on a road per hour [11]. According to different periods of statistical movement, it can be divided into daily traffic flow, hourly traffic flow, and 15-minute traffic flow. The traffic flow within 15 minutes is called short-term traffic flow. The simple traffic flow collection is as follows:

$$Q = n * \frac{p}{t} \quad (1)$$

Here, Q is the traffic flow (vehicles), p is the minimum sampling period specified by the project, t is the actual statistical time interval, and n is the number of vehicles passing through a certain road section within the statistical time interval [12].

2.2.2. Speed. Speed is the distance the vehicle travels on the road per unit time. The speed in the traffic flow parameter generally refers to the average speed of the road section. Assuming that there is a vehicle passing through a certain section of the road during a certain statistical period, the vehicle speeds are, respectively, $v_1, v_2, v_3, \dots, v_n$, then the average speed formula of the road section traffic flow in the t period is as follows:

$$v_T = \frac{1}{n} \sum_{i=1}^n v_i \quad (2)$$

2.2.3. Traffic Density. Traffic density refers to the density of vehicles on a lane, that is, the number of vehicles on a lane per unit length at a certain moment, also known as traffic density. The traffic density reflects the number of vehicles on the road segment at the current time point, and the formula can be expressed as follows:

$$k = \frac{n}{l} \quad (3)$$

Here, n is the number of vehicles on a certain road section, l is the length of the road section, and k is the traffic density. Through the traffic flow parameter relationship model, it can be seen that the combination of traffic volume and traffic density can more intuitively and accurately evaluate the traffic state. For example, when the traffic flow is zero, by analyzing whether the traffic density is at the maximum or also zero, we can determine whether the road has few cars or is congested to a standstill [13, 14]. Although the traffic density and traffic volume can be used well together, the data collection is not big, and it is rarely used in practice.

2.2.4. Travel Time. Driving time refers to the time required for a vehicle to travel from two adjacent control points in the same direction to a specific road section. This article calculates the travel time of a section of road. Two intersections (x_1 or x_2 or x_3 or x_4) arrive at the same vehicle at y to calculate the travel time. First, take the passing time of the same vehicle through two adjacent control points, and take the time difference to take the travel time of the road segment. The travel time of different vehicles is collected every 5 minutes. To a large extent, 60% of the average of the total travel time is used to calculate the average travel time of the road segment [15].

2.3. Machine Learning. Machine learning is a type of machine or computer that uses experience to improve and enhance its own performance and capabilities. Among them, experience is very important. However, in a computer environment, experience refers to data. Therefore, machine learning must involve data analysis. Use machine learning algorithms to analyze data sets and discover patterns in the data. When encountering new data, you can make relatively accurate predictions. This is also a hot spot for the application and development of modern machine learning.

According to the different characteristics of the types of data processed, machine learning is generally divided into four learning methods, which are supervised learning, unsupervised learning, semisupervised learning, and reinforcement learning [16]. Machine learning can be divided into these four types according to whether the training data has labels and the form of the algorithm output.

2.3.1. Supervised Learning. Supervised learning is a widely used learning method in machine learning. Its main characteristics are as follows: in the learning process, each input training data has a clear label. The learning model analyzes

and processes these labeled data and continuously learns and trains to adjust the parameters of the learning model until the expected accuracy rate is reached and the learning is completed. After that, the trained model can be used to predict the new unlabeled data and output the result.

2.3.2. Unsupervised Learning. The characteristics of unsupervised learning are mainly that the data used for learning and training is unlabeled, and the unsupervised learning model directly uses its own mechanism to discover the internal rules of the input data set to be predicted and generates the corresponding prediction criteria.

2.3.3. Semisupervised Learning. Semisupervised learning is a learning method that combines supervised learning and unsupervised learning. It differs from the former two. What is more, during the training process, not all the data in the training data set are unlabeled, and there will be artificially added labels to improve the learning results. The purpose of using this learning method is to reduce the cost or price paid for marking each sample.

2.3.4. Reinforcement Learning. Reinforcement learning's, also known as reinforcement learning, goal is to pass an agent through the environment due to changes in its actions. The rewards and punishments are given to optimize the action set, which is also called the strategy set.

2.4. Refined Recognition Method of Traffic State

2.4.1. The Division of Road Section Traffic Status. There are many indicators for evaluating traffic conditions. Generally speaking, traffic flow, integrity rate, travel speed, travel time, and delay time are defined as the main indicators to measure traffic conditions.

This article divides the road section traffic conditions into four types: barrier-free, slow-moving, congestion, and intersection locked. Accessibility means that most vehicles in line can be released at the green light at the entrance. Slow travel means that most of the queued vehicles cannot be released after the green light and must wait for many signal cycles. Traffic congestion has the characteristics of time and space, and the spatial distribution of traffic congestion will also show different characteristics. The slow-moving state caused by the large number of vehicles is also a kind of congestion. Congestion means that the length of the line has reached the congestion detection point within the road section. Interval lock refers to the failure of the intersection function and the queued vehicles cannot move for a long time [17].

2.4.2. Process of Judging Traffic Status. According to the traffic state discrimination parameters and the division of the four traffic states of the road section, the traffic state discrimination process is shown in Figure 1. A_1 , A_2 , and A_3 are three detectors; B is the vehicle time occupancy rate; B_{\min} is the minimum preset threshold of vehicle time occupancy

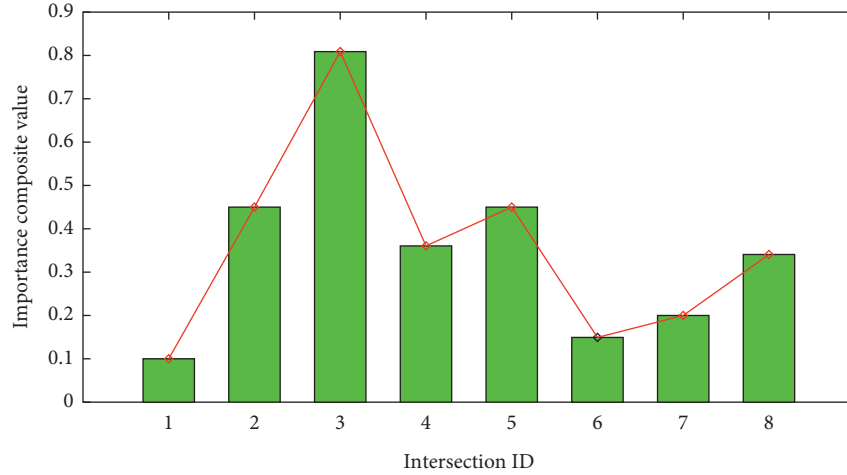


FIGURE 1: Comprehensive value of the importance of traffic intersections.

rate; and B_{\max} is the maximum preset threshold value of vehicle time occupancy rate [18].

2.4.3. Calculation Method of Traffic State

- (1) In the process of traffic state recognition, there are problems of tail length weight and traffic density weight. Different vehicle tail length measurement methods will measure vehicle loading length and delayed occupation length. The traffic density and tail length algorithms used in this program are defined as follows:

When the road section is short and there are no other entrances and exits in the middle, the traffic density algorithm is used to determine the result. In other cases, the vehicle tail length algorithm should be used to determine the result [19].

Determine the traffic conditions in the community. In this article, the cross section detector is used to determine the traffic conditions in a small area. This method is within the interval (total multiplication of the signal period), and subsequently the minimum length of time of the motor vehicle in the interval is predetermined. And compare the maximum threshold with the maximum and minimum values to obtain three types of discrimination effects:

When $B \leq B_{\min}$, the queued vehicles are not queued to the section detector [20].

When $B \geq B_{\max}$, the queued vehicles have passed the section detector, and within one green light time, the queue at the detector cannot be dissipated.

When $B = 100\%$, the intersection is locked.

- (2) Calculation of the length of the tail of a motor vehicle: Assuming that the saturation is x , the method of calculating the length of the tail of the vehicle can be divided into irregular state, saturated state, and supersaturated state, then the critical saturation value x_0 is

$$x_0 = 0.56 + \frac{gt}{500}. \quad (4)$$

When $x \leq x_0$, the number of vehicles in line at the red light is

$$Q = c_i q. \quad (5)$$

When in saturation and oversaturation, when $x > x_0$, the number of queued vehicles during the red light period is

$$Q = \frac{Gt}{4} \left[x - 1 + \sqrt{(x - 1)^2 + \frac{12(x - x_0)}{Gt}} \right]. \quad (6)$$

Here, G is the capacity, $C = S\chi$; t is the collection time, and g, x is the saturation within the collection interval.

According to the above judgments and calculations, the number of tails in no-load, saturated, and supersaturated states is taken. Then, the length of the tail of the motor vehicle is

$$L = \frac{Q(L + l)}{n}. \quad (7)$$

Here, L is the length of the vehicle, and its vehicle length is 5 m; l is the vehicle spacing, and its distance is 1 m; and n is the number of entrance lanes.

- (3) Calculation of traffic density: When the road section is short and there are no other entrances and exits in the middle, the traffic density algorithm is used to determine the road section of the traffic condition. The number of vehicles Q_t on the road during t time is

$$Q_t = Q_0 + Q_1 - Q_2. \quad (8)$$

Here, Q_1 and Q_2 are, respectively, the traffic volume entering and exiting the road section within the collection

interval t and Q_0 is the initial traffic volume of the road section. Then, the traffic density is

$$k = \frac{Q_t}{L}. \quad (9)$$

3. Machine Learning Traffic State Fine Recognition Experiment

3.1. Process of Fine Recognition of Traffic Status. The traffic state recognition in the intelligent transportation system needs to ensure strong real-time performance, so the use of state classification based on prior knowledge can effectively reduce the calculation time and quickly obtain the recognition result. The basic process of applying fuzzy clustering technology to real-time traffic status recognition is as follows: first, select appropriate parameters that can describe traffic conditions, and extract these parameter values from uncontaminated historical traffic operating data. Because the minimum period of urban traffic operation is generally 24 hours, the time span of the selected data is not less than the minimum period interval. Then, use fuzzy clustering algorithm to classify the data, get the cluster center, determine the traffic state represented by each cluster of data, and get the prior knowledge of state recognition represented by the cluster center. Finally, the membership function is used to calculate the membership of the traffic data tuples collected in real time for different cluster centers, which is the membership of different traffic states. The maximum membership state is selected as the result of the current road traffic state, and the result is displayed to the user, and the traffic state recognition is completed.

3.2. Improvement of Traffic State Recognition Algorithm. With the development of technology, the discrimination algorithm is also improving. According to different sources of input data, the improved discrimination algorithm can be divided into ACI algorithm based on fixed detector and ACI algorithm based on mobile detector.

3.2.1. Fixed Detector: Two-Stage ACI Algorithm Based on HOG + SVM. The combination of HOG feature and SVM classifier has been widely used in pedestrian detection and face recognition, and many scholars have verified its good effect in the field of traffic state recognition. This paper implements a HOG + SVM classifier for positioning. Exit the traffic sign area. The realization process is as follows:

- (1) *Data Preparation.* Preprocess the traffic data to remove the random components in the data; divide the data set to form a subset of the HOG + SVM training data and the test subset; estimate the predicted value of all data in chronological order and calculate the value of the input variable.
- (2) *HOG + SVM Model Calibration.* Use the input variable data of the upstream and downstream of the target road section to determine the number of

hidden nodes in the upstream and downstream HOG + SVM model and their connection weights.

- (3) Determine the decision threshold and distinguish traffic conditions. According to the traffic conditions corresponding to each data group in the data set, in accordance with the requirements to ensure the congestion crisis rate, the misjudgment rate and the average crisis time, and so on, the decision-making and threshold values of the upstream and downstream HOG + SVM models are optimized, and the traffic index is judged accordingly. And use the “or” operation to fuse the decision results and give the traffic state of the target road section.

3.2.2. Motion Detector: ACI Algorithm Based on Road Travel Time. Mobile traffic detectors are the main technology for collecting dynamic traffic flow information in the future. It not only obtains more intuitive and useful travel time, travel speed, and other road traffic flow parameters, but also has good scalability and scalability economy. Therefore, the ACI algorithm developed based on this data has a better effect of judging traffic congestion.

Motion detection technology can receive real-time travel time data of road sections. Therefore, when determining the expected travel time, the traffic state of the destination road section can be determined according to the current travel time data. The travel time data of different road segments in the same period can also be used to distinguish what is happening in the congestion type. The algorithm flow is as follows:

- (1) Data preparation: preprocess the obtained average travel time data, remove random components, and form the travel time sequence $T_i(t)$ of the i th road section
- (2) Determine the expected travel time for each road section
- (3) Calculate the delay $T_i(t)$ of the travel time of each section
- (4) Judging the crowded state: if $T(t)$ is greater than the established threshold K_i , it can be considered that there is congestion in the i th road section

3.3. Intelligent Recognition System of Traffic State Based on Deep Learning

3.3.1. Data Processing. Before the design and training of the network, the first thing to do is to collect and process data. What needs to be noted in the data collection process is the following: (1) Data needs to be collected with different devices, including different mobile phone cameras, different cameras, and devices with different resolutions. (2) Different lighting needs to be taken care of during the data collection process, different environments. (3) The data collection scene needs to be as large as possible or collect various pictures from the Internet. These practices are mainly to make the collected data as comprehensive as possible. Only

as comprehensive as possible can the probability of error in the subsequent actual use process be small.

After collecting the data, we also need to label the data. The content of the label includes the extraction of the position of the traffic light and the classification of the type of the traffic light. After processing the data, we need to divide the data into three categories: 60% of the data is used for network training, 30% of the data is used for testing, and 10% of the data is used for verification.

3.3.2. Network Design. First, the image is passed through FASTER-RCNN to obtain the detection result, and the target area is extracted. The extracted image is preprocessed to make the image the same size, and then the changed image is classified through the classification network. Then, the traffic light area obtained by Faster-RCNN is deducted from the original image, and the obtained images are unified into the same size and then sent to the image classification network to further classify the image. If the results obtained by ftP-RCNN are the same as those obtained by the subsequent classification network, the results are considered correct. If they are inconsistent, re-detection will be conducted.

4. Refined Discriminant Analysis of Urban Traffic Status Based on Deep Learning

4.1. State Analysis of Urban Traffic Intersections. According to the calculation method of the index weight value in the comprehensive evaluation method of the intersection, first determine the judgment matrix composed of five indicators, and then verify the consistency of it to obtain the consistency index value of 0.068. Obviously, this value is less than 0.1, so it can be considered as calculated. The obtained index weight values have good consistency. The specific data and calculation results are shown in Table 1.

From the data analysis in Table 2, we can see that the indicators with weights from high to low are average delay, saturation, queue length, proximity centrality, and degree centrality. Specific analysis shows that because the impact of intersections on the road network is more caused by changing traffic flow, the existence of traffic flow and its randomness make the evaluation index of traditional traffic engineering have a higher weight; secondly, in traditional traffic engineering, the average delay has a relatively high weight ratio because people are more sensitive to driving speed and travel time in the process of participating in traffic; finally, in the two indicators of complex network theory, proximity centrality has comparative centrality. A higher weight ratio exists because whether the intersection in the road network is in the core position and whether it has better accessibility can more directly affect its importance.

According to the road network structure diagram, the parameter values of the centrality and proximity centrality of each intersection can be calculated. At the same time, in the VISSIM software, run the road network simulation for 4500 simulation seconds. Among them, each road section is set according to the actual situation with a flow input ranging from 200 to 700 pcu/h, and 500 simulation seconds are set as

a measurement cycle to obtain the average value of the saturation, average delay, and queue length in each cycle, a total of 8 cycles. In order to make the simulation data relatively real and complete, discard the first few cycles, the last few cycles, and the cycle data with more incomplete data, and select the fourth cycle data. The final index values are shown in Table 2.

Combining the abovementioned index parameters, using the method of calculating the comprehensive value of importance in the intersection importance evaluation of multi-index decision-making described in this chapter, the result shown in Figure 1 can be obtained.

The comparative analysis shows that among the 8 intersections, the first three most important intersections are intersections 2, 3, and 5, respectively. Only the total importance of these three intersections accounts for 40%. A reasonable explanation for this result is that both of the three intersections 2 and 3 are on the main road and have a large traffic volume, which has a greater impact on the operation efficiency of the road network; in the structural layout, 5 and 9 are relatively located. The central location of the road network area makes them have a higher influence. Judging from the raw data, intersections 5 and 9 bear more traffic distribution pressure than intersection 3.

4.2. Refined Discriminant Analysis of Urban Traffic. In order to verify the effectiveness of the above method, this paper uses VISSIM traffic simulation software to construct a traffic section, input the simulation environment of continuous changes in traffic volume, and input the traffic volume in the test section. When the time is 0–1000 s, the traffic volume is 500 pcu (standard car equivalent number), in a smooth state; when the time is 1000–2000 s, the traffic volume is 700 pcu, which is in a slow state; when the time is 2000–3000 s, the traffic volume is 1000 pcu, in a congested state; when the time is 3000–4000, the traffic volume is 1350 pcu, and the intersection is locked. In the whole process of traffic volume change, the interval vehicle speed, travel time, vehicle density, and queue length of the road section are collected, and the change characteristics of road section information are compared and analyzed.

The simulation data structure shows that when the traffic volume gradually increases from 500 pcu to 1350 pcu, the changing trends of different indicators are shown in Figure 2. According to the data analysis in the table, the traffic volume of 1–13 seconds may be 500 pcu; the traffic volume of 14–26 s is 700 pcu; the traffic volume of 27–39 s is 1000 pcu, and the traffic volume during 40–51 s is 1350 pcu. In addition, the speed of the space may fluctuate frequently throughout the process. Compared with travel time, the curve of section density and tail length has the best normality. Therefore, the use of vehicle tail length and traffic density algorithms can effectively distinguish road traffic conditions.

4.3. Analysis of the Intelligent Transportation System Based on Deep Learning. Adjust according to the priority of each direction of the intersection. Assuming that the current is an intersection, there are four intersection directions,

TABLE 1: Judgment matrix and the weight of each indicator.

Index	Saturation	Average delay	The length of queue	Degree centrality	Proximity centrality
Saturation	3	0.3	6	4	0.23
Average delay	2	1	4	4	0.47
The length of queue	0.3	0.2	1	2	0.12
Degree centrality	0.3	0.2	0.3	1	0.06
Proximity centrality	0.3	0.2	0.4	3	0.12

TABLE 2: Index values of traffic intersections.

Intersection ID	Saturation	Average delay	The length of queue	Degree centrality	Proximity centrality
1	0.11	10	1.2	0.12	0.3
2	0.13	5	0.7	0.12	0.3
3	0.26	243	27	0.15	0.3
4	0.5	259	121	0.15	0.38
5	0.4	24	22	0.18	0.38
6	0.4	35	87	0.18	0.38
7	0.5	322	45	0.22	0.45
8	0.3	122	33	0.22	0.45

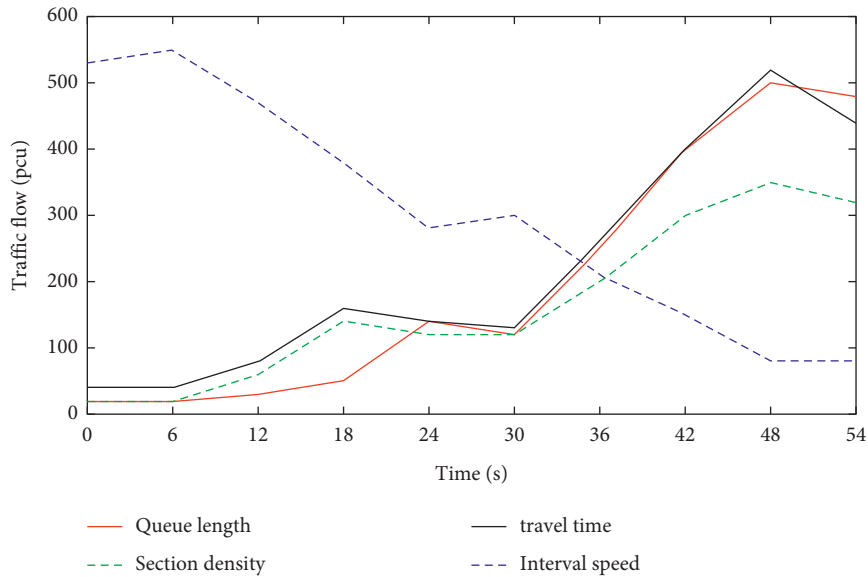


FIGURE 2: Change trend process of road parameters.

represented by E, S, W, and N, respectively; the two directions that are passing are positive, and the remaining two directions are negative. When the state of the direction with the highest priority is positive, the transit time t_1 second is increased, and so on.

In order to verify the feasibility of the experimental plan, a traffic congestion model is established, assuming a fixed intersection scene, and each car in the scene is moving forward at an equal speed. Suppose that the traffic lights at the intersection are all t_1 and the initial number of vehicles on the roads in the four directions is a , and random b vehicles will be added at time t_1 . That is, for the general situation without the adjustment function, the number of vehicles in the four directions of the intersection at each time point after the end of the traffic is N . In the general case without the adjustment function, the changes in the number

of vehicles in the four directions of the intersection at each time point after the end of the traffic are simulated, and the result is shown in Figure 3.

After adding intelligent adjustment, it will have an impact on the transit time and then affect the number of vehicles in the four directions of the intersection at each time point after the end of the traffic. Among them, the adjustment time T is obtained after the congestion level is determined according to the number of vehicles obtained by the vehicle detection module in the roadside unit. The value of T is not absolutely fixed and can be set according to the actual situation in practical applications. But here, different fixed values of T are assigned to different congestion levels, and the change in the number of vehicles N in the four directions of the intersection at each time point after the end of the traffic is simulated when the adjustment function is

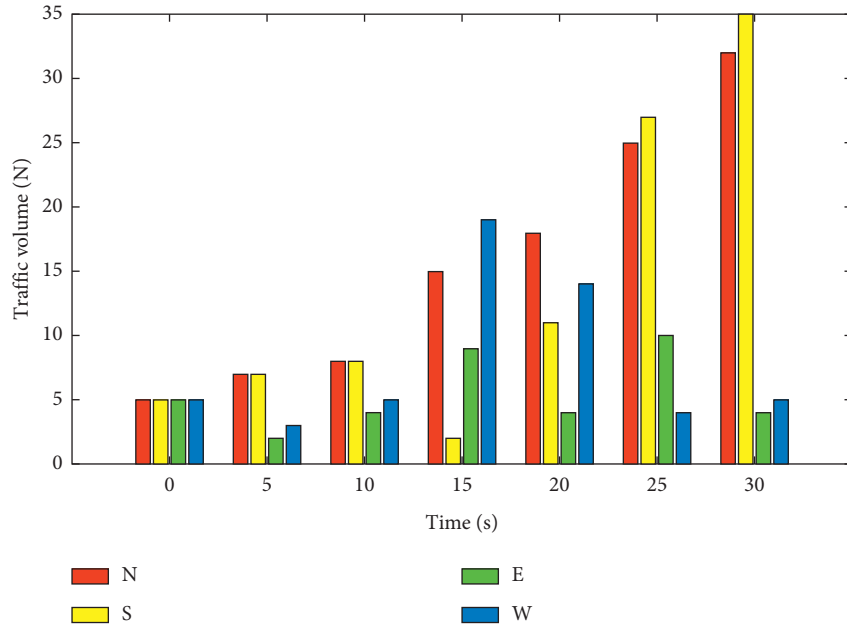


FIGURE 3: Simulation effect of the general traffic system.

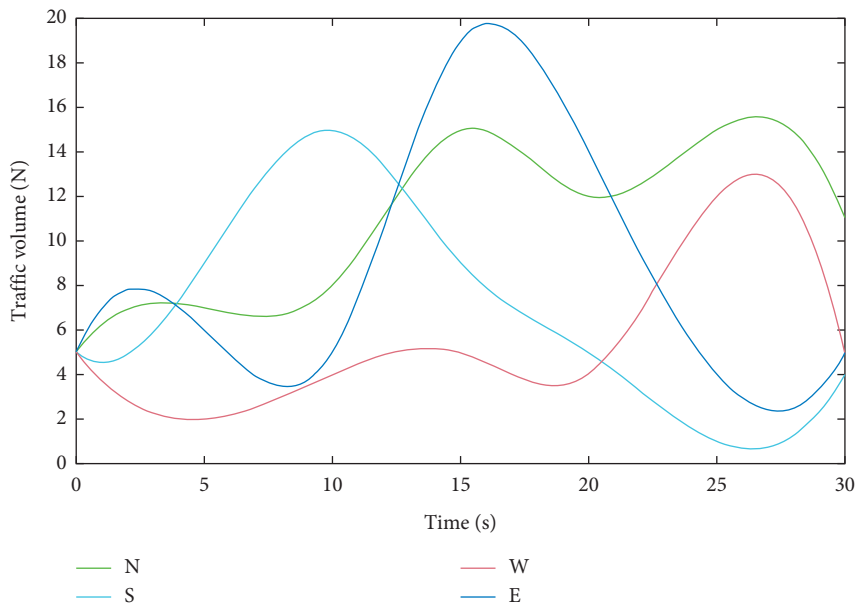


FIGURE 4: Traffic system effect after adding regulation.

added so as to facilitate contrast with the general situation above. The simulation result is shown in Figure 4.

As can be seen from the above simulation results, when the random value B is large, that is, there are more vehicles coming into the intersection in a certain direction in a certain period of time, the congestion at the intersection without the adjustment function will tend to be aggravated and it will take a long time to recover. After the adjustment function is added, the congestion at the intersection is relatively stable and can be restored in a relatively short period of time. This shows that the adjustment of traffic lights is effective, and the vehicle detection function based on

the improved traffic recognition algorithm is the basis for the realization of vehicle statistics, congestion judgment, and adjustment functions.

5. Conclusions

For the identification of traffic state, the domestic and foreign identification methods are studied and summarized. The classic urban traffic state discrimination methods include California algorithm, McMaster method, exponential smoothing method, and standard deviation method. These algorithms are simple to operate, but the false alarm rate is

relatively high, and they are generally studied for expressways. Urban roads are more complex, and more appropriate algorithms need to be explored.

The urban road traffic system itself is an operating system with very complex logic. There are many variable factors that affect the system, with strong time-varying and spatial differences. Although this article focuses on traffic flow prediction and traffic state subproblems in the field of traffic systems and does some research work, there are still a lot of problems that need to be analyzed and discussed.

The improved traffic recognition algorithm only targets three types of dynamic targets and does not integrate the static target detection model. For static targets, only the optimization of the data set is done. Static objects do not affect the identification of traffic flow, because although these static objects are traffic participants, their impact on traffic is almost zero. Such processing may cause the redundancy problem of the system loading model, and the optimization is not thorough. If the system design needs to be verified on the spot, large-scale road traffic scenarios and equipment are needed. The research in this article does not yet support such a costly verification test.

Data Availability

The data that support the findings of this study are available from the author upon reasonable request.

Conflicts of Interest

The author declares no conflicts of interest regarding the publication of this paper.

Acknowledgments

This work was supported by the Foundation of the 2021 Key Scientific Research Project of Neijiang Normal University (No. 2021ZD08).

References

- [1] Y. Chen, Z. Lin, X. Zhao, G. Wang, and Y. Gu, "Deep learning-based classification of hyperspectral data," *Ieee Journal of Selected Topics in Applied Earth Observations and Remote Sensing*, vol. 7, no. 6, pp. 2094–2107, 2017.
- [2] T. Taleb, K. Samdanis, B. Mada, and Flinck, "On multi-access edge computing: a survey of the emerging 5G network edge cloud architecture and orchestration," *IEEE Communications Surveys & Tutorials*, vol. 19, no. 3, pp. 1657–1681, 2017.
- [3] C. Werner, T. Bedford, and J. Quigley, "Sequential refined partitioning for probabilistic dependence assessment," *Risk Analysis*, vol. 38, no. 12, pp. 2683–2702, 2018.
- [4] G. Litjens, T. Kooi, B. E. Bejnordi, A. Setio, and V. D. Ciomp, "A survey on deep learning in medical image analysis," *Medical Image Analysis*, vol. 42, no. 9, pp. 60–88, 2017.
- [5] D. Shen, G. Wu, and H. I. Suk, "Deep learning in medical image analysis," *Annual Review of Biomedical Engineering*, vol. 19, no. 1, pp. 221–248, 2017.
- [6] X. Wang, L. Gao, S. Mao, and S. Pandey, "CSI-based fingerprinting for indoor localization: a deep learning approach," *IEEE Transactions on Vehicular Technology*, vol. 66, no. 1, pp. 763–776, 2017.
- [7] D. Ravi, C. Wong, F. Deligianni, Berthelot, J. Andreu-Perez, and B. Lo, G. Z. Yang, "Deep learning for health informatics," *IEEE Journal of Biomedical and Health Informatics*, vol. 21, 2017.
- [8] X. X. Zhu, D. Tuia, L. Mou et al., "Deep learning in remote sensing: a comprehensive review and list of resources," *IEEE Geoenvironment & Remote Sensing Magazine*, vol. 5, no. 4, pp. 8–36, 2018.
- [9] W. Hou, X. Gao, D. Tao, and X. Li, "Blind image quality assessment via deep learning," *IEEE Transactions on Neural Networks and Learning Systems*, vol. 26, no. 6, pp. 1275–1286, 2017.
- [10] Y. Tom, H. Devamanyu, P. Soujanya, and E. Cambria, "Recent trends in deep learning based natural language processing [review article]," *IEEE Computational Intelligence Magazine*, vol. 13, no. 3, pp. 55–75, 2018.
- [11] M. D. De Assuncao, A. D. S. Veith, and R. Buyya, "Distributed data stream processing and edge computing: a survey on resource elasticity and future directions," *Journal of Network and Computer Applications*, vol. 103, pp. 1–17, 2018.
- [12] Z. Li, W. M. Wang, G. Liu, L. Liu, J. He, and G. Q. Huang, "Toward open manufacturing: a cross-enterprises knowledge and services exchange framework based on blockchain and edge computing," *Industrial Management & Data Systems*, vol. 118, no. 9, pp. 303–320, 2018.
- [13] K. Zhang and Y. Mao, "Mobile-edge computing for vehicular networks: a promising network paradigm with predictive off-loading," *IEEE Vehicular Technology Magazine*, vol. 12, no. 2, pp. 36–44, 2017.
- [14] H. Li, K. Ota, and M. Dong, "Learning IoT in edge: deep learning for the Internet of things with edge computing," *IEEE Network*, vol. 32, no. 1, pp. 96–101, 2018.
- [15] Y. Mao, J. Zhang, S. H. Song, and Letaief, "Stochastic joint radio and computational resource management for multi-user mobile-edge computing systems," *IEEE Transactions on Wireless Communications*, vol. 16, no. 9, pp. 5994–6009, 2017.
- [16] G. Ananthanarayanan, P. Bahl, B. Bodik, and Chintalapudi, "Real-time video analytics: the killer app for edge computing," *Computer*, vol. 50, no. 10, pp. 58–67, 2017.
- [17] X. Chen, Q. Shi, L. Yang, and Xu, "ThriftyEdge: resource-efficient edge computing for intelligent IoT applications," *IEEE Network*, vol. 32, no. 1, pp. 61–65, 2018.
- [18] Q. Yuan, H. Zhou, J. Li, and Liu, "Toward efficient content delivery for automated driving services: an edge computing solution," *IEEE Network*, vol. 32, no. 1, pp. 80–86, 2018.
- [19] X. Zehui, Z. Yang, N. Dusit, P. Wang, and Z. Han, "When mobile blockchain meets edge computing," *IEEE Communications Magazine*, vol. 56, no. 8, pp. 33–39, 2017.
- [20] E. Ahmed, A. Ahmed, I. Yaqoob, and Shuja, "Bringing computation closer toward the user network: is edge computing the solution?" *IEEE Communications Magazine*, vol. 55, no. 11, pp. 138–144, 2017.

Research Article

Outdoor Clothing Design for Traffic Safety Based on Big Data and Artificial Intelligence

Ya Zhou  and Yun Shi

School of Fine Arts and Design, Zhanjiang Science and Technology College, Zhanjiang 524003, Guangdong, China

Correspondence should be addressed to Ya Zhou; 201904020037@stu.zjsru.edu.cn

Received 18 February 2022; Revised 20 May 2022; Accepted 30 May 2022; Published 7 July 2022

Academic Editor: Sang-Bing Tsai

Copyright © 2022 Ya Zhou and Yun Shi. This is an open access article distributed under the Creative Commons Attribution License, which permits unrestricted use, distribution, and reproduction in any medium, provided the original work is properly cited.

With the development of technologies in various fields, more and more technologies have been applied to safety clothing, which has led to the rapid development of safety clothing. The improvement of living standards is accompanied by the change of consumption concepts. Consumers' requirements for clothing products have become more artistic, healthier, and more ecological, and they look forward to more and better safety clothing to meet their health needs. In this context, this article studies traffic safety outdoor clothing design based on big data (BD) and AI. This article introduces the design method of outdoor safety clothing for traffic based on BD and machine learning in artificial intelligence (AI) and did two experiments. To this end, this paper adopts a Deep Belief Network (DBN), which is trained layer by layer through Restricted Boltzmann Machine (RBM), and successfully solves the problems of lack of a large number of labeled samples and easy to fall into local optimum. The first experiment is to test the accuracy of various machine learning algorithms for clothing size measurement. The results obtained are as follows: the predicted value of the DBN neural network is the closest to the actual value, the average prediction accuracy of DBN for the cuff size is 90%, and the average prediction accuracy for the neck circumference is 91.5%. The second experiment is to investigate the functional needs and performance concerns of children and outdoor workers. The results of the experiment are as follows: for children, 79.9% of people want clothing to have a positioning function, which accounts for the highest proportion. For outdoor workers, the most important clothing function they need is eye-catching style, and 90.1% of those choose this option. In terms of clothing performance concerns, most people choose to care very much, and the second most people choose to care about comfort.

1. Introduction

1.1. Background. With safety as the main purpose, emphasizing a healthy, comfortable, green, and environmentally friendly living environment is what modern people yearn for and look forward to. In the face of the complexity of the traffic environment, the differences in human coping capabilities, and the chaos of special groups, it is necessary to understand the close relationship between clothes and the human body and use the special functions of clothes to reduce traffic accidents. The design of safety clothing requires the use of technologies in multiple disciplines, such as electronic information technology, biological science technology, 3D printing technology, bionic technology, new material technology, and human-computer interaction

technology. It is the product of the integration of technological development and clothing. BD is a collection of superlarge amounts of data. The application of BD is the result of the development of modern information technology, and it is also an important tool to promote the development of information technology. Applying BD to the design of outdoor clothing for traffic safety and designing clothing based on AI-related technologies will make the safety performance of clothing more secure.

1.2. Significance. Traffic safety is an important safety issue in people's daily life. Complicated traffic conditions, heavy traffic, and people's low awareness of traffic safety are all important causes of traffic accidents. Traffic accidents are

constantly happening every day, so it is necessary to reduce the occurrence of traffic safety accidents through some means. Therefore, it is very meaningful to combine intelligent technology, BD technology, and clothing technology to design clothing that guarantees traffic safety. Intelligence is regarded as one of the development trends in safety clothing. Application innovation is the core of the development of smart clothing in the network age, innovation with user safety as the core and the soul of the development of safety clothing. BD is currently an important way for people to use information. The analysis of data enables people to better grasp and use information. The design of traffic safety clothing utilizes the information processing capabilities of BD and combines the key technologies of AI. It is believed that the design of safety clothing will get a breakthrough development.

1.3. Related Work. Both BD and AI are new technologies in the Internet era, and their applications have spread to various fields, and many scholars have conducted research on them. Xu et al. examined the privacy issues related to data mining from a broader perspective, studied different methods to ensure sophisticated data, and also put forward some preliminary ideas for future research directions. These methods are designed to decompose the associations between various customers in data mining scenarios, and each customer has their own assessment of sensitive information [1]. Kuang et al. proposed a unified tensor model and ihosvd method. Experimental results show that the proposed unified tensor model and ihosvd method are effective for BD representation and dimensionality reduction, but the research lacks detailed design [2]. Yaoxue and Zhang gave an overview of the topic of big data and conducted a comprehensive investigation on how cloud computing and related technologies respond to the challenges brought by big data. Then, Yaoxue analyzed the shortcomings of cloud computing when BD encountered the Internet of Things and introduced two promising computing paradigms. Finally, he summarized some open challenges and future directions to promote continuous research in this evolving research field. The disadvantage is that the study lacks specific cases [3]. Zhang et al. proposed a cyber-physical system for patient-centric healthcare applications and services called health CPS, which is based on BD analysis technology. The results of this study show that cloud and BD technology can be used to improve the performance of medical systems so that humans can enjoy various intelligent services. The research shows relatively little on the data [4]. Rathore et al. proposed a real-time BD analysis architecture for remote sensing satellite applications. The architecture has the ability to partition, load balance, and process only useful data in parallel. Therefore, the use of Earth observation systems can effectively analyze real-time remote sensing big data. In addition, the proposed architecture is able to store the incoming raw data in order to perform offline analysis on a large number of stored dumps when needed [5]. Rongpeng and Li tried to emphasize one of the most basic characteristics of the revolutionary technology in the 5G era and

further introduced the basic concepts of AI. He discussed the relationship between AI and candidate technologies in 5G cellular networks, demonstrating the effectiveness of AI in managing and orchestrating cellular network resources. Rongpeng envisions that 5G cellular networks with AI capabilities will make acclaimed ICT promoters a reality. This research has good ideas but no convincing reasons [6].

1.4. Innovation. The innovation of this article is (1) Combining big data, AI, and traffic safety outdoor clothing design, it introduces the traffic safety outdoor clothing design method based on BD and AI and proposes some algorithms, which is a methodological innovation. (2) It designed experiments to test the clothing size measurement method based on AI and did a questionnaire survey. By investigating the two groups most in need of outdoor traffic safety, this article understands their expectations of clothing functions and their attention to various performances of clothing. This is an experimental innovation.

2. Road Safety Outdoor Clothing Design Method Based on BD and AI

2.1. Clothing Design Based on AI. This chapter mainly uses traditional machine learning methods and improved deep belief networks to intelligently design the size of safety clothing and studies the methods of establishing neural network models.

2.1.1. Construction of Clothing Data Set. The constructed data set is divided into two parts: the data measured by the traditional measurement master and the data produced by the advanced Boke intelligent CAD software. Performing net body size data collection and clothing model size data collection [7]. The collected net body size data includes items such as height, upper arm circumference, hip circumference, net sitting circumference, and net waist circumference. The collected clothing model size data includes back length, neck circumference, trouser length, foot opening, front wave, back wave, front small crotch width, and back small crotch width. And ensuring that the collected clothing model size data and the net body size data establish a one-to-one correspondence.

2.1.2. Machine Learning Algorithm Design. AI is developing rapidly. As the core of AI, machine learning is also excellent in the rapid development of AI, and it has attracted more and more people's attention [8]. The following describes the application of machine learning related algorithms in the intelligent design of safety clothing.

(1) BP Algorithm Size Intelligent Design. BP network, in fact, is also a kind of multilayer perceptron and is currently the most widely used neural network. The BP network training process is divided into two steps, one is forward propagation to obtain the output result, and the other is backpropagation to transmit the error back to the input and then adjust the

model parameters. Finally, a neural network model of $6 \times 12 \times 10$ is formed. The result of data normalization is shown in the left image of Figure 1, and the small shoulder width is shown in the right image of Figure 1.

(2) *Linear Algorithm Size Intelligent Design*. The least square method is also called the least square method. The least square method can achieve the goal of minimizing errors. The sum of squared errors between the obtained data and the actual data can be minimized, and the derivation Formula is as follows [9]:

$$\log L(\theta) = \prod_{i=1}^m \frac{1}{\sqrt{2\pi\sigma}} \exp\left(-\frac{(y^i - \theta^t x^i)^2}{2\sigma^2}\right). \quad (1)$$

Expand and simplify

$$\begin{aligned} \sum_{i=1}^m \log \frac{1}{\sqrt{2\pi\sigma}} \exp\left(-\frac{(y^i - \theta^t x^i)^2}{2\sigma^2}\right) \\ = m \log \frac{1}{\sqrt{2\pi\sigma}} - \frac{1}{\sigma^2} \cdot \frac{1}{2} \sum_{i=1}^m (y^i - \theta^t x^i)^2. \end{aligned} \quad (2)$$

Simplify the least square method by combining the log-likelihood formula to obtain the following least square method formula. After logarithmic transformation, the larger the likelihood function value, the better.

$$J(\theta) = \frac{\left[\sum_{i=1}^m (y^i - \theta^t x^i)^2\right]}{2}. \quad (3)$$

When using ordinary least squares regression, the residual sum of squares and similar variance items are used to evaluate the fitting effect of the model. The model evaluation method of the following formula [10]:

$$R^2 = 1 - \frac{\sum_{i=1}^m (\hat{y}_i - y_i)^2}{\sum_{i=1}^m (y_i - \bar{y}_i)^2}. \quad (4)$$

In the formula, the numerator of the score is the residual sum of squares, and the denominator is a similar variance term.

Establish a linear regression formula by deriving the formula of least squares regression and construct a loss function to solve the parameters a and b when the loss function is minimum, as shown in the following formula:

$$\hat{y} = ax + b. \quad (5)$$

In the formula, \hat{y} represents the predicted value.

2.1.3. Improved Deep Belief Network. The Deep Belief Network (DBN) is composed of several restricted Boltzmann machines and a layer of backpropagation network. Its structure is shown in Figure 2 [11].

Its structure is shown in Figure 2. The training process of DBN mainly includes two parts, namely unsupervised layer-by-layer pretraining, using RBM layer-by-layer training as

the pretraining stage, each layer of the RBM network is trained independently and unsupervised, and the RBM of the previous layer is output. The value is taken as the RBM input value of the next layer; the other part is to use the supervised improved BP network as the fine-tuning stage, and the error between the output value obtained by the network training and the expected output value is propagated back layer by layer, and the entire Deep belief network to fine-tune the weights.

(1) *Restricted Boltzmann Machine*. The basic idea of a restricted Boltzmann machine (RBM) is to satisfy self-learning unsupervised learning. It can fit the input parameters to the maximum extent so that the difference between the reconstructed data and the actual input parameters becomes the smallest. It has been widely used in speech recognition, document processing, image recognition, face recognition, etc. However, at present, RBM is mainly used to initialize the parameters of the neural network and extract features during data preprocessing. At present, RBM is mainly used to initialize neural network parameters and extract features in data preprocessing. Each RBM consists of a visible layer and a hidden layer. Its structure is shown in Figure 3. In the figure, h represents the hidden layer, W represents the weight, and V represents the visible layer [12].

Let the reconstructed visible layer neurons calculate the state of the hidden layer neurons again, and then the state of the new hidden layer neurons can be obtained. If the state of the hidden layer or visible layer neuron is determined [13], the activation probability of its unit is as follows:

$$p\left(\frac{h_j = 1}{v; \theta}\right) = f\left(c_j + \sum_{i=1}^I w_{ij} v_i\right), \quad (6)$$

$$p\left(\frac{v_j = 1}{h; \theta}\right) = f\left(b_j + \sum_{i=1}^I w_{ij} h_i\right).$$

In the formula, the function f represents the sigmoid function.

(2) *Backpropagation Network*. Backpropagation network (BP) is a supervised classifier trained according to the error backpropagation algorithm, which can achieve the effect of fine-tuning the entire deep belief network model. The backpropagation network (BP) has the following three formulas in the selection of the optimal number of units in the hidden layer of the network structure:

$$\begin{cases} l < \sqrt{a+b} + c, \\ l < n - 1, \\ l = \log_2 n. \end{cases} \quad (7)$$

In the formula, a , b , and l represent the number of nodes in the output layer, input layer, and hidden layer, and c is a constant. Since the Sigmoid activation function is used, it can be seen in the figure that when the output is close to 1, the rate of change of the Sigmoid curve is close

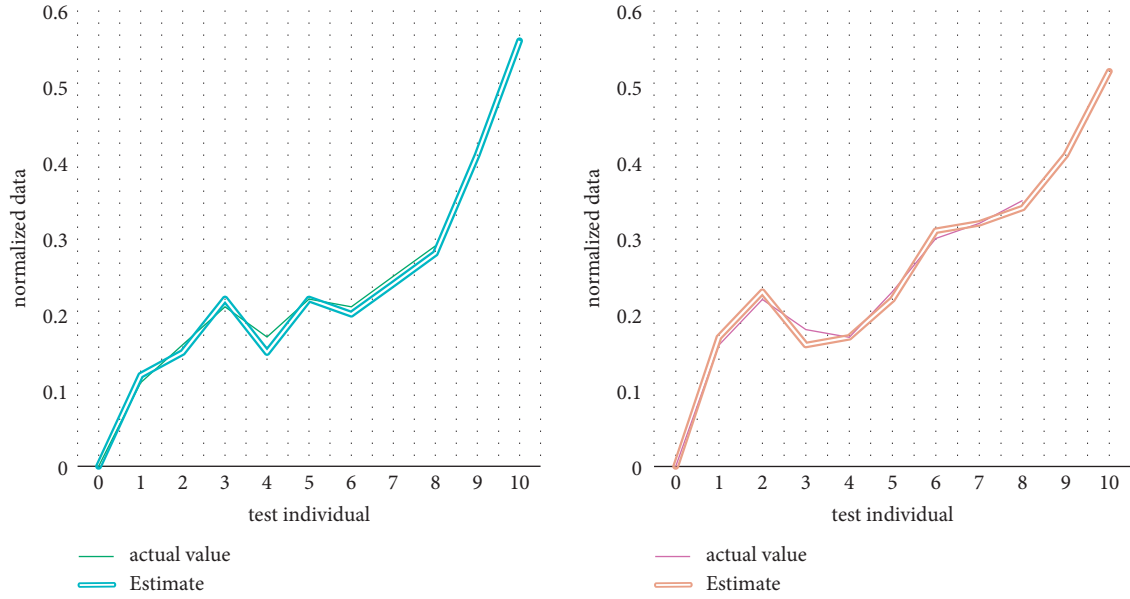


FIGURE 1: BP algorithm results of neck circumference and small shoulder width.

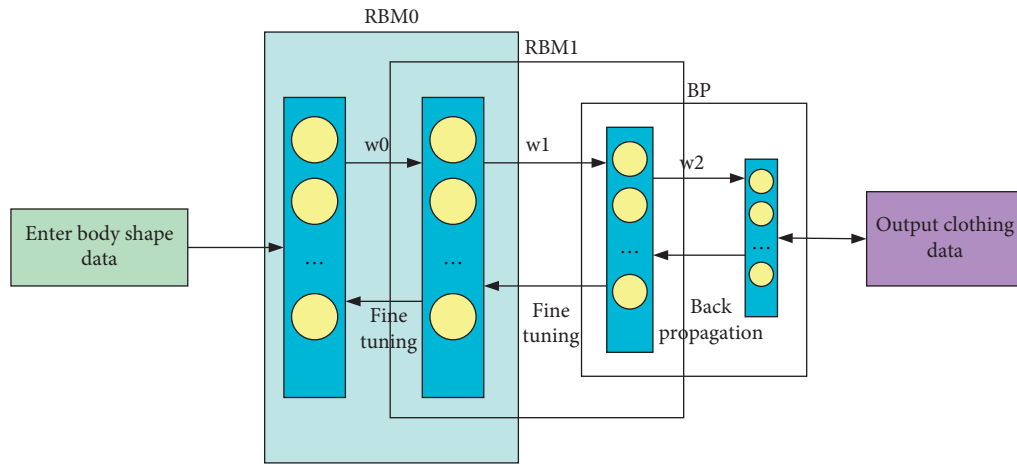


FIGURE 2: Deep belief network structure.

to 0. At this time, the value of $\sigma'(z)$ is small, which will cause the learning rate of the BP neural network to be relatively slow., in order to change the influence on the learning rate of the BP neural network, This paper uses the cross-entropy cost function [14]:

$$C = -\frac{1}{k} \sum_X [y_0 \ln y + (1 - y_0) \ln (1 - y)], \quad (8)$$

where k represents the total training data and y_0 is the expected output value.

(3) *The Realization of Deep Belief Network Model.* Due to the different units of input data and output data, there will be a certain error in the training of the DBN neural network. In the process of BP neural network, the sigmoid function is regarded as an excitation function. Because the result of the

sigmoid function is in $(0, 1)$, the data of the training sample set should be normalized and then resized to a uniform size. The formula is as follows:

$$y = \frac{x_0 - x_{\min}}{x_{\max} - x_{\min}}. \quad (9)$$

In the formula, y represents the standardized data and x_0 represents the original data.

2.1.4. *Wearable Clothing Based on Artificial Intelligence.* Under the system of “human intelligent clothing environment,” wearable clothing has more and more functions. In the design of smart clothing with technical design as the key element, technology determines the overall performance of smart clothing. It will not only directly affect the functionality, comfort, and interaction of smart clothing but also

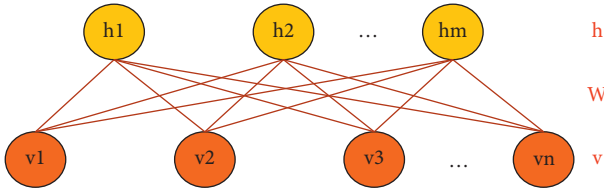


FIGURE 3: RBM structure diagram.

indirectly affect the appearance fashion of clothing. Therefore, the improvement of technology is undoubtedly a double-edged sword. We should not only ensure the wearability of smart clothing but also “hide” the electronic devices in smart clothing as much as possible.

The positioning function is an important function of wearable clothing. This function is mainly used for children. Children belong to relatively vulnerable groups due to their physical and mental particularity, and the problem of loss is an important problem for children, which mostly concerns parents. Therefore, this function is also the most important function of children’s outdoor safety clothing.

Safety protection function is also one of the important functions of intelligent wearable clothing, especially for outdoor workers and cyclists. Multiple reflective strips are installed on the body and trousers of such clothes to improve night safety. In order to prevent accidents, airbag modules are added in important parts of clothing, such as the neck, shoulder, chest, back, and hip, and collision sensors are set at the same time. When the contact point is impacted, the control unit will automatically inflate the airbag quickly so as to protect important parts of the body and improve safety guarantee.

2.2. Clothing Design Based on Big Data

2.2.1. Big Data. BD generally refers to a kind of data collection, which is very large and contains more data than the amount of general data analysis, so it is called “big data.” The concept of BD was put forward in the context of human beings entering the era of data. BD means the ability to collect and analyze large amounts of data generated in society [15]. BD is a collection of a large number of various data forms. This collection has high value and high technical requirements for data processing. At the same time, it is accompanied by high data security and information security risks.

2.2.2. Clothing Algorithm Design Based on Big Data. The relevant algorithms of the BD analysis module in this chapter are essentially an application of collective wisdom. It is to collect useful information from traffic safety clothing usage information to help obtain statistically significant conclusions on safety clothing. These conclusions are not available to us with a small amount of data and can reflect the essential elements of safety clothing. This chapter uses a collaborative filtering algorithm to design [16].

First, we use the Sqoop-based BD collection module to investigate people’s preferences for safety clothing in a distributed manner and convert these records into a simple triple:

$$\langle \text{UserID}, \text{ItemID}, \text{Preference} \rangle. \quad (10)$$

Then, use metrics such as Euclidean distance, cosine similarity, etc., to calculate the similarity between users. In essence, Euclidean distance represents the true distance between two points in a multidimensional space, and its calculation formula is as follows:

$$d(x, y) = \sqrt{\sum (x_i - y_i)^2}. \quad (11)$$

The similarity expressed by Euclidean distance is as follows:

$$\text{sim}(x, y) = \frac{1}{1 + d(x, y)} = \frac{1}{1 + \sqrt{\sum (x_i - y_i)^2}}. \quad (12)$$

The Pearson correlation coefficient represents the ratio between the covariance and standard deviation between two triples, as follows:

$$\rho(x, y) = \frac{\text{cov}(x, y)}{\sigma_x \sigma_y} = \frac{\sum x_i y_i - \sum x_i y_i / N}{\sqrt{(\sum x_i^2 - (\sum x_i)^2 / N)(\sum y_i^2 - (\sum y_i)^2 / N)}}. \quad (13)$$

$\text{cov}(x, y)$ represents the covariance, and $\sigma_x \sigma_y$ is the standard deviation.

Use x, y to represent triples and N represents the number of triples [17]. The calculation Formula of cosine similarity is as follows:

$$\cos \alpha = \frac{\sum x_i y_i}{\sqrt{\sum x_i^2} \sqrt{\sum y_i^2}}. \quad (14)$$

In summary, different recommendation methods are formed in this system to realize the recommendation process. Then according to the algorithm evaluation mechanism, the optimal method is automatically selected, and the algorithm is submitted to the distributed platform to run, and the final result is obtained, as shown in Figure 4.

2.2.3. Algorithm Evaluation. The accuracy rate represents the ratio of the number of retrieved documents to the total number of retrieved documents [18]. The recall rate represents the ratio of the number of retrieved related documents to the number of all related documents. They are used as evaluation indicators in the field of information retrieval and statistical classification. Defined by confusion matrix: retrieved (True), not retrieved (False), relevant (Positive), and irrelevant (Negative), as shown in Table 1.

2.2.4. Decoding of Collaborative Influence Factors Based on Cloud Computing. According to the three-step process of grounded theoretical concept generation, step-by-step decoding, and construction of the theory, the first step is to extract the smallest decoding unit for safety clothing design influencing factors from document analysis, field research,

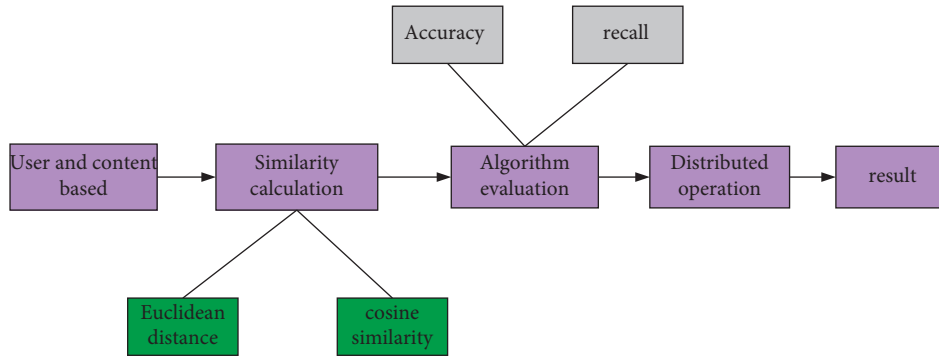


FIGURE 4: Recommendation process.

and expert interview records [19]. In order to obtain the necessary synergy influencing factors of safety clothing design, the survey results were screened by two methods: average score value and full score frequency.

(1) *Average Score Value*. First, summarize the scores of each expert for each indicator, and then calculate the average score of each item according to the following formula:

$$V_i = \frac{\sum_{j=1}^{b_j} x_{ij}}{b_j}, \quad i = 1, 2, \dots, n; \quad j = 1, 2, \dots, b, \quad (15)$$

V_i represents the average score of index i , b_j represents the number of experts evaluating index j , and x_{ij} refers to the score of the i th expert on index j . The larger the average score, the more important the indicator.

(2) *Frequency of Full Marks*. The frequency of full score refers to the ratio of the number of experts who give full marks to the i index to the total number of experts who evaluate the i index, namely:

$$f_i = \frac{b_j}{b_i}. \quad (16)$$

Among them, f_i represents the frequency with which index i gets a perfect score, b_j represents the number of experts who scored a perfect score for index j , and b_i represents the total number of experts who evaluated the index i .

2.3. Outdoor Traffic Safety Clothing Design. At present, outdoor traffic safety clothing is mainly used for outdoor workers such as traffic police, sanitation workers, and cyclists. Due to their special work requirements, they need to wear eye-catching clothing to protect their own safety. Nowadays, due to the rapid development of technology, safety clothing is not only specially designed in colors, but also high-tech means such as BD and AI technology can be introduced to design.

2.3.1. Clothing Design Process. With the rapid development of science and technology and the mutual penetration of various fields, many new technologies and methods have emerged. Smart safety clothing will inevitably develop in a multifunctional and comfortable direction. Designers must

carefully test the accuracy and power consumption of safety function components when formulating the development process of intelligent safety clothing products. And it organically combines these properties with the basic elements of clothing, thus retaining other factors that may be equally important to consumers under the premise of emphasizing safety functions [20].

(1) *Combination of Intelligent Interactive Equipment and Wearer's Clothing*. Smart safety clothing includes clothing and accessories that make up a smart system. According to the method of use, it can be divided into four categories: headwear, wristbands, pendants, and body wear. Regardless of the device, the goal of research and development is to improve the portability, wearability, and safety performance of the product according to the user's physical, psychological, and living conditions under the premise of satisfying the preset component functions.

(2) *Standardization of the Research and Development Model of Intelligent Safety Clothing*. Targeting the characteristics of human-computer interaction, the combination of smart interactive devices and wearer's clothing, and the multi-interaction methods of smart interactive devices and mobile terminals, this research conducts a comprehensive and systematic exploration of the research and development model of smart interactive wearer safety clothing. It puts forward a set of theoretical models with high operability and relatively universal in a certain range and explores the theoretical basis for the industrialization of interactive wearable clothing. Figure 5 is a typical frame diagram of information sharing in multiple interactive modes.

2.3.2. Design Principles of Outdoor Traffic Safety Clothing

(1) *Principles of Zoning Design*. Elements such as points, lines, and surfaces of clothes design are the basic composition methods. The study of zoning design is dedicated to solving the contradiction between the size of the safety factor and the appearance of the clothing. The zoning design cleverly divides the front and back of the clothes into a layered system of areas and the main fabric of the clothes and seamlessly connects and combines them according to the

TABLE 1: Accuracy and recall.

Actual class	Assigned class			
	Positive Negative Total	Positive True positive (TP) False positive (FP) TP + FP	Negative False negative (FN) True negative (TN) FN + TN	Total TP + FN FP + TN TP + FP + FN + TN

needs of the design appearance. The influencing factors of zoning design include clothing wearing environment, functional indicators, monitoring accuracy, wearing performance, and decorative effects.

(2) *Principles of Human-Computer Interaction*. Although people live in the real world, they increasingly rely on the information exchange brought about by the virtual world. Based on the development of network technology, it is possible to achieve good communication between clothes and other online worlds. Clothing designers and consumers have clearly guided that clothing and accessories are the most primitive but the most natural wearable clothing, always inseparable. Compared with many wearables as additional accessories, wearing clothes seems to have no extra burden at all. Smart safety clothes are based on the interaction of three parts, namely the interaction of body, climate, and clothes. In the interactive system, the body, climate, and clothes form an interdependent relationship. The body and the environment exist objectively, so people can only change their clothes to adapt to the body and the environment.

2.3.3. *Current Situation of Outdoor Traffic Safety Clothing*. Due to the special professional needs of outdoor workers such as traffic police, sanitation workers, and cycling athletes, most of the current outdoor traffic safety clothes are designed for these practitioners. Traffic police on-duty clothing is related to traffic safety. Reasonable and efficient traffic police clothing design will provide a favorable guarantee for China's road traffic safety. Within the scope stipulated by law, the modeling setting of traffic police clothing, the proportion of color area, and the design of details, styles, and structural processes need to be more scientific and reasonable. Giving the functionality of traffic police clothing styles has become an urgent problem to be solved. Figure 6 shows the clothing of Chinese traffic police. It can be seen that the clothing has bright color, comfortable style, and reasonable design, which is in line with the professional characteristics of traffic police.

With the rise of cycling, the development of cycling clothing in the industry is also advancing by leaps and bounds. It is one of the most potential types of intelligent clothing and fabrics. In order to reduce the resistance of the wind, the riding clothes mostly adopt the close-fitting style. During cycling, the upper body of the human body keeps leaning forward, and the arms lean forward, so the length of the front piece is shorter than that of the back piece, and the sleeves are designed to cut forward. In the process of cycling, the wearer also has functional needs for color. The color can be used as a warning for people to express each

other's rationality when riding so that they can use color to express each other's rationality and avoid each other's movement. At the same time, on the premise of meeting the aesthetic effect of clothing, the fabric of clothing should also have the properties of adapting to the expansion of body movement, efficient perspiration, moisture permeability, warmth preservation, wind resistance, sun resistance, water washing resistance, and so on. Figure 7 shows a classic cycling suit.

3. Outdoor Clothing Design for Traffic Safety Based on BD and AI

3.1. Clothing Design Experiment Based on AI

3.1.1. *The Overall Design of the Experiment*. This chapter conducts experiments based on the Linear algorithm, BP algorithm, and DBN algorithm introduced in 3.1. This chapter uses these three algorithms to predict the cuff size and neck size of the human body and then compares them with the actual values to explore the prediction accuracy of these algorithms.

3.1.2. *Algorithm Flow Design*. A linear algorithm is a traditional machine learning algorithm, the process of which has been described in the previous article, so I will not repeat it here.

(1) *BP Algorithm Process*. The BP network training process is divided into two steps. The first is to calculate the output of each unit of the hidden layer and the output layer and calculate the square error $E(i)$ between the output result and the actual value. If all $E(i)$ meet the requirements, the training ends. If the requirements are not met, recalculate until the parameter $E(i)$ meets all the requirements. Its work flowchart is shown in Figure 8.

(2) *DBN Algorithm Flow*. The training of the DBN network mainly includes unsupervised layer-by-layer pretraining of RBM and supervised fine-tuning of BP and DBN network structure. The training steps of the deep belief neural network are shown in Figure 9.

In unsupervised pretraining, the human body shape data is assigned to the output layer as input data, and the CD algorithm is used to train the input layer. After the training, the RBM0 parameter reaches the highest value. With the help of the trained RBM0, the value of the hidden layer is obtained, the data of the input layer is regarded as the data of the input layer, and RBM1 is formed with the second hidden layer. The training method is used to train the RBM1, and

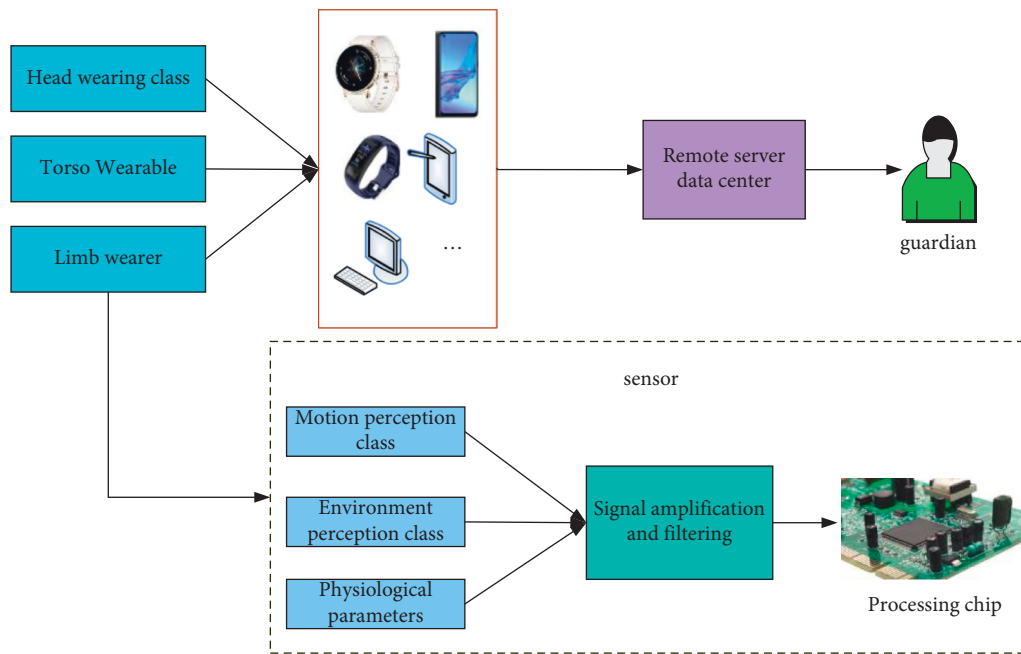


FIGURE 5: Multi-interaction information sharing framework diagram.



FIGURE 6: Chinese traffic police clothing.

finally, the optimal parameters of the RBM1 network are obtained.

3.1.3. Experimental results and analysis. The Linear algorithm, BP algorithm, and DBN algorithm are used to predict the cuff size according to the steps described, and the actual values of the cuff size and the size predicted by the three algorithms are counted, and the results are shown in Figure 10.

It can be seen from the figure that among the three algorithms, the cuff value measured by the linear algorithm

is the farthest from the actual value. The predicted value of the DBM algorithm is the closest to the true value. It can be seen that the DBM algorithm has the highest accuracy for the predicted value of the size. In order to better verify this conclusion, we have done another neck circumference measurement experiment, and the results are shown in Figure 11.

In the measurement of neck circumference, the predicted values of the three algorithms are relatively close, and there is no significant difference. However, the measured value of the DNB algorithm is still the closest to the true value, so it can be seen from the two experiments



FIGURE 7: Cycling clothes.

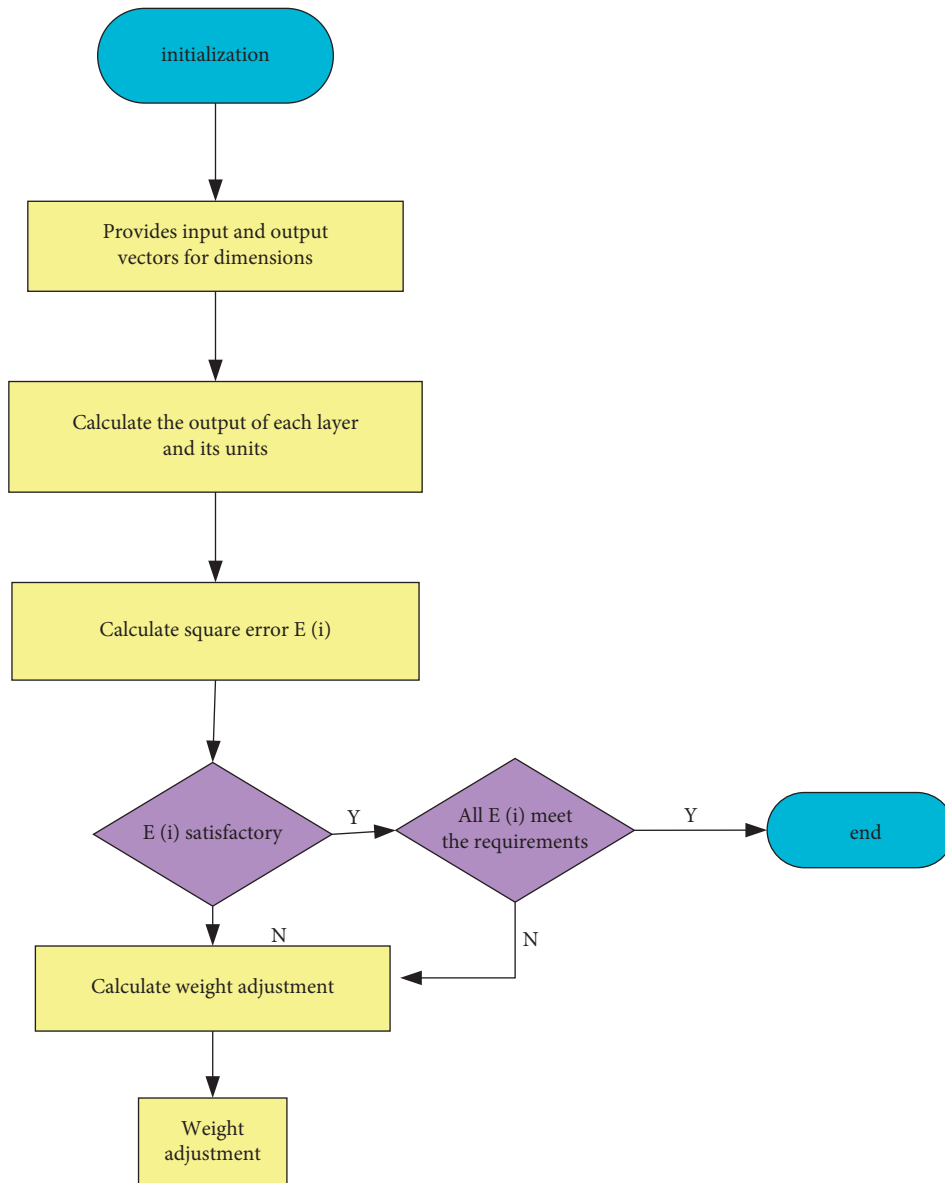


FIGURE 8: BP algorithm flowchart.

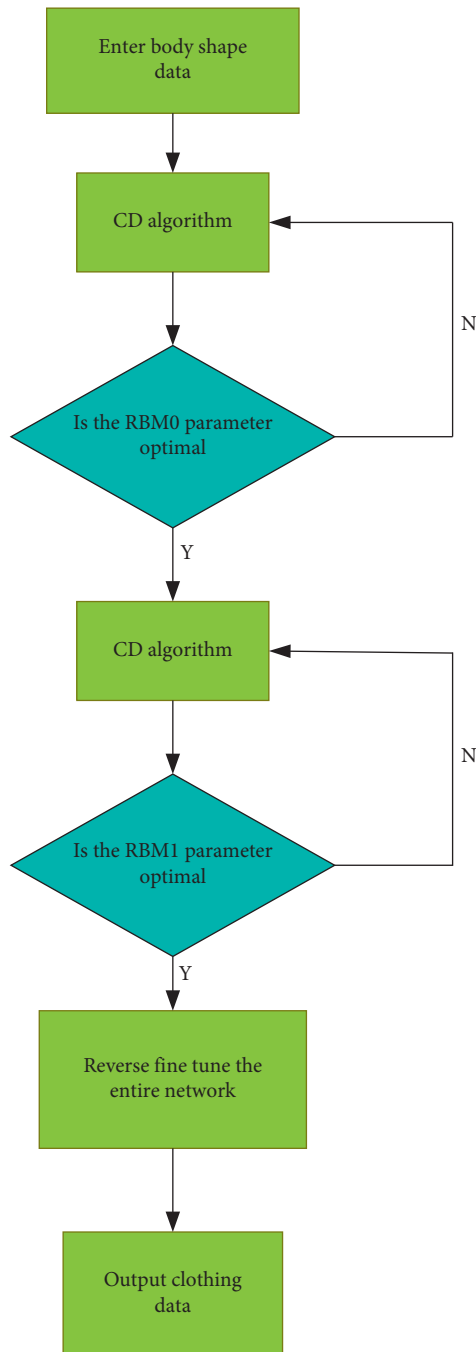


FIGURE 9: DBN network training flowchart.

that the prediction of DBN is the closest to the true value compared to the predicted value of the other two algorithms. And in the measurement of cuff size, DBN's average prediction accuracy rate for different samples is 90%. In the measurement of neck circumference, the average prediction accuracy of DBN for different samples is 91.5%. Although there is a certain error between the predicted value of the DBN neural network and the actual value, this deviation is normal for clothing structure design. At the same time, for 15 different test samples, the effects predicted by the DBN neural network model are also different. For example, the accuracy of the neck

circumference is higher than that of the waist circumference. After analysis, it is found that, on the one hand, the data source of the output layer is inconsistent with the data source of the input layer. The data of the input layer is the child's body shape data, and the data of the output layer is the sample size of children's clothing. On the other hand, the training sample set is not large enough. If there is more data for scientific training, the accuracy of this model will be further improved [21, 22].

3.2. Survey on Demand for Outdoor Traffic Safety Clothing. This questionnaire conducted market research and analysis for the two major groups of people who most need outdoor traffic safety clothing. The two major groups are children and outdoor workers. Children have poor self-management skills, weak traffic awareness, and are petite. Outdoor workers often need to work outdoors. The working place is generally on the street, outside the building, and there are many opportunities for contact with vehicles and pedestrians. Therefore, these two types of people are more likely to encounter traffic hazards, so there is a high demand for outdoor traffic safety clothing. The purpose of this experiment is to understand the functional needs and performance concerns of these two groups of people for safety clothing so as to grasp the overall development direction of safety clothing design in the later period. It clarifies the market positioning and future development direction of safety clothing, promotes the process of industrialization of safety clothing, and better meets people's consumer needs [23].

3.2.1. Experimental Method. This test method adopts the questionnaire method, and the contents of the questionnaire are set as follows: Questions are, respectively, asked about the functional expectations of the two types of clothing and the degree of attention to the clothing performance. A total of 300 questionnaires were received in this survey, of which 286 were valid questionnaires, including 144 questionnaires on children's outdoor traffic safety clothing and 142 outdoor workers' safety clothing questionnaires.

3.2.2. Survey Results of Clothing Function Questionnaire. This study first investigated the functions that parents hope that children's safety clothing has, and the results obtained are shown in Table 2.

It can be seen from the table that 79.9% of people hope that clothing has a positioning function, which accounts for the highest proportion. The second is the reminder function, such as a real-time reminder of location information, mood changes, and physical signs changes. It can also be seen that the biggest pain point for parents is that they are afraid of children getting lost when traveling with them. Therefore, when designing children's safety clothing, it is necessary to focus on the design of the positioning function, then the reminder function should be designed well, the clothing style should be eye-catching, and the design of the physical sign monitoring function should be paid attention to.

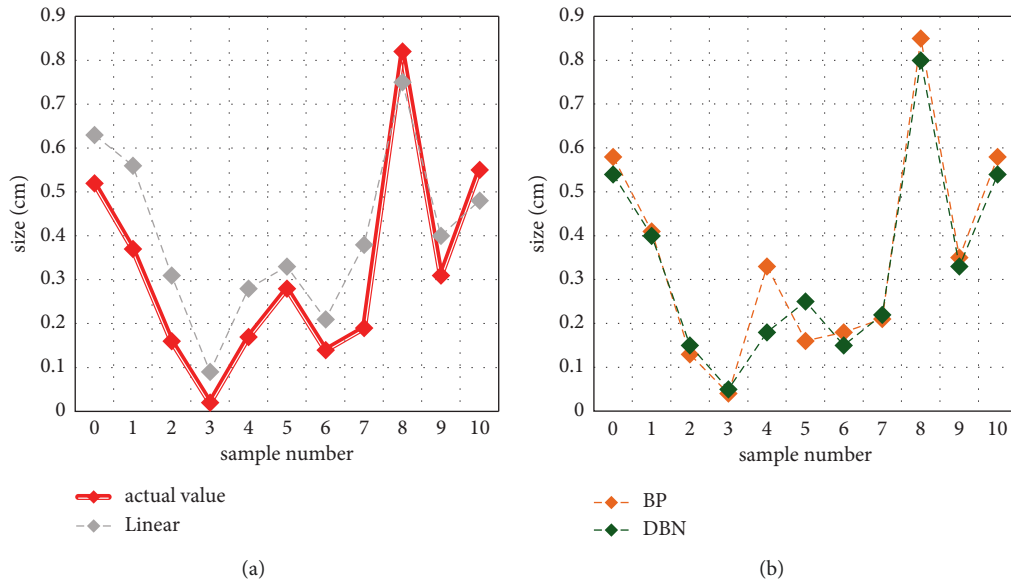


FIGURE 10: Cuff size of different algorithms: (a) The cuff data is not normalized (b) The cuff data is normalized.

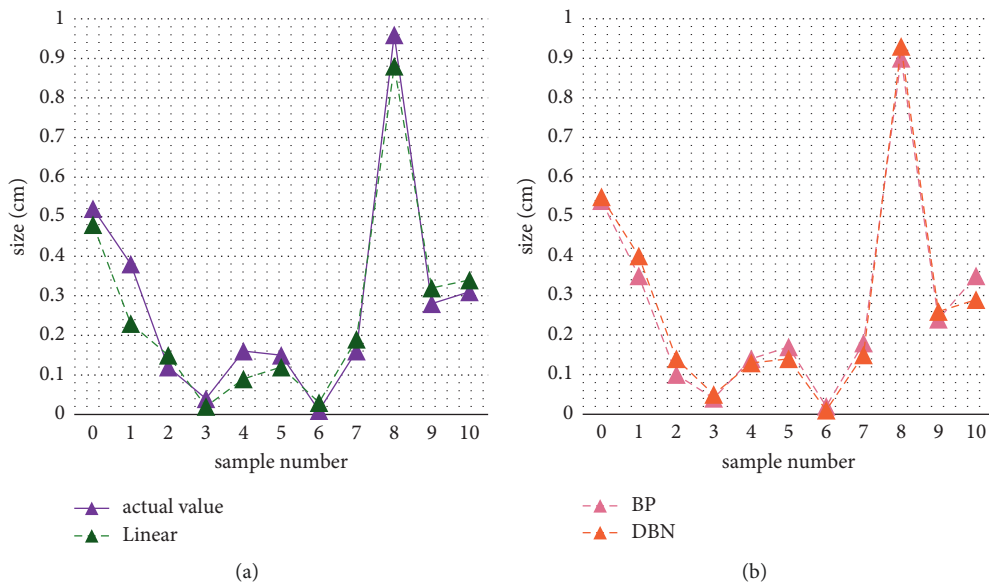


FIGURE 11: Neck size of different algorithms: (a) Experimental result of cuff. (b) Experimental result of neck circumference.

TABLE 2: The functions expected of children’s clothing.

Function	Number of people	Proportion (%)
Positioning function	115	79.9
Bold style	77	53.5
Sign monitoring	69	48.0
Real-time reminder	103	71.5
Other	21	14.6

TABLE 3: The functions expected of outdoor worker clothing.

Function	Number of people	Proportion (%)
Bold style	128	90.1
Sign monitoring	73	51.4
Control temperature	105	74.0
Antifouling property	98	69.0
Other	13	9.2

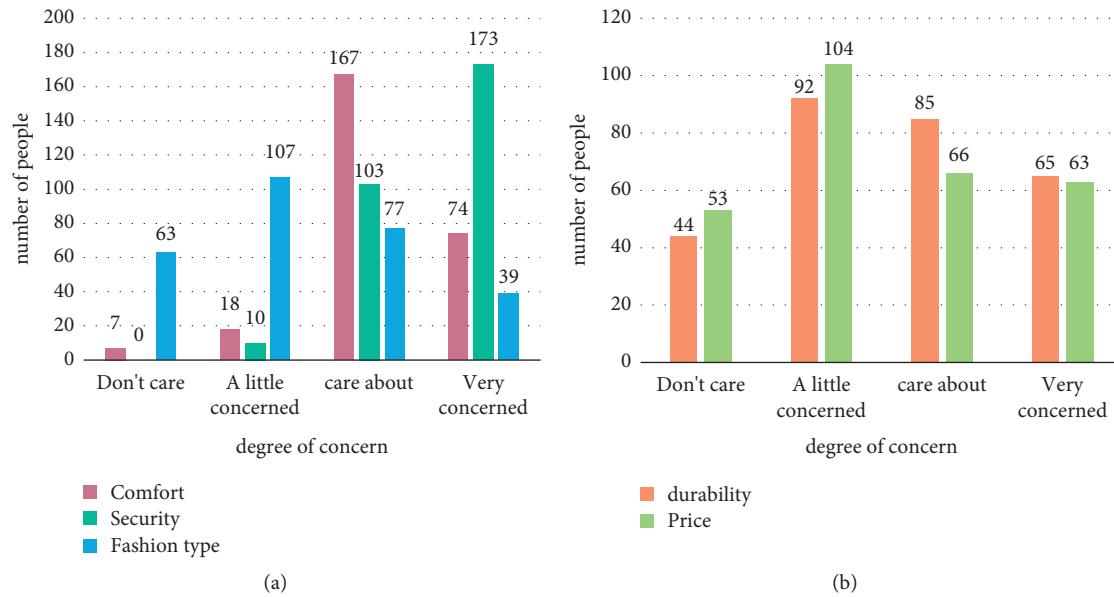


FIGURE 12: Statistics of the degree of attention to clothing performance.

Next, this study counts the functions that outdoor workers expect safety clothing to have, as shown in Table 3.

It can be seen from the table that for outdoor workers, the most important clothing function is eye-catching style, and 90.1% of those choose this option. The second place is temperature control. Because outdoor workers work outdoors, their temperature is always too cold or too hot. This feature can give them comfort to a great extent. It can be seen that when designing traffic safety clothing for outdoor workers, the style and temperature control function design should be considered as much as possible. In addition, the functions of physical sign monitoring and antifouling should also be considered.

3.2.3. Survey Results of Clothing Performance Questionnaire. In the experiments in this chapter, we investigated the clothing performance expectations of the two groups of people. The performances are comfort, safety, fashion, durability, and price. It counts people's attention to each performance and makes statistics on the results of the questionnaires of the two groups of people, and the results are shown in Figure 12.

It can be seen from the figure that among these five properties, 0 people choose not to care about safety, and most people, 173 people, choose to care about safety very much. Proof that safety should be the basic function of safety clothing. The second most concerning choice is the comfort of the clothing. 74 people chose this option. It proves that in all the performance, safety and comfort are the most concerned by people. Therefore, in the clothing design of outdoor traffic safety, the designer should pay more attention to these two aspects of performance.

4. Discussion

How to ensure one's own safety and eliminate the potential safety hazards caused by the surrounding environment to

the human body has become a current hot topic. As an indispensable clothing industry for people's lives, safety clothing has developed rapidly in recent years and has become an important branch of the clothing industry, and it has also been warmly welcomed by people. The design stage of safety clothing is the front end of the clothing production chain, which determines the performance, cost, and impact of the entire product on people, society, and the environment. Smart safety clothing needs to continuously improve the stability and reliability of the system, pay more attention to the interaction between the clothing itself and the environment, and have a more comprehensive understanding of market needs. It is necessary to break down the barriers between clothing design and engineering, strengthen interdisciplinary cooperation, and better reflect the impact of the interaction between smart safety clothing and humans.

5. Conclusion

This article introduces the design method of traffic outdoor safety clothing based on BD and AI machine learning, introduces many related algorithms, and also introduces the principles and processes of traffic outdoor safety clothing design. It did two experiments. The first experiment was to test the accuracy of various machine learning algorithms for clothing size measurement. The results are obtained: In the clothing performance concern, 173 people choose to care about safety the most, and the second most concern is the comfort of the clothing. 74 people choose this option. It can be seen that when designing clothing, children's clothing should pay the most attention to positioning functions, and outdoor worker clothing should pay the most attention to eye-catching styles. In terms of performance, whether it is children's clothing or outdoor workers, safety should be the most basic, followed by the comfort of clothes. After the comparison of the predicted value and the actual value

obtained by DBN, BP, Bagging, and Linear training, respectively, it is concluded that the deep belief neural network (DBN) model established in this paper has higher accuracy than BP, Bagging, and Linear, and can directly improve the efficiency of model design and realize large-scale customized production. It is believed that after training with more data in the later stage, the network will be further improved, and at the same time, it can further design and develop intelligent clothing model sizes directly generated from 3D human body data: Fashion design system.

Data Availability

No data were used to support this study.

Conflicts of Interest

There are no potential conflicts of interest in this study.

Acknowledgments

This work was supported by “The Research on the costume design of Zhanjiang style tourism under the background of Tourism City construction” (ZJ21YB48), in 2021, Philosophy and Social Sciences Program of Zhanjiang, “Research on the design and development of tourism clothing based on the regional characteristics of Zhanjiang” (2021B01063), in 2021, the non funded Science and Technology Research Project of Zhanjiang Science and Technology Bureau, and “Research on literal translation and free translation of architectural decoration language of ancient folk houses in Leizhou in modern design under the development of research and creation economy” (GD20XYS15), in 2020, the “13th five year plan” Philosophy Social Science Discipline Co-Construction Project of Guangdong Province.

References

- [1] L. Xu, C. Jiang, and J. Wang, “Information security in big data: privacy and data mining,” *IEEE Access*, vol. 2, no. 2, pp. 1149–1176, 2017.
- [2] L. Kuang, F. Hao, and L. T. Yang, “A tensor-based approach for BD representation and dimensionality reduction,” *IEEE Transactions on Emerging Topics in Computing*, vol. 2, no. 3, pp. 280–291, 2017.
- [3] Z. Yaoxue and J. Zhang, “A survey on emerging computing paradigms for big data,” *Chinese Journal of Electronics*, vol. 26, no. 1, pp. 1–12, 2017.
- [4] Y. Zhang, M. Qiu, C.-W. Tsai, M. M. Hassan, and A. Alamri, “Health-CPS: healthcare cyber-physical system Assisted by cloud and big data,” *IEEE Systems Journal*, vol. 11, no. 1, pp. 88–95, 2017.
- [5] M. Rathore, A. Paul, and A. A. hmad, “Real-time BD analytical architecture for remote sensing application,” *Ieee Journal of Selected Topics in Applied Earth Observations and Remote Sensing*, vol. 8, no. 10, pp. 4610–4621, 2017.
- [6] L. Rongpeng and Z. Li, “Intelligent 5G: when cellular networks meet AI,” *IEEE Wireless Communications*, vol. 24, no. 5, pp. 175–183, 2017.
- [7] H. Lu, Y. Li, and C. Min, “Brain intelligence: go beyond AI,” *Mobile Networks and Applications*, vol. 23, no. 7553, pp. 368–375, 2017.
- [8] Y. Zheng, “Urban computing: enabling urban intelligence with big data,” *Frontiers of Computer Science*, vol. 11, no. 1, pp. 1–3, 2017.
- [9] H. Xing, A. Qian, and R. C. Qiu, “A BD architecture design for smart grids based on random matrix theory,” *IEEE Transactions on Smart Grid*, vol. 8, no. 2, pp. 674–686, 2017.
- [10] Y. Wang, L. Kung, and T. A. Byrd, “Big data analytics: understanding its capabilities and potential benefits for healthcare organizations,” *Technological Forecasting and Social Change*, vol. 126, pp. 3–13, 2018, JAN.
- [11] C. S. Calude and G. Longo, “The deluge of spurious correlations in big data,” *Foundations of Science*, vol. 22, no. 3, pp. 595–612, 2017.
- [12] M. Janssen, H. van der Voort, and A. Wahyudi, “Factors influencing big data decision-making quality,” *Journal of Business Research*, vol. 70, pp. 338–345, 2017, JAN.
- [13] L. Zhou, S. Pan, J. Wang, and A. V. Vasilakos, “Machine learning on big data: opportunities and challenges,” *Neurocomputing*, vol. 237, pp. 350–361, 2017, MAY10.
- [14] Y. Zhang, S. Ren, Y. Liu, and S. Si, “A big data analytics architecture for cleaner manufacturing and maintenance processes of complex products,” *Journal of Cleaner Production*, vol. 142, pp. 626–641, 2017, PT.2.
- [15] H. Cai, B. Xu, L. Jiang, and A. V. Vasilakos, “IoT-based big data storage systems in cloud computing: perspectives and challenges,” *IEEE Internet of Things Journal*, vol. 4, no. 1, pp. 75–87, 2017.
- [16] S. Athey, “Beyond prediction: using big data for policy problems,” *Science*, vol. 355, no. 6324, pp. 483–485, 2017.
- [17] M. Nasr, A. E. D. Mahmoud, M. Fawzy, and A. Radwan, “Artificial intelligence modeling of cadmium(II) biosorption using rice straw,” *Applied Water Science*, vol. 7, no. 2, pp. 823–831, 2017.
- [18] J. Lemley, S. Bazrafkan, and P. Corcoran, “Deep Learning for Consumer Devices and Services: pushing the limits for machine learning, artificial intelligence, and computer vision,” *IEEE Consumer Electronics Magazine*, vol. 6, no. 2, pp. 48–56, 2017.
- [19] R. Chatila, K. Firth-Butterflied, J. C. Havens, and K. Karachalios, “The IEEE global initiative for ethical considerations in artificial intelligence and autonomous systems [standards],” *IEEE Robotics and Automation Magazine*, vol. 24, no. 1, p. 110, 2017.
- [20] X. Yang, H. Li, L. Ni, and T. Li, “Application of artificial intelligence in precision marketing,” *Journal of Organizational and End User Computing*, vol. 33, no. 4, pp. 209–219, 2021.
- [21] N. Man, K. Wang, and L. Liu, “Using computer cognitive atlas to improve students’ divergent thinking ability,” *Journal of Organizational and End User Computing*, vol. 33, no. 6, pp. 1–16, 2021.
- [22] L. Li and J. Zhang, “Research and analysis of an enterprise E-commerce marketing system under the big data environment,” *Journal of Organizational and End User Computing*, vol. 33, no. 6, pp. 1–19, 2021.
- [23] D. Hassabis, D. Kumaran, C. Summerfield, and M. Botvinick, “Neuroscience-inspired artificial intelligence,” *Neuron*, vol. 95, no. 2, pp. 245–258, 2017.

Research Article

A New Approach to Regional Traffic Estimation for Intelligent Transport Systems

Minghe Yu ¹, Jianhua Feng,² Tianmiao Zhang,³ and Tiancheng Zhang ³

¹School of Software, Northeastern University, Shenyang 110169, China

²Department of Computer Science, Tsinghua University, Beijing 100084, China

³School of Computer Science and Engineering, Northeastern University, Shenyang 110169, China

Correspondence should be addressed to Minghe Yu; yuminghe@mail.neu.edu.cn

Received 30 January 2022; Accepted 1 June 2022; Published 28 June 2022

Academic Editor: Sang-Bing Tsai

Copyright © 2022 Minghe Yu et al. This is an open access article distributed under the Creative Commons Attribution License, which permits unrestricted use, distribution, and reproduction in any medium, provided the original work is properly cited.

With the great development of urban transportation systems, immediate urban traffic information has become an essential resource for the public. Traffic estimation is to predict current or future traffic situation (traffic speed and/or volume) in a road or a region of a city, and can benefit our daily life from many aspects, such as routing planning and traffic management. Existing works focus on estimating future traffic for individual road segments from a perspective of fine-grained level. This paper presents a new approach to estimating future traffic from a perspective of coarse-grained level, by which we estimate the traffic situation of a region, instead of an individual road segment. We propose a new concept about regional traffic named Ω -region, which aims to reflect the traffic situation of a region precisely. Two challenges in the regional traffic estimation problem are how to partition the road network into reasonable regions and how to estimate the regional traffic effectively. To address these challenges, first we define reasonable regions Ω -regions with traffic situations so that the all the road segment in the region has similar traffic. Then, we propose a three-phase partition method to divide the road network into Ω -regions based on historical trajectory data. Thirdly, we propose an effective linear-based model to estimate regional traffic. Experimental results on real-world dataset show that our proposed method achieves high performance.

1. Introduction

With the great development of urban transportation systems, immediate urban traffic information has become an essential resource for the public. Many human activities, such as path planning, traffic management, and city's infrastructure construction plan, are related to the awareness of urban traffic. Nowadays, many large metropolises in the world suffer from constant traffic congestion with their undergoing rapid economic growth. To mitigate the burden of the underlying road networks, efficient traffic management is of great importance, and metropolitan-scale traffic estimation is valuable to traffic management and to build smart city. To obtain precise traffic information for future plans, many existing studies [1–7] have been focused on the future traffic estimation, which aim to predict the urban traffic situations for the nearby time

periods. These works provide very fine-grained level of traffic estimation; i.e., they try to predict the future traffic for each individual road segments. However, these works are quite difficult to realize and thus they are hard to put into practical applications. This is because (1) their approaches are often developed based on the foundation that they are aware of the details of current traffic which, in fact, are difficult to retrieve. Existing methods, including obtaining the current traffic through the deployed traffic cameras and probing buses/taxis, can only retrieve sparse part of the current traffic. (2) Sometimes, the traffic situation of an individual road segment is irregular, which means the variation of its traffic flow is not similar with its adjacent roads. Therefore, the methods developed from general observations do not work effectively on regions, since we cannot assure that the traffic of every road segment in a region is uniform.

In this paper, we present an approach to estimating future traffic situation from a new perspective of coarse-grained level, regional traffic. The regional traffic is considered as the sum of vehicles appears in a region which consists of several adjacent road segments. A road can be one-way or two-way, and the traffic flows on the two directions in a two-way road usually are different. But they impact the traffic situation in a region together since the vehicles on two ways of a road pass the same junctions. Therefore, we combine the traffic flows of a two-way road into a single traffic for regional traffic estimation. There are many approaches to defining regions in a road network, for example, by grid, by population region, or by administration district. We propose a new way to define the region by traffic situation and name it as Ω -region, which has the property: all the traffic situations of road segments within it must be similar (see Section 3). There are certain advantages using the regional traffic. First, it can reflect both the regional traffic and the individual traffic since all the traffic situation within an Ω -region is similar. And the individual traffic can be easily deduced by the regional traffic as we can obtain the traffic ratio of each road segment in the region. Second, it can avoid the sparse problem of retrieving the current traffic since it is estimated in a coarse-grained level. Meanwhile, there are many practical applications of utilizing regional traffic estimation. Here, we give two examples. The regional traffic model can help our routing plan and is more expressive than using individual traffic estimation because in our daily life, when we are planning a path and trying to avoid traffic congestions, we usually consider to avoid congested regions rather than to remember all the individual congest road segments. We can also benefit traffic management with regional traffic estimation. Traffic polices in a city are usually assigned to certain regions to maintain traffic order. By detecting the congested region, the traffic polices can be made more judiciously.

However, there are several challenges to estimate regional traffic. First, we need to divide the road network into reasonable regions Ω -regions. To guarantee that the road segments within a region have similar traffic situation, we consider the historical trajectory data over the road segments and proposed a three-phase partition method to find those regions correctly. Second, we need to estimate the regional traffic precisely. To this end, we propose a linear-based model by considering the traffic of the region as well as the traffic of its neighborhood regions. To the best of our knowledge, it is the first study to estimate the reasonable regional traffic. In this paper, we make the following contributions.

- (1) We propose the concept of reasonable regional traffic and formulate the problem of regional traffic estimation.
- (2) We propose a three-phase partition method to divide the road network into Ω -regions by clustering historical trajectory data.
- (3) We propose an effective linear-based model to estimate regional traffic in Ω -regions.

- (4) We conduct experiments on real metropolitan traffic datasets, and the results show that our proposed methods achieve high performance.

The rest of the paper is organized as follows. We present the reviews of related works in Section 2. The preliminaries are defined in Section 3, and then we introduce how to generate Ω -regions in Section 4. We discuss how to estimate the future traffic for Ω -regions in Section 5. Experimental results are reported in Section 6. Finally, we conclude the paper in Section 7.

2. Related Works

Traffic estimation or modeling has been attracted many attentions from the researching community in recent years. Existing studies mainly focus on two categories:

Current traffic estimation. Current traffic estimation is based on partial observed traffic information from monitoring cameras and probing vehicles [4, 8, 9]. Traffic situations of a road network are usually modeled as a road-time matrix, where each entry stands by a traffic situation of a road segment in a specific time period. By assuming the adjacent road network may have similar traffic situation, matrix factorization [4, 8–11]-based methods are proposed to estimate the missing value of the matrix. In addition, Liu et al. [12] present GPTE, which utilizes nonlinear correlation modeling to represent real-time road network for traffic speed prediction. H-ARIMA [13] provided by Pan et al. utilizes both historical traffic patterns and current traffic speed for hybrid traffic prediction.

Future traffic estimation. Plenty approaches have been put into future traffic estimation [2, 3, 14–21]. A general method is developed over the basic hidden Markov model, which focuses on reflecting the evolvement of traffic through time. Other features (e.g., the scale of road segments and the traffic signals) that will affect traffic are also considered and incorporated into their models. Typically, future traffic estimation is used to predict traffic speed and volume. Ma et al. [22] study traffic speed prediction with deep learning theory. They represent network traffic as images with an image-based method and utilize convolutional neural network to extract spatio-temporal features. Wang et al. [23] utilize error feedback recurrent convolutional neural network (eRCNN) to capture complicated interactions of traffic speeds for prediction, which introduces separate error feedback neurons into the model and captures prediction errors to achieve high accuracy. Zhang et al. [24] study city crowd flow prediction. They consider both spatial dependency and temporal property and employ the residual neural network framework to dynamically aggregate them to predict the final traffic of crowds. There are also some works that focus on vehicular network to prediction future location of vehicle [25–27]. These methods provide essential and novel strategies, including vehicle coordinate normalization and context feature mining, to

improve the accuracy of prediction and efficiency of delivery ratio.

Recently, some works focus on regional traffic [28–31]. Zhu et al. [29] design a spatio-temporal attention mechanism to capture dynamic impact, including the number of vehicles in the accident and the amount of the injured people, of both local and global regions to predict traffic accident risk. Wang et al. [30] study regional traffic volume of the highway network in holidays and propose a holiday traffic growth model to predict holiday traffic based on seasonality, holiday, and trend components. Liu et al. [31] and Kang et al. [28] work on regional traffic prediction. In their works, a road network is partitioned into a grid map based on the longitude and latitude, and a region is represented by a grid.

These works are different from our work. We propose a new concept about regional traffic, the reasonable region Ω -region. An Ω -region is a subgraph of road network, which is consisted of several connected road segments with similar traffic situation. As far as we know, this is the first study on reasonable regional traffic estimation. To solve the problem, we first study how to generate those regions based on the historical traffic information. Next, we study how to predict future regional traffic effectively. We find the regional traffic in a coarse-grained level follows a linear relationship; thus, we propose an effective linear-based model to estimate regional traffic.

3. Preliminaries

Road Network. We model the road network as an undirected graph $G = (V, E)$, where V is the vertex set and E is the edge set. Each vertex of V is composed by a pair of geo-coordinates, i.e., latitude, longitude. Figure 1(a) shows an example of road network.

Region. We define the region based on the road network. A region is a disjointed subgraph of G . The road network G consisted of k disjoint subgraphs $G_1 = (V_1, E_1)$, $G_2 = (V_2, E_2)$, \dots , $G_k = (V_k, E_k)$, where $E_1 \cap E_2 \cap \dots \cap E_k = \emptyset$. We denote $|\mathcal{E}_i|$ as the number of edges in G_i .

Regional Traffic. We focus on traffic volume for regional traffic in this paper. To measure the traffic volume in a region, we utilize the vehicle trajectories. A trajectory T is a series of geo-coordinates which is generated by the GPS devices of moving vehicles, i.e., $T = (ts_i, lat_i, lng_i) (1 \leq i \leq T)$, where ts_i is its timestamp, lat_i is the latitude of the vehicle, and lng_i is the longitude. Given a region G_i and a time interval $P_t = [P_s, P_e]$, the regional traffic $R(G_i, P_t)$ is defined as the average number of vehicles which appear within the edges of subgraph G_i between the time P_s and P_e . Formally,

$$\mathcal{R}(\mathcal{G}_x, \mathcal{P}_t) = \frac{|\{\mathcal{T} | ts_i \in [P_s, P_e], (lat_i, lng_i) \in \mathcal{G}_x\}|}{|\mathcal{G}_x|} \quad (1)$$

Problem Statement. In this paper, we study two problems. (1) Given a road network work G , we first study how to divide the road network into reasonable regions G_1, \dots, G_k , which is named Ω -region. All the road segments within the Ω -region have similar traffic situations as the traffic(s) on a one-way road or a two-way road are considered as a single one (we will introduce the details in Section 4). (2) Given a time interval P_t and an Ω -region G_i , we predict the regional traffic $R(G_i, P_t)$ based on previous traffics P_{t-1}, P_{t-2}, \dots of the road network.

Example 1. Figure 1(b) shows the regional traffic on the road network of Figure 1(a). The points shown on the edge are the trajectories of the vehicles for a given time period P_t . We divide the original road network G into nine regions, in which some edges are clustered into four regions, i.e., G_1, G_2, G_3 , and G_4 . Within these regions, we use four colors, i.e., dark red, red, orange, and yellow, to represent different traffic situations. In particular, $R(G_1, P_t) = 1$, $R(G_2, P_t) = 2$, $R(G_3, P_t) = 3$, and $R(G_4, P_t) = 7$.

4. Regional Traffic

4.1. Basic Idea. Intuitively, the traffic situations of two close locations are usually similar. If one place is suffered from heavy traffic jams, the nearby places will be jammed too. For example, in Beijing, the West Railway Station is a place where traffic congestions happen frequently, while the nearby place Gongzhufen is also always suffered from heavy traffic. This is because that the traffic situations in one place can easily affect the nearby place on the road network, as the vehicles have to move from one road segment to the adjacent one. In this section, we study how to divide the road network into separate regions with the property that the road segments within a region have similar traffic situations. A naive method is to divide the road network according to the spatial proximity, e.g., to partition the road network into grids. However, such method does not consider the traffic conditions on the road segments. Apparently, the traffic situations vary for some connected road segments (e.g., segments connected through crosses or main roads); thus, it cannot guarantee the consistency of traffic situations in those divided partitions by gridding.

To this end, we devise a novel method to find Ω -region named REGION, which considers both the graph topology and the trajectories together in the region partitioning. We first attach each trajectory to the nearest edge on the road network, and then we construct a new graph by assigning the weight of edges as the amounts of trajectories appear in the corresponding segments. Finally, we iteratively merge the edges that are connected both on road network and with similar amounts of trajectories by utilizing hierarchical clustering technique. Next, we formally introduce our method.

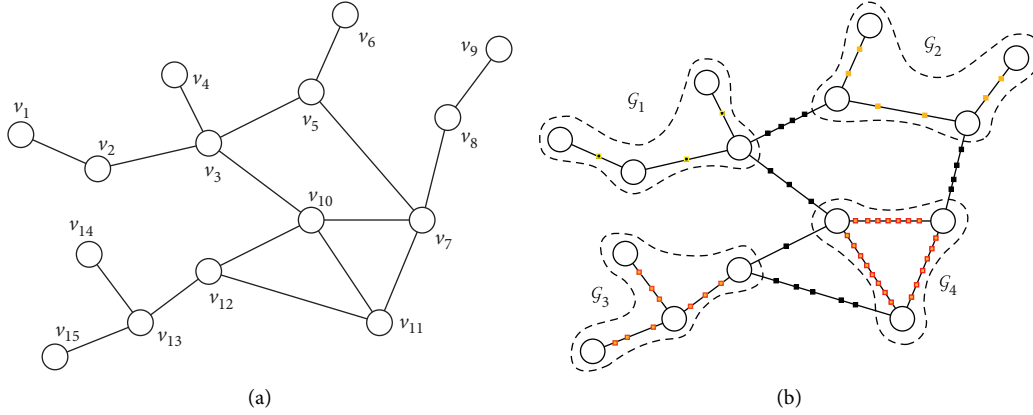


FIGURE 1: An example of the road network with trajectories. (a) A road network. (b) Regional traffic.

4.2. Region Finding

REGION involves three phases: (1) trajectory positioning; (2) graph building; and (3) hierarchical clustering. In this section, we discuss these three phases in detail.

Trajectory Positioning. For each trajectory $T = (ts_i, lat_i, lng_i)$, we find an edge $e \in E$ that is closest to (lat_i, lng_i) . We can use the linear scan to find the closest edge. To speed up this procedure, we build the quadtree to hierarchically index all the edges of the road network and employ the best-first search algorithm to find the nearest edge. We omit the details of this, as it is not the focus of this paper.

Graph Construction. Based on the results of trajectory positioning, we construct a new graph $G' = (V, E)$. For each edge (segment) $e \in E$, we assign a weight, which is denoted by $w(e)$. The weight is assigned as the amount of trajectories which lies on edge e . The $w(e)$ is defined by

$$\omega(e) = |\{\mathcal{T} | \mathcal{T} \in e\}|. \quad (2)$$

The weight can reflect the historical traffic situations. If the amounts of two close edges differ greatly, they are very likely to have different traffic situations. Therefore, those two edges should not be partitioned into the same region.

Hierarchical Clustering. We adopt a hierarchical clustering to generate the regions. First, we initialize each edge $e \in E$ as an independent group. Then, we iteratively merge two groups together by two rules. The first rule is that two groups, i.e., G_1 and G_2 , are topologically adjacent. The second rule is that the difference of the average weight between two groups is less than a threshold λ , i.e., $|\bar{w}(\mathcal{E}_1) - \bar{w}(\mathcal{E}_2)| \leq \lambda$, where $\bar{w}(\mathcal{E}_x) = \sum \omega(e \in \mathcal{E}_x) / |\mathcal{E}_x|$. We stop this process until the difference of the group weight is larger than λ . λ reflects the granularity of the regions we retrieve. If λ is small, we can obtain many small consistent regions; otherwise, we will divide the road network into less larger regions. λ is decided and tuned by applications

and experiences. We demonstrate the pseudo-code of this procedure in Algorithm 1 in Figure 2.

In Algorithm 1 in Figure 2, we first assign a weight to each edge (line 4) and count adjacent edges (line 6–7). Meanwhile, we initialize a queue Q to store the edges as independent groups (line 8). For each group G_x in Q , we calculate the difference of the average weight between its adjacent group and it, respectively (line 12). If there is an adjacent group $G_{x'}$ satisfying the condition, we merge it with G_x as G_y , and update adjacent groups of G_y and all the other groups containing G_x and $G_{x'}$ (line 13–18). Finally, we push G_y into queue Q (line 20). Otherwise, we consider G_x as a generated region, that is, Ω -region, and push it into set T (line 22). We repeat these steps until Q becomes empty, and all the regions in T are the Ω -regions from the graph of road network (line 23).

Example 2. Figure 3 shows the process of the hierarchical clustering. First, we use different colors to label the edges which initially belong to different groups. Then, we find two groups which are connected on the road network and have the average weight within the threshold λ . We combine these two groups together. We repeat this procedure until we cannot find any two groups that the difference of their average weight is smaller than λ . In Figure 3, we finally divide the road network into nine regions.

5. Traffic Estimation

In this section, we discuss how to estimate the traffic situation of a given region for next period of time.

5.1. Fundamental. In daily life, vehicles always move along a path of road segments. Since we have already divided the road network into regions, the vehicles have only three options to get the destination: (1) stay in the current region, (2) go in, or (3) go out to other regions. For example, in Figure 1, suppose a car is heading to v_8 from v_{13} . The path from v_{13} to v_8 is $v_{12} \rightarrow v_{10} \rightarrow v_7 \rightarrow v_8$. It will leave the region G_3 at v_{12} , and then it has to bypass several regions like G_4 to arrive at the region G_2 . Therefore, given a specific

Algorithm 1: Region (\mathcal{G}, λ)

Input: \mathcal{G} : the graph of road network
 λ : the threshold to tune the granularity of regions

Output: T : the set containing the generated regions $\{G_1, \dots, G_k\}$

```

1  Begin
2  Queue  $Q = \emptyset$ ;
3  for  $e \in \mathcal{E}$  do
4     $w(e)$  = number of trajectories on  $e$ ;
5     $G_e = \{e\}$ ;
6    for each adjacent edge  $e'$  of  $e$  do
7       $\mathcal{A}(G_e).add(G_{e'})$ 
8     $Q.push(G_{e'})$ ;
9  while  $Q \neq \emptyset$  do
10    $G_x = Q.pop()$ ;  $G_y = \emptyset$ ;
11   for each  $G_{x'} \in \mathcal{A}(G_x)$  do
12     if  $Abs\left(\frac{\sum_{e \in G_x} w(e)}{|G_x|} - \frac{\sum_{e \in G_{x'}} w(e)}{|G_{x'}|}\right) < \lambda$  then
13        $G_y = G_x \cup G_{x'}$ ;
14        $\mathcal{A}(G_y) = \mathcal{A}(G_x) \cup \mathcal{A}(G_{x'})$ ;
15       for each  $G_{x''} \in \mathcal{A}(G_x) \cup \mathcal{A}(G_{x'})$  do
16          $\mathcal{A}(G_{x''}).remove(G_x, G_{x'})$ ;
17          $\mathcal{A}(G_{x''}).add(G_y)$ ;
18       break;
19   if  $G_y \neq \emptyset$  then
20      $Q.push(G_y)$ ;
21   else
22      $T.add(G_x)$ ;
23 return  $T$ ;
24 end

```

FIGURE 2: Region finding algorithm.

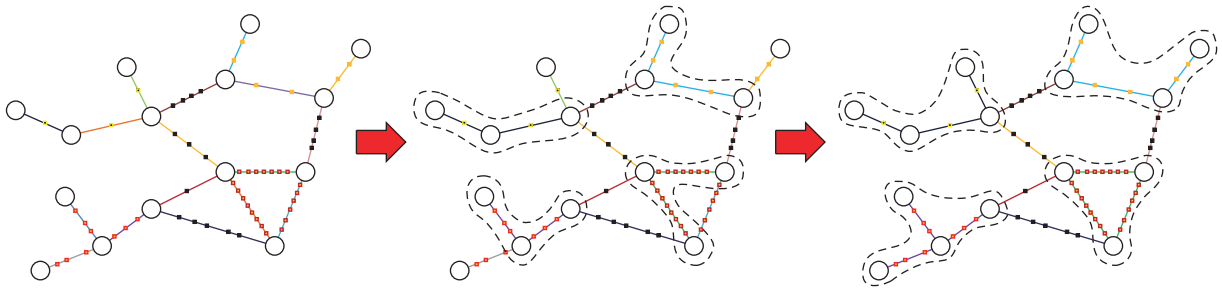


FIGURE 3: The process of the hierarchical clustering.

region, the traffic condition of such region will only be affected by the traffic situation of adjacent regions in the previous period of time. If one region is suffering from the traffic jams, it will then give an impact on the adjacent regions sometime later. Moreover, according to the closure property of the regions on road network, the vehicles that go out from a region must go in another adjacent region, while the total amount of transitions is unchanged.

The above facts indicate that we can use the linear model to address this problem. Next, we formally define our model. We denote our method by LINEST.

5.2. Estimation Model. First of all, we divide the daily time into m intervals, i.e., P_1, P_2, \dots, P_m . We denote the adjacent regions of a given region G_x by $\mathcal{A}(G_x)$, where the adjacent

regions of G_x are the regions that connected to G_x with at least one edge in G . Given a specific region G_x at the time interval P_t , our goal is to estimate the regional traffic $R(G_x, P_{t+1})$, $R(G_x, P_{t+2})$, etc., based on $\mathcal{R}(\mathcal{G}'_{\mathcal{G}' \in \mathcal{A}(G_x)}, \mathcal{P}_t)$.

According to the previous analysis, we use a linear model to depict the relationship among this regional traffic, which is shown as

$$\mathcal{R}(G_x, \mathcal{P}_t) = \alpha_0 + \sum_{\mathcal{G}' \in \mathcal{A}(G_x)} \alpha_{\mathcal{G}'} \cdot \mathcal{R}(G', \mathcal{P}_{t-1}). \quad (3)$$

Equation (2) has good interpretability. The parameters $\alpha_1, \alpha_2, \dots, \alpha_{G'}$ in equation (2) indicate the proportions of vehicles that transport between the regions G_x and $\mathcal{A}(G_x)$ from the previous period of time to the current period. The parameter α_0 is a constant factor which suggests the usual traffic situation at the current period of a day.

Notice that, as we have divided the daily time into m intervals P_1, P_2, \dots, P_m , thus, for a single region G_x , we can use m distinct models for a single day. This is because that the underlying patterns of vehicles' moving are different within a whole day. For example, in the morning, the cars are prone to move to downtown area, while in the evening, those cars tend to drive off from downtown. Based on this observation, we separately treat m models for region G_x within a day.

Equation (2) also suggests that we can employ the technique of linear regression to solve the parameters $\alpha_1, \alpha_2, \dots, \alpha_{G'}$. Our problem can be formulated by the linear regression as follows:

$$\mathcal{R}(G_x, \mathcal{P}_t) = X_{t-1} \beta_t + \varepsilon, \quad (4)$$

where $\beta_t = [\alpha_{t_0}, \alpha_{t_1}, \alpha_{t_2}, \dots, \alpha_{t_{|\mathcal{A}(G_x)|}}]^T$ and X is a $n \times (|\mathcal{A}(G_x)| + 1)$ matrix, where n rows describe the traffic situations of region G_x and its neighbors in $\mathcal{A}(G_x)$ at time period P_{t-1} during n different days (n can be understood as the number of training data used to solve β_t). To minimize the overall sum of squared estimating errors, i.e., $\sum \varepsilon$ (given a region, we can compute a standard variation of vehicles' amounts over edges within the region; the average standard variation is the mean of the standard variations over all regions), we use its close-form solution, which is shown below.

$$\hat{\beta}_t = (X_{t-1}^T X_{t-1})^{-1} X_{t-1}^T \mathcal{R}(G_x, \mathcal{P}_t). \quad (5)$$

We take the learned parameters into equation (2) to estimate the regional traffic $R(G_x, P_{t+1})$.

6. Experiments

In this section, we first introduce the datasets and experimental settings. Then, we present the experimental results and analysis of comparative performance.

6.1. Experiment Setup

6.1.1. Dataset. To evaluate our method, we used the detailed road network of Beijing in 2012. The vertex size is 1,278,984,

and the edge size is 2,402,784. We also obtained the trajectory data of taxis in Beijing from October 2012 to December 2012. The total number of trajectories is 3.05 billion. We divided a daytime into 96 intervals; i.e., each interval lasts 15 minutes.

6.1.2. Baseline Methods. As we discuss in Section 2, regions in the existing methods are defined as a grid, which is constructed by directly dividing map based on geo-coordinates. Therefore, these works are not comparable with ours. To prove the effectiveness of our methods, we collect the ground truth data and compare our methods REGION and LINEST with two baseline methods GRID and HISTORY, respectively.

- (i) GRID. GRID is a straightforward method to divide road network. It utilized geo-coordinates to divide road network directly.
- (ii) HISTORY. We collected historical data of road network in Beijing as the ground truth data. And HISTORY is computed as the average amounts of vehicles based on only historical data.

6.1.3. Evaluation Metrics. We implemented REGION and LINEST with Python 3.4. All experiments were run on a Linux 10.0.4 machine with a 3.2 GHz CPU and 8 GB RAM.

6.2. The Effectiveness of REGION. We evaluated the effectiveness of REGION. First, we tested the number of generated regions by varying the threshold λ as 32, 64, 128, and 256. Figure 4(a) shows the results. We can see that the number of regions decreases greatly with the increase of λ ; this is because the region finding algorithm will merge more road segments into regions when λ is large. We generated total 274 K regions when $\lambda = 32$, and if $\lambda = 512$, we obtained 40 K regions.

Next, we tested the average standard variations of the amounts of vehicles which appear on the edges within corresponding regions (given a region, we can compute a standard variation of vehicles' amounts over edges within the region; the average standard variation is the mean of the standard variations over all regions). If the road segments within a region have similar traffic situation, it will have a small standard variation. Otherwise, the standard variation will be large. Figure 4(b) shows the average standard variations when we varied λ . We compared REGION with GRID, which divided road network into regions based on their geo-coordinates. The number of grids is determined by the corresponding regions of REGION. For example, if $\lambda = 32$, we generate 274 K grids. We can see that REGION outperforms GRID with a much smaller standard variation, which means that the traffic situations in regions generated by REGION are more consistent than the regions obtained from GRID. In addition, we also show the evolvment of average standard variation over recent 20 days in

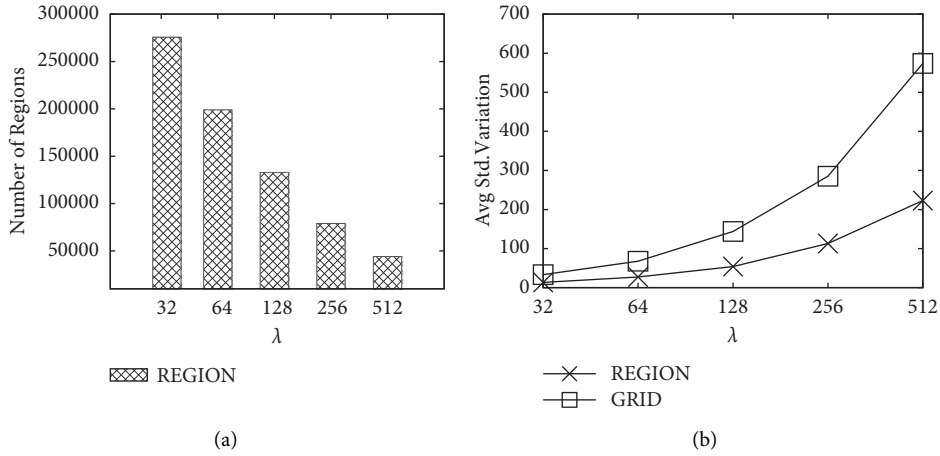


FIGURE 4: Varying threshold λ . (a) Number of generated regions. (b) Average standard variations.

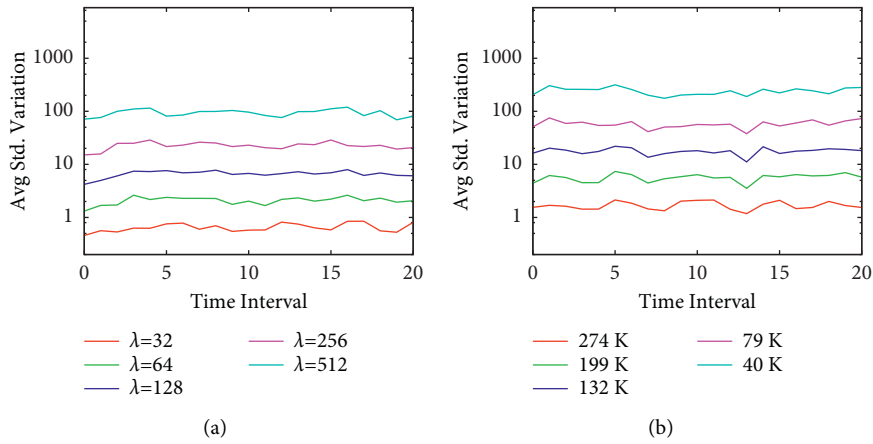


FIGURE 5: Average standard variations over 20 days. (a) REGION. (b) GRID.

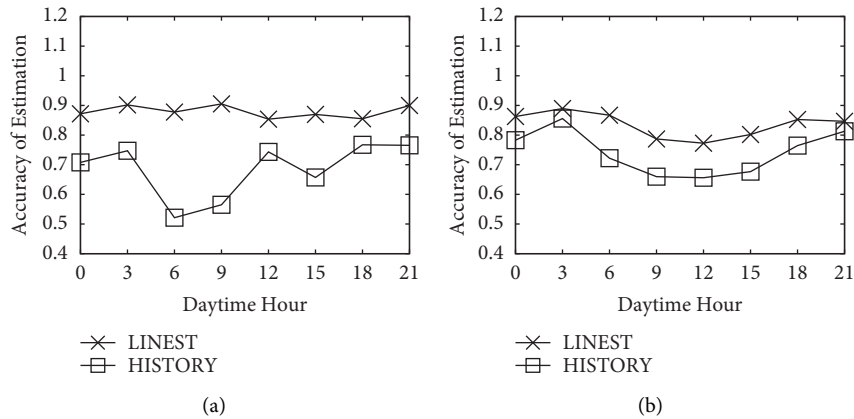


FIGURE 6: Regional traffic estimation. (a) Downtown. (b) Uptown.

Figure 5. It shows that REGION can reach a very stable performance over different days.

6.3. Regional Traffic Estimation. We evaluated the effectiveness of LINEST by using the accuracy ratio computed as follows:

$$\text{Accuracy} = 1 - \frac{\sum \text{Abs}(\mathcal{R}(\mathcal{E}_x, \mathcal{P}_t) - \mathcal{R}(\mathcal{E}_{\bar{x}}, \mathcal{P}_t))}{\sum \mathcal{R}(\mathcal{E}_x, \mathcal{P}_t)}, \quad (6)$$

where $\mathcal{R}(\mathcal{E}_{\bar{x}}, \mathcal{P}_t)$ is the estimating value of regional traffic and $\text{Abs}(\mathcal{R}(\mathcal{E}_x, \mathcal{P}_t) - \mathcal{R}(\mathcal{E}_{\bar{x}}, \mathcal{P}_t))$ is the estimating error. The trajectories within the last week are extracted as test

datasets. We further divide the test data into two categories: *Downtown* and *Uptown*. *Downtown* is the region located within the fourth ring road of Beijing (the center area of Beijing). *Uptown* is the other region of Beijing. We reported the accuracy by varying the hours of daytime. We compared LINEST with HISTORY, which computed as the average amounts of vehicles from only historical data. The results are shown in Figure 6. LINEST achieved very high performance comparing with HISTORY. The average accuracy reaches 90%. For example, the accuracy of downtown at 9 am can reach 91.2%. We also found that the performance increases from the uptown area to the downtown area, which indicates the linear model is more fit to the traffic situations of downtown.

7. Conclusion

In this paper, we study the regional traffic estimation problem. We first discussed how to divide road network into reasonable regions. We propose a three-phase region generating algorithm by clustering historical trajectory data. Next, we studied how to estimate future regional traffic effectively. By considering the linear relationship between the regional traffics, we proposed a linear-based model. Experimental results on read dataset show our method achieves high performance. In the next step, we will further optimize the algorithm to adapt to dynamic traffic estimation. In the future, we can consider on how to improve our model for granular-level transportation by constructing regions in higher dimension on the premise of ensuring the effectiveness of the existing model.

Data Availability

The data used to support the findings of this study have not been made available because these data are from our co-operative company. They only authorize us to use data for analysis, but not publish data.

Conflicts of Interest

The authors declare that they have no conflicts of interest.

Acknowledgments

This work was supported by the Fundamental Research Funds for the Central Universities (N2117001).

References

- [1] H. Yuan and G. Li, "A survey of traffic prediction: from spatio-temporal data to intelligent transportation," *Data Science and Engineering*, vol. 6, no. 1, pp. 63–85, 2021.
- [2] Y. Qi and S. Ishak, "Stochastic approach for short-term freeway traffic prediction during peak periods," *IEEE Transactions on Intelligent Transportation Systems*, vol. 14, no. 2, pp. 660–672, 2013.
- [3] B. Yang, C. Guo, and C. S. Jensen, "Travel cost inference from sparse, spatio-temporally correlated time series using Markov models," *Proceedings of the VLDB Endowment*, vol. 6, no. 9, pp. 769–780, 2013.
- [4] Y. Wang, Y. Zheng, and Y. Xue, "Travel time estimation of a path using sparse trajectories," in *Proceedings of the 20th SIGKDD conference on Knowledge Discovery and Data Mining (KDD 2014)*, pp. 25–34, ACM, New York, NY, USA, August 2014.
- [5] J. Snowdon, O. Gkoutouna, A. Zufle, and D. Pfoser, "Spatiotemporal traffic volume estimation model based on GPS samples," in *Proceedings of the the Fifth International ACM SIGMOD Workshop*, pp. 1–6, ACM, New York, NY, USA, 2018.
- [6] L. Lin, J. Li, F. Chen, J. Ye, and J. Huai, "Road traffic speed prediction: A probabilistic model fusing multi-source data," *IEEE Transactions on Knowledge and Data Engineering*, vol. 30, no. 7, pp. 1310–1323, 2018.
- [7] T. Liebig, N. Piatkowski, C. Bockermann, and K. Morik, "Route planning with real-time traffic predictions," *Information Systems*, vol. 1226, pp. 83–94, 2014.
- [8] J. Shang, Y. Zheng, W. Tong, E. Chang, and Y. Yu, "Inferring gas consumption and pollution emission of vehicles throughout a city," in *Proceedings of the 20th SIGKDD conference on Knowledge Discovery and Data Mining*, pp. 1027–1036, ACM, New York, NY, USA, 2014.
- [9] Y. Zhu, Z. Li, H. Zhu, M. Li, and Q. Zhang, "A compressive sensing approach to urban traffic estimation with probe vehicles," *IEEE Transactions on Mobile Computing*, vol. 12, no. 11, pp. 2289–2302, 2013.
- [10] T. Darwish and K. Abu Bakar, "Traffic density estimation in vehicular ad hoc networks: A review," *Ad Hoc Networks*, vol. 24, pp. 337–351, 2015.
- [11] A. Kaminska-Chuchmala, "Spatial internet traffic load forecasting with using estimation method," *Procedia Computer Science*, vol. 35, pp. 290–298, 2014.
- [12] Z. Liu, P. Zhou, Z. Li, and M. Li, "Think like A graph: Real-time traffic estimation at city-scale," *IEEE Transactions on Mobile Computing*, vol. 18, no. 10, pp. 2446–2459, 2019.
- [13] B. Pan, U. Demiryurek, and C. Shahabi, "Utilizing real-world transportation data for accurate traffic prediction," in *Proceedings of the 2012 IEEE 12th International Conference on Data Mining*, pp. 595–604, IEEE, Brussels, Belgium, December 2012.
- [14] L. Chen and C. L. P. Chen, "Ensemble learning approach for freeway short-term traffic flow prediction," in *Proceedings of the 2007 IEEE International Conference on System of Systems Engineering*, pp. 1–6, IEEE, San Antonio, TX, USA, April 2007.
- [15] R. Herring, A. Hofleitner, P. Abbeel, and A. Bayen, "Estimating arterial traffic conditions using sparse probe data," in *Proceedings of the 13th International IEEE Conference on Intelligent Transportation Systems*, pp. 929–936, IEEE, Funchal, Portugal, September 2010.
- [16] H. Yuan, G. Li, Z. Bao, and L. Feng, "Effective travel time estimation: When historical trajectories over road networks matter," in *Proceedings of the SIGMOD/PODS '20: International Conference on Management of Data*, pp. 2135–2149, ACM, New York, NY, USA, 2020.
- [17] R. Shi, Z. Mo, and X. Di, "Physics-informed deep learning for traffic state estimation: A hybrid paradigm informed by second-order traffic models," *IEEE Transactions on Intelligent Transportation Systems*, pp. 540–547, 2021, AAAI, AAAI Press.
- [18] M. Sederlin, X. Ma, and J. Jin, "A hybrid modelling approach for traffic state estimation at signalized intersections," in *Proceedings of the 2021 IEEE International Intelligent*

- Transportation Systems Conference (ITSC)*, pp. 3604–3609, IEEE, Indianapolis, IN, USA, September 2021.
- [19] M. X. Wang, W. C. Lee, T. Y. Fu, and G. Yu, “Learning embeddings of intersections on road networks,” in *Proceedings of the the 27th ACM SIGSPATIAL International Conference*, pp. 309–318, 2019.
- [20] X. Zhan, Y. Zheng, X. Yi, and S. V. Ukkusuri, “Citywide traffic volume estimation using trajectory data,” *IEEE Transactions on Knowledge and Data Engineering*, vol. 29, no. 2, pp. 272–285, 2017.
- [21] H. Yuan, G. Li, Z. Bao, and L. Feng, “An effective joint prediction model for travel demands and traffic flows,” in *Proceedings of the 2021 IEEE 37th International Conference on Data Engineering (ICDE)*, pp. 348–359, IEEE, New York, NY, USA, 2021.
- [22] X. Ma, Z. Dai, Z. He, J. Ma, Y. Wang, and Y. Wang, “Learning traffic as images: A deep convolutional neural network for large-scale transportation network speed prediction,” *Sensors*, vol. 17, no. 4, p. 818, 2017.
- [23] J. Wang, Q. Gu, J. Wu, G. Liu, and Z. Xiong, “Traffic speed prediction and congestion source exploration: A deep learning method,” in *Proceedings of the 2016 IEEE 16th International Conference on Data Mining (ICDM)*, pp. 499–508, IEEE, Barcelona, Spain, December 2016.
- [24] J. Zhang, Y. Zheng, and D. Qi, “Deep spatio-temporal residual networks for citywide crowd flows prediction,” *AAAI*, pp. 1655–1661, 2017.
- [25] L. Zhao, Y. Liu, A. Y. Al-Dubai, A. Y. Zomaya, G. Min, and A. Hawbani, “A novel Generation-Adversarial-network-based vehicle trajectory prediction method for intelligent vehicular networks,” *IEEE Internet of Things Journal*, vol. 8, no. 3, pp. 2066–2077, 2021.
- [26] L. Zhao, Z. Li, A. Y. Al-Dubai et al., “A novel prediction-based temporal graph Routing Algorithm for Software-defined vehicular networks,” *IEEE Transactions on Intelligent Transportation Systems*, pp. 1–16, 2021.
- [27] L. Zhao, T. Zheng, M. Lin, A. Hawbani, J. Shang, and C. Fan, “SPIDER: A Social computing Inspired predictive Routing Scheme for Softwarized vehicular networks,” *IEEE Transactions on Intelligent Transportation Systems*, pp. 1–12, 2021.
- [28] Y. Kang, J. Li, S.-J. Lee, and H. Li, “Generative adversarial network-based regional epitaxial traffic flow prediction,” *Advances in Natural Computation, Fuzzy Systems and Knowledge Discovery*, vol. 1075, pp. 804–814, 2019.
- [29] L. Zhu, T. Li, and S. Du, “TA-STAN: A deep spatial-temporal attention learning framework for regional traffic accident risk prediction,” in *Proceedings of the 2019 International Joint Conference on Neural Networks (IJCNN)*, pp. 1–8, IEEE, Budapest, Hungary, September 2019.
- [30] Z. Wang, Y. Chen, J. Su et al., “Measurement and prediction of regional traffic volume in holidays,” in *Proceedings of the 2019 IEEE Intelligent Transportation Systems Conference (ITSC)*, pp. 486–491, IEEE, Auckland, New Zealand, October 2019.
- [31] Z. Liu, M. Huang, Z. Ye, and K. Wu, “Deeprtp: A deep spatio-temporal residual network for regional traffic prediction,” in *Proceedings of the 2019 15th International Conference on Mobile Ad-Hoc and Sensor Networks (MSN)*, pp. 291–296, IEEE, Shenzhen, China, December 2019.

Research Article

Research on the Development Model of Rural Tourism Based on Multiobjective Planning and Intelligent Optimization Algorithm

Lu Yang¹ and Xiaoying Dong ²

¹ZhengZhou Tourism College, Zhengzhou 451464, China

²Xi'an FanYi University, Xi'an 710105, China

Correspondence should be addressed to Xiaoying Dong; dxy2010054@xafy.edu.cn

Received 18 February 2022; Revised 8 March 2022; Accepted 18 March 2022; Published 23 May 2022

Academic Editor: Sang-Bing Tsai

Copyright © 2022 Lu Yang and Xiaoying Dong. This is an open access article distributed under the Creative Commons Attribution License, which permits unrestricted use, distribution, and reproduction in any medium, provided the original work is properly cited.

In order to improve the effect of rural tourism development, this study combines multiobjective planning and intelligent optimization algorithms to analyze the development mode of rural tourism and further deals with the problem of multisensor target tracking under unknown input interference conditions by designing a tourism network consensus algorithm. The algorithm adopts a distributed multisensor fusion structure combined with consensus estimation, and each sensor first performs two-level information filtering estimation and unknown input parameter estimation locally. The experimental research results show that the rural tourism development model based on multiobjective planning and intelligent optimization algorithm proposed in this study can play an important role in the development of rural tourism.

1. Introduction

Tourism products have the characteristics of different places, changes, and differences, and it is more convenient and efficient to publicize and promote through the mode of Internet interconnection. In the era of micromedia, the public began to use mobile terminals to obtain relevant consultation, exchange experiences, and reservations for scenic spots through the Internet in the process of tourism selection, which changed the traditional tourism marketing model. The rural tourism marketing model in the micromedia era is that the majority of tourists choose the information of the tourism destination through the Internet. Tourists choose their favorite rural tourism destinations according to their personal preferences. Moreover, managers and operators of rural tourism strengthen interaction and communication with each other and with tourists through the Internet. Tourists can post comments through WeChat and Weibo, which can subtly enhance the popularity and reputation of tourism companies. The connection between tourists and operators can promote the development of the rural tourism

industry, thereby driving the development of the local tourism economy.

The sinking tourism market represented by rural areas has broadened the growth space of online consumption and has become a new bright spot in the growth of Internet consumption. In the era of micromedia, rural tourists can publish their itinerary or travel strategies through WeChat, Weibo, and other methods for rural tourism routes, accommodation, travel experience, etc. Taking Weibo as an example and browsing the Weibo of a tourist attraction, we can see the comments of netizens on the relevant tourist attractions, tourist accommodation, or travel itinerary planning, strategies, and suggestions and opinions from senior tourists. Moreover, novel business models have driven the transformation of traditional consumption patterns.

The combination of operators of modern tourism enterprises and advanced Internet technology has changed the traditional mode of operation. Operators no longer distribute travel information through the traditional methods of distributing leaflets or mass information but publish tourism information through WeChat and Weibo public

accounts and update it to meet the comprehensive and personalized tourism needs of rural tourists. For managers and tourism operators of rural tourism destinations, the use of Internet technology to release and publicize the latest tourism routes, contact information, and tourism products not only saves the cost of publicity but also expands the scope of information dissemination, especially The promotion of tourism packages is carried out on a regular basis according to the needs of the public, which further enhances the influence of rural tourism. For example, in the parent-child interaction in the farm, combining the Internet of Things technology and tourists' favorite "sweep" function, tourists can experience farming activities such as picking melons and fruits, making tofu, and making cheese while recognizing animals and plants. The user purchase provides a vivid experience interface, which combines education and entertainment, and shopping in tourism, which is conducive to the sustainable development of rural tourism. In the era of micromedia, rural tourism has accelerated the development of the tourism industry and promoted the vigorous development of the rural economy. On the other hand, it promoted the construction of rural network infrastructure.

Based on the above analysis, this study combines multiobjective planning and intelligent optimization algorithm to analyze the development mode of rural tourism, so as to improve the analysis effect of rural tourism development path.

2. Related Work

The rapid development of science, technology, and economy has greatly reduced the demand for mass tourism products such as traditional sightseeing tourism products [1]. Literature [2] classifies the development mode of rural tourism into five categories: demand-pull, supply-push, intermediary-influence, support-effect, and mixed-drive. Literature [3] believes that government promotion is the main driving force in the early stage of rural tourism development; with the development of rural tourism, market driving force has gradually become the main driving force, and the government mainly plays the role of supervision. Literature [4] believes that relying on natural landscapes to develop rural tourism is suitable to adopt pastoral agricultural tourism mode and return to nature tourism mode and farmhouse tourism mode. Literature [5] believes that the three development models based on regional tourism resources, oriented by the development and management of the main body, and relied on the type of tourism product projects are the main models of rural tourism development in Beautiful China. Literature [6] found that the development mode of rural tourism is mainly scenic based, urban based, and primitive ecological (the old and young, borderless, and poor areas). Literature [7] believes that there are two rural tourism development modes in the Erhai Lake area: the mode of participation of community residents guided by grassroots organizations and the mode of community residents leading. Literature [8] believes that according to the main body of management, the main models of rural tourism development can be divided into government led, enterprise led, collective led, and individual led.

Tourism is an information-intensive and information-dependent industry, and tourism informatization has become one of the hotspots in tourism research. Literature [9] proposes that policy selection, personnel training, network security, and technology adoption are the needs of tourism informatization. Literature [9] proposes that policy selection, personnel training, network security, and technology adoption are the basic issues that need to be considered in tourism informatization. Literature [10] analyzed the limitations of the traditional tourism value chain and the impact of tourism informatization on the tourism value chain in the context of tourism informatization and reconstructed the new tourism value chain. Reference [11] analyzes the problems encountered in the process of tourism informatization and proposes solutions. Literature [12] proposes a networked system and development countermeasures for urban tourism information consulting services. Literature [13] proposes measures such as developing rural tourism mobile SMS mode, strengthening website construction, improving infrastructure construction, raising public awareness, strengthening talent training and introduction, and promulgating relevant policies and regulations for rural tourism informatization construction. Literature [14] analyzed the constraints and opportunities of rural tourism informatization construction in Yunnan and proposed countermeasures and platform construction measures for rural tourism informatization construction. Literature [15] discussed the influence mechanism and main manifestations of informatization on the development of tourism industry, aiming at establishing office automation network, business management network, public service network, and comprehensive tourism information database and pointed out that informatization can transform the tourism industry development model, enhance the competitiveness of the tourism industry, and optimize the tourism development environment. Reference [16] discusses the development mode of the intelligent management system of tourist attractions. Literature [14] proposed digital tourism service, pointing out that digital tourism is a tourism information service system based on the network environment, and it is a space centered on "3S" technology, database technology, decision support system, network technology, electronics, and virtual reality technology. The information technology system is the combination of economy, tourism, and information science and technology. Literature [17] constructed the overall framework of the digital tourism system and proposed the realization idea of the tourism application information system. Literature [18] studies the multimedia tourism intelligent navigation system, designs, and develops the tourism intelligent navigation system platform, which has the functions of online virtual tour, tourism itinerary planning, autonomous navigation, and rescue. Literature [19] starts from the realization method and realization of intelligent tourism. The concept of smart tourism is described from the perspective of goals, but the essence of smart tourism is insufficiently explored. Literature [20] believes that smart tourism has not changed the basic characteristics and inherent requirements of the development of the tourism industry and the whole chain of

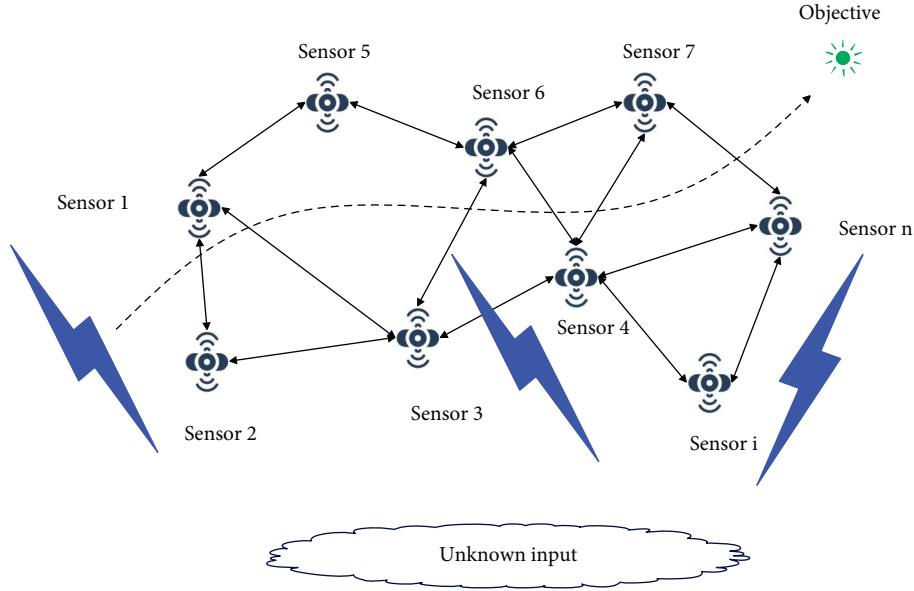


FIGURE 1: Target tracking with multiple sensors affected by unknown inputs.

tourism services to generate wisdom effect and create wisdom value.

3. Multiobjective Programming and Intelligent Optimization Algorithms

A multisensor target tracking scenario affected by unknown inputs is shown in Figure 1. Each sensor node in the multisensor network is equipped with a detection function module, a communication function module, and a data processing function module. The detection function module of the node has the functions of real-time detection of targets and acquisition of target observation information. The communication function module has the function of transmitting the observation information of the sensor itself or the estimated information processed by the data processing module to its neighbor nodes; at the same time, it has the function of receiving the data information of the neighbor nodes. The data processing module has the functions of local data processing and consensus data fusion. Therefore, this study designs the detection function module of all nodes in the sensor network to detect the target measurement information. The target state estimation, sensor bias estimation, and unknown parameter estimation are obtained by filtering estimation locally through the information processing module. Then, through the communication function module, the state estimation and unknown parameter estimation of itself are exchanged and transmitted with the information of the neighbor nodes. Then, in the data processing module, the estimated information of the network consensus is fused, the system deviation is further corrected, and the information is repeatedly exchanged for consensus fusion to finally obtain the global consistency estimation of the target state.

Based on the above description, considering a sensor consisting of n sensors, this section proposes the following multisensor discrete system model:

$$\mathbf{x}_{k+1} = \mathbf{A}_k \mathbf{x}_k + \boldsymbol{\zeta}_k, \quad (1)$$

$$\mathbf{b}_{k+1}^i = \mathbf{B}_k^i \mathbf{b}_k^i + \mathbf{D}_k^i \boldsymbol{\mu}_k + \boldsymbol{\omega}_k^i, \quad (2)$$

$$\mathbf{y}_{k+1}^i = \mathbf{H}_{k+1}^i \mathbf{x}_{k+1} + \mathbf{N}_{k+1}^i \mathbf{b}_{k+1}^i + \mathbf{v}_{k+1}^i. \quad (3)$$

Among them, $\mathbf{x}_k \in \mathfrak{R}^n$ is the target state quantity at time k , $\boldsymbol{\mu}_k \in \mathfrak{R}^q$ is the unknown input, $\mathbf{y}_k^i \in \mathfrak{R}^m$ is the observation quantity of the i -th sensor system at time k , and $\mathbf{b}_k^i \in \mathfrak{R}^p$ is the deviation of the i th sensor system at time k . $\mathbf{A}_k, \mathbf{B}_k^i, \mathbf{N}_k^i, \mathbf{H}_k^i$ is a known transition matrix of appropriate dimension. We assume that $m^i > p^i > q^i$, \mathbf{D}_k^i is a column full rank matrix. The noises $\boldsymbol{\zeta}_k, \boldsymbol{\omega}_k^i$ and \mathbf{v}_k^i are uncorrelated zero-mean white noises, and the noises of each sensor are also uncorrelated with each other, satisfying $E\{\boldsymbol{\zeta}_k \boldsymbol{\zeta}_k^T\} = \mathbf{F}_k \boldsymbol{\delta}_{k-1}$, $E\{\mathbf{v}_k^i \mathbf{v}_k^{iT}\} = \mathbf{R}_k^i \boldsymbol{\delta}_{k-1}$, $E\{\boldsymbol{\omega}_k^i \boldsymbol{\omega}_k^{iT}\} = \mathbf{S}_k^i \boldsymbol{\delta}_{k-1} \cdot \mathbf{F}_k \mathbf{R}_k^i$ and \mathbf{S}_k^i are their respective covariance matrices.

The information filtering vector and its information matrix transformation formula are as follows:

$$\mathbf{Y} = \mathbf{P}^{-1} = \frac{\mathbf{P}}{\mathbb{1}}, \quad \mathbf{y} = \mathbf{Y}\mathbf{x}. \quad (4)$$

Among them, “ \backslash ” represents the left division operator, “ \mathbf{y} ” represents the information vector, “ \mathbf{Y} ” is the information matrix, “ \mathbf{x} ” represents the filter estimated value, and “ \mathbf{P} ” is the estimated error covariance.

Then, according to formula (4), the matrix inverse transformation can be performed to predict the stateless deviation information vector $\bar{\mathbf{y}}_{k+1k}^{b,i}$ and its information matrix $\bar{\mathbf{Y}}_{k+1k}^{b,i}$. Similarly, it is easy to obtain the predicted state information vector $\mathbf{y}_{k+1k}^{x,i}$ and its information matrix $\mathbf{Y}_{k+1k}^{x,i}$ by inverse transformation.

Theorem 1. The algorithm updates the stateless bias information vector $\tilde{\mathbf{y}}_{k+1|k+1}^{b,i}$ and its information matrix $\tilde{\mathbf{Y}}_{k+1|k+1}^{b,i}$ as follows:

$$\begin{aligned}\tilde{\mathbf{Y}}_{k+1|k+1}^{b,i} &= \tilde{\mathbf{Y}}_{k+1|k}^{b,i} + \tilde{\mathbf{I}}_{k+1}^{b,i}, \\ \tilde{\mathbf{y}}_{k+1|k+1}^{b,i} &= \tilde{\mathbf{y}}_{k+1|k}^{b,i} + \tilde{\mathbf{i}}_{k+1}^{b,i}.\end{aligned}\quad (5)$$

Among them, $\tilde{\mathbf{b}}_{k+1|k}^i = \bar{\mathbf{B}}_k^i (\tilde{\mathbf{Y}}_{k|k}^{b,i} / \tilde{\mathbf{y}}_{k|k}^{b,i}) + \mathbf{D}_k^i \Pi_k^i \mathbf{y}_{k+1}^i + \Theta_k^i \tilde{\mathbf{i}}_{k+1}^{b,i} = \mathbf{N}_{k+1}^{iT} \mathbf{R}_{k+1}^{i-1} \mathbf{y}_{k+1}^i$, $\tilde{\mathbf{I}}_{k+1}^{b,i} = \mathbf{N}_{k+1}^{iT} \mathbf{R}_{k+1}^{i-1} \mathbf{N}_{k+1}^i$. The algorithm updates the state information vector $\mathbf{y}_{k+1|k+1}^{x,i}$ and its information matrix $\mathbf{Y}_{k+1|k+1}^{x,i}$ as follows:

$$\begin{aligned}\mathbf{Y}_{k+1|k+1}^{x,i} &= \mathbf{Y}_{k+1|k}^{x,i} + \mathbf{I}_{k+1}^{x,i}, \\ \mathbf{y}_{k+1|k+1}^{x,i} &= \mathbf{y}_{k+1|k}^{x,i} + \mathbf{i}_{k+1}^{x,i}.\end{aligned}\quad (6)$$

Among them, $\tilde{\mathbf{x}}_{k|k}^i = \mathbf{Y}_{k|k}^{x,i} / \mathbf{y}_{k|k}^{x,i}$, $\tilde{\mathbf{G}}_{k+1}^i = L^i (\mathbf{N}_{k+1}^i (\tilde{\mathbf{Y}}_{k+1|k}^{b,i} / \mathbb{I})) (\mathbf{N}_{k+1}^{iT} + \mathbf{R}_{k+1}^i) L^{iT}$, $\tilde{\mathbf{i}}_{k+1}^{x,i} = \mathbf{S}_{k+1|k}^{iT} \tilde{\mathbf{G}}_{k+1}^{i-1} \tilde{\mathbf{r}}_{k+1}^i$.

The prediction and update information vector $\mathbf{y}_{k+1|k+1}^{\beta,i}$ and information matrix $\mathbf{Y}_{k+1|k+1}^{\beta,i}$ of β are expressed as follows:

$$\mathbf{y}_{k+1|k+1}^{\beta,i} = \mathbf{y}_{k+1|k}^{\beta,i} + \mathbf{i}_{k+1}^{\beta,i}, \frac{n!}{r!(n-r)!} \quad (7)$$

$$\mathbf{\beta}_{k+1|k+1}^i = \mathbf{Y}_{k+1|k+1}^{\beta,i} \setminus \mathbf{y}_{k+1|k+1}^{\beta,i}. \quad (8)$$

$$\mathbf{Y}_{k+1|k+1}^{\beta,i} = \mathbf{Y}_{k+1|k}^{\beta,i} + \mathbf{I}_{k+1}^{\beta,i} = \tilde{\mathbf{y}}_{k+1|k+1}^{b,i}. \quad (9)$$

Among them, the value of $\mathbf{Y}_{k+1|k}^{\beta,i} = \tilde{\mathbf{y}}_{k+1|k}^{b,i}$, $\mathbf{y}_{k+1|k}^{\beta,i} = \mathbf{Y}_{k+1|k}^{\beta,i} \beta_{k+1|k}^i$, $\mathbf{I}_{k+1}^{\beta,i} = \tilde{\mathbf{I}}_{k+1}^{b,i} = \mathbf{N}_{k+1}^i \mathbf{R}_{k+1}^{i-1} \mathbf{N}_{k+1}^i$, $\mathbf{i}_{k+1}^{\beta,i} = -\mathbf{N}_{k+1}^{iT} \mathbf{R}_{k+1}^{i-1} \mathbf{H}_{k+1}^i \beta_{k+1|k}^i = \Gamma_{k+1}^i + (\mathbf{Q}_k^{bxi} - \Gamma_{k+1}^i \mathbf{Q}_k^x) \mathbf{y}_{k+1|k}^{x,i}$, $\Gamma_{k+1}^i = \Theta_k^i \mathbf{S}_{k+1|k}^i \tilde{\mathbf{Q}}_k^{b,i} \tilde{\mathbf{r}}_{k+1}^i$ is the same as the formula.

Proof. It can be expressed as follows:

$$\begin{aligned}\tilde{\mathbf{K}}_{k+1}^{b,i} &= \tilde{\mathbf{P}}_{k+1|k}^{b,i} \mathbf{N}_{k+1}^{iT} L^{iT} (\tilde{\mathbf{G}}_{k+1}^i)^{-1} \\ &= \tilde{\mathbf{P}}_{k+1|k}^{b,i} \mathbf{N}_{k+1}^{iT} L^{iT} \left(L^i \left(\mathbf{N}_{k+1}^i \tilde{\mathbf{P}}_{k+1|k}^{b,i} \mathbf{N}_{k+1}^{iT} + \mathbf{R}_{k+1}^i \right) L^{iT} \right)^{-1} \\ &= \tilde{\mathbf{P}}_{k+1|k}^{b,i} \mathbf{N}_{k+1}^{iT} L^{iT} \left(L^i \left(\mathbf{N}_{k+1}^i \tilde{\mathbf{P}}_{k+1|k}^{b,i} \mathbf{N}_{k+1}^{iT} + \mathbf{R}_{k+1}^i \right) L^{iT} \right)^{-1} (L^i \mathbf{R}_{k+1}^i L^{iT}) (L^i \mathbf{R}_{k+1}^i L^{iT})^{-1} \\ &= \tilde{\mathbf{P}}_{k+1|k}^{b,i} \mathbf{N}_{k+1}^{iT} L^{iT} (L^i \mathbf{R}_{k+1}^i L^{iT})^{-1} - \tilde{\mathbf{P}}_{k+1|k}^{b,i} \mathbf{N}_{k+1}^{iT} L^{iT} \left(L^i \left(\mathbf{N}_{k+1}^i \tilde{\mathbf{P}}_{k+1|k}^{b,i} \mathbf{N}_{k+1}^{iT} + \mathbf{R}_{k+1}^i \right) L^{iT} \right)^{-1} \\ &\quad \left(L^i \left(\mathbf{N}_{k+1}^i \tilde{\mathbf{P}}_{k+1|k}^{b,i} \mathbf{N}_{k+1}^{iT} \right) L^{iT} \right) (L^i \mathbf{R}_{k+1}^i L^{iT})^{-1} \\ &= \left(\mathbb{I} - \tilde{\mathbf{K}}_{k+1}^{b,i} L^i \mathbf{N}_{k+1}^i \right) \tilde{\mathbf{P}}_{k+1|k}^{b,i} \mathbf{N}_{k+1}^{iT} L^{iT} (L^i \mathbf{R}_{k+1}^i L^{iT})^{-1} \\ &= \tilde{\mathbf{P}}_{k+1|k+1}^{b,i} \mathbf{N}_{k+1}^{iT} L^{iT} (L^i \mathbf{R}_{k+1}^i L^{iT})^{-1} \\ &= \tilde{\mathbf{P}}_{k+1|k+1}^{b,i} \mathbf{N}_{k+1}^{iT} \mathbf{R}_{k+1}^{i-1} (L^i)^{-1}.\end{aligned}\quad (10)$$

Then, there is

$$\mathbb{I} - \tilde{\mathbf{K}}_{k+1}^{b,i} L^i \mathbf{N}_{k+1}^i = \tilde{\mathbf{P}}_{k+1|k+1}^{b,i} \left(\tilde{\mathbf{P}}_{k+1|k}^{b,i} \right)^{-1}. \quad (11)$$

Then, it can be expressed as follows:

$$\begin{aligned}
\tilde{\mathbf{b}}_{k+1|k+1}^i &= \tilde{\mathbf{b}}_{k+1|k}^i + \tilde{\mathbf{K}}_{k+1}^{b,1} \tilde{\mathbf{r}}_{k+1}^i \\
&= \left(\mathbb{I} - \tilde{\mathbf{K}}_{k+1}^{b,i} L^i N_{k+1}^i \right) \tilde{\mathbf{b}}_{k+1|k}^i + \tilde{\mathbf{K}}_{k+1}^{b,i} L^i \mathbf{y}_{k+1}^i \\
&= \tilde{\mathbf{P}}_{k+1|k+1}^{b,i} \left(\tilde{\mathbf{P}}_{k+1|k}^{b,i} \right)^{-1} \tilde{\mathbf{b}}_{k+1|k}^i + \tilde{\mathbf{P}}_{k+1|k+1}^{b,i} \mathbf{N}_{k+1}^{i,T} \mathbf{R}_{k+1}^{i,-1} L^{i,-1} L^i \mathbf{y}_{k+1}^i \\
\left(\tilde{\mathbf{P}}_{k+1|k+1}^{b,i} \right)^{-1} \tilde{\mathbf{b}}_{k+1|k+1}^i &= \left(\tilde{\mathbf{P}}_{k+1|k}^{b,i} \right)^{-1} \tilde{\mathbf{b}}_{k+1|k}^i + N_{k+1}^{i,T} \mathbf{R}_{k+1}^{i,-1} L^{i,-1} L^i \mathbf{y}_{k+1}^i \\
&= \left(\tilde{\mathbf{P}}_{k+1|k}^{b,i} \right)^{-1} \tilde{\mathbf{b}}_{k+1|k}^i + N_{k+1}^{i,T} \mathbf{R}_{k+1}^{i,-1} \mathbf{y}_{k+1}^i.
\end{aligned} \tag{12}$$

It is easy to obtain $\tilde{\mathbf{y}}_{k+1|k}^{b,i}$ according to the definition of the information matrix. By connecting the above formula, formula (4) can be proved.

By taking formula (7) into it, we get

$$\tilde{\mathbf{P}}_{k+1|k+1}^{b,i} = \tilde{\mathbf{P}}_{k+1|k}^{b,i} - \tilde{\mathbf{P}}_{k+1|k+1}^{b,i} N_{k+1}^{i,T} \mathbf{R}_{k+1}^{i,-1} N_{k+1}^i \tilde{\mathbf{P}}_{k+1|k}^{b,i}. \tag{13}$$

By inverse matrix transformation of this formula, we can get

$$\begin{aligned}
\left(\tilde{\mathbf{P}}_{k+1|k+1}^{b,i} \right)^{-1} &= \left(\tilde{\mathbf{P}}_{k+1|k}^{b,i} \right)^{-1} + N_{k+1}^{i,T} L^i \left(L^i \mathbf{R}_{k+1}^i L^{i,T} \right)^{-1} L^i N_{k+1}^i \\
&= \left(\tilde{\mathbf{P}}_{k+1|k}^{b,i} \right)^{-1} + N_{k+1}^{i,T} L^i \left(L^{i,T} \right)^{-1} \mathbf{R}_{k+1}^{i,-1} L^{i,-1} L^i N_{k+1}^i \\
&= \left(\tilde{\mathbf{P}}_{k+1|k}^{b,i} \right)^{-1} + N_{k+1}^{i,T} \mathbf{R}_{k+1}^{i,-1} N_{k+1}^i.
\end{aligned} \tag{14}$$

Then, formula (3) is proved.

Substituting formula (8) into it, we get

$$\begin{aligned}
\beta_{k+1|k+1}^i &= \beta_{k+1|k}^i - \tilde{\mathbf{K}}_{k+1}^{b,i} \mathbf{S}_{k+1|k}^i \\
&= \left(\mathbb{I} - \tilde{\mathbf{K}}_{k+1}^{b,i} L^i N_{k+1}^i \right) \beta_{k+1|k}^i - \tilde{\mathbf{K}}_{k+1}^{b,i} L^i \mathbf{H}_{k+1}^i \\
&= \tilde{\mathbf{P}}_{k+1|k+1}^{b,i} \left(\tilde{\mathbf{P}}_{k+1|k}^{b,i} \right)^{-1} \beta_{k+1|k}^i - \tilde{\mathbf{P}}_{k+1|k+1}^{b,i} \mathbf{N}_{k+1}^{i,T} \mathbf{R}_{k+1}^{i,-1} \mathbf{H}_{k+1}^i.
\end{aligned} \tag{15}$$

Then,

$\left(\tilde{\mathbf{P}}_{k+1|k+1}^{b,i} \right)^{-1} \beta_{k+1|k+1}^i = \left(\tilde{\mathbf{P}}_{k+1|k}^{b,i} \right)^{-1} \beta_{k+1|k}^i - N_{k+1}^{i,T} \mathbf{R}_{k+1}^{i,-1} \mathbf{H}_{k+1}^i$, and formula (9) is proved.

In order to improve the tracking accuracy, this study designs parameter estimation for unknown input. The unknown parameters in the system are estimated in turn using the bias estimates derived in the previous section. The bias dynamic equation of the multisensor network in formula (2) can be rewritten as follows:

$$\begin{aligned}
\mathbf{D}_k^i \boldsymbol{\mu}_k &= \mathbf{b}_{k+1}^i - \mathbf{B}_k^i \mathbf{b}_k^i - \omega_k^i \\
&= \hat{\mathbf{b}}_{k+1|k+1}^i - \mathbf{B}_k^i \hat{\mathbf{b}}_{k|k}^i + \left(\hat{\mathbf{b}}_{k+1|k+1}^i - \mathbf{B}_k^i \hat{\mathbf{b}}_{k|k}^i - \omega_k^i \right) \\
&= \bar{\mathbf{b}}_k^i + \phi_k^i.
\end{aligned} \tag{16}$$

Among them, $\bar{\mathbf{b}}_k^i \triangleq \hat{\mathbf{b}}_{k+1|k+1}^i - \mathbf{B}_k^i \hat{\mathbf{b}}_{k|k}^i$, $\phi_k^i \triangleq \hat{\mathbf{b}}_{k+1|k+1}^i - \mathbf{B}_k^i \hat{\mathbf{b}}_{k|k}^i - \omega_k^i$, $\hat{\mathbf{b}}_{k+1|k+1}^i \triangleq \hat{\mathbf{b}}_{k+1}^i - \hat{\mathbf{b}}_{k+1|k+1}^i$. It is easy to know $E(\phi_k^i) = 0$. The deviation equations of sensor node i and its neighbor

nodes can be expressed in the form of equation (13). Therefore, these equations can be combined, and formula (13) can be expressed as follows:

$$\mathbf{D}_k \boldsymbol{\mu}_k = \mathbf{B}_k + \phi_k. \tag{17}$$

Among them, $\mathbf{D}_k \triangleq \text{col}\{\mathbf{D}_k^j: j \in J_i\}$, $\mathbf{B}_k \triangleq \text{col}\{\bar{\mathbf{b}}_k^j: j \in J_i\}$, $\phi_k \triangleq \text{col}\{\phi_k^j: j \in J_i\}$.

Further, according to the principle of least squares estimation, equation (14) can be transformed into the following equation, so as to obtain the estimation of the unknown input parameters of the i -th sensor node:

$$\begin{aligned}
\hat{\boldsymbol{\mu}}_k^i &= \left(\mathbb{D}_k^T \mathbb{D}_k \right)^{-1} \mathbb{D}_k^T \mathbf{B}_k, \\
\mathbf{Y}_k^{\mu,i} &= \mathbb{D}_k^T \mathbb{D}_k.
\end{aligned} \tag{18}$$

Then, there is $\mathbf{y}_k^{\mu,i} = \mathbb{D}_k^T \mathbb{B}_k$.

Although each sensor network has different biases, sensor networks are all affected by unknown inputs. Therefore, it is advisable to design a network to achieve consistent consensus on unknown inputs, so that unknown parameters can be accurately estimated.

The multisensor communication network topology is usually represented by the adjacency matrix in graph theory, and the communication connection of the nodes in the sensor network is often represented by the adjacency matrix. The topology of the sensor network is represented by defining an undirected graph $G = (V, E)$. Among them, V is the node set in the multisensor network, $V = \{1, 2, \dots, n\}$, and each element in the set corresponds to a sensor. E represents the set of edges in the graph G , the elements in $E \subseteq V \times V$, E are called edges, which are represented as unordered pairs of elements in V , and an edge represents two-way communication between the two sensors. The number of edges associated with V_i is called the degree of a point V_i , and the degree of a graph is equal to the sum of the degrees of the points. $A_i = \{j \in V, (j, i) \in E\}$ represents the set of neighbor nodes that can communicate with sensor i , and n represents the number of sensor nodes.

For graph $G = (V, E)$, $|V| = n$, $|E| = m$, the $n \times n$ -order matrix $J = [a_{ij}]_{i,j=1}^n$ is an adjacency matrix, which is expressed as follows:

$$a_{ij} \begin{cases} 1 & \text{if } (j, i) \notin E \\ 0 & \text{otherwise} \end{cases}. \tag{19}$$

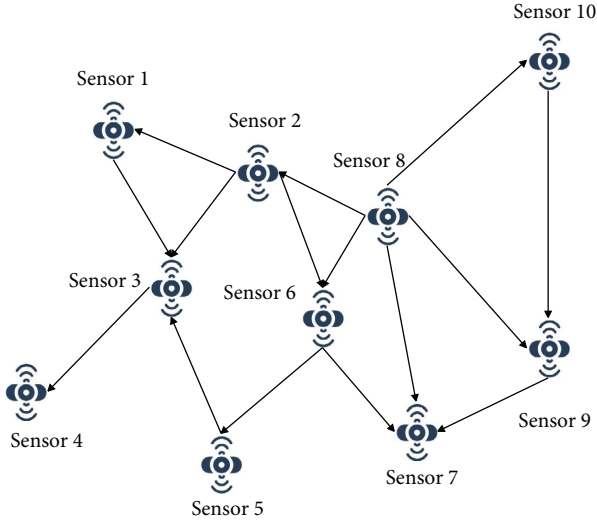


FIGURE 2: Sensor network communication topology.

Among them, $a_{ij} = 1$ refers to the existence of a communication link between sensor i and sensor j and $a_{ij} = 0$ refers to the absence of communication between sensor i and sensor j . According to the adjacency matrix, the connection and communication of the sensor network can be well represented, and it has a wide range of applications in multisensor fusion algorithms.

During the operation of the entire network, the node set V and the edge set E of the network change dynamically, that is to say, the connection relationship between nodes is allowed to change during the operation of the sensor network, and nodes can be directly added or removed. However, due to the limited communication capability of each sensor, it is impossible to send its own information to every other node in one communication cycle. Taking 10 sensors as an example, Figure 2 shows the network communication topology diagram composed of 10 sensors.

The adjacency matrix corresponding to the sensor network in Figure 2 is shown in formula (17):

$$J = \begin{bmatrix} 0 & 1 & 1 & 0 & 0 & 0 & 0 & 0 & 0 & 0 \\ 1 & 0 & 1 & 0 & 0 & 1 & 0 & 1 & 0 & 0 \\ 1 & 1 & 0 & 1 & 1 & 0 & 0 & 0 & 0 & 0 \\ 0 & 0 & 1 & 0 & 0 & 0 & 0 & 0 & 0 & 0 \\ 0 & 0 & 1 & 0 & 0 & 1 & 0 & 0 & 0 & 0 \\ 0 & 1 & 0 & 0 & 1 & 0 & 1 & 1 & 0 & 0 \\ 0 & 0 & 0 & 0 & 0 & 1 & 0 & 1 & 1 & 0 \\ 0 & 1 & 0 & 0 & 0 & 1 & 1 & 0 & 1 & 1 \\ 0 & 0 & 0 & 0 & 0 & 0 & 1 & 1 & 0 & 1 \\ 0 & 0 & 0 & 0 & 0 & 0 & 0 & 1 & 1 & 0 \end{bmatrix}. \quad (20)$$

Since the sensor bias is not only affected by the unknown input but also includes the sensor's own bias, the bias of each sensor is unique to itself, and consistency filtering cannot be performed. However, the unknown input received by the

sensor network is consistent, so it can achieve a consistent consensus on the unknown parameters.

According to the network topology, the matrix Time_{i*j} is defined in this study to represent the minimum number of times that the information of node i is transmitted to node j , that is, the shortest path of information transmission. The matrix Time_{i*j} is an $n * n$ matrix, and the matrix element Time_{ij} represents the minimum number of transfers required to transmit information from the i -th node to the j -th node. Taking Figure 2 as an example, the shortest path to transmit information from sensor 1 to sensor 9 is as follows: sensor 1 -> sensor 2 -> sensor 8 -> sensor 9. Since it is passed 3 times, $\text{Time}_{1*9} = 3$. For different network communication topologies, the matrix Time_{i*j} will also be different. It can be seen that according to the matrix Time_{i*j} , the communication situation of each sensor can be known, and it can be seen which nodes can obtain the most global information in the least number of iterations. The matrix Time_{i*j} of the multisensor network shown in Figure 2 can be expressed as formula (17):

$$\text{Time}_{i*j} = \begin{bmatrix} 0 & 1 & 1 & 2 & 2 & 2 & 3 & 2 & 3 & 3 \\ 1 & 0 & 1 & 2 & 2 & 1 & 2 & 1 & 2 & 2 \\ 1 & 1 & 0 & 1 & 1 & 2 & 3 & 2 & 3 & 3 \\ 2 & 2 & 1 & 0 & 2 & 3 & 4 & 3 & 4 & 4 \\ 2 & 2 & 1 & 2 & 0 & 1 & 2 & 2 & 3 & 3 \\ 2 & 1 & 2 & 3 & 1 & 0 & 1 & 1 & 2 & 2 \\ 3 & 2 & 3 & 4 & 2 & 1 & 0 & 1 & 1 & 2 \\ 2 & 1 & 2 & 3 & 2 & 1 & 1 & 0 & 1 & 1 \\ 3 & 2 & 3 & 4 & 3 & 2 & 1 & 1 & 0 & 1 \\ 3 & 2 & 3 & 4 & 3 & 2 & 2 & 1 & 1 & 0 \end{bmatrix}. \quad (21)$$

This study defines ρ as a set, where $\rho(i) = \sum_{j=1}^n \text{Time}_{ij}$ is the sum of the minimum number of iterations for node i to receive information from all other nodes. Within the limited number of iterations, the smaller the sum of the minimum number of iterations for a node to receive information from other nodes, the more information the node obtains from other nodes. Therefore, the communication volume of a node is designed in this study to represent the amount of information obtained by the node, which is inversely proportional to $\rho(i)$. The smaller $\rho(i)$ is, the greater the communication volume is, and the more information is obtained.

This study defines Δ to represent the node traffic, and its expression is as follows:

$$\Delta(i) = \frac{1}{\rho(i)}. \quad (22)$$

A sensor with more neighbor nodes potentially has more information throughput, and its status in the sensor network is equivalent to a core node. This study defines Ω_{\max} as the sensor with the most neighbor nodes, which represents the node that exchanges the most information in the sensor network. Then, this study designs the consistency weight

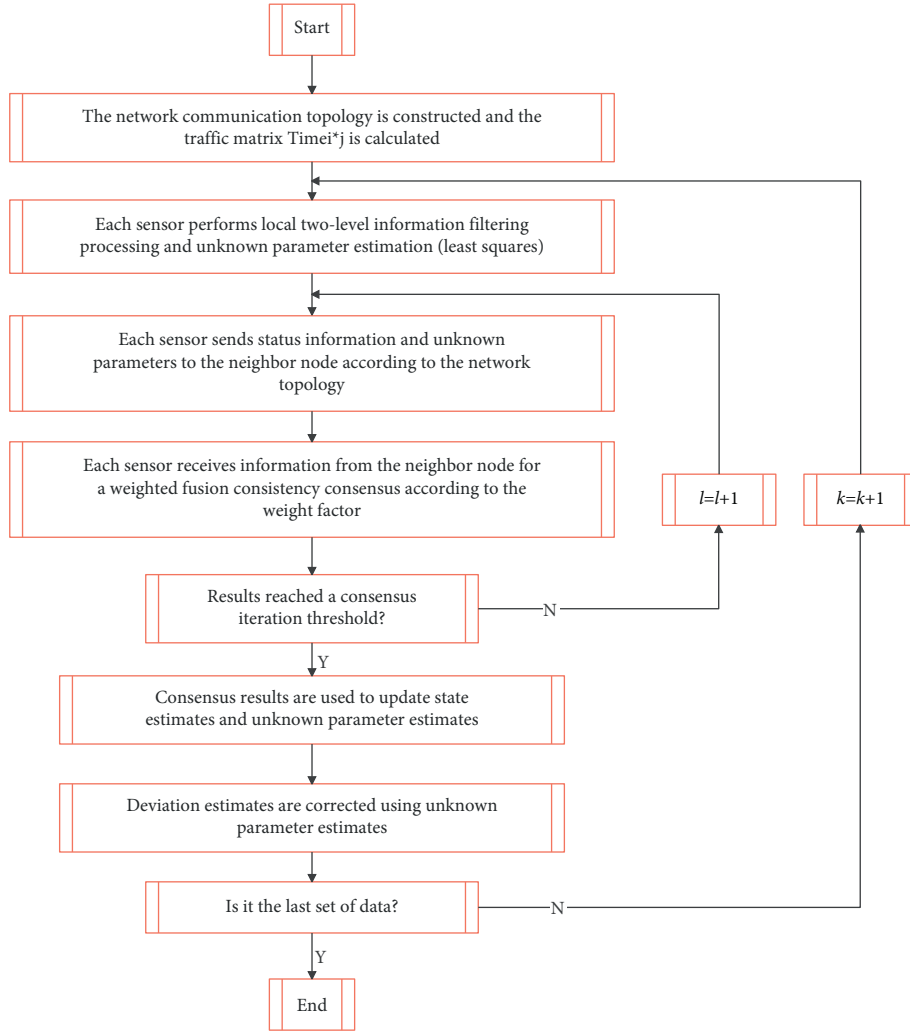


FIGURE 3: Block diagram of the algorithm flow.

factor according to the traffic of the node, so that the greater the traffic of the node, the higher the importance of the node, and the estimated value of the node is closer to the global optimal estimated value of all the information in the sensor.

Consistency estimation theory means that in a multi-sensor network, the arbitrary initial state of each node for any sensor has

$$\lim_{t \rightarrow \infty} \|x_i(t) - x_j(t)\| = 0. \quad (23)$$

That is, all sensors eventually reach a common consistent state, and all sensors have the same estimated state of the target.

In a sensor network, the basis for judging the good performance of the system is the unbiased estimation of the mean initial state of the node as the target state. If each sensor is in an initial state, each node of the sensor network can quickly reach the average consistency of the initial value; it is considered that for the target in any fixed time state, the entire network has achieved consistent tracking of the target. In the discrete-time case, the most commonly used mathematical model for consensus estimation is expressed as follows:

$$x_i(k+1) = x_i(k) + \varepsilon \sum_{j \in N_i} w_{ij} (x_j(k) - x_i(k)) \quad i \in V. \quad (24)$$

Among them, ε represents the iteration step size, and the value range is as follows:

$$0 < \varepsilon < \frac{1}{\theta} \quad \theta = \max_i \left(\sum_{i \neq j} a_{ij} \right). \quad (25)$$

In an undirected graph, w_{ij} represents the weight that sensor i assigns to sensor j .

Since the sensor nodes exchange information with each other, the greater the communication volume of a node, the more times the node communicates with other sensors, and the greater the impact on other sensors in the process of network consensus. Therefore, when designing the data fusion weight factor, the relative situation between nodes should be considered, and the consistency weight factor should be designed by corresponding to the relative size of the communication between the two sensor nodes. The consistency weight factor is determined by the traffic between node i and node j . According to the average consensus

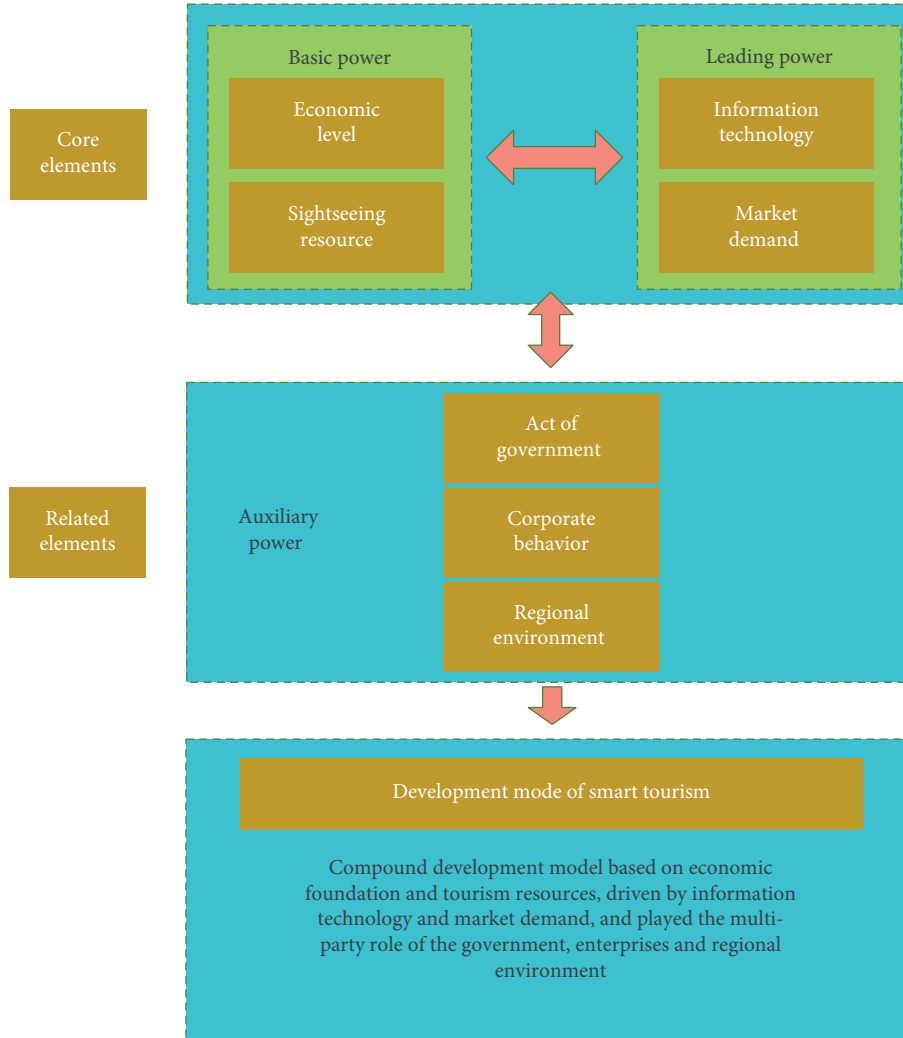


FIGURE 4: Dynamic mechanism of rural smart tourism development.

fusion criterion, $\mathbf{U}(l) = [\mathbf{u}_{ij}(l)]$ denotes the linear weighting matrix of the state estimation iteration l step, and \mathbf{u}_{ij} denotes the weight of node j at sensor node i . The initial design weight factor is determined in the form of $\Delta(j)/\Delta(i)$. The greater the traffic $\Delta(j)$ of the neighbor node j , the greater the weight factor, and the local information will make more corrections to its own information according to the weight factor. Then, the estimation accuracy of the node with small communication traffic will be corrected at a faster speed than the estimation accuracy of the node with large communication traffic. In order to ensure that the consistency weight factor does not modify the local too much and cause the information to be cluttered in the iterative process, this study defines the following weighting matrix rules:

$$\begin{cases} \mathbf{u}_{ij}(l+1) = \frac{\Delta(j)}{\Delta(i)} * \frac{\min_{j=1,2,\dots,n}\{\Delta(f)\}}{\max_{f=1,2,\dots,n}\{\Delta(f)\}} * \Omega_{\max} & j \in J_i \\ \mathbf{u}_{ij}(l+1) = 0 & j \notin J_i \end{cases} \quad (26)$$

The second half of this formula is to ensure that $\mathbf{u}_{ij} \in (0, 1)$ enables the network to converge.

According to formulas (1)–(3), after sensor i performs l consistent fusion, its state estimation and unknown parameter weighting coefficient matrix is $\mathbf{U}(l)$, and its corresponding global optimal information vector and information matrix are as follows:

$$\begin{cases} \mathbf{y}_{k|k}^{x,i}(l+1) = \mathbf{y}_{k|k}^{x,i}(l) + \sum_{j \in J_i} \mathbf{u}_{ij}(l) (\mathbf{y}_{k|k}^{x,j}(l) - \mathbf{y}_{k|k}^{x,i}(l)) \\ \mathbf{Y}_{k|k}^{x,i}(l+1) = \mathbf{Y}_{k|k}^{x,i}(l) + \sum_{j \in J_i} \mathbf{u}_{ij}(l) (\mathbf{Y}_{k|k}^{x,j}(l) - \mathbf{Y}_{k|k}^{x,i}(l)) \\ \mathbf{y}_k^{\mu,i}(l+1) = \mathbf{y}_k^{\mu,i}(l) + \sum_{j \in J_i} \mathbf{u}_{ij}(l) (\mathbf{y}_k^{\mu,j}(l) - \mathbf{y}_k^{\mu,i}(l)) \\ \mathbf{Y}_k^{\mu,i}(l+1) = \mathbf{Y}_k^{\mu,i}(l) + \sum_{j \in J_i} \mathbf{u}_{ij}(l) (\mathbf{Y}_k^{\mu,j}(l) - \mathbf{Y}_k^{\mu,i}(l)) \end{cases} \quad (27)$$

Then, the global optimal state estimation and unknown parameter estimation can be expressed as follows:

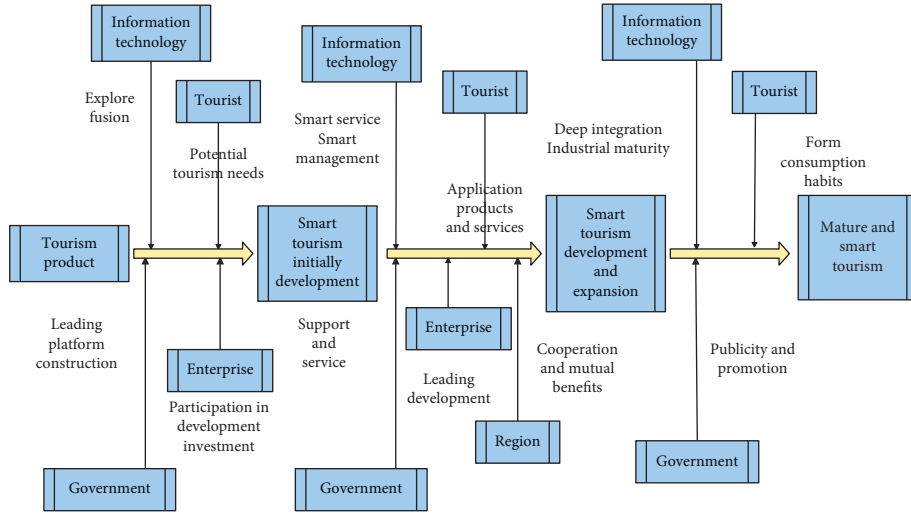


FIGURE 5: Rural smart tourism development model.

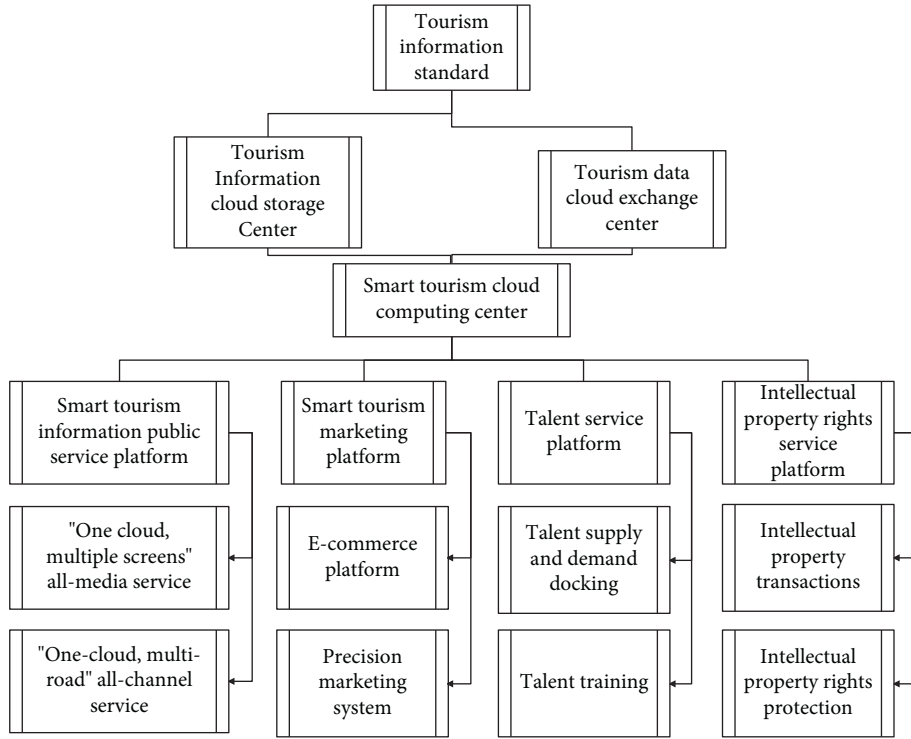


FIGURE 6: Construction system of rural smart tourism public service platform.

$$\begin{aligned} \hat{\mathbf{x}}_{k|k}^i(l+1) &= \mathbf{Y}_{k|k}^{r,i}(l+1) \setminus \mathbf{y}_{k|k}^{xi}(l+1), \\ \hat{\boldsymbol{\mu}}_k^i(l+1) &= \mathbf{Y}_k^{\mu,i}(l+1) \setminus \mathbf{y}_k^{\mu,i}(l+1). \end{aligned} \quad (28)$$

The distributed consistent data fusion algorithm continuously improves the state estimation accuracy of each sensor through iteration. The fused state estimation is fed back to each sensor to continue to use the unknown parameter estimation to correct the deviation, so that the state of the sensor and the estimation accuracy of the deviation are improved in both aspects. This iterative update method makes the neighbor nodes with high traffic have higher

weights, and each sensor collects the neighbor information iteratively, so that the updated value of each sensor is more accurate. By repeating this cycle, eventually, the state estimates of all sensors will gradually reach an agreement.

After the unknown input global estimate $\hat{\boldsymbol{\mu}}_k^i$ obtained through the consensus estimation of the network consensus, it is put into the local to correct the local bias estimate. According to formula (2), the following deviation estimate can be obtained:

$$\hat{\mathbf{b}}_{k+1|k+1}^i = \mathbf{B}_k^i \hat{\mathbf{b}}_{k|k}^i + \mathbf{D}_k^i \hat{\boldsymbol{\mu}}_k^i. \quad (29)$$

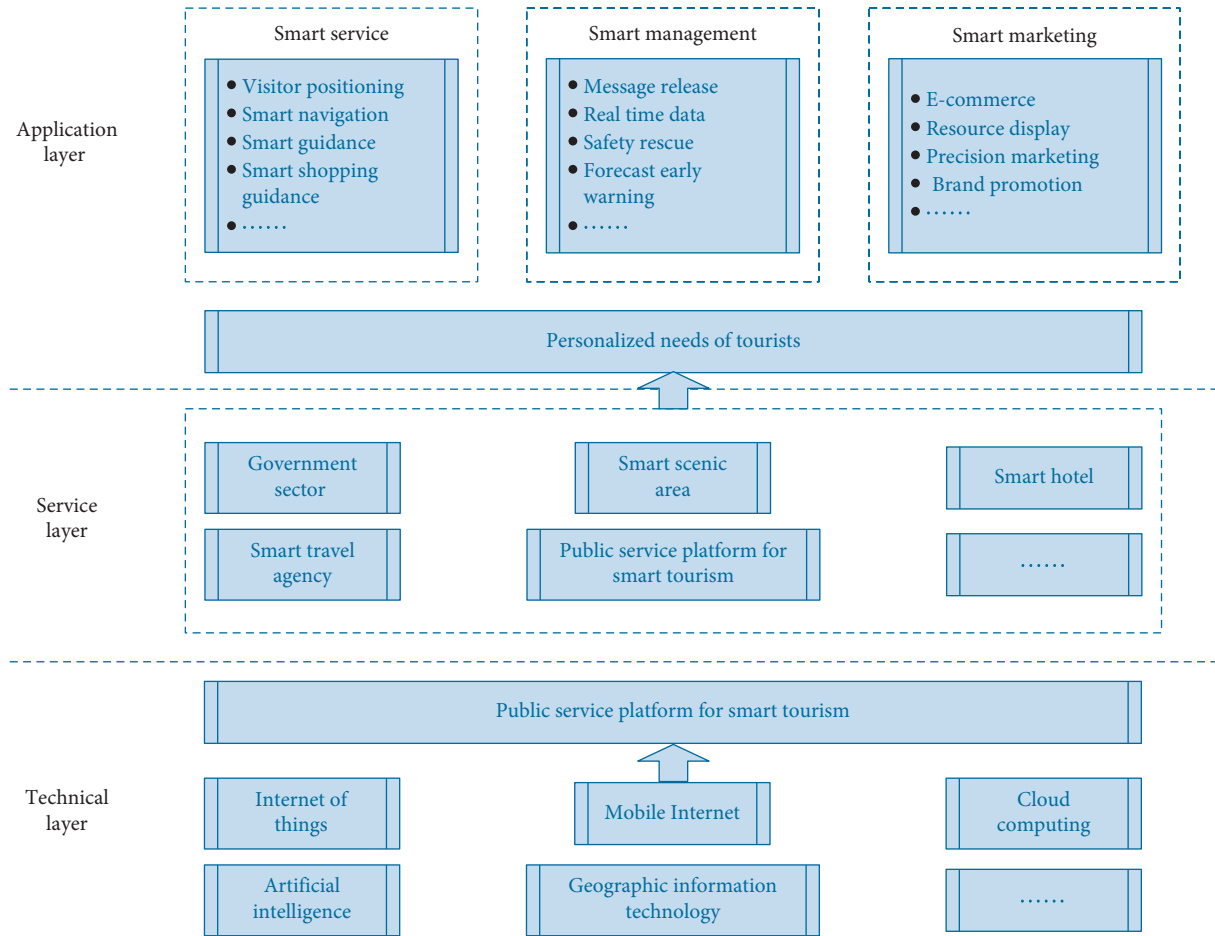


FIGURE 7: Diagram of rural smart tourism system.

TABLE 1: Planning effect of rural tourism development model.

Number	Tourism plan	Number	Tourism plan	Number	Tourism plan
1	93.23	25	91.06	49	89.62
2	90.53	26	87.98	50	90.28
3	93.45	27	89.13	51	89.44
4	89.50	28	92.36	52	89.13
5	90.85	29	91.95	53	89.17
6	89.54	30	93.77	54	90.75
7	88.82	31	91.73	55	92.97
8	87.15	32	93.28	56	93.18
9	90.20	33	90.00	57	88.62
10	93.50	34	92.11	58	91.29
11	91.36	35	87.32	59	87.23
12	87.54	36	92.26	60	88.27
13	91.27	37	87.93	61	92.20
14	89.55	38	89.44	62	93.19
15	93.50	39	90.42	63	92.70
16	88.32	40	87.43	64	91.18
17	91.05	41	88.46	65	92.09
18	93.55	42	91.01	66	93.79
19	92.74	43	87.38	67	89.78
20	92.80	44	91.00	68	90.04
21	89.17	45	91.79	69	91.99
22	87.31	46	93.25	70	90.11
23	92.76	47	89.50	71	93.79
24	90.10	48	89.18	72	90.73

So far, the estimated value $\hat{\mathbf{b}}_{k+1|k+1}^i, \hat{\mathbf{x}}_{k+1|k+1}^i, \hat{\mu}_k^i$ can be output as the final estimation result after the k th sampling, as shown in Figure 3. \square

4. Research on the Development Model of Rural Tourism Based on Multiobjective Planning and Intelligent Optimization Algorithm

Combined with the previous intelligent optimization algorithm and multiobjective planning sensor algorithm, the rural tourism development model of this study is constructed. According to the analysis of the driving factors of rural smart tourism development, it can be seen that the core factors promoting the development of rural smart tourism are information technology, market demand, economic level, and tourism resources, and the relevant factors are government behavior, corporate behavior, and regional environment. The economic level provides financial guarantee, and tourism resources provide resource attractiveness, both of which are the basis for the development of smart tourism. The application of information technology and the update of market demand are the leading factors to promote the development of smart tourism in Changshu, and the government, enterprises, and regional environment are the external driving forces. The particularity of the

TABLE 2: The effect of rural tourism development model.

Number	Tourism development	Number	Tourism development	Number	Tourism development
1	76.29	25	75.31	49	72.97
2	84.52	26	79.43	50	76.88
3	81.33	27	83.50	51	74.14
4	83.42	28	80.22	52	74.71
5	70.91	29	84.58	53	77.00
6	81.87	30	83.86	54	70.10
7	78.94	31	74.90	55	84.82
8	75.27	32	82.70	56	83.50
9	76.10	33	77.07	57	78.17
10	83.00	34	73.28	58	74.10
11	76.52	35	81.92	59	79.30
12	73.31	36	70.34	60	84.69
13	74.61	37	72.93	61	84.70
14	74.63	38	75.48	62	77.33
15	81.99	39	76.82	63	69.56
16	74.17	40	69.74	64	77.66
17	70.66	41	79.08	65	73.33
18	78.26	42	84.40	66	83.97
19	79.86	43	76.51	67	81.27
20	83.85	44	79.99	68	75.35
21	81.86	45	79.33	69	75.55
22	80.39	46	79.08	70	81.25
23	75.48	47	83.79	71	76.78
24	77.28	48	75.10	72	79.92

development conditions of smart tourism determines that the mode of regional smart tourism development is based on the economic foundation and tourism resources. Moreover, it is driven by information technology and market demand and is a compound development model, in which the government, enterprises, and the regional environment play multiple roles, as shown in Figure 4.

This study analyzes the development model of rural smart tourism. Under the action of dynamic factors, the development of smart tourism is divided into three stages, as shown in Figure 5.

The construction system of the smart tourism public service platform is shown in Figure 6.

Rural smart tourism will go through the initial stage and the development stage. Under the interaction of driving factors such as tourism resources, economic level, market demand, information technology, government behavior, corporate behavior, and regional environment, through multiple efforts and joint development, a mature smart tourism system will be built. It specifically covers the technical layer, service layer, and application layer and realizes the whole process, all media, and all time and space services of tourism information. Moreover, it realizes the optimal utilization of rural tourism resources, promotes the optimization and upgrading of the tourism industry and improves the quality of rural tourism. At the same time, the smart tourism system can be promoted as the framework system of rural smart tourism, providing reference for the development of other rural smart tourism. Figure 7 shows the smart tourism system diagram.

Through the above research, a good rural smart tourism development model is constructed. Next, the effectiveness of

the smart tourism development model proposed in this study is verified. This study combines the intelligent simulation method to verify the effect of the rural tourism development model and count the effect of tourism planning and the evaluation of the effect of the rural tourism development model. The statistical test results are listed in Tables 1 and 2.

From the above research, we can see that the rural tourism development model based on multiobjective planning and intelligent optimization algorithm proposed in this study can play an important role in the development of rural tourism.

5. Conclusion

In the process of the development of the rural tourism industry, in the context of the micromedia era, whether it is rural tourists making Internet financial payments or operators publishing information through the Internet platform, Internet technology plays a very important role in it. Moreover, the development of rural tourism has forced the construction of network infrastructure to a certain extent. On the other hand, rural tourism e-commerce has become a new business operation model that provides online payment, financial trade, and comprehensive services. This study combines multiobjective planning and intelligent optimization algorithm to analyze the development mode of rural tourism, so as to improve the analysis effect of rural tourism development path. The experimental research results show that the rural tourism development model based on multiobjective planning and intelligent optimization algorithm proposed in this study can play an important role in the development of rural tourism.

Data Availability

The labeled dataset used to support the findings of this study is available from the corresponding author upon request.

Conflicts of Interest

The authors declare that they have no conflicts of interest.

Acknowledgments

This work was supported by the Xi'an FanYi University.

References

- [1] K. Nam, C. S. Dutt, P. Chathoth, and M. S. Khan, "Blockchain technology for smart city and smart tourism: latest trends and challenges," *Asia Pacific Journal of Tourism Research*, vol. 26, no. 4, pp. 454–468, 2021.
- [2] C. D. Huang, J. Goo, K. Nam, and C. W. Yoo, "Smart tourism technologies in travel planning: the role of exploration and exploitation," *Information & Management*, vol. 54, no. 6, pp. 757–770, 2017.
- [3] T. Brandt, J. Bendler, and D. Neumann, "Social media analytics and value creation in urban smart tourism ecosystems," *Information & Management*, vol. 54, no. 6, pp. 703–713, 2017.
- [4] A. K. Tripathy, P. K. Tripathy, N. K. Ray, and S. P. Mohanty, "iTour: the future of smart tourism: an IoT framework for the independent mobility of tourists in smart cities," *IEEE consumer electronics magazine*, vol. 7, no. 3, pp. 32–37, 2018.
- [5] E. Sigalat-Signes, R. Calvo-Palomares, B. Roig-Merino, and I. García-Adán, "Transition towards a tourist innovation model: the smart tourism destination," *Journal of Innovation & Knowledge*, vol. 5, no. 2, pp. 96–104, 2020.
- [6] H. Lee, J. Lee, N. Chung, and C. Koo, "Tourists' happiness: are there smart tourism technology effects?" *Asia Pacific Journal of Tourism Research*, vol. 23, no. 5, pp. 486–501, 2018.
- [7] C. Koo, L. Mendes-Filho, and D. Buhalis, "Guest editorial," *Tourism Review*, vol. 74, no. 1, pp. 1–4, 2019.
- [8] T. Zhang, C. Cheung, and R. Law, "Functionality evaluation for destination marketing websites in smart tourism cities," *Journal of China Tourism Research*, vol. 14, no. 3, pp. 263–278, 2018.
- [9] M. A. C. Ruíz, S. T. Bohorquez, and J. I. R. Molano, "Colombian tourism: proposal app to foster smart tourism in the country," *Advanced Science Letters*, vol. 23, no. 11, pp. 10533–10537, 2017.
- [10] W. Wang, N. Kumar, J. Chen et al., "Realizing the potential of the Internet of Things for smart tourism with 5G and AI," *IEEE Network*, vol. 34, no. 6, pp. 295–301, 2020.
- [11] I. Guerra, F. Borges, J. Padrão, J. Tavares, and M. H. Padrão, "Smart cities, smart tourism? The case of the city of Porto," *Revista Galega de Economía*, vol. 26, no. 2, pp. 129–142, 2017.
- [12] Y. Topsakal, M. Bahar, and N. Yüzbaşıoğlu, "Review of smart tourism literature by bibliometric and visualization analysis," *Journal of Tourism Intelligence and Smartness*, vol. 3, no. 1, pp. 1–15, 2020.
- [13] S. Joshi, "Social network analysis in smart tourism driven service distribution channels: evidence from tourism supply chain of Uttarakhand, India," *International Journal of Digital Culture and Electronic Tourism*, vol. 2, no. 4, pp. 255–272, 2018.
- [14] F. Femenia-Serra, B. Neuhofer, and J. A. Ivars-Baidal, "Towards a conceptualisation of smart tourists and their role within the smart destination scenario," *Service Industries Journal*, vol. 39, no. 2, pp. 109–133, 2019.
- [15] C. Koo, F. Ricci, C. Cobanoglu, and F. Okumus, "Special issue on smart, connected hospitality and tourism," *Information Systems Frontiers*, vol. 19, no. 4, pp. 699–703, 2017.
- [16] H. Abdel Rady and A. Khalf, "Towards smart tourism destination: an empirical study on Sharm El Sheikh city, Egypt," *International Journal of Heritage, Tourism and Hospitality*, vol. 13, no. 1, pp. 78–95, 2019.
- [17] T. Pencarelli, "The digital revolution in the travel and tourism industry," *Information Technology & Tourism*, vol. 22, no. 3, pp. 455–476, 2020.
- [18] C. J. P. Abad and J. F. Álvarez, "Landscape as digital content and a smart tourism resource in the mining area of cartagena-La unión (Spain)," *Land*, vol. 9, no. 4, pp. 1–22, 2020.
- [19] Z. Ghaderi, P. Hatamifar, and J. C. Henderson, "Destination selection by smart tourists: the case of Isfahan, Iran," *Asia Pacific Journal of Tourism Research*, vol. 23, no. 4, pp. 385–394, 2018.
- [20] T. T. Nguyen, D. Camacho, and J. E. Jung, "Identifying and ranking cultural heritage resources on geotagged social media for smart cultural tourism services," *Personal and Ubiquitous Computing*, vol. 21, no. 2, pp. 267–279, 2017.

Research Article

Coordinated Development of Urban Intelligent Transportation Data System and Supply Chain Management

Qian Chen 

School of Logistics Management and Engineering, Zhuhai College of Science and Technology, Zhuhai 519041, Guangdong, China

Correspondence should be addressed to Qian Chen; chenqian@zcst.edu.cn

Received 16 February 2022; Revised 2 April 2022; Accepted 15 April 2022; Published 4 May 2022

Academic Editor: Sang-Bing Tsai

Copyright © 2022 Qian Chen. This is an open access article distributed under the Creative Commons Attribution License, which permits unrestricted use, distribution, and reproduction in any medium, provided the original work is properly cited.

With the development of the urban economy, the number of people using various means of transportation is also increasing, resulting in a huge workload of the traffic data system and prone to errors. Supply chain management can formulate a reasonable production plan according to the comprehensive information data generated by the supply chain management system, such as market demand analysis, purchasing demand analysis, and supplier assessment and evaluation. Therefore, this paper proposes the coordinated development of urban intelligent transportation data system and supply chain management, so as to improve the overall efficiency of the logistics system and the level of customer service. This paper aims to study the importance and advantages of the coordinated development of urban intelligent transportation data system and supply chain management. As can be seen from the data in Table 2, the percentage of people using a car increased by 18.2% in 2015, and by 2020, the percentage of people using a car increased by 36.9%. As shown in Figure 10, the traditional urban traffic data management system has the disadvantages of large amount of data and various and complex data types. Among them, the percentage of large amount of data is between 70% and 75%, and the percentage of diverse and complex data is between 62% and 68%. It can be seen that the number of people using cars is increasing, resulting in an increasing workload for the transportation system. On this basis, the intelligent traffic data system should be used to solve this problem and the coordinated development of the intelligent traffic data system and supply chain management can achieve a win-win situation.

1. Introduction

With the rapid increase in the number of motor vehicles, traffic problems have gradually become a worldwide problem. In order to solve traffic problems efficiently and reliably, all countries vigorously develop intelligent transportation systems. Intelligent transportation system is a system that collects and processes traffic information and monitors traffic conditions through modern technology. Traffic data with different structures and complex sources are often stored in intelligent transportation systems. These traffic data contain the inherent laws of the traffic system. Efficient and accurate analysis of traffic data and rational use play a critical role in improving traffic safety and minimizing traffic congestion. The supply chain management system may manage information, logistics, and capital in a fully integrated manner, allowing for coordination and integration.

Transportation plays an important role in urban life, and it is also an important factor restricting urban economic growth and the improvement of residents' living standards. Whether it is to facilitate people's lives or promote social and economic development, high-quality urban transportation is very important. With the rapid development of urbanization, the number of cars is also increasing. People suffer from traffic jams while enjoying the convenience of cars. Urban traffic quality is related to people's tourism efficiency and life happiness index.

The innovation of this paper is as follows: (1) The theoretical knowledge of intelligent transportation data system and supply chain management is introduced, and data mining is used to analyze how data mining plays a role in the research on the coordinated development of intelligent transportation data system and supply chain management. (2) The advantages of the intelligent traffic data system are analyzed in detail, and it is found through experiments that

the intelligent traffic data system based on data mining can handle the work better.

2. Related Work

With the rapid development of the economy, the society is also making continuous progress. Liu Yi found that, in a smart city, the intelligent transportation system is very important, and it can make the lives of residents more convenient. The massive data of the Internet of Things can improve the happiness index. Although the scholar put forward his own point of view, there is no specific data to support [1]. Shaukat N found that the use of fossil fuels in transportation became less and less with the advent of hybrid vehicles. Hybrid electric vehicles are not only environmentally friendly, but also inexpensive; therefore, it is necessary to explore and solve these problems. He found electric vehicle batteries to be a promising solution that would help store excess energy and feed it back to the main grid during periods of high demand, which would save energy. The scholar proposed a solution to the problem but did not verify the practicability of the method [2]. Lin J discovered that public vehicle systems can improve traffic efficiency and vehicle occupancy rate, so he proposed an edge computing-based public vehicle system. In vehicle control systems, it not only improves traffic efficiency and vehicle occupancy rate, but also improves traffic efficiency by making travelers more and more satisfied. Although the scholar proposed that edge computing can be applied to public vehicle systems, there is no experimental object to prove the reliability of the experiment [3]. Babar M discovered that a large number of smart devices or objects are connected to each other, expanding the scale of the digital world. Due to the rapid increase in the novelty and number of embedded devices, IoT has become central to transportation system considerations. At the heart of citizens' quality of life is intelligent transportation. In vehicle control systems, this entails the employment of devices and sensors. He presented a big data analytics-based intelligent transportation system architecture. The scholar only proposed an intelligent transportation system architecture using big data analysis and did not specifically describe the usage and characteristics of the architecture [4]. The main purpose of Samarayake is to conduct research on the development of a conceptual framework for supply chains. He developed an integrated framework to integrate components in the supply chain. This framework can provide an integrated approach to the implementation of components but also allows flexibility. The framework proposed by this scholar has not been used in real life, and there is no example to illustrate, so the practicability of the framework has not been confirmed [5]. Rajeev A found that the increasing demand for products and their consumption puts pressure on supply chains, and industrial production brings serious pollution and environmental disasters. To address this problem he proposes a conceptual framework for classifying various problems. Although the scholar proposed a framework, the various factors were not explained or classified [6]. Vanalle RM found that the

impact of manufacturing activities on the environment is receiving increasing attention. Manufacturers have taken green supply chain management very seriously to reduce environmental pollution and improve work efficiency at the same time. He explores the pressures observed in automotive supply chain suppliers, using least squares structural equation modeling to process the data. But the scholar did not describe how to use the least squares structural equation model to process the data [7]. Tiwari S found that big data analytics can play a big role in supply chain management. In the current competitive environment, a large amount of work data has brought many challenges to the workers in the supply chain; he did not mention how to play a role [8].

3. Concepts of Intelligent Transportation Data System and Supply Chain Management

Only by analyzing and summarizing massive data can data mining technology be fully utilized [9]. Data mining technology integrates data and then filters useful data to improve people's work efficiency [10]. The application of intelligent transportation is shown in Figure 1.

As shown in Figure 1, from the perspective of the urban traffic management department, millions of traffic flow data and vehicle activity data can be obtained every day using traffic detection devices such as induction coils, radar, GPS, and high-speed cameras [11].

The use of cars is no longer a luxury, and more and more people are buying cars. This paper investigates the number of people who bought cars from 2011 to 2018, as shown in Figure 2.

As shown in Figure 2: The number of selected vehicle trips in 2011 was 56.42 million, and the number of selected vehicle trips in 2018 was 356.73 million, an increase of 300.31 million. More and more people choose to drive for short-term travel and urban life. The continuous increase in the number of people and vehicles and the saturation of urban roads have caused a lot of trouble, reducing people's travel efficiency and also causing the loss of economic benefits and the decline of life [12].

The word "supply chain management" refers to the process of reducing the cost of a supply chain's operation, from purchasing to fulfilling the final client's full process into a single process with the appropriate information system computer management technology [13]. The application of intelligent transportation system (ITS) in supply chain management (SCM) system can improve the efficiency of traffic management, as shown in Figure 3.

As shown in Figure 3: In addition to the establishment of relatively complete urban highway transportation system infrastructure, the infrastructure of each enterprise in the supply chain must also create conditions for information synchronization at each stage of the supply chain [14], but also a traffic information service and an important basic support for road control. In order to reflect the situation of road traffic in real time, we must first be able to mine the data information of traffic flow in time and analyze it accurately [15], as shown in Figure 4.

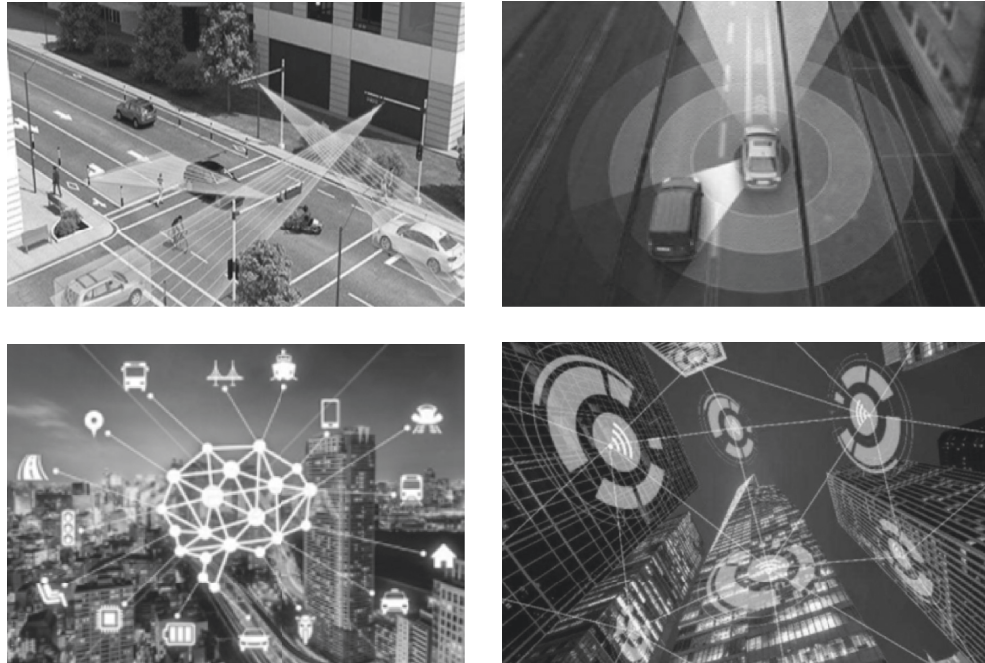


FIGURE 1: Applications of intelligent transportation.

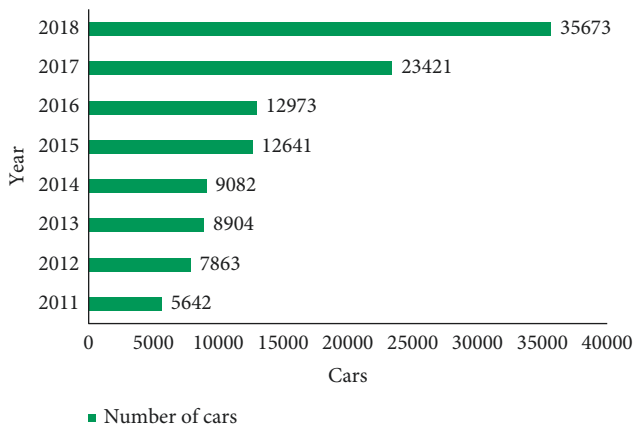


FIGURE 2: The number of people who bought a car, 2011–2018.

As shown in Figure 4: The primary problem facing the current traffic is that as time goes by, more and more traffic data are generated, and its types are also more and more difficult to identify.

The timely and effective collection and utilization of these traffic big data can find the reasons for the existence of urban traffic congestion, which can solve targeted problems, lay a foundation for the smooth traffic, and provide detailed information for the decision-making of government departments [16]. As the main data analysis technology, data mining technology plays an important role in effectively collecting traffic data, as shown in Figure 5.

As shown in Figure 5: The main advantage of an intelligent transportation system lies in the timely and efficient processing of information. The gathering, processing, and analysis of data are among the main functions. It can make better use of current traffic infrastructure, reducing traffic congestion and pollution,

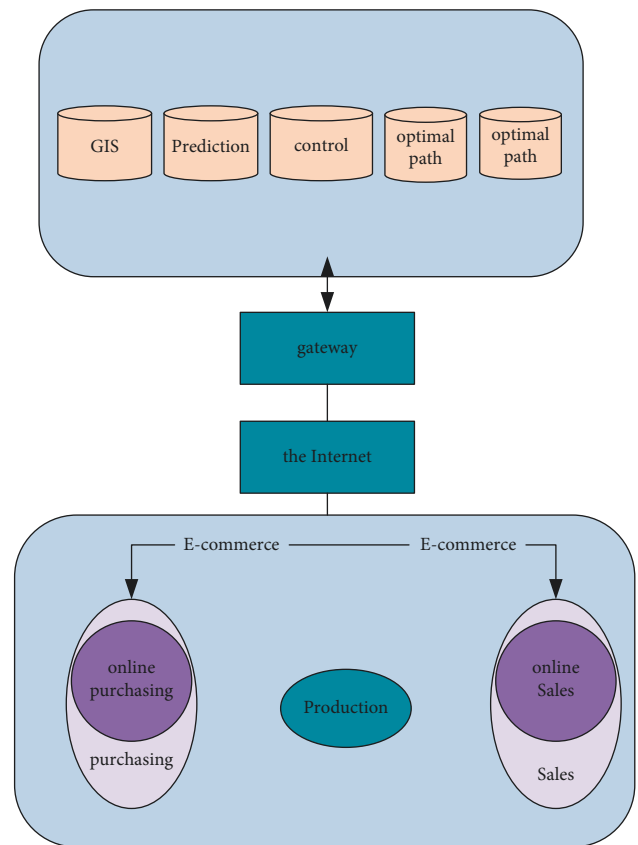


FIGURE 3: Schematic diagram of the system structure for the coordinated development of urban ITS and SCM.

ensuring traffic safety, and increasing transportation efficiency. To increase the utilization efficiency of traffic resources and reduce traffic congestion, the construction

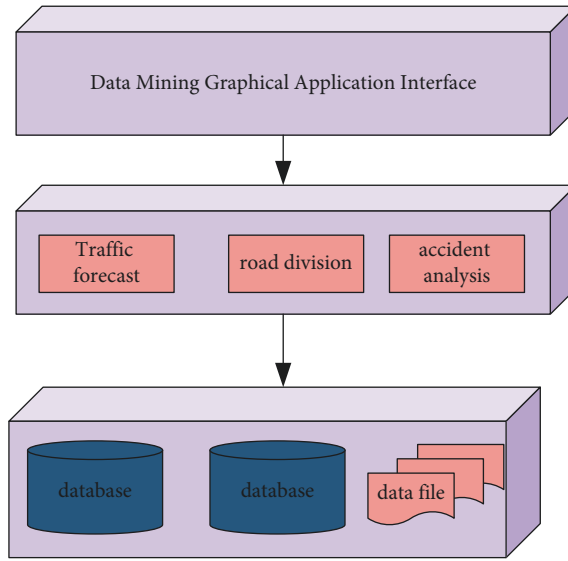


FIGURE 4: Architecture of intelligent transportation data mining application platform.

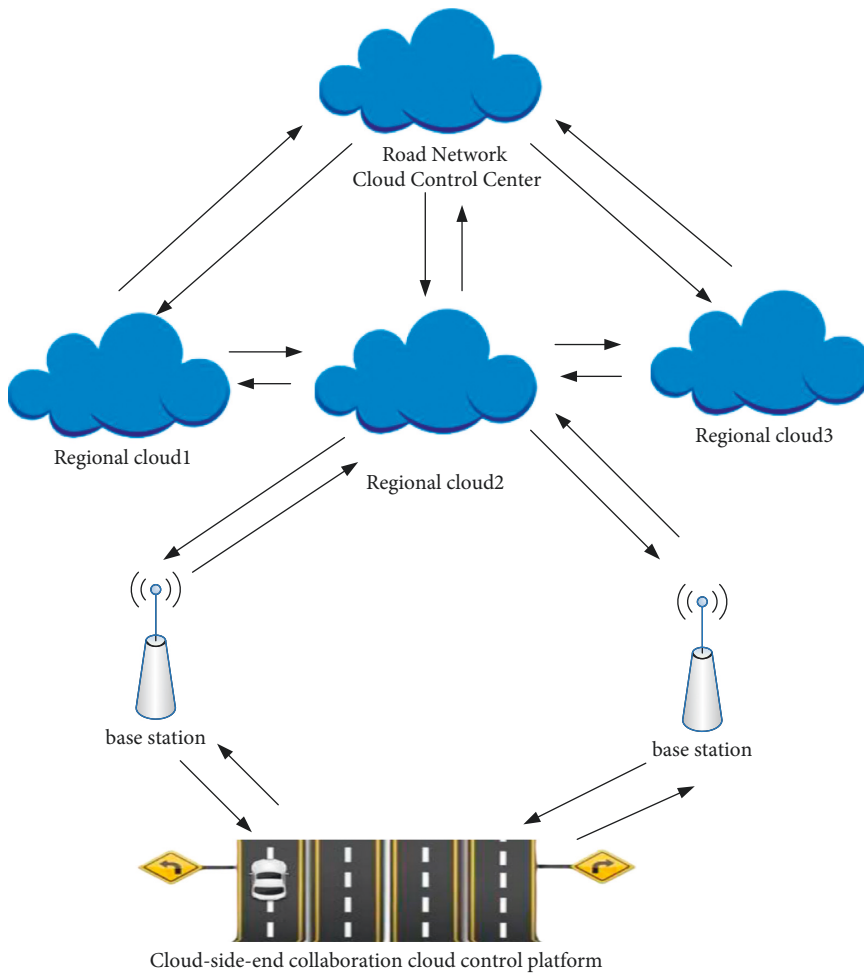


FIGURE 5: Structure diagram of collected traffic data.

of a comprehensive intelligent transportation system is critical [17].

4. Data Mining Algorithm Applied in Intelligent Transportation System

4.1. BP Neural Network Prediction Model. This structure is simple to understand, the calculating function is powerful, and it is simple to implement [18]. One of the most extensively used neural network models is the BP neural network, which is a multilayer feedforward network trained using the error backpropagation technique. A vast number of input-output pattern mapping associations can be learned and stored by a BP network. Its structure is shown in Figure 6.

As shown in Figure 6, each layer of the BP neural network comprises an endless number of nodes, and each node represents a neuron [19].

The following components make up the three-layer BP network learning process.

4.1.1. Input Mode Forward Propagation. The process of learning convergence is also the forward propagation process of the input pattern. Set the input vector to A_k ; then there is

$$A_k = a_1^k, a_2^k, \dots, a_n^k \quad (1)$$

In (1), set the desired output vector as B_k , which is

$$B_k = b_1^k, b_2^k, \dots, b_q^k \quad (2)$$

In equation (2), $k = 1, 2, \dots, n$; n is the logarithm of the learning mode, calculated as S_j as

$$S_j = \sum_{i=1}^n w_{ij} a_i - \theta_j \quad (3)$$

It is

$$f(a) = \frac{1}{1 + \exp(-a)} \quad (4)$$

4.1.2. Backpropagation of Output Error. If these data are wrong or contradict expectations, the network needs to be modified. Calibration errors are usually caused by collision-caused stream corruption and read and write offsets, and this is a calibration error [20]. Output layer correction error:

$$d_t^k = (b_t^k - c_t^k) f(o_t^k) \quad (5)$$

The correction error equation is

$$e_j^k = \left(\sum_{i=1}^q w_{ij} d_t^k \right) f(s_j^k) \quad (6)$$

The traffic data prediction research in this paper uses the BP neural network, and the gradient descent method applied in it requires the activation function to have continuous derivatives, and the activation function belongs to a linear

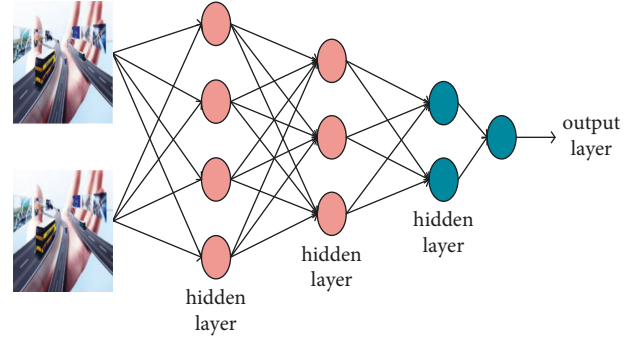


FIGURE 6: BP neural network.

function [21, 22]. Gradient descent is a popular first-order optimization approach for addressing unconstrained optimization problems. It is one of the simplest and most well-known methods. In addition, the input traffic data structure of this study is complex. When processing complex data, it is necessary to complete the approximation of higher-order functions, and an appropriate nonlinear function should be used as the activation function. Therefore, the final use of this research is the nonlinear function sigmoid function [23, 24]. It is

$$f(a) = \frac{1}{1 + e^{-a}} - 1, \quad -1 < f(a) < 1. \quad (7)$$

In the optimization process of the traffic data prediction neural network, it will be applied to the derivative function $1/(1 + e^{-a})$ of the bipolar S function, and the derivative function of the bipolar S function is

$$f(a) = \frac{2ae^{-a}}{(1 + e^{-a})^2} \quad (8)$$

The daily activity period $(1 + e^{-a})^2$ of human beings is roughly fixed, and the vehicle base in the traffic system is large, and the instantaneous change of traffic conditions has little effect on the overall traffic conditions at a fixed period of time every day. Especially after being classified according to the cycle, it can be considered that the vehicle changes in the same period of any Monday in the short term will basically fluctuate within a small range [25].

Taking historical vehicle speed data as input data and predicting vehicle speed in each period as output data, a neural network is established [26, 27]. Among them, a_i is the speed of a certain fixed road section in a certain period of a certain day, and b is the corresponding output predicted value. The prediction equation is as follows:

$$b = G(a_i, \theta) \quad (9)$$

When the neural network is in the learning state, it is necessary to give the neural network a certain initial value, which is a process of optimizing the network by using the objective function. After learning to obtain a stable neural network that meets the actual needs, it can enter the working state of the neural network.

4.2. Cluster Analysis Algorithm (K-Means Algorithm). The clustering method first regards each classification object as a separate class and then selects a pair of classification objects in turn according to the principle of the smallest distance and forms a new class. In this section, an aggregation-based approach is required to segment the traffic data stream; therefore, the K-means clustering algorithm is chosen as the basic algorithm.

K-means algorithm is shown in Figure 7.

As shown in Figure 7: Traffic flow is divided into two peak periods: morning peak and evening peak. In order to improve work efficiency, clustering is required to classify traffic.

The K-means is suitable for processing large-scale datasets and is very efficient and scalable. The K-means algorithm uses distance as a similarity evaluation metric and the farther the two objects, the lower the similarity.

The main task of the data preprocessing step is to standardize the vehicle speed data. Calculate the average absolute deviation S_f , and the absolute deviation is calculated as

$$S_f = \frac{(|a^{1f} - m_f|) + (|a^{2f} - m_f|) + \dots + (|a^{nf} - m_f|)}{n}, \quad (10)$$

here, a^{1f}, \dots, a^{nf} is the n-dimensional quantity of the vehicle speed, and the average value of f is $2 m_f$ as the transformation standard. If calculating the normalized measure of vehicle speed divided by traffic period, it can refer to

$$Z_{if} = \frac{(a^{if} - m_f)}{S_f}. \quad (11)$$

The choice of the number of classifications K in the clustering algorithm has a significant impact on the clustering results. The selection of the K initial cluster center points determines the final clustering result. The criterion for judging the current clustering performance uses the squared difference distance. J of the distances from the object to its cluster centroid is shown in

$$J = \max \sum_{i=1}^k \sum_{a \in c_i} di \text{ st}(c_i, a)^2. \quad (12)$$

The principle of object division is determined by the distance between the object to be classified and the center of each group.

4.3. Support Vector Machine Algorithm for Traffic Congestion Events. Support Vector Machines (SVM) are suitable for classification problems. It mainly searches for the best big data-based urban intelligent bus management system algorithm among the load types of the model based on limited sample information.

The basic principle of SVM is to complete data classification by finding the optimal hyperplane, for example, as shown in Figure 8.

As shown in Figure 8: On a two-dimensional plane, there are two types of samples, orange triangles and green circles, denoted by H1 and H2, respectively. It can be seen that the data in this example is linearly separable, and the straight line in the middle is its hyperplane, which can completely separate the two types of samples.

When classifying data, it is necessary to measure the quality of the current solution by the classification interval or other good indicators. Among them, a represents the sample vector. Bring the sample data point into $g(a)$; if it is greater than 0, it is considered to be class H1; if it is less than 0, it is class H2.

A hyperplane in a two-dimensional plane can be represented by a linear function such as

$$g(a) = wa + b. \quad (13)$$

When classifying, the computer consists of a vector (a_i, b_i) and a label for each sample, as in

$$D_i = (a_i, b_i). \quad (14)$$

Therefore, the interval from a sample point to a certain hyperplane is as follows:

$$\delta_i = b_i (wa_i + b). \quad (15)$$

If a sample belongs to this category, according to (15), b_i and $wa_i + b$ results are both greater than 0 or less than 0. Normalize w and b and replace them with $w/\|w\|$ and $b/\|w\|$, respectively; then the interval becomes

$$\delta_i = \frac{1}{\|w\|} |g(a_i)|. \quad (16)$$

But the above process is to solve the classification problem; what this paper needs is to complete the prediction problem of traffic data. Support Vector Machine Regression (SVR) is an algorithm developed on the basis of SVM, as shown in Figure 9.

As shown in Figure 9: Support vector machine regression is to find a smooth curve $f(a)$ by training the sample data, so that more training samples can be included in the region formed between $f(a) + w$ and $f(a) - w$. In the M-dimensional feature space, the classification hyperplane or approximation function is constructed as follows:

$$f(a) = \sum_{i=1}^m w\varphi(a) + b. \quad (17)$$

Among them, the input sample is transformed by φ , and the insensitive loss function is defined as follows:

$$L_w(a_i, b_i, f) = \max\{0, |b_i - f(a_i)| - w\}. \quad (18)$$

After processing the original traffic flow data, the Euclidean distance is used to measure the similarity search and matching. The Euclidean distance is defined as follows: Assuming that the speeds of the two modes PX_1 and PX_2 are v_1 and v_2 , respectively, and the flow rates are f_1 and f_2 , respectively, then the distance between the two modes is

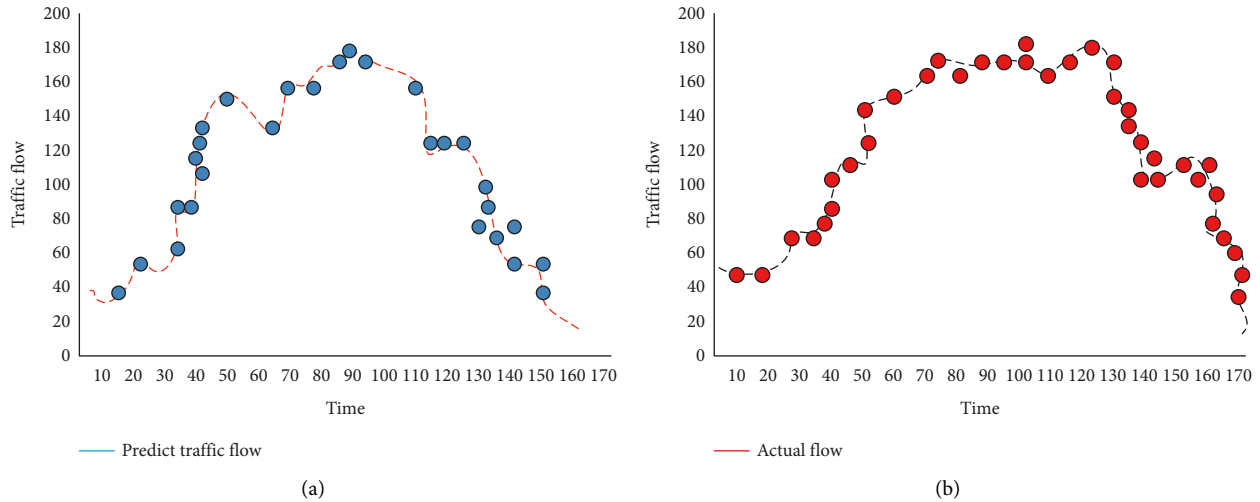


FIGURE 7: Statistical graph of predicted and actual traffic flow by K-means algorithm. (a) Prediction of traffic flow by K-means algorithm. (b) Actual flow of traffic.

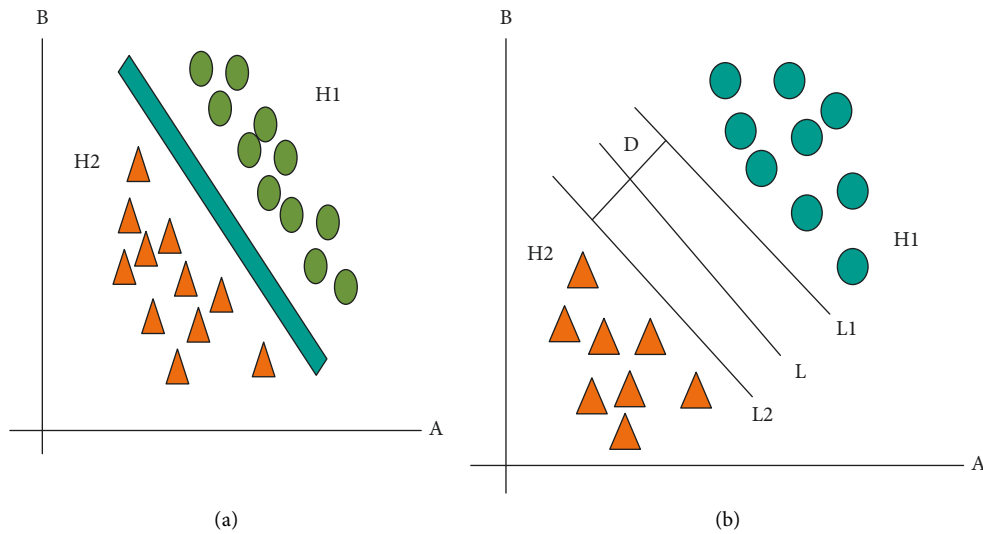


FIGURE 8: The basic principle of SVM is to find the optimal hyperplane by (a) basic principle of SVM; (b) optimal hyperplane.

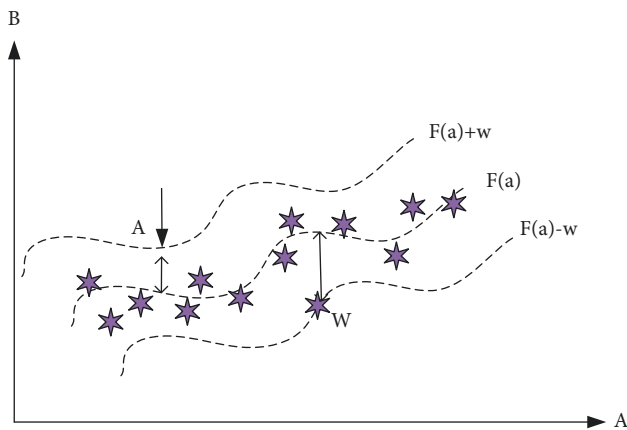


FIGURE 9: Support vector machine regression.

$$D(PX_1, PX_2) = \sqrt{w_1(v_1, v_2)^2 + w_2(f_1 - f_2)^2}. \quad (19)$$

At present, the methods used to test the accuracy of the prediction results of the algorithm model include average error (AE). The comparison of several algorithms is shown in Table 1.

As shown in Table 1: The sensitivity of the average error is 56%, the working efficiency is 43%, and the working error is 0.35, while the sensitivity of the root mean square error is 72%, the working efficiency is 67%, and the working error is 0.16. The square root error is more advantageous. It can reflect the effect of the algorithm well, so this method is adopted in this paper. During the detection process, traffic flow data and all data in the pattern are recorded.

The predicted value is A_1 , the number of samples is n , and the calculation equation of the root mean square error (RMSE) is

TABLE 1: Comparison table of 3 algorithms.

Algorithm	Sensitivity (%)	Work efficiency (%)	Error rate
AE	56	43	0.35
MSE	59	46	0.32
RMSE	72	67	0.16

$$\text{RMSE} = \sqrt{\frac{\sum_{i=1}^n (A_i - A_1)^2}{n}}. \quad (20)$$

To sum up, it can be seen that the parallel machine learning algorithm maintains a consistent prediction effect, and the neural network shows better performance in processing large-scale data.

5. Experiment and Analysis of Intelligent Transportation Data System and Supply Chain Management

5.1. Experiment and Analysis of the Characteristics of the Intelligent Traffic Data System. After decades of sustained high-speed and stable development of China's economy, the development of road transportation has been greatly promoted, which makes road traffic one of the main economic entities. For a long time to come, transportation will be adjusted with the rapid economic development and the development of other industries. In recent years, the construction of basic software and hardware facilities for road traffic has continued to increase, and the number of motor vehicles has increased exponentially. In addition, the number of trips on traffic roads is also increasing, and large-scale traffic projects have been put into construction, such as railways, subways, and light rail transits, resulting in increasing traffic congestion in key urban areas, and the number of traffic accidents has always been high.

This paper analyzes the growth rate of population, the growth rate of automobiles, and the traffic accidents from 2015 to 2020, as shown in Table 2 and 3.

As shown in Table 2 and 3: the number of traffic incidents in 2015 was 6532, accounting for 15%, and the fatality rate caused by traffic accidents was 2%; the number of traffic incidents in 2020 is 267,845, accounting for 35%, and the fatality rate due to traffic accidents is 10%. The percentage of traffic accidents increased by 20%, and the fatality rate increased by 8%. As a result, traffic accidents are increasing.

This paper compares the management of traffic data using traditional technologies and intelligent transportation systems, as shown in Figure 10.

As shown in Figure 10: There are many types of urban traffic big data, and it is difficult to manage, process, and analyze it in a short time using traditional technologies. Its specific characteristics are as follows: First: the amount of data is huge. The structured data obtained from the urban traffic management department reaches more than 100 GB every day. If it includes media data such as road surveillance videos and mobile phone photos, the amount of data is even greater. And the volume of data imported from related industries and domains, social networks, and public services will be even greater. Second: There are various

TABLE 2: Population growth rate and vehicle growth rate, 2015–2020.

Year	Population growth rate (%)	Car growth rate (%)
2015	12.5	18.2
2016	13.6	23.5
2017	16.9	25.2
2018	21.3	27.0
2019	23.6	33.7
2020	23.2	36.9

TABLE 3: Traffic accidents and fatalities from 2015 to 2020.

Year	Number of security incidents	Percentage	Mortality rate (%)
2015	6532	15	2
2016	7898	19	3.5
2017	8096	21	4.9
2018	15672	24	9
2019	16790	29	10
2020	267845	35	11.6

types of data. From the perspective of data sources, in addition to the data of the transportation industry, there are other data that may affect the transportation industry such as meteorology, environment, and population. Regarding data types, it is divided into structured data and unstructured data.

The characteristics of intelligent transportation data through data mining are as follows:

- (1) Rich in value. The big data of urban traffic has rich value. According to scientific analysis, people can obtain necessary traffic information in real time and accurately, so traffic management departments can provide powerful data analysis for emergency decision-making. Intelligent traffic data systems can not only maintain social stability, but also reduce economic losses.
- (2) It has obvious timeliness. Decisions such as traffic management and urban planning focus more on the analysis of the latest data. That is to say, there are far fewer historical data references to determine traffic management and city planning than recent data. Among them, the percentage of rich value is 76%–80%, and the percentage with obvious timeliness is 71%–73%. It can be seen that the intelligent traffic data system has more advantages.

5.2. Experiment and Analysis of the Combination of Intelligent Transportation Data System and Supply Chain Management.

This paper compares the benefits, customer service levels, and work efficiency of the entire logistics system after applying the intelligent transportation system in the supply chain management system, as shown in Table 4.

As shown in Table 4, after the supply chain management system is applied to the intelligent transportation system, the overall efficiency of the logistics system, customer service level, and work efficiency have been improved.

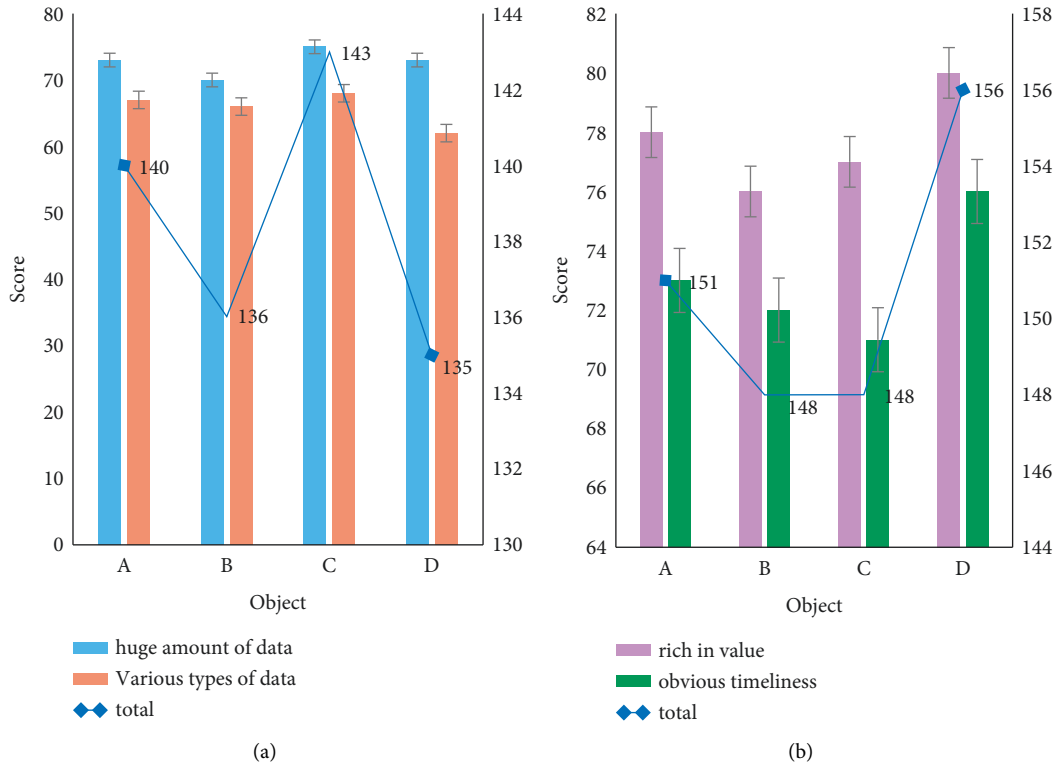


FIGURE 10: Traditional technologies and intelligent transportation systems manage traffic data. (a) Characteristics of traditional technologies in traffic management. (b) Characteristics of intelligent transportation systems in traffic management.

TABLE 4: Efficiency after ITS application in supply chain management system.

Analysis object	The benefits of the logistics system (%)	Customer service level (%)	Work efficiency (%)
Single supply chain management	45	51	49
Single intelligent transportation system	42	53	50
Combining the two	78	89	86

6. Discussion

This paper analyzes how to research the coordinated development of urban intelligent transportation data system and supply chain management based on data mining, expounds the related concepts of intelligent transportation data system and supply chain management, and studies the relevant theories of data mining. It explores the importance of the coordinated development of urban intelligent transportation data systems and supply chain management and discusses the role of urban intelligent transportation data systems through survey methods. Finally, it takes the integration of data mining in the coordinated development of urban intelligent transportation data system and supply chain management as an example to analyze the relationship between them.

This paper also makes reasonable use of neural network and cluster analysis. With the widening application of neural network and cluster analysis, its importance has gradually become prominent; many scholars have begun to combine neural network with data mining. Neural networks can effectively predict the information of the traffic data system

to get the results people want. Finally, we learned that the coordinated development of urban intelligent transportation data system and supply chain management is of great significance. Through experimental analysis, this paper shows that, with the rapid development of urban economy, the application of urban intelligent traffic data system can greatly improve work efficiency. The coordinated development of urban intelligent transportation data system and supply chain management has improved the efficiency of logistics work and promoted the economic development of enterprises.

7. Conclusions

With the economic development in recent years, cities have become more and more prosperous, but this has also led to more and more congested traffic roads, which has brought difficulties to the processing of traffic data. In this context, this paper proposes an intelligent traffic data system and the coordinated development with supply chain management, which not only greatly improves the work efficiency in traffic management, but also reduces traffic accidents. This paper

provides a clear description around the basic concepts of ITS and supply chain management. It proposes data mining technology based on the need to process a large amount of data in the traffic system. In the method part, based on data mining, the function of neural network and cluster analysis in traffic data processing is introduced in detail. In the experimental analysis, the traffic accidents that occurred in recent years are analyzed, which reflects the importance of the application of the intelligent traffic data system. In the experiment, not only the shortcomings of traditional traffic data processing methods, but also the advantages of intelligent traffic data systems are analyzed. Finally, the application of intelligent transportation system in supply chain management system is summarized, and it is found that the coordinated development of intelligent transportation data and supply chain management is of great significance to the transportation industry.

Data Availability

Data sharing is not applicable to this article as no new data were created or analyzed in this study.

Conflicts of Interest

The author states that this article has no conflicts of interest.

References

- [1] Y. Liu, X. Weng, J. Wan, X. Yue, H. Song, and A. V. Vasilakos, "Exploring data validity in transportation systems for smart cities," *IEEE Communications Magazine*, vol. 55, no. 5, pp. 26–33, 2017.
- [2] N. Shaukat, B. Khan, S. M. Ali et al., "A survey on electric vehicle transportation within smart grid system," *Renewable and Sustainable Energy Reviews*, vol. 81, no. 1, pp. 1329–1349, 2017.
- [3] J. Lin, W. Yu, X. Yang, P. Zhao, H. Zhang, and W. Zhao, "An edge computing based public vehicle system for smart transportation," *IEEE Transactions on Vehicular Technology*, vol. 69, no. 11, pp. 12635–12651, 2020.
- [4] M. Babar and F. Arif, "Real-time data processing scheme using big data analytics in internet of things based smart transportation environment," *Journal of Ambient Intelligence and Humanized Computing*, vol. 10, no. 10, pp. 4167–4177, 2019.
- [5] P. Samaranyake, "A conceptual framework for supply chain management: a structural integration," *Supply Chain Management*, vol. 10, no. 1, pp. 47–59, 2017.
- [6] A. Rajeev, R. K. Pati, S. S. Padhi, and K. Govindan, "Evolution of sustainability in supply chain management: a literature review," *Journal of Cleaner Production*, vol. 162, no. sep.20, pp. 299–314, 2017.
- [7] R. M. Vanalle, G. M. D. Ganga, M. Godinho Filho, and W. C. Lucato, "Green supply chain management: an investigation of pressures, practices, and performance within the Brazilian automotive supply chain," *Journal of Cleaner Production*, vol. 151, no. MAY10, pp. 250–259, 2017.
- [8] S. Tiwari, H. M. Wee, and Y. Daryanto, "Big data analytics in supply chain management between 2010 and 2016: insights to industries," *Computers & Industrial Engineering*, vol. 115, no. JAN, pp. 319–330, 2017.
- [9] A. C. Cagliano, A. De Marco, and C. Rafele, "E-grocery supply chain management enabled by mobile tools," *Business Process Management Journal*, vol. 23, no. 1, pp. 47–70, 2017.
- [10] M. Papert and A. Pflaum, "Development of an ecosystem model for the realization of internet of things (IoT) services in supply chain management," *Electronic Markets*, vol. 27, no. 3, pp. 1–15, 2018.
- [11] D. Das, "Development and validation of a scale for measuring Sustainable Supply Chain Management practices and performance," *Journal of Cleaner Production*, vol. 164, no. oct.15, pp. 1344–1362, 2017.
- [12] S. K. Jauhar, M. Pant, and R. Dutt, "Performance measurement of an Indian higher education institute: a sustainable educational supply chain management perspective," *International Journal of System Assurance Engineering and Management*, vol. 9, no. 1, pp. 180–193, 2018.
- [13] A. Buczak and E. Guven, "A survey of data mining and machine learning methods for cyber security intrusion detection," *IEEE Communications Surveys & Tutorials*, vol. 18, no. 2, pp. 1153–1176, 2017.
- [14] I. Kavakiotis, O. Tsave, A. Salifoglou, N. Maglaveras, I. Vlahavas, and I. Chouvarda, "Machine learning and data mining methods in diabetes research," *Computational and Structural Biotechnology Journal*, vol. 15, no. C, pp. 104–116, 2017.
- [15] V. Chaurasia and S. Pal, "A novel approach for breast cancer detection using data mining techniques," *Social Science Electronic Publishing*, vol. 3297, no. 1, pp. 2320–9801, 2017.
- [16] X. Yan and L. Zheng, "Fundamental analysis and the cross-section of stock returns: a data-mining approach," *Review of Financial Studies*, vol. 30, no. 4, pp. 1382–1423, 2017.
- [17] R. E. Chandler, K. Juhlin, J. Fransson, O. Caster, I. R. Edwards, and G. N. Norén, "Current safety concerns with human papillomavirus vaccine: a cluster Analysis of reports in VigiBase," *Drug Safety*, vol. 40, no. 1, pp. 81–90, 2017.
- [18] J. B. Varley, A. Miglio, V.-A. Ha, M. J. van Setten, G.-M. Rignanese, and G. Hautier, "High-throughput design of non-oxide p-type transparent conducting materials: data mining, search strategy, and identification of boron phosphide," *Chemistry of Materials*, vol. 29, no. 6, pp. 2568–2573, 2017.
- [19] T. Emoto, T. Yamashita, T. Kobayashi et al., "Characterization of gut microbiota profiles in coronary artery disease patients using data mining analysis of terminal restriction fragment length polymorphism: gut microbiota could be a diagnostic marker of coronary artery disease," *Heart and Vessels*, vol. 32, no. 1, pp. 39–46, 2017.
- [20] H. Hong, P. Tsangaratos, I. Ilia, J. Liu, A.-X. Zhu, and W. Chen, "Application of fuzzy weight of evidence and data mining techniques in construction of flood susceptibility map of Poyang County, China," *The Science of the Total Environment*, vol. 625, no. JUN.1, pp. 575–588, 2018.
- [21] S. K. Biswas, D. Devi, and M. Chakraborty, "A hybrid case based reasoning model for classification in internet of things (iot) environment," *Journal of Organizational and End User Computing*, vol. 30, no. 4, pp. 104–122, 2018.
- [22] O. Ibrahim Khalaf, C. Andrés Tavera Romero, A. Azhagu Jaisudhan Pazhani, and G. Vinuja, "VLSI implementation of a high-performance nonlinear image scaling algorithm," *Journal of Healthcare Engineering*, vol. 2021, Article ID 6297856, 10 pages, 2021.

- [23] L. Ogiela, M. R. Ogiela, and H. Ko, "Intelligent data management and security in cloud computing," *Sensors*, vol. 20, no. 12, p. 3458, 2020.
- [24] O. I. Khalaf and G. M. Abdulsahib, "Energy efficient routing and reliable data transmission protocol in WSN," *International Journal of Advances in Soft Computing and Its Applications*, vol. 12, no. 3, pp. 45–53, 2020.
- [25] M. Adil, J. Ali, M. Attique et al., "Three byte-based mutual authentication scheme for autonomous Internet of Vehicles," *IEEE Transactions on Intelligent Transportation Systems*, 2021.
- [26] Z. Lv, Y. Li, H. Feng, and H. Lv, "Deep learning for security in digital twins of cooperative intelligent transportation systems," *IEEE Transactions on Intelligent Transportation Systems*, 2021.
- [27] C.-H. Chen, "An arrival time prediction method for bus system," *IEEE Internet of Things Journal*, vol. 5, no. 5, pp. 4231–4232, 2018.

Research Article

Evaluation Method of Ecological Tourism Carrying Capacity of Popular Scenic Spots Based on Set Pair Analysis Method

Xiangrong Yan 

Wuhan Technical College of Communications, Wuhan 430065, China

Correspondence should be addressed to Xiangrong Yan; yanxiangrong1964@163.com

Received 18 February 2022; Revised 15 March 2022; Accepted 31 March 2022; Published 5 May 2022

Academic Editor: Sang-Bing Tsai

Copyright © 2022 Xiangrong Yan. This is an open access article distributed under the Creative Commons Attribution License, which permits unrestricted use, distribution, and reproduction in any medium, provided the original work is properly cited.

By making adaptive adjustments to the tourism activities and tourism structure carried out in the tourist area, the natural resources of the scenic area can be protected while pursuing economies of scale. Moreover, it achieves a benign interaction between scenic spot development, planning, carrying capacity, and benefits, so that the scenic spot can develop sustainably under the condition of grasping the carrying capacity and restrictive conditions. This paper combines the set pair analysis method to evaluate the ecological tourism carrying capacity of scenic spots, so as to improve the quantitative effect of ecological tourism carrying capacity of scenic spots. In addition, this paper introduces the fuzzy analytic hierarchy process to determine the weight of the evaluation indicators and combines the set pair analysis method to establish a comprehensive evaluation model. The research results show that the evaluation method of ecotourism carrying capacity of popular scenic spots based on set pair analysis proposed in this paper has a good effect.

1. Introduction

Examining the carrying capacity of tourism environment from the perspective of stakeholder theory can promote the cross-integration of different disciplines such as management, tourism science, and environmental science. Studying tourism issues from the perspective of management theory objectively involves the cross-integration of a variety of disciplines. For example, management experts believe that [1] tourist attractions should consciously strengthen the awareness of marketing services, expand the tourist attraction of scenic spots, and enhance the awareness of tourism services, so that more tourists can experience beautiful natural scenery and high-quality tourism services. The tourism environment researchers believe that [2, 3] the carrying capacity of the scenic environment and the impact of foreign tourism culture on local traditional cultural values, customs, ideology, and natural resources should be considered while developing tourism. At the same time, while attracting foreign tourists, we should pay attention to the protection of the cultural traditions of the local residents in the scenic area, avoid the impact of foreign culture on the

local culture, and pay more attention to the protection of the ecological environment and natural resources. Therefore, the cross-study of different disciplines will find some new theories and new viewpoints, and the fusion of many theories and viewpoints can create a new knowledge system. This avoids single theoretical research from falling into a loop and falling into a one-sided research paradigm and enriches and improves the knowledge system of tourism-related disciplines [3].

Environmental damage and cultural conflicts brought about by tourism are getting bigger and bigger. “Smoke-free industry” faces the embarrassment of “smoke.” While developing the tourism industry, some countries only pursue the speed of development without paying attention to the negative effects brought by the tourism industry. They resort to excessive or even predatory exploitation of natural resources such as tourist attractions, blind construction of tourist facilities, and extensive use of scenic spots. At the same time, the influx of tourists into the scenic spot poses a challenge to the environmental carrying capacity of the scenic spot. Many tourist scenic spots have a series of problems such as ecosystem destruction, environmental

pollution, and the decline of traditional culture and the normal life of residents in the scenic spots.

Tourism and leisure have become the first choice for people to go out and play. Tourism in various places has developed rapidly. The rapid development of tourism has attracted a large number of tourists to gather in tourist destinations within a certain period of time. The density of tourists has increased significantly, exceeding local tourism. The environmental capacity brings problems such as environmental pollution, resource shortage, and traffic congestion to the tourist destination and seriously damages the local tourism ecological environment. During the peak tourist season, it is necessary to control the number of tourists, reduce the pressure on the environmental capacity of the tourist destination, and keep the tourist density within a reasonable range so that the ecological environment carrying capacity of the tourist destination and the sense of tourist experience will not decline.

This paper combines the set pair analysis method to evaluate the ecological tourism carrying capacity of scenic spots, improve the quantitative effect of ecological tourism carrying capacity of scenic spots, and provide theoretical reference for the follow-up sustainable development of tourist scenic spots.

2. Related Work

Wee et al. [4] believe that the tourist experience of tourists has not reached the best state, so it is necessary to study the carrying capacity of the tourism environment, limit a certain number of tourists, and develop tourism within the range allowed by the tourism environment, so that most tourists get a good travel experience. Lepage only conducted basic research on the carrying capacity of tourism environment but did not conduct in-depth research. From the perspective of classification of biophysical capacity, social and cultural capacity, psychological capacity, management capacity, and so on, Do et al. [5] proposed that the tourism environment capacity is within a certain time and a certain space range, and tourists can obtain a good tourism experience without destroying it. The activity intensity is improved that the tourism environment can bear under the condition that tourists can obtain a good tourism experience and do not damage the environment. Mykola et al. [6] believe that the tourism environment capacity is the level of tourists that the tourism resources of a certain area can accept under the condition that they are not destroyed. Simanjuntak and Rumondang Banjarnahor [7] mainly used observational experiments, icon analysis, case analysis, and other methods to study the carrying capacity of tourism environment. Tourism has become a frequent recreational activity for residents, and the environmental problems caused by tourism have become more and more prominent. As a result, the research on the carrying capacity of tourism environment has once again become the tipping point of research [8]. Trang et al. [9] believe that the carrying capacity of the tourism environment is the quality of resources that the natural environment can accept without being damaged to an unacceptable degree.

Kongbuamai et al. [10] made a brand-new attempt to the concept of tourism environmental capacity and the method of calculating capacity and creatively used the multifactor analysis method to determine the tourism environmental capacity. Kisiel et al. [11] made an in-depth theoretical discussion and proposed that the tourism environment capacity should include two aspects: one is the natural environment capacity, and the other is the sensing environment capacity, that is, the capacity to accommodate tourists on the basis of ensuring a good tourism experience for tourists. On the basis of theoretical analysis, quantitative research is also made, and improvement measures are proposed from both macro and microaspects. Rahmawati et al. [12] divided the tourism environment capacity into two categories: basic tourism environment capacity and non-basic tourism environment capacity. Milla et al. [13] determined the connotation of tourism environmental carrying capacity and established the definition of tourism environmental carrying capacity. It is believed that tourism environmental carrying capacity should include four indicators: natural environment carrying capacity, resource space carrying capacity, economic carrying capacity, and psychological carrying capacity. Rahmawati et al. [14] proposed that nature reserves should pay attention to both ecological protection and resource development and should take a sustainable development path. Dzhandzhugazova et al. [15] focused on the early warning system of the environmental carrying capacity of tourist attractions, proposed that the environmental early warning system of scenic spots should include a weight module, an indicator module, a prediction module, and a warning area module, and analyzed the application of each module in the early warning system. Scenic spots should establish an early warning system for the environmental carrying capacity of tourist attractions according to the number of tourists they receive. Adamchuk [16] established a quantitative evaluation model for the comprehensive carrying capacity of scenic spots based on the product matrix vector length method and obtained a favorable measure of the comprehensive carrying capacity of scenic spots. Cvijanović et al. [17] constructed the measurement formulas of ecotourism environment capacity, natural resource environment capacity, tourism space environment capacity, social ecotourism environment capacity, and tourist ecotourism environment capacity by using the theoretical speculation method and empirical measurement method. Mohanty et al. [18] analyzed the cumulative effect of tourism activities on environmental capacity and established a formula for calculating tourism environmental capacity by using the quantitative relationship between environmental factors and Pareto optimality. Kalchenko et al. [19] proposed a tourism environmental carrying capacity measurement model with length, area, and recreational facilities as limiting factors and measured the environmental carrying capacity through the design of the model.

3. Set Pair Analysis Method

It analyzes and studies the relationship and transformation between objective things from the three aspects of similarities, differences, and opposites and uses the degree of

connection to describe the various uncertainties of the system, thereby transforming the dialectical understanding of uncertainty into a mathematical tool for quantitative analysis.

We give sets A and B and set the set pair composed of these two sets to be denoted as $H = (A, B)$. On the background of a specific problem, the characteristics of the set pair H are analyzed, and the connection degree expression of the two sets is established.

$$\mu_{(A,B)} = \frac{S}{N} + \frac{F}{N}i + \frac{P}{N}j. \quad (1)$$

Then, formula (1) can be rewritten as

$$\mu_{(A,B)} = a + bi + cj. \quad (2)$$

Formula (2) should satisfy the normalization condition:

$$a + b + c = 1. \quad (3)$$

In formulas (1) and (2), i is the difference degree coefficient; j is the opposite degree coefficient. i and j have dual meanings. The first implication is that i and j are used as coefficients for the degree of difference and the degree of oppositeness, respectively. The second meaning is that the values of i and j are not taken into account, and it only acts as a marker at this time. The highest level of connection is the tourism resource carrying capacity level of the evaluated city. The set composed of the index values of the evaluated city is A, the set composed of the corresponding level I standard index values is B1, the set composed of the corresponding level II standard index values is B2, and the set composed of the corresponding level III standard index values is B3. If $\mu_{(A,B_1)} > \mu_{(A,B_2)} > \mu_{(A,B_3)}$, the tourism resource carrying capacity of the evaluated city belongs to level I. Therefore, the determination of the degree of connection is the key to the analysis of the set pair.

From the definition of connection degree, it can be known that a , b , and c in formula (2) are determined by the similarities and differences of the set pairs. Therefore, in practical applications, attention should be paid to the definition of the criteria for the discrimination of the same, the different, and the opposite. In the evaluation problem studied in this section, the criterion for the identification of similarities, differences, and opposites is as follows: when the evaluation indicators are within the discussed level range, they are considered to be the same. When the evaluation indicators are in separate standard levels, they are considered to be opposites. When the evaluation index is in the adjacent standard level, it is considered to be different.

It is easy to obtain from the definition and criterion of connection degree:

$$\mu_{(A,B_1)} = \frac{S_1}{N} + \frac{F_1}{N}i + \frac{P_1}{N}j, \quad (4)$$

where N is the total number of evaluation indicators, S is the number of indicators whose index value is within the level I standard, F is the number of indicators whose index value is within the level II standard, and P is the number of indicators whose index value is within the level III standard. Similarly, the expression for $\mu_{(A,B_2)}$, $\mu_{(A,B_3)}$ can be obtained.

Definition 1. The object is taken as the domain of discourse, denoted as X. The membership degrees of A and A are:

$$\mu_A(x) = a + c, \mu_{A^c}(x) = b. \quad (5)$$

The two are, respectively, called the deterministic degree of membership (referred to as the degree of certainty) and the degree of uncertainty membership (referred to as the degree of difference). According to the definition of fuzzy complement, there are

$$\mu_A(x) + \mu_{A^c}(x) = 1. \quad (6)$$

Definition 2. Deterministic information is a domain, which is denoted by Y. The fuzzy subset B^c in Y is defined as identity information and opposite information, respectively. Then, the membership degree of the extracted information x about B^c is

$$\mu_A(x) = a, \mu_{A^c}(x) = c. \quad (7)$$

They are, respectively, called the same degree of membership (referred to as the same degree) and the opposite degree of membership (referred to as the opposite degree).

Therefore, formula (2) becomes the deterministic and uncertain fuzzy structure function formula in the information sense, which gives the fuzzy description of the same, different, and antithetical set pairs on a certain characteristic. Therefore, it is called the fuzzy connection degree expression of set pair. The expression of fuzzy connection degree can conceptually describe the uncertainty of objective objects and subjective cognition relatively completely and can describe various uncertainty problems extensively and deeply.

We use the determination of the difference degree coefficient i in $\mu_{(A,B_1)} = S_1/N + F_1/Ni + P_1/Nj$ as an example to further illustrate its value method. The value of a certain index in the class I standard is x , $x \in [S_{(1)}, S_{(2)}]$, and $S_{(1)}$ and $S_{(2)}$ are the limit values of the class I and class II standards of the index. The proximity of x to $S_{(1)}$ is $S_{(1)}/x$, and the proximity of x to $S_{(2)}$ is $x/S_{(2)}$. When $x = S_{(1)}$ or $x = S_{(2)}$, $S_{(1)}/x + x/S_{(2)}$ takes the maximum value of $1 + S_{(1)}/S_{(2)}$. The two can be regarded as the affirmation and negation of the closeness of x to its level I standard, that is, the degree of identity and opposition of the set pair (x, b_1) . Then, there is

$$a = \frac{S_{(1)}S_{(2)}}{(S_{(1)} + S_{(2)})x}, c = \frac{x}{S_{(1)} + S_{(2)}}. \quad (8)$$

Since $a+b+c=1$, the difference can be obtained as

$$b = 1 - a - c = 1 - \frac{S_{(1)}S_{(2)}}{(S_{(1)} + S_{(2)})x} - \frac{x}{S_{(1)} + S_{(2)}} \quad (9)$$

$$= \frac{(S_{(2)} - x)(x - S_{(1)})}{(S_{(1)} + S_{(2)})x}$$

From this, we can get

$$\begin{aligned} \mu_{(x,b_1)} &= \frac{S_{(1)}S_{(2)}}{(S_{(1)} + S_{(2)})x} \\ &+ \frac{(S_{(2)} - x)(x - S_{(1)})}{(S_{(1)} + S_{(2)})x} i \\ &+ \frac{x}{S_{(1)} + S_{(2)}} j. \end{aligned} \tag{10}$$

The value process of the difference coefficient i is also the decomposition process. By substituting the value of i into the expression for $\mu_{(A,B_1)}$, we get

$$\begin{aligned} \mu_{(A,B_1)} &= \left(\frac{S_1}{N} + \frac{F_1}{N} \times \frac{S_{(1)}S_{(2)}}{(S_{(1)} + S_{(2)})x} \right) \\ &+ \frac{F_1}{N} \times \frac{(S_{(2)} - x)(x - S_{(1)})}{(S_{(1)} + S_{(2)})x} i \\ &+ \left(\frac{F_1}{N} \times \frac{x}{S_{(1)} + S_{(2)}} + \frac{P_1}{N} \right) j. \end{aligned} \tag{11}$$

Comparing formulas (4) and (11), it can be seen that the value process of i is a further analysis process of uncertainty. It is a process of in-depth understanding of the system, which can obtain more effective information and make the evaluation results more accurate and reliable. The final i value can take the average value of the corresponding items of the n i values.

The key link of the AHP method is to establish a judgment matrix, and whether the judgment matrix is scientific and reasonable directly affects the effect of the AHP method. Through analysis, it is found that there are the following problems:

- (1) It is very difficult to test whether the judgment matrix is consistent.

To check whether the judgment matrix is consistent, it is necessary to find the maximum characteristic root λ_{\max} of the judgment matrix and judge whether λ_{\max} is equal to the order n of the judgment matrix. If $\lambda_{\max} = n$ is consistent, when the order n is large, the workload of calculating λ_{\max} accurately is very large.

- (2) When the judgment matrix is not consistent, it is necessary to adjust the elements of the judgment matrix to make it consistent. This does not rule out that the judgment matrix can be made consistent after several times of adjustment, inspection, readjustment, and reinspection.
- (3) The consistency of judgment matrix is significantly different from that of human thinking.

In order to solve the above problems, Yao Min et al. introduced the concept of fuzzy consistent matrix, improved AHP, and proposed a fuzzy analytic hierarchy process (FAHP) based on fuzzy induced matrix. The research on this method has achieved certain results.

Then, its connection degree expression is

$$\mu(A, B_1) = \sum_{i=1}^s u_i + \sum_{k=1}^f t_k i_k + \sum_{j=1}^p v_j j, \tag{12}$$

where i_k represents the difference coefficient between sets A and B1 reflected on the index with the weight of sample set A. Similarly, the expression for $\mu_{(A,B_2)}, \mu_{(A,B_3)}$ can be obtained.

Step 4. Determination of the difference degree coefficient i_k in the connection degree expression.

We take the value of i in the expression $\mu_{(A,B_1)}$ as an example and set a certain index whose value of the sample index is within the range of level II standard as x_k and $S_{(1)}^k, S_{(2)}^k$ as the limit of level I and II of the index. Then, according to the point of view of fuzzy connection degree, to determine the value of the difference degree coefficient c is to determine the similarity, difference, and anti-fuzzy connection degree between x_k and the index level I standard post, which is expressed as $\mu_{(x_k, b_1^k)} = a + bi + cj$, that is, the values of i_k are a_k, b_k, c_k , respectively. Among them, a_k is the same degree, b_k is the difference degree, and c_k is the opposite degree. The fuzzy connection degree between x_k and its class I standard b_1^k is determined from the closeness characteristic, the closeness between x_k and $S_{(1)}^k$ is $S_{(1)}^k/x_k$, and the closeness between x_k and $S_{(2)}^k$ is $x_k/S_{(2)}^k$. When $x = S_{(1)}$ or $x = S_{(2)}$, $S_{(1)}/x + x/S_{(2)}$ takes the maximum value of $1 + S_{(1)}/S_{(2)}$. The two can be regarded as the affirmation and negation of the closeness of x to its level I standard, that is, the degree of identity and opposition of the set pair (x, b_1) . Then, there is

$$\begin{aligned} a_k &= \frac{S_{(1)}^k S_{(2)}^k}{(S_{(1)}^k + S_{(2)}^k)x_k}, \\ c &= \frac{x_k}{S_{(1)}^k + S_{(2)}^k}. \end{aligned} \tag{13}$$

Because $a_k + b_k + c_k = 1$, the degree of difference can be obtained as

$$\begin{aligned} b_k &= 1 - a_k - c_k = 1 - \frac{S_{(1)}^k S_{(2)}^k}{(S_{(1)}^k + S_{(2)}^k)x_k} - \frac{x_k}{S_{(1)}^k + S_{(2)}^k} \\ &= \frac{(S_{(2)}^k - x_k)(x - S_{(1)}^k)}{(S_{(1)}^k + S_{(2)}^k)x_k}. \end{aligned} \tag{14}$$

From this, we can get

$$\begin{aligned} \mu_{(x_k, b_1^k)} &= a_k + b_k i + c_k j = \frac{S_{(1)}^k S_{(2)}^k}{(S_{(1)}^k + S_{(2)}^k)x_k} \\ &+ \frac{(S_{(2)}^k - x_k)(x - S_{(1)}^k)}{(S_{(1)}^k + S_{(2)}^k)x_k} i + \frac{x_k}{S_{(1)}^k + S_{(2)}^k} j. \end{aligned} \tag{15}$$

It can be seen that the value process of the difference degree coefficient i_k is the decomposition process of the difference degree of sets A and B reflected on the index x_k with the weight t_k .

Step 5. Calculate the value of the connection degree.

By taking $\mu(A, B_1)$ as an example and substituting the values of i_k into formula (15), respectively, we get

$$\begin{aligned} \mu(A, B_1) &= \sum_{i=1}^s u_i + \sum_{k=1}^f t_k (a_k + b_k i + c_k j) + \sum_{i=1}^P v_i j \\ &= \left(\sum_{i=1}^s u_i + \sum_{k=1}^f t_k a_k \right) + \sum_{k=1}^f t_k b_k i \\ &\quad + \left(\sum_{k=1}^f t_k c_k + \sum_{i=1}^P v_i \right) j. \end{aligned} \tag{16}$$

At this time, $i = 0, j = -1$ in formula (16). This method of value selection reflects that on the basis of fully mining the information contained in the evaluation samples.

Step 6. The grade of the evaluation sample is determined by comparing the value of the degree of connection between the evaluation sample index value set and each evaluation grade standard index value set. The grade with a larger connection degree value is the water quality grade of the evaluation sample. By determining the grade of the evaluation sample A as an example, if $\mu_{(A, B_1)} > \mu_{(A, B_2)} > \mu_{(A, B_3)}$, the grade of the evaluation sample A is grade I.

4. Evaluation System of Ecotourism Carrying Capacity of Popular Scenic Spots

The environmental carrying capacity of ecotourism is that with the rise of ecotourism in the world, the sustainable development of tourism is emphasized on the basis of the carrying capacity of the tourism environment, that is, the intensity of tourism activities. It does not damage the present and future generations and also emphasizes the continuity and fairness of the intensity of tourism activities between human generations. Figure 1 shows the relationship between the carrying capacity of ecotourism, the carrying capacity of the tourism environment, and the capacity of the tourism environment.

There is a correlation between the ecological environment of a tourist destination and its surrounding stakeholders, and a large number of stakeholders are gathered around the tourist destination. These stakeholders directly or indirectly related to the scenic spot are divided into three levels: core stakeholders, strategic stakeholders, and peripheral stakeholders, as shown in Figure 2.

The factors involved in tourist attractions are intertwined and complex. In the process of determining the index system process, the availability, operability, and statisticability of the index must be fully considered, and the index system constructed can objectively reflect its impact on the bearing capacity. Therefore, the construction of the tourism

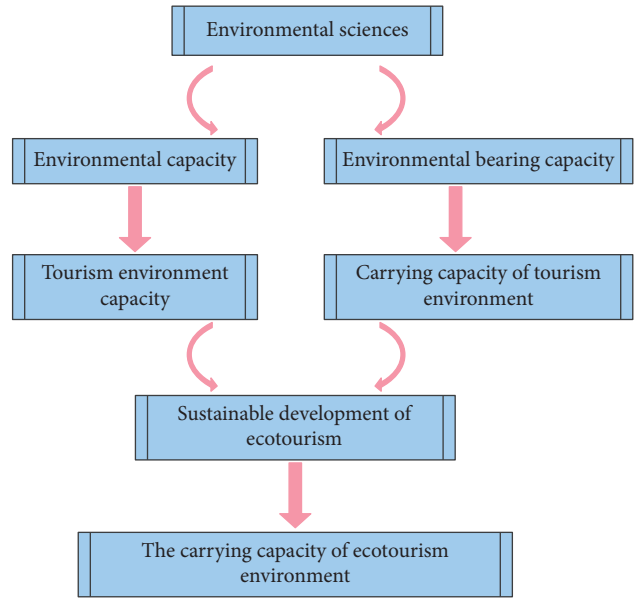


FIGURE 1: The relationship between the carrying capacity of ecotourism, the carrying capacity of the tourism environment, and the capacity of the tourism environment.

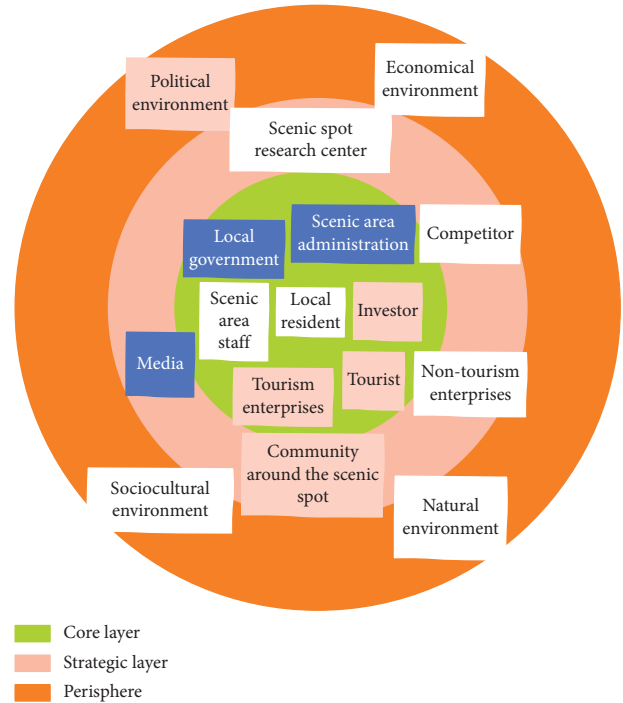


FIGURE 2: Stakeholder hierarchy diagram of tourist scenic spots.

environmental carrying capacity index system goes through the following processes (Figure 3).

From the perspective of stakeholders, the environmental carrying capacity of East Lake Scenic Spot is discussed, so that it can achieve various levels within the scope of the environmental carrying capacity of the scenic spot, and the interest demands of various major stakeholders will ultimately

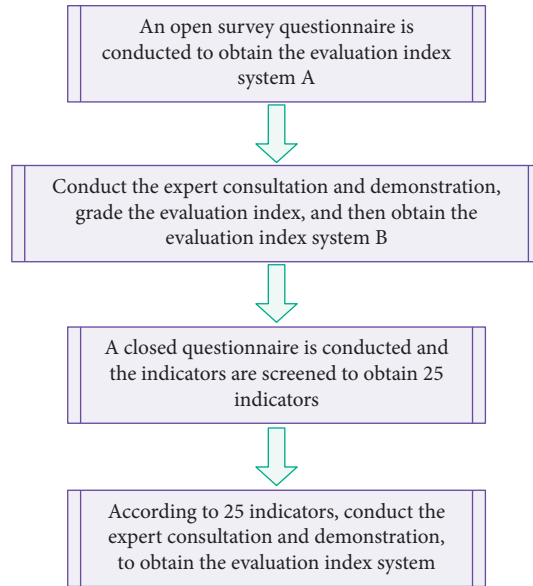


FIGURE 3: Flowchart of the construction index of tourism environmental carrying capacity.

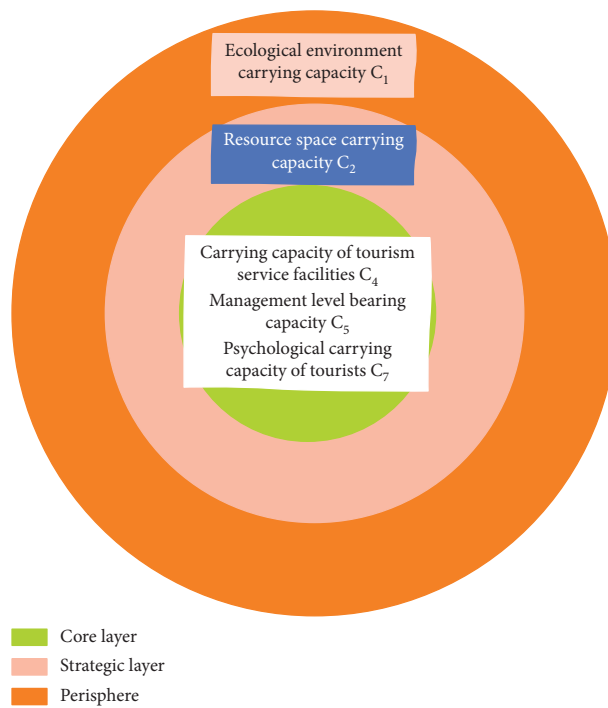


FIGURE 4: Relationship between the restrictive indicators of tourism environmental carrying capacity and stakeholders.

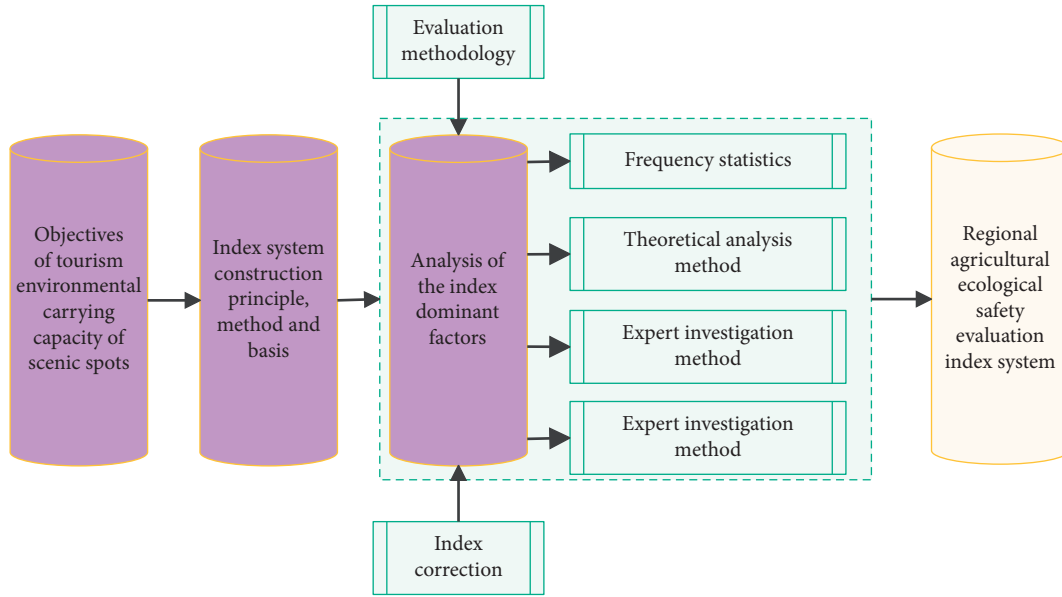


FIGURE 5: Evaluation index system of tourism environment carrying capacity.

serve the realization of scenic spot management goals, as shown in Figure 4.

The expert consultation method is to further seek the opinions of relevant experts and adjust the indicators on the basis of initially proposing evaluation indicators. This study will comprehensively use these four methods (Figure 5). Finally, a better evaluation index system of tourism environment carrying capacity will be obtained.

The clear-level evaluation index system of ecotourism carrying capacity of tourist attractions was constructed (Figure 6). The entire evaluation index system consists of 36 indicators, which belong to 10 domain layers and 3 criterion layers.

The comprehensive conceptual system of tourism environmental carrying capacity divides the value of the carrying capacity component according to different tourism environmental elements and contents. The composition

system of the researched tourism environmental carrying capacity is shown in Figure 7.

Based on the above analysis, the model proposed in this paper is validated on the basis of the above research model. The ecological tourism carrying capacity of popular scenic spots is evaluated, and the analysis is carried out in the form of simulation test, and the evaluation effect of the model in this paper in the carrying capacity of the tourism environment is counted, and the results shown in Figure 8 are obtained.

From the above cluster analysis, it can be seen that the method proposed in this paper performs well in the cluster analysis. Next, the performance of the model proposed in this paper in the evaluation of ecotourism carrying capacity is evaluated, and the results shown in Table 1 are obtained.

From the above research, it can be seen that the evaluation method of ecotourism carrying capacity of popular

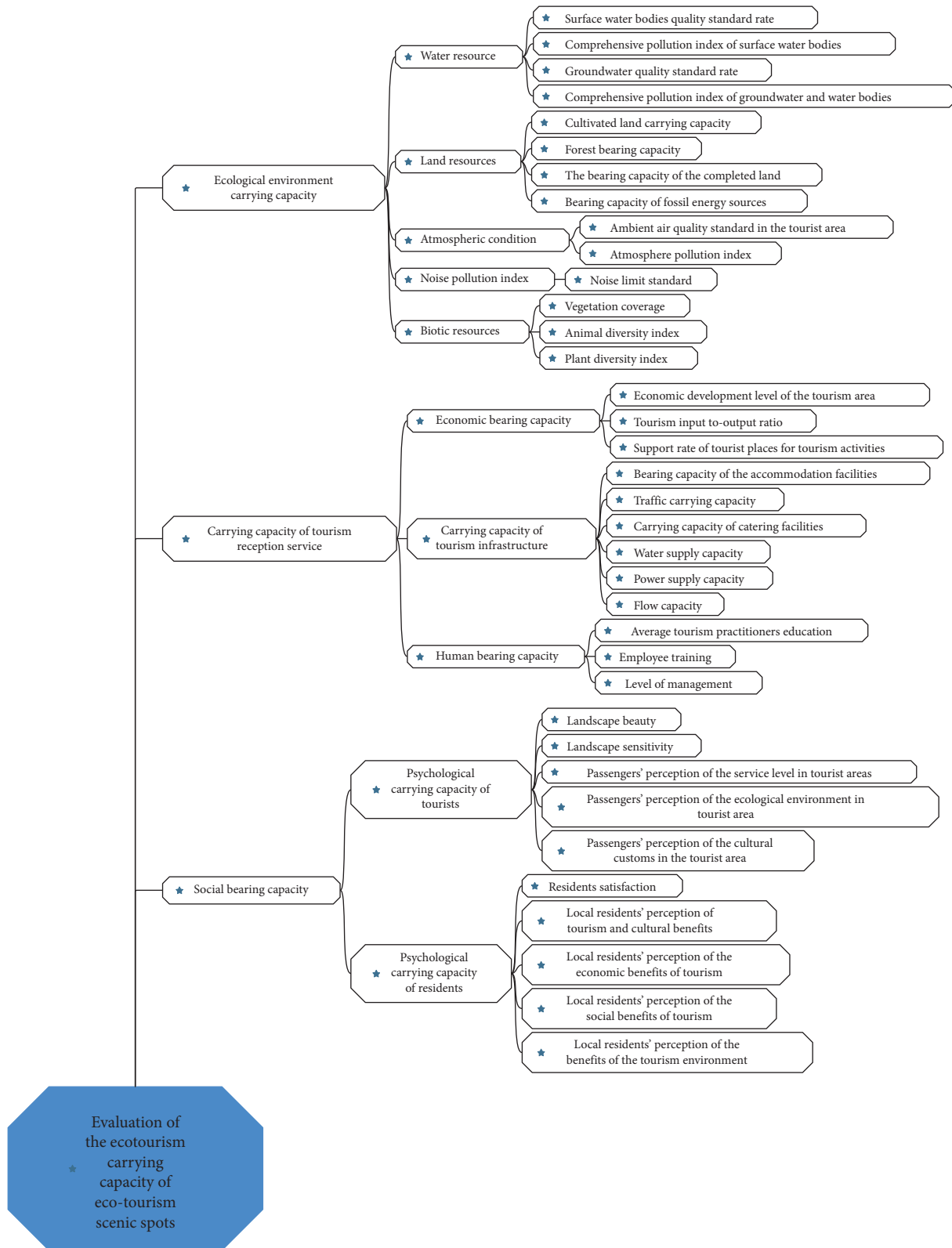


FIGURE 6: Evaluation index system of ecotourism carrying capacity of tourist attractions.

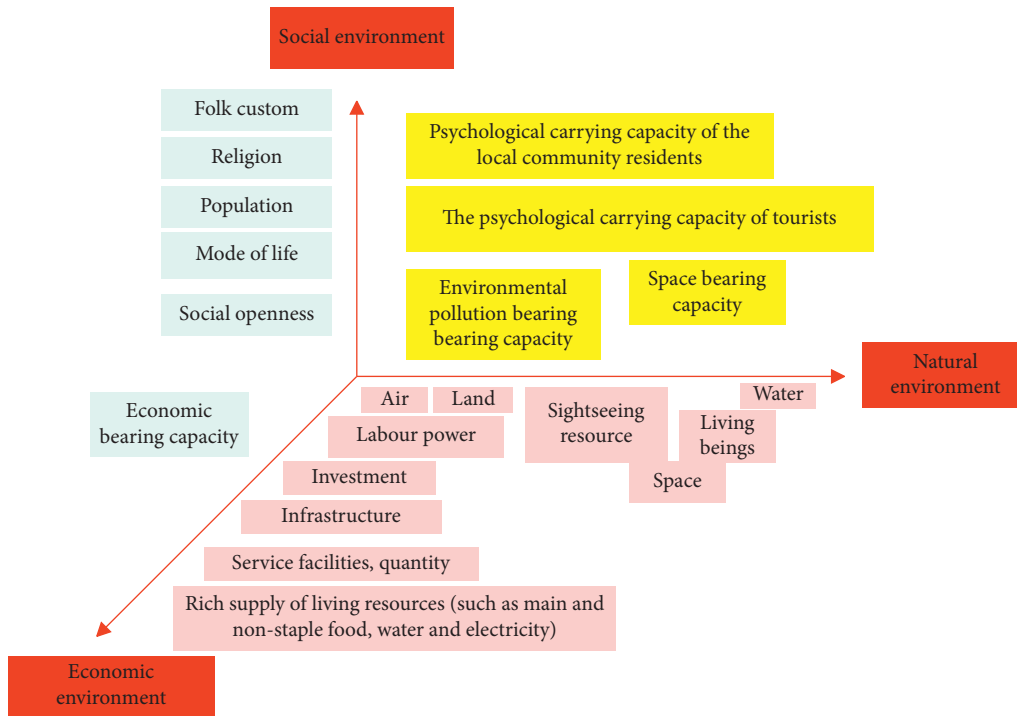


FIGURE 7: Composition system of tourism environment carrying capacity.

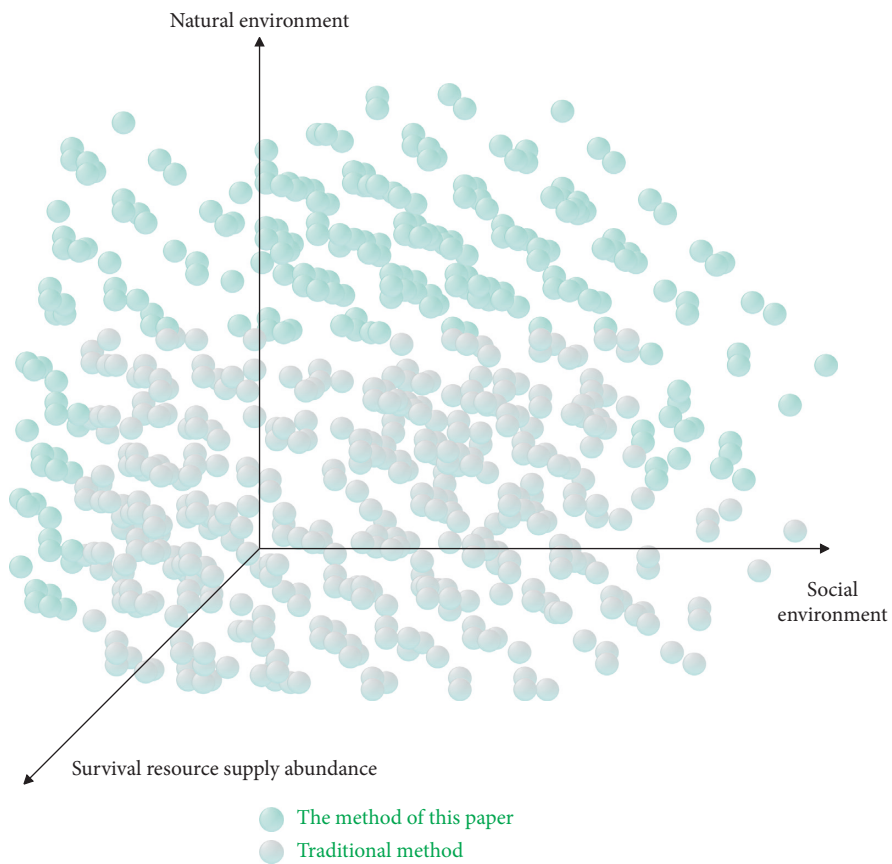


FIGURE 8: Cluster analysis of the effectiveness of the method proposed in this paper.

TABLE 1: Performance evaluation of the model proposed in this paper in the evaluation of ecotourism carrying capacity.

Num	Model evaluation	Num	Model evaluation	Num	Model evaluation
1	94.61	21	89.94	41	93.96
2	87.25	22	92.08	42	91.38
3	94.94	23	89.32	43	88.57
4	91.63	24	88.89	44	91.00
5	89.08	25	90.83	45	88.32
6	89.44	26	88.26	46	93.85
7	88.08	27	93.58	47	87.27
8	90.11	28	87.14	48	93.41
9	95.28	29	87.35	49	87.71
10	92.66	30	93.66	50	87.33
11	90.42	31	94.43	51	90.68
12	87.75	32	93.69	52	94.97
13	87.81	33	95.22	53	87.38
14	95.75	34	93.78	54	93.45
15	88.90	35	92.67	55	90.17
16	91.76	36	87.87	56	93.79
17	94.32	37	94.81	57	88.80
18	88.64	38	95.06	58	91.44
19	94.68	39	91.13	59	88.85
20	88.77	40	89.95	60	95.03

scenic spots based on set pair analysis proposed in this paper has a good effect.

5. Conclusion

The research on the environmental carrying capacity of tourist attractions can reasonably determine the service management level, environmental facilities, and resource development status of scenic spots and provide rational suggestions for scientifically formulating scenic spot management plans and management measures. At the same time, it can monitor the resource development status of the scenic spot, the level of service management, the number of tourists, and other factors in real time. Therefore, the research on the environmental carrying capacity of tourist attractions not only improves the service management level of the scenic spots but also makes various environmental facilities and resource conditions in the scenic spots in a benign interactive state, and finally the tourist satisfaction of tourists is sublimated. This paper combines the set pair analysis method to evaluate the ecological tourism carrying capacity of the scenic spots and improves the quantitative effect of the ecological tourism carrying capacity of the scenic spots.

Data Availability

The labeled dataset used to support the findings of this study is available from the corresponding author upon request.

Conflicts of Interest

The author declares that there are no conflicts of interest.

Acknowledgments

This study was sponsored by Wuhan Technical College of Communications.

References

- [1] Y. Yusof, K. Jusoff, Y. Ibrahim, and Z. Awang, "The influence of green practices by non-green hotels on customer satisfaction and loyalty in hotel and tourism industry," *International Journal of Green Economics*, vol. 11, no. 1, pp. 1–14, 2017.
- [2] I. Andersson and L. James, "Altruism or entrepreneurialism? The co-evolution of green place branding and policy tourism in Växjö, Sweden," *Urban Studies*, vol. 55, no. 15, pp. 3437–3453, 2018.
- [3] C. Irazábal, "Coastal urban planning in the 'green republic': tourism development and the nature-infrastructure paradox in Costa Rica," *International Journal of Urban and Regional Research*, vol. 42, no. 5, pp. 882–913, 2018.
- [4] H. Wee, N. A. Mustapha, and M. S. Anas, "Characteristic of green event practices in mice tourism: a systematic literature review," *International Journal of Academic Research in Business and Social Sciences*, vol. 11, no. 16, pp. 271–291, 2021.
- [5] A. D. Do, Q. V. Nguyen, D. U. Nguyen, Q. H. Le, and D. U. Trinh, "Green supply chain management practices and destination image: evidence from Vietnam tourism industry," *Uncertain Supply Chain Management*, vol. 8, no. 2, pp. 371–378, 2020.
- [6] I. Mykola, A. Vadym, P. Anatoliy, H. Yurii, and R. Nataliia, "Features of the content and implementation of innovation and investment projects for the development of enterprises in the field of rural green tourism," *International Journal of Management*, vol. 11, no. 3, pp. 304–315, 2020.
- [7] M. Simanjuntak and A. Rumondang Banjarnahor, "Re-investigating the roles of green service-scape to improve tourism performance marketing service dominant logic perspective: a literature review," *Quantitative Economics and Management Studies*, vol. 2, no. 4, pp. 214–232, 2021.
- [8] Z. Lili, "Retracted article: prediction of air pollutants and rural green tourism factors based on dynamic migration," *Arabian Journal of Geosciences*, vol. 14, no. 17, pp. 1777–7, 2021.
- [9] H. L. T. Trang, J.-S. Lee, and H. Han, "How do green attributes elicit pro-environmental behaviors in guests? The case of

- green hotels in Vietnam,” *Journal of Travel & Tourism Marketing*, vol. 36, no. 1, pp. 14–28, 2019.
- [10] N. Kongbuamai, Q. Bui, H. M. A. U. Yousaf, and Y. Liu, “The impact of tourism and natural resources on the ecological footprint: a case study of ASEAN countries,” *Environmental Science and Pollution Research*, vol. 27, no. 16, pp. 19251–19264, 2020.
- [11] R. Kisiel, J. Zielińska-Szczepkowska, and D. Taradejna, “Natural and cultural resources of Green Kurpie as drivers of tourism development,” *Ekonomia i Środowisko-Economics and Environment*, vol. 65, no. 2, 15 pages, 2018.
- [12] R. Rahmawati, A. R. Suprapti, S. R. H. Pinta, and P. Sudira, “Green entrepreneurship: a study for developing eco-tourism in Indonesia,” *The Journal of Asian Finance, Economics and Business*, vol. 8, no. 5, pp. 143–150, 2021.
- [13] V. Milla, A. Villalobos, L. Wallbott, and M. Lederer, “Green and social beyond a postcard scene? Sustainable tourism in Costa Rica and vietnam,” *Sociology*, vol. 8, no. 2, pp. 50–67, 2020.
- [14] R. Rahmawati, S. Soenarto, A. R. Suprapti, R. Handayani, and P. Sudira, “Green entrepreneurship development strategy based on local characteristic to support eco-tourism continuous,” *Jurnal Manajemen*, vol. 23, no. 2, pp. 257–273, 2019.
- [15] E. A. Dzhandzhugazova, E. L. Iljina, A. N. Latkin, A. R. Davydovich, and V. V. Siganova, “Problems of development of ecological tourism on the territory of national parks of Russia,” *Ekoloji*, vol. 28, no. 107, pp. 4913–4917, 2019.
- [16] O. Adamchyk, “Innovative sources of increasing the competitiveness of rural green tourism enterprises,” *University Economic Bulletin*, no. 46, pp. 38–45, 2020.
- [17] D. Cvijanović, D. Sekulić, and D. Pavlović, “Are green hotels suitable for the development of entrepreneurship in tourism?” *Ekonomika preduzeća*, vol. 66, no. 7-8, pp. 424–432, 2018.
- [18] S. Mohanty, S. Mishra, and A. Mohanty, “Green human resource management: a review of integration of environment and hrm practices in hotel industry,” *Journal of Environmental Management and Tourism*, vol. 12, no. 6, pp. 1572–1575, 2021.
- [19] S. V. Kalchenko, A. O. Hutorov, L. S. Bezuhla, O. A. Leushina, T. V. Popova, and O. V. Dorokhov, “Managing the SOCIO-economic development OF small forms OF green tourism,” *Series II: Forestry Wood Industry Agricultural Food Engineering*, vol. 14, no. 1, pp. 141–152, 2021.

Research Article

The Shared Transportation Industry in China: Examining the Influence of Regional Environmental Factors on New Venture Formation

Yan Zhou,¹ Sangmoon Park ,² Justin Zuopeng Zhang ,³ and Xin Rong ⁴

¹Logistics and E-commerce College, Zhejiang Wanli University, Ningbo, China

²College of Business Administration, Kangwon National University, Chuncheon, Republic of Korea

³Department of Management, Coggin College of Business, University of North Florida, Jacksonville, FL 32224, USA

⁴Audit Department, Zhejiang Wanli University, Ningbo, China

Correspondence should be addressed to Sangmoon Park; venture@kangwon.ac.kr and Xin Rong; rongxin@zwu.edu.cn

Received 26 January 2022; Accepted 11 April 2022; Published 4 May 2022

Academic Editor: Sang-Bing Tsai

Copyright © 2022 Yan Zhou et al. This is an open access article distributed under the Creative Commons Attribution License, which permits unrestricted use, distribution, and reproduction in any medium, provided the original work is properly cited.

China's shared transportation industry is leading innovation, driving employment, and promoting regional economic growth. China's aggressive efforts to promote the development of various transportation sectors motivate our investigation of this emerging industry. We examine the influence of regional environmental factors on new venture formation using a dataset encompassing newly established bike-sharing startups in 257 cities in China from 2015 to 2019. The empirical results show that entrepreneurial capital, entrepreneurial support policies, and urban auxiliary infrastructure positively impact the formation of new ventures. However, no significant relationship exists between industrial policy, competitive urban infrastructure, and new business formation. This study expands the scope of the existing research studying the characteristics of entrepreneurial space, offers inspiration for future startups entering the field of shared transportation in choosing entrepreneurial locations, and provides theoretical guidance for the government in formulating policies to attract entrepreneurial activities.

1. Introduction

The concept of the sharing economy has promoted the emergence of a new consumption model that has globally become popular due to its successful performance in addressing wasted resources caused by overcapacity [1]. The sharing economy has also promoted the emergence and popularization of a new business model. The emergence of the internet allows platforms to integrate offline idle goods or personal services with network technology and to provide them to users at a lower price. The commercial operation of internet network platforms such as Uber and Airbnb marked the beginning of the sharing economy. These firms not only led the development of the global sharing economy while enlightening the world about its potential but also provided a realistic foundation for a feasible business model for the sharing economy.

The sharing economy in China has rapidly developed in the past decade, playing an essential role in promoting economic growth, employment, innovation, and sustainable urban development. The sharing economy has become one of China's national economic development strategies and a vital driving force in the transformation and development of the service industry. In particular, the great attention and participation of the entire population in the sharing of transportation have made it an inseparable part of the daily life of ordinary people. Shared transportation alleviates traffic congestion, reduces environmental pollution, and satisfies short-distance travel needs. Consumers and government agencies in all regions have welcomed shared transportation services, and the industry has experienced tremendous growth by forming new ventures.

Entrepreneurship has always been regarded as an important means of promoting sustainable economic

development [2]. The higher the entry rate of new enterprises, the fiercer the competition will be, which is conducive to economic growth. Economic development practitioners and public decision-makers have focused their attention and resources on activities that support entrepreneurship to promote the development of local economies.

Prior empirical studies indicate that a large agglomeration trend can significantly differ in entrepreneurship rates in different countries and regions [3–6]. Regional differences in entrepreneurship rates are interpreted as differences in available or identifiable opportunities [7]. The entrepreneurship research on the regional dimension is premised on entrepreneurial opportunities in the regional environment. The entrepreneurial environment, such as the intermediary between entrepreneurs and their place of entrepreneurship, its relative merits, and the number of entrepreneurial opportunities, has a direct role in determining regional entrepreneurial activities.

Many regional determinants affecting the formation of new firms have been empirically validated. Examples of such determinants include the availability of venture capital, a skilled workforce, proximity to universities, the availability of support services, unemployment level, employment opportunities, the availability of productive resources, efficient public infrastructure, knowledge and R&D, human resources, population growth, economic base, local government support and policies, and agglomeration effects [8–13]. However, the existing studies focusing on the influence of the regional environment on the formation of new ventures have mainly considered the United States or European countries such as the United Kingdom, the Netherlands, and Italy. In recent years, the startup rate in China has dramatically increased, and the nascent GEM [14] report scored China with 5.3 points for its nascent entrepreneurship rate, ranking it 34th worldwide. China's entrepreneurial environment and urban infrastructure are also improving. However, under China's political background, the influence of the existing entrepreneurial environment on the formation of new ventures has never been deeply explored. Empirical research on regional differences in specific industries is also a field neglected by scholars [15, 16].

This study aims to fill this gap. We discuss whether and why the regional environment is important for an industry where market demand exceeds expectations and is almost unconstrained by space. This background is highly relevant to the future development of the shared transportation industry, the implementation of regional strategic management, and the cultivation of regional entrepreneurship. Combining the development characteristics of the shared transportation industry and China's period of rapid growth, we consider three aspects of the literature stream: venture capital, local government support and policies, and public infrastructure. Using a dataset of 307 bike-sharing startups in 257 Chinese cities from 2015 to 2019, we demonstrate the importance of regional environments for new venture formation. In other words, we find that regional venture capital, entrepreneurial policy, and urban auxiliary infrastructure are good predictors of the formation of new ventures, but we find no evidence for the effectiveness of industrial policy and

competitive urban infrastructure in startup promotion or restraint.

This study proceeds according to the following structure. The second section reviews the previous research and proposes hypotheses. The third section introduces the research methods, and the fourth section collates the analysis results. The fifth section is the discussion part. The sixth section is the conclusions, limitations, and future research directions.

2. Regional Determinants of Entrepreneurship

2.1. Regional Entrepreneurship. In recent years, entrepreneurs have created employment opportunities, introduced new innovations, and made significant contributions to regional economic development. Regional entrepreneurship has become an important means of promoting regional economic development. This has attracted many scholars devoted to studying the topic [6, 17–19]. Scholars in various disciplines, such as regional economic sociology, management, and geographic economics, have conducted in-depth studies on the relationship between entrepreneurship and regional development from different perspectives. Each discipline has focused on the influence of regional characteristics on the formation of new firms. The first type of research emphasizes traditional industrial organization theory and investigates the impact of industrial structure on the ability to establish new enterprises. In particular, the industrial organization approach is used to test whether the market structure hinders or accelerates the formation of new firms [20, 21]. The other type of research takes labor market theory as a starting point. Regional conditions often affect the entrepreneurship rate among enterprises, so the local social and economic environment is crucial for cultivating entrepreneurship [22]. This study explores the impact and importance of the market environment and social variables on entrepreneurial decision-making based on labor market theory.

2.2. Venture Capital. Although venture capitalists seek out the most promising new ventures for investment, there is a highly localized investment pattern in selecting investment opportunities [23–25]. The two roles of venture capitalists can explain this. The first is the preinvestment role, which mainly focuses on identifying and evaluating opportunities. The second is the postinvestment role, which facilitates the monitoring of new ventures and provides value-added services to investee firms [26].

Venture capitalists have two important tasks to accomplish when looking for an investment target. First, venture capitalists must have access to information about the existence of investment opportunities and their characteristics. Second, they must be able to assess the quality of these opportunities [26]. In every stage, from seeking investment opportunities to evaluating those opportunities, these tasks cannot be separated from the interpersonal relationships in the social network because these relationships are the primary path for information transmission within the

community of actors. Some sociological studies have provided the theoretical basis for this behavior, for example, Granovetter's [27] strength of weak ties theory and Burt's [28] structural holes theory. According to these theories, the strength of social networks and the structure of professional relationships influence the identification of investment opportunities by venture capitalists. Venture capitalists usually obtain timely information about high-quality investment opportunities in the field through their network relationships. The limited diffusion of reliable information among networks plays a central role in forming venture capital exchange relationships [26]. At the same time, because social relationships tend to form in geographical and social spaces, network relationships will positively influence the distribution space of investment activities in terms of generating indications regarding investment opportunities.

The role of venture capitalists or venture capital institutions after investment can also explain the phenomenon of investment localization. In addition to providing financial support to investment targets, venture capitalists also need to provide expertise to startups and monitor their management after selecting investment targets. Venture capitalists spend much time building and strengthening their social networks so that they can monitor the activities of other venture capital firms and markets [29]. The effective geographic radius over which insurance investment companies tend to invest has been found to be limited to a travel time of one to two hours from their offices [30]. Geographical proximity helps reduce the travel time and material cost of monitoring. It can also improve the relationship with the investment company and avoid communication conflict between the managers or entrepreneurs at the target firm to reduce agency problems and ultimately achieve the expected returns on the investment goals.

Due to the localized investment characteristics of venture capital, to increase the likelihood of receiving investment, startups treat proximity to local venture capital firms as a strategic means to obtain venture capital. The history of the development of China's shared transportation industry shows that it has been highly dependent on the support of venture capital. Therefore, in this case, the activity of various regional venture capital institutions will profoundly impact the formation of shared transportation startups. Consequently, we propose the following hypothesis:

H1: Venture capital activity in various regions will positively impact the formation of shared transportation startups.

2.3. Policy Environment. The positive effects of government policies on entrepreneurial formation can be explained by the outsider assistance theory [31, 32]. The assistance theory begins with the assumption that the knowledge possessed by entrepreneurs or teams of entrepreneurs is the most critical advantage held by new ventures. However, no entrepreneur has perfect knowledge, so the knowledge and other resource gaps must be addressed through preparation before and during the initiation process. Therefore, entrepreneurs often increase their knowledge in two ways: through preparation

or seeking outside advice or mentoring. Both are valuable means of acquiring knowledge; however, each method has its limitations, so a third method is proposed: preparing for entrepreneurship through professional guidance, which can minimize or eliminate the respective limitations of the entrepreneur and produce the greatest benefit. External assistance can be used as a knowledge resource, and the provision of guidance during the entrepreneurial process can affect new venture performance [31, 32]. This theory is applied to the startup phase of the entrepreneurial process and is used to test whether a connection with external assistance programs and a relationship with entrepreneurs who have already conducted planning activities such as market research, business plans, and financial plans will contribute to startup results.

The most common form of external assistance is government policy assistance. Government assistance is considered as a means of encouraging knowledge spillovers or positive externalities (social returns exceed private returns) [33]. Storey [34] believed that although entrepreneurs were motivated to acquire knowledge, they could not quickly gain the knowledge or experience they needed without government-funded assistance programs. Government policy support also reduces the capital cost of new enterprises when they acquire knowledge resources. The Chinese government has issued various intervention-type policies to help small- and medium-sized enterprises or startups to develop and become established. Small- and medium-sized enterprises and startups are also receptive to preferential treatments and benefits from government policies. The Chinese government has also given strong support to entrepreneurs. According to the 2016 Global Entrepreneurship Index, China ranks 3rd among 62 countries regarding the impact of government policies and related support on entrepreneurship. The Chinese government's support for entrepreneurship is mainly embodied in some specific micropolicies that focused on supporting groups or individuals to solve business-related or social problems. Micropolicies are mainly reflected in the following four aspects: entrepreneurship training, facilities, loans, tax reduction, and entrepreneurship exemptions. These policies have created a good entrepreneurial environment and have significantly helped new enterprises.

In the context of "mass entrepreneurship and mass innovation," the Chinese government has also formulated support plans for entrepreneurship according to the characteristics of various industries, especially the sharing economy, including the shared transportation industry. As a new green transportation tool, shared transportation has received special attention and support from the government. Specific incentive measures include the rational layout of transportation networks and parking facilities, the establishment and construction of parking spots, and the encouragement of relevant social organizations and industrial technology alliances to develop standards and systems related to the shared transportation industry. Local governments have also signed strategic cooperation agreements with companies to actively introduce shared transportation infrastructure from the government's perspective. All these actions send positive signals and have an essential impact on

the formation of new ventures. Therefore, we propose the following hypotheses:

H2-1: The policies in various regions relevant to the shared transportation industry will positively impact the formation of new ventures.

H2-2: The entrepreneurship policies in various regions will positively impact the formation of shared transportation startups.

2.4. Urban Infrastructure. The relationship between urban infrastructure and entrepreneurship has received little attention from scholars, but a few studies have empirically tested the positive effect of infrastructure on the regional entrepreneurship rate [35, 36].

The primary theoretical basis for the positive impact of infrastructure on the regional entrepreneurship rate is the argument that infrastructure can stimulate entrepreneurial opportunities, promote interaction between industries within regions, and increase the knowledge spillover effect. New entrepreneurs can seize these opportunities by establishing new companies [35, 36]. New infrastructure investment also helps facilitate the flow of capital goods, ideas, and people [35], potentially improving the connections between industries within an area. Increased interaction and connection contribute to the spillover of knowledge. The knowledge spillover effect refers to the correlation effect generated by knowledge receivers and demanders who digest and absorb innovative knowledge and promote enterprise development and economic growth [37]. A stronger knowledge spillover effect within a region means that enterprises acquire more low-cost and valuable knowledge from outside, which is more favorable for the establishment and development of enterprises.

As an external driver, infrastructure investment creates space for new economic activities [38] and supports the development or expansion of growth centers or the aggregation of economic activity in a region [39, 40]. Existing businesses may strategically relocate to an infrastructure-supported growth hub. The development of new infrastructure will also attract risk-takers and proactive entrepreneurs who are alert and ready to act on the exploitable opportunities it brings. In this way, infrastructure investment allows entrepreneurs to build new companies or expand existing ones in newly created or expanded markets [41]. In either case, infrastructure investment can serve as an approach to improving the potential to establish new businesses [36].

As a new means of transportation, shared transportation is a form of urban infrastructure built by private investment. It is a type of urban infrastructure that requires private investment and involves the maintenance and development of public interests, that is, it provides residents with unlimited short-term travel services. When shared transportation emerged in China, the development goals pursued by various companies were to provide more convenient public transportation connections, solve short-distance travel problems, alleviate traffic pressure, and mitigate environmental pollution.

In addition to private cars, the three types of public transportation vehicles, buses, subways, and taxis are the most frequently used in daily travel, but there are alternatives and some competition. With the rise of shared transportation, the shared transportation industry has become a new component of the urban public transportation system. As a transportation tool providing advantages in short-distance travel, shared transportation services largely rely on other public transportation tools, especially traditional tools such as subways and buses. Due to fixed bus and subway routes, bike sharing has become the most convenient and efficient way to connect subway and bus stations with residential areas. According to a survey on the main reasons for shared bike use, 36.8% of users use shared bikes as a part of their commute [42]. In public transportation, taxis offer convenient routes, timing, and location availability, which conflict with the characteristics of shared transportation services, so taxis have become the most direct source of competition. Therefore, in the shared transportation industry, the development of regional transportation infrastructure has become an important factor that must be considered because it affects the formation and future development of new ventures. Therefore, we propose the following hypotheses:

H3-1: The degree of development of a city's auxiliary transportation facilities will positively impact the formation of shared transportation startups.

H3-2: The degree of development of urban competitive transportation facilities will negatively impact the formation of shared transportation startups.

3. Data and Methods

This study uses a dataset of Chinese bike-sharing startups to test the proposed hypotheses. As a typical representative of China's shared transportation industry, bike sharing has become the field with the highest participation among the population. More details about the data collection, independent variables, dependent variables, and data analysis are described below.

3.1. Data. We constructed the bike-sharing enterprise dataset in three steps based on a combination of public data and survey data. In the first step, we identified 509 bike-sharing-related enterprises with business licenses registered in mainland China through the National Enterprise Credit Information Publicity System provided by the State Administration for Industry and Commerce. Second, we used the Tianyancha database to examine the business scope of each enterprise in detail and excluded 116 enterprises that did not include keywords such as sharing, sharing bikes, sharing transportation, or sharing economy. We manually sorted the basic information for each company, including the year of establishment, registered address, and registered capital. A bike-sharing enterprise must have its own brand and app as a precondition to entering the market. This study assumes that the enterprise remains in the product design or strategic deployment stage if there is no app. Therefore, in

the third step, we searched the mobile apps under the name of each enterprise in the Android and iOS mobile app stores, and apps were not found for 83 enterprises. We excluded these enterprises and ultimately created a dataset of 310 bike-sharing startups.

The data relating to Chinese cities are obtained from the China City Statistical Yearbook 2016, 2017, and 2018 released by the National Bureau of Statistics of China. The development of China's coastal and inland provinces is extremely uneven, and the use of provincial-level data will cause serious endogeneity problems. Therefore, we abandon the traditional research method of taking provinces as the unit and instead use cities at or above the prefecture level, representing the main part of China's prefecture-level administrative regions. Of the 297 prefecture-level cities, 38 belonged to the five ethnic minority autonomous regions and were excluded because the cultural customs, administrative policies, and systems in these regions of China are quite different from those of other cities. We also excluded an island and a military city far from mainland China. Ultimately, we identified 257 cities in 22 provinces.

The relevant venture capital data in each region come from the PEdaily database. The PEdaily database is the ZeroIPO's most comprehensive public database on venture capital information in China. There are no specific restrictions on the enterprise characteristics of investment institutions when collecting data, such as the investment field, investment stage, investment nature, and capital type, except that the registration location of the enterprises must be in mainland China. Foreign-funded enterprises that have registered industrial and commercial information in China are also included. The aim is to determine the level of venture capital activity in the region. The data on venture capital firms were eventually collected in all 257 cities.

3.2. Dependent Variable. The dependent variable in this study uses the cumulative number of new bike-sharing enterprises in each city as the measurement unit, excluding the company's branches or the new institutions created by a change in location or name, and the number of cities in which the enterprises have expanded. By the end of 2019, a total of 310 new bike-sharing enterprises had been established in China, of which 3 were not located in the 257 prefecture-level cities ultimately selected in this study. Therefore, these 3 enterprises are excluded, and the distribution of 307 enterprises in various cities in China is analyzed. In this study, bike-sharing startups that are no longer in business or announced their withdrawal from the market are not excluded because such events do not influence the purpose of our study. Cross-sectional data are formed according to the registration time and place of the enterprises.

3.3. Independent Variables. The venture capital variable is a dichotomous variable that captures whether a venture capital institution was registered in the city for industry and commerce as of December 31, 2019. A city with at least one venture capital institution is 1, and a city without a venture

capital institution is 0. For the measurement of policy, this study considers two aspects. The first is the support of local governments for the bike-sharing business. The government's support for bike-sharing can be measured by the following two factors: (1) relevant policy documents promoting and encouraging the development of green transportation or bike-sharing in the city have been issued and are published on the websites of various local governments, (2) and bike-sharing projects have been officially introduced in the name of the government. Cities with government support have a value of 1 for this variable, and cities without support are assigned 0. The second aspect is the support given by local governments to startups. The preferential policies provided by local governments for startups include (1) exemption from administrative charges, (2) provision of small secured loans, (3) vocational training subsidies, (4) tax reduction and exemption, (5) rent-free startup space in the local pioneer park, and (6) cancellation of household registration restrictions and house purchase restrictions. Cities that have any of these policies are set to 1, and those that do not are set to 0.

Two variables were used to measure the city's public facilities. As the best solution to short-distance travel, the shared transportation industry is a supplement to public transportation tools such as buses and subways. Therefore, to capture auxiliary transportation facilities in cities, this study measures the density of the mass transportation system by the number of traffic routes in each city using data from China's public transportation information network. Taxis represent the strongest competitor in the shared transportation industry. Therefore, to capture the city's competitive transportation facilities, the second variable is the number of taxi vehicles per ten thousand people. The data come from the China City Statistical Yearbook, and the average number of taxis in each city in 2016, 2017, and 2018 was calculated.

3.4. Control Variables. This study also controls for some of the variables that influence the formation of bike-sharing startups. The development of bike-sharing services cannot be separated from the population and economic conditions of the city, so the population variables and economic variables are controlled. The population variables are population density, i.e., the number of registered residents of the administrative area of the city (unit: square kilometers). The economic variable is the average per capita GDP of each city in 2016, 2017, and 2018. Because Shanghai, Tianjin, and other cities have clear regulations requiring bike-sharing operators to allocate personnel for vehicle maintenance, maintenance, and transportation at a proportion of no less than 5% of the total number of shared vehicles, labor variables are also controlled in this study. The current labor force was measured using the proportion of workers in the tertiary industry. Shared bikes are unshielded vehicles. According to the White Paper on Shared Bikes and Urban Development released by Mobike in 2017, air quality will affect consumers' use intention and usage duration. Therefore, air quality in a city is also

included due to its potential to affect the formation of bike-sharing startups. The average PM2.5 of each city in 2016, 2017, and 2018 was used to measure air quality. As a kind of human capital, well-educated people possess both general labor skills and specialized skills. Areas with a dense representation of citizens with a higher education background will generate more entrepreneurial activities, so we also control the variable representing human capital using the number of college students per ten thousand residents [16].

3.5. Methods. At present, the measurements of entrepreneurship in the existing empirical research are almost all based on the number of new enterprises established [43, 44] or the firm entry rate [16, 45]. The main purpose of this study is to determine the external environmental factors that influence the establishment of shared transportation startups, so it is appropriate to use the number of startups established in each region to measure the degree of entrepreneurial activity. Moreover, the new business model for bike sharing in China was established only 4 years ago, so panel data analysis is not suitable for measurement. Therefore, in this study, the number of new enterprises established is the cumulative number of enterprises established in each region until 2019. These are non-negative integer count data, and the model estimation method should use Poisson's regression.

The basic condition for Poisson's regression is that the mean of the number is equal to its variance. In this study, the mean value of the dependent variable was 1.195, the variance was 20.603, and the variance in the explained variable was greater than the mean value, indicating the existence of overdispersion, which does not conform to the premise of Poisson's regression, so negative binomial regression was used for the estimation. However, the number of new enterprises established in different regions is very unbalanced, and there are a large number of zero values in the data. The excessive overdispersion may also be caused by the high probability of zero, which will lead to the zero-inflation problem. Therefore, a zero-inflation negative binomial regression model is used to test the data. In the zero-inflated negative binomial regression model, the 95% confidence interval of the alpha is (0.364, 1.668), so the null hypothesis of alpha = 0 can be rejected at the significance level of 5%; that is, negative binomial regression can be used. Furthermore, the Vuong statistic is -2.20 , $\Pr > z = 0.986$, less than -1.96 , and not significant [46], so zero-inflated negative binomial regression is rejected, and standard negative binomial regression should be used. In short, based on the required tests for the above models, negative binomial regression is the most consistent analysis method for testing the data in this study.

4. Results

4.1. Results of the Basic Analysis. Table 1 shows the statistical description of each variable. Among the 257 prefecture-level cities, an average of 1.195 bike-sharing startups were

TABLE 1: Descriptive statistics.

Variable	Obs	Mean	Std. dev.	Min	Max
Firm	257	1.195	4.539	0	45
Density	257	468.215	346.832	5.811	2537.518
GDP per capita	257	65933.55	134000	13589.67	2160000
Labor	257	53.118	21.678	18.07	284.953
Air quality	257	49.396	15.998	15.3	94.733
Human capital	257	192.78	251.343	9.795	1283.629
Venture capital	257	0.716	0.452	0	1
Policy bike sharing	257	0.35	0.478	0	1
Policy entrepreneurship	257	0.214	0.411	0	1
Auxiliary facilities	257	129.035	191.049	5	1461
Competition facilities	257	7.657	8.558	0.388	50.465

established in each city. The city with the most registered companies was Beijing, where 45 bike-sharing startups have chosen to establish their business. In the three years, the average population density was 468.215 people per square kilometer, and the per capita GDP was 65,933.55 yuan. The labor force in the tertiary industry accounted for 53.18%, and the air pollution was 49.396 per cubic meter on average, which is approaching a light pollution level. The average number of college students in each city was 192.78 per 10,000 people. With at least one registered venture capital institution, the number of cities accounted for 71.6% (184 cities). Cities where local government has issued policies to support bike sharing account for 35% of all cities, specifically 90 cities. Only 55 cities, accounting for 21.4% of the total, have issued policies to support entrepreneurial enterprises, and these are almost all among the largest major cities in China. For the public transport infrastructure in each city, there are 129 bus lines in each city on average, and there are 7.657 taxis per 10,000 people on average.

Table 2 shows the correlation between the variables. It can be seen from the table that most variables do not have a high correlation. The lack of correlation proves some of the relationships discussed in the theory section, but there were some high correlations between the variables, which was not surprising given the reality and the nature of the variables. For example, there was a positive correlation between the number of firms and the number of auxiliary public facilities (bus routes) in the city ($r = 0.741$). Although the correlation coefficient is relatively high, this is because shared bikes are designed from the very beginning to supplement the existing public transportation in the city, as they aim to solve the "last kilometer" problem. Such a starting point makes it necessary to have a high connection between shared bikes and buses, which also extends to consumers' search for and cognition of shared bikes and buses. Subsequent regression analysis also showed statistically significant and theoretical signs. To increase the accuracy of the analysis, the multicollinearity of each variable was measured before the analysis. The analysis results show that the average VIF = 1.82, which proves no multicollinearity between the variables.

TABLE 2: Matrix of correlations.

Variables	(1)	(2)	(3)	(4)	(5)	(6)	(7)	(8)	(9)	(10)	(11)
(1) Firm	1.000										
(2) Density	0.416*	1.000									
(3) GDP per capita	0.092	0.107	1.000								
(4) Labor	0.028	-0.238*	-0.052	1.000							
(5) Air quality	0.036	0.291*	0.015	-0.099	1.000						
(6) Human capital	0.275*	0.261*	0.095	-0.007	0.028	1.000					
(7) Venture capital	0.151*	0.257*	0.129*	-0.135*	0.124*	0.289*	1.000				
(8) Policy bike sharing	0.255*	0.269*	0.152*	-0.106	0.030	0.357*	0.245*	1.000			
(9) Policy entrepreneurship	0.382*	0.375*	0.085	-0.068	0.196*	0.594*	0.308*	0.253*	1.000		
(10) Auxiliary facilities	0.741*	0.528*	0.117	-0.066	0.030	0.557*	0.301*	0.360*	0.548*	1.000	
(11) Competition facilities	0.484*	0.141*	0.057	0.015	-0.110	0.548*	0.139*	0.216*	0.396*	0.513*	1.000

4.2. Negative Binomial Regression Analysis Results.

Table 3 shows the negative binomial regression analysis results for venture capital, policy support, urban infrastructure, and bike-sharing startup formation in each city. To ensure consistency in the analysis results, a nested model was selected to test robustness. Model 1 provides the analysis results, including only control variables. Model 2 is the test result of Hypothesis 1, Model 3 is the test result of Hypothesis 2-1 and Hypothesis 2-2, Model 4 is the test result of Hypothesis 3-1 and Hypothesis 3-2, and Model 5 is the full model including all variables.

First, Model 1 provides only statistical results, including all control variables. Among the control variables, population density ($\beta=0.002$, $p<0.01$) and human capital ($\beta=0.003$, $p<0.01$) have a positive influence on the formation of bike-sharing startups in each city. Model 2 is a test of Hypothesis 1. According to the test results, cities with venture capital institutions are more likely to attract bike-sharing startups than cities without venture capital institutions. Thus, the presence of venture capital firms has a positive impact on the formation of bike-sharing startups ($\beta=1.136$, $p<0.05$), so Hypothesis 1 is supported.

The strong influence of venture capital on the formation of startups is also in line with the development of bike sharing in China. The rapid expansion of bike sharing in a short period of time is largely due to the active support of venture capital. Among the 307 startups discussed in this study, 63 (20%) were supported by venture capital funds at least once. In addition, 72% of these venture capital firms and bike-sharing startups are located in the same city, proving that venture capital firms prefer local enterprises when choosing investment target companies. To increase the probability of obtaining venture capital, bike-sharing startups prioritize starting businesses in cities with venture capital institutions as one of their development strategies.

Model 3 is the result of testing Hypotheses 2-1 and 2-2. Cities with clear policy support for bike sharing are more likely to attract bike-sharing startups than cities without such support. Although it has a positive impact when all variables are taken into account, bike-sharing policy support does not impact startup formation, so we reject Hypothesis 2-1 ($\beta=0.397$, ns). Cities with entrepreneurial policy support are more attractive to bike-sharing startups than cities without such support, and entrepreneurial policy support positively impacts the formation of startups ($\beta=1.506$, $p<0.01$). Therefore, the analysis results support Hypothesis 2-2.

The impact of policy on the formation of bike-sharing startups also varies according to the type of policy. In the early days of bike-sharing development, the central government issued a series of policy documents actively promoting “green transportation” to ease traffic pressure and protect the environment, and local governments followed suit. Policies such as those attracting investment, providing government procurement opportunities, and reducing taxes have positively signaled the development of the green transportation industry, and thus bike sharing was born as a concept and a project. In the stage of rapid development for bike sharing, a series of social problems emerged, such as

random bike parking and damaged or lost vehicles. Shared bikes became a new form of garbage and created traffic pressure, leading the central government to quickly issue several management policies on shared bikes to control the situation, with many cities even issuing “investment prohibition orders,” which greatly affected the confidence in bike-sharing startups. Our analysis results also verify this phenomenon, which is positive when considering the influence of the bike-sharing support policy on the formation of startups alone ($\beta=0.674$, $p<0.05$). However, after the entry of other influencing factors, the attractiveness of this policy weakens, and it ultimately has no significant impact on the formation of startups ($\beta=0.397$, ns).

For entrepreneurs, the entrepreneurship policies issued by the government are more attractive to them, such as those providing training courses for startup companies in business management, prioritizing business sites, and reducing taxes or offering exemptions. Meanwhile, in recent years, after the central government made it clear that talent is the number one resource and innovation is the number one driving force for China’s future development, and local governments launched a symbolic “talent war.” In the past, when developing the economy, most localities regarded only land, minerals, and other resources as resources, while only a few regarded “human resources” as the most valuable resources for economic development. The change in the central government’s direction for development also prompted local governments to introduce very strong measures to attract all kinds of talent, including entrepreneurial and innovative talent; the introduced policies include adjustments in the hukou system for households, subsidized housing, and child prioritization in school. Both entrepreneurship policies and talent policies are more practical and specifically focused on helping new enterprises and entrepreneurs. The effects of these local policies are empirically tested in this study, which finds that they have a positive and significant impact on attracting the formation of bike-sharing startups.

Model 4 examines the impact of urban infrastructure on the formation of bike-sharing startups. In urban infrastructure, the more advanced auxiliary facilities there are, the more likely they will attract new bike-sharing startups to the city, supporting Hypothesis 3-1 ($\beta=0.004$, $p<0.01$). Competition facilities do not affect startup formation, so hypothesis 3-2 ($\beta=-0.003$, ns) is rejected.

The positive impact of urban infrastructure on the formation of bike-sharing startups is mainly reflected in the degree of development of auxiliary transportation facilities in the city. Bike-sharing services are mainly aimed at consumers who need to travel short distances. According to a basic survey of 20,000 bike-sharing users conducted by iiMedia Research, 50.8% of users use shared bikes for 10–30 minutes, and 36.8% use shared bikes for commuting. Although the average use price of buses is 1.33 yuan per unit of time, which makes them strongly competitive with shared bikes in the use price, the convenience of shared bikes in terms of both use route and use timing creates a competitive relationship between the two modes of transportation. Bike-sharing startups have developed strategies to supplement public transportation from their early days, such as buses or

TABLE 3: Negative binomial regression analysis results.

	Model 1	Model 2	Model 3	Model 4	Model 5
Density	0.002*** (4.28)	0.002*** (4.52)	0.001*** (3.60)	0.001** (2.03)	0.000 (1.29)
GDP per capita	0.000 (1.02)	0.000 (0.65)	0.000 (0.90)	0.000 (1.22)	0.000 (0.94)
Labor	0.006 (0.72)	0.007 (0.97)	0.003 (0.40)	-0.008 (-0.94)	-0.004 (-0.55)
Air quality	0.002 (0.25)	0.000 (-0.01)	-0.005 (-0.52)	0.004 (0.48)	-0.001 (-0.16)
Human capital	0.003*** (4.27)	0.003*** (4.45)	0.001** (2.19)	0.001*** (2.71)	0.000 (0.86)
Venture capital		1.136** (2.45)			0.758* (1.81)
Policy bike sharing			0.674** (2.35)		0.397 (1.55)
Policy entrepreneurship			1.506*** (4.48)		0.899*** (2.97)
Auxiliary facilities				0.004*** (5.53)	0.003*** (4.77)
Competition facilities				-0.003 (-0.20)	-0.007 (-0.42)
Constant	-2.958*** (-4.34)	-3.582*** (-5.01)	-2.288*** (-3.87)	-1.796*** (-3.04)	-2.317*** (-3.48)
N	257	257	257	257	257
Pseudo- R^2	0.143	0.153	0.181	0.210	0.236
Chi-square	88.207	94.491	111.819	129.267	145.532
Log-likelihood	-263.969	-260.827	-252.163	-243.439	-235.307

*** $p < 0.01$, ** $p < 0.05$, and * $p < 0.1$ (T values are in parentheses).

subways. Combined with the research results of this study, it can be once again confirmed that when choosing where to establish their business, shared transportation startups will inevitably consider the current urban traffic situation of the location, which is also determined by the service characteristics and development strategy of shared transportation.

In China, there has always been controversy about the fact that many entrepreneurs, scholars, and the media regard the taxi industry as competition for shared bikes. In some areas, taxi drivers even stole hundreds of shared bikes in the middle of the night to prevent the development of shared bike services. However, it can be seen from the research in this study that bike-sharing startups do not regard the taxi industry as a competitor, and they do not avoid entering the market of a city because there are many taxis. This result is related to the use price of shared bikes, the main use scenarios, and the use distance. From 2015 to 2020, the starting taxi fare in 36 large- and medium-sized cities in China was 9.54 yuan per taxi (Price Monitoring Center of National Development and Reform Commission of China). The use price of shared bikes is 2 yuan per hour on average, which is more advantageous for short-distance trips. At the same time, in the use scenario, shared bikes are mainly used to change vehicles at work when the traffic conditions are the most complicated and congested, and the use of shared bikes can reduce travel time more than taking a taxi. Although some scholars have verified that an increase in bike-sharing reduces bus use [47], it also reduces the use of cars, taxis, and illegal motorcycles. However, these issues are not the focus of this study. We hope to explore the influence of shared transportation industry relationships from the perspective of urban public transportation in future research.

5. Discussion

The rapid growth of shared transportation startups in China in a short period has contributed to the rise of this industry. Residents' high demand for transportation has driven the industry's market potential to exceed expectations. The industry provides a supplement to a city's existing

transportation system, and it is almost free from any spatial and geographical restrictions. The shared transportation industry, among all sectors, must be considered innovative and accessible. This research aims to explore whether and why the regional environment is vital to forming new industries. We used regional data in China to analyze the regional differences influencing the formation of shared transportation startups. This study focuses on financial capital, policy, and urban infrastructure. The research results prove that regional factors have a substantial impact on the formation of startups.

With an average of 1.195 bike-sharing startups being established in each of China's 257 cities and 307 companies clustered in 75 cities, there is a severe imbalance in the startup rates among cities. We find strong evidence for the relationship between financial capital, entrepreneurial policy, urban ancillary transport facilities, and new firm formation, but the results for industrial policy and urban competitive transport facilities are surprising.

First, the development of China's venture capital industry has played a positive role in promoting China's regional economy [48], which is inseparable from the strategic development mode of venture capital institutions focusing on investment for regional startups. As Von Burg and Kenney [49] observe, venture capital promotes the emergence of area networking. Shared transportation startups seem to pursue the advantages of venture capital industry agglomeration and rely more on gaining attention and investment through geographical proximity to venture capital. The lack of venture capital in a surrounding area can discourage startups from setting up in a given area. Competition may be fiercer in regions favored by venture capital but that does not deter entrepreneurs from entering the market. From another point of view, to narrow the gap in regional development or break the imbalance, the government can also begin by reforming the regional layout of venture capital institutions. In remote cities, we can learn from the general model of government-funded venture capital to provide opportunities for more technology-based and new business model startups to obtain financial support.

Second, the window of opportunity for developing shared transportation in China comes from some social problems that need to be solved, such as traffic congestion and environmental pollution. To solve these social problems and improve conditions, the Chinese government has formulated a series of policy solutions. As Hammond [50] said, the changes in politics and hierarchy in non-Western countries such as China provide more opportunities for individual decision-making. Entrepreneurs are seizing the opportunities and advantages of policy entrepreneurship to connect problems and solutions and quickly create businesses. However, we find that public policy presents challenges in terms of shaping and promoting the entrepreneurship of new business models based on technology. Different types of policy support have diverging effects on attracting the creation of startups. Through innovative destruction, shared transportation and the sharing economy have brought rapid growth, but they also face many controversial issues. The government is trying to correct the market failure of the bike-sharing economy while regulating the industry and protecting the public interest. In the theory of public interest, the transformation of the three roles of government as protector, coordinator, and regulator [51] inhibits the formation of new ventures. The government's continued negative attitude toward the sharing economy and unclear regulatory role have dampened entrepreneurs' enthusiasm. In the future, the government can learn from the management of shared transportation. On the premise of protecting the public interest, the responsibilities and management boundaries of the government should be clarified, and solutions to the challenges brought by the development of new industries should be provided.

Third, our results partially support the relationship between urban infrastructure and entrepreneurship; in particular, they confirm Audretsch et al.'s [35] conjecture of a positive relationship between specific types of infrastructure and specific industrial contexts. However, in this study, this particular type of infrastructure is also limited to infrastructure that has auxiliary functionality for the industry. However, another interesting and fortunate finding is that competitive infrastructure has no impact on entrepreneurial activities. With the advancement of urbanization and the rapid development of digital reform, traditional urban infrastructure provides the basis for realizing the shared transportation part of the smart city concept [52]. Smart cities based on high-tech infrastructure will be the ultimate goal of future urban transformation [53]. A wealth of innovation and market opportunities triggered by emerging technologies [54], such as the internet of things [55–57], machine learning [58, 59], and deep learning [60–62], are driving the creation of new businesses. Many scholars have proposed that an increasing number of new business models have been created in this process. In the future, smart city infrastructure will be more closely related to entrepreneurship, with higher entrepreneurial activity in smart cities than in other cities [41, 63, 64]. Our results also provide some new evidence for this hypothesis.

The potential contributions of this research include the following aspects. (1) A new academic contribution of this

study is its deepened understanding of the role of entrepreneurial policies and urban infrastructure at different stages or in different forms that may promote or inhibit the formation of new firms. The subdivision of the external factors affecting entrepreneurial activities expands the research framework of entrepreneurial spatial characteristics. It also enriches the literature on entrepreneurship policy and infrastructure and entrepreneurship research. (2) The results of this study are particularly valuable to entrepreneurs entering the field of shared transportation as the adoption of the shared transportation business model is globally growing. The choice of business location will affect the survival and development of enterprises. The spillover effect brought by financial capital, preferential policies, infrastructure development, and entrepreneurial opportunities in the regional environment will bring substantial benefits to the establishment of enterprises. Therefore, prospective entrepreneurs entering a new market by starting a new business should take full advantage of the potential spillover benefits in regions with active financial capital, a more inclusive political environment, and better infrastructure to increase their future competitiveness. (3) Local governments can also use this study as a theoretical reference when formulating policies related to promotion or management in the field of the sharing economy. On the one hand, the government should continue to promote policy support for entrepreneurship and innovation, especially in small- and medium-sized cities. Micropolicies should be introduced as an important means to attract new enterprises and talent. At the same time, policy should realize the importance of balancing the development of various industries in a region; integrating government, enterprise, and talent in development; and providing precise and substantive assistance to enterprises and talent. On the other hand, Samila and Sorenson [65] observe that venture capital has become a catalyst for the commercialization of new products. Because the government wants to encourage new businesses to enter a region, it must recognize the importance of funding them. It is important to not only promote the healthy development of venture capital institutions in the region but also to attract startups through policies such as simplifying and optimizing the application for government support funds or expanding the target of fund support to reduce the sole dependence of startups on venture capital.

6. Conclusions, Limitations, and Future Research Directions

This study is part of a general study on the shared transportation industry. A new discussion of the formation of the shared transportation industry from the perspectives of system, economy, society, and geographic space can help us better understand this new business model and the logic driving the development of new ventures. Although existing patterns have demonstrated the importance of regional context, our study extends the traditional types of variables used in regional venture research. The regional environment is a complex ecosystem, and the detailed differentiation of influencing factors is a neglected and not fully studied topic.

By subdividing the types of variables, we believe that our research has clarified the potential impact of regional environmental factors on the formation of industries. In addition, the improvement of China's entrepreneurial ecological environment has promoted the growth of entrepreneurial activities.

The research in this study also has some limitations. First, due to data restrictions, we cannot include other variables that form determinants for startups, such as the unemployment rate and agglomeration effects. The business model of the sharing economy is an emerging product based on the rapid development of the internet, so there has only been a short development period for this industry. Some particularities of this industry that have not been explored may limit our interpretation of the analytical results. In future research, data information will be updated, and changes in some influencing factors of the shared transportation industry will be redetermined and detected under a more rational development environment. At the same time, we also suggest that attention should be given to the internal factors affecting the establishment of enterprises through interviews or questionnaires with founders. Moreover, the development of the whole industry should be considered from more perspectives.

Second, the study involved only one country, China. The special political environment in China makes government intervention in the market or industry more efficient, and the policies issued by the central government become a framework and a source of guidance used by local governments to formulate and implement specific policies. Therefore, whether the research results of this study apply to countries under other systems and with other political environment variables must also be considered. We also hope to verify this phenomenon through scholars in other countries.

Third, as shared transportation is the most rapidly developing industry and the most accepted by the market under the sharing economy, business success in shared transportation has popularized the concept of the sharing economy. However, other startups in the sharing economy, such as shared space, shared knowledge, and other industries, are catching up. The Chinese government has paid much more attention to the transportation-sharing industry. We cannot determine whether this industrial learning will affect our results when applied to other sharing industries. In the future, a full discussion of other sharing industries and even the sharing concept itself will be necessary.

Despite some limitations, this study presents one of the first studies to explore new enterprises in the sharing economy. We believe that our research provides a [66] visual result for scholars and managers. We also hope to arouse more discussions with policymakers and managers to further promote the healthy and sustainable development of this field.

Data Availability

No new data were created or analyzed in this study. Data sharing is not applicable to this article.

Conflicts of Interest

The authors declare that they have no conflicts of interest.

Acknowledgments

This paper was supported by the Scientific Research and Innovation Team Project of the Zhejiang Wanli University in 2020.

References

- [1] Y. Zhou, S. Park, Q. Wang, J. Z. Zhang, and A. Behl, "The survival of bike-sharing startups in China: an empirical analysis of the influencing factors," *Kybernetes*, 2022, In press.
- [2] J. Ge, H. Sun, and Y. Chen, "Technology entrepreneurship of large state-owned firms in emerging economies," *Journal of Global Information Management*, vol. 28, no. 4, pp. 120–134, 2020.
- [3] S. M. Cheng and H. Q. Li, "Spatially varying relationships of new firm formation in the United States," *Regional Studies*, vol. 45, no. 6, pp. 773–789, 2011.
- [4] A. Kangasharju, "Regional variations in firm formation: panel and cross-section data evidence from Finland," *Papers in Regional Science*, vol. 79, no. 4, pp. 355–373, 2005.
- [5] H. Okamuro and N. Kobayashi, "The impact of regional factors on the startup ratio in Japan," *Journal of Small Business Management*, vol. 44, no. 2, pp. 310–313, 2006.
- [6] Y. Zhou and S. Park, "The regional determinants of the new venture formation in China's car-sharing economy," *Sustainability*, vol. 13, no. 1, p. 74, 2020.
- [7] J. Knoben, R. Ponds, and F. van Oort, "Employment from new firm formation in The Netherlands: agglomeration economies and the knowledge spillover theory of entrepreneurship," *Entrepreneurship & Regional Development*, vol. 23, no. 3–4, pp. 135–157, 2011.
- [8] P. Bishop, "Knowledge diversity and entrepreneurship following an economic crisis: an empirical study of regional resilience in Great Britain," *Entrepreneurship & Regional Development*, vol. 31, no. 5–6, pp. 496–515, 2019.
- [9] C. D. Calá, "Sectoral and regional determinants of firm dynamics in developing countries: evidence for low-medium- and high-tech manufacturing in Argentina," *CEPAL Review*, vol. 124, pp. 121–142, 2018.
- [10] A. Colombelli and F. Quatraro, "New firm formation and regional knowledge production modes: Italian evidence," *Research Policy*, vol. 47, no. 1, pp. 139–157, 2018.
- [11] M. Li, S. J. Goetz, M. Partridge, and D. A. Fleming, "Location determinants of high-growth firms," *Entrepreneurship & Regional Development*, vol. 28, no. 1–2, pp. 97–125, 2016.
- [12] H. Qian, Z. J. Acs, and R. R. Stough, "Regional systems of entrepreneurship: the nexus of human capital, knowledge and new firm formation," *Journal of Economic Geography*, vol. 13, no. 4, pp. 559–587, 2013.
- [13] U. Shrivastava, L. Ofstein, and D. Golhar, "Direct and indirect effects of ICT infrastructure, skills, and use on entrepreneurship: a cross-country empirical investigation," *Journal of Global Information Management*, vol. 29, no. 6, pp. 1–25, 2021.
- [14] Gem, "Global report," 2020, <https://www.gemconsortium.org/report/gem-2019-2020-global-report>.
- [15] P. Johnson, "Differences in regional firm formation rates: a decomposition analysis," *Entrepreneurship: Theory and Practice*, vol. 28, no. 5, pp. 431–446, 2004.

- [16] F. Lasch, F. Robert, and F. Le Roy, "Regional determinants of ICT new firm formation," *Small Business Economics*, vol. 40, no. 3, pp. 671–686, 2013.
- [17] D. Baumgartner, M. Pütz, and I. Seidl, "What kind of entrepreneurship drives regional development in European non-core regions? a literature review on empirical entrepreneurship research," *European Planning Studies*, vol. 21, no. 8, pp. 1095–1127, 2013.
- [18] R. Sternberg, "Do EU regional policies favour regional entrepreneurship? empirical evidence from Spain and Germany," *European Planning Studies*, vol. 20, no. 4, pp. 583–608, 2012.
- [19] L. Trettin and F. Welter, "Challenges for spatially oriented entrepreneurship research," *Entrepreneurship & Regional Development*, vol. 23, no. 7-8, pp. 575–602, 2011.
- [20] C. Capozza, S. Salomone, and E. Somma, "Local industrial structure, agglomeration economies and the creation of innovative startups: evidence from the Italian case," *Entrepreneurship & Regional Development*, vol. 30, no. 7-8, pp. 749–775, 2018.
- [21] S. Cheng, "Business cycle, industrial composition, or regional advantage? A decomposition analysis of new firm formation in the United States," *The Annals of Regional Science*, vol. 47, no. 1, pp. 147–167, 2011.
- [22] M. S. Castaño, M. T. Méndez, and M. Á. Galindo, "The effect of social, cultural, and economic factors on entrepreneurship," *Journal of Business Research*, vol. 68, no. 7, pp. 1496–1500, 2015.
- [23] E. Norton and B. H. Tenenbaum, "Specialization versus diversification as a venture capital investment strategy," *Journal of Business Venturing*, vol. 8, no. 5, pp. 431–442, 1993.
- [24] R. Martin, C. Berndt, B. Klagge, and P. Sunley, "Spatial proximity effects and regional equity gaps in the venture capital market: evidence from Germany and the United Kingdom," *Environment & Planning A*, vol. 37, no. 7, pp. 1207–1231, 2005.
- [25] Y. Fu and S. H. Ng, "Local bias and performance of venture capital institutions: evidence from the Chinese venture capital market," *Journal of Asia Business Studies*, vol. 15, no. 1, pp. 174–197, 2021.
- [26] O. Sorenson and T. E. Stuart, "Syndication networks and the spatial distribution of venture capital investments," *American Journal of Sociology*, vol. 106, no. 6, pp. 1546–1588, 2001.
- [27] M. S. Granovetter, "The strength of weak ties," *American Journal of Sociology*, vol. 78, no. 6, pp. 1360–1380, 1973.
- [28] R. S. Burt, *Structural Holes: The Social Structure of Competition*, Harvard University Press, Cambridge, MA, USA, 2009.
- [29] R. Chen and Z. Qiu, "Dynamics of venture capital syndication: Perspective of information," 2019, <https://ssrn.com/abstract=3475874>.
- [30] C. Mason and R. Harrison, "Why 'business angels' say no: a case study of opportunities rejected by an informal investor syndicate," *International Small Business Journal*, vol. 14, no. 2, pp. 35–51, 1996.
- [31] J. J. Chrisman and W. E. McMullan, "A preliminary assessment of outsider assistance as a knowledge resource: the longer-term impact of new venture counseling," *Entrepreneurship: Theory and Practice*, vol. 24, no. 3, pp. 37–53, 2000.
- [32] J. J. Chrisman, E. McMullan, and J. Hall, "The influence of guided preparation on the long-term performance of new ventures," *Journal of Business Venturing*, vol. 20, no. 6, pp. 769–791, 2005.
- [33] C. Shu, M. Gu, C. Liu, and D. B. Audretsch, "The role of the government in the knowledge spillover theory of entrepreneurship: a firm-level analysis," *IEEE Transactions on Engineering Management*, pp. 1–15, 2020.
- [34] D. J. Storey, "Entrepreneurship, small and medium sized enterprises and public policies," in *Handbook of Entrepreneurship Research*, Springer, Boston, MA, USA, 2003.
- [35] D. B. Audretsch, D. Heger, and T. Veith, "Infrastructure and entrepreneurship," *Small Business Economics*, vol. 44, no. 2, pp. 219–230, 2015.
- [36] D. L. Bennett, "Infrastructure investments and entrepreneurial dynamism in the US," *Journal of Business Venturing*, vol. 34, no. 5, Article ID 105907, 2019.
- [37] S. Zhao, Y. Jiang, and S. Wang, "Innovation stages, knowledge spillover, and green economy development: moderating role of absorptive capacity and environmental regulation," *Environmental Science and Pollution Research*, vol. 26, no. 24, pp. 25312–25325, 2019.
- [38] P. Davidsson, "Entrepreneurial opportunities and the entrepreneurship nexus: a re-conceptualization," *Journal of Business Venturing*, vol. 30, no. 5, pp. 674–695, 2015.
- [39] M. J. Moseley, *Growth Centres in Spatial Planning*, Pergamon Urban and Regional Planning, Elsevier, Hoboken, NJ, USA, 2013.
- [40] F. Perroux, "Economic space: theory and applications," *Quarterly Journal of Economics*, vol. 64, no. 1, pp. 89–104, 1950.
- [41] C. Richter, S. Kraus, and P. Syrjä, "The smart city as an opportunity for entrepreneurship," *International Journal of Entrepreneurial Venturing*, vol. 7, no. 3, pp. 211–226, 2015.
- [42] iiMedia Research, *China Shared Bikes Development Status Research*, iiMedia Research, Guangzhou, China, 2018.
- [43] C. He and S. Zhu, "What facilitates new firm formation in China?" in *Evolutionary Economic Geography in China*, Springer, Berlin, Germany, 2019.
- [44] J. Koo and K. R. Cho, "New firm formation and industry clusters: a case of the drugs industry in the US," *Growth and Change*, vol. 42, no. 2, pp. 179–199, 2011.
- [45] N. Bosma, A. Van Stel, and K. Suddle, "The geography of new firm formation: evidence from independent startups and new subsidiaries in The Netherlands," *International Entrepreneurship and Management Journal*, vol. 4, no. 2, pp. 129–146, 2008.
- [46] Q. H. Vuong, "Likelihood ratio tests for model selection and non-nested hypotheses," *Econometrica*, vol. 57, no. 2, pp. 307–333, 1989.
- [47] K. B. Campbell and C. Brakewood, "Sharing riders: how bikesharing impacts bus ridership in New York city," *Transportation Research Part A: Policy and Practice*, vol. 100, pp. 264–282, 2017.
- [48] Y. Jin, Q. Zhang, L. Shan, and S. P. Li, "Characteristics of venture capital network and its correlation with regional economy: evidence from China," *PLoS One*, vol. 10, no. 9, Article ID e0137172, 2015.
- [49] U. Von Burg and M. Kenney, "Venture capital and the birth of the local area networking industry," *Research Policy*, vol. 29, no. 9, pp. 1135–1155, 2000.
- [50] D. R. Hammond, "Policy entrepreneurship in China's response to urban poverty," *Policy Studies Journal*, vol. 41, no. 1, pp. 119–146, 2013.
- [51] C. G. Reddick, Y. Zheng, and T. Liu, "Roles of government in regulating the sharing economy: a case study of bike sharing in China," *Information Polity*, vol. 25, no. 2, pp. 219–235, 2020.
- [52] B. Zhang, G. Peng, F. Xing, and S. Chen, "Mobile applications in China's smart cities: state-of-the-art and lessons learned,"

- Journal of Global Information Management*, vol. 29, no. 6, pp. 1–18, 2021.
- [53] B. Choudhuri, P. R. Srivastava, S. Gupta, A. Kumar, and S. Bag, “Determinants of smart digital infrastructure diffusion for urban public services,” *Journal of Global Information Management*, vol. 29, no. 6, pp. 1–27, 2021.
- [54] M. Yao, D. Ye, G. Yang, H. Shi, and X. Zheng, “Are entrepreneurial capabilities and prior knowledge the silver bullet for the generation of new digital venture ideas in a digital context?” *Journal of Global Information Management*, vol. 29, no. 6, pp. 1–17, 2021.
- [55] A. Almomani, A. Al-Nawasrah, W. Alomoush, M. Al-Abweh, A. Alrosan, and B. B. Gupta, “Information management and IoT technology for safety and security of smart home and farm systems,” *Journal of Global Information Management*, vol. 29, no. 6, pp. 1–23, 2021.
- [56] C. H. Huang, T. C. Chou, and S. H. Wu, “Towards convergence of ai and IoT for smart policing: a case of a mobile edge computing-based context-aware system,” *Journal of Global Information Management*, vol. 29, no. 6, pp. 1–21, 2021.
- [57] G. Peng, P. D. Clough, A. Madden, F. Xing, and B. Zhang, “Investigating the usage of IoT-based smart parking services in the borough of westminster,” *Journal of Global Information Management*, vol. 29, no. 6, pp. 1–19, 2021.
- [58] L. C. Cheng, H. W. Hu, and C. C. Wu, “Spammer group detection using machine learning technology for observation of new spammer behavioral features,” *Journal of Global Information Management*, vol. 29, no. 2, pp. 61–76, 2021.
- [59] P. R. Srivastava and P. Eachempati, “Intelligent employee retention system for attrition rate analysis and churn prediction: an ensemble machine learning and multi-criteria decision-making approach,” *Journal of Global Information Management*, vol. 29, no. 6, pp. 1–29, 2021.
- [60] P. Du and H. Shu, “Exploration of financial market Credit scoring and risk management and prediction using deep learning and bionic algorithm,” *Journal of Global Information Management*, vol. 30, no. 9, pp. 1–29, 2022.
- [61] H. Hou, K. Tang, X. Liu, and Y. Zhou, “Application of artificial intelligence technology optimized by deep learning to rural financial development and rural governance,” *Journal of Global Information Management*, vol. 30, no. 7, pp. 1–23, 2022.
- [62] Y. Wu, D. Zhu, Z. Liu, and X. Li, “An improved BPNN algorithm based on deep learning technology to analyze the market risks of A+H shares,” *Journal of Global Information Management*, vol. 30, no. 7, pp. 1–23, 2022.
- [63] P. Lombardi, S. Giordano, H. Farouh, and W. Yousef, “Modelling the smart city performance,” *Innovation: The European Journal of Social Science Research*, vol. 25, no. 2, pp. 137–149, 2012.
- [64] E. Tranos and D. Gertner, “Smart networked cities?” *Innovation: The European Journal of Social Science Research*, vol. 25, no. 2, pp. 175–190, 2012.
- [65] S. Samila and O. Sorenson, “Venture capital as a catalyst to commercialization,” *Research Policy*, vol. 39, no. 10, pp. 1348–1360, 2010.
- [66] W. H. Hung, C. L. Tseng, F. K. Chang, and C. F. Ho, “Effects of utilitarian and hedonic emotion on the use of online banking services,” *Journal of Global Information Management*, vol. 29, no. 6, pp. 1–20, 2021.

Research Article

Finite-Element Analysis of Vertical Displacement of Laminated Rubber Bearing under Earthquake Action for Disaster Resilience of the Smart City

Denglian Yang  and Yanli Liu 

Yunnan Science & Technology Research Institute of Highway, Kunming 650000, Yunnan, China

Correspondence should be addressed to Yanli Liu; 181911805@nuaa.edu.cn

Received 7 January 2022; Revised 27 January 2022; Accepted 31 January 2022; Published 30 April 2022

Academic Editor: Sang-Bing Tsai

Copyright © 2022 Denglian Yang and Yanli Liu. This is an open access article distributed under the Creative Commons Attribution License, which permits unrestricted use, distribution, and reproduction in any medium, provided the original work is properly cited.

With the construction and development of smart cities, higher requirements have been put forward for the prediction and control of major natural disasters. For the prevention of earthquake disasters in super high-rise buildings, the rubber bearings of high-rise seismic isolation structures may have the risk of tensile damage in high-intensity areas, which has always been an urgent problem to be solved. In this paper, a unidirectional horizontal compression-shear experiment with 400% large deformation was conducted on the laminated rubber bearing (LNR500), and the relationship curve of vertical displacement with horizontal displacement of the bearing was obtained. According to the experimental data, an ideal elastic-plastic principal structure model was selected for the steel and a Yeoh principal structure model was selected for the rubber material, and the finite element analysis was carried out for the bearing. The time course curves of displacement, velocity and acceleration of the vertical and horizontal deformation of the laminated rubber bearing under the earthquake were obtained.

1. Introduction

The commonly used form of seismic isolation in the foundation isolation can be divided into rubber bearing, friction pendulum isolation bearing and reset spring and plane slide plate parallel system, the first two are more common [1]. Laminated rubber bearing is proposed by Kelly [2] in 1978, the bearing is formed by a layer of steel plate and a layer of rubber staggered arrangement. The vertical ultimate tensile stress of the laminated rubber bearing is much smaller than the vertical ultimate compressive stress, and the rubber bearing of the high-rise seismic isolation structure may have the risk of tensile damage and overturning in the high-intensity zone. For this reason, there are many designs and researches on the isolation tensile device [3, 4], but the effect of bearing deformation on the use of tensile devices is less considered. Especially the rubber of the bearings is mostly assumed to be incompressible material, and the vertical deformation is almost ignored, and the increase of

vertical deformation displacement of the bearing will reduce the spacing between the upper and lower flange plates, which may lead to the device failure or even damage if the tensile device does not leave enough working clearance. So, the vertical deformation of rubber bearing should be taken into consideration.

Since the 1970s, laminated rubber bearings began to be widely used, so a large number of experts and scholars conducted in-depth studies on the modeling of mechanical properties of laminated rubber bearings, large deformation cyclic response and simulation of deformation characteristics under seismic action. More classical early models such as Koh et al. [5, 6] proposed a two-degree-of-freedom model considering fluid deformation and shear deformation for simulating the effects of vertical loads on the mechanical properties of laminated rubber bearings, which assumed the contact surface as a spring model and gave insufficient consideration to the effects of damping.

The currently used intrinsic model of rubber is based on two theories [7]: one is based on the mechanics of continuous media and the other is based on a thermodynamic statistical approach. The Mooney-Rivlin intrinsic model [8] retains only the linear part and it is the simplest hyperelastic model. The Neo-Hookean and Yeoh intrinsic model [9, 10] in general it is seen as an extension of the previous form and in many cases it can be closer to the experimental data than the Mooney-Rivlin form. However, the drawback is the same, they are both linear functions and cannot describe the nonlinear behavior of rubber materials. However, the Yeoh instantonal model shows the softening phase of the rubber and can perfectly express the large deformation, so the Yeoh instantonal model is more commonly used in large deformation simulation. Ogden instantonal model [11], Ogden strain energy function with three main elongations as variables, the order N can be taken from 1 to 6, the order is too small accuracy is not enough, too large strain energy function and practical value is not much, engineering is generally used. The Ogden $N=3$ form is commonly used in engineering. The above principal structure models are widely used, such as: Wang et al. [12] improved the bi-directional coupling restoring force model for lead-core laminated rubber bearing, and used DABIS to compare the unidirectional and bi-directional seismic response of the base isolation structure of lead-core laminated rubber bearing, and the results concluded that the influence of bi-directional seismic action should be considered when determining the maximum displacement of the bearing. Ohsaki et al. [13] modeled the laminated rubber bearing with ABAQUS finite element analysis software and discretized it into hexahedral solid units, in which the Ogden hyperelastic principal model of natural rubber was selected, and simulated the deformation characteristics of the laminated rubber bearing under static and seismic effects. The Yeoh intrinsic model used in this paper is based on the method of continuous medium mechanics.

2. Laminated Rubber Bearing Mechanical Performance Test Research

The test includes two parts: the first part is the material property test of rubber and steel. In the material property test, the steel plate material is Q235 steel, the steel mainly carries out uniaxial tensile test; the rubber material carries out uniaxial tensile and pure shear test to provide the basis for the material parameters in ABAQUS; the second part is the unidirectional horizontal compression shear test of the laminated rubber bearing, which is compared and analyzed with the results of the finite element simulation analysis afterwards to ensure the reliability of the simulation data.

The laminated rubber bearing consists of flange plate, rubber layer and steel plate layer, the force subject is rubber layer and steel plate layer, flange plate mainly plays the role of connection and force transfer. Because the steel and rubber in the laminated rubber bearing is easier to deformation, so relatively speaking, the deformation of the flange plate is negligible, also has a large number of bearing simulation papers will be the flange plate as a nondeformable rigid body.

2.1. Pure Shear Test of Rubber. The density of the bearing rubber was 1.05 g/cm^3 and the initial bulk modulus K_0 was 400 MPa, and the pure shear test which is shown in Figure 1 and uniaxial tensile test of the rubber were carried out in this paper. The shear test of rubber in this paper was carried out on a SANS universal material testing machine, and the gripper was loaded slowly at a speed of 50 mm/min until the specimen was damaged by loading, and the whole deformation process was recorded, as shown in Figures 2 and 3.

In this test, six rubber specimens were used, and the data were taken as the average of six tests. The rubber shear stress-strain curve is plotted in Figure 4. From the data, it can be seen that the stress-strain curve is close to a straight line when the horizontal strain is less than 250%; when the horizontal strain is greater than 250%, the rubber has an obvious period of stiffness strengthening; and when the horizontal strain reaches 450%, the specimens are damaged. Because simple shear can be seen as pure shear plus rotation [14], therefore, at strains greater than 250%, the principal stress of the shear ellipse within the rubber is skewed, and the rubber is subjected to shear in addition to tensile, so that the apparent strength increase can be seen only at a later stage.

2.2. Rubber Uniaxial Tensile Test. The tensile test of rubber in this paper was carried out on SANS universal material testing machine, as shown in Figure 5. The rubber tensile specimens should be dumbbell-shaped as shown in Figure 6. The number of specimens is 3. The width of the narrow part are 6.01 mm; the thickness are 2.35 mm, 2.26 mm, 2.28 mm; the length is 33 mm; the lead gauge clamping spacing is $l_0 = 25 \text{ mm}$.

The test results were taken as the average of three test results. The rubber tensile stress-strain curve is plotted in Figure 7. From the test, it can be seen that the ultimate tensile strength of the rubber is 21.84 MPa and the ultimate tensile strain is 738%; the rubber monotonic tensile curve is nonlinear, its elastic modulus is variable, the initial elastic modulus is about 1 MPa, and the later strength is obviously higher than the earlier one.

2.3. Uniaxial Tensile Test of Steel. The instrument used in this test is an electronic universal testing machine, and the strain rate during yielding of the metal material should be determined between 0.00025/s and 0.0025/s. Plate thickness, tensile area, elongation gauge clamping spacing. Width of both ends of the specimen, width of the narrow part of the specimen. The shape of the test piece and test photo are shown in Figures 8 and 9. Based on the dimensional information, the loading rate can be calculated as follows:

$$\begin{aligned} u &= l \varepsilon_e \\ &= 120 \times 0.00025 \sim 0.0025 \times 60 \\ &= \frac{1.8 \sim 18 \text{ mm}}{\text{min}} \end{aligned} \quad (1)$$

Therefore, the test loading rate of 2 mm/min. test temperature for the room temperature, the number of test pieces

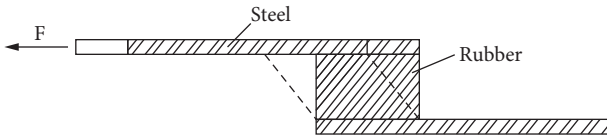


FIGURE 1: Pure shear test rubber specimen force mode.



FIGURE 2: SANS universal material testing machine.

a total of 3. Steel and laminated rubber bearing steel plate layer is the same, are Q235 steel.

The results were taken as the average of three tests and the results are shown in the Table 1.

2.4. Bearing Horizontal Compression Shear Test. The test object is a 500 mm diameter laminated rubber bearing (LNR500), and the main monitoring data are, under the compression shear state, the lateral displacement, vertical displacement and horizontal force of the bearing. The variables controlled by the tester are horizontal displacement and vertical pressure. In the test of 400% limit shear, bearing top surface pressure is 12 MPa and the number of test bearing is 3. The test machine for this experiment is 1500 t electro-hydraulic servo compression shear test machine (FJS1W5001) as shown in Figure 10. When doing 400% large deformation, 4 displacement gauges were evenly arranged around the bearing, and the displacement gauges were adsorbed under the upper flange plate, which could move with the flange plate movement, and the displacement gauges were kept



FIGURE 3: Rubber test piece and steel plate connection diagram.

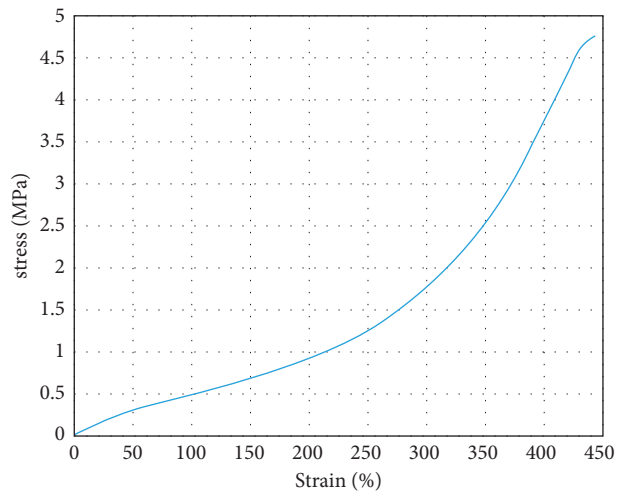
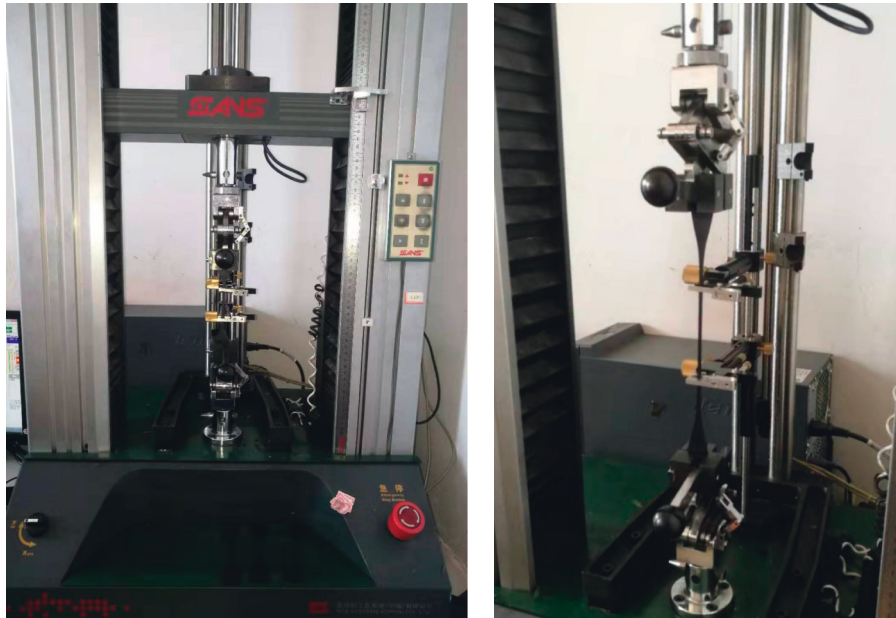


FIGURE 4: Graph of rubber shear stress-strain curve.

perpendicular to the lower flange plate when moving, as shown in Figures 11–13.

The data of bearing reaction force and bearing transverse displacement can be read from the monitoring data inside the testing machine, and the bearing vertical displacement is read from the monitoring data of displacement meter, and the data is collected once every 0.02 s interval. The test adopts the way of controlled displacement, the maximum displacement reaches 377 mm. the data is taken from the average of 3 bearing test data.



(a) (b)

FIGURE 5: Graph of rubber tensile test.

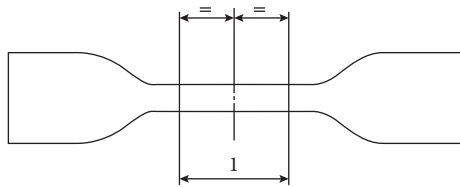


FIGURE 6: Dumbbell-shaped specimen shape.

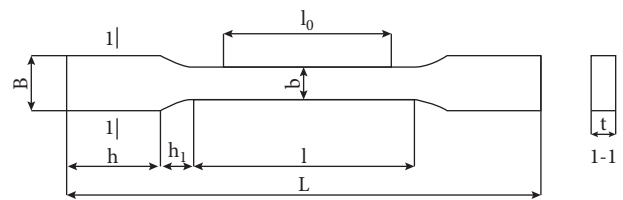


FIGURE 8: Diagram of the plate strip head specimen.

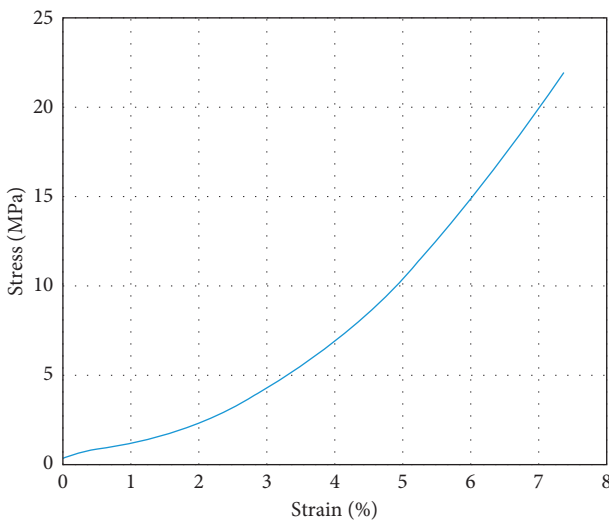


FIGURE 7: Graph of rubber tensile stress-strain curve.

In the graph of the relationship between horizontal displacement and vertical displacement, it can be observed that when the horizontal displacement is 0, there is a section of displacement vertical change section, this section is the beginning of the test, the static pressure

stage of the rubber bearing, this stage of the press slowly apply pressure until the bearing upper pressure reaches 12 MPa, then keep the pressure onstant and shear the bearing. In the static pressure stage, the height of the bearing vertical drop is 2.89 mm on average, and with the increase of lateral displacement, the pressed area is reduced from a whole circular surface to a shuttle-shaped area.

If we set the lateral displacement as X and the bearing diameter as R , we can deduce the formula of shuttle area as follows:

$$S = 2R^2 \arccos\left(\frac{x}{2R}\right) - x\sqrt{R^2 - \frac{x^2}{4}} \quad (2)$$

As can be seen from Figures 14 and 15, after the horizontal displacement reaches the maximum, the vertical drop height of the bearing is 9.55 mm, the thickness of the rubber layer is 92.96 mm, and the drop percentage is 10.27%, which is negligible compared with the whole floor, but this displacement is not negligible compared with the tensile device set in the seismic isolation layer. Because as the displacement increases, the vertical load remains unchanged, but the compressed area becomes smaller, as shown in the Figure 16. So accordingly, the



FIGURE 9: Steel tensile test.

TABLE 1: Steel tensile test data sheet.

Specimen number	Yield strength (MPa)	Tensile strength (MPa)	Elongation (%)	Elastic modulus (MPa)
1	288.1	458.2	25.3	201400
2	281.7	431.6	29.8	198300
3	302.5	439.4	30.0	196000
Average value	290.8	443.1	28.4	198567



FIGURE 10: Field test setup diagram.

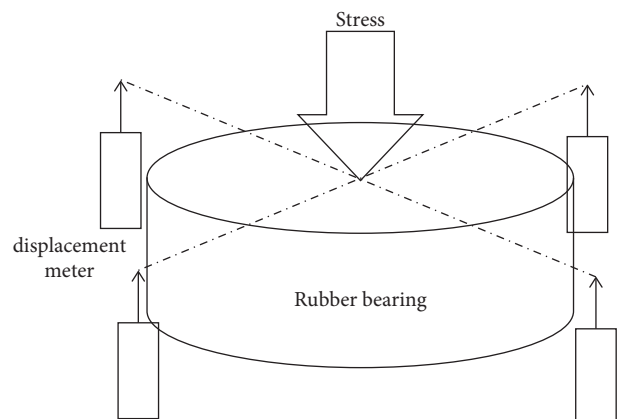


FIGURE 11: Schematic diagram of the relative position of the displacement meter and the bearing.

vertical stiffness will be reduced, so the vertical displacement is produced. Therefore, the rubber cannot be simply regarded as incompressible material in the finite element simulation.

The vertical pressure is 12 MPa, then the upper pressure can be calculated as 2355 kN. Converting the test results into the relationship between displacement and stiffness, then the relationship curve are plotted in Figures 17 and 18.

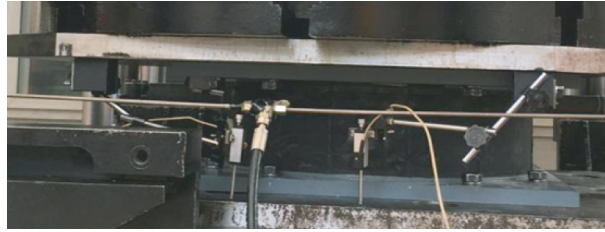


FIGURE 12: Schematic diagram of the installation of the bearing and displacement meter.

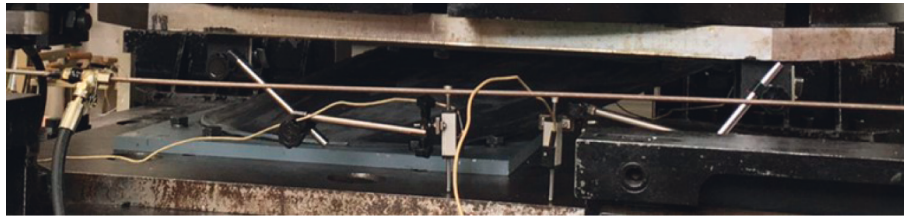


FIGURE 13: 400% ultimate shear bearing deformation diagram.

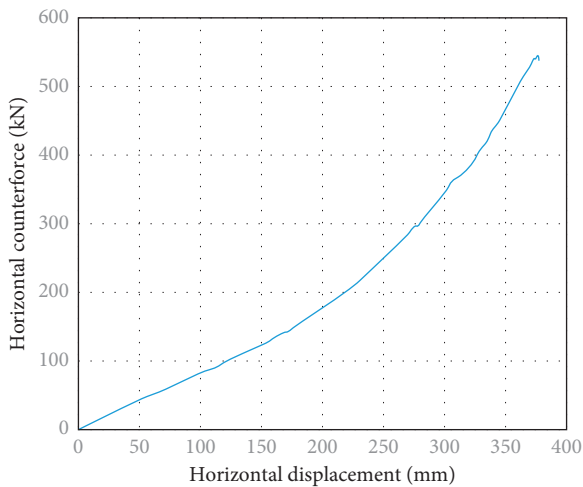


FIGURE 14: Relationship between horizontal reaction force and horizontal displacement of LNR500.

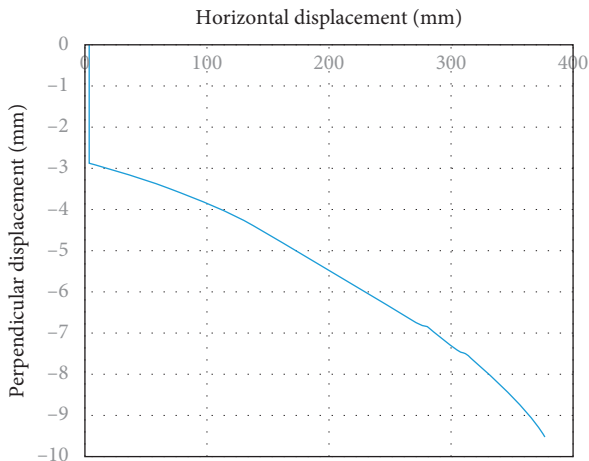


FIGURE 15: Relationship between vertical displacement and horizontal displacement of LNR500.

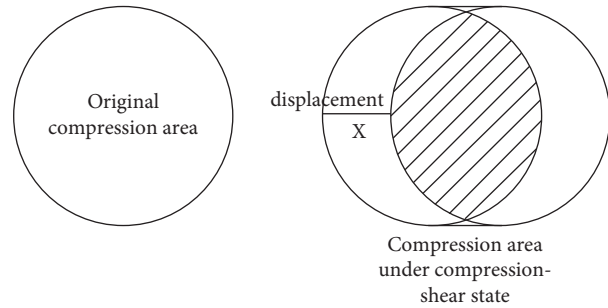


FIGURE 16: Bearing compression shear state under pressure area reduction.

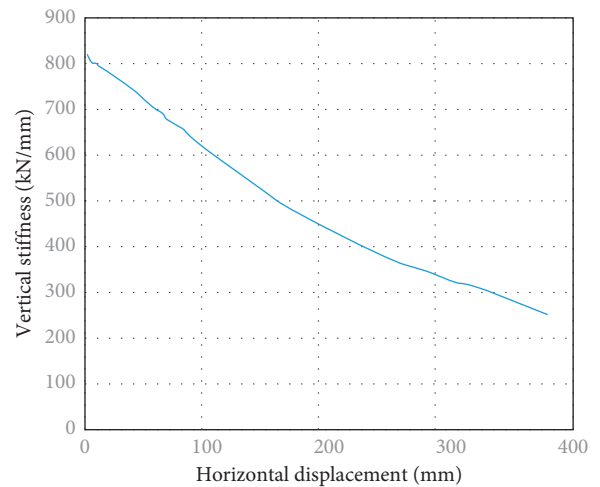


FIGURE 17: Relationship between vertical stiffness and horizontal displacement.

The initial vertical stiffness of the laminated rubber bearing LNR500 is 814.88 kN/mm, with the increase of horizontal displacement, the vertical stiffness decreases, when the horizontal deformation reaches 100%, the vertical

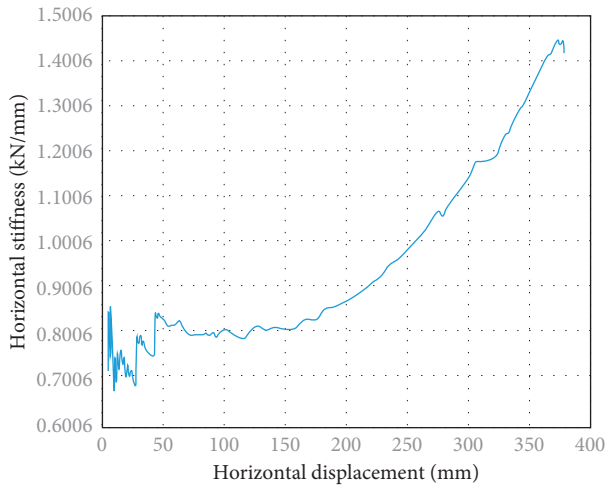


FIGURE 18: The relationship between horizontal stiffness and horizontal displacement.

stiffness is 620.83 kN/mm, down 23.74%; when it reaches 200%, the vertical stiffness is 449.72 kN/mm, down 44.74%; when it reaches 300%, the vertical stiffness 342.46 kN/mm, a decrease of 57.97%; when reaching 400%, the vertical stiffness is 246.48 kN/mm, a decrease of 69.75%. It can be seen that the vertical stiffness decreases faster, but its magnitude decreases with the increase of horizontal displacement, and the rate of decline in the later period is slower than that in the earlier period.

Since the horizontal reaction force data read by the press shear is more shaky during the experiment, the relationship curve between horizontal stiffness and horizontal displacement also fluctuates somewhat. The initial horizontal stiffness is about 0.8 kN/mm; when the deformation reaches between 100% and 200%, the horizontal stiffness changes slowly and even has a decreasing trend, the lowest is about 0.79 kN/mm; when the horizontal displacement reaches 377 mm, that is, when 400% limit shear displacement is reached, the horizontal stiffness is the largest, reaching 1.4 kN/mm.

3. Bearing Finite Element Static Simulation

3.1. Bearing Finite Element Modeling. The bearing studied in this paper is a lead-free core laminated rubber bearing (LNR500). The thickness of each layer of steel plate is 3 mm, 15 layers in total; and the thickness of each layer of rubber is 5.81 mm, 16 layers in total, as shown in Figure 19. The middle of this bearing is hollow, the aperture is 80 mm. there is a thin layer of rubber around the bearing as a protective layer, because it does not participate in the force analysis, the flange plate mainly plays the role of connection and force transfer, compared with the rubber and steel plate, its deformation is negligible, so the simulation are discarded. The contact surface of the rubber layer and steel plate layer of the bearing model is chosen to bind the connection as shown in Figure 20.

This laminated rubber bearing is made of Q235 steel with an elastic modulus of $E = 198567$ MPa, Poisson's ratio

$\mu = 0.25$, yield strength = 290.8 MPa, tensile strength = 443.1 MPa, and elongation $\delta = 28.4\%$. The ideal elastic-plastic intrinsic model is chosen for the simulation of steel in this paper as shown in Table 2.

In this paper, the Yeoh intrinsic structure model is chosen for the rubber material. The Yeoh model parameters were obtained from the experimental results. Although the usual value is negative because it mainly describes the state of rubber in the softening stage, the softening of rubber in this paper is not obvious enough, so it is positive. Parameter settings are shown in Table 3. The density of rubber is 1.05 g/cm³.

According to the test process data of 400% ultimate shear, the upper pressure should be 12.06 MPa. U2 that is, the Y-direction displacement is 377 mm.

4. Analysis Results and Comparison

Observation of the resultant stress clouds reveals that:

- (1) As can be seen from Figure 21, initially in the pure pressure state, the vertical displacement of all parts of the bearing is 0. All units in the bearing are in compression, and the relative displacement of the upper unit of the bearing is the largest, 2.89 mm.
- (2) As can be seen from Figure 22, when the horizontal displacement reaches 75 mm (when the horizontal shear reaches 81.5%), the left lower part of the bearing has a more obvious unit with positive vertical displacement, at this time the bearing should be in local tension, and after reaching 150%, the bearing is in tension very obviously.
- (3) As can be seen from Figure 23, when the 400% ultimate compression shear state is finally reached, the number of units with positive vertical displacement in the left half of the bearing increases significantly, and the tensile area inside the bearing is larger at this time.

In the previous section, it was also mentioned that there is local tension inside the bearing in compression shear state, which is partly responsible for the increase in horizontal stiffness of the bearing, and this resultant diagram also corresponds to this statement. The stress cloud diagram of the middle layer unit of the bearing is as shown in Figures 24–29. There is a relatively obvious stress concentration in the middle where there is a hole, from the diagram it is also obvious to observe the location of the middle compressive zone, which is a shuttle-shaped area. S11, S22, S33 are positive values of tensile stress, from the diagram it is also obvious to observe the local tensile situation.

The data monitored in the test are the horizontal displacement of the upper part of the bearing, the horizontal reaction force and the vertical displacement of the height drop of the bearing. In order to make the simulation results correspond to them, in the course output, the horizontal displacement (Y direction), horizontal reaction force (Y direction) and vertical displacement (Z direction) of the upper surface of the bearing are selected to be output. After

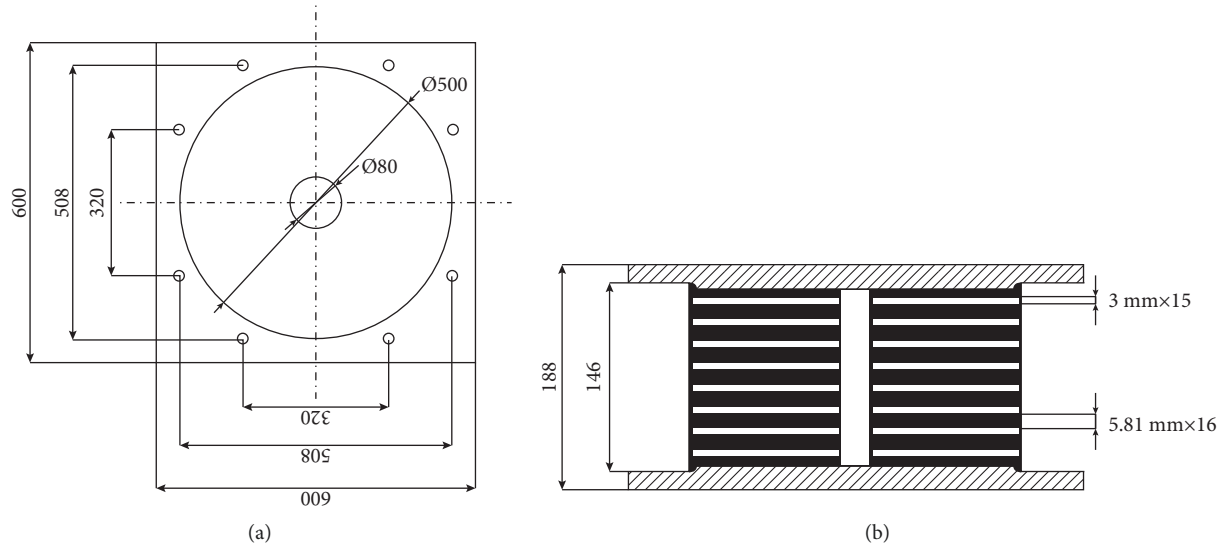


FIGURE 19: Dimensional drawing of LNR500.

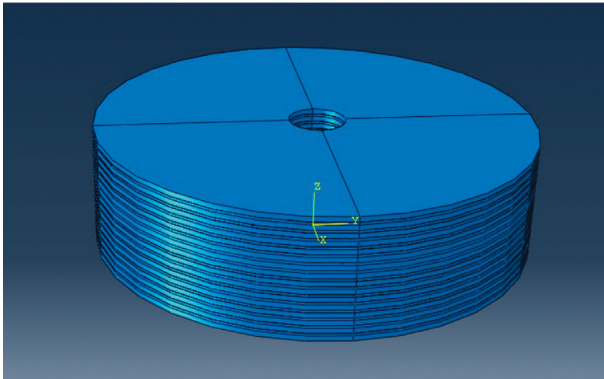


FIGURE 20: Geometric model of LNR500 in ABAQUS.

TABLE 2: Relationship between stress and plastic strain in steel.

Real stress (MPa)	Plastic strain
291	0
443.1	1

TABLE 3: Table of parameters of the Yeoh model for rubber materials.

C10	C20	C30	D1	D2	D3
0.23	0.0013	0.000176	0.00504	0.005	0.000005

processing the obtained simulation data, the following curve is obtained. Compare the simulation result with the test result data curve.

The relationship curves of horizontal reaction force and horizontal displacement are in good agreement. Simulation results of vertical displacement: at the initial compression stage, the test data is 2.89 mm and the simulation data is 2.90 mm; when the lateral displacement reaches 377 mm, the test data is 9.54 mm and the simulation data is 9.81 mm; the maximum error of the intermediate data is 8.91%, not more

than 10%, and the vertical displacement-horizontal displacement relationship curve matches well. In the test, when the press shear pushes the upper part of the bearing to produce horizontal displacement, the pressure exerted on the upper part of the bearing cannot be kept completely consistent, so the error within 10% is within the allowable range. Then the test data derived from the simulation is further converted into the relationship between stiffness and displacement, and the comparison is as shown in Figures 30–33.

The finite element simulation shows the characteristics of the change of stiffness of the rubber bearing in three different stages. The starting bearing stiffness is low, 0.7 kN/mm. In the actual project, the equivalent horizontal stiffness is taken as the corresponding shear stiffness at 100% deformation, 0.81 kN/mm. In the middle deformation, there is a softening stage, and its stiffness change has a plateau period. The horizontal stiffness is 1.4 kN/mm when 400% ultimate deformation is reached.

The change curve of vertical stiffness is more linear compared with horizontal stiffness, and the initial vertical stiffness and the vertical stiffness at 400% are basically consistent with the test results. In the middle deformation, there is a slight difference due to the relationship of the error of the test itself and the influence of the simulation error, but the error at the maximum error between the simulation data and the test data in this paper is 9.09%, not more than 10%, and it is still considered to be in good agreement.

5. Bearing Finite Element Dynamic Simulation

5.1. Finite Element Simulation of the Bearing under Seismic Action. The structure chosen in this paper is an asymmetric L-shaped structure, and the structural form of this project is determined to be cast-in-place concrete frame structure. The horizontal displacement of the bearing is generally not more than 250% of the thickness of the bearing rubber layer for a building with few floors. Within this range, the calculation

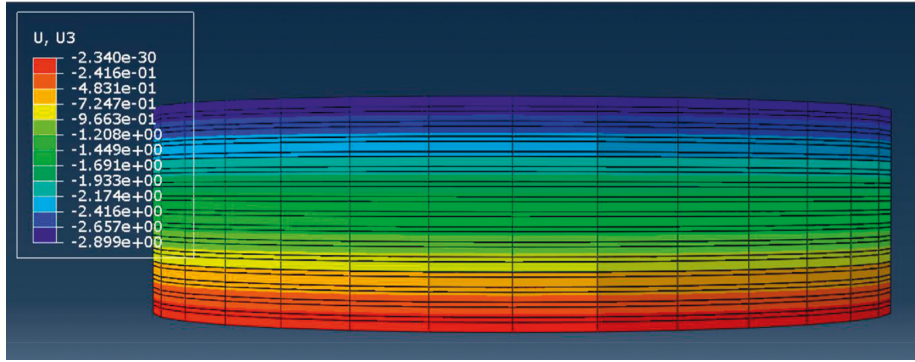


FIGURE 21: The vertical displacement cloud of the bearing under pure pressure.

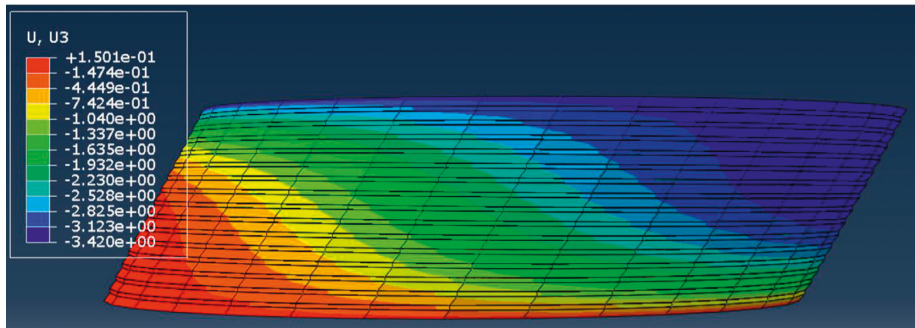


FIGURE 22: Vertical displacement cloud of the bearing when the horizontal displacement is 75 mm.

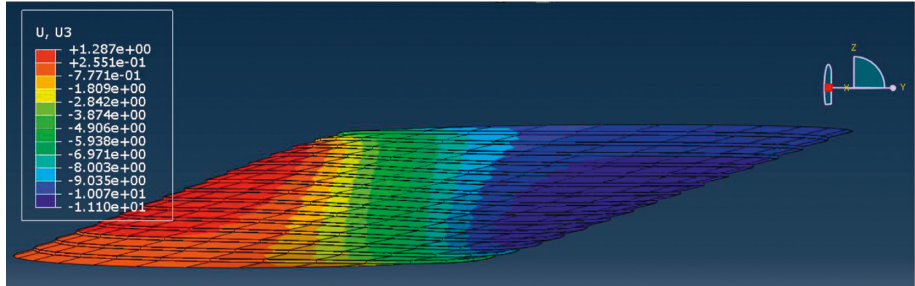


FIGURE 23: Vertical displacement cloud of the bearing under 400% ultimate compression shear.

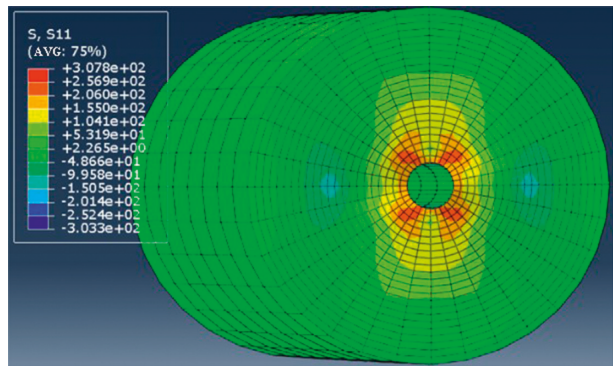


FIGURE 24: Stress cloud of middle layer S11 in 400% compression shear.

errors of both ETABS and ABAQUS software are relatively small and can be used simultaneously. The number of upper floors is 4, with a seismic isolation layer underneath and no

designed basement. The height of the building structure is 15.6 m and the width is 28.1 m. The building structure is shown in Figure 34.

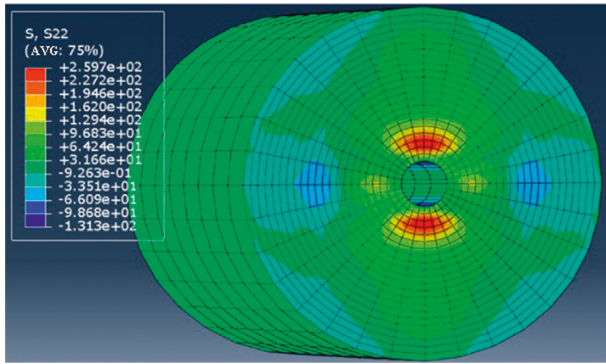


FIGURE 25: Stress cloud of middle layer S22 in 400% compression shear.

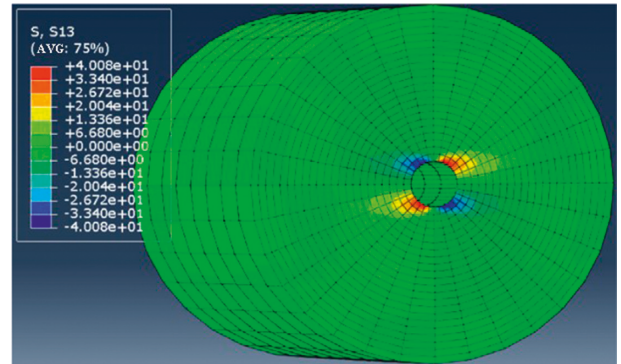


FIGURE 28: Stress cloud of middle layer S13 in 400% compression shear condition.

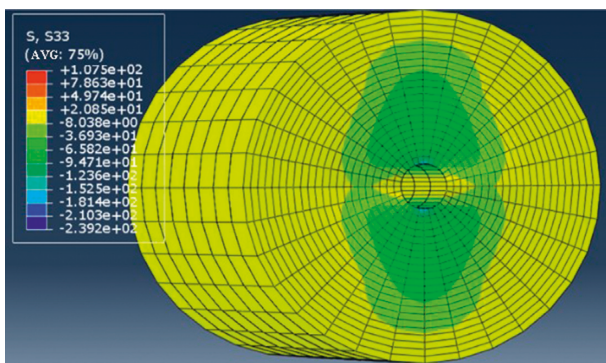


FIGURE 26: Stress cloud of intermediate layer S33 in 400% compression shear condition.

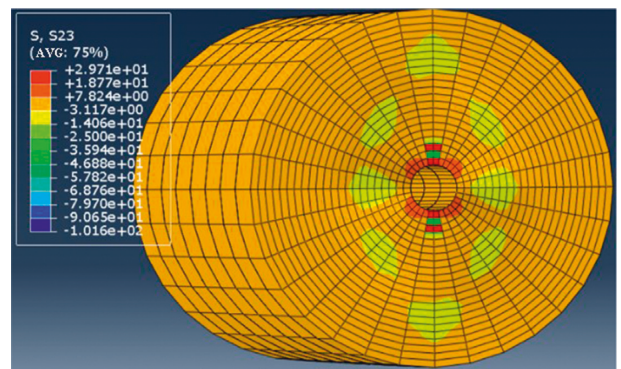


FIGURE 29: Stress cloud of intermediate layer S23 in 400% compression shear condition.

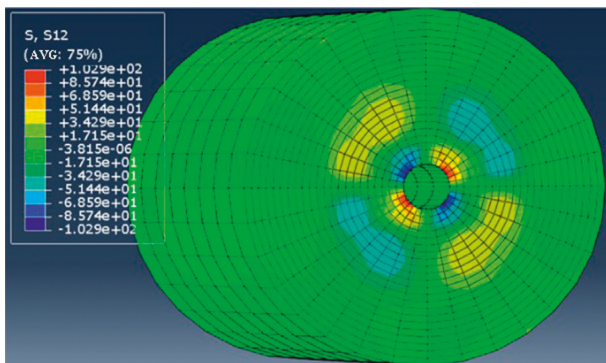


FIGURE 27: Stress cloud of intermediate layer S12 in 400% compression shear condition.

In the engineering design, two artificial waves and five natural waves are generally selected for seismic waves, for a total of seven waves. The specific information of the selected seismic waves is in Tables 4 and 5. The seismic waves are shown in Figures 35 and 36. The side slope amplification factor is 1.1. Except for REN1 and REN2, which are artificial waves, the other five entries are all natural waves.

The seismic waves information is input into ETABS by defining the time course function.

The following two guidelines need to be followed for the seismic isolation design [15]: to take the expectation of a moderate earthquake at the site where the structure is

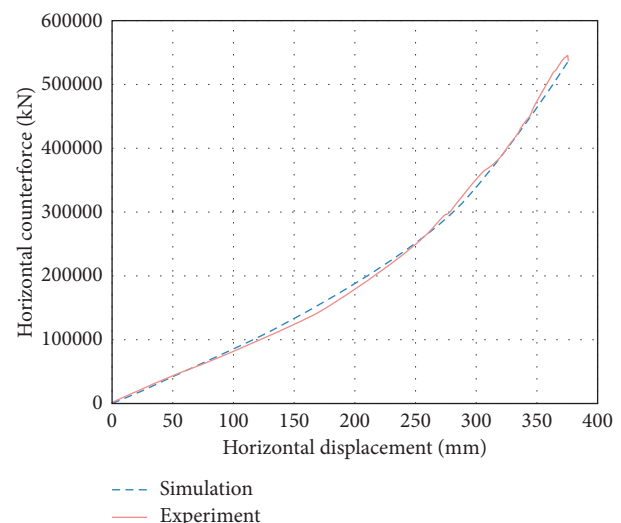


FIGURE 30: Comparison of horizontal reaction force—horizontal displacement relationship curve.

located during its lifetime as the basis for design; to take the most severe earthquake that may occur at the site as a test of structural safety, and to better study the deformation characteristics of the bearings when tensile stresses occur in

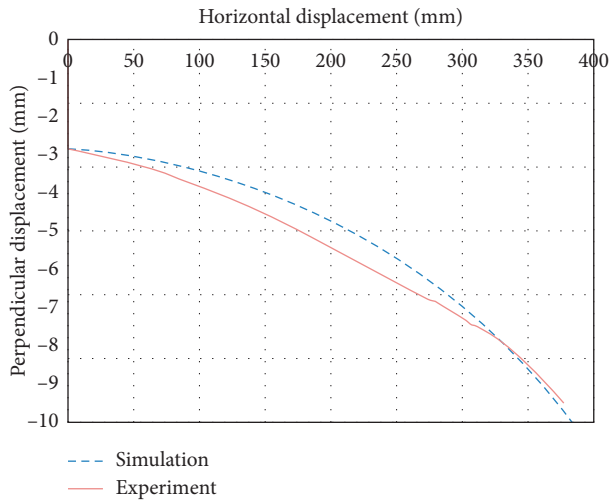


FIGURE 31: Comparison of vertical displacement-horizontal displacement relationship curve.

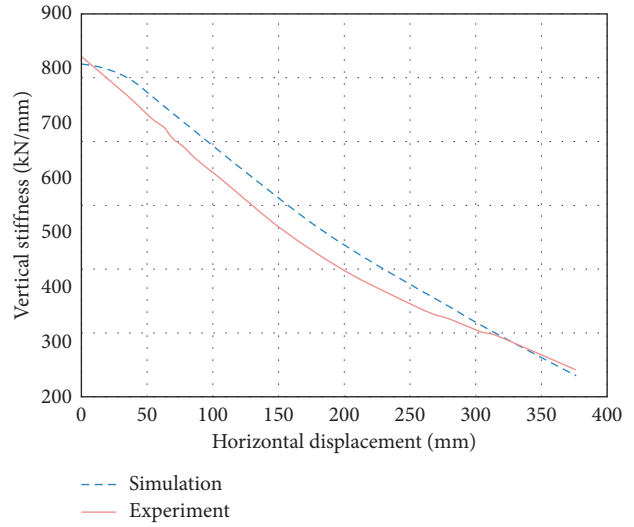


FIGURE 33: Comparison of vertical stiffness-horizontal displacement relationship curve.

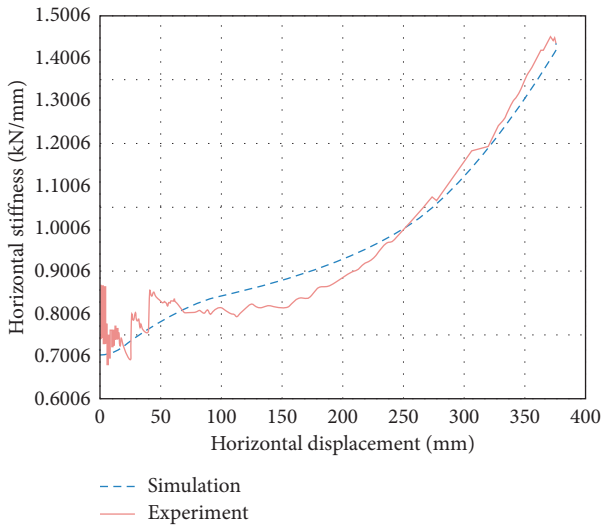


FIGURE 32: Comparison of horizontal stiffness-horizontal displacement relationship curve.

the laminated rubber bearings, the bearings No. 3 and No. 25 were set as LNR500, for seismic isolation analysis. The design scheme is shown in Figure 37.

The eccentricity of the structure was first checked and the maximum eccentricity was 1.77% in Table 6, which satisfied the requirement.

Load combinations.

Combination (1): $1.0 \times$ representative value of gravity load + $1.0 \times$ horizontal earthquakes - $0.5 \times$ vertical earthquakes.

Combination (2): $1.0 \times$ representative value of gravity load - $1.0 \times$ horizontal earthquakes - $0.5 \times$ vertical earthquakes.

Combination (3): $1.0 \times$ representative value of gravity load + $1.0 \times 45^\circ$ horizontal earthquake - $0.5 \times$ vertical earthquake.



FIGURE 34: Floor model diagram.

Combination (4): $1.0 \times$ representative value of gravity load + $1.0 \times 225^\circ$ horizontal earthquake - $0.5 \times$ vertical earthquake.

The change in data is small because fewer bearings were changed, but due to the replacement of bearings, three more bearings produced positive axial forces, and No. 3 and No. 25 remained the bearings subjected to the greatest axial tension, and No. 3 was subjected to slightly greater tensile stress than No. 25.

This paper focuses on the analysis of the tensile situation of the seismic isolation bearing, so the force situation under the most unfavorable load combination of tensile

TABLE 4: Timing information table.

Abbreviation of time schedule	Full name of the time schedule	The maximum value of seismic acceleration is used for earthquake preparedness (cm/s ²)	The maximum value of seismic acceleration is used for rare earthquakes (cm/s ²)	Acquisition interval	Number of collection points
REN1	ACC5	200	400 * 1.1	0.02	1501
REN2	RZ17	200	400 * 1.1	0.02	1501
ELC	ELCENTRO	200	400 * 1.1	0.02	1501
LWD	LWD_DEL AMO BLVD_90_nor	200	400 * 1.1	0.02	1770
N90	NORTHRNWH090	200	400 * 1.1	0.02	2000
N94	NGA_949NORTHR.ARL_FN	200	400 * 1.1	0.02	1998
TAF	TAFT S69	200	400 * 1.1	0.02	2720

TABLE 5: Duration schedule of the seven time course response spectra.

Schedule Name	The time corresponding to the first 10% of the maximum value of this seismic wave (S)	The time corresponding to 10% of the last time the maximum value of this seismic wave was reached (S)	Effective duration of the wave (S)	Structure cycle (S)	Ratio
REN1	2.020	23.100	21.08	2.437	8.7
REN2	0.540	17.440	16.90	2.437	6.9
ELC	0.861	29.174	28.313	2.437	11.6
LWD	0.037	33.638	33.601	2.437	13.8
N90	2.060	16.681	14.62	2.437	6.0
N94	2.180	24.180	22.00	2.437	9.0
TAF	1.048	45.398	44.35	2.437	18.2

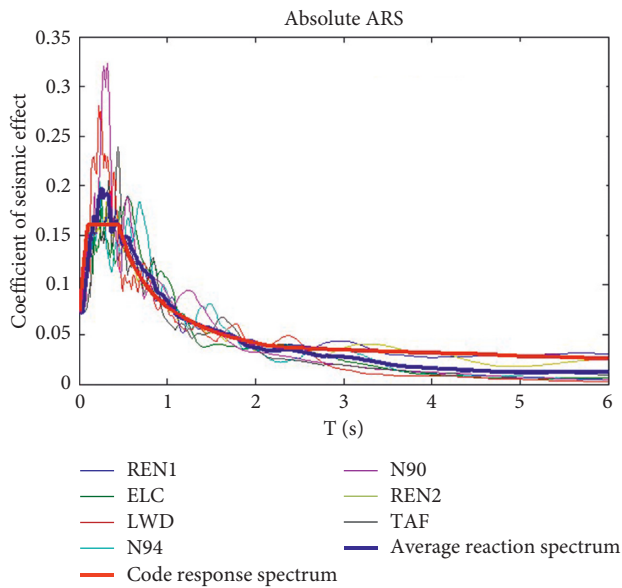


FIGURE 35: 7 time course response spectra with canonical response spectra curves.

stress is mainly analyzed. By the table display function of the resultant data, the time course curve of the upper force of each bearing can be obtained. The model used in this section analyzes a total of 4 load combinations, and 7 waves are analyzed under each combination, each wave is divided into 2 cases of X- and Y-inputs, and there are 2 research bearings, No. 3 and No. 25. If the force conditions under each load combination of each bearing are all analyzed, there are 112 time curves in total, which is too many, so the

representative ones should be selected as the research objects.

From Table 7, it is known that under the action of the rare earthquake, the maximum tensile stress of the bearing is 0.28 MPa in combination (1), which appears in bearing No. 3 LNR500; in combination (2), the maximum tensile stress of the bearing is 0.26 MPa, which appears in bearing No. 28 LNR500; when the horizontal earthquake is 45 degrees, the maximum tensile stress of the bearing is 0.25 MPa, which appears in bearing No. 3. When the horizontal earthquake is 225 degrees, the maximum tensile stress of the bearing is 0.25 MPa, which appears in No. 3 bearing LNR500. No. 3 and No. 25 are the same kind of bearing, but the tensile force at the location of No. 3 bearing is greater, so No. 3 bearing is the main object of study. The laminated rubber bearing selected for this study is a circular bearing, there is no bearing deformation characteristics related to the direction of deformation, so the four load combinations to select the relatively large upper force of the bearing combination (1).

In the load combination (1), the time-course curves of the force condition of No. 3 bearing are plotted in Figures 38–44.

Observing the above 14 sets of force time curves, it is obvious that the upper force of the bearing is greater when the seismic wave is input from the Y direction than when it is input from the X direction. Among the seven waves, REN1 and REN2 showed the largest fluctuations in the upper force of the bearing when they were input.

6. Analysis of the Results

The detailed seismic isolation analysis of this engineering case has been carried out by ETABS above, and the

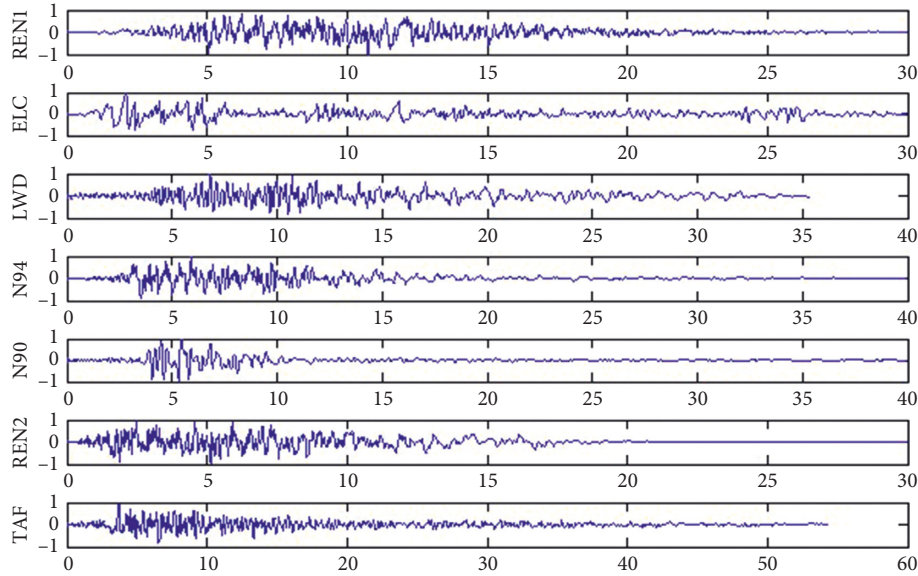


FIGURE 36: Comparison of reaction spectrum and acceleration time curve.

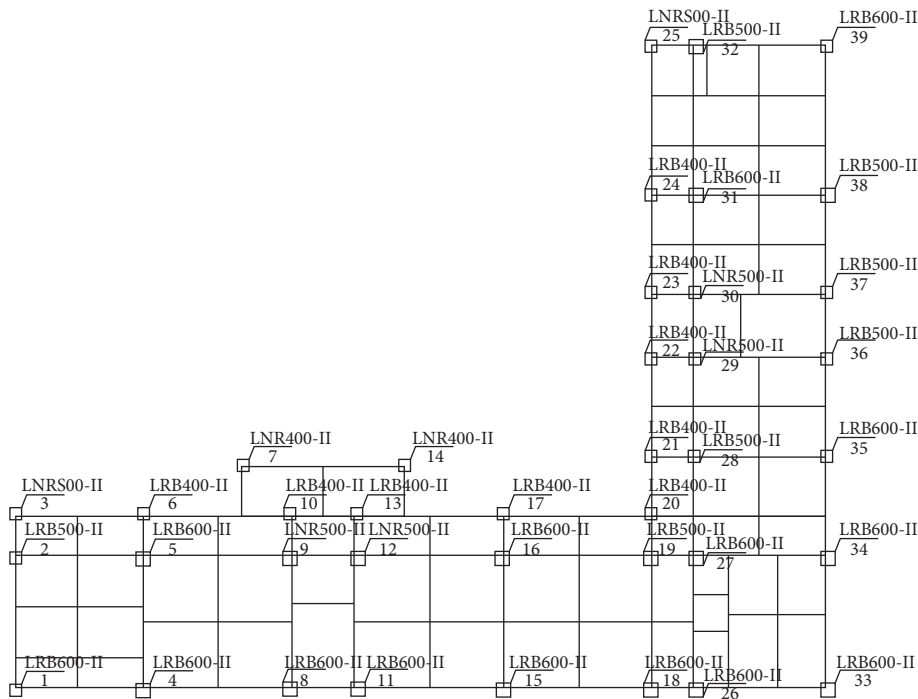


FIGURE 37: Arrangement of bearing design.

TABLE 6: Eccentricity of seismic isolation structure.

Global coordinate	Center of gravity (m)	Rigid heart (m)	Eccentric distance (m)	Torsional stiffness (kN·m)	Stretch radius (m)	Eccentricity
X	31.61	31.39	0.35	18368102	19.54	1.09%
Y	12.33	12.67	0.21			1.77%

maximum horizontal displacement of the bearing in the seismic isolation layer does not exceed 250% of the thickness of the bearing rubber layer, within this range, the calculation error of ETABS and ABAQUS can be controlled within 10%,

so the analysis results above can be put into ABAQUS for a more accurate calculation of bearing No. 3.

The above total 14 force time curves, 7 of which have upper pressure greater than 0 and 7 of which do not exist, are inputted

TABLE 7: Maximum tensile stress and minimum axial force under different load combinations.

Standoffs number	Stand model	Combination (1)		Combination (2)		Combination (3)		Combination (4)	
		Axial force(kN)	Tensile stress (MPa)	Axial force(kN)	Tensile stress (MPa)	Axial force(kN)	Tensile stress (MPa)	Axial force(kN)	Tensile stress (MPa)
1	LRB600	-79	-0.28	-80	-0.28	-71	-0.25	-71	-0.25
2	LRB500	-90	-0.46	-91	-0.46	-81	-0.41	-81	-0.41
3	LNR500	54	0.28	52	0.26	50	0.25	50	0.25
4	LRB600	-158	-0.56	-158	-0.56	-167	-0.59	-167	-0.59
5	LRB600	-220	-0.78	-220	-0.78	-215	-0.76	-215	-0.76
6	LRB400	-12	-0.09	-12	-0.09	-29	-0.23	-29	-0.23
7	LNR400	-21	-0.17	-21	-0.17	-17	-0.14	-17	-0.14
8	LRB600	-108	-0.38	-107	-0.38	-97	-0.34	-96	-0.34
9	LNR500	-112	-0.57	-112	-0.57	-106	-0.54	-106	-0.54
10	LRB400	-32	-0.25	-31	-0.25	-23	-0.18	-21	-0.17
11	LRB600	-108	-0.38	-107	-0.38	-93	-0.33	-93	-0.33
12	LNR500	-112	-0.57	-111	-0.57	-104	-0.53	-105	-0.54
13	LRB400	-31	-0.25	-30	-0.24	-24	-0.19	-22	-0.18
14	LNR400	-21	-0.17	-21	-0.16	-18	-0.14	-18	-0.14
15	LRB600	-146	-0.52	-145	-0.51	-161	-0.57	-161	-0.57
16	LRB600	-202	-0.72	-204	-0.72	-210	-0.74	-210	-0.74
17	LRB400	-21	-0.16	-19	-0.15	-39	-0.31	-38	-0.31
18	LRB600	-72	-0.25	-72	-0.26	-59	-0.21	-59	-0.21
19	LRB500	-94	-0.48	-95	-0.48	-101	-0.52	-103	-0.52
20	LRB400	-43	-0.34	-43	-0.35	-41	-0.32	-41	-0.33
21	LRB400	1	0.01	-1	-0.01	2	0.02	4	0.03
22	LRB400	3	0.03	1	0.01	1	0.00	0	0.00
23	LRB400	2	0.02	2	0.02	3	0.03	4	0.03
24	LRB400	-7	-0.06	-8	-0.06	-21	-0.17	-22	-0.17
25	LNR500	37	0.19	36	0.18	32	0.16	32	0.16
26	LRB600	-132	-0.47	-132	-0.47	-112	-0.40	-112	-0.40
27	LRB600	-188	-0.67	-187	-0.66	-205	-0.73	-206	-0.73
28	LRB500	-116	-0.59	-114	-0.58	-122	-0.62	-121	-0.61
29	LNR500	-103	-0.53	-104	-0.53	-95	-0.48	-96	-0.49
30	LNR500	-99	-0.50	-98	-0.50	-91	-0.47	-91	-0.46
31	LRB600	-193	-0.68	-192	-0.68	-191	-0.68	-190	-0.67
32	LRB500	-115	-0.59	-115	-0.59	-108	-0.55	-108	-0.55
33	LRB600	-104	-0.37	-103	-0.37	-91	-0.32	-91	-0.32
34	LRB600	-164	-0.58	-164	-0.58	-174	-0.62	-174	-0.62
35	LRB600	-90	-0.32	-90	-0.32	-99	-0.35	-99	-0.35
36	LRB500	-102	-0.52	-102	-0.52	-100	-0.51	-100	-0.51
37	LRB500	-97	-0.50	-97	-0.49	-95	-0.48	-95	-0.48
38	LRB500	-111	-0.57	-111	-0.56	-126	-0.64	-125	-0.64
39	LRB600	-81	-0.29	-81	-0.29	-71	-0.25	-71	-0.25

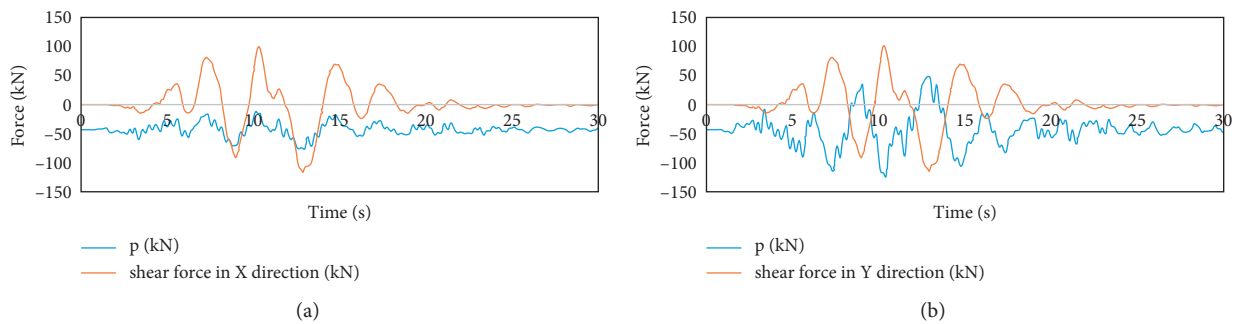


FIGURE 38: REN1 seismic waves under the bearing force time curve. (a) X-directional input. (b) Y-directional input.

into the LNR500 model that has been built in ABAQUS before in turn, after calculating the displacement, velocity and acceleration time curves of the bearing deformation in the

earthquake. They are compared and analyzed to get what are the characteristics of the changes of the bearing in the cases where tensile stresses appear and those where they do not.

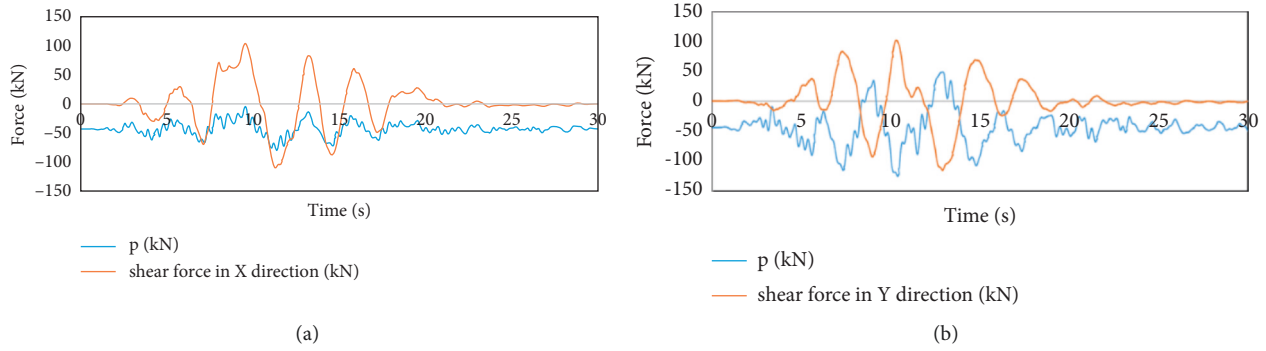


FIGURE 39: REN2 seismic waves under the bearing force time curve. (a) X-directional input. (b) Y-directional input.

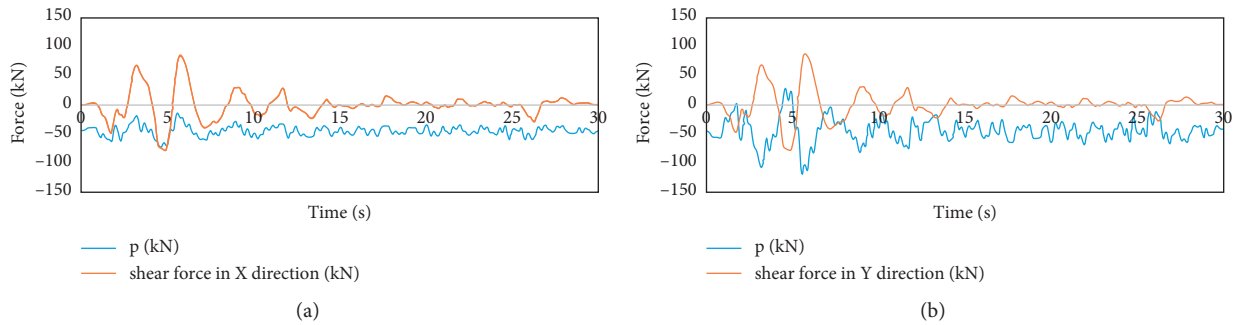


FIGURE 40: Time course curve of bearing force under ELC seismic wave. (a) X-directional input. (b) Y-directional input.

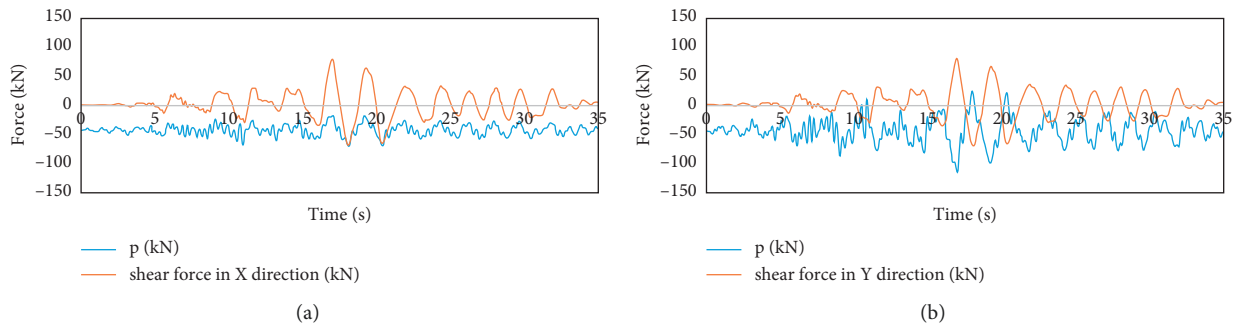


FIGURE 41: Time course curves of bearing stresses under LWD seismic waves. (a) X-directional input. (b) Y-directional input.

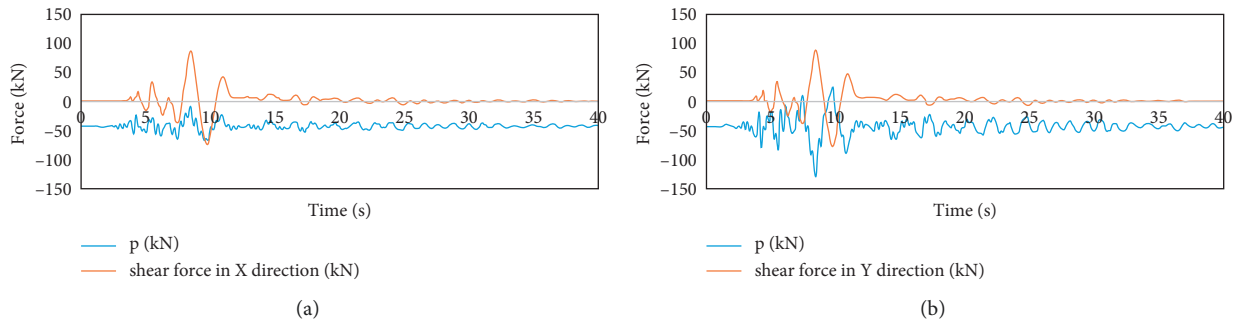


FIGURE 42: Time course curve of bearing force under N90 seismic wave. (a) X-directional input. (b) Y-directional input.

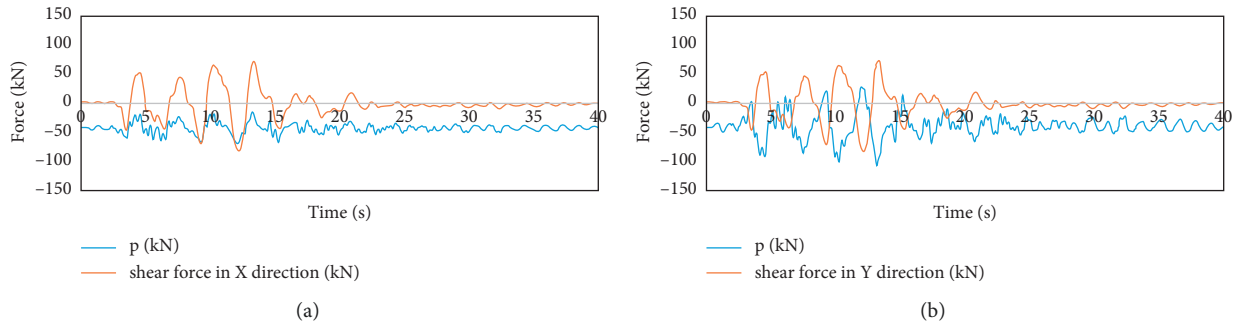


FIGURE 43: Time course curve of bearing force under N94 seismic wave. (a) X-directional input. (b) Y-directional input.

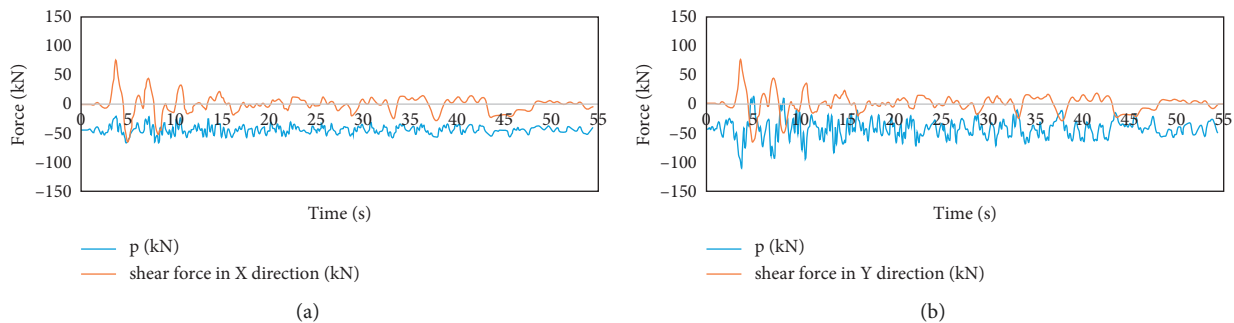


FIGURE 44: Time course curves of bearing stresses under TAF seismic waves. (a) X-directional input. (b) Y-directional input.

In order to observe the connection between displacement, velocity and acceleration of bearing deformation more intuitively, the displacement, velocity and acceleration time curves were drawn on one graph, as shown in Figures 45–58. However, since they are not of one order of magnitude, especially the acceleration is generally relatively large. Therefore, when drawing the graph, the acceleration needs to be reduced by a certain multiple, and the vertical displacement also has a smaller value, so it needs to be enlarged by a certain multiple. For example, in the horizontal deformation in Figure 45, the acceleration unit is labelled as 20 mm/s^2 , which means the acceleration is reduced by 20 times; while in the vertical deformation in Figure 45, the displacement unit is labelled as 0.5 mm , which means the displacement is enlarged by 2 times.

In ABAQUS, a total of 14 sets of dynamic analysis were done, and the above 28 sets of time-course curves were obtained. In each set of curves, the highest frequency of change was acceleration, followed by velocity, and the lowest was displacement.

This paper is prepared for the reference of the tensile device, so in the exploration of the first to define under what circumstances to determine the bearing in the tensile situation, in order to determine when the bearing is in what condition when the tensile device needs to play a role. In this paper, the laminated rubber bearing tension not only need to consider the upper bearing pressure less than 0, but also need to consider the horizontal displacement of the larger case, the simulation results in preceding paragraphs found that the LNR500 horizontal displacement of 75 mm that is, the horizontal shear of 81.5% or so, the bearing should start

to have local tension, after reaching 150% , the bearing tension is more obvious, comprehensive Considering, this paper considers that when the upper pressure of the bearing is positive and the horizontal displacement of the bearing is greater than 200% of the thickness of the rubber layer, i.e. 186 mm , the bearing is considered to be in tension.

Observation and comparison of the above graphs will show that when the displacement of the bearing deformation is relatively large, its velocity in the adjacent time period is also larger, but the acceleration is not necessarily larger, in this case most of the time course curve changes are characterized by a smaller acceleration in a certain time period, its nearby displacement is larger. And the load combination with larger maximum displacement, its corresponding maximum acceleration is not necessarily proportional, take the two different cases of REN2's X-direction input and Y-direction input as an example, it is known from the previous subsection that the upper force of the bearing is larger when Y-direction input, and there is the case that the upper vertical force is positive. Horizontal acceleration is 9.81 mm/s^2 , maximum vertical displacement is 0 mm , and maximum vertical acceleration is 0.59 m/s^2 ; when REN2 is input from Y direction, the maximum horizontal displacement corresponding to bearing deformation is 109.57 mm , maximum horizontal acceleration is 6.85 mm/s^2 , maximum vertical deformation is 0.09 mm , and maximum vertical acceleration is also 0.59 m/s^2 . input horizontal displacement is 5.59% larger than the maximum horizontal displacement in Y direction input, but its maximum horizontal acceleration is 43.21% larger; the vertical displacement in Y direction input is obviously larger, but its maximum vertical acceleration is the same.

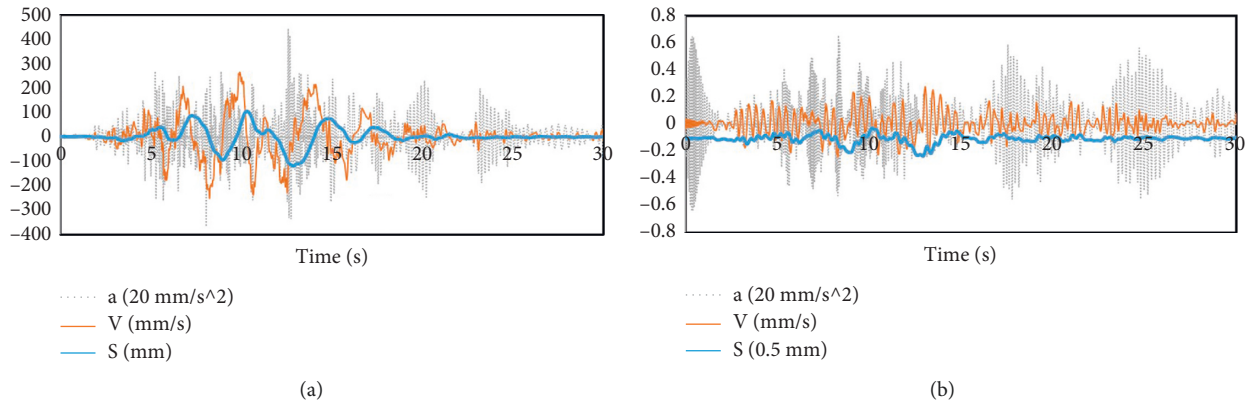


FIGURE 45: Time course curves of displacement, velocity and acceleration of bearing deformation when REN1 is input from X direction. (a) Horizontal deformation. (b) Vertical deformation.

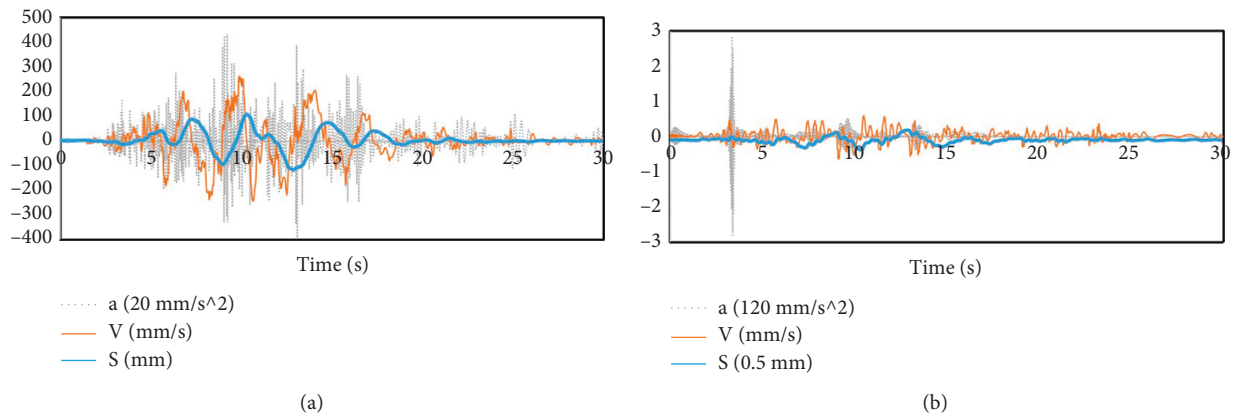


FIGURE 46: Time course curves of displacement, velocity and acceleration of bearing deformation when REN1 is input from Y direction. (a) Horizontal deformation. (b) Vertical deformation.

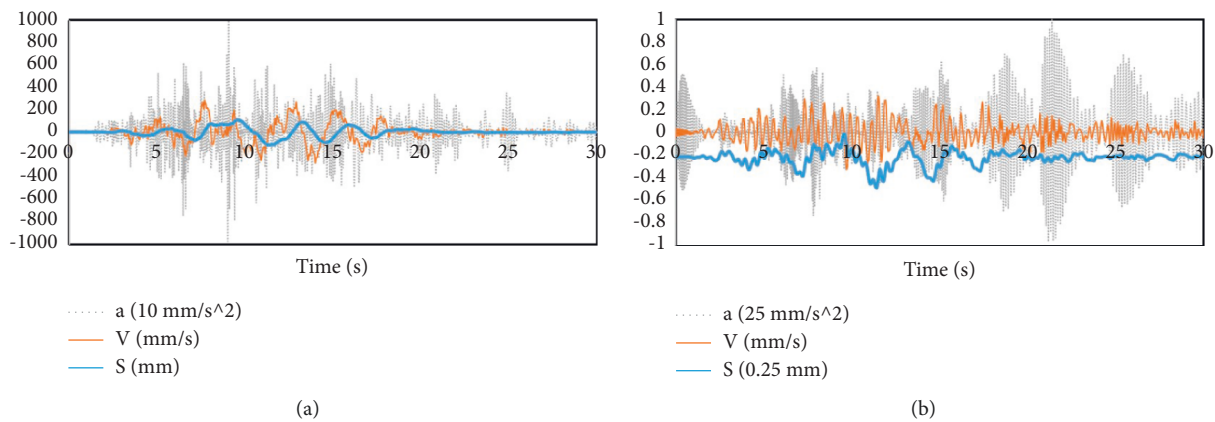


FIGURE 47: Time course curves of displacement, velocity and acceleration of bearing deformation when REN2 is input from X direction. (a) Horizontal deformation. (b) Vertical deformation.

Such deformation characteristics may not be conducive to the role of acceleration-controlled tensile devices, but the use of velocity-controlled tensile devices can be considered. As the case model used in this paper is small, the horizontal displacement and vertical

displacement of the bearing are not particularly large, and when the horizontal displacement is close to 200% of the thickness of the rubber layer and the vertical displacement is greater than 0, the maximum velocity near its corresponding position is close to 350 mm/s . Therefore,

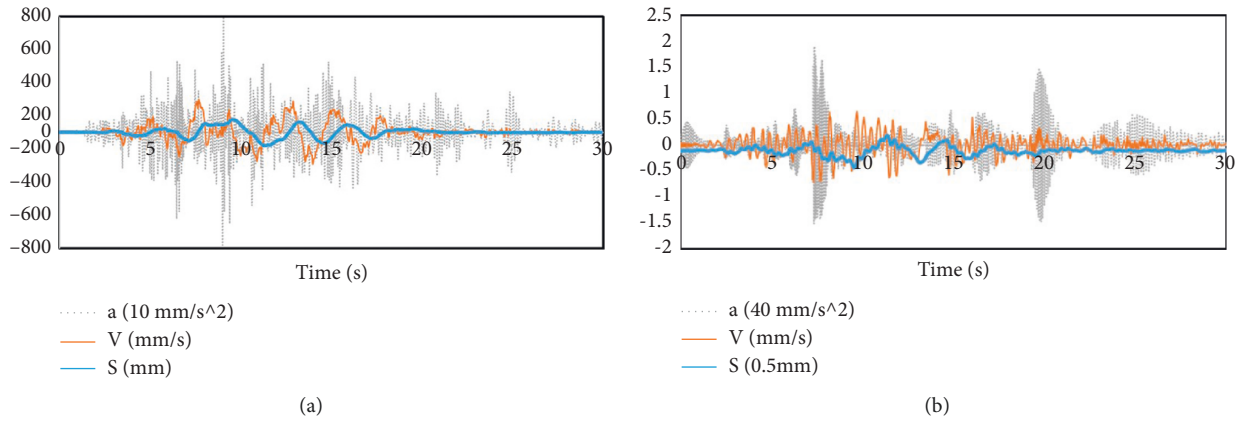


FIGURE 48: Time course curves of displacement, velocity and acceleration of bearing deformation when REN2 is input from Y direction. (a) Horizontal deformation. (b) Vertical deformation.

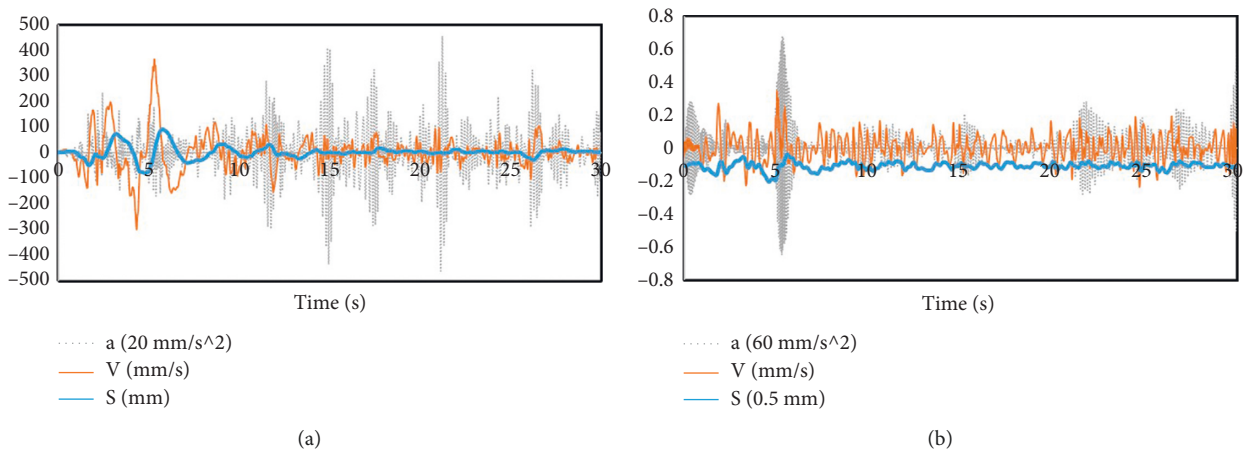


FIGURE 49: Time course curves of bearing deformation displacement, velocity and acceleration when ELC is input from X direction. (a) Horizontal deformation. (b) Vertical deformation.

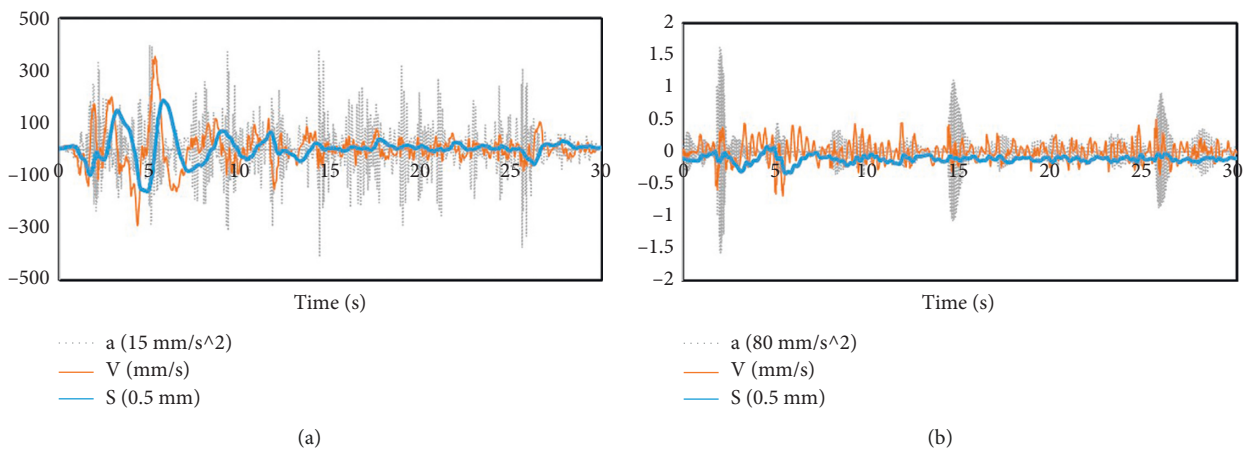


FIGURE 50: Time course curves of bearing deformation displacement, velocity and acceleration when ELC is input from Y direction. (a) Horizontal deformation. (b) Vertical deformation.

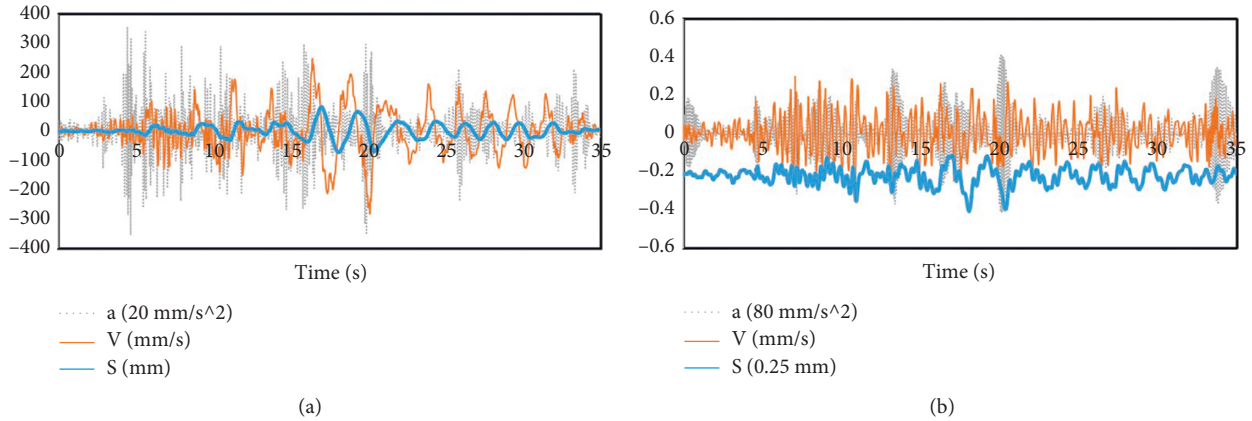


FIGURE 51: Time course curves of bearing deformation displacement, velocity and acceleration when LWD is input from X direction. (a) Horizontal deformation. (b) Vertical deformation.

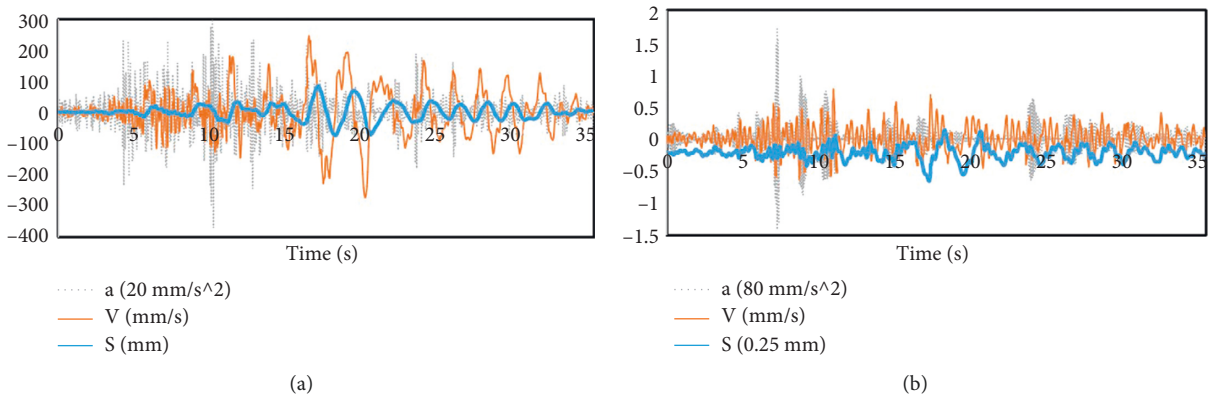


FIGURE 52: Time course curves of bearing deformation displacement, velocity and acceleration when LWD is input from Y direction. (a) Horizontal deformation. (b) Vertical deformation.

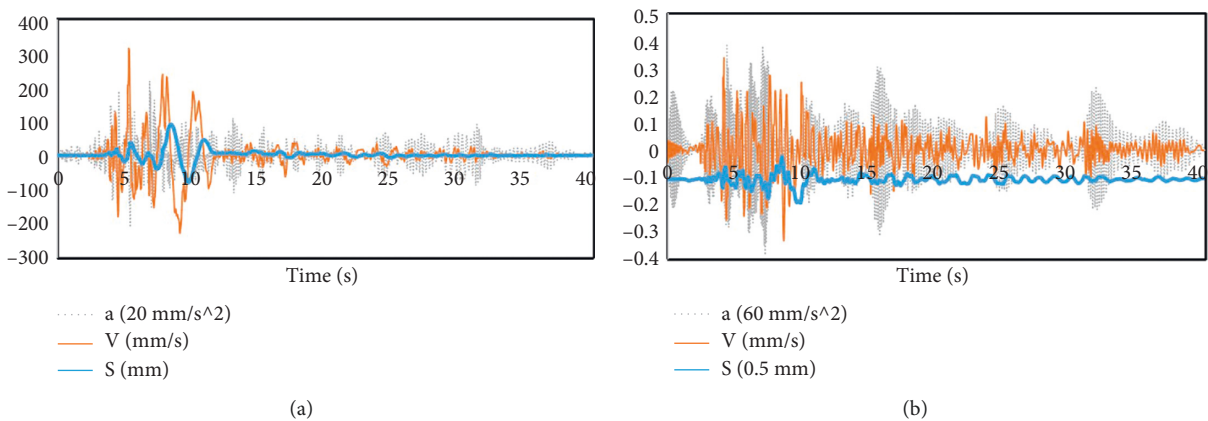


FIGURE 53: Time course curves of bearing deformation displacement, velocity and acceleration when N90 is input from X direction. (a) Horizontal deformation. (b) Vertical deformation.

considering all aspects, this paper believes that the velocity-controlled tensile device of LNR500 can be considered to set the action velocity at 400 mm/s (0.4 m/s),

that is, when the bearing deformation speed reaches 0.4 m/s , the tensile device then starts to play the tensile effect.

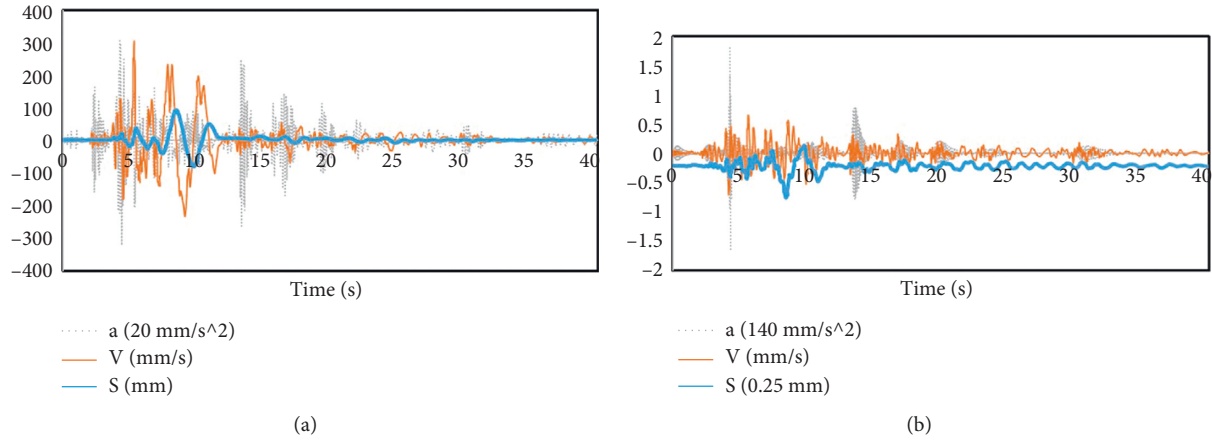


FIGURE 54: Time course curves of bearing deformation displacement, velocity and acceleration when N90 is input from Y direction. (a) Horizontal deformation. (b) Vertical deformation.

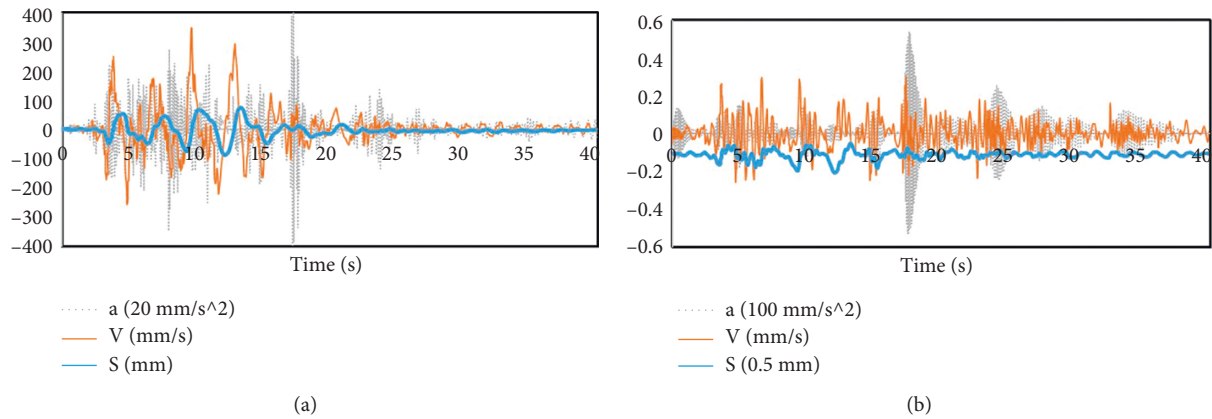


FIGURE 55: Time course curves of bearing deformation displacement, velocity and acceleration when N94 is input from X direction. (a) Horizontal deformation. (b) Vertical deformation.

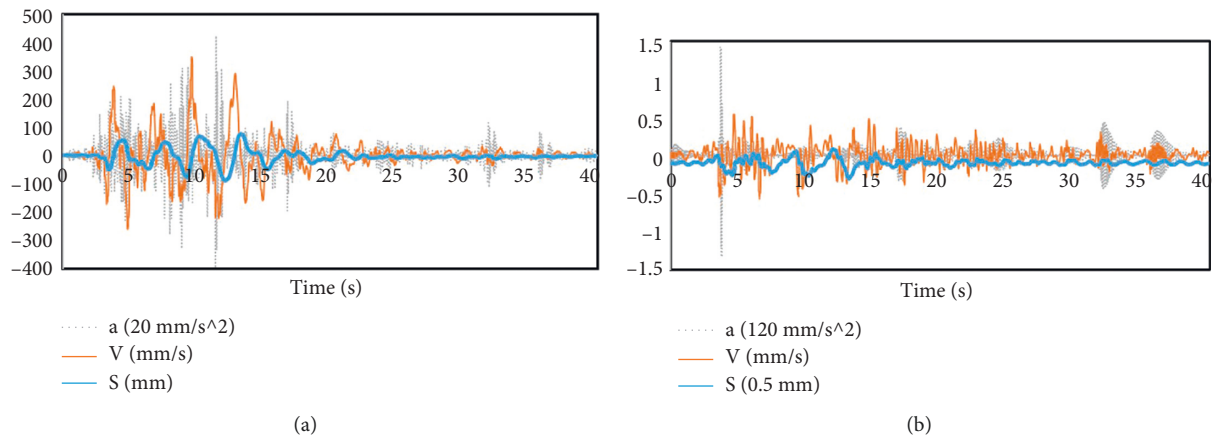


FIGURE 56: Time course curves of bearing deformation displacement, velocity and acceleration when N94 is input from Y direction. (a) Horizontal deformation. (b) Vertical deformation.

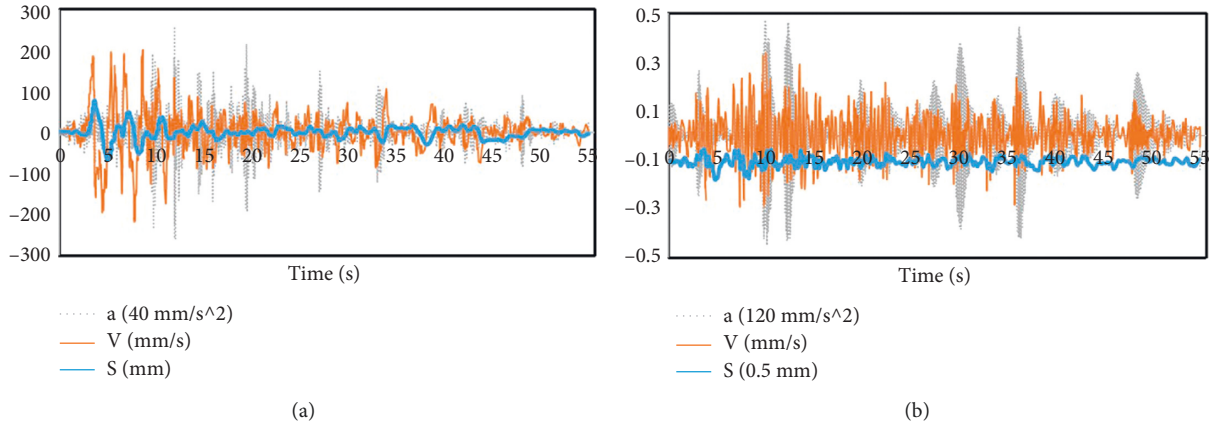


FIGURE 57: Time course curves of bearing deformation displacement, velocity and acceleration when TAF is input from X direction. (a) Horizontal deformation. (b) Vertical deformation.

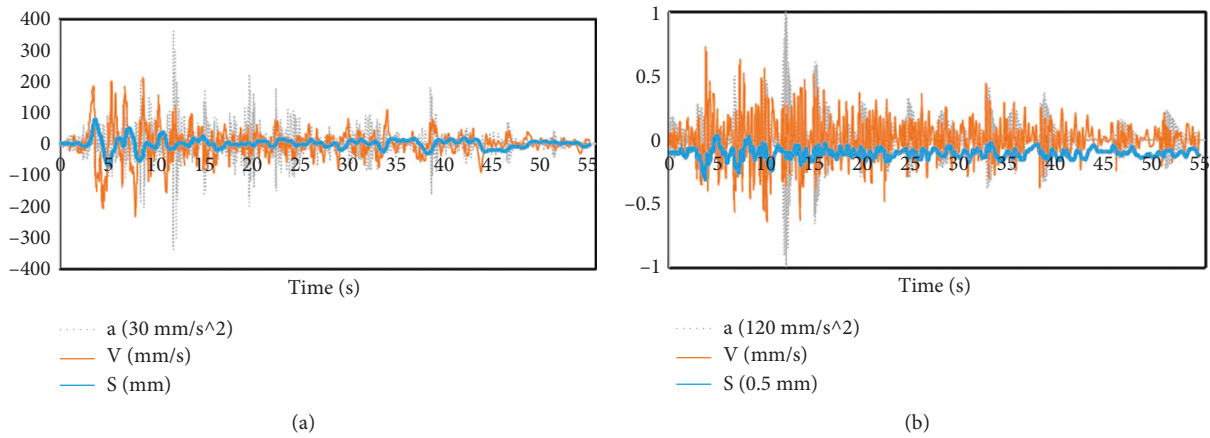


FIGURE 58: Time course curves of bearing deformation displacement, velocity and acceleration when TAF is input from Y direction. (a) Horizontal deformation. (b) Vertical deformation.

7. Conclusion

With the increase of seismically isolated buildings, the weakness of poor tensile capacity of seismic isolation bearings is also increasingly highlighted. For this reason, the design research of seismic isolation bearing tensile devices is also emerging. However, the deformation of the bearing itself in the earthquake process is relatively complex, and its deformation characteristics will have certain influence on the performance of the tensile device. In order to study the tensile device more reasonably and make the research results more reliable, the deformation characteristics of the seismic isolation bearing should be studied more thoroughly first. In this paper, three sets of materiality tests, 400% compression shear test of LNR500 bearing and 400% compression shear test of LNR500 bearing were firstly conducted; the materiality parameters obtained from the tests were applied, and the static analysis of the correlation between vertical displacement and horizontal displacement was carried out on LNR500 bearings with finite element analysis software, and the relationship curves between horizontal stiffness of the bearing and vertical stiffness and horizontal displacement of

the bearing were obtained. The relationship curves between the horizontal stiffness and vertical stiffness of the bearing and the horizontal displacement of the upper part of the bearing were obtained; seismic isolation analysis was carried out for an actual engineering case, and the results of the upper force time course of the bearing were imported into ABAQUS software, and dynamic analysis was carried out for LNR500 to obtain the displacement, velocity and acceleration time course curves of the horizontal and vertical deformation of the bearing. After the comprehensive analysis, the following conclusions were obtained.

- (1) When the bearing is in compression-shear state, the bearing's compressed area will be reduced because of the increase of the upper horizontal displacement, resulting in the reduction of the vertical stiffness of the bearing, thus increasing the vertical displacement, so this part of the displacement should be taken into account when designing the tensile device to guarantee the vertical clearance. In general, the maximum horizontal displacement of the bearing in the seismic isolation structure under the action of earthquake does not exceed 250% of the thickness of

the rubber layer, corresponding to the tensile device of LNR500 should retain the vertical clearance of 5 mm.

- (2) In the simulation of large deformation of rubber bearing, Yeoh and Ogden models are commonly used, and Yeoh model is used in this paper. Usually in the bearing finite element simulation, rubber is often assumed to be incompressible model, this paper also simulates the compression model and incompressible model in the simulation, the results show that the vertical stiffness of the incompressible model of the bearing is larger, the numerical analysis results and test results are very big difference; and the horizontal stiffness of the incompressible model simulation is also larger than the compressible model, and the error will increase with the increase of horizontal displacement, when the horizontal displacement is greater than 320% of the thickness of the rubber layer, the relative error of the two horizontal stiffnesses is more than 10%. Therefore, in the simulation modeling stage of the research process of tensile device, the rubber should use compressible model.
- (3) The vertical stiffness and horizontal stiffness of the laminated rubber bearing will change with the change of horizontal displacement of the upper part of the bearing, and the change has the following law (the correlation can also be established by the method of this paper for bearings of different materials or different diameters): the vertical stiffness of the bearing decreases nearly linearly with the increase of horizontal displacement is about 1.55 kN/mm².
- (4) The research and design analysis of the speed-controlled tensile device and acceleration-controlled tensile device show that when the LNR500 deformation displacement is large and the tensile force is usually small, and this deformation characteristic is not conducive to the acceleration-controlled tensile device to play its role, so it is not recommended to use; and there is generally a large change speed in this time period, and this speed is about 0.4 m/s, so it is recommended that the velocity-controlled tensile device designed for LNR500 should be designed to act at a velocity of 0.4 m/s.

The types of tensile devices can be roughly divided into three categories: displacement controlled tensile devices, speed controlled tensile devices and acceleration controlled tensile devices. The static analysis is mainly for the displacement controlled tensile device, and the dynamic analysis is mainly for the speed controlled tensile device and the acceleration controlled tensile device. The research results of this paper provide some reference data for the design research of LNR500 tensile device, and also provide some research ideas for the tensile devices of other bearings in the future. However, the static and dynamic analysis of the laminated rubber bearing is carried out in this paper, but it

mainly assumes the state of the floor without overturning, under this state, the vertical displacement of the bearing is small, and the reference significance of its deformation is more limited. If we want to better explore the deformation characteristics of the bearing when it is under tension in the earthquake, we should find a large engineering case with a larger aspect ratio to do the analysis, and take the overturning displacement into consideration.

Data Availability

The dataset can be accessed upon request.

Conflicts of Interest

The authors declare that they have no conflicts of interest regarding this work.

Acknowledgments

This work was supported by the Science and Technology Program of Yunnan Transportation Department with 2017(A)03.

References

- [1] H. Yu-xian, *Earthquake Engineering*, Seismological Press, China, 2006.
- [2] J. M. Kelly, "Experimental results of an earthquake isolation system using natural rubber bearing," Report No. UCB/EERC-78/03, University of California, California, CA, USA, 1978.
- [3] C. Peng, Y. Zhou, L. Lu, L. Jiang, K. Hu, and G. Qu, "Experimental research on mechanical performance of tension-resistant device for rubber bearings," *Journal of building structures*, vol. 38, no. 7, pp. 113–119, 2017.
- [4] X. Yan, Y. Zhang, H. Wang, and W. Lushun, "Shaking table test for the structure with three-dimensional base isolation and overturn resistance devices," *Engineering Mechanics*, vol. 27, no. 5, pp. 91–96, 2010.
- [5] C. G. Koh and J. M. Kelly, "A simple mechanical model for elastomeric bearings used in base isolation," *International Journal of Mechanical Sciences*, vol. 30, no. 12, pp. 933–943, 1988.
- [6] J. M. Kelly, *Earthquake-resistant Design with Rubber*, Springer-Verlag, London, 1997.
- [7] X. Li and X. Yang, "A review of elastic constitutive model for rubber materials," *China Elastomerics*, vol. 15, no. 1, pp. 52–60, 2005.
- [8] W. Wang, T. Deng, and S. Zhao, "Determination for material constants of rubber Mooney-Rivlin model," *Special purpose rubber products*, vol. 25, no. 4, pp. 8–10, 2011.
- [9] O. H. Yeoh, "Characterization of elastic properties of carbon-black-filled rubber vulcanizates," *Rubber Chemistry and Technology*, vol. 63, no. 5, pp. 792–805, 1990.
- [10] O. H. Yeoh, "Some forms of the strain energy function for rubber," *Rubber Chemistry and Technology*, vol. 66, no. 5, pp. 754–771, 1993.
- [11] R. W. Ogden, "Large deformation isotropic elasticity: on the correlation of the theory and experiment for compressible rubberlike solids," *Proceedings of Royal Society of London Series A*, vol. 328, pp. 567–583, 1972.
- [12] J. Wang, P. Guan, and Q. Yao, "Analysis of bilateralseism iceresponse of base-isolated structures with lead rubber

- bearings,” *Earthquake Engineering and Engineering Vibration*, vol. 25, no. 1, pp. 133–137, 2005.
- [13] M. Ohsaki, T. Miyamura, M. Kohiyama, T. Yamashita, M. Yamamoto, and N. Nakamura, “Finite-element analysis of laminated rubber bearing of building frame under seismic excitation,” *Earthquake Engineering & Structural Dynamics*, vol. 44, no. 11, pp. 1881–1898, 2015.
- [14] X. Luo, “The relation between simple shear and pure shear in rubber,” *Acta Polymerica Sinica*, vol. 1994, no. 4, pp. 385–391, 1994.
- [15] A. Li, *Vibration Control for Building Structures: Theory and Applications*, Springer, Berlin, Germany, 2020.

Research Article

Mathematical Model and Algorithm of Multi-Index Transportation Problem in the Background of Artificial Intelligence

Junfang Cao 

College of Continuing Education, Xuchang Vocational Technical College, Xuchang 461000, Henan, China

Correspondence should be addressed to Junfang Cao; caojunfang@xcitc.edu.cn

Received 16 February 2022; Revised 9 March 2022; Accepted 25 March 2022; Published 26 April 2022

Academic Editor: Sang-Bing Tsai

Copyright © 2022 Junfang Cao. This is an open access article distributed under the Creative Commons Attribution License, which permits unrestricted use, distribution, and reproduction in any medium, provided the original work is properly cited.

The development of artificial intelligence has brought rapid changes to human life and brought great convenience to human activities. The development of various modes of transportation has also brought convenience to people's travel and commodity transactions, but it has also added more issues that need to be carefully considered. Because of the diversification of transportation methods, transportation problems also arise many fields, such as air transportation, water transportation, and land transportation. The development of mathematical models and algorithms for transportation problems is also in full swing, and it is a major trend to introduce mathematical models and algorithms into the solution of transportation problems. This paper deals with the multi-index transportation problem by establishing a multi-index mathematical model and algorithm to find a scientific transportation method for the goods to be transported, so as to save the cost and time of transportation. Experiments show that the mathematical model established in this paper has high efficiency for solving the multi-index transportation problem. At the same time, the most suitable transportation method can also be selected for the transportation of goods, and the route planned by the mathematical model and algorithm can reduce the risk to 12.34%.

1. Introduction

The transportation problem is a special form of common linear programming, which has both the common properties of linear programming and its own characteristics and algorithms. It is a problem that needs to be solved according to a certain algorithm, and it means mainly to solve the problem of high freight in the transportation route. And, with the improvement of the economic level, the transportation problem has also begun to receive extensive attention. Nowadays, the production of commodities is often divided into multiple places. Therefore, based on the current transportation network, it is one of the problems that need to be solved to make a reasonable plan to transport the goods to various sales places and reduce the transportation cost [1, 2]. The competition in today's transportation market is also extremely fierce, such as the logistics industry and the transportation of fruits and vegetables. Therefore, it is very necessary to choose a reasonable transportation solution to

ensure the transportation time and safety. Today's commodities need to face a lot of transportation, and the number of production and sales places is also large. For the transportation problems that need to be faced with a lot of transportation and a large number of production and sales places, a method is needed to establish a new model to solve the problems of how to allocate and transport materials and rationally arrange transportation capacity. This is because the theoretical and practical significance of the traffic problem is very important [3, 4].

By establishing mathematical models to solve traditional transportation problems, artificial intelligence technology is used to make multi-index decisions for the transportation of goods, so as to choose the best route for transportation of goods, improve the efficiency of transportation, and improve the problem of unbalanced production and sales. At the same time, it can also reduce the cost of transportation, reduce the damage of goods during transportation, and ensure the quality of goods [5, 6]. Artificial intelligence

technology plays a major role in the transportation problems of the logistics industry. Because the goods transported by logistics are of various types and sizes, the use of artificial intelligence can quickly classify these goods and provide suitable transportation solutions to promote the efficiency of commodity transportation and ensure the integrity of the goods. At the same time, it can also strengthen the control of transportation time and provide scientific and quantitative decision support for transportation. At the same time, through artificial intelligence technology and mathematical models and algorithms, the multi-index experimental transportation problem can ensure the quality of the goods during the transportation and reduce unnecessary losses.

In order to improve the transportation problem, many scholars have done research on it. Among them, Hu et al. studied the mathematical model of container transportation planning in the port area and proposed a tabu search algorithm to establish this model. The findings show the extent to which internal (ITT) and external transport processes interact and the potential to improve overall operations when using the proposed comprehensive optimization [7]. Borndoerfer et al. proposed the development of mathematical models and optimization methods for railway transportation to solve many related problems in the railway planning process. They introduced a new sorting method, and an example shows that the new projection method provides a good method for fuzzy algorithms to deal with transportation problems [8]. Kawa and Anholcer presented the results of a quantitative study with a random sample of 300 cargo service transport providers in Poland involving exclusion constraints in transport, which confirms that exclusion factors are an important part of the activities of freight transport enterprises [9]. Kukharchyk discussed solving cost optimization problems in transportation problems with mathematical models, noting that all these criteria are meaningful in such tasks where the traffic volume is predetermined [10]. Although their research has a certain reference for the solution of transportation problems, Hu et al.'s research has no specific data and Borndoerfer et al.'s research lacks specific examples. Although the research of Kawa et al. has examples, it only considers one factor that affects the transportation problem. The research of Kukharchyk has not written specific research results and is not convincing.

The mathematical models and algorithms established in this paper have the following innovations: (1) This paper uses the genetic algorithm to build the model, which helps the mathematical model to make multi-index decision-making, so that it can quickly and accurately find out the transportation problem, so as to seek the optimal solution to the problem. (2) This paper fully considers various uncertain factors and certain factors that affect transportation and grasps transportation problems through mathematical models, so as to make the most accurate multi-index decision-making. (3) This paper combines artificial intelligence technology with mathematical models and algorithms of multi-index transportation problems. Artificial intelligence can be described as mathematical models and algorithms that provide accurately implemented data, so that the freight and risk factors of each route can be calculated.

2. Mathematical Model-Building Method for Multi-Index Transportation Problems

2.1. Artificial Intelligence and Transportation. Transportation is one of the important factors of economic development. Good transportation can promote economic development and strengthen business exchanges between regions [11–14]. Just as the current international trade can be completed by air transportation, railway transportation, and other transportation methods, its transportation time will be greatly shortened, convenient, and fast. The current development of artificial intelligence technology also provides a good opportunity for the development of transportation. The current application of artificial intelligence in the transportation industry is shown in Figure 1.

There are many applications of artificial intelligence in transportation, such as traffic lights in Figure 1, GPS positioning and navigation systems during travel, and intelligent communication within vehicles, all of which belong to artificial intelligence technology. The unmanned driving technology currently under development needs to be controlled by artificial intelligence technology. When we need to reach a new destination in the process of traveling, we need to use navigation. Usually, artificial intelligence technology and algorithms are used to determine the optimal route. At the same time, this method can also be used to avoid traffic-congested road sections, save travel time, and reduce the energy consumption of travel tools [15].

Intelligent transportation is a hot spot in the development of transportation in the world today [2, 16, 17]. It aims to build a safe, convenient, efficient, and green transportation system, relying on the existing transportation infrastructure and means of transportation, through the integrated application of modern information, communication, control, and other technologies. It is an important symbol of the modern transportation industry to fully meet the diverse needs of public travel and cargo transportation [18]. In the process of aircraft transportation, the communication between the air and the ground is always maintained, so as to know the status of the aircraft during transportation, and it is also convenient for the airport staff to prepare for the response when it is about to arrive at the airport. These all need to rely on artificial intelligence technology and communication technology [19].

AI technology can also provide better transportation decisions based on the size and nature of the cargo. It is possible to arrange and schedule the whole road transportation more reasonably and effectively adjust the traffic density, so as to maximize the utilization of the line and avoid traffic congestion [20]. In air transportation, artificial intelligence technology can also be used to check before the take-off of cargo transportation, which can more accurately identify whether the air transportation means is faulty, so as to reduce the possibility of risks. At the same time, it can also be used in the external fuselage wing structure system of the aircraft, the aircraft flight control system, and the electrical system to ensure the use time of air vehicle parts [21]. AI technology can also coordinate the transportation of various types of transportation, as shown in Figure 2.

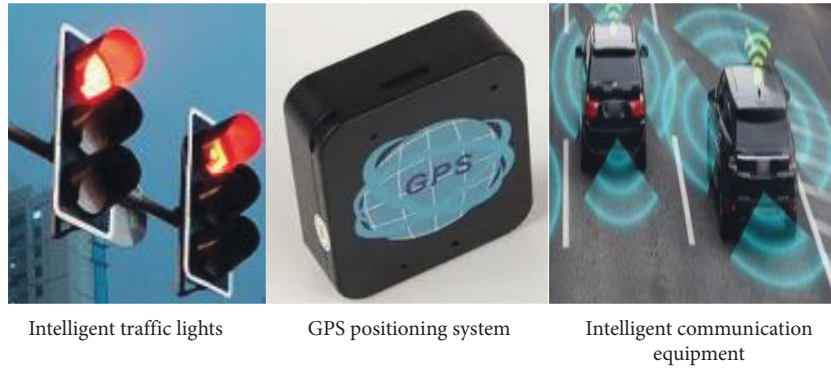


FIGURE 1: The use of artificial intelligence in transportation.

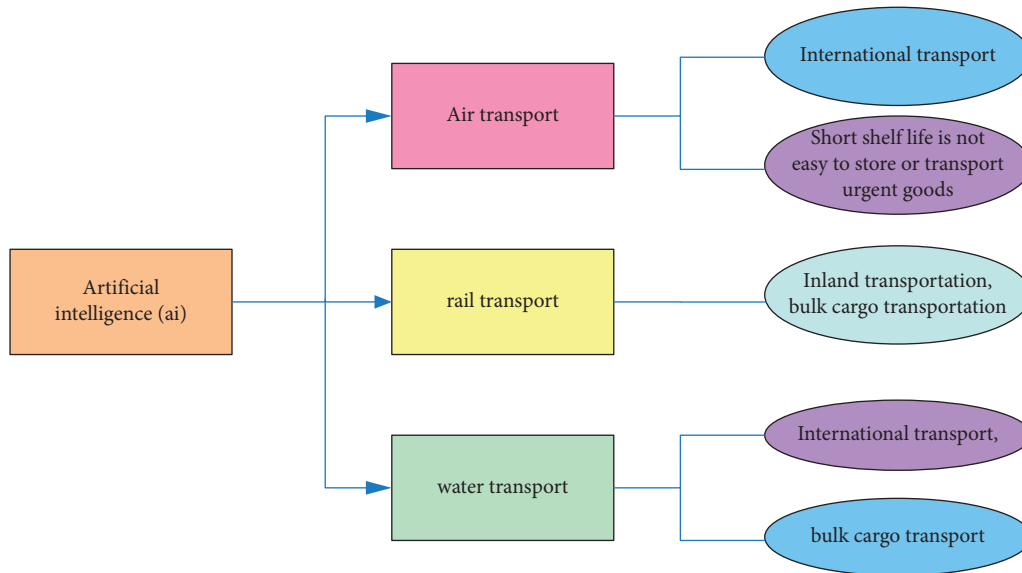


FIGURE 2: AI coordination of modes of transport.

Under the coordination of artificial intelligence, the problem of transportation of goods can be well solved and if the transportation of goods can be seamlessly connected to various modes of transportation, the time cost can be reduced. For example, in the transportation of some fresh vegetables, they can be transported by air to the city where the destination is located and then connected by road transportation through communication technology, which can save a lot of transportation time. At the same time, the transportation can also select the best running route in combination with the algorithm to ensure the quality of the goods. Therefore, the development of transportation under the background of artificial intelligence is faster, more practical, and safer, and the coordination ability of operation is also strong.

2.2. Transportation Issues. The transportation problem is the problem of solving the transportation route of the commodity between the place where the commodity is produced and the place where the commodity is needed and getting the commodity safely to the place of demand. In traditional transportation problems, all supply and demand related to transportation and transportation costs are already

determined values. Because traditional transportation can only follow the traditional route, there will be no other running routes [22]. However, with the diversification of transportation modes and the development of transportation, the available routes are gradually increasing and transportation problems are also increasing. The existing transportation problems are divided into six types, as shown in Figure 3.

The transportation problems shown in Figure 3 include general transportation problem, network transportation problem, maximum flow problem, shortest path problem, task assignment problem, and production planning problem. The general transportation problem refers to conventional ordinary transportation methods, such as railway and road transportation, as well as transportation modes that require transshipment of combined vehicles. We need codistribution optimized for overland transport to achieve the best route and save as much cost as possible. The network transportation problem generally refers to the problems in the logistics industry, and network transportation generally refers to logistics distribution and express delivery [23]. For example, the things purchased on the current online shopping platform need to be shipped by express. Because of the convenience of shopping on the platform, this is generally a

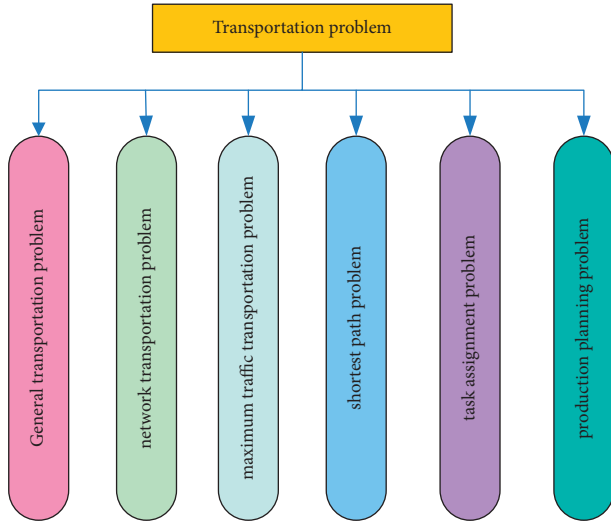


FIGURE 3: Shipping issues.

multimodal transportation method with various types and needs. The schematic diagram is shown in Figure 4.

It can be seen that the multiple categories in Figure 4 refer to different kinds of commodities. Multidemand means that buyers in different places may need the same kind of goods or different kinds of goods, and they need to take different transportation methods for this. In the choice of transportation modes, it is necessary to determine the optimal relationship between transportation cost, transportation efficiency, and transportation mode through the model and, at the same time, the optimization problem of reverse logistics transportation should be considered in the optimization of logistics transportation from the demand place to the supply place and the best transportation route should be found based on the back-and-forth transportation route, which improves the efficiency of logistics network transportation [24].

The maximum flow problem, also known as the F problem, is a problem of using an algorithm to allocate the traffic size of the transportation network, but it does not consider the most distributed problem of the amount of traffic, so it is insufficient to a certain extent. The maximum flow problem provides a theoretical basis for the actual transportation network, and a reasonable and convenient transportation route can be formulated by analyzing the flow in the running route. By studying the maximum flow problem, we can get a good understanding of the risk in the actual transportation, so as to avoid the loss caused by the risk as much as possible [25]. In the logistics transportation, not only the route selection but also the centralized transportation is required, so the shortest path and the centralized transportation mode are considered [26]. Due to the particularity of the transportation of dangerous and hazardous goods, the problem of transportation routes is very important and the time risk must also be considered.

2.3. Mathematical Model and Algorithm of the Transportation Problem. The mathematical model in the transportation problem is used for the final determination of the low-cost and high-safety transportation route by measuring the cost of

transportation, time cost, and other costs between the production and sales places. Simply put, it is a means to improve transportation safety and reduce costs by controlling some factors. This provides a better proposal for transportation between the production and sales locations. Multiobjective decision-making of transportation problems is carried out through artificial intelligence technology, mathematical model, and genetic algorithm. Among them, artificial intelligence technology enables mathematical models and algorithms to autonomously make predictions based on actual conditions and plays a solid role in the process of planning paths of mathematical models and algorithms [27]. Of course, artificial intelligence technology also needs to navigate the transportation between production and sales to avoid deviating from the original transportation route. The ultimate goal of the multi-index transportation problem is to minimize the total transportation cost [28].

To this end, we need to understand the main sources of transportation problems, places of demand, transportation costs, output, demand, etc. [29]. The schematic diagram of transportation problems is shown in Figure 5.

In Figure 5, if there are i production places, S_i ($i = 1, 2, 3, \dots$) for a commodity, and the output of each production place is U_i ($i = 1, 2, 3, \dots$), and there are j demand places, Q_j ($j = 1, 2, 3, \dots$) for this commodity, the required quantity of commodities in each demand place is G_j ($j = 1, 2, 3, \dots$). Then, there is a need for transportation between the place of origin and the place of demand. The transportation cost and the amount of transportation in the transportation problem will be generated, which are represented by T_i and M_j , respectively, and the matrix of the total transportation cost is expressed as follows:

$$[T] = \begin{bmatrix} T_1 & \dots & T_i \\ \dots & T_{2i} & \dots \\ T_i & \dots & T_1 \end{bmatrix}. \quad (1)$$

And, the matrix of shipping quantities is expressed as follows:

$$[M] = \begin{bmatrix} M_1 & \dots & M_j \\ \dots & M_{2j} & \dots \\ M_j & \dots & M_1 \end{bmatrix}. \quad (2)$$

To this end, we need to establish a mathematical model of multiple indicators as follows:

$$\sum_{j=1}^i T_e \geq M_j, \quad (j = 1, 2, 3, \dots). \quad (3)$$

Formula (3) represents that the production quantity T_e of the production place exceeds the shipped quantity of this production place, which is also a phenomenon under normal circumstances. However, usually, the quantity of a commodity shipped will not exceed the production quantity of the origin. The quantity of products arriving at the place of demand will not be lower than the quantity of commodities required by the place of demand, so its mathematical model can be expressed as follows:

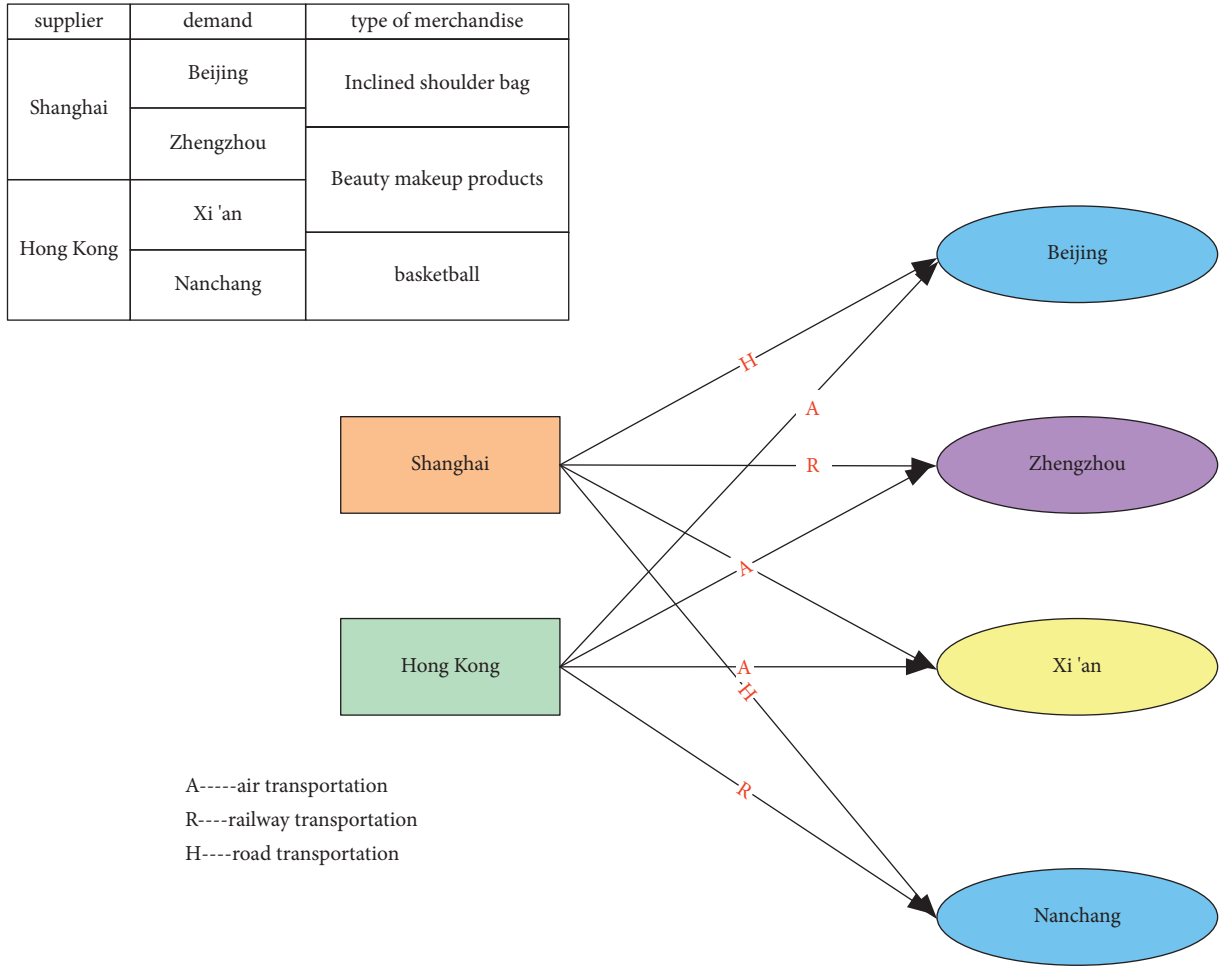


FIGURE 4: Multimodal transport with multiple types and demands.

$$\sum_{i=1}^j M_j \geq Y_e, \quad (j = 1, 2, 3 \dots). \quad (4)$$

Here, Y_e represents the total quantity of goods required by the demand place. So, in general, the mathematical model of the transportation problem is as follows:

$$\begin{aligned} \min T * M &= \sum_{j=1}^i \sum_{i=1}^j T_e * Y_e, \\ \text{s.t. } \sum_j G_1 &\leq U_1 (i, j = 1, 2, 3 \dots), \\ \sum_j G_1 &\geq T_e, \\ \text{s.t. } \sum_i M_j &\geq G_1 (i, j = 1, 2, 3 \dots), \\ \sum_i Y_e &\leq G_1, \\ T_e \geq 0, M_j \geq 0, U_1 \geq 0, Y_e &\geq 0 (e = 1, 2, 3 \dots i, j). \end{aligned} \quad (5)$$

For the multi-index transportation problem, it is necessary to achieve multiple goals in transportation; that is, to

find the optimal node in the case of multiple goals, the linear programming function of the multi-index transportation problem is as follows:

$$\begin{aligned} F(x) &= 1, (M_j \geq Y_e), \\ F(x) &= \frac{T_i - 1}{M_j - Y_e}, (Y_e \leq M_j \leq M_{2j}), \\ f(x) &= 0, (Y_e = M_j). \end{aligned} \quad (6)$$

Through the above-mentioned explicit planning, the initial optimal nodes of the timeline multiobjective transportation problem are obtained and then the genetic algorithm is used for further calculation. In transportation problems, it is also necessary to use intelligent algorithms to calculate the variables in the model. Transportation problems mainly include products, vehicles, demand locations, time, constraints, and objective functions [30]. The algorithm in the transportation problem is mainly divided into the genetic algorithm and the Hopfield neural network algorithm. The genetic algorithm is a global optimal search optimization algorithm. The flowchart of the genetic algorithm is shown in Figure 6.

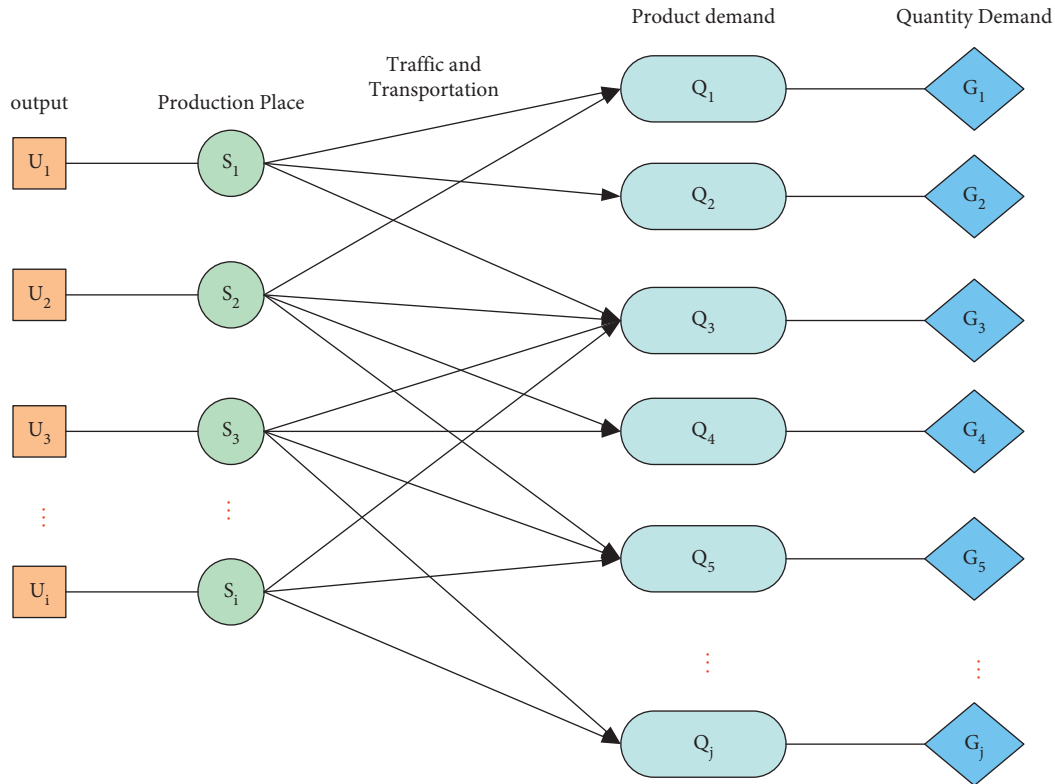


FIGURE 5: Schematic diagram of the transportation problem.

Assume that the output of the product production place is U , the production place is i , the quantity of products required by the demand place is G , and the demand place has j . When the quantity of demand places is greater than the quantity of production places, then the planning of transportation cost T and quantity M of products transported is as follows:

$$T = M * g. \quad (7)$$

Here, g is the unit price of commodity transportation. Then, the genetic algorithm is used to calculate the freight of multiple routes, and then, the transportation route is selected by comparing the freight. If there is only one production place X , but there are two demand places, there are two transportation routes Y_1 and Y_2 and the quantity of goods required by demand places Y_1 and Y_2 are G_1 and G_2 , respectively. Then, there are two transportation schemes. The first is to ship all the commodities from the two demand places from the production place and then transport them between the two demand places. The second is to transport the goods to the two demand places. The ultimate goal of the transportation problem is to reduce the freight; then, the freight of the first transportation scheme is calculated as follows:

$$\begin{aligned} T_1 &= G_1 * g + G_2 * g, \\ T_2 &= M * g + (M - G_1) * g, \\ M &< U. \end{aligned} \quad (8)$$

In this way, if $T_1 < T_2$, the transportation route of option 1 will be selected, and if $T_1 > T_2$, the transportation route of option 2 will be selected for commodity transportation. Moreover, with the development of today's society,

transportation problems are complex, so we need to combine artificial intelligence technology and establish mathematical models and algorithms to more efficiently solve multi-index transportation problems. At the same time, it can also ensure the quality of items in the process of transportation, so that the cost of transportation can be minimized [10]. Of course, some steep slopes and curves will be encountered during transportation, which will increase the risk of transportation. Therefore, the planning of the i transportation route also needs to consider the transportation risk. The calculation formula of transportation risk is as follows:

$$\text{Risk} = \frac{n + t}{L} * 100\%. \quad (9)$$

Here, n refers to the number of steep slopes encountered in the transportation route, while t represents the number of curves in the transportation route and L represents the total length of the transportation route. Therefore, the multi-index transportation problem should not only minimize the freight but also reduce the risk factor to ensure the least cost loss of goods during transportation.

3. Experiment and Analysis of the Multi-Index Transportation Problem

3.1. Statistics of Cargo Transportation Indicators

3.1.1. *Experiment 1.* This experiment assumes that there are 4 places of supply and 4 places of demand for a certain commodity. In the experiment, the mathematical model and

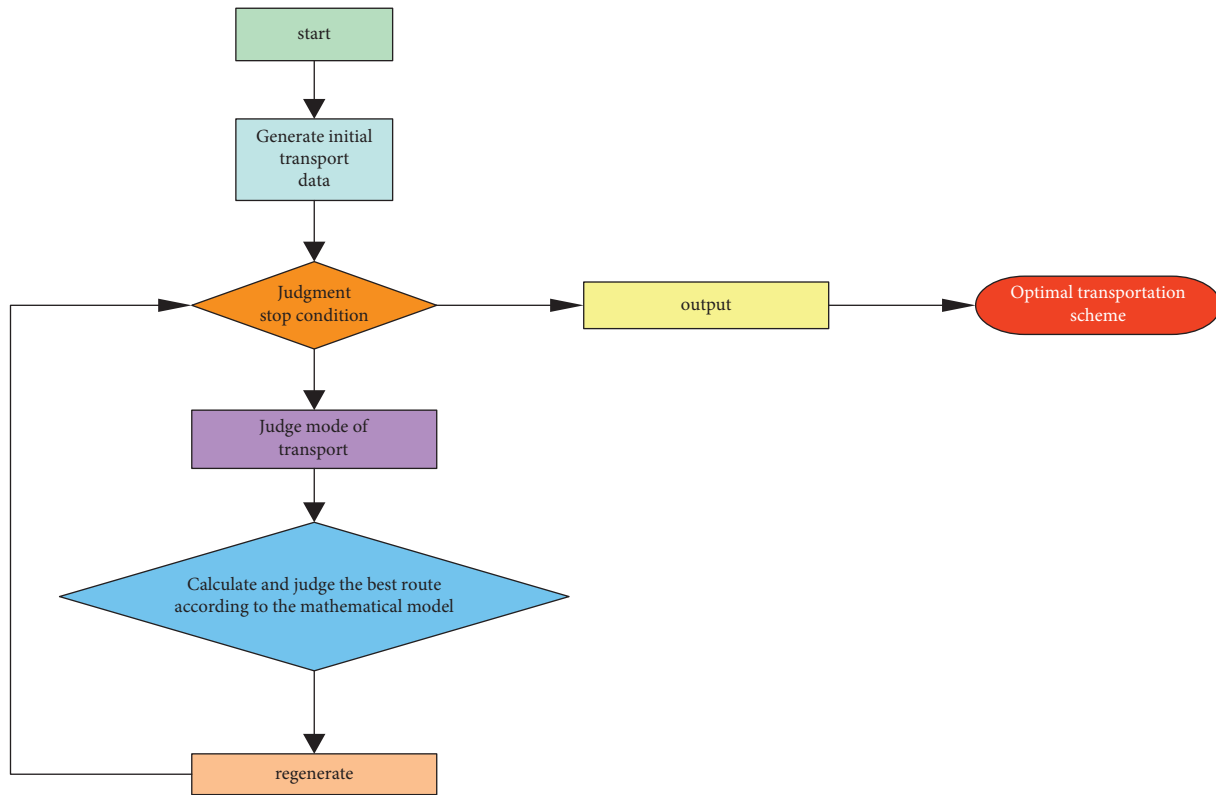


FIGURE 6: Genetic algorithm flow.

algorithm of multiobjective transportation problem and artificial intelligence technology will be used to analyze the freight, time, quality of goods, and transportation mode in the transportation process for statistics; while planning the best transportation route, it can also ensure the quality of the goods. In the transportation of goods, the means of transportation that need to be used will not be single, so there are many indicators that need to be considered. The means of transportation and related parameter assignments that need to be used this time are shown in Table 1.

Table 1 shows the maximum capacity and transportation costs of various means of transportation, which are used to calculate the transportation costs between the supply and demand locations in the later period and plan the optimal route between the supply and demand locations through mathematical models and algorithms. Among them, road transportation is the most flexible, so the planning of each transportation route requires road transportation, and the amount of commodities required between the supply and demand places is shown in Table 2.

In this way, it is necessary to plan the transportation route between the demand place and the supply place, and it is necessary to evaluate the freight, risk, and other indicators of the transportation route. According to the demand in the demand place in Table 2, the actual quantity of goods that the supply place needs to send is the supply quantity of the goods required by the demand place. For this reason, we need to calculate the transportation cost and transportation risk rate of various transportation methods.

The freight rate of a single shipping method calculated by mathematical models and algorithms and the shipping risk rate identified by artificial intelligence technology are shown in Figure 7.

The risk rate is calculated by taking into account the curves, steep slopes, and other influencing factors that need to be passed in the transportation route. In Figure 7(a), the shipping cost is the lowest for the transportation mode from the supply place to the demand place, while the freight cost of air freight is the highest, followed by railway and expressway. From the point of view of freight, the best mode of transport for demand a is rail, and the best transport for demand b is air. In Figure 7(b), the risk of air transport is the lowest overall, followed by rail transport. From other perspectives, because the transportation routes between different supply and demand places will be different, the standard of risk assessment is to assess the required operation route between the two places. But from a single means of transport and risk, rail transport is the best mode of transport.

3.2. Planning of Combined Transportation Routes

3.2.1. Experiment 2. This experiment still uses the data in Experiment 1 and plans a combined route, in which the shipping cost of the combined route will be changed. For better calculation, we recalculated the freight of the combined route, and the freight of the combined route is shown in Table 3.

TABLE 1: Assignment of means of transportation and related parameters (units: t and yuan).

Way of transportation	Shipping	Highway	Railway	Airport
Minimum processing capacity (t)	10000	2500	8000	2000
The loading point disaster recovery limit (t)	8000	2000	4000	1000
Fixed charge for loading point (Wanyuan)	5	7	8	9
Variable cost per unit	1.2	0.7	0.9	0.5

TABLE 2: Quantity of goods.

Place of supply	1	2	3	4
Quantity delivered (t)	32000	23000	30000	19000
Place of demand	a	b	c	d
Quantity demand (t)	20000	14000	24000	15000

Then, the freight and transportation risk rates required by the supply and demand places of a and b are shown in Figure 8.

Shown in Figure 8(a) are the shipping costs and risks of various combined routes used in a supply location. It can be seen from Figure 8(a) that the combination of air and road transportation has the highest transportation cost, but the lowest risk rate, while road transportation has the highest risk rate among all transportation methods. Compared with other modes of transportation, such as the combination of shipping and road and the combination of rail and road, the combination of shipping and road is extremely risky. In general, it is most suitable to use railway and road transportation, where the freight is moderate and the risk is lower, the total loss will be smaller, and the quality of the goods will be guaranteed. What is shown in Figure 8(b) is the comparison of the transportation combination mode adopted by the demand place b from the supply place. It can be seen from Figure 8(b) that the cost and risk of road transportation are extremely high, while the cost of the combination of air and road transportation is slightly lower than that of road transportation, the risk is extremely low, and the time required for air transportation is shorter. Therefore, the transportation mode of the place of demand b can be a combination of air transportation and road transportation.

Then, the mathematical model and the algorithm are compared to the best transportation methods obtained by comparing the specific data as shown in Figure 9.

As can be seen from Figure 9, among the three modes of transport in a demand place, the combined transport mode of rail and road has the lowest risk and freight. Therefore, through the planning route a of the mathematical model and artificial intelligence technology, the transportation of goods in demand should be carried out by a combination of railway transportation and road transportation. And, the mode of transportation at the place of demand b should also be a combination of railway and road transportation, because the freight and risk rate of this combination are the lowest.

3.3. Experimental Summary. From the above experiments, in the solution of transportation problems that introduce mathematical models and algorithms of artificial intelligence technology, the freight and risk factors of various routes can

be calculated more accurately. The optimal transport among these transport modes can be guided from the transport combinations verified in the experiments. In Experiment 1, the freight and risk rate generated by a single means of transportation were measured, and it was found that railway transportation is the most suitable for transporting commodities. Experiment 2 compared some of the combined transportation methods and found that the distance between each supply and demand location and the amount of goods transported will affect the level of freight and risk. Through the final comparison, it is found that the railway plus road transportation method has the lowest freight and risk and is the most suitable for transporting commodities.

4. Discussion

This paper has a certain understanding of the application of artificial intelligence technology in transportation, advanced traffic extends in all directions, and there are many intersections. These require traffic lights to coordinate, and artificial intelligence technology is involved in traffic lights [31]. The application of artificial intelligence technology in transportation can prevent many traffic accidents, so artificial intelligence promotes the development of transportation, for example, it can enter the station through face recognition at the gate channel of the entering station. And, it also improves the efficiency of people's travel and reduces the time cost of people's travel. To a certain extent, it has played a great role in the development of transportation. Artificial intelligence technology has also played an invaluable role in cross-border commodity transportation. It can plan transportation routes in advance, avoid unnecessary risks, reduce losses caused by accidental risks in the transportation process, and greatly promote the development of international trade.

This paper makes a certain analysis of the multi-index transportation problem. Multi-index refers to multiple goals, that is, multiple goals need to be achieved in the process of transportation. For example, minimizing the cost of transportation is the most important goal to consider in transportation issues. The second is to ensure the quality of the goods, ensure that the goods are in good condition during transportation, and reduce the damage of the goods caused by collisions. Then, there is the transportation time. The length of the transportation time has a certain relationship with the length of the transportation route. When planning a route, it is necessary to consider all factors of supply and demand, and in this process, it is also necessary to assess the risk of the route. Routes are planned to reduce transportation costs and avoid losses due to risks. The establishment of the mathematical model of the transportation

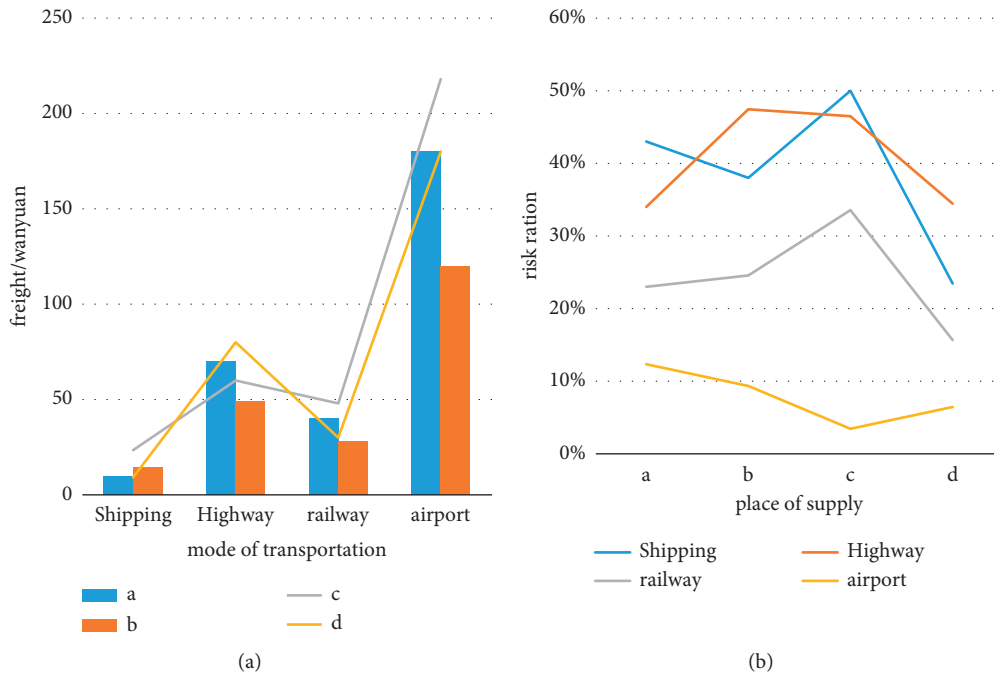


FIGURE 7: (a) Freight and (b) risk rates for a single shipping method.

TABLE 3: Combined route freight (unit: yuan/t).

Array mode	$S+H$	$R+H$	$A+H$	H
Minimum processing capacity (t)	20000	14000	24000	15000
Fixed charge for loading point (Wanyuan)	6	7.5	8	7
Variable cost per unit	1.2	0.3	0.2	1.4

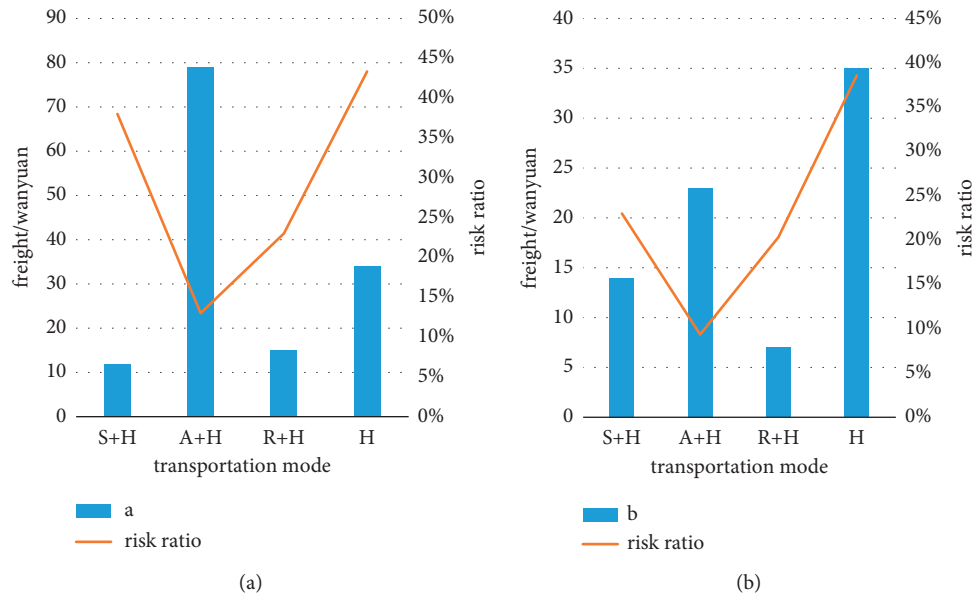


FIGURE 8: Freight and risk rates for a and b. (a) a demand place. (b) b demand place.

problem is to better calculate the transportation cost in the intricate route map and then use the genetic algorithm to find the optimal words to filter the route, which is the most effective way.

The experiments in this paper have estimated the transportation costs and risks required by several transportation modes using mathematical models and algorithms. In the process of estimation, artificial intelligence

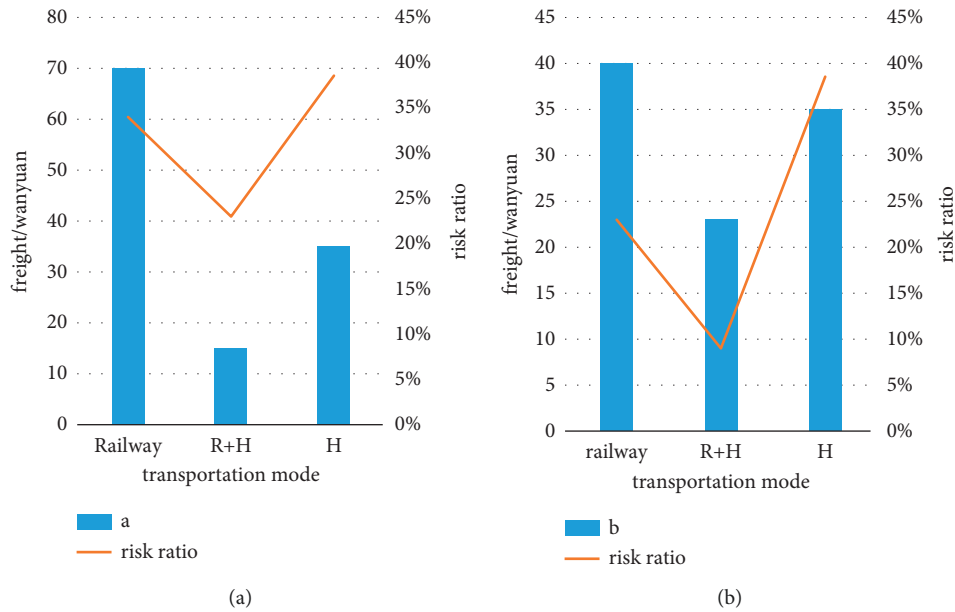


FIGURE 9: Optimal roadmap. (a) Route comparison of a demand place. (b) b demand place route comparison.

technology is also used to plan the route. Because the number of supply and demand places is different, there are many ways to combine various routes and the diversification of transportation means also increases the difficulty of route planning. Therefore, artificial intelligence technology can be used to list all passable transportation routes, and then, mathematical models and algorithms can be used to estimate the risk rate of transportation routes for transportation costs. This can greatly improve the efficiency of route planning and also provide a more reliable guarantee for the transportation of goods.

5. Conclusions

This paper combines mathematical models and algorithms for transportation problems with artificial intelligence. Artificial intelligence can facilitate the planning of transportation routes with mathematical models and algorithms in transportation problems and can also provide the data required in mathematical models and algorithms to estimate the freight and risks of transportation routes. In the multi-index transportation problem, the genetic algorithm can perform the optimal evaluation of the increasingly complex transportation routes and can accurately promote the estimated data of the mathematical model of the transportation routes. The experimental structure of this paper shows that the multi-index transportation problem model and algorithm combined with artificial intelligence technology can promote the planning of commodity transportation routes and minimize both freight and risk. And, it can also choose the optimal transportation route from the consideration of the sum and realize the multi-index problem of line transportation. Therefore, the research in this paper has great reference value for solving the problem of commodity transportation, which can promote the efficiency of upper-screen transportation, reduce transportation costs, and

avoid some unnecessary losses. However, because the factors affecting the transportation problem are complex, the research in this paper still fails to take into account all the influencing factors. It is hoped that all the factors can be taken into account in later research to make the mathematical model and algorithm of the transportation problem more practical.

Data Availability

The data that support the findings of this study are available from the author upon reasonable request.

Conflicts of Interest

The author declares no conflicts of interest.

References

- [1] Y. Zhen, K. Zhou, H. Fang et al., "Research on hybrid artificial intelligence optimization algorithm for grain transportation," *Journal of computer*, vol. 31, no. 2, pp. 35–44, 2020.
- [2] Z. Lv, S. Zhang, and W. Xiu, "Solving the security problem of intelligent transportation system with deep learning," *IEEE Transactions on Intelligent Transportation Systems*, vol. 22, 2020.
- [3] R. Zhang, P. Xie, C. Wang, G. Liu, and S. Wan, "Classifying transportation mode and speed from trajectory data via deep multi-Scale learning," *Computer Networks*, vol. 162, Article ID 106861, 2019.
- [4] Y. Liu, Y. Jing, and Y. Lu, "Research on quantitative remote sensing monitoring algorithm of air pollution based on artificial intelligence," *Journal of Chemistry*, vol. 2020, no. 2, pp. 1–7, 2020.
- [5] S.-B. Tsai and K. Wang, "Using a novel method to evaluate the performance of human resources in green logistics enterprises," *Ecological Chemistry and Engineering S*, vol. 26, no. 4, pp. 629–640, 2019.

- [6] Y. Chen, W. Zheng, W. Li, and Y. Huang, "The robustness and sustainability of port logistics systems for emergency supplies from overseas," *Journal of Advanced Transportation*, vol. 2020, 10 pages, 2020.
- [7] Q. Hu, F. Corman, B. Wiegman, and G. Lodewijks, "A tabu search algorithm to solve the integrated planning of container on an inter-terminal network connected with a hinterland rail network," *Transportation Research Part C: Emerging Technologies*, vol. 91, no. 7, pp. 15–36, 2018.
- [8] R. Borndorfer, T. Klug, L. Lamorgese, M. Carlo, R. Markus, and S. Thomas, "Recent success stories on integrated optimization of railway systems," *Transportation Research Part C: Emerging Technologies*, vol. 74, pp. 196–211, 2017.
- [9] A. Kawa and M. Anholcer, "Exclusionary constraints in transport - results of quantitative research," *Logforum*, vol. 16, no. 4, pp. 573–592, 2020.
- [10] A. G. Kukharchyk, "Transport task OF optimization OF costs with multimodal transportation," *Economic Innovations*, vol. 19, no. 2, pp. 157–163, 2017.
- [11] W. V. Hoeve, *Integration of constraint programming, artificial intelligence, and operations research*, Springer International Publishing, Manhattan, NY, USA, 2018.
- [12] Z. Lv, Y. Li, H. Feng, and H. Lv, "Deep Learning for Security in Digital Twins of Cooperative Intelligent Transportation Systems," *IEEE Transactions on Intelligent Transportation Systems*, 2021.
- [13] C.-H. Chen, "A cell probe-based method for vehicle speed estimation," *IEICE - Transactions on Fundamentals of Electronics, Communications and Computer Sciences*, vol. E103.A, no. 1, pp. 265–267, 2020.
- [14] H. Song, R. Srinivasan, T. Sookoor, and S. Jeschke, *Smart Cities: Foundations, Principles and Applications*, Wiley, Hoboken, NJ, USA, 2017.
- [15] S. Stüdl, M. Corless, R. H. Middleton, and R. Shorten, "On the AIMD algorithm under saturation constraints," *Automatic Control, IEEE Transactions on*, vol. 62, no. 12, pp. 6392–6398, 2017.
- [16] Z. Lv, X. Li, W. Wang, B. Zhang, J. Hu, and S. Feng, "Government affairs service platform for smart city," *Future Generation Computer Systems*, vol. 81, pp. 443–451, 2018.
- [17] Z. Lv, R. Lou, and K. Singh, "AI Empowered Communication Systems for Intelligent Transportation Systems," *IEEE Transactions on Intelligent Transportation Systems*, vol. 22, 2020.
- [18] M. Mouna and B. Sadok, "Firework algorithm for multi-objective optimization of A multimodal transportation network problem - ScienceDirect," *Procedia Computer Science*, vol. 112, no. 34, pp. 1670–1682, 2017.
- [19] Z. Liping and W. Guoyuan, "Dynamic lane grouping at isolated intersections: problem formulation and performance analysis," *Transportation Research Record*, vol. 2311, no. 1, pp. 152–166, 2018.
- [20] W. B. Daszczuk, "Measures of structure and operation of automated transit networks," *IEEE Transactions on Intelligent Transportation Systems*, vol. 21, no. 7, pp. 2966–2979, 2020.
- [21] G. Cao, "Research on the application of artificial intelligence algorithm in logistics distribution route optimization," *Paper Asia*, vol. 34, no. 5, pp. 35–38, 2018.
- [22] F. Shabani-Naeeni and R. G. Yaghin, "Integrating data visibility decision in a multi-objective procurement transport planning under risk: a modified NSGA-II," *Applied Soft Computing*, vol. 107, no. 1, pp. 107–167, 2021.
- [23] K. Huang, C. Lu, and M. Lian, "Research on modeling and algorithm for three-echelon location-routing problem," *Xitong Gongcheng Lilun yu Shijian/System Engineering Theory and Practice*, vol. 38, no. 3, pp. 743–754, 2018.
- [24] M. A. Arslanov, S. M. Minatullaev, and A. A. Filippov, "Mathematical model OF the organization OF passengers' transportation IN stopping-trans-relocation points with a multiple change OF passenger traffic," *Vestnik SibADI*, vol. 15, no. 3, pp. 362–371, 2018.
- [25] G. Wang, A. Chen, S. Kitthamkesorn et al., "A multi-modal network equilibrium model with captive mode choice and path size logit route choice," *Transportation Research Part A: Policy and Practice*, vol. 136, no. 25, pp. 293–317, 2020.
- [26] Y. Yeh and C. Low, "Mathematical modelling for a multi-product inventory routing problem with split delivery," *Applied Mathematics and Applied Physics*, no. 9, pp. 1607–1612, 2017.
- [27] M. T. Alonso, R. Alvarez-Valdes, M. Iori, and F. Parreño, "Mathematical models for multi container loading problems with practical constraints," *Computers & Industrial Engineering*, vol. 127, pp. 722–733, 2019.
- [28] S. Singh, S. K. Chauhan, and K. Deep, "A Bi-criteria multi-index bulk transportation problem," *Annals of Pure and Applied Mathematics*, vol. 16, no. 2, pp. 479–485, 2018.
- [29] M. G. Mnif and S. Bouamama, "Multi-objective optimization methods for transportation network problems," *International Journal of Operations Research and Information Systems*, vol. 11, no. 1, pp. 1–36, 2020.
- [30] M. M. Acharya, A. Gessesse, R. Mishra, and S. Acharya, "Multi-objective stochastic transportation problem involving three-parameter extreme value distribution," *Yugoslav Journal of Operations Research*, vol. 29, no. 35, p. 36, 2019.
- [31] Z. Song, Y. He, and L. Zhang, "Integrated planning of park-and-ride facilities and transit service," *Transportation Research Part C: Emerging Technologies*, vol. 74, pp. 182–195, 2017.

Research Article

Urban Traffic State Estimation with Online Car-Hailing Data: A Dynamic Tensor-Based Bayesian Probabilistic Decomposition Approach

Wenqi Lu ^{1,2}, Ziwei Yi ^{1,2}, Dongyu Luo ³, Yikang Rui ^{1,2}, Bin Ran ^{1,2}, Jianqing Wu,⁴ and Tao Li⁵

¹School of Transportation, Southeast University, Nanjing, Jiangsu 211189, China

²Joint Research Institute on Internet of Mobility, Southeast University and University of Wisconsin-Madison, Southeast University, Nanjing 211189, China

³Key Laboratory of Transport Industry of Big Data Application Technologies for Comprehensive Transport, Beijing Jiaotong University, Beijing 10044, China

⁴School of Qilu Transportation, Shandong University, Jinan 250002, China

⁵Shandong Hi-speed Construction Management Group Co., Ltd., Jinan 250000, China

Correspondence should be addressed to Yikang Rui; 101012189@seu.edu.cn

Received 2 January 2022; Accepted 4 March 2022; Published 26 April 2022

Academic Editor: Sang-Bing Tsai

Copyright © 2022 Wenqi Lu et al. This is an open access article distributed under the Creative Commons Attribution License, which permits unrestricted use, distribution, and reproduction in any medium, provided the original work is properly cited.

Timely and precise traffic state estimation of urban roads is significant for urban traffic management and operation. However, most of the advanced studies focus on building complex deep learning structures to learn the spatiotemporal feature of the urban traffic flow, ignoring improving the efficiency of the traffic state estimation. Considering the benefit of the tensor decomposition, we present a novel urban traffic state estimation based on dynamic tensor and Bayesian probabilistic decomposition. Firstly, the real-time traffic speed data are organized in the form of a dynamic tensor which contains the spatiotemporal characteristics of the traffic state. Then, a dynamic tensor Bayesian probabilistic decomposition (DTBPD) approach is built by decomposing the dynamic tensor into the outer product of several vectors. Afterward, the Gibbs sampling method is introduced to calibrate the parameters of the DTBPD models. Finally, the real-world traffic speeds data extracted from online car-hailing trajectories are employed to validate the model performance. Experimental results indicate that the proposed model can greatly reduce computational time while maintaining relatively high accuracy. Meanwhile, the DTBPD model outperforms the state-of-the-art models in terms of both single-step-ahead and multistep-ahead traffic state estimation.

1. Introduction

With the rapid advancement of urbanization, urban traffic congestion has become a critical problem in the construction of smart cities [1]. It may take place when the traffic demand is beyond the capacity of the road network, resulting in more traffic accidents, severe air pollution, and increased fuel consumption [2]. As a significant part of the intelligent transportation system and automated vehicle technology [3], accurate estimation of the urban road network traffic state in the near future is very important for

traffic management and planning in reducing traffic congestion. By providing accurate and comprehensive network state estimation information, human-driven vehicles and connected automated vehicles (CAV) can optimize travel paths and generate lane-changing recommendations [4]. Fleet management companies are capable of operating the dispatch system more efficiently [5]. Traffic management agencies can update the control plan in real time to improve control performance. Besides, the traffic policy-making department can analyze emerging needs and evaluate the policy impact [6, 7].

During these years, many approaches have been proposed for the estimation traffic state of the urban roads including statistical models [8], artificial-based intelligent models [9], and deep learning-based models [10]. From the perspective of the research objects, the macroscopic parameters of the lane sections, intersection, link sections, and road networks, such as travel speed, volume, and density, are usually considered as the estimated targets [11].

However, the challenges of the urban traffic state estimation still exist as follows. (1) The collection of urban traffic data may still rely on stationary detectors or cameras, which is expensive and inflexible. It is not usually a realistic choice to deploy sufficient detectors on low-level roads such as secondary roads and access roads. The traffic states of some low-level roads are always neglected though they may have a significant influence on the future state of the urban network [11]. (2) Though the deep learning-based models are capable of learning the spatiotemporal feature of urban traffic state, the performance of these methods is partly influenced by the quantity and quality of the research data. Achieving a well-trained deep learning model is time-consuming, and it is difficult to update the parameters of the trained models in a short time.

Nowadays, the massive trajectory data of various car-hailing companies have become a popular and alternative source for analyzing traffic operation and traffic emissions [12–14], and it also provides the basis for the urban traffic state estimation since the trajectory data are high-precision, high-resolution, and widely distributed. In addition, the tensor-based approaches turn out to be efficient for dealing with traffic data due to their ability to capture the multimode relevance of data [15–18], and it provides a new perspective on modeling.

Inspired by the rise of ride-hailing trajectory data and the benefit of tensor mode, this paper proposes a traffic state estimation model based on dynamic tensor Bayesian probabilistic decomposition (DTBPD). Firstly, the concept of the dynamic tensor is introduced to form the urban spatiotemporal data into the tensor pattern. Then a higher-order Bayesian matrix factorization model is established based on CANDECOMP/PARAFAC (CP) decomposition. Meanwhile, the Gibbs sampling algorithm is established to perform inference on the element of the Bayesian decomposition model. Finally, we utilize the urban traffic speed data captured from online car-hailing trajectory data provided by the Didi company to validate the feasibility of the DTBPD approach under the scenarios of different types of roads. As far as the authors know, this is the first time that a dynamic tensor-based probabilistic paradigm has been employed for urban traffic state estimation.

The main contributions of this paper can be summarized as follows:

- (1) The traffic speeds of the urban network are organized in the form of the dynamic tensor pattern with consideration of the spatiotemporal features for the first time.
- (2) We propose a dynamic tensor Bayesian probability decomposition structure that is capable of modeling

the dynamic tensor in real time with highly spatiotemporal data and provide a Gibbs sampling algorithm for estimating model parameters.

- (3) The traffic speeds of the urban network are extracted from the online car-hailing trajectory data of Didi company and used for validating the efficiency of the DTBPD model under multiple scenarios. Experimental results demonstrate that the DTBPD model is not only accurate but also time-saving during the calibration process.

In the next section, a general overview of related work on urban traffic estimation is provided. Section 3 gives the basic definition of tensor decomposition. The methodology of the DTBPD model is introduced in Section 4. In Section 5, trajectory data description and preprocessing with data analysis are provided. The results and discussion of the experiments are introduced in Section 6. Some conclusions and future work are discussed in Section 7.

2. Related Work

The methods for estimating traffic state usually can be categorized into two classes including the parametric methods and nonparametric methods.

The common parametric methods include the statistical method, time-series method, and Kalman filter method [11]. In the time series method, the most common method is the Autoregressive integrated moving average model (ARIMA) and Ahmed and Cook [19] applied it to the traffic state estimation. Since ARIMA is only applicable to several scenarios with continuous and sufficient historical data, many scholars extended the ARIMA such as seasonal ARIMA (SARIMA) [20]. Another typical nonparametric approach is Kalman filter-based methods. Using the information of CAVs, Emami et al. [21] gave a faded memory Kalman filter to forecast the short-term flow at urban arterials. However, the parametric methods normally have fixed structures and are unable to fully learn the spatiotemporal characteristics of traffic flow.

With the development of mobile communication networks and big data, the nonparametric methods represented by machine learning models emerged to deal with the above issues [22–24]. For example, Castro-Neto et al. [25] built an online support vector machine model considering normal conditions and abnormal conditions such as accidents. Sun et al. [26] proposed a dynamic process K-nearest Neighbor method, which enables KNN parameters to be self-adjusted and robust without the need to predefine models or train parameters.

In addition, the excellent performance of deep learning (DL) in processing massive data has also attracted extensive attention, and it has been widely used in computer vision, semantic recognition, and automatic driving. In recent years, DL-based models [27–31] have been introduced into traffic flow estimation. Lv et al. [32] proposed a deep architecture model considering the temporal and spatial characteristics of the traffic flow by employing the autoencoder. To solve the long-term dependence in the

prediction process, some variants of recurrent neural networks (RNN), such as long short-term memory (LSTM) neural network [33], Gated recurrent unit (GRU) neural network [34], and Transformer [35] were proposed and applied to learning the temporal characteristics for the traffic state estimation. Ma et al. [36] represented traffic flow data as images and used a convolutional neural network-based architecture to estimate the traffic state in a large network. Furthermore, some DL-based combination models [37–40] have been proposed to improve the ability to learn spatiotemporal features and the robustness of the estimation. Wu et al. [41] proposed a traffic flow prediction model with a hybrid DL neural network, where convolutional neural networks (CNN) and RNN were used to extract spatiotemporal features, respectively, and an attention mechanism was introduced to determine the importance of historical data. Li et al. [42] employed a deep fusion model combining stacked restricted Boltzmann machines to forecast the accident duration. To capture the spatial and temporal dependences simultaneously, Zhao et al. [43] constructed a novel neural network-based traffic forecasting method named T-GCN, which combines the graph convolutional network (GCN) [44] and the GRU for traffic forecasting. Although the DL-based traffic state estimation approaches can fully mine the potential characteristics of the traffic flow, DL-based traffic state estimation approaches take a long time to train or calibrate the models, resulting in inconvenient and inflexible updates of the parameters [45]. Meanwhile, tuning the parameters of a DL-models reasonably is a very difficult task and highly depends on experience, which prevents these models from being used in practice [29].

To tackle the above problem, tensor-based methods [18, 46–48] have become new solutions for traffic estimation issues due to their efficient architecture to mine temporal and spatial correlations of the traffic flow. Ran et al. [49] built a Tucker decomposition-based imputation method for the traffic state estimation of the floating car system. Further, Ran et al. [50] provided a high accuracy low-rank tensor completion (HaLRTC) algorithm for estimating missing traffic speed data, and it can address the extreme case where the data of a long period of one or several weeks are completely missing [51]. However, these models rely on trace norm minimization to find a low-rank approximation to the original incomplete tensor, and they are often prone to overfitting when the missing rate is large. To address this issue, Bayesian inference methods such as the Markov chain Monte Carlo algorithm and variational inference have been designed and used for tensor decomposition [52]. For instance, Tang et al. [53] constructed a tensor decomposition method to estimate traffic flow parameters of signalized intersections with collected vehicle trajectories. Using the large-scale and sparse GPS data generated by taxicabs, Tang et al. [54] established a novel tensor-based Bayesian probabilistic model for estimating the travel time of the road links. To efficiently capture the spatiotemporal characteristics of traffic flow with tensor pattern and improve the performance of the tensor decomposition approach, we combine the concept of the dynamic tensor with the Bayesian probabilistic decomposition (DTBPD) for the first

time. By establishing a Gibbs sampling algorithm to estimate the proposed model constantly and dynamically, the future traffic state data in dynamic tensor can be generated efficiently and stably.

3. Tensor Basis

3.1. Dynamic Tensor. Tensors known as multidimensional arrays are higher-order generalizations of vectors and matrices. The d^{th} -order tensor is denoted as $\mathbf{X} \in \mathbb{R}^{I_1 \times I_2 \times \dots \times I_d}$. Each dimension of a multidimensional array is called a mode. A sequence of d^{th} -order tensors $\mathbf{X}_1, \mathbf{X}_2, \mathbf{X}_3, \dots, \mathbf{X}_T$ with $\mathbf{X}_t \in \mathbb{R}^{I_1 \times I_2 \times \dots \times I_d}$ ($1 \leq t \leq T$) can be denoted as a $(d+1)^{\text{th}}$ -order tensor stream where T is the maximum index of the time intervals. Figure 1 indicates an example of the tensor stream of the d^{th} -order $\mathbf{X}_t \in \mathbb{R}^{I_1 \times I_2 \times \dots \times I_d}$.

In the task of making traffic speed estimation of urban traffic state, only spatiotemporal characteristics of the tensors from several previous time intervals in the tensor stream are necessary. Therefore, a sliding time window H at time interval t is employed to localize the tensor stream into a small one, which can be written as $\tilde{\mathbf{X}}_t = \{\mathbf{X}_{t-H+1}, \mathbf{X}_{t-H+2}, \dots, \mathbf{X}_t\}$. Figure 2 reveals the tensor stream separated by employing a sliding time window.

3.2. CANDECOMP/PARAFAC Decomposition. Let $\tilde{\mathbf{X}} \in \mathbb{R}^{I_1 \times I_2 \times \dots \times I_d}$ be the dynamic tensor containing the observed historical values and missing values to be forecasted, where I_k is the dimension along the k^{th} way $k \in \{1, 2, \dots, d\}$. x_{i_1, i_2, \dots, i_d} ($1 \leq i_k \leq I_k$) is a value of an entry in $\tilde{\mathbf{X}}$. The idea of CP decomposition is to approximate $\tilde{\mathbf{X}}$ by calculating the sum of R rank-one component tensors as follows:

$$\tilde{\mathbf{X}} = \sum_{r=1}^R \mathbf{a}_r^1 \circ \mathbf{a}_r^2 \circ \dots \circ \mathbf{a}_r^d, \quad (1)$$

where \circ represent the outer product of two vectors. $\mathbf{a}_r^k \in \mathbb{R}^{I_k}$ is the r^{th} column vector of the decomposed factor matrix $A \in \mathbb{R}^{I_k \times R}$ and $\mathbf{a}_r^1 \circ \mathbf{a}_r^2 \circ \dots \circ \mathbf{a}_r^d$ is a rank-one tensor. R is the CP rank of the tensor $\tilde{\mathbf{X}}$. Correspondingly, the element $\tilde{x}_{i_1, i_2, \dots, i_d}$ in the tensor $\tilde{\mathbf{X}}$ is written as follows:

$$\begin{aligned} \tilde{x}_{i_1, i_2, \dots, i_d} &= \sum_{r=1}^R a_{i_1, r}^1 a_{i_2, r}^2 \dots a_{i_d, r}^d, \\ &= 1, 2, \dots, I_1, \dots, i_d \\ &= 1, 2, \dots, I_d, \end{aligned} \quad (2)$$

where $a_{i_k, r}^k$ is the element with an index of (i_k, r) in the factor matrix $A_k \in \mathbb{R}^{I_k \times R}$.

4. Dynamic Tensor-Based Bayesian Probabilistic Decomposition Approach

This section demonstrates a dynamic tensor-based Bayesian probabilistic decomposition approach for estimating the urban traffic states. As a common indicator of evaluating the traffic states, the average speed of the vehicle on a link

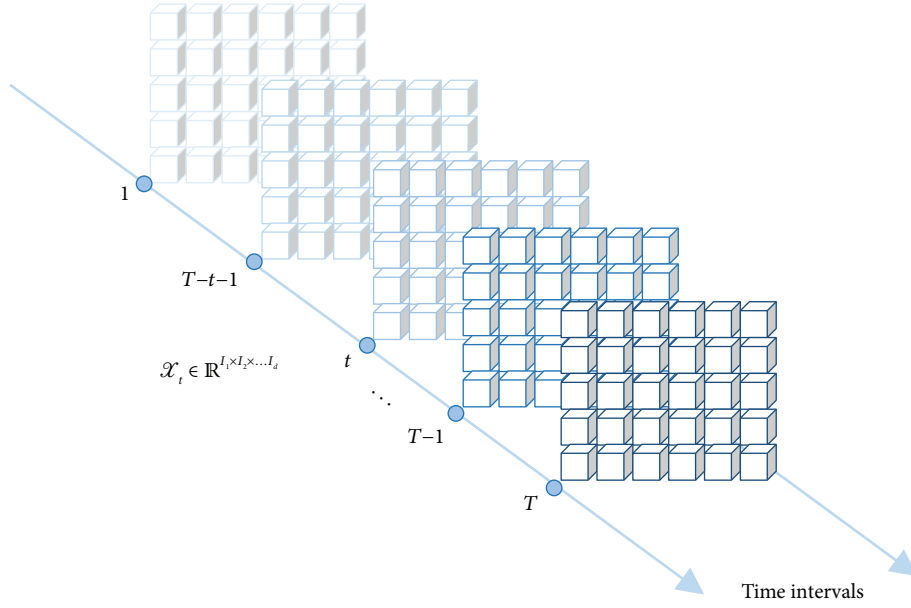


FIGURE 1: The schematic diagram of a d^{th} -order tensor stream.

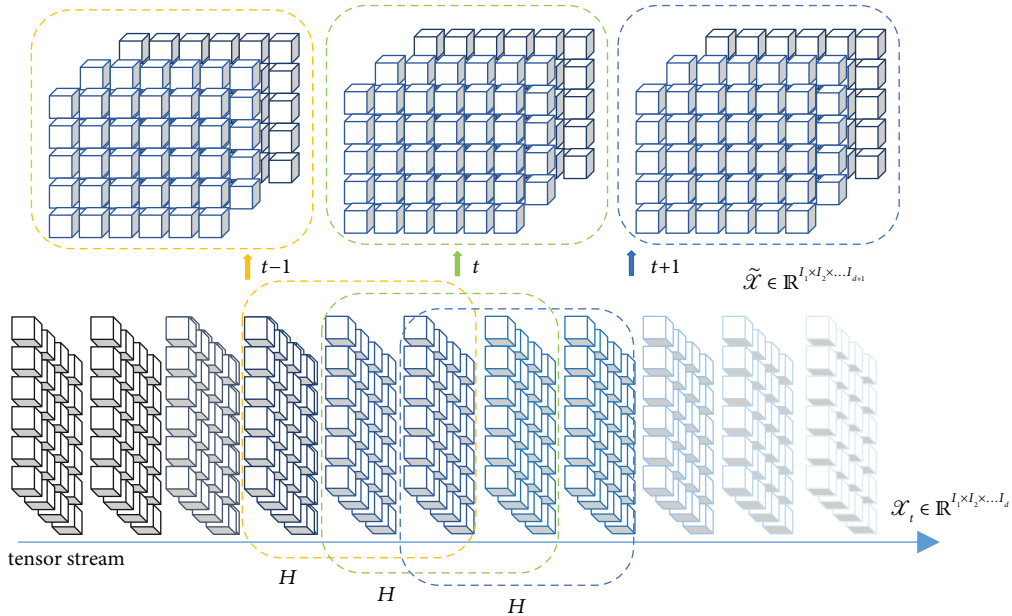


FIGURE 2: The divided tensor stream with a time horizon.

section during a time interval is utilized to represent the traffic state.

4.1. Problem Statement. Road network speed estimation is to predict the traffic speed in the future by using the speed data of the existing historical time.

Define $\bar{X} \in \mathbb{R}^{I_1 \times I_2 \times \dots \times I_n}$ as the n^{th} -order tensor flow represented by road network speed data. I_1, \dots, I_n represent different dimensions of the tensor, such as the number of link sections, the number of days in different weeks, the number of time intervals, and other dimensions. The dynamic tensors $\tilde{X} \in \mathbb{R}^{I_1 \times \dots \times H \times \dots \times I_n}$ can be extracted from the tensor stream with the sliding time window set as H . Note

that $\tilde{X} \in \mathbb{R}^{I_1 \times \dots \times H \times \dots \times I_n}$ contains the traffic speeds to be estimated with the prediction horizon set as P and $1 \leq P \leq H$.

If I_i represents the sliding time window of the dynamic tensor, the value of the I_i can be represented as H , which includes the traffic speeds of the time intervals that need to be estimated. Assume P defines the estimation horizon and $1 \leq P \leq H$; therefore, the state estimation can be written as follows:

$$\bar{y}^{I_n \times P} = f\left(\tilde{X}^{I_1 \times \dots \times H \times \dots \times I_n}\right), \quad (3)$$

where \bar{y} represents the traffic flow data to be estimated. $f(\cdot)$ denotes the estimation model.

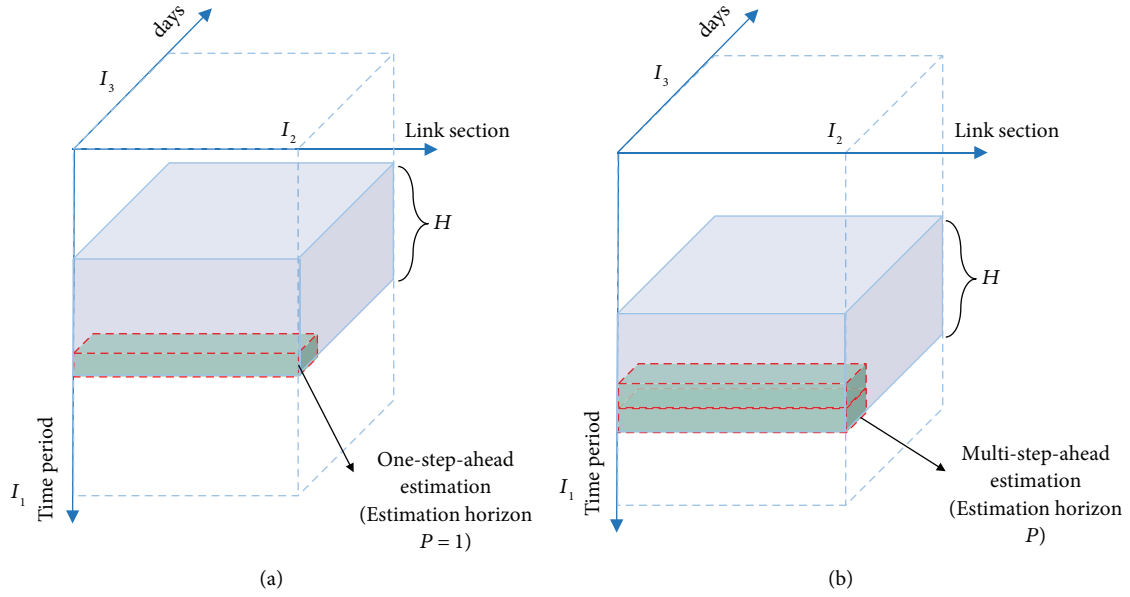


FIGURE 3: Example of the dynamic tensor with traffic speeds to be estimated. (a) One-step ahead estimation; (b) multistep ahead estimation.

Figure 3 shows the example of the dynamic tensor extracted from the tensor stream with three dimensions, where I_1 represents the periods, I_2 represents the number of the research link sections, and I_3 represents the number of days in different weeks. In addition, Figure 3 indicates two cases including the one-step-ahead prediction and multi-step-ahead estimation, respectively. Note that the iterated strategy indicated by Zhan et al. [55], which takes the estimated value as the input, was utilized to realize multistep ahead estimation.

4.2. Tensor-Based Bayesian Probabilistic CP Decomposition.

This section introduces the Bayesian probabilistic CP decomposition utilized to produce the predicted value in a dynamic tensor $\tilde{\mathbf{X}}$. Assume $\tilde{\mathbf{X}}$ is a 3rd-order tensor and according to the definition of the CP decomposition, we have the following:

$$\tilde{\mathbf{X}} = \sum_{r=1}^R \mathbf{a}_r \circ \mathbf{b}_r \circ \mathbf{c}_r, \quad (4)$$

where \mathbf{a}_r , \mathbf{b}_r , and \mathbf{c}_r represent the r -th row of the factor matrix $\mathbf{A} \in \mathbb{R}^{I_1 \times R}$, $\mathbf{B} \in \mathbb{R}^{I_2 \times R}$, and $\mathbf{C} \in \mathbb{R}^{I_3 \times R}$.

Suppose that the noise term of the measured entry $p \in P_o$ in the approximation obeys independent Gaussian distribution as follows:

$$x_p \sim \mathbf{N}(\hat{x}_p, \sigma^{-1}), \quad (5)$$

where $\mathbf{N}(\cdot)$ stands for the Gaussian distribution and σ is the precision item which is equal to the inverse of the covariance. Note that σ is a universal parameter for all elements.

To construct model on the tensor data adequately, flexible prior distributions are placed over both the precision item σ and the factor matrices. To be specific, the prior

distributions over the row vectors in all factor matrices are assumed to obey multivariate Gaussians.

$$\begin{aligned} \mathbf{a}_i &\sim \mathbf{N}(\mu_a, (\Lambda_a)^{-1}), i = 1, 2, \dots, I_1, \\ \mathbf{b}_j &\sim \mathbf{N}(\mu_b, (\Lambda_b)^{-1}), j = 1, 2, \dots, I_2, \\ \mathbf{c}_k &\sim \mathbf{N}(\mu_c, (\Lambda_c)^{-1}), k = 1, 2, \dots, I_3. \end{aligned} \quad (6)$$

The key concept of the fully Bayesian scheme is to treat the hyperparameters including σ , $\theta_a \equiv \{\mu_a, \Lambda_a\}$, $\theta_b \equiv \{\mu_b, \Lambda_b\}$, and $\theta_c \equiv \{\mu_c, \Lambda_c\}$ as random variables. According to the related work done by Salakhutdinov and Mnih [56], Tang et al. [54], and Chen et al. [52], conjugate Gaussian-Wishart priors can be set on the hyperparameters $\mu_a, \mu_b, \mu_c \in \mathbb{R}^{R \times 1}$ and $\Lambda_a, \Lambda_b, \Lambda_c \in \mathbb{R}^{R \times R}$ as follows:

$$\begin{aligned} p(\theta_a) &\sim \mathbf{N}(\mu_a, (\beta_0 \Lambda_a)^{-1}) \times \mathbf{W}(\Lambda_a | W_0, \nu_0), \\ p(\theta_b) &\sim \mathbf{N}(\mu_b, (\beta_0 \Lambda_b)^{-1}) \times \mathbf{W}(\Lambda_b | W_0, \nu_0), \\ p(\theta_c) &\sim \mathbf{N}(\mu_c, (\beta_0 \Lambda_c)^{-1}) \times \mathbf{W}(\Lambda_c | W_0, \nu_0), \end{aligned} \quad (7)$$

where $\mathbf{G}(\cdot)$ is a Gamma distribution. $\mathbf{W}(\cdot)$ represents a Wishart distribution with ν_0 degrees of freedom and a $R \times R$ scale matrix W_0 . $\mathbf{W}(\cdot)$ can be written as follows:

$$\mathbf{W}(\Lambda^k | W_0, \nu_0) = \frac{1}{C} |\Lambda^k|^{(\nu_0 - R - 1)/2} \exp\left\{-\frac{1}{2} \text{tr}(W_0^{-1} \Lambda^k)\right\}, \quad (8)$$

where $\text{tr}(\cdot)$ defines the trace function of a square matrix, which is the sum of all elements on its main diagonal.

Next, the precision item σ in (5) needs to be estimated. Under the assumption of Gaussian distribution, the parameters reflect the noise level. Under the scenario of urban traffic state estimation, the data is constantly updated with time, so the precision is unknown, and it is unable to be

completely captured by the reciprocal of the variance of all historical data. To improve the robustness of the model, the conjugate gamma distribution prior $\mathbf{G}(\cdot)$ is set for the precision item and it can be expressed as follows:

$$\sigma \sim \mathbf{G}(\tilde{W}_0, \tilde{v}_0), \quad (9)$$

where \tilde{W}_0 and \tilde{v}_0 represent the shape parameter and the rate parameter, respectively.

And we have the following:

$$p(\sigma) \sim G(\tilde{W}_0, \tilde{v}_0) = \frac{\tilde{v}_0^{\tilde{W}_0} \sigma^{\tilde{W}_0 - 1} \exp(-\tilde{v}_0 \sigma)}{\Gamma(\tilde{W}_0)}. \quad (10)$$

In this way, the distribution of the traffic speeds to be estimated in \tilde{X} can be obtained by the Bayesian inference algorithm as follows:

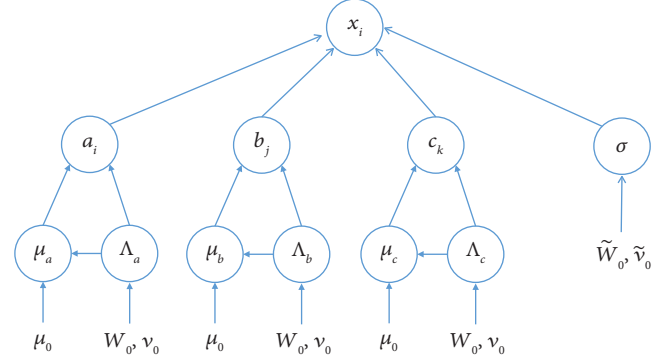


FIGURE 4: Graphical model for the DTBPD approach with 3rd-order tensor.

$$p(\hat{x}_p | \tilde{X}) = \int p(\hat{x}_p | \mathbf{a}, \mathbf{b}, \mathbf{c}, \sigma) p(A, B, C, \sigma, \theta_a, \theta_b, \theta_c | \tilde{X}) d\{A, B, C, \sigma, \theta_a, \theta_b, \theta_c\}, p \in P_e \quad (11)$$

Figure 4 indicates the graphical model which describes the generation procedure of the Bayesian probabilistic CP decomposition. Note that μ_0 , \tilde{v}_0 , \tilde{W}_0 , v_0 , and W_0 are hyperparameters that should be given in advance.

4.3. Markov Chain Monte Carlo Model. Considering the distribution of the speeds in the near future by (11) is a multidimensional integral, numerical methods can be applied to solve this issue. By treating $p(\hat{x}_p | \tilde{X})$ as the expectation of $p(\hat{x}_p | A, B, C, \sigma)$ over the posterior distribution $p(A, B, C, \theta_a, \theta_b, \theta_c, \sigma | \tilde{X})$, $p(\hat{x}_p | \tilde{X})$ can be estimated by averaging the samples from this posterior distribution. To sample from the complicated posterior distribution that is hard to sample directly, a novel Gibbs sampling algorithm is provided to perform inference on the graphical model. Gibbs sampling algorithm is a widely used Markov Chain Monte Carlo-based approach for Bayesian inference. According to the computation details of conditional distribution discussed in reference [52, 54, 57], an efficient Gibbs sampling algorithm is summarized in Algorithm 1.

By running the Gibbs sampling algorithm several times under a stationary state, the estimation traffic speeds can be written as follows:

$$p(\hat{x}_p | \tilde{X}) = \frac{1}{M} \sum_{t=1}^M \mathbf{N} \left(\sum_{r=1}^R a_{ir}(t) b_{jr}(t) c_{kr}(t), \sigma_t^{-1} \right), \quad (12)$$

where \tilde{X} represents measured dynamic tensor. \hat{x}_p is an entry to be predicted and M is the number of iteration. $a_{ir}(t)$ is the (i, r) entry in the factor matrix A during the t -th iteration. $b_{jr}(t)$ is the (i, r) entry in the factor matrix B during the t -th iteration. $c_{kr}(t)$ is the (i, r) entry in the factor matrix C during the t -th iteration. σ_t^{-1} defines precision item during the t -th iteration.

5. Experiment

5.1. Trajectory Data Description and Preprocessing. The data used in this paper mainly include trajectory data and urban network data. The online car-hailing trajectory data of Xi'an provided by the Didi open project (<https://outreach.didichuxing.com/research/opendata/>) is employed to extract the trajectory data to capture the traffic speeds of the urban network. The network data were extracted from the open street map (OSM) to provide the map information of Xi'an city.

Since the trajectory data set used has the advantages of the high sampling frequency, wide coverage, and high precision, it is suitable for representing the traffic state. The original online car-hailing trajectory data covers about 60 square kilometers range of Xi'an city from Nov 1 to Nov 30 in 2016. The attributes of original datasets include driver ID, order ID, timestamp, longitude, latitude, and description. The sampling interval of trajectory is 2~4 seconds and the trajectory point can be mapped to the network.

Figure 5 illustrates the preprocessing of the original trajectory data, which can obtain the initial experiment datasets. As shown in Table 1, the initial experiment datasets include six attributes including the Driver_ID, Order_ID, Time Label, Longitude, Latitude, and Velocity.

5.2. Experiment Data and Analysis. To ensure the effectiveness of the experiment, we processed road network speed data for four weeks from Nov 1 to Nov 28 in 2016 as the experimental data. The data of the first 23 days were taken as historical data, and the data of the last 5 days were taken as testing data. Figure 6 provides the research scope of the experiment. As shown in Figure 6, the research scope area includes 64 roads including types of expressways, arterial roads, and secondary roads. To ensure a sufficient number of vehicles at each time interval and avoid inaccuracy or

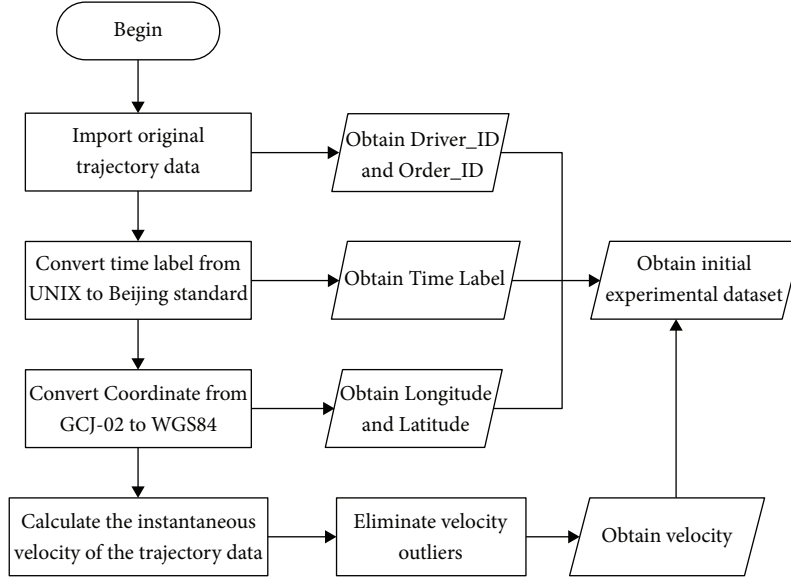
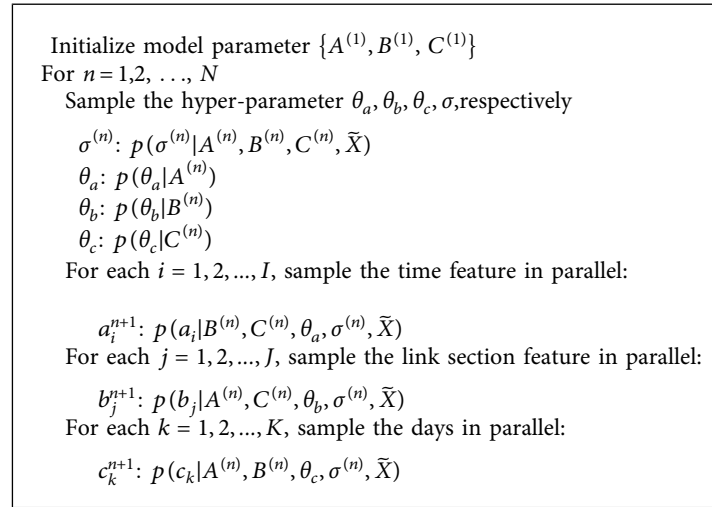


FIGURE 5: The preprocessing of the original trajectory data.



ALGORITHM 1: Gibbs sampling for the DTBPD approach.

missing data caused by too long time interval, the travel speeds of the online car-hailing vehicle were average at each research road with a time interval of 5 min and each day is divided into 288 time intervals.

Figure 7 provides the average number of online car-hailing orders within the research area during different time intervals in a day. Considering the insufficient number of online car-hailing may lead to the inaccurate acquisition of traffic conditions, we select the periods from 8:00 to 22:00 when the number of orders is relatively large and sufficient taxis are running in the range of the research networks.

Figure 8 demonstrates the speed distribution of three different grades of roads in the study time range on a certain day. It can be seen from Figure 8 that in terms of speed distribution, the average speed of the expressway is the highest, and that of the secondary road is the lowest among the three types of roads, which is consistent with the

functional design of the roads. In addition, the speeds of all roads decreased significantly during the period of 17:00 to 19:00 and the speeds of the expressways fluctuated most sharply among the three kinds of roads.

5.3. Spatiotemporal Analysis of Urban Traffic Data. Urban traffic flow data are complex and related to spatiotemporal dependency. Organizing the multidimensional traffic flow data into an appropriate tensor pattern is of importance to improve the efficiency and robustness of the traffic state estimation. In this section, the Pearson correlation coefficient is utilized to analyze the spatiotemporal characteristics of urban traffic. Since the residents usually travel regularly and urban traffic data often have certain periodic similarities, Figure 9 indicates the temporal dependency analysis of the urban roads from multiple perspectives. Based on the



FIGURE 6: The research scope area.

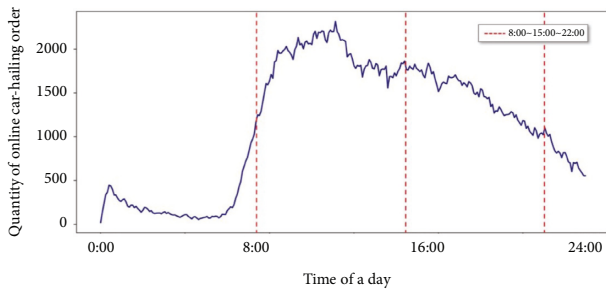


FIGURE 7: The average number of online car-hailing orders at time intervals in a day.

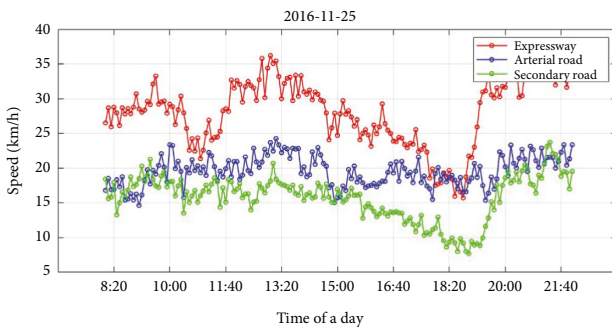


FIGURE 8: Comparison of the average speeds of the three kinds of roads in a day.

traffic speeds of a road link (ID = 63) during a day, Figure 9(a) illustrates that the traffic state of the same section varies greatly with the hours, indicating a shorter sliding time window may be suitable for dynamic tensor construction. As shown in Figure 9(b), the traffic state during

days in a week shows a significant correlation with a correlation coefficient larger than 0.60. Meanwhile, Figures 9(c) and 9(d) demonstrate the high relevance of the traffic state among days in different weeks. As shown in Figures 9(c) and 9(d), these four days are all Thursday and the correlation coefficients among them are larger than 0.75. Hence, the dynamic tensor construction should consider more days with high relevance including the days in the same weeks and the days in different weeks.

Figure 10 indicates the spatial dependency analysis of the urban network by using the traffic speeds series data of all road links in the research scope during a day. It can be found that the road link on the network demonstrates spatial correlation in different degrees due to the connectivity of the urban road network. In general, the road links present high relevance with their upstream road section, downstream sections, or adjacent sections. Hence, this paper selects the highly correlated road links to construct dynamic tensors.

5.4. Baseline Model and Performance Indexes. To verify the effectiveness of the DTBPD model, several advanced deep learning-based models and tensor-based models are applied as the baseline models, including the LSTM [58], GRU [34], FDL [59], T-GCN [43], smooth PARAFAC tensor completion model (SPC) [60], HaLRTC [50], and BGCP model [52]. The parameters of the baseline models are indicated as follows:

LSTM: To solve the long-term dependency of RNN, the LSTM structure was established whose memory block contains forget gate, the input gate, and the output gate. To reduce overfitting issues, the dropout rate was set as 0.1.

GRU: As a variant of the LSTM with a simpler structure, the GRU model only combines the forget

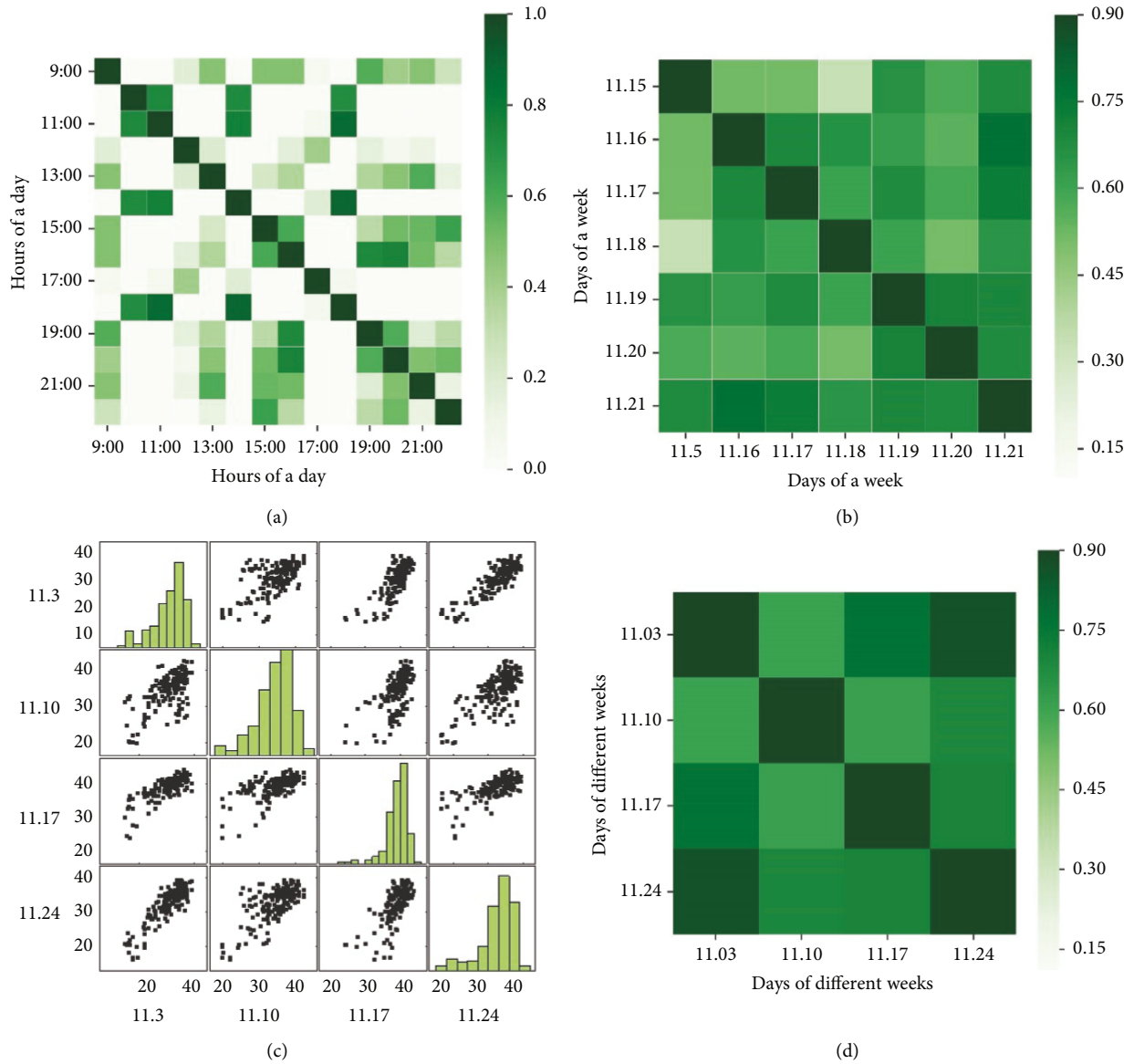


FIGURE 9: Temporal dependency analysis of the urban roads. (a) Correlation coefficient matrix of traffic state of different hours in a day; (b) correlation coefficient matrix of traffic state of different days in weeks; (c) speed scatter diagram of the Thursdays in different weeks; (d) correlation coefficient matrix of the Thursdays in different weeks.

gate and the input gate of the LSTM into a single update gate. Besides, there is a reset gate in a hidden unit of the GRU.

FDL: It is a combination model proposed by Gu et al. [59] and it fuses the LSTM and GRU layer, which can fully mine the spatiotemporal features with the selected input.

T-GCN: T-GCN [43] integrates the graph convolutional network and gated recurrent units to model spatial dependence and temporal dependence, respectively. There is one GRU layer in the hidden layers of the T-GCN model.

SPC: SPC is a smooth PARAFAC tensor-based completion model by combining the smooth PARAFAC decomposition and the efficient selection of models to

minimize the tensor rank. Quadratic variation is employed as a strategy with parameter ρ chosen as [0.3 0.3 0.3].

HaLRTC: It is a high accuracy low-rank tensor completion approach employed by Ran et al. [50]. The parameter α is set as [1/3, 1/3, 1/3] and the parameter ρ is set as 0.01.

BGCP: It is a Bayesian decomposition-based tensor proposed by Chen et al. [52], which extends the Bayesian matrix factorization [56] to a higher-order case to learn the underlying statistical patterns in spatiotemporal traffic data.

In addition, the input time step of all the DL-based models is set as 5 and the input variable includes 64 link sections. For the LSTM, GRU, FDL, and T-GCN, the hidden

units in hidden layers are chosen as 200 and the epochs are all set as 200 with the batch size set as 64. To test the models fairly, the optimizer of three DL-based models is chosen as the Adam. For the tensor-based model, the input tensor contains the historical data of all road sections during the days in the week and the same days in the previous 4 weeks, indicating the dynamic tensors' dimension of the days and road sections 11 and 64, respectively. The low rank of the DTBPD algorithm is set as 30 and the MCMC-based sampling algorithm is run for 500 iterations. Note that the data of the first 23 days are utilized for training the DL-based model with the data of the last 5 days for testing these models.

To test the performance of the DTBPD approaches and compare it to the baseline models, the mean absolute percentage error (MAPE) and root mean square error (RMSE) were used to analyze the experimental results.

$$MAPE = \frac{1}{k} \sum_{n=1}^k \left| \frac{\widehat{\varphi}_k - \varphi_k}{\varphi_k} \right| \times 100\%, \quad (13)$$

$$RMSE = \sqrt{\frac{1}{k} \sum_{n=1}^k (\widehat{\varphi}_k - \varphi_k)^2},$$

where $\widehat{\varphi}_k$ represents the estimated speed value and φ_k represents the ground-truth value. k is the number of testing speed data.

We utilize computer with Intel(R) Core(TM) i7-11800H CPU @ 4.6 GHz and 32 GB memory to conduct the experiment. Python 3.68 with TensorFlow 2.0 and Keras 2.0 is employed to implement the proposed model and baseline models.

6. Result and Discussion

6.1. Comparison of the DTBPD Approaches with Different Parameters. In this section, we test the DTBPD models by tuning up the low rank and the sliding time window, which are the two critical parameters of the DTBPD approach. We select the low rank from [5, 15, 30, 50, 100]. The sliding time windows are chosen from the set [6, 12, 24, 36, 48], which corresponds to the time of [0.5 h, 1 h, 2 h, 3 h, 4 h]. It can be learned from Figure 9, the MAPE and RMSE of the DTBPD model decrease with the increase of the low rank. As shown in Figure 11, the RMSE does not improve obviously with a large low rank. Hence, we set the low rank of the DTBPD as 30. In addition, the performance of the proposed model improves firstly and then drops with the increase of the sliding time window. This may be because the temporal feature of the traffic speed may drop if the distance between the historical data and the speed to be forecasted becomes larger, which may introduce more invalid temporal information and affect the performance of the DTBPD model. Since the proposed model can mine the characteristics of the traffic flow effectively, the sliding time window can be set as 12 which is most efficient for estimating traffic state in the future.

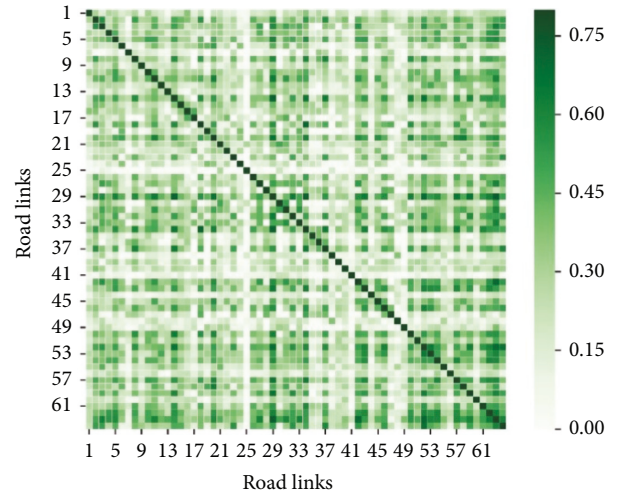


FIGURE 10: Spatial dependency analysis of the urban roads.

Figure 12 demonstrates the average MAPE and RMSE values of the DTBPD model at each time interval under different sliding time windows. It can be observed from Figure 10 that estimation errors of the starting period of the day are larger than those of other periods, which may be due to the composition of tensors considering the discontinuous traffic flow from the previous day. Figure 12 reveals that change trends of MAPE and RMSE are similar under different sliding time windows, indicating that the model is stable for different data ranges.

6.2. Performance Comparison of the Different Models.

This section compares the overall performance of the DTBPD model with the baselines by taking the five-day estimation results as a whole. Tables 2 and 3 provide the MAPEs and RMSEs of the model at different types of roads. To be specific, the estimation error of all models at the expressways is little larger than those of the arterial road and secondary road. This may be since the values of the traffic speeds at expressways are relatively larger than those of the arterial roads and secondary roads, and the fluctuation of the traffic speeds at expressways are more violent. From the performance of the different models, it can be learned from Tables 2 and 3, the DTBPD outperforms the DL-based models and the tensor-based models, with improvements of 7.49% and 9.25% on MAPE and RMSE compared with those of the T-GCN model, which is the best DL-based predictor among the models. Since the T-GCN model combines the GCN and the GRU model, it shows better performance in learning the spatiotemporal characteristics than RNN-based models including the LSTM, GRU, and FDL. Meanwhile, the SPC and HaLRTC model also provides accurate and stable performance at the expressway and arterial road compared with the LSTM and GRU. Besides, the DTBPD model comes best among these models, which outperforms the BGCP model with improvements of 6.68% and 7.34% on MAPE and RMSE, respectively. Since the proposed model utilizes the dynamic input structure and Bayesian probabilistic CP decomposition, the traffic feature with high dependency can

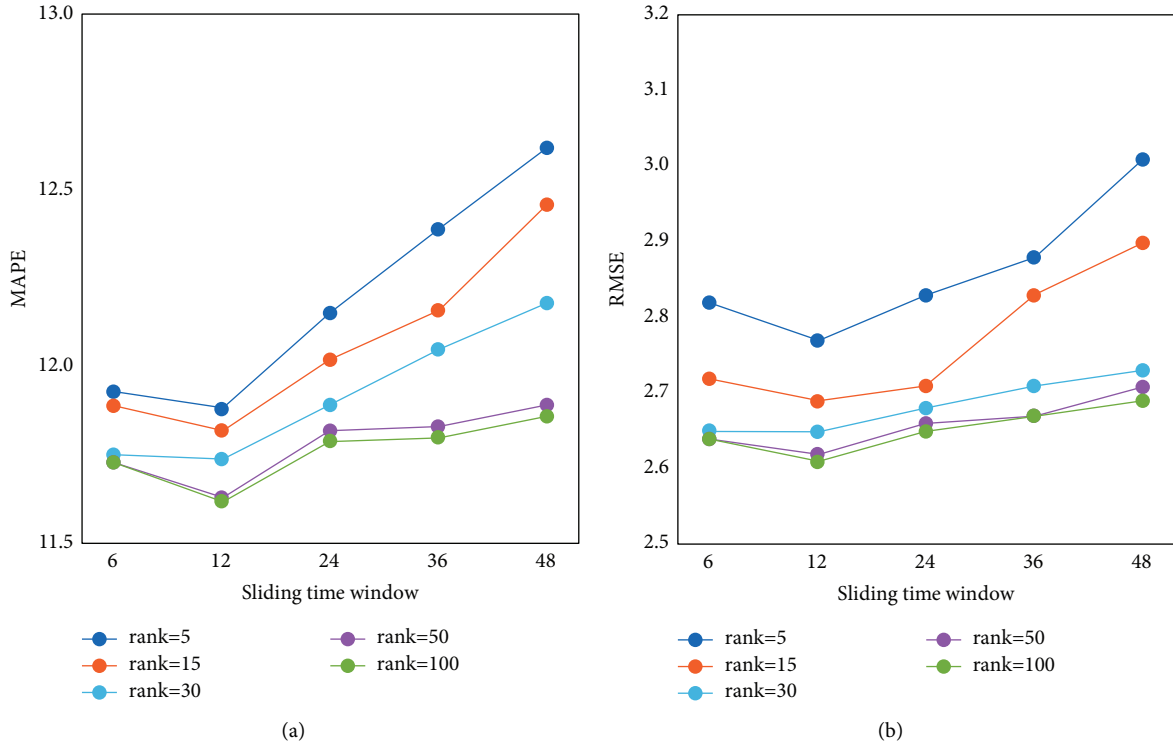


FIGURE 11: Comparison of the DTBPD model with different parameters. (a) MAPE; (b) RMSE.

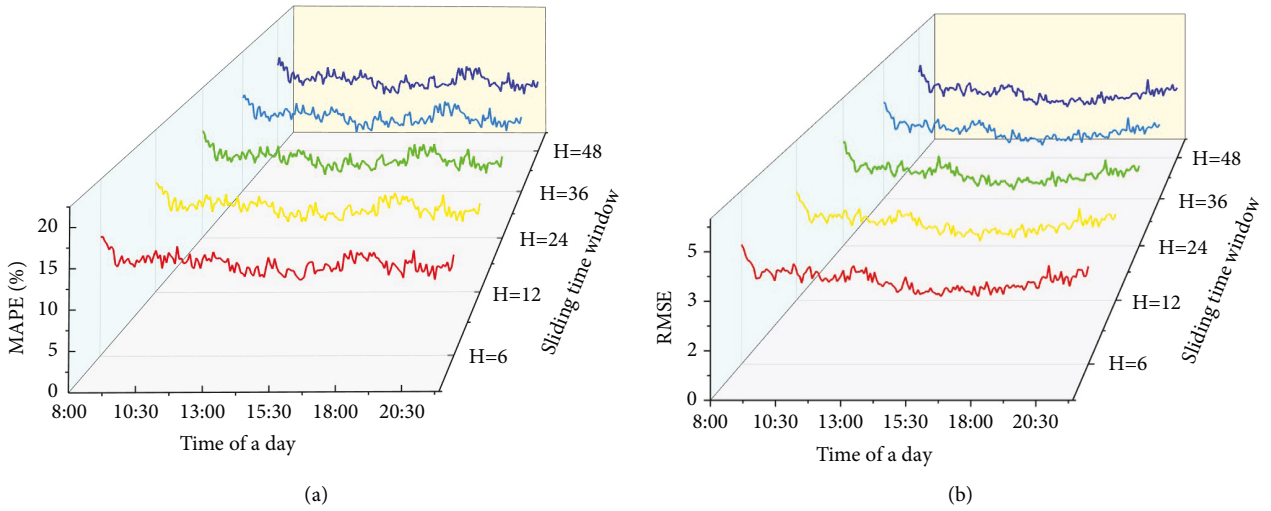


FIGURE 12: Average estimation speed of different time intervals with different sliding time windows. (a) MAPE; (b) RMSE.

TABLE 1: Examples of initial experimental datasets.

Driver_ID	Order_ID	Time Label	Longitude	Latitude	Velocity
0f8...322	5d6...891	2016/11/1 18:45:56	108.9425396	34.2667061	25.28
0f8...322	5d6...891	2016/11/1 18:45:59	108.9425496	34.2669360	30.62
0f8...322	5d6...891	2016/11/1 18:46:02	108.9425496	34.2670260	11.97
0f8...322	5d6...891	2016/11/1 18:46:05	108.9425495	34.2671659	18.63
0f8...322	5d6...891	2016/11/1 18:46:14	108.9425495	34.2674858	15.97
0f8...322	5d6...891	2016/11/1 18:46:17	108.9425495	34.2673958	11.97

TABLE 2: The overall performance of different models in terms of MAPE (%).

Models	Different types of roads			Total
	Expressway	Arterial road	Secondary road	
LSTM	13.87	13.72	13.32	13.64
GRU	13.54	13.03	12.88	13.16
FDL	13.04	12.98	12.58	12.88
T-GCN	12.82	12.71	12.44	12.69
SPC	13.85	13.67	13.45	13.65
HaLRTC	13.93	13.81	13.49	13.78
BGCP	12.77	12.78	12.03	12.58
DTBPD	11.86	11.83	11.51	11.74

TABLE 3: The overall performance of different models in terms of RMSE.

Models	Different types of roads			Total
	Expressway	Arterial road	Secondary road	
LSTM	3.42	3.29	3.13	3.32
GRU	3.26	3.18	3.12	3.19
FDL	3.19	3.13	3.03	3.12
T-GCN	3.03	2.99	2.82	2.92
SPC	3.36	3.25	3.02	3.20
HaLRTC	3.46	3.23	3.11	3.26
BGCP	2.92	2.94	2.74	2.86
DTBPD	2.73	2.76	2.40	2.65

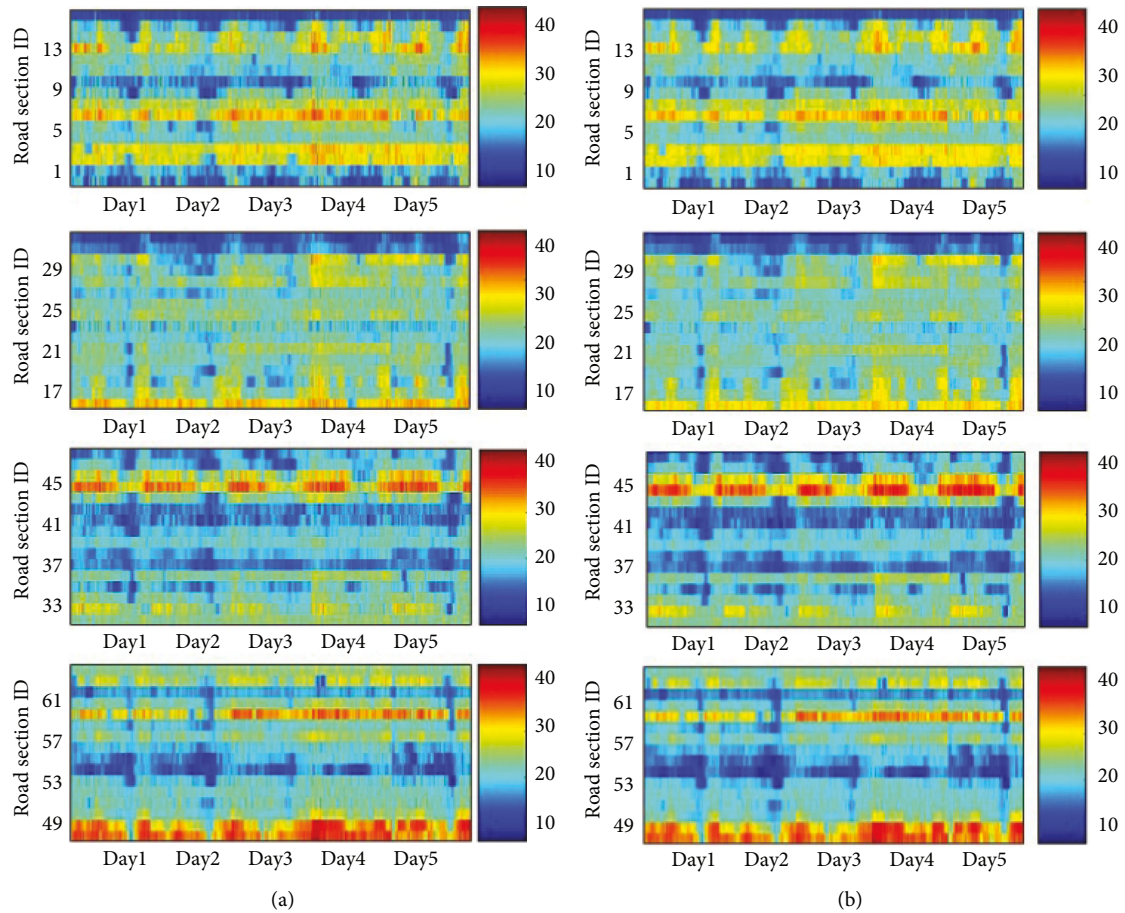


FIGURE 13: Comparison between the ground-truth and estimated data during the 5 days. (a) Ground-truth data; (b) estimated data.

TABLE 4: Comparison of time consumption between the DTBPD model and DL-based models.

Model	Training time consumption or calibration time consumption (s)
LSTM	380.35
GRU	310.40
FDL	774.08
T-GCN	823.31
DTBPD	2.49

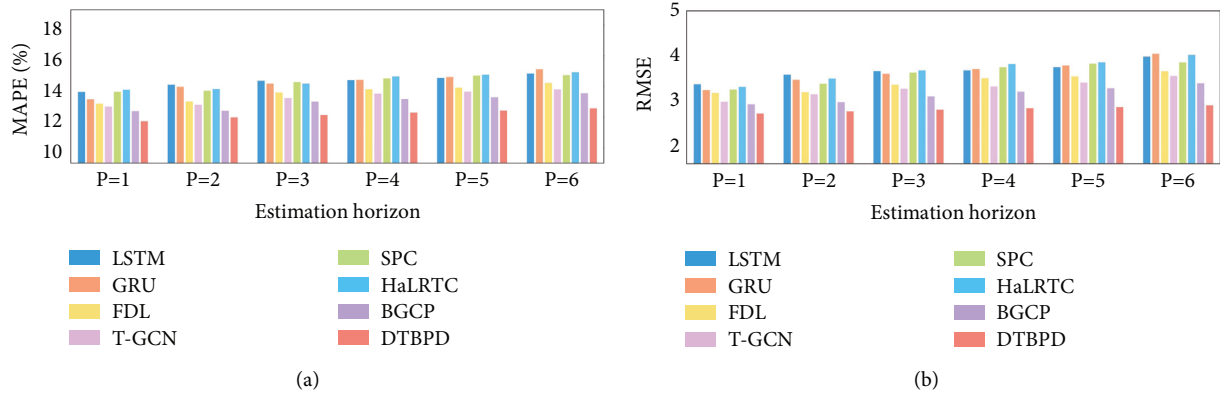


FIGURE 14: Comparison of different models with longer estimation horizons. (a) MAPE; (b) RMSE.

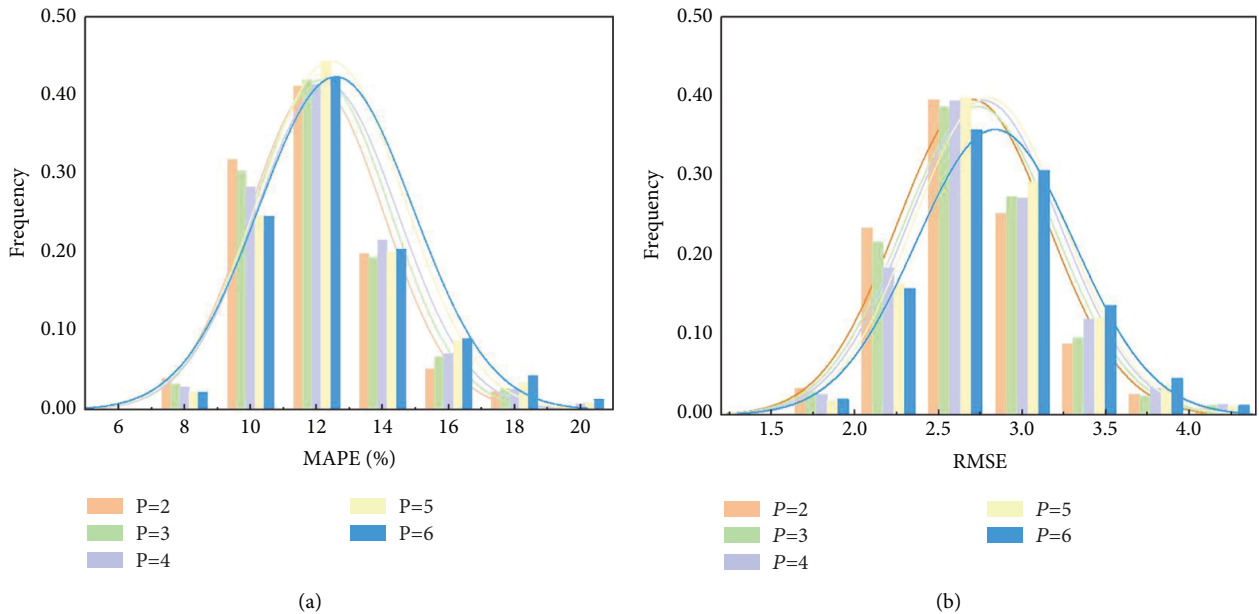


FIGURE 15: The error distribution of the DTBPD model with the increase of the estimation horizon. (a) MAPE; (b) RMSE.

be organized and mined in the tensor structure constantly. With the efficient decomposition approach, the calibrated factor matrices are capable of estimating the missing values in the dynamic tensor accurately.

Figure 13 gives the performance comparison between the ground-truth data and estimated data under the single-step-ahead estimation horizons. From the heat map, it is observed that the DTBPD model has a very good fitness

under normal and abnormal scenarios at different link sections. Note that even during the peak period when the traffic speed fluctuates significantly, the DTBPD can still estimate the traffic speed accurately. Meanwhile, even in different types of link sections where the traffic state presents differentiated features, the DTBPD model is capable of presenting similar estimation performance by using the dynamic tensor to consider the relative temporal characteristics and using the Gibbs sampling approach to approximate the factor matrix of the tensor.

Table 4 demonstrates the time consumption of the DTBPD model and the DL-based models. Since the DTBPD model needs to estimate the parameters of the model at each step, Table 4 provides its average time consumption for a single step. For the DL-based model, the update parameter in the model structure needs to train it with historical data, which spends much more time than the DTBPD model. Hence, compared with the DL-based models, the simple structure of the proposed model only needs a few seconds to calibrate the model, which is flexible and time-saving. In addition, the proposed model can adjust the composition of tensor data dynamically by using the sliding time window, which may protect the model from abnormal data and make the model robust.

6.3. Comparison of Different Models with Longer Estimation Horizons. Figure 14 provides the comparison of the different models with the extension of the estimation horizon from 5 mins to 30 mins. As shown in Figure 14, the MAPE and RMSE of different models rise slightly with the increase of the estimation horizon. Note that the DTBPD model still indicates obvious advantages over the LSTM, GRU, FDL, T-GCN, SPC, HaLRTC, and BGCP models when the estimation horizon $P=6$, which means that this tensor-based model can efficiently infer the evolution trend of the traffic state.

Figure 15 provides the distributions of the MAPE and the RMSE estimated by the BTBPD approach with the 5-day dataset. As indicated in Figure 15, the errors of the proposed model are generally normal distribution. When the number of the estimation horizon increases from 2 to 6, the fitting curve moves to the right gradually and the prediction error gradually increases. This may be because the more step to estimate, the more estimated values in the historical data may enlarge the estimated error [55].

7. Conclusion

Massive online car-hailing trajectory data have become a popular and significant source for analyzing the urban traffic status, which is fundamental for reducing traffic congestion and constructing smart cities. This paper proposes a dynamic tensor-based Bayesian probabilistic decomposition approach for urban traffic state estimation. Firstly, the urban traffic speed data are formed into the dynamic tensor mode to fully mine the spatiotemporal characteristics of the traffic state. Secondly, the Bayesian probabilistic decomposition approach is introduced to decompose the tensor with speed

to be estimated into a product of several vectors. Thirdly, the Gibbs sampling algorithm is proposed to calibrate the parameter of the proposed DBTPD models. Finally, the urban traffic speed data were extracted from the online car-hailing trajectory data of Didi Company to examine the accuracy and robustness of the DBTPD model.

Some findings can be summarized as follows. (1) The DBTPD model can well capture the spatiotemporal characteristics of the urban traffic state with a sliding sampling structure and Bayesian probabilistic decomposition approach. (2) The proposed outperforms the benchmark model including the LSTM, GRU, FDL, T-GCN, SPC, HaLRTC, and BGCP model in terms of the one-step-ahead estimation and multistep-ahead estimation. (3) The calibration time consumption of the DBTPD model is much less than those of the DL-based model, which indicates the proposed model is practical.

Some further research areas should be investigated. On the one hand, multisource data such as geographic information data or pedestrian flow data can be introduced to improve the accuracy of data estimation. On the other hand, the Bayesian probabilistic decomposition approach can be applied to multidimensional tensors, which consider more spatiotemporal characteristics for enhancing the robustness of the DBTPD model.

Data Availability

The trajectory data used to support the findings of this study are available from the corresponding author upon request.

Conflicts of Interest

The authors declare that there are no conflicts of interest regarding the publication of this manuscript.

Authors' Contributions

Wenqi Lu was responsible for conceptualization, investigation, methodology, software, and writing—original draft preparation and review and editing. Ziwei Yi was responsible for visualization, methodology, and writing—original draft preparation. Dongyu Luo performed formal analysis and data curation. Yikang Rui was responsible for conceptualization, validation, and project administration. Bin Ran was responsible for project administration and supervision. Jianqing Wu performed formal analysis. Tao Li reviewed and edited the manuscript.

Acknowledgments

This research was supported by the National Natural Science Foundation of China (Grant no. 41971342), the Key Research and Development Program of Shandong Province (Grant no. 2020CXGC010118), the Fundamental Research Funds for the Central Universities, China (Grant no. 3221002145D), and the Scientific Research Foundation of Graduate School of Southeast University, China (Grant no. YBPY2161).

References

- [1] J. Lu, B. Li, H. Li, and A. Al-Barakani, "Expansion of city scale, traffic modes, traffic congestion, and air pollution," *Cities*, vol. 108, Article ID 102974, 2021.
- [2] X. Qian, T. Lei, J. Xue, Z. Lei, and S. V. Ukkusuri, "Impact of transportation network companies on urban congestion: evidence from large-scale trajectory data," *Sustainable Cities and Society*, vol. 55, Article ID 102053, 2020.
- [3] Z. Chen, X. Lin, Y. Yin, and M. Li, "Path controlling of automated vehicles for system optimum on transportation networks with heterogeneous traffic stream," *Transportation Research Part C: Emerging Technologies*, vol. 110, pp. 312–329, 2020.
- [4] D. Tian, G. Wu, P. Hao, K. Boriboonsomsin, and M. J. Barth, "Connected vehicle-based lane selection assistance application," *IEEE Transactions on Intelligent Transportation Systems*, vol. 20, no. 7, pp. 2630–2643, 2019.
- [5] L. Chen, A. H. Valadkhani, and M. Ramezani, "Decentralised cooperative cruising of autonomous ride-sourcing fleets," *Transportation Research Part C: Emerging Technologies*, vol. 131, Article ID 103336, 2021.
- [6] E. Jenelius and H. N. Koutsopoulos, "Travel time estimation for urban road networks using low frequency probe vehicle data," *Transportation Research Part B: Methodological*, vol. 53, pp. 64–81, 2013.
- [7] E. Jenelius and H. N. Koutsopoulos, "Probe vehicle data sampled by time or space: consistent travel time allocation and estimation," *Transportation Research Part B: Methodological*, vol. 71, pp. 120–137, 2015.
- [8] T. T. Tchraikian, B. Basu, and M. O'Mahony, "Real-time traffic flow forecasting using spectral analysis," *IEEE Transactions on Intelligent Transportation Systems*, vol. 13, no. 2, pp. 519–526, 2011.
- [9] Z. Mingheng, Z. Yaobao, H. Ganglong, and C. Gang, "Accurate multisteps traffic flow prediction based on SVM," *Mathematical Problems in Engineering*, vol. 2013, pp. 1–8, Article ID 418303, 2013.
- [10] Y. Zhang, M. Lu, and H. Li, "Urban traffic flow forecast based on FastGCRNN," *Journal of Advanced Transportation*, vol. 2020, pp. 1–9, Article ID 8859538, 2020.
- [11] E. I. Vlahogianni, M. G. Karlaftis, and J. C. Golias, "Short-term traffic forecasting: where we are and where we're going," *Transportation Research Part C: Emerging Technologies*, vol. 43, pp. 3–19, 2014.
- [12] D. Sun, K. Zhang, and S. Shen, "Analyzing spatiotemporal traffic line source emissions based on massive didi online car-hailing service data," *Transportation Research Part D: Transport and Environment*, vol. 62, pp. 699–714, 2018.
- [13] J. Chen, W. Li, H. Zhang et al., "GPS data in urban online ride-hailing: a simulation method to evaluate impact of user scale on emission performance of system," *Journal of Cleaner Production*, vol. 287, Article ID 125567, 2021.
- [14] B. Zhang, S. Chen, Y. Ma, T. Li, and K. Tang, "Analysis on spatiotemporal urban mobility based on online car-hailing data," *Journal of Transport Geography*, vol. 82, Article ID 102568, 2020.
- [15] H. Tan, G. Feng, J. Feng, W. Wang, Y.-J. Zhang, and F. Li, "A tensor-based method for missing traffic data completion," *Transportation Research Part C: Emerging Technologies*, vol. 28, pp. 15–27, 2013.
- [16] Z. Ma, H. N. Koutsopoulos, L. Ferreira, and M. Mesbah, "Estimation of trip travel time distribution using a generalized Markov chain approach," *Transportation Research Part C: Emerging Technologies*, vol. 74, pp. 1–21, 2017.
- [17] W. Lu, T. Zhou, L. Li, Y. Gu, Y. Rui, and B. Ran, "An improved tucker decomposition-based imputation method for recovering lane-level missing values in traffic data," *IET Intelligent Transport Systems*, vol. 16, no. 3, pp. 363–379, 2022.
- [18] Y. Han and Z. He, "Simultaneous incomplete traffic data imputation and similarity pattern discovery with bayesian nonparametric tensor decomposition," *Journal of Advanced Transportation*, vol. 2020, pp. 1–10, Article ID 8810753, 2020.
- [19] M. S. Ahmed and A. R. Cook, "Analysis of freeway traffic time-series data by using box-jenkins techniques," *Transportation Research Record*, vol. 722, pp. 1–9, 1979.
- [20] B. M. Williams and L. A. Hoel, "Modeling and forecasting vehicular traffic flow as a seasonal ARIMA process: theoretical basis and empirical results," *Journal of Transportation Engineering*, vol. 129, no. 6, pp. 664–672, 2003.
- [21] A. Emami, M. Sarvi, and S. A. Bagloee, "Short-term traffic flow prediction based on faded memory Kalman Filter fusing data from connected vehicles and Bluetooth sensors," *Simulation Modelling Practice and Theory*, vol. 102, Article ID 102025, 2020.
- [22] H. P. Lu, Z. Y. Sun, and W. C. Qu, "Big data-driven based real-time traffic flow state identification and prediction," *Discrete Dynamics in Nature and Society*, vol. 2015, Article ID 284906, 11 pages, 2015.
- [23] Z. Song, F. Sun, R. Zhang, Y. Du, and C. Li, "Prediction of road network traffic state using the NARX neural network," *Journal of Advanced Transportation*, vol. 2021, pp. 1–17, Article ID 2564211, 2021.
- [24] J. Rice and E. vanZwet, "A simple and effective method for predicting travel times on freeways," *IEEE Transactions on Intelligent Transportation Systems*, vol. 5, no. 3, pp. 200–207, 2004.
- [25] M. Castro-Neto, Y.-S. Jeong, M.-K. Jeong, and L. D. Han, "Online-SVR for short-term traffic flow prediction under typical and atypical traffic conditions," *Expert Systems with Applications*, vol. 36, no. 3, pp. 6164–6173, 2009.
- [26] B. Sun, W. Cheng, P. Goswami, and G. Bai, "Short-term traffic forecasting using self-adjusting k-nearest neighbours," *IET Intelligent Transport Systems*, vol. 12, no. 1, pp. 41–48, 2018.
- [27] L. Li, L. Qin, X. Qu, J. Zhang, Y. Wang, and B. Ran, "Day-ahead traffic flow forecasting based on a deep belief network optimized by the multi-objective particle swarm algorithm," *Knowledge-Based Systems*, vol. 172, pp. 1–14, 2019.
- [28] L. Li, B. Du, Y. Wang, L. Qin, and H. Tan, "Estimation of missing values in heterogeneous traffic data: application of multimodal deep learning model," *Knowledge-Based Systems*, vol. 194, Article ID 105592, 2020.
- [29] Y. Rui, W. Lu, Z. Yi, R. Wu, and B. Ran, "A novel hybrid model for predicting traffic flow via improved ensemble learning combined with deep belief networks," *Mathematical Problems in Engineering*, vol. 2021, no. 2, pp. 1–16, Article ID 7328056, 2021.
- [30] Y. Hou, Z. Deng, and H. Cui, "Short-term traffic flow prediction with weather conditions: based on deep learning algorithms and data fusion," *Complexity*, vol. 2021, pp. 1–14, Article ID 6662959, 2021.
- [31] J. Liu, X. Wang, Y. Li, X. Kang, and L. Gao, "Method of evaluating and predicting traffic state of highway network based on deep learning," *Journal of Advanced Transportation*, vol. 2021, pp. 1–9, Article ID 8878494, 2021.
- [32] Y. Lv, Y. Duan, W. Kang, Z. Li, and F. Y. Wang, "Traffic flow prediction with big data: a deep learning approach," *IEEE*

- Transactions on Intelligent Transportation Systems*, vol. 16, 2015.
- [33] X. Luo, D. Li, nt(ancestor::ref)"=2?^!"count(..!name)"=1? ^!"count(following-sibling::name)" and >Y. Yang, and S. Zhang, "Spatiotemporal traffic flow prediction with KNN and LSTM," *Journal of Advanced Transportation*, vol. 2019, pp. 1–10, Article ID 4145353, 2019.
- [34] F. Rui, Z. Zuo, and L. Li, "Using LSTM and GRU neural network methods for traffic flow prediction," in *Proceedings of the 2016 31st Youth Academic Annual Conference of Chinese Association of Automation (YAC)*, pp. 324–328, Wuhan, China, November 2016.
- [35] H. Yan, X. Ma, and Z. Pu, "Learning dynamic and hierarchical traffic spatiotemporal features with transformer," *IEEE Transactions on Intelligent Transportation Systems*, pp. 1–14, 2021.
- [36] X. Ma, Z. Dai, Z. He, J. Ma, Y. Wang, and Y. Wang, "Learning traffic as images: a deep convolutional neural network for large-scale transportation network speed prediction," *Sensors*, vol. 17, no. 4, 2017.
- [37] L. Zhao, D. Wei, Y. Dongmei, C. Gan, and G. Jianhua, "Short-term traffic flow forecast based on combination of K nearest neighbor algorithm and support vector regression," *Journal of Highway and Transportation Research and Development*, vol. 34, no. 5, pp. 122–128, 2017.
- [38] Y. Liu, H. Zheng, X. Feng, and Z. Chen, "Short-term traffic flow prediction with Conv-LSTM," in *Proceedings of the 2017 9th International Conference on Wireless Communications and Signal Processing*, pp. 1–6, Nanjing, China, October 2017.
- [39] Y. Gu, W. Lu, X. Xu, L. Qin, Z. Shao, and H. Zhang, "An improved bayesian combination model for short-term traffic prediction with deep learning," *IEEE Transactions on Intelligent Transportation Systems*, vol. 21, no. 3, pp. 1332–1342, 2020.
- [40] S. Guo, Y. Lin, S. Li, Z. Chen, and H. Wan, "Deep spatial-temporal 3D convolutional neural networks for traffic data forecasting," *IEEE Transactions on Intelligent Transportation Systems*, vol. 20, no. 10, pp. 3913–3926, 2019.
- [41] Y. Wu, H. Tan, L. Qin, B. Ran, and Z. Jiang, "A hybrid deep learning based traffic flow prediction method and its understanding," *Transportation Research Part C: Emerging Technologies*, vol. 90, no. 5, pp. 166–180, 2018.
- [42] L. Li, X. Sheng, B. Du, Y. Wang, and B. Ran, "A deep fusion model based on restricted Boltzmann machines for traffic accident duration prediction," *Engineering Applications of Artificial Intelligence*, vol. 93, Article ID 103686, 2020.
- [43] L. Zhao, Y. Song, C. Zhang et al., "T-GCN: a temporal graph convolutional network for traffic prediction," *IEEE Transactions on Intelligent Transportation Systems*, vol. 21, no. 9, pp. 3848–3858, 2020.
- [44] S. Guo, Y. Lin, N. Feng, C. Song, and H. Wan, "Attention based spatial-temporal graph convolutional networks for traffic flow forecasting," *Proceedings of the AAAI Conference on Artificial Intelligence*, vol. 33, pp. 922–929, 2019.
- [45] W. Lu, Z. Yi, W. Liu, Y. Gu, Y. Rui, and B. Ran, "Efficient deep learning based method for multi-lane speed forecasting: a case study in Beijing," *IET Intelligent Transport Systems*, vol. 14, no. 14, pp. 2073–2082, 2020.
- [46] W. Chen, J. An, R. Li, and G. Xie, "Tensor-train fuzzy deep computation model for citywide traffic flow prediction," *IEEE Access*, vol. 7, Article ID 120581, 2019.
- [47] M. Bhanu, J. Mendes-Moreira, and J. Chandra, "Embedding traffic network characteristics using tensor for improved traffic prediction," *IEEE Transactions on Intelligent Transportation Systems*, vol. 22, no. 6, pp. 3359–3371, 2021.
- [48] J. Liao, J. Tang, W. Zeng, and X. Zhao, "Efficient and accurate traffic flow prediction via incremental tensor completion," *IEEE Access*, vol. 6, Article ID 36897, 2018.
- [49] B. Ran, L. Song, J. Zhang, Y. Cheng, and H. Tan, "Using tensor completion method to achieving better coverage of traffic state estimation from sparse floating car data," *PLoS One*, vol. 11, no. 7, Article ID e0157420, 2016.
- [50] B. Ran, H. Tan, Y. Wu, and P. J. Jin, "Tensor based missing traffic data completion with spatial-temporal correlation," *Physica A: Statistical Mechanics and Its Applications*, vol. 446, pp. 54–63, 2016.
- [51] E. Acar, D. M. Dunlavy, T. G. Kolda, and M. Mørup, "Scalable tensor factorizations for incomplete data," *Chemometrics and Intelligent Laboratory Systems*, vol. 106, no. 1, pp. 41–56, 2011.
- [52] X. Chen, Z. He, and L. Sun, "A Bayesian tensor decomposition approach for spatiotemporal traffic data imputation," *Transportation Research Part C: Emerging Technologies*, vol. 98, pp. 73–84, 2019.
- [53] K. Tang, C. Tan, Y. Cao, J. Yao, and J. Sun, "A tensor decomposition method for cycle-based traffic volume estimation using sampled vehicle trajectories," *Transportation Research Part C: Emerging Technologies*, vol. 118, Article ID 102739, 2020.
- [54] K. Tang, S. Chen, Z. Liu, and A. J. Khattak, "A tensor-based Bayesian probabilistic model for citywide personalized travel time estimation," *Transportation Research Part C: Emerging Technologies*, vol. 90, pp. 260–280, 2018.
- [55] X. Zhan, S. Zhang, W. Y. Szeto, and X. Chen, "Multi-step-ahead traffic speed forecasting using multi-output gradient boosting regression tree," *Journal of Intelligent Transportation Systems*, vol. 24, no. 2, pp. 125–141, 2020.
- [56] R. Salakhutdinov and A. Mnih, "Bayesian probabilistic matrix factorization using Markov chain Monte Carlo," in *Proceedings of the 25th International Conference on Machine Learning*, pp. 880–887, Association for Computing Machinery, NY, USA, July 2008.
- [57] L. Xiong, X. Chen, T.-K. Huang, J. Schneider, and J. G. Carbonell, "Temporal collaborative filtering with bayesian probabilistic tensor factorization," in *Proceedings of the 2010 SIAM international conference on data mining*, pp. 211–222, Milan, Italy, December 2010.
- [58] X. Ma, Z. Tao, Y. Wang, H. Yu, and Y. Wang, "Long short-term memory neural network for traffic speed prediction using remote microwave sensor data," *Transportation Research Part C: Emerging Technologies*, vol. 54, pp. 187–197, 2015.
- [59] Y. Gu, W. Lu, L. Qin, M. Li, and Z. Shao, "Short-term prediction of lane-level traffic speeds: a fusion deep learning model," *Transportation Research Part C: Emerging Technologies*, vol. 106, pp. 1–16, 2019.
- [60] T. Yokota, Q. Zhao, and A. Cichocki, "Smooth PARAFAC decomposition for tensor completion," *IEEE Transactions on Signal Processing*, vol. 64, no. 20, pp. 5423–5436, 2016.

Research Article

Seismic Analysis of Reticulated Shell Structure Based on Sensor Network for Smart Transportation Seismic Isolation Bearings

Jun Peng  and Yufei Li

College of Agricultural and Hydraulic Engineering, Suihua University, Suihua 152001, Heilongjiang, China

Correspondence should be addressed to Jun Peng; 171841220@masu.edu.cn

Received 18 February 2022; Revised 19 March 2022; Accepted 31 March 2022; Published 22 April 2022

Academic Editor: Sang-Bing Tsai

Copyright © 2022 Jun Peng and Yufei Li. This is an open access article distributed under the Creative Commons Attribution License, which permits unrestricted use, distribution, and reproduction in any medium, provided the original work is properly cited.

Earthquakes are one of the most frequent and inevitable natural disasters that occur on Earth. The most important seismic isolation device used in the isolation technology is the isolation bearing, but the limited structure of the isolation bearing is not suitable for the seismic isolation and shock absorption of smart transportation buildings. Therefore, it is very important to improve the new generation of seismic isolation structures with good seismic isolation effect, stable performance, and economical performance. It is very important to study the structural composition of the isolation bearing and the rigidity of the isolation structure. Isolation bearings are designed to resist and absorb the energy of seismic shocks by installing substructures in the structure. Active control involves installing sensors on the structure and its foundation to determine how the structure responds to seismic action. In this paper, based on the intelligent transportation of the sensor network, the reticulated shell structure of the isolation bearing is analyzed. By introducing the architecture and network layout of the sensor network, it is beneficial to obtain more accurate seismic data in complex and difficult terrain. This paper analyzes the technical principle of seismic isolation technology, which can effectively avoid the upward transmission of ground vibration by increasing the flexibility and proper damping of the system. From the experimental data of the seismic response of the ground-isolated structure to the near-field pulsation and far-field vibration, the total energy of the ground-isolated structure under the near-field pulsed ground motion is the largest. The seismic isolation effect of the reticulated shell structure of the seismic isolation bearing prevents more than 80% of the seismic energy from being transmitted to the superstructure.

1. Introduction

Over the past three decades, China's economy has boomed and the construction of large-scale technical buildings has achieved remarkable results. The emergence of large-scale transportation facilities with various large volumes and complex spatial forces makes the seismic behavior of these large-scale buildings in the event of earthquakes very important. In order to improve the seismic behavior of space structures, researchers began to introduce the theory of seismic isolation of space structures and initially developed seismic load reduction and isolation technologies for such structures. The traditional seismic design resists the seismic action of the structure's own bearing capacity, stiffness, and flexibility, that is, relying on the structure itself to consume

seismic energy, which is uneconomical and cannot achieve the desired effect. At present, people have turned their attention to seismic isolation research, and domestic and foreign structural shock absorption and seismic isolation technologies have developed rapidly.

Large-scale spatial structures have developed rapidly in recent decades. Large space structure is not only a structural system for large space structures, such as large stadiums and hangars but also widely used in large public buildings, such as transportation hubs and conference centers. With the development of the national economy and the improvement of infrastructure, the demand for large profile structures is increasing every day. However, most structures are flexible systems with low damping ratios, which cause relatively high vibrations under dynamic loads, affecting the normal use of

the structure, which in turn affects safety. The study found that the use of seismic isolation technology or adding damping devices to the structure can effectively reduce the degree of damage to building facilities caused by earthquakes. China is geographically located in an earthquake-prone area. Large buildings often have a large number of people, and the personal and property losses caused by earthquakes may be huge. Therefore, the seismic behavior of large spatial structures is a topic that structural designers and researchers need to consider.

This paper is based on isolation technology to reduce the loss caused by the earthquake. The earthquake-isolated traffic building can effectively reduce the damage to the superstructure in the earthquake disaster, thereby greatly reducing the maintenance and repair costs after the earthquake. In the reticulated shell structure management model of the intelligent transportation isolation bearing, the intelligent transportation model based on the sensor network is adopted and combined with the road traffic conditions, such as the traffic flow speed, road characteristics, and other guidance models, network data is collected to realize the intelligent transportation operation.

2. Related Work

Wu Q conducted a high deformation horizontal displacement test on LRB600 and LRB1100 (LRB600, LRB1100: vibration isolation rubber bearing), and the deformation index was 400%. The results show that the bending stiffness after installation increases when the displacement strain reaches 240%, the hardening stiffness increases with the displacement strain, and when the displacement strain reaches 400%, the hardening stiffness increases by a factor of 1.5. He compared the seismic response, elastoplastic response spectrum, and plastic energy dissipation state of LRB of the traditional bilinear model and the proposed multilinear model, respectively. The results show that for large earthquakes, the hardening of the bearing weakens the seismic isolation capability of the LRB, the acceleration of the superstructure increases by 30%–50%, and the plastic energy dissipation of the structure increases, and the superstructure enters a state of plastic deformation. Therefore, without considering the hardening of the supports, the seismic response of the structure will be underestimated [1]. Hong et al. present a framework for seismic analysis of high-speed interconnected bridge systems with pendulum friction bearing isolation. Using computer simulation techniques, he performed dynamic simulations of seismic isolation systems for five railway bridges under seismic conditions. He considered a 35-degree-of-freedom (DOF) train consisting of eight 4-axle passenger cars and modeled the FPB with force elements including nonlinear spring and damper properties and hysteresis functions. The results show that replacing CSB with FPB with a friction coefficient of not less than 0.05 can greatly reduce the dynamic response of the train [2]. Recently, the number of base-isolated buildings for general commercial buildings is increasing due to the high seismic performance of the seismic isolation system. On the other hand, for nuclear power plants (NPPs), although there has

been a lot of research to apply isolation systems, no plants for base isolation have been built in Japan. Recent seismic regulations require an assessment of seismic safety, including the eventual conduct of national nuclear power plants. Therefore, the final behavior of national nuclear power plants employing seismic isolation systems must also take into account the residual risk of earthquakes: for example, hardening in horizontal deformation or rupture of seismic isolators. The seismic response prediction method based on energy balance and its design method will be regarded as the seismic safety evaluation of large horizontal deformation area. Hiraki et al. especially proposed a mechanical energy balance evaluation scheme for studying the extreme behavior of large deflection regions, which can estimate the mechanical energy conversion based on the experimental records of the relationship restoring force and shear deflection on the base isolation layer. However, it has not been widely used [3]. The seismic capacity and continuous operation of bridges after earthquakes are important seismic design criteria. Mohebbi et al. explore a new concept for seismic protection of monolithic piers that uses sliding bearings to separate the superstructure from the piers. The effect of sliding bearings on the seismic response of a representative 3-span monolithic highway bridge is investigated. By sliding the bearing, the shear force of the pier is limited to the design friction of the bearing. Furthermore, since the displacement requirement of the bridge is governed by the equal displacement rule, it was found that the ductility requirement of the bridge pier is not sensitive to the friction force of the sliding bearing [4]. In order to solve the problem of three-dimensional isolation of high-rise buildings, Yan et al. introduced the prototype structure, model structure, and vibration test system. He conducted vibration tests and showed that although the three-dimensional vibration isolation bearings placed at the bottom of the substructure differed in the shape and damping mechanism of the vibration isolation, the natural vibration period of the structure was prolonged both horizontally and vertically. The simulation results are consistent with the experimental results. The isolated base structure has an obvious damping effect on the seismic response of the main structure of different groups [5]. Qingning et al. applied friction-slip isolation theory to study the seismic isolation performance of curved bridges. He studied the relationship between stress, strain, and displacement of rubber friction-slip isolation under two typical working conditions, established the constitutive slip-friction relationship, and obtained and analyzed the friction-slip calculation method and energy dissipation mechanism. Combined with shaking table test, the effects of different types of seismic waves and different acceleration loads on the failure state and seismic isolation effect of bridge piers with different stiffness are analyzed. The research shows that the cracks in the drawings are mainly flexible cracks, and the stiffness of the drawings has a greater influence on the crack position; the bearing is mainly damaged by shearing. In a strong earthquake, the acceleration response of the bearing is basically independent of the type of seismic wave but related to the friction coefficient between the bearing and the bearing. Moreover, the effect of

friction-slip isolation bearings increases with the loading level [6]. Wireless sensor networks (WSNs) are an important technology for the Internet of Things (IoT) and smart applications. In intelligent transportation systems (ITS), WSNs play an important role in safe and efficient traffic management. Therefore, there is a huge demand for energy-efficient WSNs with dynamic resource allocation in vehicles and infrastructure. Mukherjee A proposed a model of multiple-input multiple-output (MIMO) technology in WSNs to solve the problem of cluster head (CH) identification for MIMO sensor networks by using a back-propagation neural network (BPNN). Due to the influence of dynamic and real-time environments, traditional CH identification has the problem of insufficient location identification. Therefore, in order to obtain more precise localization accuracy, the proposed work uses BPNN combined with distributed gradient descent technique to calculate the location of unknown CH. This reduces distance estimation errors and further uses particle swarm optimization techniques to obtain optimal weights and thresholds for the network. The advantage of particle swarm optimization is that it is simple and easy to implement, and there are not many parameters to adjust. This work is validated through mathematical analysis, simulations, and comparisons with the state-of-the-art [7]. The above studies provide a detailed analysis of the seismic isolation capability and the application of sensor networks. It is undeniable that these studies have greatly promoted the development of the corresponding fields. We can learn a lot from methodology and data analysis. However, in the field of intelligent transportation, there are relatively few studies on the reticulated shell structure of the isolation bearing, and it is necessary to fully apply these theories to the research in this field.

3. Combination Analysis of the Smart Transportation of Sensor Network and the Reticulated Shell Structure of the Isolation Bearing

Earthquakes are sudden and heavy-weight disasters that cause heavy economic losses and casualties. Located between the Asia-Europe earthquake zone and the Pacific Rim region, China is a country with frequent seismic activities and many seismic waves. Seismic waves are vibrations propagating from the source of the earthquake in all directions and refer to the elastic waves that are generated from the source and radiate to the surroundings. Seismic waves appear in strong objects after being perceived by the source and have various properties [8]. Seismic waves can be divided into two categories according to their performance range, namely surface waves and body waves, and body waves are further divided into longitudinal waves (P waves) and transverse waves (S waves).

In seismology, the wave impedance is the product of the density of the medium and the velocity of the wave. The wave impedance is related to the radiation source. The radiation source is low impedance, and the electromagnetic wave

generated is also low impedance, and vice versa. The wave impedance is also related to the distance from the observation point to the radiation source. When the distance is greater than 1/6 of the wavelength, the wave impedance is 377 ohms regardless of the radiation source impedance. And the distance between the radiation source and the radiation source is less than 1/6 wavelength is called the near field area, and the far field area is more than 1/6 wavelength. The wave impedance affects the motion of the wave and the state of wave propagation at the boundary between the two media. Table 1 shows wavelength propagation rates and wave impedance reference values for different regions [9].

The complexity of the subsurface structure and the existence of many unstable boundaries in the near-surface environment and the fact that the media parameters may be different in different regions mean that the propagation velocity of seismic waves in the subsurface is not consistent [10].

3.1. The Main Structure of Unconstrained Concrete. Concrete materials used in structural models can be divided into constrained concrete and unconstrained concrete. The stress-strain curve under uniaxial loading of unconstrained concrete can be determined by the following formula:

$$\sigma = (1 - e_c)F_c \varepsilon, \quad (1)$$

$$e_c = \begin{cases} 1 - \frac{\rho_c m}{m + x^m - 1}, & x \leq 1, \\ 1 - \frac{\rho_t}{\varphi_c (x - 1)^2 + x}, & x > 1, \end{cases}$$

$$x = \frac{\varepsilon}{\varepsilon_{c,r}}$$

$$\rho_c = \frac{e_{c,r}}{F_c \varepsilon_{c,r}}$$

$$m = \frac{F_c \varepsilon_{c,r}}{F_c \varepsilon_{c,r} - e_{c,r}}$$

Among them, φ_c is the value of the descending part of the concrete compressive strength curve; $e_{c,r}$ is the representative value of the concrete compressive strength. $\varepsilon_{c,r}$ is the maximum value of concrete compressive strength corresponding to the compressive strength $e_{c,r}$ value; e_c is the failure evolution parameter of concrete compressive strength.

3.2. Constrained Concrete Main Structure. Confined concrete can solve the shortcomings of crack width development, easy crushing, and poor ductility of concrete members. Confined concrete can also be divided into reinforced concrete and stirrup concrete. Concreting uses external constraints to improve its original compressive properties and compressive strength and ductility. High-strength stirrups are used in the beams, columns, nodes, and hoops in the walls of concrete structures to constrain the

TABLE 1: Propagation speed and wave impedance of waves in different media.

Media name	Rock layer	Soil	Clay	Limestone
Speed (m/s)	300~13000	200~800	1800~2400	3200~5500
Density (kg/cm ³)	1.4~2	1.1~2	1.5~2.2	2.3~3
Wave impedance (g/s * cm ² * 10 ⁴)	4.2~26	2.2~16	27~52.8	73.6~165

concrete to form a constrained concrete structure system. And the uniaxial stress-strain curve of stirrup concrete is calculated according to the following formula:

$$\begin{aligned}
 e_c &= \frac{e'_{cc} x s}{s + x^s - 1}, \\
 x &= \frac{\varepsilon_c}{\varepsilon_{cc}}, \\
 \varepsilon_{cc} &= \varepsilon_{co} \left[5 \left(\frac{e'_{cc}}{e'_{co}} - 1 \right) + 1 \right], \\
 s &= \frac{F_c}{F_c - F_{sec}}, \\
 F_c &= 5000 \sqrt{e'_{co}}, \\
 e'_{cc} &= e'_{co} \left(2.254 \sqrt{1 + \frac{7.94 e'_1}{e'_{co}}} - \frac{2e'_1}{e'_{co}} - 1.254 \right).
 \end{aligned} \tag{2}$$

Among them, e'_{cc} is the strength of the constrained concrete, $e'_{co}, \varepsilon_{co}$ is the compressive strength and the maximum strength of the unconstrained concrete, generally taking $\varepsilon_{co} = 0.002$; F_c, F_{sec} is the tangent modulus and secant modulus of the concrete.

The traditional seismic structure mainly uses the plastic deformation and energy dissipation of the main structure after yielding against lateral force to dissipate the force of the earthquake. In the structural design of building facilities, on the one hand, by reducing the bottom stiffness of the building structure, the effect of earthquakes on the building is reduced. On the other hand, it is to increase the interface of components, enhance the rigidity of the bottom of the structure, and improve the resistance of the building itself. The principle of seismic isolation technology is to increase the self-correction time of the system itself, thus exceeding the characteristic period of the object and the bearing time of the superstructure. By maintaining the flexibility of the system and good damping, the vibration to the ground is effectively avoided so that the upper system is in a flexible position and the safety of the system is ensured [11]. As the damping of the system increases, the vibration isolation efficiency gradually decreases, but with the increase of the frequency ratio, the vibration isolation efficiency increases. When the system damping increases, the equipment quality also has a certain influence on the vibration isolation efficiency. By prolonging the oscillation time of the system, according to the response scenario, the acceleration of the vibration is reduced, the distortion of the protected system under the action of the earthquake becomes no longer

significant, and the response to the seismic force is reduced [12]. This is considered a key direction for future research, as it contributes more to the safety within system facilities than the usual simple design of system rigidity and function.

As the load-bearing member of the structural system, the main function of the bearing is to transmit the upper bearing force of the supporting structure and ensure the harmonious deformation of the upper and lower parts of the structure [13]. In the event of a sudden earthquake, the bearing is the direct part of the lower part where the seismic force is transmitted. Initially, the widely used steel bearings in the project failed to provide significant seismic isolation during large earthquakes, and the seismic forces were almost entirely transferred to the superstructure, resulting in complete structural failure [14].

The continuous evolution of structural design concepts and the continuous development of various building materials are conducive to the rapid development and application of large-frame buildings. Among them, the reticulated shell structure, as an important element of large-scale space structure, has gradually won the resonance of designers with its beautiful architectural form and has been used more and more widely [15]. The reticulated shell structure is a new type of space structure derived from thinness and characteristics. It is a net-like body based on rods, and the rods are formed according to certain rules. Its form is the structure of the organizer, forming the overall structure of the space frame. It has both the force transmission characteristics of the rod system and the structural characteristics of the shell. The force is mainly transmitted point-to-point through the two directions of tension, compression, or displacement in the shell, and the force transmission process is very clear [16].

At present, the commonly used shell structures at home and abroad are divided into single-layer shell structure, prestressed shell structure, ribbon cable support shell structure, single-layer fork-roll shell structure, etc. There are many forms of reticulated shell structures, such as spherical reticulated shells, hyperbolic plane reticulated shells, and hyperbolic, parabolic reticulated shells, which can be combined in various forms in the design [17]. This opens up a wide range of possibilities for designing buildings with large gaps to create different plan shapes and new unique architectural forms. It has been widely used in engineering practice due to its reasonable structural tension, high stiffness, low weight, beautiful and diverse shapes, and good technical and economic performance [18].

For the seismic isolation principle of reticulated shell structures, the structural oscillation control of spatial grids can be divided into three categories.

- (1) The energy dissipation support system is located in the lower part of the structure.

- (2) Dissipating energy and reduce vibration by installing isolation bearings, including sliding bearings and viscoelastic bearings.
- (3) Installing dampers on the upper part of the reticulated shell structure for vibration isolation.

By reasonably arranging the seismic isolation bearings, the sliding bearings can form an effective seismic isolation layer. During the seismic activity, the sliding of the bearings and the expansion and contraction of the large coil springs will consume a certain amount of energy. At the same time, the self-sustained seismic period of the structure far from the optimal period of the site is prolonged, and the seismic response is weakened to a certain extent [19].

In order to make up for the high cost of lines, maintenance problems, expensive and difficult lines in the traditional wired seismic data acquisition system in the field, in the whole system design, wireless communication technology is chosen to replace the communication work using a large number of communication cables in the traditional seismic data acquisition system [20]. The use of wireless transmission solutions facilitates the distributed deployment of seismic measurement units and enables efficient seismic operations in complex terrain. Wireless data transmission includes data communication between the receiving computer and each receiving unit and network communication between adjacent wireless communication units [21]. Table 2 is a comparison of the main technical indicators of wireless communication technology.

As a self-organized and distributed network centered on data transmission and exchange, sensor network provides data from a large number of sensor nodes. Real-time monitoring, joint exchange of data and information, and transmission of monitoring data are enabled even under very difficult conditions [22]. Therefore, wireless sensor network has been widely used in many fields, and its use in earthquake monitoring can provide a more real and reliable information basis for earthquake prevention and rescue. A wireless sensor network consists of some randomly distributed sensor nodes, which together constitute a wireless sensor network architecture [23]. Sensor nodes are self-organizing and capable of monitoring objects in real-time, collecting information, and sending data wirelessly. Wireless sensor networks detect, collect, process, and transmit sensor data, which is their most basic function.

Wireless sensor network is a comprehensive intelligent system that integrates sensor technology, MEMS, embedded technology, network communication technology, and information computing technology [24]. The sensor network is configured and managed by the user through the control node. The data collected by the sensor node is transmitted to other sensor nodes in the form of jump connection through the network, and the control node provides monitoring and retrieval of monitoring data. The architecture of the sensor network is shown in Figure 1.

The sensor node consists of a sensor module, a processor module, a wireless communication module, and a power supply module, as shown in Figure 2. The sensor module is

responsible for information collection and data transmission in the monitoring area [25]. The processor is usually an embedded processor. The wireless communication module is responsible for wireless communication with other parts of the system, exchanging control information, and sending and receiving data. The power supply unit provides the power needed to operate the sensor components and typically uses a small battery.

MEMS sensor is one of the earliest products widely used in commerce, and it is also one of the fastest growing technologies in MEMS technology. MEMS stands for Micro-Electro-Mechanical Systems, which are integrated devices or systems composed of electronic and mechanical components manufactured through large-scale processing processes, compatible with integrated circuits, and ranging in size from small to millimeters. In particular, it combines computers, sensors, and actuators to change the way nature is perceived and managed. Compared with traditional sensors, it has the characteristics of small size, light weight, low cost, low power, high reliability, suitable for mass production, easy integration, and intelligence. Its micro- or nanoscale size enables it to achieve some functions that traditional mechanical sensors cannot.

MEMS accelerometers are usually attached to an external object so that the motion of the object is represented by the motion of the accelerometer. When the accelerometer is accelerated together with an external object, the mass moves in the opposite direction under the influence of the inertial force acting on the spring. As shown in Figure 3(a), the spring and damper can quantify the motion of an object. The laws of physics show that there is a one-to-one correspondence between acceleration and displacement: as the acceleration changes, the displacement of the mass also changes, and the change in acceleration can be represented by the change in displacement. At the same time, it can be seen from Figure 3(b) that with the change of mass displacement, the capacitance between the stationary glass and the moving glass also changes accordingly. That is, C_{x_1} and C_{x_2} change due to the change of the distance between the plates, and the mathematical expression is as follows:

$$\begin{aligned} C_{x_1} &= \frac{\varepsilon\varepsilon_0 S}{d-x}, \\ C_{x_2} &= \frac{\varepsilon\varepsilon_0 S}{d+x}. \end{aligned} \quad (3)$$

Among them, C_{x_1} and C_{x_2} , respectively, represent the two capacitances between the fixed glass and the movable glass, where $\varepsilon_0 = 8.854 \times 10^{-12} F/m$ is the dielectric constant of the vacuum; ε is the relative permittivity of the medium between the plates, which is 1 in air; S is the covering area (m^2) of the plates; x is the displacement of the mass block, and d is the distance between the fixed glass and the movable glass.

The change in capacitance will be displayed by voltage, specifying V_p for the input voltage signal and V_s for the output voltage. The relationship between the output voltage and the input voltage is as follows:

TABLE 2: Comparison of main technical indicators of wireless communication technology.

Technical standards	Operating band	Transmission rate	Standby time	Transmission distance (m)	Main uses
WiFi	2.4 GHz	11 Mbps	1~6 hours	10~100	Wireless LAN
Bluetooth	2.4 GHz	1 Mbps	1~3 weeks	0~10	Personal network
ZigBee	868/915 MHz, 2.4 GHz	20~250 kbps	6~24 months	10~75	Sensor networks

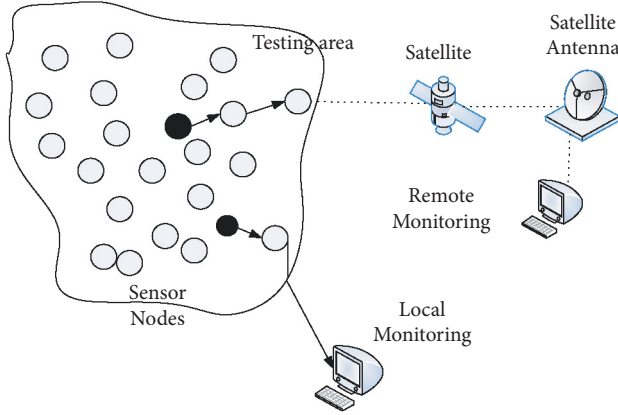


FIGURE 1: Architecture of a sensor network.

$$V_s = \frac{C_{x_1} - C_{x_2}}{C_{x_1} + C_{x_2}} V_p. \quad (4)$$

By measuring the change in voltage, the displacement change of the mass can be obtained. Voltage and displacement have a linear relationship, which is expressed as follows:

$$V_s = \frac{x}{d} V_p. \quad (5)$$

According to Newton's second law, the motion direction of the mass block is opposite to that of the object, and the relationship between the mass block displacement and acceleration is expressed as follows:

$$\begin{aligned} F &= kx \\ &= -ma, \end{aligned} \quad (6)$$

where k is the stiffness coefficient of the spring; m is the mass of the mass. Therefore, the relationship between the external acceleration and the output voltage is expressed as follows:

$$\begin{aligned} a &= \frac{kx}{m} \\ &= \frac{kdV_s}{mV_p}. \end{aligned} \quad (7)$$

It can be concluded from the above formula that there is a one-to-one correspondence between the acceleration and the output voltage, and the acceleration can be quantified by the change of the output voltage.

In view of the randomness and uncertainty of wireless seismic sensors in practical use, the P-wave components captured by seismic waves are biased. In this paper, a self-correction method of accelerometer position based on

longitudinal wave measurement is proposed, which can automatically detect the rotation correction of installation direction and coordinates, and the corrected accelerometer can be used to eliminate the influence of sensor positioning.

The accelerometer position correction method is divided into two parts: first, the data collected by the accelerometer are compared and analyzed, a vertical axis is selected, and then the coordinate rotation on the selected axis is corrected, and the sensor data is self-corrected.

Sensor self-calibration method:

3.3. Identifying the Installation Direction and Selecting the Vertical Coordinate Axis. The simulation diagram of the sensor coordinate system is shown in Figure 4(a). During the installation process of the MEMS sensor, there is usually an included angle between the Z-axis and the gravitational acceleration. This is because a mass block is added to the acceleration sensor, so it will always be affected by gravity. As long as the measurement axis is not perpendicular to gravity, the inclination angle between the sensor and gravity can be measured. Let the included angle be θ . At this time, the gravitational acceleration will produce a projected component on the xyz coordinate axis. There is the following relation:

$$\cos \theta = \frac{g_r}{g}. \quad (8)$$

The axis with the smallest angle θ , that is, the axis with the largest gravitational acceleration projection, is chosen as the reference direction. Where g_x , g_y and g_z are the component modulus of the gravitational acceleration on the xyz axis, and g is the gravitational acceleration value at rest. r is the axial direction corresponding to the maximum value of g_x , g_y and g_z , ie the chosen reference direction. g_r is the modulus of the gravitational acceleration component on the reference axis.

3.4. Coordinate Rotation Correction. The coordinate rotation model is shown in Figure 4(b), where g is the gravitational acceleration at rest and g_r is the mode of the gravitational acceleration component on the reference axis. G is the acceleration value when the accelerometer moves after calibration, G_r is the acceleration value when the reference axis is selected, where

$$g = \sqrt{g_x^2 + g_y^2 + g_z^2}. \quad (9)$$

The accelerometer values at rest and in motion on the reference axis should be measured under conditions g_r and G_r , respectively. Since the angle between the reference axis and the gravitational acceleration is constant at rest and in

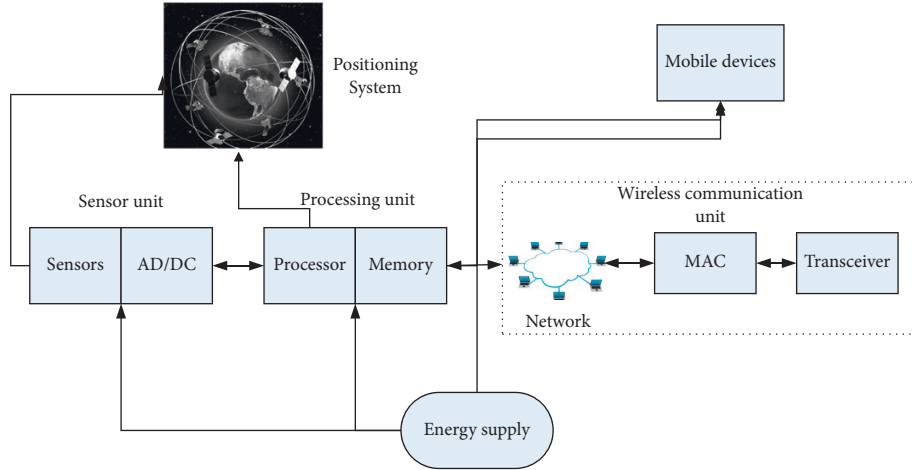


FIGURE 2: Node structure of the sensor.

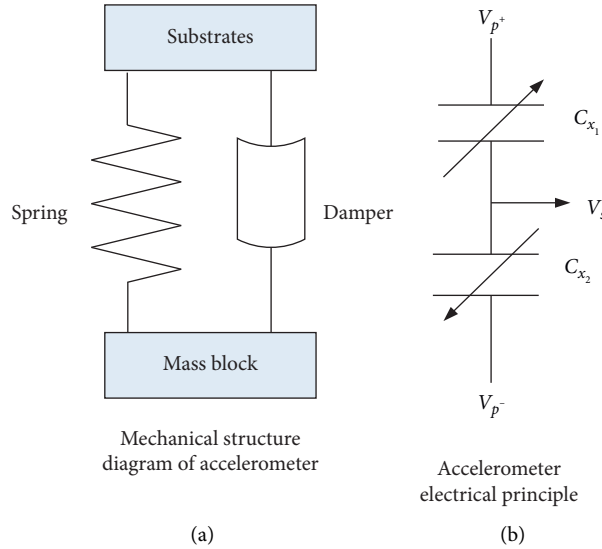


FIGURE 3: Schematic diagram of the working principle of accelerometer. (a) Mechanical structure diagram of accelerometer. (b) Accelerometer electrical principle.

motion, it can be concluded that the acceleration values at rest and in motion are also proportional. It follows that:

$$\begin{aligned} \cos \theta &= \frac{g_r}{g} \\ &= \frac{G_r}{G}. \end{aligned} \tag{10}$$

Corrected G value for accelerometer motion:

$$G = \frac{g}{g_r} G_r. \tag{11}$$

(g/g_r) is the correction coefficient in the above formula, which is used to adjust the collected data. The adjusted value deducts the value of the gravitational acceleration to obtain the actual value of the acceleration a , as shown in the following formula:

$$a = \frac{g}{g_r} G_r - g. \tag{12}$$

The above formulas allow for self-correction of the accelerometer position, which in turn translates the correction into more precise data, thereby eliminating the effect of the accelerometer position on seismic data acquisition. The accelerator position self-correction algorithm eliminates the influence of accelerometer placement position, which is beneficial to the placement of wireless seismic sensors in the field, which can be used to obtain more accurate seismic data in complex terrain.

The sensor network first uses the physical layer of the data collection and transmission module to detect road traffic conditions, such as traffic flow speed, traffic flow size, lane occupancy, road characteristics, and other traffic indicators, as shown in Figure 5.

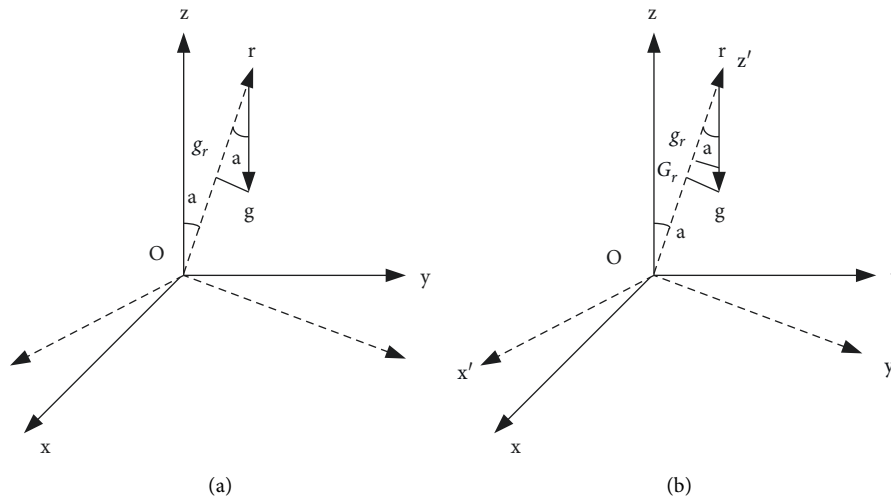


FIGURE 4: Simulation diagram of sensor coordinate system and schematic diagram of rotation model.

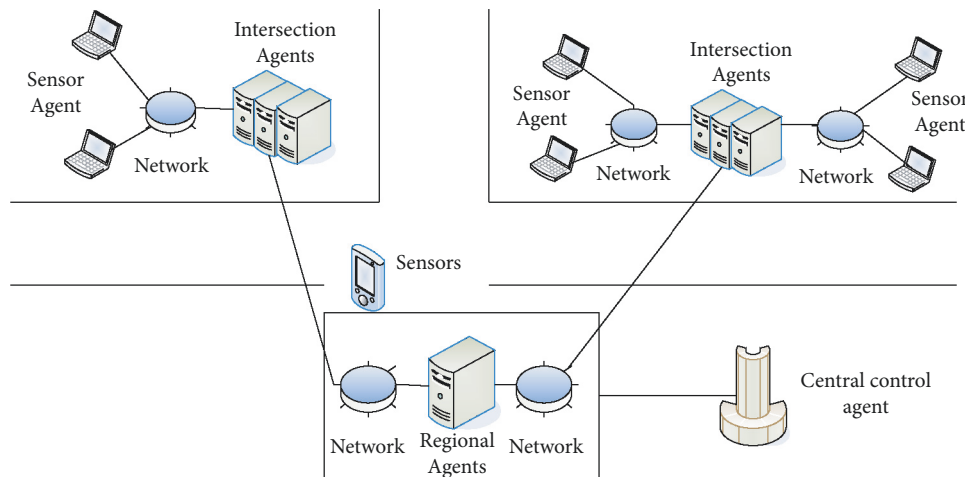


FIGURE 5: Network layout of the model.

Seismic sensor networks include detectors, differential low-pass filters for attenuating radio signals, amplifier circuits, low-pass filters, A/D conversion circuits, microprocessors, and data storage units. The detector is used to detect the vibration signal and convert it into a voltage regulation; since the RF signal appears as a DC distortion output in the area where the RF signal is strong, different low frequency parameters are used to reduce the interference of the RF signal. The signal output is not very strong, so it is very important to design the same amplifier circuit, which is mainly used to increase the reception of the small signal of the sensor, and the frequency of the vibration signal caused by the human body or the vehicle is lower than 150 Hz. To prevent noise signals from entering the A/D module (analog-to-digital conversion), the filter circuit behind the built-in amplifier circuit is low-pass, and the power control module provides a stable power supply with low ripple factor. Figure 6 is a schematic diagram of the sensor network application function.

As can be seen from Figure 6, the sensor output signal goes through the delay mode and then enters the A/D for data conversion, and another signal enters the comparator, and the output of the comparator is used as an external signal. Another approach to system optimization is to set thresholds in the node detection software and use the results to compare the A/D-evaluated values to the thresholds. When the excitation system is executed, the received data is stored in memory as valid data. The memory is used to store the data after A/D conversion. After the assembly process is completed, the CC2530-based wireless transceiver reads the data and sends it to the sink node. A/D data retrieval, memory read and write, and signal detection are all implemented by FPGA.

4. Seismic Experimental Design of Reticulated Shell Structure for Isolation Bearings

The analytical model is a double-layer spherical reticulated shell structure with a span arrangement of 60 meters, a rise-

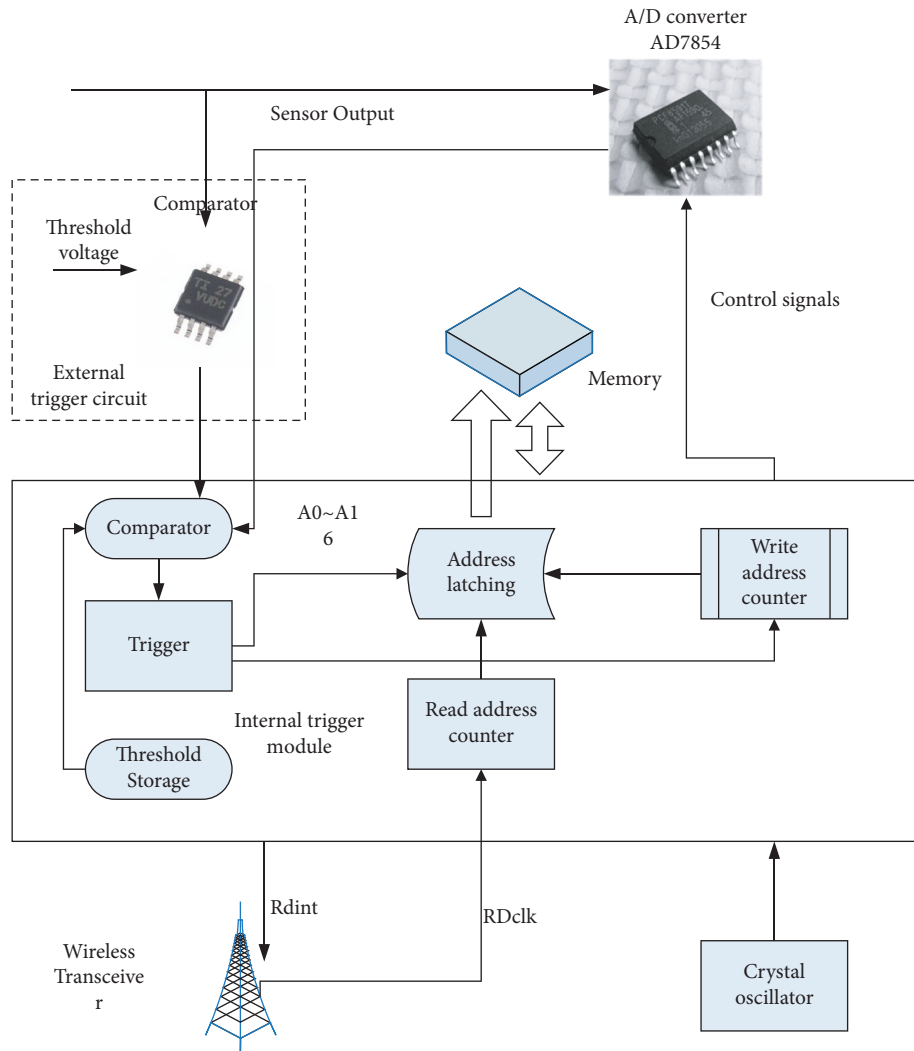


FIGURE 6: Schematic diagram of the hardware working principle of sensor network nodes.

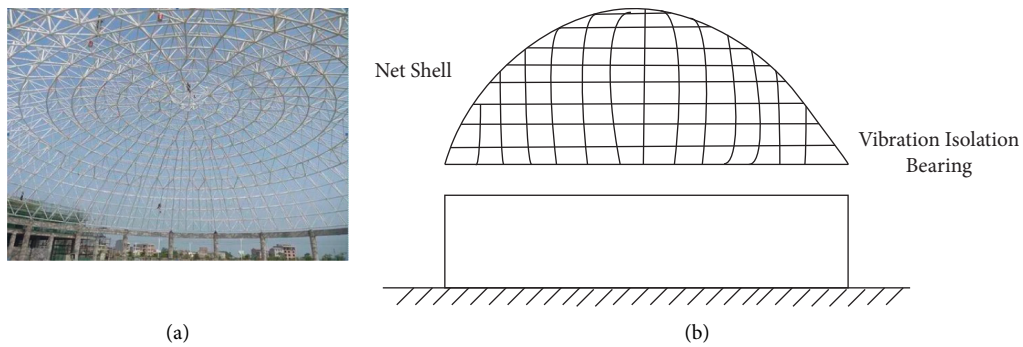


FIGURE 7: Double-layer spherical mesh shell structure model and arrangement scheme.

span ratio of 0.2, and a thickness of the reticulated shell of 2 meters, supported by the bottom chord. This structural model is shown in Figure 7(a). Five kinds of steel pipes (seamless Q235 steel pipes) of 114×6 , 133×8 , 140×7.5 , 152×8 , and 159×8 are used as reinforcement for the reticulated shell, and the roof load is assumed to be 1 kN/m^2 . In the numerical simulation, the space element member

model is used for all the stressed members of the reticulated shell. In order to ensure the overall rigidity of the reticulated shell structure, a steel box with a size of $0.8 \times 0.6 \times 0.05 \text{ m}$ is installed on the bottom support of the lattice window. For the multidimensional isolation condition, the isolation bearing is installed at the bottom of the box part of the reticulated shell frame structure, as shown in Figure 7(b).

TABLE 3: Seismic isolation bearing parameters.

Projects	Vibration isolation bearing parameters	Projects	Vibration isolation bearing parameters
Effective diameter (mm)	300	Equivalent horizontal stiffness (KN/m)	882
Height (mm)	105	Stiffness before yielding (KN/m)	3120
Equivalent damping ratio (%)	27.5	Stiffness after yielding (KN/m)	475

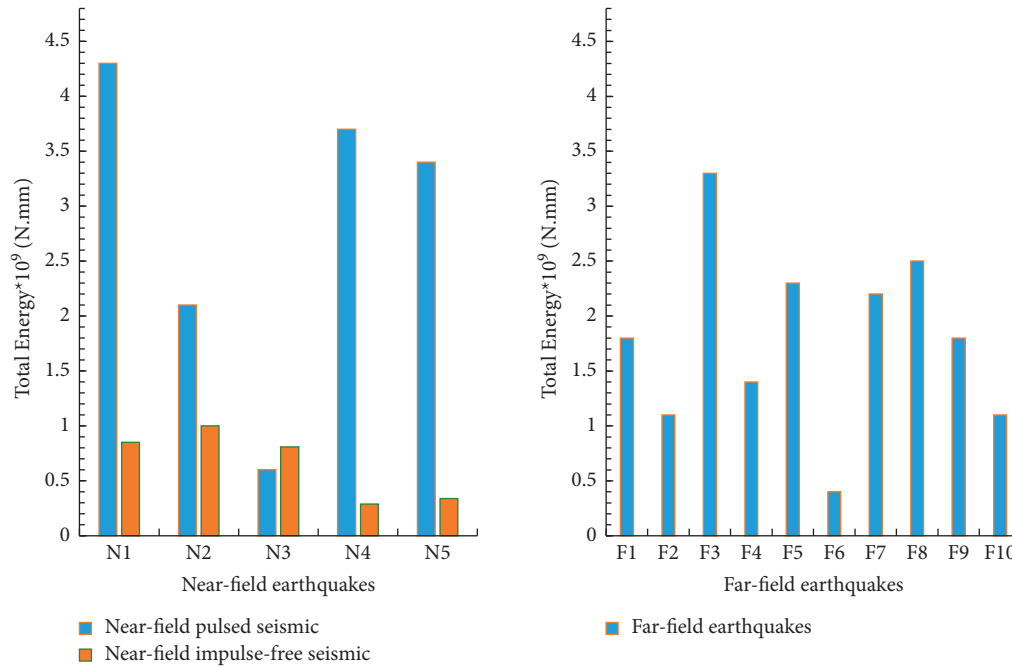


FIGURE 8: Earthquake energy input.

The load-bearing structure of the lower part of the reticulated shell is assumed to be a rigid structure, and its reinforcement for earthquake effects is not considered. Q345 steel is considered to be an ideal elastic-plastic material with a modulus of elasticity of $2.06 \times 10^5 \text{ N/mm}^2$ and a mass density of 7850 kg/m^3 according to the Von Mises yield criterion. The isolation bearing model was created in ABAQUS using C3D8R solid elements for the slider and base elements, while the reticulated shell uses quadratic interpolated Timoshenko beam elements B32 Sandwich beam elements. Simulations are performed with a coupling device. The material properties of the structural elements and reticulated shell structures are determined and coupled with the MSFB using contact and constraint functions to form the overall structural model.

The parameters of the seismic isolation bearings used are shown in Table 3.

5. Seismic Experimental Analysis of the Reticulated Shell Structure of the Isolation Bearing

Since near-field earthquakes and far-field earthquakes have different ground vibration characteristics, their effects on the

seismic response of the structure are also very different. It was found that the seismic response of ground-isolated structures to near-field pulsations and far-field vibrations was analyzed in this paper. From Figure 8, it can be seen that the total energy of the ground isolation structure in the far field is greater than the total energy of the near-field unpulsed ground vibration but less than the total energy of the near-field ground vibration pulse. Therefore, the total energy of the basic isolation structure under the near-field pulse ground motion is the largest. That is to say, the seismic response of the basic isolation structure under the near-field pulse ground motion is the largest.

The seismic isolation bearing of the reticulated shell structure made of seismic isolation is placed between the foundation and the foot of the building and is separated by a seismic isolation layer so that more than 80% of the seismic energy cannot be transmitted to the superstructure, which effectively reduce the impact and damage of earthquakes on the overall structure or structural components. However, the failure of the isolation support impairs the ability to absorb seismic energy, which is reflected in the variation in the degree of ground energy dissipation at each height of the upper floors. As shown in Figure 9, for different seismic waves, the energy consumed by the seismic fortification is

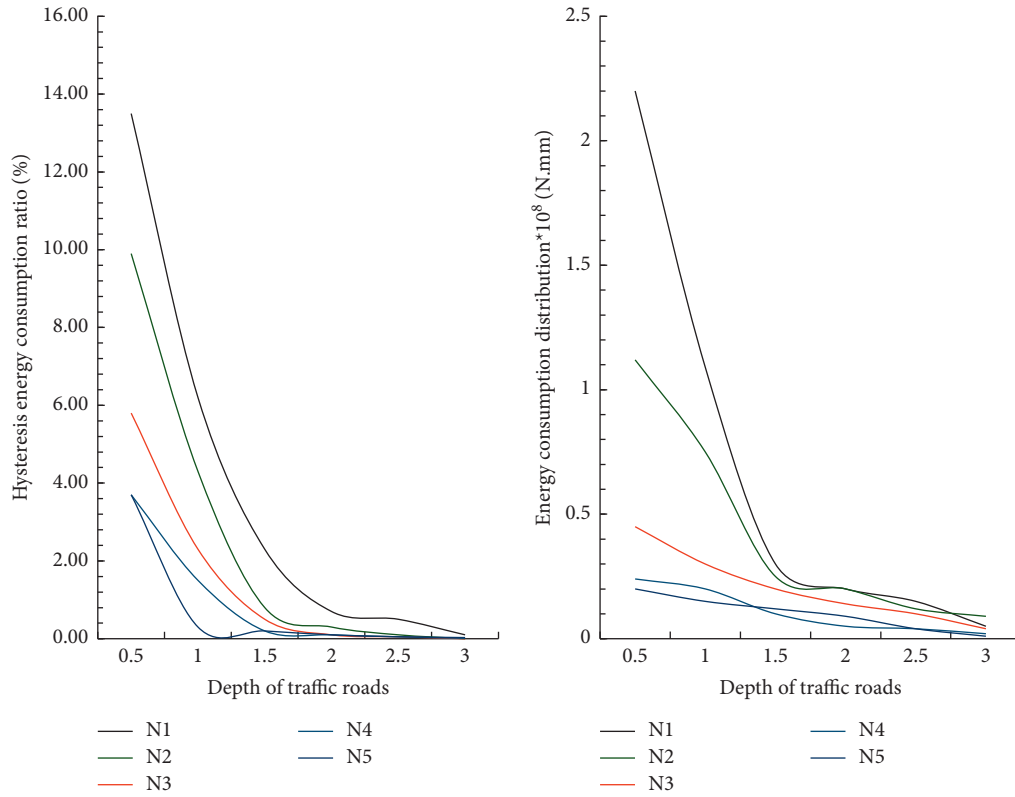


FIGURE 9: Energy consumption distribution of the reticulated shell structure of the isolation bearing.

TABLE 4: Mechanical performance parameters of isolation bearings.

Peak acceleration	0.01 g			0.02 g		
Vertical pressure (kN)	25	35	45	25	35	45
Equivalent stiffness (kN/mm)	1.186	1.674	2.140	0.981	1.24	1.401
Energy consumption per unit cycle (J)	200	341	410	420	658	942
Equivalent damping ratio	0.331	0.374	0.401	0.215	0.284	0.325

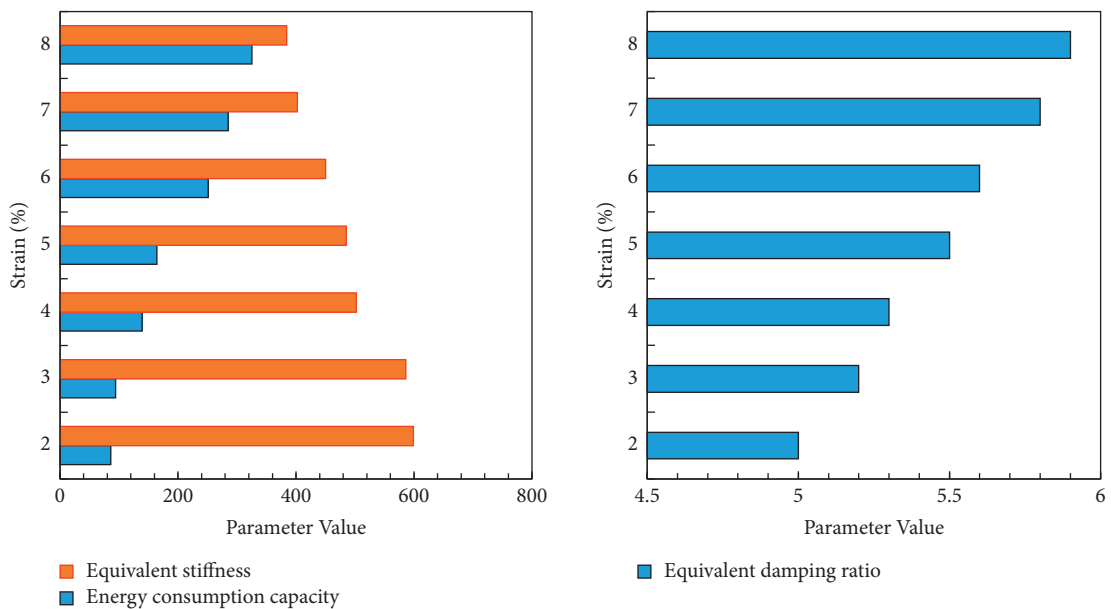


FIGURE 10: Cyclic loading test of isolation bearings.

different, but the hysteretic energy dissipation of the upper ground structure follows the principle of “upper low and lower higher”. That is, the hysteretic energy dissipation of the superstructure decreases as the height increases, so the location of the first layer is a priority in the structural design. Therefore, the location of the ground floor is the focus of the structural design.

For a simple harmonic excitation performance test, the effect of changing the vertical stress on the hysteresis behavior of the bearing was investigated by changing the magnitude of the vertically applied force when a waveform with a sinusoidal function was introduced. Table 4 shows the values of three mechano-mechanical parameters, namely equivalent stiffness, energy loss per unit cycle, and equivalent damping ratio. Figure 10 depicts the cyclic loading test of the isolation bearing.

When the maximum acceleration increased from 0.01 g to 0.02 g, the equivalent stiffness and equivalent damping ratio of the isolation bearing decreased, while the energy dissipated per unit cycle increased significantly. At a given maximum acceleration, the equivalent stiffness and equivalent damping ratios dissipated per unit cycle increase with increasing vertical force.

6. Conclusion

Most earthquakes are not felt by humans because they are low in magnitude or occur in remote areas, but some earthquakes occur near us, and if the earthquake is strong, it can cause serious personal safety threats and economic losses. China is one of the countries in the world that has experienced many earthquakes and is greatly affected by earthquakes. Earthquakes are inherently random, and their mechanisms are complex and variable. Even though a lot of time and effort has been invested in earthquake prediction at home and abroad, there is still no significant effect. In order to reduce the number of victims caused by earthquakes, it is necessary to improve the seismic performance of building facilities and the ability to resist collapse caused by strong earthquakes so as to greatly reduce the losses caused by the collapse. The reticulated shell structure has both the force transmission characteristics of the rod system and the structural properties of the shell. The force is mainly transmitted point by point through the tension, pressure, or shear force in two directions in the shell, and the force transmission process is very clear. At this stage, the spatial reticulated shell structural system is a structural system with broad development prospects. In the optimization of seismic performance, this paper only studies the energy dissipation capacity of the reticulated shell structure of the seismic isolation bearing. The material selection of the isolation bearing and the shape of the bearing of the isolation bearing have not been studied, which is the deficiency of this paper.

Data Availability

Data sharing is not applicable to this article as no new data were created or analyzed in this study.

Conflicts of Interest

The authors state that this article has no conflicts of interest.

Acknowledgments

This work was supported by K1802006 (Science and technology research project of Suihua University) (Application Research on “Internet +” and building energy saving mode).

References

- [1] Q. Wu, W. He, W. Liu, Y. Weixin, and Q. Chuan, “Large deformation hardening model of lead rubber bearings and elastic-plastic analysis for a structure with seismic isolation,” *Zhendong yu Chongji/Journal of Vibration and Shock*, vol. 36, no. 15, pp. 90–97, 2017.
- [2] X. Hong, W. Guo, and Z. Wang, “Seismic analysis of coupled high-speed train-bridge with the isolation of friction pendulum bearing,” *Advances in Civil Engineering*, vol. 2020, no. 44, pp. 1–15, 2020.
- [3] T. Hiraki, K. Kanazawa, and H. Kitamura, “Mechanical energy evaluation method for seismic isolation systems with rubber bearings under large deflection,” *Journal of Structural and Construction Engineering (Transactions of AIJ)*, vol. 82, no. 731, pp. 75–85, 2017.
- [4] A. Mohebbi, K. L. Ryan, and D. H. Sanders, “Seismic protection of the piers of integral bridges using sliding bearings,” *Journal of Earthquake Engineering*, vol. 21, no. 7–8, pp. 1365–1384, 2017.
- [5] X. Yan, Q. Ai, H. Mao, and X. Xiaoyong, “Multi-dimensional seismic response analysis of three-dimensional seismic-isolation mega-sub structure,” *China Civil Engineering Journal*, vol. 50, no. 5, pp. 36–46, 2017.
- [6] L. I. Qingning, M. Cheng, J. Yin, L. Yan, and X. Liao, “Analysis and experimental study on performance of curved bridge sliding seismic isolation,” *World Earthquake Engineering*, vol. 33, no. 1, pp. 34–40, 2017.
- [7] A. Mukherjee, D. K. Jain, P. Goswami, Q. Xin, L. Yang, and J. J. P. C. Rodrigues, “Back propagation neural network based cluster head identification in MIMO sensor networks for intelligent transportation systems,” *IEEE Access*, vol. 8, no. 1, Article ID 28524, 2020.
- [8] M. Mousa, K. Sharma, and C. G. Claudel, “Inertial measurement units-based probe vehicles: automatic calibration, trajectory estimation, and context detection,” *IEEE Transactions on Intelligent Transportation Systems*, vol. 19, no. 10, pp. 3133–3143, 2018.
- [9] Z. Liu and S. Zhang, “Artificial neural network-based method for seismic analysis of concrete-filled steel tube Arch bridges,” *Computational Intelligence and Neuroscience*, vol. 2021, no. 2, pp. 1–10, 2021.
- [10] M. A. Nabian and H. Meidani, “Deep learning for accelerated seismic reliability analysis of transportation networks,” *Computer-Aided Civil and Infrastructure Engineering*, vol. 33, no. 6, pp. 443–458, 2018.
- [11] H. Malik and W. Zatar, “Agent based routing approach to support structural health monitoring-informed, intelligent transportation system,” *Journal of Ambient Intelligence and Humanized Computing*, vol. 11, no. 3, pp. 1031–1043, 2020.
- [12] Y. Peng, X. Cao, Y. Chao, Z. Xiao, X. Xi, and D. Wu, “Proactive drone-cell deployment: overload relief for a cellular network under flash crowd traffic,” *IEEE Transactions on*

- Intelligent Transportation Systems*, vol. 18, no. 10, pp. 2877–2892, 2017.
- [13] M. Gao, W. Ping, C. Yong, R. Chen, and D. Cai, “Design and verification of a rail-borne energy harvester for powering wireless sensor networks in the railway industry,” *IEEE Transactions on Intelligent Transportation Systems*, vol. 18, no. 99, pp. 1596–1609, 2017.
- [14] Z. Zhang and S. Chen, “Real-time seam penetration identification in arc welding based on fusion of sound, voltage and spectrum signals,” *Journal of Intelligent Manufacturing*, vol. 28, no. 1, pp. 207–218, 2017.
- [15] C. Li, G. Zhang, Y. Mao, and X. Zhao, “A data aggregation privacy protection algorithm based on fat tree in wireless sensor networks,” *Security and Communication Networks*, vol. 2021, no. 8, pp. 1–9, 2021.
- [16] S. Salgadoe, F. Lu, and F. Lu, “An Anomaly Detection Model for Ultra Low Powered Wireless Sensor Networks Utilizing Attributes of IEEE 802.15.4e/TSCH,” *Journal of Communications*, vol. 14, no. 5, pp. 335–341, 2019.
- [17] T. Jinjun, W. Hua, W. Yinhai, L. Xiaoyue, and L. Fang, “Hybrid prediction approach based on weekly similarities of traffic flow for different temporal scales,” *Transportation Research Record*, vol. 2443, no. 1, pp. 21–31, 2018.
- [18] F. Chao, Z. He, R. Feng et al., “Predictive trajectory-based mobile data gathering scheme for wireless sensor networks,” *Complexity*, vol. 2021, no. 2, pp. 1–17, 2021.
- [19] W. Zhou, J. S. Berrio, S. Worrall, and E. Nebot, “Automated evaluation of semantic segmentation robustness for autonomous driving,” *IEEE Transactions on Intelligent Transportation Systems*, vol. 21, no. 5, pp. 1951–1963, 2020.
- [20] W. Yang, X. Sun, M. Wang, and P. Liu, “Vertical stiffness degradation of laminated rubber bearings under lateral deformation,” *Construction and Building Materials*, vol. 152, no. oct.15, pp. 310–318, 2017.
- [21] D. Wang, Y. Zhang, C. Wu, X. Guofeng, and H. Wencheng, “Seismic performance of base-isolated AP1000 shield building with consideration of fluid-structure interaction,” *Nuclear Engineering and Design*, vol. 353, Article ID 110241.1, 2019.
- [22] W. He, Y. Huang, and W. Liu, “Seismic responses of a nuclear plant isolated structure supported by rubber bearings with a multi-factor coupled mechanical model,” *Zhendong yu Chongji/Journal of Vibration and Shock*, vol. 37, no. 17, pp. 72–78, 2018.
- [23] Q. Han, B. Wang, and J. Jia, “Seismic response analysis of isolated offshore bridge with friction sliding bearings,” *Earthquakes and Structures*, vol. 16, no. 6, pp. 641–654, 2019.
- [24] T. Yamauchi, H. Kitamura, M. Nagano et al., “Study on application of seismic deformation method for pile top seismic isolation buildings,” *Journal of Structural and Construction Engineering (Transactions of AIJ)*, vol. 83, no. 743, pp. 69–79, 2018.
- [25] Y. Shi, J. M. Xuan, J. Yao, and Z. -Y. Zhang, “Analysis of seismic performance of long span rail transit bridge,” *Bridge Construction*, vol. 47, no. 6, pp. 42–47, 2017.

Research Article

Data Transmission Control of Vehicle Ad Hoc Network in Intelligent Transportation Systems for Smart Cities

Zhenhua Li  and Guicai Yu 

College of Physical Science and Engineering, Yichun University, Yichun Jiangxi, China

Correspondence should be addressed to Zhenhua Li; yclzh2011@163.com and Guicai Yu; guicai.yu@gmail.com

Received 17 February 2022; Accepted 29 March 2022; Published 22 April 2022

Academic Editor: Sang-Bing Tsai

Copyright © 2022 Zhenhua Li and Guicai Yu. This is an open access article distributed under the Creative Commons Attribution License, which permits unrestricted use, distribution, and reproduction in any medium, provided the original work is properly cited.

The superposition of various application data streams in smart cities can intensify the load of vehicular networks in intelligent transportation systems, which can have an impact on the popularity of smart cities. To improve the performance of large amount of data transmission in telematics, this study proposes a scheme to determine the network state using congestion parameters and routing parameters and matches different data transmission amounts according to different states of the network. The scheme first considers the possibility of the network congestion state. Once congestion is judged to occur, the amount of data sent is reduced, and reducing the data backlog can further mitigate the possibility of congestion formation on the network. Secondly, after rejecting the possibility of congestion, the routing situation of the network needs to be judged, in such cases, whether a change in vehicles in the multi-hop path leads to a path change or an interruption of the data transmission path. Congestion parameters and routing parameters evaluate the state of the network, and the size of the congestion window is appropriately limited by the routing parameters to prevent excessive data volume from causing backlogs in the vehicular network. Experimental simulations show that the proposed scheme exhibits good performance in both linear and crossover vehicular networking scenarios. The research results provide a useful reference for the data transmission of telematics in smart cities.

1. Introduction

The smart city has become the central vision of current urban development. It includes access to customer needs through data collected from a variety of interconnected sensors, devices, and people. The analysis of data is used to improve the efficiency of people's lives in the city and can even solve urban problems such as transportation and network connectivity. The focus of smart cities is based on the operability of service models and connected scenarios [1]. Such services are expected to reduce capital and infrastructure costs while improving the efficiency of service delivery within the smart city framework and enabling customers to use applications remotely from anywhere in the world via the Internet of things (IoT).

In smart cities, intelligent transportation systems carry a large number of data interactions, but the path of their transmission changes dynamically, which can lead to many

problems in the transmission of data. Vehicular ad hoc network (VANET) plays an important role in the intelligent transportation system, and the characteristics of its bearer data transmission are mainly reflected in the large capacity, and multiple applications and applications of wireless networks share the transmission protocol [2–4]. This puts new requirements on the transmission of VANET bearer data, whose protocol must have high compatibility and be able to avoid congestion caused by large-capacity data. The intelligent transportation system is designed to support the smart city vision, and the IoT can be applied to the intelligent transportation system and smart city to form an advanced platform for new applications; however, various issues and challenges have emerged. One of the main problems is the data backlog formed by the overlapping transmission of various data, and this backlog is very likely to cause network congestion; in addition, data are faced with random data loss in the IoT of smart cities, coupled with the fact that changes

in the location of vehicles in the path can lead to constant changes in the transmission path, which makes it more difficult to effectively control the transmission of data. [5–7].

Based on this, researchers have conducted a lot of research on the data transmission of the vehicle network formed by intelligent transportation in smart cities [8–10]. However, due to the superposition of various application data in smart cities are very easy to cause backlog loss; in addition, different network states will lead to the sending of data that cannot accurately match the sending volume, resulting in the problem of large data transmission fluctuations and low rates. Therefore, how to accurately determine the state of the vehicular network in smart cities and adjust the data transmission according to different states becomes an urgent problem to be solved.

2. Related Work

Intelligent transportation system occupies a very key position in the construction and application of smart cities, and researchers have conducted a lot of research work on traffic system and data processing and transmission in smart cities.

2.1. Intelligent Transportation System for Smart Cities. Xiong et al. [11] briefly reviewed the progress of intelligent transportation system (ITS) research and discussed the problems encountered in the development of ITS, thus providing a useful reference for subsequent researchers. With the widespread deployment and application of 5G, the use of 5G to support intelligent transportation systems has become a hot research topic. Data are collected through various sensors using 5G for communication, which supports the necessary communication infrastructure required for smart cities. Gohar et al. [12] discuss the technical support of 5G for ITS and key issues for subsequent research in several dimensions based on the characteristics of smart cities and intelligent transportation systems. The VANET suffers from many shortcomings similar to wireless multi-hop networks, such as intermittent connection interruptions, high bit error rates, and intense data access competition. However, VANET has been successfully used in intelligent transportation systems to realize many applications in smart cities. Considering that UAVs have the characteristics of line-of-sight communication, load balancing, flexibility, and cost control, Raza et al. [13] proposed a UAV-assisted vehicular self-organizing network architecture for smart cities, and the test results showed that UAV-assisted vehicular networking can effectively improve the robustness of network architecture for smart cities and provide a useful option for future smart city applications.

The integration of various transportation technologies in an intelligent transportation system makes it possible to be used in smart city architecture. Zhao and Jia [14] provide a literature review on how intelligent transportation systems can contribute to the environmental sustainability of smart cities, noting that the data required by a large number of vehicle terminals may result in a backlog of large volumes of data that must be processed by intelligent transportation

systems in smart cities to ensure efficient transportation by controlling traffic flow and preventing accidents. The concept of smart cities was first proposed in the early 1990s. Subsequently, based on the development of various information technologies, the study of smart cities has achieved certain results [15]. Smart cities are the way to the future development of cities, which are bound to contribute to the improvement of the quality of life of the residents with the development of information and communication technologies (ICT) and transportation technologies. There is no doubt that the requirements for smart cities in modern intelligent transportation systems are getting higher and higher, and various new information technology developments have made the combination of smart cities and intelligent transportation closer and closer. Meanwhile, modern information technologies such as cloud computing [16], blockchain, and Internet of things [17] have their own advantages in facing the processing of large volumes of traffic data, so it is especially important for the above study to use cloud computing to deal with automatic monitoring and management of vehicle flow during traffic congestion. In addition, blockchain and IoT for model evaluation of intelligent transportation systems in smart cities are evident for the improvement of the quality of life of residents in sustainable urban transportation systems.

2.2. Data Transmission Control for Intelligent Transportation Systems. Joseph et al. [18] provide a comprehensive overview of five intelligent transportation system projects (TIME, Sentient Transport, EVT, DynaCHINA, Traffic-View) with a focus on the collection, transmission, and analysis of focused traffic and vehicle data. The authors point out that providing intelligent service to drivers is particularly important for future intelligent systems, followed by an introduction to intelligent data identification and data collection in the railroad environment. The data connection of Telematics and various transportation vehicles can promote the effective data transmission in smart cities. In the process of data transmission, real-time transmission control and traffic system will generate a large amount of transmission data, and Sumalee and Ho [19] analyzed the problems that need to be paid attention to data transmission in the intelligent transportation systems, especially in the connected vehicle to build the intelligent transportation system. Considering the recent rise of IoT technologies, Sodhro et al. [20] proposed an IoT-driven intelligent transmission system control scheme aimed at supporting future IoT-driven vehicle-to-vehicle (V2V) multimedia transmission communication. The scheme analyzes the communication performance of the proposed scheme over V2V in terms of QoS metrics such as green (i.e., energy efficiency), sustainability (i.e., less battery charging consumption), reliability (i.e., less packet loss), and availability (i.e., more coverage). Zhang and Lu [21] studied the vehicle communication network in IoT-based intelligent transportation system, and model simulation tests by OPNET modeler showed that AODV protocol outperforms DSR protocol in terms of throughput, average network delay,

routing load, packet loss rate, and average routing hops, which is more suitable for the network communication of intelligent transportation system.

The magnitude of traffic flow in intelligent transportation systems is particularly important in the transmission and processing of data, and the prediction of various traffic flows is also the focus of research on intelligent transportation data transmission in smart cities. Zhang et al. [22] proposed a scheme based on a quantum particle swarm optimization strategy. The scheme metaphorically incorporates a genetic simulated annealing algorithm into the initialization of traffic flow data according to the characteristics of the transmission data of traffic flow in smart transportation and applies a radial basis neural network prediction model to optimize the parameters. The simulation results show that the proposed algorithm can reduce the error of data prediction and play a more stable role in the transmission of data in the intelligent transportation system. Similarly, for the traffic congestion problem caused by high traffic volume, Saharan et al. [23] effectively managed the problem of data transmission in intelligent transportation by developing a dynamic pricing strategy. Firstly, the authors provide a literature review and analysis of dynamic pricing techniques, followed by an in-depth discussion of various problems solved by dynamic pricing techniques, evaluation of parameters and their limitations, and, finally, an analysis of future dynamic pricing applications for intelligent transportation systems. Intelligent control of traffic in smart cities has an important impact on enhancing the transmission of data. To improve the efficiency of intersection vehicles, Lv et al. [24] modeled intersection vehicles using artificial intelligence techniques that have developed rapidly in recent years and used dynamic scheduling algorithms to improve the communication network in intelligent transportation systems. Finally, the effectiveness of the proposed model and the improved scheme was evaluated by simulation tests. The results show that the model can be used to predict the passage time of queued vehicles at intersections with a small error and a high success rate of data transmission. Suryadithia et al. [25] provide a detailed discussion of the technical barriers encountered in intelligent transportation systems, starting with a review of the literature on various intelligent transportation technologies in recent years, followed by an example of intelligent transportation research and providing examples of applications that can be used in intelligent transportation systems.

The layout of the organization of the rest of this study is as follows. Section 3 describes the proposed congestion control algorithm. Section 4 goes through the experimental simulations. The last section concludes the study and gives relevant conclusions.

3. Data Transmission in Intelligent Transportation Systems

Data for smart cities come from a variety of interconnected sensors, and sensor data from these devices are critical to intelligent transportation systems. The ITS vehicle network is the core component of the smart city. The current

widespread use of a large number of wireless communication technologies can lead to low performance of traditional transmission protocols. Meanwhile, the large-capacity data transmission generated by various sensors poses new challenges to the data transmission system of telematics. In the multi-hop network built by telematics, there will be a large amount of interaction data between the sender and receiver of the vehicle, and these data will experience various network states, such as congestion in telematics, loss of data in the wireless link, change in vehicle building path, or even interruption of data transmission. However, the above situations cannot be directly identified in these interaction data, which create an obstacle to efficient data processing in smart cities.

3.1. Data Interaction Problems in Smart Cities. The amount of data interaction in a smart city is very large. The multi-hop network built by VANET, various sensor data, and application data forms a huge pressure on the transmission system, where the biggest risk faced is the congestion caused by the backlog of transmission data. The judgment of data congestion in the network is round-trip time (RTT) timeout, and the sender of data in the telematics network directly reduces the amount of data transmission, but the guideline of this judgment is exposed to many misjudgments, especially for vehicle-based transmission systems with wireless communication technology. One of the main misjudgment cases that the wireless link caused is data loss, and this data loss is caused by a variety of reasons, such as various interference to the wireless channel, competition caused by the media access, and link bandwidth limitations. The characteristics of this data loss are very different from the case of data loss caused by congestion, and data loss in wireless links often occurs randomly. There should also be a big difference between the data sender's handling of random loss and congestion backlog loss. The former only needs to retransmit the lost random data, and the amount of data sent can still be maintained at a larger amount to improve the transmission efficiency of the network.

In addition, the driving path of vehicles in the traffic system is not a stable path, which adversely affects the construction of multi-hop routing in vehicular networks. When multiple vehicles build multi-hop transmission paths, the data transmission in multi-hop networks can form stable transmission routes. However, when there is an unexpected accident and temporary parking among multi-hop vehicles, the path of data transmission will be interrupted, and the data transmission will be disordered or even lost when looking for a suitable vehicle to build a multi-hop path. At this time, the data sender needs to reconstruct a stable transmission path and reduce or even temporarily stop the transmission of data. In the extreme case, the transmission path of data is irreversibly restored and the data connection of multi-hop network is interrupted. At this time, the sender of data should find a new transmission path as soon as possible to build a stable multi-hop transmission route, and the sender of data should suspend or stop sending data until a new transmission path is established.

Considering that the interaction of data in smart cities is very frequent and various applications will overlay different types of data, making the transmission of data face the risk of congestion caused by backlogs, and congestion is the first network state to be considered in the above two cases. Once congestion is judged to occur, the amount of data sent is reduced. Secondly, in the case of rejecting congestion, the routing situation of the network needs to be judged, and in such cases, whether a change in the multi-hop path occurs due to a change in vehicles or an interruption in the data transmission path.

3.2. Determination of Transmission Status. The sharp increase in the amount of data in smart cities may bring the risk of congestion, and the above analysis shows that in the process of data transmission, it is necessary to first determine whether congestion occurs in the car network in smart transportation and then determine the change in routing. The amount of information for judging the network state in the interaction of data in the transmission protocol is very small. This section first defines two parameters for judging the congestion state, congestion parameter $C_1(t)$ and congestion parameter $C_2(t)$, which are used to judge the congestion of the network in terms of time and throughput, respectively. In the state of negative congestion, then two parameters are defined to determine the state of routing, routing parameter $R_1(t)$ and routing parameter $R_2(t)$, which determine the state of routing from the proportion of out-of-order packets and the proportion of packet loss rate in the network, respectively.

The congestion parameter $C_1(t)$ is defined as follows:

$$C_1(t) = |R_{i+1}(t) - S_{i+1}(t)| - |R_i(t) - S_i(t)|. \quad (1)$$

The congestion parameter $C_1(t)$ is used to determine the state of the network easily by the difference between the timestamp of the sender and the receiver, where $S_{i+1}(t)$ is the timestamp included in the packet sent by the server in telematics, and $R_{i+1}(t)$ is the timestamp in the packet returned by the end device after receiving the data. There is no doubt that the difference between these two reflects all the time that the data have experienced. The congestion parameter $C_1(t)$ is the difference between the time experienced by $i+1$ packets and i packets. If the difference between the two fluctuates widely, it indicates that the time experienced by $i+1$ packets and i packets varies widely. Equation (1) can not only calculate the difference between the time stamps but also calculate the time difference between the sender's continuous data transmission and the receiver's continuous data reception; the above equation can be organized as follows:

$$C_1(t) = |R_{i+1}(t) - R_i(t)| - |S_{i+1}(t) - S_i(t)|. \quad (2)$$

The above equation shows that the initial value of the congestion parameter $C_1(t)$ is the initial difference between the timestamps of the sender and the receiver, which reflects the initial network condition of the vehicular network. However, only the difference in the timestamp intelligently reflects the change in time fluctuation, and it cannot directly reflect the congestion state value of the network. Therefore, the congestion parameter $C_2(t)$ is introduced and defined as follows:

$$C_2(t) = \frac{D(t)}{|S_{i+1}(t) - S_i(t)|}. \quad (3)$$

$D(t)$ is the number of packets received in two consecutive packet sending intervals, and the value reflects the data transmission rate in a very short time interval. In the case of stable data transmission, the value varies very little. As with the congestion parameter $C_1(t)$, the congestion state of the network is not directly reflected by the amount of data transmitted in a short time only. However, combining these two parameters together can give a good indication of the congestion status of the network. Firstly, when the congestion parameter $C_1(t)$ is larger and the congestion parameter $C_2(t)$ is smaller, it means that the packet has experienced a long time on the transmission path and the data transmission is very small, so it is obvious that a serious data backlog has occurred in the data, and then, it can be directly judged that the network is congested. On the contrary, when the congestion parameter $C_1(t)$ is larger and the congestion parameter $C_2(t)$ is larger, it cannot be directly determined that the network is sending congestion. In this case, there is a possibility of random data loss resulting in an increase in the time taken for the data to be transmitted. When the congestion parameter $C_1(t)$ is small and the congestion parameter $C_2(t)$ is large, the path of data transmission may change, resulting in a sharp increase in the amount of data sent, and it is not possible to determine whether congestion has occurred. When the congestion parameter $C_1(t)$ is small and the congestion parameter $C_2(t)$ is small, there is a possibility of serious data congestion or a large amount of random data loss or even path interruption, which requires further judgment, so it cannot be directly determined whether the network is congested. When congestion is determined, it is necessary to reduce the amount of data sent. Other cases can jump to the routing parametric feedback after determining the congestion parametric feedback. The above process is shown in Figure 1.

After negating the state of congestion, the data may experience a change in transmission path or interruption, so other parameters need to be introduced to determine the state of the network. The proposed scheme uses two parameters for the evaluation of the routing state, the routing parameter $R_1(t)$ and the routing parameter $R_2(t)$. These two parameters are the proportion of out-of-order packets and the proportion of packet loss rate in the vehicular network, respectively.

The routing parameter $R_1(t)$ is defined as follows:

$$R_1(t) = \frac{P_{\text{out-of-seq}}(t)}{|N(i+1) - N(i)|}. \quad (4)$$

In the above equation, $P_{\text{out-of-seq}}(t)$ is the number of out-of-order packets in the interval time, and $N(i+1)$ is the maximum value of out-of-order packets received by the receiver. The amount of data transmission carried in the intelligent transportation system in a smart city is relatively large, and congestion caused by data overload can lead to a large amount of data loss, but the interference of the wireless link can also lead to random loss of data due to errors in the transmission process. Therefore, the ratio of out-of-order packets within a certain time does not directly reflect a

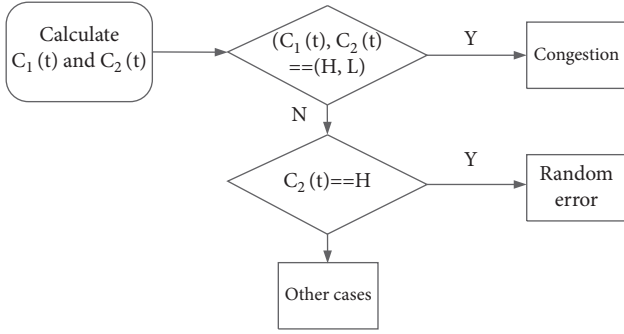


FIGURE 1: Congestion parameter feedback network condition.

certain state of the network, such as path changes or congestion. It needs to be considered with the help of other network state judgments and parameters. Therefore, it is necessary to introduce a second routing parametric $R_2(t)$, defined as follows:

$$R_2(t) = \left| \frac{1 - P_{\text{total}}(t)}{|N(i+1) - N(i)|} \right|. \quad (5)$$

In the above equation, $P_{\text{total}}(t)$ is the number of received packets in the interval time and $N(i+1)$ is the maximum value of out-of-order packets received by the receiver. The routing parameter $R_2(t)$ reflects the probability of data loss in the network, and the value reflects the state of the wireless link error. Again, a single routing parameter $R_2(t)$ does not directly determine that a link error has occurred in the network.

Congestion occurs in the network, and link disruptions may also cause fluctuations in this value. If two congestion parameters are combined to negate the congestion state, routing parameter $R_1(t)$ and routing parameter $R_2(t)$ can each reflect a different state of the network. When routing parameter $R_1(t)$ increases, it can be determined that a path change has occurred in the network, while when routing parameter $R_2(t)$ increases, it can be determined that a link error has occurred. The former case does not need to change the sending state of data, and the latter case only needs to resend the lost data, and the sending state of the network can still be maintained. When all the above states are excluded, if the congestion parameter $C_2(t)$ is extremely low, it can be determined that the data transmission path is interrupted and the sending state of the network should be temporarily stopped or even suspended. The above process is shown in Figure 2.

3.3. Window Optimization. Even if the original congestion window adjustment strategy is used when congestion occurs, it still faces the problem of excessive data transmission. After all, in a smart city where wireless channel transmission is dominant, excessive data competition for the available medium interface will only aggravate the data loss, so this scheme optimizes the transmission window appropriately.

The main parameter affected by the wireless link is the routing parameter $R_2(t)$, which reflects the degree of data loss in the vehicular network. The probability of data loss in the link is common for wireless channels, and the routing parameter $R_2(t)$ measures the probability of error in the

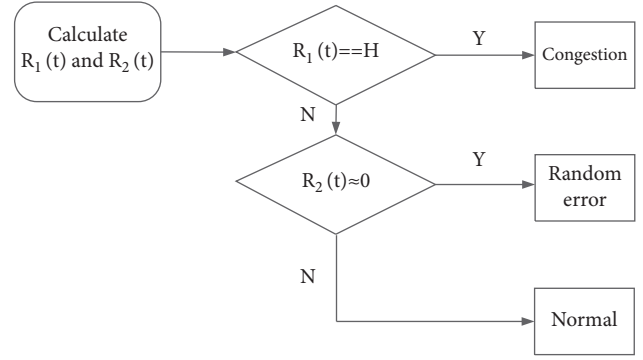


FIGURE 2: Routing parameter feedback network status.

wireless link. The proposed scheme gives the optimized congestion window by combining the routing parameter $R_2(t)$ and the upper bound on the bandwidth delay product of the vehicular network. The conventional transmission scheme follows the following rule in maintaining the increase in the congestion window.

$$W_{i+1} = W_i + \frac{1}{W_i}. \quad (6)$$

For vehicular networks where wireless links often lose data, the transmission of large amounts of data can add to the transmission pressure of multi-hop networks, so it is necessary to restrict the above windows appropriately. The proposed scheme uses an interval that limits the congestion window.

$$W_{i+1} \in \alpha \times BDP_{\text{upperlimit}}. \quad (7)$$

α is the window fading factor, $BDP_{\text{upperlimit}}$ is the upper limit of the bandwidth delay product within a multi-hop vehicular network, which generally does not exceed $(k \times P + l \times Q)$, P and Q are the size of the forward and reverse data transmission in the vehicular network, respectively. The k and l are the corresponding number of hops, respectively. The size of the congestion window is limited in the above equation to prevent excessive data volume from stressing the transmission of the vehicular network. This is extremely beneficial for the network transmission system of intelligent transportation systems in smart cities.

4. Result Analyses and Discussion

The routes formed by vehicles in the connected vehicle transportation system of a smart city are mainly in the form of straight lines and intersections. As shown in Figures 3 and 4, in the linear telematic system, vehicles mainly form traffic flow in two opposite directions, and these vehicles can build stable multi-hop transmission relay points. In particular, the lanes in the same direction can form a relatively stationary vehicular network topology map. The intersection form of vehicular networking is more complicated than the linear form of vehicular networking, and the traffic flows in different directions have different transmission paths in different lanes, which is extremely easy to cause interruptions of transmission paths and changes in routes for vehicular



FIGURE 3: Vehicular ad hoc networking for linear routes in intelligent transportation.

networking with wireless links. The simulation of the experiment is firstly carried out in the linear vehicular network, as shown in Figure 5, the topology diagram of the vehicle network by 12 vehicles statically constructing the simulation.

At the MAC layer based on the commonly used IEEE 802.11 scheme with a distance of 200 m between nodes, simulations are performed to test the transmission performance of the classical scheme 1 [26], scheme 2 [27], and scheme 3 [28] and improved algorithms.

The data flow formed by the dynamic overlay of various applications in the smart city builds a huge traffic volume, especially in the car network built by multiple sensors, and the multipoint sensing of data on multiple application data again forms the overlay of data flow that will inevitably intensify the transmission pressure of the network. Figure 6 shows the transmission rate of scheme 1 at six hops, which has been a great success in wired networks, but the transmission rate of this scheme fluctuates greatly in the vehicular network of smart cities, as seen in the figure, the transmission rate fluctuates between 120kps and 170kps, scheme 1 mainly adopts additive increase and multiplicative decrease (AIMD) scheme, the random packet loss is more serious in the vehicle network, the scheme will encounter serious performance degradation and the random loss of data, the scheme is considered to be caused by congestion, and in the transmit window will directly adjust the transmit window to 1. This will greatly reduce the efficiency of the network data transmission.

Figure 7 shows the data transmission efficiency of the proposed scheme at six hops. As seen in the figure, the data transmission rate improves significantly and fluctuates around 210kps. Overall, the data fluctuate less around 200kps. This has an important role in the stable data transmission of the telematics. Considering the proposed scheme in combination with different congestion parameters and routing parameters in the network can fully reflect the different states of the network, so that the data sending rate can be reasonably adjusted. Considering the demand for different application data from terminal devices in smart cities, congestion is bound to form in the network, and once the data backlog is formed in the network, the possibility of the congestion state of the network is considered first. Once congestion is judged to occur, the amount of data sent is reduced to reduce the probability of further formation of data backlog on the network. Secondly, after rejecting the possibility of congestion, the routing situation of the network needs to be judged, and in such cases, whether a change in vehicles in the multi-hop path leads to a path change or an interruption of the data transmission path occurs. The



FIGURE 4: Vehicular ad hoc networking for cross-routes in intelligent transportation.



FIGURE 5: Simulation model of network in linear route.

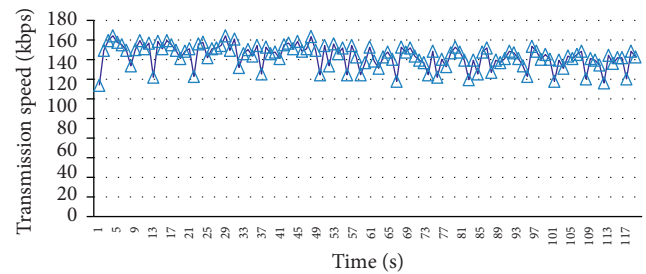


FIGURE 6: Throughput of scheme 1.

proposed scheme fully considers the different parameters of congestion and routing, which plays an important role in balancing the backlog of data in the network. Also, a stable data transmission environment reduces external disturbances and is friendly to various applications.

Figure 8 shows the transmission rates of the four schemes at different hop counts. From the figure, it can be seen that at 2 hops, different schemes have higher transmission rates than other hops. Due to the less number of hops, there is less interference between various vehicles, and to avoid random data loss caused by data access at the same time, the access mechanism will use a silent waiting scheme to adjust the competing interference of different data access, which will reduce the waiting time in the transmission of data and improve the efficiency of data transmission per unit of time. In addition, in the range of 4 hops to 12 hops, the transmission rate of data of all four schemes decreases to different degrees. It can be seen that the interference between vehicles increases when the number of hops increases, which will wait longer for the access of large amount of data. Although the waiting time increases additionally, the data reduce the data loss caused by competition when multiple data streams are accessed and avoid data retransmission. Similarly, scheme 1 uses the additive increase and multiplicative decrease (AIMD) scheme, and in wireless links where random packet loss is serious, the scheme determines that congestion is sent in the network when data are lost randomly, and the sending window is adjusted to 1 directly in the sending window,

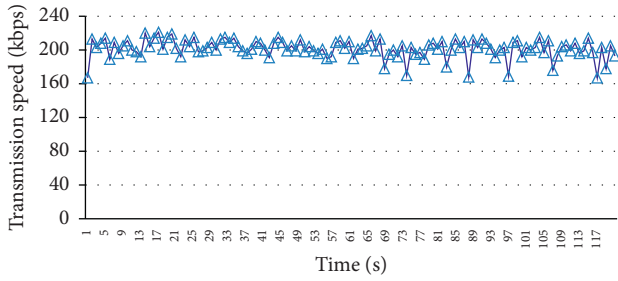


FIGURE 7: Throughput of the proposed scheme.

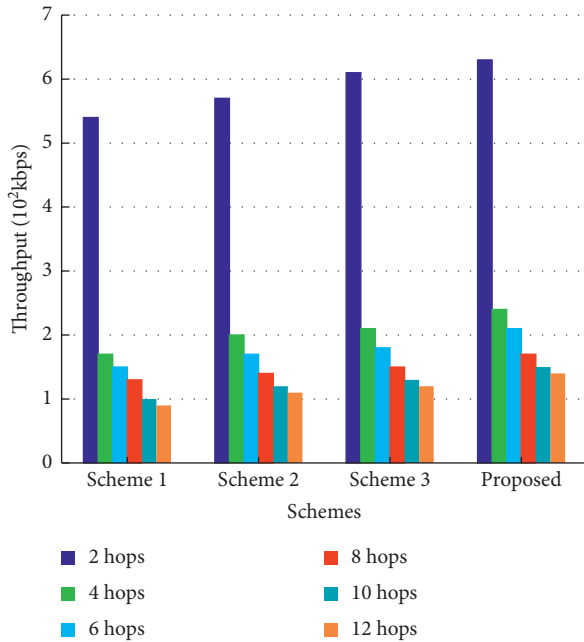


FIGURE 8: Transmission rates of the four schemes at different hop counts.

which greatly reduces the network efficiency of data transmission in the network. Scheme 2 can handle the random data loss well, but still adopts the strategy of scheme 1 in the congestion window adjustment, which obviously also reduces the data sending rate. Scheme 3 provides good feedback on the state of the network with reasonable judgment, so the data transmission rate is significantly improved based on scheme 2. The proposed scheme makes full use of the advantages of the previous three schemes not only to accurately determine the state of the data in the network but also to reasonably adjust the size of the congestion window. Therefore, the transmission rate is the highest among these schemes.

Table 1 shows the tests for different data streams, as the data transmission path of telematics in the traffic system is relatively fixed. As shown in Figures 3 and 4, two cross-streams and four parallel data streams are used in the simulation for testing. The proposed scheme shows the best transmission rate in two cases as seen in the table. The proposed scheme can fully reflect the different states of the network when combining different congestion parameters and routing parameters in the network, so that the data

TABLE 1: Transmission rates of different data streams (10^2 kbps).

	2 cross	4 parallel
Scheme 1	1.51	3.17
Scheme 2	1.57	3.21
Scheme 3	1.61	3.34
Proposed	1.66	3.48

sending rate can be reasonably adjusted. The medium access control of data in two cross-flow scenario will be more intense. The proposed scheme is still able to judge the state of the network well enough to reasonably adjust the amount of data sent. In four parallel data streams, although the transmission paths of data and cross-streams are not the same, more data streams will likewise aggravate the competition of data transmission, thus leading to the occurrence of random data loss. This makes it particularly important to determine the different states of the network, and the proposed scheme still shows a high performance in this scenario.

5. Conclusion

The vehicular network in smart cities plays an important role in carrying data transmission for various applications. In this study, we try to start from the judgment of the network state and try to judge the network state more accurately through the very little feedback information in the network, to provide a basis for the adjustment of the congestion window. The proposed scheme first defines two parameters to determine the congestion state, which are time and throughput to determine the congestion of the network. In the state of negative congestion, two parameters are then defined to determine the state of routing, which are judged from the proportion of out-of-order packets and the proportion of packet loss rate in the network, respectively. The size of the congestion window is adjusted according to the four different parameters mentioned above to match different network states. To distinguish between congestion and random loss caused by data backlog, this study combines the above different parameters to solve the data transmission problem according to the characteristics of smart cities, and the proposed scheme is simulated and compared with other three schemes, and the results show that the proposed scheme has certain advantages under different hop counts and data flows. The data from VANET in smart cities will increase dramatically, which poses new challenges for high-capacity data analysis, especially today when cloud computing and big data analysis are increasingly important. Future research will not only focus on data transmission enhancement but also combine the analysis of big data to refine the required feature data and better provide personalized services.

Data Availability

The data used to support the findings of this study are available from the corresponding author upon reasonable request and with the permission of funders.

Conflicts of Interest

The authors declare that they have no conflicts of interest.

Acknowledgments

This work was supported by the Jiangxi Provincial Natural Science Foundation (20212BAB202029) and the Science and Technology Foundation of Jiangxi Provincial Education Department (grant no. GJJ201601).

References

- [1] S. P. Gayialis, G. D. Konstantakopoulos, E. P. Kechagias, and G. A. Papadopoulos, "An advanced transportation system based on internet of things," in *Proceedings of the 10th Annual International Conference on Industrial Engineering and Operations Management (IEOM 2020)*, pp. 10–12, United Arab Emirates, Dhaka, Bangladesh, December 2020.
- [2] J. Wang, T. Yamamoto, and K. Liu, "Role of customized bus services in the transportation system: insight from actual performance," *Journal of Advanced Transportation*, vol. 2019, Article ID 6171532, 14 pages, 2019.
- [3] H. Wang, L. Xu, Z. Yan, and T. A. Gulliver, "Low-complexity MIMO-FBMC sparse channel parameter estimation for industrial big data communications," *IEEE Transactions on Industrial Informatics*, vol. 17, no. 5, pp. 3422–3430, 2020.
- [4] P. Zheng, S. Quan, and W. Chu, "Analysis of market competitiveness of container Railway transportation," *Journal of Advanced Transportation*, vol. 2021, Article ID 5569464, 8 pages, 2021.
- [5] H. Wang, P. Xiao, and X. Li, "Channel parameter estimation of mmWave mimo system in urban traffic scene: a training channel-based method," *IEEE Transactions on Intelligent Transportation Systems*, pp. 1–9, 2022.
- [6] H. Ding, X. Li, and Y. Cai, "Intelligent data transportation in smart cities: a spectrum-aware approach," *IEEE/ACM Transactions on Networking*, vol. 26, no. 6, pp. 2598–2611, 2018.
- [7] L. Zong, F. H. Memon, X. Li, H. Wang, and K. Dev, "End-to-end transmission control for cross-regional industrial Internet of Things in Industry 5.0," *IEEE Transactions on Industrial Informatics*, vol. 18, no. 6, pp. 4215–4223, 2022.
- [8] S. Sundaresan, K. S. Kumar, R. Nishanth, Y. H. Robinson, and A. J. Kumar, "Artificial intelligence and machine learning approaches for smart transportation in smart cities using blockchain architecture," *Blockchain for Smart Cities*, Elsevier, Amsterdam, The Netherlands, pp. 35–56, 2021.
- [9] H. Wang, X. Li, R. H. Jhaveri et al., "Sparse Bayesian learning based channel estimation in FBMC/OQAM industrial IoT networks," *Computer Communications*, vol. 176, pp. 40–45, 2021.
- [10] A. Gohar and G. Nencioni, "The role of 5G technologies in a smart city: the case for intelligent transportation system," *Sustainability*, vol. 13, no. 9, p. 5188, 2021.
- [11] Z. Xiong, H. Sheng, W. G. Rong, and D. E. Cooper, "Intelligent transportation systems for smart cities: a progress review," *Science China Information Sciences*, vol. 55, no. 12, pp. 2908–2914, 2012.
- [12] A. Gohar and G. Nencioni, "The role of 5G technologies in a smart city: the case for intelligent transportation system," *Sustainability*, vol. 13, no. 9, pp. 1–24, 2021.
- [13] A. Raza, S. H. R. Bukhari, F. Aadil, and I. Zeshan, "An UAV-assisted VANET architecture for intelligent transportation system in smart cities," *International Journal of Distributed Sensor Networks*, vol. 17, no. 7, pp. 1–17, 2021.
- [14] L. Zhao and Y. Jia, "Intelligent transportation system for sustainable environment in smart cities[J]," *International Journal of Electrical Engineering Education*, pp. 1–19, 2021.
- [15] S. Telang, A. Chel, A. Nemade, and K. Geetanjali, "Intelligent transport system for a smart city," *Security and Privacy Applications for Smart City Development*, Springer, Cham, pp. 171–187, 2021.
- [16] C. Liu and L. Ke, "Cloud assisted Internet of things intelligent transportation system and the traffic control system in the smart city," *Journal of Control and Decision*, pp. 1–14, 2022.
- [17] K. Abbas, L. A. A. Tawalbeh, A. Rafiq, and M. Ammar, "Convergence of blockchain and IoT for secure transportation systems in smart cities," *Security and Communication Networks*, vol. 2021, Article ID 5597679, 13 pages, 2021.
- [18] A. D. Joseph, A. R. Beresford, J. Bacon et al., "Intelligent transportation systems," *IEEE Pervasive Computing*, vol. 5, no. 4, pp. 63–67, 2006.
- [19] A. Sumalee and H. W. Ho, "Smarter and more connected: future intelligent transportation system," *IATSS Research*, vol. 42, no. 2, pp. 67–71, 2018.
- [20] A. H. Sodhro, M. S. Obaidat, Q. H. Abbasi, P. Pace, and S. Pirbhulal, "Quality of service optimization in an IoT-driven intelligent transportation system," *IEEE Wireless Communications*, vol. 26, no. 6, pp. 10–17, 2019.
- [21] H. Zhang and X. Lu, "Vehicle communication network in intelligent transportation system based on internet of things," *Computer Communications*, vol. 160, pp. 799–806, 2020.
- [22] D. Zhang, J. Wang, H. Fan, Z. Ting, G. Jinxin, and Y. Peng, "New method of traffic flow forecasting based on quantum particle swarm optimization strategy for intelligent transportation system," *International Journal of Communication Systems*, vol. 34, no. 1, pp. 1–20, 2021.
- [23] S. Saharan, S. Bawa, and N. Kumar, "Dynamic pricing techniques for Intelligent Transportation System in smart cities: a systematic review," *Computer Communications*, vol. 150, pp. 603–625, 2020.
- [24] Z. Lv, R. Lou, and A. K. Singh, "AI empowered communication systems for intelligent transportation systems," *IEEE Transactions on Intelligent Transportation Systems*, vol. 22, no. 7, pp. 4579–4587, 2020.
- [25] R. Suryadithia, M. Faisal, A. S. Putra, S. A. Shaheen, and R. Finson, "Technological developments in the intelligent transportation system (ITS)," *International Journal of Services Technology and Management*, vol. 2, no. 3, pp. 837–843, 2021.
- [26] J. Padhye, V. Firoiu, D. F. Towsley, and J. F. Kurose, "Modeling TCP Reno performance: a simple model and its empirical validation," *IEEE/ACM Transactions on Networking*, vol. 8, no. 2, pp. 133–145, 2000.
- [27] C. P. Fu and S. C. Liew, "TCP VenO: TCP enhancement for transmission over wireless access networks," *IEEE Journal on Selected Areas in Communications*, vol. 21, no. 2, pp. 216–228, 2003.
- [28] Z. Fu, B. Greenstein, X. Meng, and S. Lu, "Design and implementation of a TCP-friendly transport protocol for ad hoc wireless networks," in *Proceedings of the 10th IEEE International Conference on Network Protocols, 2002*, pp. 216–225, IEEE, Paris, France, November 2002.

Research Article

Multidimensional Dynamics and Forecast Models of Network Public Opinions Based on the Fusion of Smart Transportation and Big Data

Guojun Sheng and Yi Guan 

College of Information and Business Management, Dalian Neusoft University of Information, Dalian 116023, Liaoning, China

Correspondence should be addressed to Yi Guan; guany@neusoft.edu.cn

Received 15 February 2022; Revised 5 March 2022; Accepted 22 March 2022; Published 7 April 2022

Academic Editor: Sang-Bing Tsai

Copyright © 2022 Guojun Sheng and Yi Guan. This is an open access article distributed under the Creative Commons Attribution License, which permits unrestricted use, distribution, and reproduction in any medium, provided the original work is properly cited.

With the increase of the world's population, the means of transportation and vehicles that adapt to the times are still difficult to cope with the increase in traffic volume. The traffic problem can be said to be a worldwide problem. However, with the development of artificial intelligence, the emergence of smart transportation has brought new development to modern transportation, and the application of smart transportation and big data is inseparable. In contemporary society, the widespread use of the Internet allows the public to fully exercise their rights to participate in social management and conduct public opinion supervision, which provides a great impetus for the development of online public opinion. However, due to the huge scale of information, some false and harmful information and opinions will inevitably be mixed into it, which will make the network public opinion unable to perform its due function smoothly. Therefore, it is necessary to carry out highly effective management activities on the network public opinion. This paper studies the multidimensional dynamics and prediction model of network public opinion based on the integration of smart transportation and big data; the aim is to design a simple and effective forecasting model to provide traffic management departments with good public opinion forecasting and analysis methods so as to make better decisions. This paper analyzes the related technologies of smart transportation and network public opinion and designs a prediction model of smart transportation network public opinion. Finally, this paper uses rough set theory to optimize the model and compares the data before and after optimization. The results are as follows: the data correlation coefficient before and after optimization is 0.988, and the two-tailed significance level is 0.471, which proves that the results before and after processing are highly correlated, and the two sets of data have no significant difference, proving that the optimization of the model is effective, simplifies the analysis process, and does not change the results.

1. Introduction

With the rapid development of social informatization, the wave of the informatization era represented by the Internet is spreading all over the world, and its influence is increasing day by day. Internet public opinion is playing an increasingly important role in the formation and popularization of social public opinion. Online public opinion is a new type of public opinion generated by the Internet. As an important part of public opinion in the entire society, online public opinion has become a force that cannot be ignored and has gradually played an irreplaceable social role. The transportation

department has many contacts and close relations with the masses and needs to pay attention to the problem of online public opinion. To be people-oriented, it is necessary to pay attention to the ideas of the masses and respect the masses' online public opinion. Facing the problem, investigating, analyzing, and correcting the problem are the responsibility of the traffic management department.

The intelligent transportation system integrates computer technology, mobile communication technology, image processing, transportation management, and other high-tech means and combines transportation tools, transportation channels, and management and control to play a

real-time, accurate, and efficient role. The Internet platform provides a place for different ideologies to compete, and it can reflect social public opinion in a relatively concentrated manner. If the online public opinion cannot be effectively controlled, it will easily be used by people with intentions, which will bring harm to the country and society. Therefore, the public security traffic management department must do a good job in online public opinion management, timely grasping the situation, correctly analyzing the news, making scientific and democratic decisions, promoting work, and improving people's lives. Therefore, it is very important to establish a multidimensional dynamic and predictive model of online public opinion for smart transportation.

The innovation of this paper is as follows: (1) proposing a prediction model of smart transportation network public opinion, designing each index of the model, and also designing the processing method of the index; (2) optimizing the prediction model of smart transportation network public opinion through rough set theory, simplifying the model, and comparing the data before and after optimization, and we found no significant difference, which proved that the optimization is effective. This model can help traffic control departments understand online public opinion, grasp the progress of online public opinion, and make more reasonable decisions.

2. Related Work

The rapid development of the Internet in the twenty-first century provides a platform for people to actively speak, and these speeches are mixed with many dangerous factors, so the management and control of online public opinion are very important. So far, many scholars have conducted research on online public opinion. Jiang, through a brief introduction to the connotation and characteristics of online public opinion in colleges and universities, discussed the innovation of ideological and political education in colleges and universities under the background of online public opinion from the perspectives of educational concepts, educational content, and educational methods, to ensure that this education plays a positive role in the new era. However, the study did not propose specific measures [1]. Zhu proposed an adaptive edge service placement mechanism based on online learning and a predictive edge service migration method based on a factor graph model, which solved the problem of edge computing service placement from the perspective of edge computing. The prediction model is also improved by using complex network topology. The results show that the improved model has the advantages of accuracy, rapidity, and adaptability and can be applied to other fields [2]. Based on the research results of domestic and foreign scholars, Wang and Hu analyzed the current situation of online public opinion governance and initially constructed a big data platform for online public opinion, realized the transformation from online public opinion management to governance, and strengthened the awareness of the rule of law in online public opinion. Finally, it provides development strategies for the government to create a healthy and green

online public opinion ecology from three aspects. The shortcoming is the lack of experiments to verify the effectiveness of the strategy [3].

In addition to online public opinion, smart transportation is also a product of the new era, bringing new opportunities for smart transportation and the Internet of goods industry. Angshuman has established a method to evaluate the various benefits of an incident management plan. This method calculates the benefits of improved air quality brought about by driver assistance services, reduced delays, reduced fuel consumption, secondary collisions, and accident management plans. The results show that this method can save drivers 7.2 million vehicle hours of accident-related delays each year. It also calculated that the annual benefit-cost ratio was 4.4:1 [4]. For cities in developing countries that are less motorized and have less developed infrastructure, less financial resources, and less institutional and technical capabilities, Chen et al. suggested to benefit from smart transportation investment: involving all public and private participants in collaboration and transparent environment, developing technical capabilities for purchasing and monitoring information services, and paying attention to basic infrastructure. But these suggestions are not specifically enough [5]. Lin proposed the design of hybrid vehicle-to-infrastructure and vehicle-to-vehicle communication networks and discussed how to efficiently manage electric vehicle charging services in charging station scenarios and distributed home charging scenarios. Then, it summarizes the open research issues related to networked electric vehicle communication technology and charging services. It is also proposed that connected electric vehicles can realize a green and intelligent transportation system. However, the discussion of the study is a bit vague and not very practical [6]. Yan discussed the development and implementation of tools and methods for evaluating the benefits and costs of these systems as part of the travel demand forecasting modeling environment. He also introduced the application of the developed tools to evaluate the two most widely deployed intelligent transportation systems: incident management and advanced traveler information system. The research results show that the method developed in this research can be used to evaluate its effectiveness [7].

3. Network Public Opinion Based on the Integration of Smart Transportation and Big Data

3.1. Data Analysis Technology in Smart Transportation

3.1.1. Data Mining Task. Data mining is also translated into data exploration and data mining. It is a method of analyzing a large amount of data stored in an enterprise through mathematical models to find different customers or market segments and to analyze consumer preferences and behaviors. Data mining tasks can be divided into statistical data mining, knowledge data mining, and unstructured data mining. According to the realized functions, data mining tasks can be divided into four types: predictive modeling, association analysis, cluster analysis, and anomaly detection.

(1) *Predictive Modeling*. According to the discreteness and continuity of target variables, predictive modeling can be divided into classification mining and regression mining. Classification mining is based on the analysis of the training data set to derive the corresponding prediction model. Sometimes people may wish to predict some unknown or missing data values. This situation is called regression. Regression is to evaluate unlabeled samples by establishing a model, or to evaluate the value interval that a sample may have [8].

(2) *Association Analysis*. Correlation characterizes the dependency between various attributes and events. Association rules are implicit expressions of the form $A \Rightarrow B$ [support, confidence]. Support reflects the usefulness of the discovered association rules, and confidence reflects the certainty of the discovered association rules.

Let I be a collection of items and D a collection of database transactions T . The association rule is an implicit formula of the form $A \Rightarrow B$, $A \subset I$, $B \subset I$, and $A \cap B = \emptyset$, and the support of the rule $A \Rightarrow B$ in the transaction set D is as follows:

$$\text{support}(A \Rightarrow B) = P(A \cap B). \quad (1)$$

Rule $A \Rightarrow B$'s confidence in transaction set D refers to the ratio of the transaction containing A and B to the transaction containing A , as follows:

$$\text{confidence}(A \Rightarrow B) = P(B \cap A). \quad (2)$$

(3) *Cluster Analysis*. The definition of clustering determines the need for a standard to characterize the similarity between data objects, so the key to clustering is the measurement of object similarity. Usually, using distance to measure the similarity of objects is the method we most often think of. The smaller the distance between two objects is, the more similar they are [9]. Cluster analysis itself is not a specific algorithm, but a task that needs to be solved in general. It can be implemented by different algorithms, which are very different in understanding the composition of clusters and how to find them effectively.

(4) *Anomaly Detection*. In general, data mining methods will try to minimize the impact of abnormal points or outliers, such as treating abnormal points as noise or discarding or repairing incorrect data. But in some special applications, it is these abnormal points that will help a lot. Data mining for these abnormal points is called anomaly detection.

3.1.2. *Data Mining Algorithm*. There are some very classic mining algorithms in data mining technology, some of which will be introduced.

(1) *Bayesian Classification*. Bayesian classification is a statistical classification method. Its analysis method is characterized by the use of probability to represent all forms of uncertainty, and learning or reasoning must be implemented

by probability rules. Bayesian classification is a classification method of predictive modeling, which can predict the possibility of a certain attribute, such as the probability that a given sample belongs to a certain class. Let X be a data sample of unknown class attributes, and A a certain assumption: the data sample X belongs to class C . The classification problem is to obtain the probability that hypothesis A holds for a given sample of observation data X , that is, the conditional probability $P(A | X)$. Bayes' theorem provides a method for calculating $P(H | A)$ when $P(X)$, $P(A)$ and $P(X | A)$ are known. The formula is as follows:

$$P(A | X) = \frac{P(X | A)P(A)}{P(X)}. \quad (3)$$

Naive Bayes classification has a smaller error rate than other classification algorithms and is widely used in text classification and other fields. The steps of naive Bayes classification are as follows: the first step is to use an n -dimensional feature vector X to characterize each data sample, describing n metrics of n attributes to the sample. The second step, for a given unknown data sample X , assumes that there are m classes of C_1, C_2, \dots, C_m , and the Bayesian classification algorithm classifies X into the class with the highest posterior probability [10]. That is, when the following conditions are met,

$$P(C_i | X) > P(C_j | X), \quad 1 \leq j \leq m, j \neq i. \quad (4)$$

Naive Bayes classification assigns unknown samples to class C_i and then maximizes $P(C_i | X)$. Among them, $P(C_i | X)$ of the largest C_i is called the largest posterior hypothesis. According to Bayes' theorem,

$$P(C_i | X) = \frac{P(X | C_i)P(C_i)}{P(X)}. \quad (5)$$

In the third step, you only need $P(X | C_i)P(C_i)$ to be the largest. If the prior probability of the class cannot be obtained, it can be assumed that these classes are of equal probability. That is, $P(C_1) = P(C_2) = \dots = P(C_m)$. According to this, $P(C_i | X)$ is maximized.

In the fourth step, the complexity of calculating $P(X | C_i)$ may be very large. In order to reduce the cost of calculating $P(X | C_i)$, assume that the class conditions are independent. That is, assume that the attribute value conditions are independent of each other. This is Bayesian classification. Get

$$P(X | C_i) = \prod_{k=1}^n P(x_k | C_i). \quad (6)$$

(2) *K-Means Algorithm*. K-Means algorithm is by far the most widely used clustering technique. The K-Means algorithm essentially implements the basic idea of clustering: the closer the data points within the class, the better, and the farther the data points between the classes, the better the algorithm. For large-scale and massive data, the scalability and operating efficiency of the algorithm are very high. The K-Means algorithm first specifies the number k value of the clusters to be divided. During initialization, k objects are

randomly selected from n data objects, representing k average values or centers. For the remaining $(n-k)$ objects, measure the distance between each of the k cluster centers, assign them to the nearest clusters, and then recalculate the centroid of each cluster. Repeat the above process cyclically until the criterion function converges; that is, the center of mass no longer changes [11]. The criterion function is shown in the following formula:

$$E = \sum_{i=1}^k \sum_{x \in C_i} |x - \bar{x}_i|^2. \quad (7)$$

3.1.3. Hadoop Technology. Hadoop is a framework for applications running on large server clusters. It is good at complex analysis of large data sets. Hadoop contains two key technologies: reliable data storage using Hadoop distributed file system (HDFS), and high-performance parallel data processing using MapReduce technology. Figure 1 shows the structure of the Hadoop distributed file system.

HDFS breaks up the input data into blocks and stores them redundantly across server clusters. In this way, it can be ensured that even if multiple nodes fail, data will not be lost. HDFS is a master/slave architecture. HDFS includes a master server client and many data servers. The NameNode is the core of the HDFS file system. It keeps a directory tree of all files in the file system and tracks where the file data of the server cluster is saved.

MapReduce is mainly used to write various distributed applications. MapReduce is a method of dividing huge tasks into discrete tasks that can be executed in parallel [12, 13]. After analyzing each discrete task, the results will be integrated into a single output. This method can eliminate the processing bottleneck of a monolithic storage system.

3.2. Internet Public Opinion Related Theories

3.2.1. Complex Social Network Theory. If you only use traditional social networks to analyze data, it is often very limited. Therefore, it is necessary to make full use of the relevant theories and analysis methods of complex networks in social network analysis. From the history of complex network research, it can be roughly divided into three stages, namely, the regular network stage, the random network stage, and the complex network stage. Generally speaking, a complex network consists of many nodes and complex connections between these nodes. The structural characteristics of the network do not depend on specific node positions or connection forms, which are the topological characteristics of complex networks. In this regard, the average path length, clustering coefficient, and degree distribution of the network are the three most basic concepts used to describe the topological properties of complex networks [14].

From the point of view of graph theory, a specific network can be abstracted as a two-tuple $G = (V, E)$, where the set V is the electric set, E is the edge set, and each edge in set E has a point pair in set V corresponding to it. The

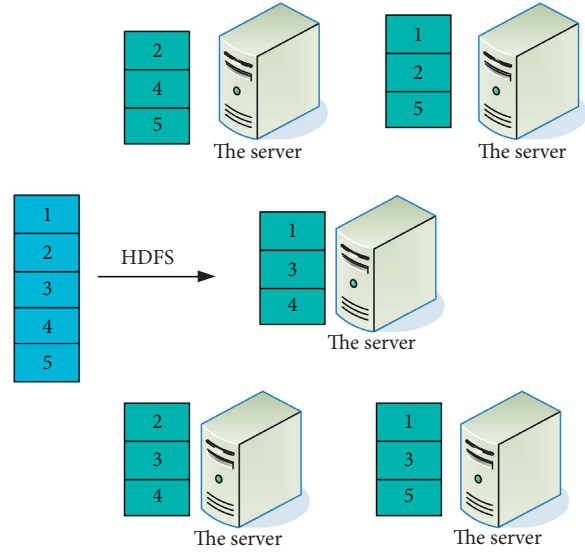


FIGURE 1: Hadoop distributed file system.

distance between nodes I and J , d_{ij} , is usually defined as the number of edges on the shortest path connecting these two nodes. The average path length D of the network is the average value of the distance between any two nodes. In a social network, it represents the number of individuals in the shortest relationship chain of two individuals, and its calculation formula is as follows:

$$D = \frac{\sum_{i=1}^N \sum_{j=1}^N d_{ij}}{N^2}. \quad (8)$$

N represents the number of nodes, for an undirected network, $d_{ij} = d_{ji}$, so it can be simplified to the following formula:

$$D = \frac{2\sum_{i \geq j} d_{ij}}{N(N-1)}. \quad (9)$$

What the agglomeration coefficient wants to reveal is the agglomeration characteristics of the network. The so-called agglomeration characteristic means that two nodes in the network that are connected to a node by an edge are likely to be connected to each other by an edge. Suppose that node i has k edges connecting it to other nodes, and these k nodes are neighboring nodes of node i [15]. If the actual number of neighboring nodes of node i is R , then the agglomeration coefficient of node i is

$$C_i = \frac{2R}{k(k-1)}. \quad (10)$$

The clustering coefficient of the entire network is the mean value of the clustering coefficients of all nodes, which is

$$C = \frac{\sum_{i=1}^N C_i}{N}. \quad (11)$$

When $C = 0$, all nodes in the network are isolated nodes without any connecting edges; when $C = 1$, the network is completely coupled, and any two nodes are directly connected.

Degree is an important concept to describe the attributes of a single node in the network. The number of neighboring nodes of a node is the degree of the node.

In a directed network, degrees are divided into out-degree and in-degree, where out-degree refers to the number of edges from node i to other nodes in the network, and the in-degree is the number of edges pointing to node i from other nodes in the network. By averaging the degrees of all nodes in the network, the average degree of the network can be obtained, usually denoted as $\langle k \rangle$.

$$\langle k \rangle = \frac{\sum_{i=1}^N k_i}{N}. \quad (12)$$

For a regular network, since all nodes have the same degree, its degree distribution is concentrated on a single peak, which is the Delta distribution. For a completely random network, its degree distribution approximately satisfies the Poisson distribution. However, a large number of studies in recent years have shown that the degree distribution of real networks does not show a Poisson distribution like random networks. Especially when the network scale is large, their degree distribution can be better described in the form of approximate power-law distribution. A network whose degree distribution conforms to a power-law distribution is usually called a scale-free network [16,17]. The images of these degree distributions are shown in Figure 2.

In addition, there is another way to describe the degree distribution of the network, namely, the cumulative degree distribution function, which represents the probability distribution of nodes with degree not less than k . Let $P(k)$ represent the cumulative degree distribution function, and its function is as follows:

$$P(k) = \sum_{k'=k}^{\infty} p(k'). \quad (13)$$

Based on the theories and methods of complex social networks, it is not only feasible but also necessary to understand the real society from the perspective of the network, especially the individuals in the network society and their interactions with each other.

3.2.2. The Element Composition of the Network Public Opinion Model. The main body of online public opinion is the various network responders participating in the online public opinion. These network responders may be reliable network communication media, or they may be the general online public. They can play different roles in the evolution of online public opinion, but they are all important components that cannot be missed in the evolution of a complete online public opinion [18]. Figure 3 shows the spread of online public opinion.

In the evolution of online public opinion, autonomous network actors mainly include grassroots netizens, opinion leaders, and online communication media. Together, they constitute the main force in the Internet space to promote the development of online public opinion. In the

evolutionary space of online public opinion, grassroots netizens constitute the largest part of the main body of online behavior; opinion leaders occupy a central position in the media information dissemination network; Internet communication media are an important actor in the evolution of online public opinion, which can quickly promote the dissemination of various online public opinion opinions and online public opinion information.

3.2.3. Construction of Online Public Opinion Aggregation Model

(1) *Build Basic Rules.* Without considering the increase and loss of people in the view aggregation space, set the group size as N , $\{1, 2, \dots, n\}$ as the individual group that constitutes N , and the social network constituted by all individuals is denoted as $G(N, E)$, where E is the number of edges in the network. Let x be a random individual in the group, and his opinion value on a certain network public opinion event or issue at time t is represented by O_x^t , and $O_x^t \in [0, 1]$. Setting individual opinions in the process of aggregation of online public opinions, which independently change over time, then

$$\begin{aligned} O_x^{t+1} &\sim \{O_x^t, O_y^t\}, \quad x \neq y \text{ and } \widehat{x, y} = 1, \\ O_y^{t+1} &\sim \{O_y^t, O_z^t\}, \quad y \neq z \text{ and } \widehat{y, z} = 1. \end{aligned} \quad (14)$$

$\widehat{x, y}$ means that there is an edge that directly connects individual x and individual y ; that is, y is a random node in the social network of individual x .

(2) *Rules for Aggregation of Online Public Opinion in a Complex Open Space.* In reality, the aggregation of group opinions also needs to consider the openness of space and its impact. In the process of the aggregation of online public opinion, the size of the virtual “discussion group” can sometimes remain the same, but more often it is constantly changing; that is, there is a flow of people in it, and at a certain moment, some individuals will be from the group, and some individuals will also join [19].

Due to the widespread celebrity effect in the Internet, it is obvious that adding edges with nonequal probability with a degree value is more in line with the actual situation of the Internet. This chapter chooses this edge addition rule to establish the relationship between newly added individuals and other individuals in the network. Figure 4 is the process of online public opinion aggregation in the open space.

Compared with a closed space where there is no increase and loss of individuals, the network structure of active groups in an open space is constantly changing. This change is reflected not only in the changes in the number of nodes and the number of nodes, but also in the changes in the connection relationship between the nodes.

3.3. Network Public Opinion Prediction Model for Smart Transportation. Smart transportation and management of network public opinion are closely related to the vital

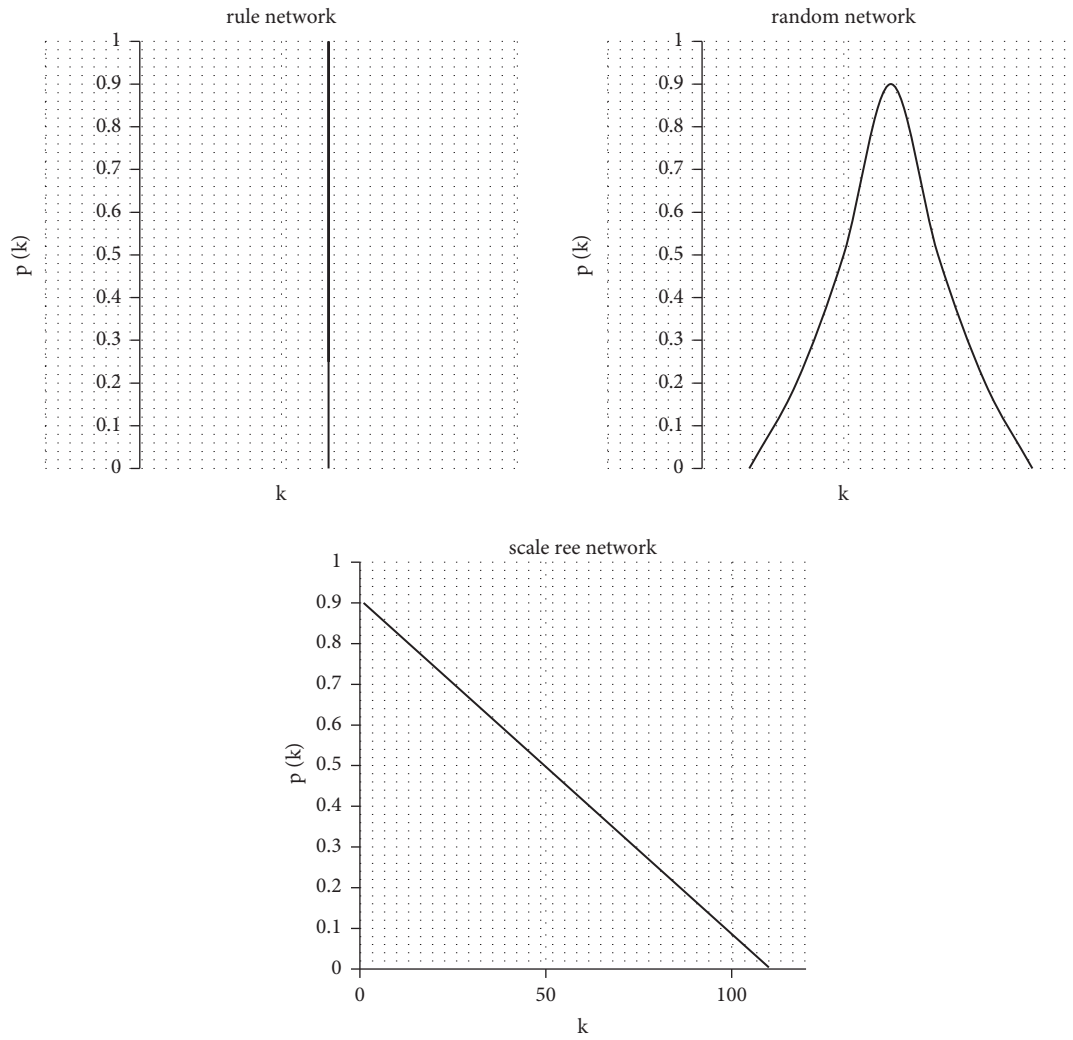


FIGURE 2: Degree distribution of the network.

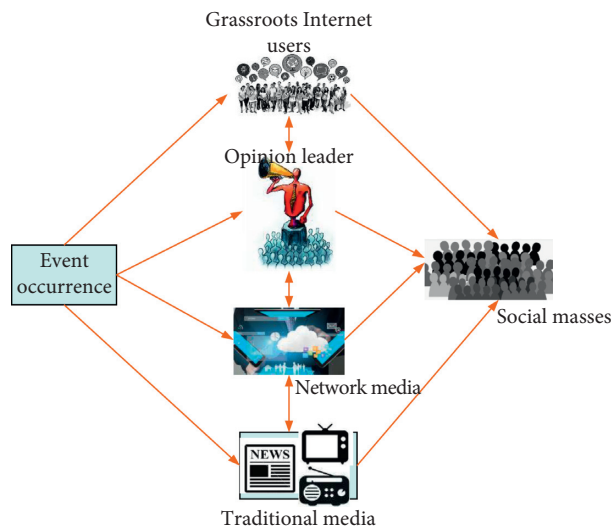


FIGURE 3: Ways of spreading online public opinion.

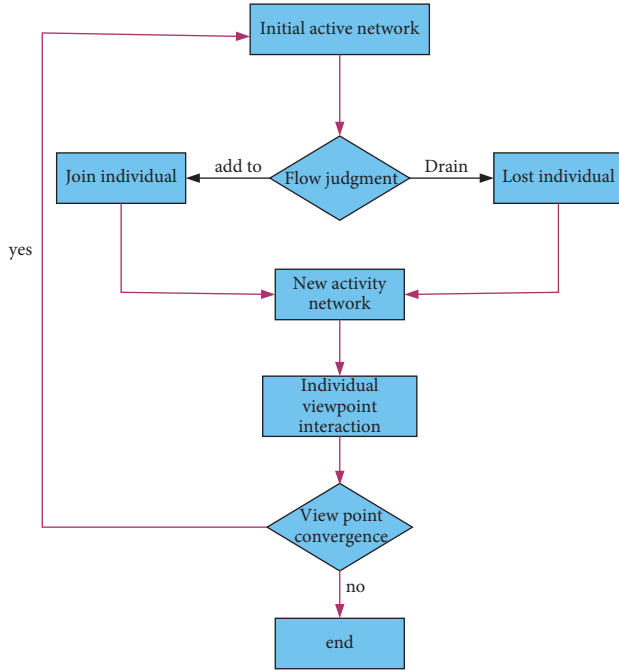


FIGURE 4: Network public opinion aggregation process.

interests of the public and are generally concerned by the public. Therefore, network public opinion is usually manifested as a hot traffic issue that urgently needs to be improved. The core idea of Analytic Hierarchy Process is to judge the importance of indicators through the decomposition of objectives. Then, establish a judgment matrix, calculate its maximum eigenvalue and eigenvector, and get different weights, which provide a basis for decision-making. This chapter uses the analytic hierarchy process to assist in the construction of an evaluation index system for smart transportation and management network public opinion.

3.3.1. Quantitative Treatment of Evaluation Indicators

(1) *Quantification of Subjective Indicators.* The quantification of each indicator in the traffic safety and management network public opinion early warning evaluation index system is an important data processing task to ensure that the indicator system is scientific, comprehensive, and accurate. For the traffic safety and management network public opinion early warning evaluation index system, all indicators can be divided into two categories: subjective evaluation and objective evaluation [20–23].

The so-called subjective evaluation index refers to the evaluation made by several evaluators on the basis of their own feelings or opinions. Subjective evaluation indicators are not expressed in numerical values. They are commonly used to describe indicators such as satisfaction, authority, authenticity, scientificity, and a certain ability. The dimensionless processing of subjective data and objective data is shown in the formula. The positive indicators are as follows:

$$Y_{ij} = \frac{x_{ij} - \min(x_{ij})}{\max(x_{ij}) - \min(x_{ij})}. \quad (15)$$

The inverse index is

$$Y_{ij} = \frac{\max(x_{ij}) - x_{ij}}{\max(x_{ij}) - \min(x_{ij})}. \quad (16)$$

In the formula, $\max(x_{ij})$ represents the maximum value of the evaluation value, and $\min(x_{ij})$ represents the minimum value.

(2) *Quantification of Objective Indicators.* The data of objective evaluation indicators for traffic safety and management network public opinion early warning evaluation can be obtained from specialized network public opinion monitoring agencies [24]. The objective indicators are as follows: public opinion time, which is calculated as the time from when public opinion is generated to disappear. Public opinion gains and losses are the official estimated economic loss. Baidu media index is obtained from Baidu index search. The number of related news is calculated as the number of originals plus the number of reposts.

(3) *Calculation of Weight Set.* The index weights are determined according to the analytic hierarchy process, which has the advantages of uniformity, practicability, and simplicity. Select 40 evaluators to form a comment group consisting of public opinion workers and public opinion researchers from the traffic police department. Based on the understanding of the problem, comments on the indicators in the indicator system are made, and the comparison results are obtained according to the following principles. Take traffic police credibility $B9 = \{C15, C16, C17\} = \{\text{legitimacy of traffic police administrative behavior, scientific traffic police administrative behavior, democratic traffic police administrative behavior}\}$ as an example, and find the weight of each indicator. The weight of the criterion layer can be obtained from the index layer calculation. Let us take the criterion layer as an example for calculation.

First find the judgment matrix, as in the following formula:

$$A = \begin{bmatrix} a_{11} & a_{12} & \cdots & a_{1m} \\ a_{21} & a_{22} & \cdots & a_{2m} \\ \cdots & \cdots & \cdots & \cdots \\ a_{m1} & a_{12} & \cdots & a_{mm} \end{bmatrix}. \quad (17)$$

Then, calculating the importance weight index, assuming $n=3$, the product of each row element is shown in the following formula:

$$M_i = a_1 \times a_{21} \times a_3, \quad i = 1, 2, 3. \quad (18)$$

Find the n -th root of M_i as follows:

$$W_i = \sqrt[n]{M_i}. \quad (19)$$

Finally, the consistency test refers to the logical consistency of judgment thinking. Here, C.I. is used for consistency check, as shown in the following formula:

$$C.I. = \frac{\lambda_{\max} - m}{m - 1}. \quad (20)$$

In the formula, m refers to the dimension of the judgment matrix A .

3.3.2. Index Weight Design. This chapter builds a model, as shown in Figure 5, to calculate the index weight. This chapter uses a graded index system for calculations. In the grading of the indicator, the red public opinion refers to the unified public opinion, and mostly negative public opinion, which needs to be solved urgently. Blue indicates that there are a large number of people participating, but a unified public opinion has not yet formed, and secondary public opinion may erupt. Green is the one that does not need attention or the public opinion event that is coming to an end.

As can be seen from the figure, the entire system is divided into three layers. The top layer is the prediction model, the second layer is layer A, and the third layer is layer B, and each element has its number.

4. Smart Transportation Network Public Opinion Prediction Model Experiment

This experiment is designed based on the network public opinion prediction model in Section 3.3. This experiment will use rough set theory to optimize the indicators in Figure 5 and evaluate the model.

4.1. Optimizing Forecast Model Indicators. The role of rough set theory is to deal with incomplete data and uncertain knowledge expression and induction. The core is to connect knowledge and classification, to equate knowledge to classification ability, and to use equivalent relations to classify and express. In this step, the rough set theory is used to process the data to make the indicators more concise without reducing the effect of the prediction model [25, 26].

4.1.1. Data Preparation. This experiment selects traffic-related Internet public opinion events in the past five years for analysis, and the way to obtain it is Baidu index, Internet public opinion report, and other websites [27–29]. Specific events and data are shown in Table 1.

Next, enter the data and perform simplified processing. The input data is shown in Table 2.

4.1.2. Data Discretization and Reduction. Rough set can only process discretized data. In view of the continuous data of the index system, the data needs to be discretized. The discretization method used in this experiment is OneRuleDiscretizer (IRD) [30]. Given a minimum value \min , each discrete interval is initialized to contain \min continuous attribute values, as far as possible by moving the dividing boundary to increase the observation value, until the

number of objects in the main decision-making interval is greater than \min .

The reduction method adopted in this experiment is attribute reduction. The attribute reduction is to remove redundant conditional attributes through algorithms and simplify the index system. The steps are as follows: (1) first, calculate the discernibility matrix of the decision table; (2) $S = \emptyset$; (3) let A be the set in the discrimination function, and $W(A)$ the weight of A . Define i as the attribute with the largest product of frequency and weight $W(A)$ in A . If the two attribute values are equal, the value is randomly selected; (4) add attribute i to set S ; (5) remove items with attribute i in A ; (6) if A is an empty set, then return to step (2); otherwise, return to step (3).

Table 3 shows the rules after reduction.

4.1.3. Index Analysis after Reduction. After normalizing the reduced index, the weight obtained is shown in Figure 6.

The simplified processing reduces the indicators of the B layer from the original 10 to 6 and removes some indicators that have little effect. It can be seen from Figure 6 that the event sensitivity weight in the public opinion sensitivity is the highest, reaching 0.4527. Therefore, the transportation department can focus on this content and make corresponding decisions. The media public opinion index can reflect the heat of public opinion very well and can play an early warning role in the early stage of public opinion, and its weight has reached 0.3072. Therefore, the traffic part should pay attention to the content of this part and understand the public opinion index of the event. For example, the Baidu index, the number of news, etc. are specific indicators that reflect the public opinion index, which can be used as a reference for decision-making by the transportation department.

4.2. Index Test of Network Public Opinion Prediction Model

4.2.1. Inspection Principle. The experiment uses a paired sample T test, which can be used to detect whether there is a one-to-one correspondence between two equal samples. This can be used to determine whether two samples are significantly different, and whether they come from subjects with the same normal distribution. The principle of inspection is to find the difference between each pair of corresponding observations and use the difference between the sample observations as a new single sample. The difference between the two samples is not obvious, and the difference at this time is almost zero. This is equivalent to a sample T test, which in principle is to test whether the overall mean difference is zero. Therefore, it is necessary to follow the normal distribution and obtain the judgment result according to the significance level. If the probability value of the test statistic is lower than the significance level, the null hypothesis is rejected, and the difference between the samples is significant; if it is higher, the null hypothesis is accepted, and no significant difference is considered at this time.

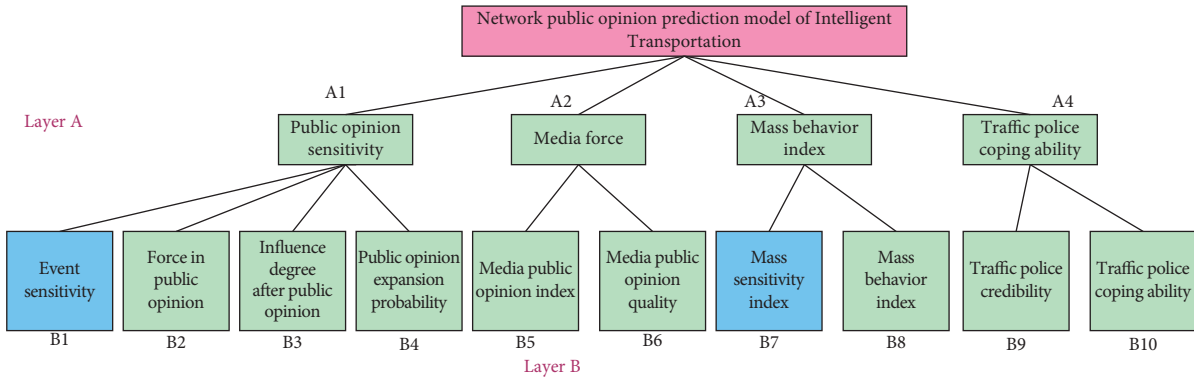


FIGURE 5: Indicator system.

TABLE 1: Events and Baidu data.

Event	Number	Baidu index (peak)	Total news
Six points will be deducted if you wear a red light	1	2510	12014
Bus falling into the river	2	3400	23095
Drunken sentence	3	2630	18319
Universal ETC payment	4	820	8915
New policy of online car Hailing	5	880	10287
Cargo Lala jumping event	6	3210	20173
Bus arson	7	190	19200

TABLE 2: Input data.

	1	2	3	4	5	6	7
B1	1	0.75	0.65	0.75	0.5	0.65	0.25
B2	0.5	0.25	0.75	0.5	0.65	0	0.5
B3	0.75	0.75	0.5	0.65	0	0	0.5
B4	0.25	0.5	0.75	0.25	0.5	0.25	0.75
B5	0	0.25	0.25	0.75	0	0.75	0.5
B6	1	0.5	0.25	0	0.25	0.65	0.75
B7	1	0.75	0.5	1	0.25	0.5	0

TABLE 3: Rules after reduction.

Arrangement	Rule
A1	B1, B2, B3
A2	B5
A3	B7
A4	B9

4.2.2. *Data Comparison.* Before testing the indicators, you need to multiply the values of different indicators by the corresponding weights, and the detailed operation will not be repeated. The settlement result and the comparison result of 7 public opinion events with the previous results are shown in Figure 7.

It can be seen from Figure 7 that the comprehensive data of each event before and after the reduction has not changed much. The numerical difference of each event before and after the reduction is between [0.2, 0.4], and the difference is relatively small. It can be seen that the reduction processing does not reduce the effectiveness of the predictive model while simplifying the data processing steps.

4.2.3. *Data Verification of the Forecast Model Index System.* First, calculate the mean, standard deviation, and standard error of the mean before and after the processing to get Figure 8 [31].

Then, calculate the correlation coefficient of the data before and after the processing, the paired test result, the two-tailed significance level, and other values, and get Figure 9.

It can be seen from Figure 8 that there is no significant difference between the standard deviation and standard error of the data before and after processing, which proves that there is no change in the structure of the model. It can be seen from Figure 9 that the correlation coefficient is 0.988, which proves that the results before and after processing are highly correlated. The paired test result is 0.712, and the two-tailed significance level is 0.471. This value is one 0.01, indicating that the null hypothesis should be accepted; that is, the two sets of data are not considered to be significantly different. In summary, there is no significant difference between the results obtained before and after processing the indicators in the model, so it is feasible to simplify and optimize the indicators of the model.

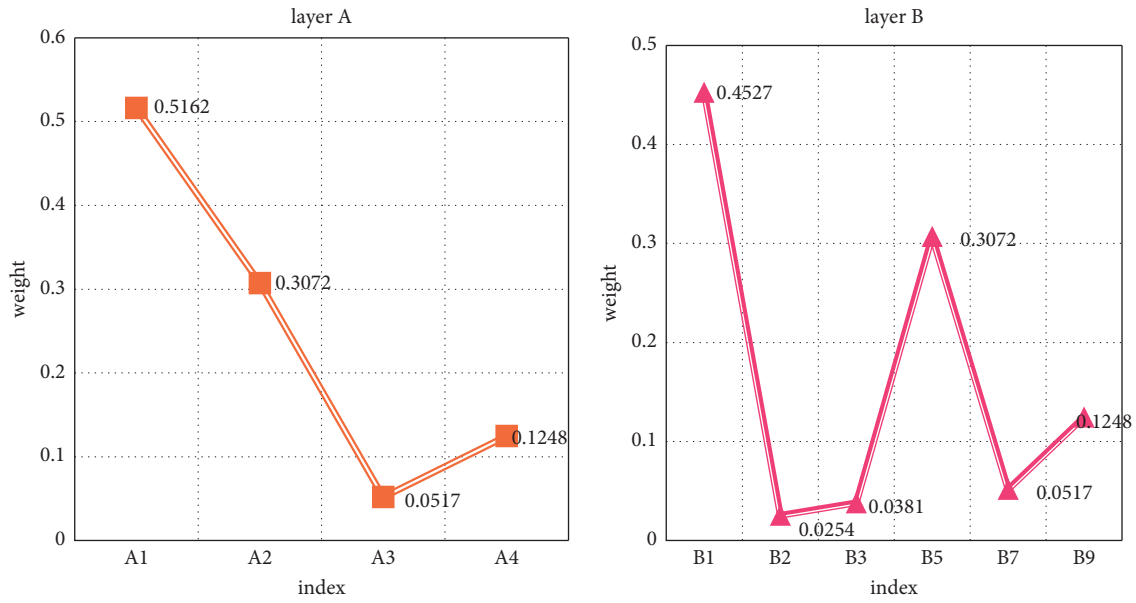


FIGURE 6: Index weights after reduction.

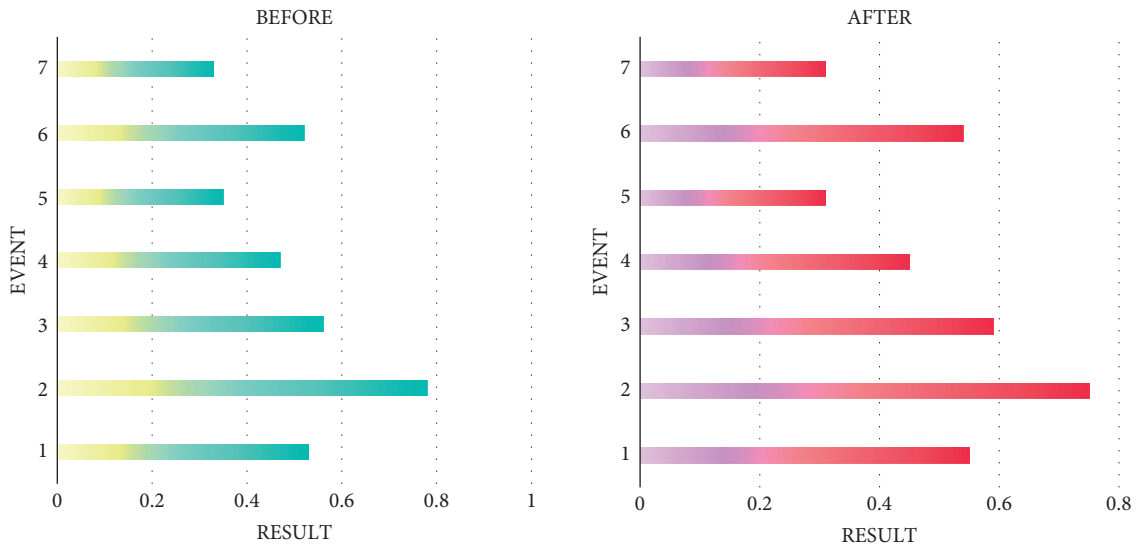


FIGURE 7: Comprehensive event data before and after processing.

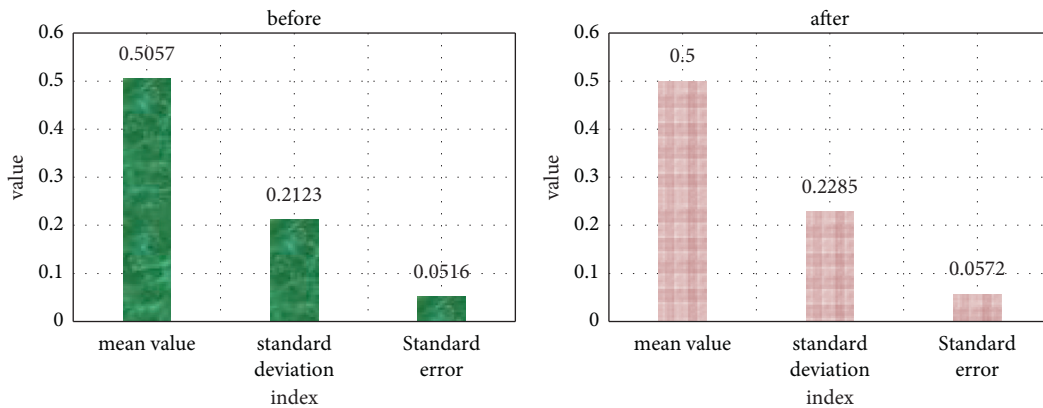


FIGURE 8: Sample statistics before and after processing.

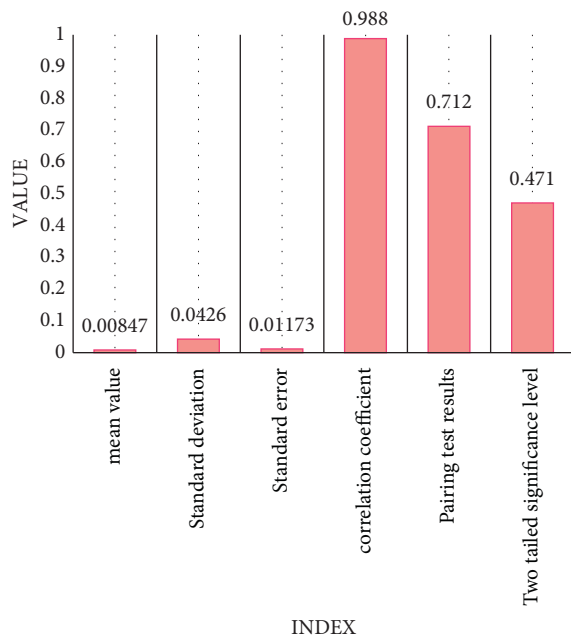


FIGURE 9: Sample inspection before and after processing.

5. Discussion

The network's timeliness, interactivity, and large amount of information are incomparable to traditional media such as television, newspapers, and radio. Internet public opinion plays an important role in the development of the country and society. This is the voice of netizens, and it reflects the overall situation of online public opinion and is an important reference material for traffic management departments to make decisions. The rapid development of social information has brought new challenges to the response capabilities of traffic management departments. Relevant departments should face online public opinion with an open and positive attitude and incorporate the use of public opinion into the necessary work of the traffic management department. It uses online public opinion to integrate decision-making and establish a feedback mechanism. Only by winning every battle in response to online public opinion can we seize the commanding heights of public opinion, firmly grasp the right to speak and initiative, change the passive situation of public opinion response, and create a better public opinion atmosphere for the smooth development of traffic management.

6. Conclusion

Internet public opinion is a double-edged sword. Governmental departments must establish a suitable and effective public opinion management mechanism and build a good public opinion environment to help make decisions and maintain social harmony. This article discusses the multi-dimensional dynamic and predictive model of network public opinion based on the integration of smart transportation and big data. First, this article analyzes the big data technology in smart transportation. Then, we introduced the

relevant theory of network public opinion and designed a prediction model of smart transportation network public opinion. Finally, this article optimized the model through experiments and calculated a variety of index data before and after optimization. It is found that the optimization not only simplifies the analysis process of network public opinion by removing some indicators with minimal influence, but also is similar to the comprehensive data result before optimization without significant difference, which proves the feasibility of the experimental optimization process. The future work is to further optimize the prediction model of online public opinion, make the analysis process of the model simpler and more efficient, and promote the prediction model of online public opinion.

Data Availability

No data were used to support this study.

Conflicts of Interest

The authors declare that the research was conducted in the absence of any commercial or financial relationships that could be construed as a potential conflict of interest.

Acknowledgments

This work was supported by Liaoning Social Science Planning Fund Project (L19BXW010).


References

- [1] H. Jiang, "Innovation of ideological and political education in colleges and universities from the perspective of network public opinion," *Journal of Contemporary Educational Research*, vol. 5, no. 7, pp. 26–30, 2021.
- [2] C. Wang and Z. X. Hu, "Research ON the governance OF government network public OPINION IN the age OF big data," *Journal on Innovation and Sustainability RISUS*, vol. 11, no. 3, pp. 4–12, 2020.
- [3] A. Guin, C. Porter, and B. Smith, "Benefits analysis for incident management program integrated with intelligent transportation systems operations: case study," *Transportation Research Record*, vol. 2000, no. 1, pp. 78–87, 2018.
- [4] Y. Chen, A. Ardila-Gomez, and G. Frame, "Achieving energy savings by intelligent transportation systems investments in the context of smart cities," *Transportation Research Part D: Transport and Environment*, vol. 54, no. jul, pp. 381–396, 2017.
- [5] C. Lin, J. Pan, Z. Lian, and X. Shen, "Networked electric vehicles for green intelligent transportation," *IEEE Communications Standards Magazine*, vol. 1, no. 2, pp. 77–83, 2017.
- [6] X. Yan, M. Hadi, and H. Ozen, "Intelligent transportation system as evaluation tool in a regional demand modeling environment: implementation in Florida standard urban transportation model structure," *Transportation Research Record*, vol. 2176, no. 1, pp. 76–83, 2018.
- [7] F.-Y. Wang, "Artificial intelligence and intelligent transportation: driving into the 3rd axial age with ITS," *IEEE Intelligent Transportation Systems Magazine*, vol. 9, no. 4, pp. 6–9, 2017.
- [8] H. G. Nathan, C. Stamatidis, and S. Srinivas, "Development of strategic plan for deployment of intelligent transportation

- system equipment: utility index decision framework," *Transportation Research Record*, vol. 2423, no. 1, pp. 68–78, 2018.
- [9] S. Zhang, T. Niu, Y. Wu et al., "Fine-grained vehicle emission management using intelligent transportation system data," *Environmental Pollution*, vol. 241, no. OCT, pp. 1027–1037, 2018.
- [10] A. A. Bhoot, N. Pirzada, M. M. Jawaid, and S. A. Memon, "Design and simulation of a rectangular E-shaped microstrip patch antenna for RFID based intelligent transportation," *International Journal of Advanced Computer Science and Applications*, vol. 9, no. 4, pp. 165–169, 2018.
- [11] H. Kazemi, Y. P. Fallah, A. Nix, and S. Wayne, "Predictive AECMS by utilization of intelligent transportation systems for hybrid electric vehicle powertrain control," *IEEE Transactions on Intelligent Vehicles*, vol. 2, no. 2, pp. 75–84, 2017.
- [12] E. Grigoreva, V. Grigoryev, I. Khvorov, Y. Raspaev, and W. Kellerer, "Techno-economic case study on dedicated RAN for an intelligent transportation system: impact of the legislation-driven costs," *Netnomics: Economic Research and Electronic Networking*, vol. 18, no. 1, pp. 23–41, 2017.
- [13] R. Salazar-Cabrera, Á. Pachón de la Cruz, and J. M. M. Molina, "Design of a public vehicle tracking service using long-range (LoRa) and intelligent transportation system Architecture," *Journal of Information Technology Research*, vol. 14, no. 1, pp. 147–166, 2021.
- [14] Z. H. Ali, S. Hagrass, and H. A. Ali, "Distributed computing architecture using fog technology for improving intelligent transportation systems in smart city," *International Journal of Computer Application*, vol. 183, no. 6, pp. 42–45, 2021.
- [15] F. Nambajemariya and Y. Wang, "Excavation of the internet of things in urban areas based on an intelligent transportation management system," *Advances in Internet of Things*, vol. 11, no. 3, pp. 113–122, 2021.
- [16] S. Syedyusuff, R. Subramaniam, and R. Vijay, "Orthogonally integrated hybrid antenna for intelligent transportation systems," *Applied Computational Electromagnetics Society*, vol. 36, no. 5, pp. 519–525, 2021.
- [17] Y. Xie, "Study on the guiding mechanism of ideological and political education in colleges and universities to network public opinion during the period of COVID-19 prevention," *Progress in Social Sciences*, vol. 2, no. 4, pp. 127–141, 2020.
- [18] A. Jolfaei, V. G. Menon, C. Lv, A. K. Bashir, Y. K. Tan, and K. Kant, "Guest editorial advanced sensing and sensor fusion for intelligent transportation systems," *IEEE Sensors Journal*, vol. 21, no. 14, pp. 15425–15426, 2021.
- [19] L. Wang, P. Sun, M. Xie et al., "Advanced driver-assistance system (ADAS) for intelligent transportation based on the recognition of traffic cones," *Advances in Civil Engineering*, vol. 2020, no. 4, pp. 1–8, 2020.
- [20] E. Suryani, R. A. Hendrawan, F. Syafa'at, and A. Az-Zahra, "Scenario model to reduce traffic congestion using intelligent transportation systems," *MATTER: International Journal of Science and Technology*, vol. 6, no. 2, pp. 54–73, 2020.
- [21] M. R. Reddy, K. G. Srinivasa, and B. E. Reddy, "Smart vehicular system based on the internet of things," *Journal of Organizational and End User Computing*, vol. 30, no. 3, pp. 45–62, 2018.
- [22] S. Wan, X. Li, Y. Xue, W. Lin, and X. Xu, "Efficient computation offloading for Internet of Vehicles in edge computing-assisted 5G networks," *The Journal of Supercomputing*, vol. 76, pp. 2547–2518, 2019.
- [23] Z. Lv, R. Lou, and A. K. Singh, "AI empowered communication systems for intelligent transportation systems," *IEEE Transactions on Intelligent Transportation Systems*, vol. 22, no. 7, pp. 4579–4587, 2020.
- [24] M. Adil, J. Ali, M. Attique et al., "Three byte-based mutual authentication scheme for autonomous Internet of Vehicles," *IEEE Transactions on Intelligent Transportation Systems*, 2021.
- [25] J. Y. Hong, H. Ko, L. Mesicek, and M. B. Song, "Cultural intelligence as education contents: exploring the pedagogical aspects of effective functioning in higher education," *Concurrency and Computation: Practice and Experience*, vol. 33, no. 2, 2019.
- [26] L. Ogiela, M. R. Ogiela, and H. Ko, "Intelligent data management and security in cloud computing," *Sensors*, vol. 20, no. 12, p. 3458, 2020.
- [27] A. Farouk, M. Zakaria, A. Megahed, and F. A. Omara, "A generalized architecture of quantum secure direct communication for N disjointed users with authentication," *Scientific Reports*, vol. 5, no. 1, pp. 16080–16117, 2015.
- [28] L. M. T. Pham, L. T. T. Tran, P. Thipwong, and W. T. Huang, "Dynamic capability and organizational performance," *Journal of Organizational and End User Computing*, vol. 31, no. 2, pp. 1–21, 2019.
- [29] L. Fabisiak, "Web service usability analysis based on user preferences," *Journal of Organizational and End User Computing*, vol. 30, no. 4, pp. 1–13, 2018.
- [30] B. Wang, B. F. Zhang, X. W. Liu, and F. C. Zou, "Novel infrared image enhancement optimization algorithm combined with DFOCS," *Optik*, vol. 224, Article ID 165476, 2020.
- [31] M. Lee, L. Mesicek, and K. Bae, "AI advisor platform for disaster response based on big data," *Concurrency and Computation: Practice and Experience*, Article ID e6215, 2021.

Research Article

Optimization of Traffic Congestion Management in Smart Cities under Bidirectional Long and Short-Term Memory Model

Yujia Zhai, Yan Wan, and Xiaoxiao Wang 

Faculty of Humanities and Arts, Macau University of Science and Technology, Avenida Wai Long, Taipa 999078, Macau, China

Correspondence should be addressed to Xiaoxiao Wang; 120212202032@ncepu.edu.cn

Received 4 January 2022; Accepted 9 February 2022; Published 1 April 2022

Academic Editor: Sang-Bing Tsai

Copyright © 2022 Yujia Zhai et al. This is an open access article distributed under the Creative Commons Attribution License, which permits unrestricted use, distribution, and reproduction in any medium, provided the original work is properly cited.

To solve the increasingly serious traffic congestion and reduce traffic pressure, the bidirectional long and short-term memory (BiLSTM) algorithm is adopted to the traffic flow prediction. Firstly, a BiLSTM-based urban road short-term traffic state algorithm network is established based on the collected road traffic flow data, and then the internal memory unit structure of the network is optimized. After training and optimization, it becomes a high-quality prediction model. Then, the experimental simulation verification and prediction performance evaluation are performed. Finally, the data predicted by the BiLSTM algorithm model are compared with the actual data and the data predicted by the long short-term memory (LSTM) algorithm model. Simulation comparison shows that the prediction results of LSTM and BiLSTM are consistent with the actual traffic flow trend, but the data of LSTM deviate greatly from the real situation, and the error is more serious during peak periods. BiLSTM is in good agreement with the real situation during the stationary period and the low peak period, and it is slightly different from the real situation during the peak period, but it can still be used as a reference. In general, the prediction accuracy of the BiLSTM algorithm for traffic flow is relatively high. The comparison of evaluation indicators shows that the coefficient of determination value of BiLSTM is 0.795746 greater than that of LSTM (0.778742), indicating that BiLSTM shows a higher degree of fitting than the LSTM algorithm, that is, the prediction of BiLSTM is more accurate. The mean absolute percentage error (MAPE) value of BiLSTM is 9.718624%, which is less than 9.722147% of LSTM, indicating that the trend predicted by the BiLSTM is more consistent with the actual trend than that of LSTM. The mean absolute error (MAE) value of BiLSTM (105.087415) is smaller than that of LSTM (106.156847), indicating that its actual prediction error is smaller than LSTM. Generally speaking, BiLSTM shows advantages in traffic flow prediction over LSTM. Results of this study play a reliable reference role in the dynamic control, monitoring, and guidance of urban traffic, and congestion management.

1. Introduction

With the continuous development of society, the process of urbanization is also accelerating and the traffic congestion is getting more and more serious. According to the data released by the Traffic Management Bureau of the Ministry of Public Security, the number of motor vehicles has reached 390 million as of the end of September 2021, of which 297 million are cars; and there are 476 million motor vehicle drivers nationwide, of which 439 million are car drivers. In the first quarter alone, the number of newly registered motor vehicles nationwide reached 27.53 million, a year-on-year increase of 4.363 million, and a growth rate of 18.83% [1]. Nowadays, it is urgent to tackle the urban traffic congestion.

With the advent of the era of big data and the rise of the “Internet +” boom, smart transportation engineering has gradually been developed [2]. Smart transportation engineering integrates vehicle networking technology, artificial intelligence (AI) technology, automatic control technology, computer technology, information and communication technology, and electronic sensor technology to build a unified cross-regional transportation information resource sharing platform and comprehensively manage information resources in the transportation field, realizing intelligent management of road operations. It is a real-time, accurate, and efficient comprehensive transportation management system that is applied to the entire ground transportation management system and established for a large-scale, all-

round function. By constructing a short-term traffic state prediction mechanism for urban roads, it can grasp the traffic conditions of traffic roads in a period of time in the future, use the prediction results for traffic guidance, improve the utilization rate of urban road resources, and alleviate the traffic pressure on the urban-congested sections [3].

In the traditional traffic flow prediction method, some scholars consider multiple factors that affect the flow, so they use multiple linear regression to predict the traffic flow, but the real-time performance is low. Kumar and Vanajakshi (2015) considered the periodicity of traffic flow, fitted a model for real-time data statistical processing, and applied the seasonal autoregressive integrated moving average (ARIMA) model to short-term traffic flow prediction. However, the nonlinear and uncertain fitting of traffic flow is poor, and it is not suitable for short-term traffic flow prediction [4]. Huang et al. (2014) proposed a deep belief network to extract traffic flow features and a top-level multitask regression two-layer deep learning model [5]. Zhang et al. (2020) adopted the fast graph convolution recurrent neural network (FastGCRNN) to model the spatiotemporal dependence of traffic flow [6]. Xia et al. (2021) developed a distributed modeling framework for traffic flow prediction on MapReduce under the Hadoop distributed computing platform, which solved the storage and computing problems existing in the single-machine learning model processing large-scale traffic flow data [7]. These deep learning models only consider one-way traffic flow data for prediction, ignoring the change law of traffic flow data after the prediction time point. With increasing emphasis on the application of traffic big data and the creation of smart transportation cities, the bidirectional long short-term memory (BiLSTM) algorithm is applied to the traffic flow prediction. The innovation of the research is to model the traffic flow data through the BiLSTM model and to analyze the influence of the time series change rules of the front and rear traffic flow on the short-term prediction. Firstly, a BiLSTM-based urban road short-term traffic state algorithm network is established based on the collected road traffic flow data, and then the internal memory unit structure of the network is optimized. After training and optimization, it becomes a high-quality prediction model. Then, the experimental simulation verification and prediction performance evaluation are performed. Results of this study play a reliable reference role in the dynamic control, monitoring, and guidance of urban traffic, and congestion management.

2. Materials and Methods

2.1. Standard LSTM Algorithm. Among various deep neural networks, recurrent neural network (RNN) is widely used in the prediction of time series, but long-term series data have caused gradient explosion and gradient disappearance [8]. Therefore, Hochreite and Schmidhuber proposed long short-term memory (LSTM) in 1997. LSTM is an improved RNN that has the function of long-term memory information and solves the problem of RNN gradient disappearance. Its structure includes a module chain structure,

but it only changes the hidden layer module structure [9]. A memory block is added to the hidden layer of LSTM to realize its memory function. The memory block is composed of a set of iteratively connected subnets. Each subnet has one or more storage units, which are connected to each other. The memory block contains three multiplication units consisting of gates: input gates, output gates, and forget gates. All three gates have a nonlinear summation function, which contains two activation functions to control the amount of data transfer [10]. The internal structure diagram of the storage unit is shown in Figure 1.

In Figure 1, the three modules were used as three storage units in the memory block, which were connected to each other, and each of them contains three multiplication units composed of gates: an input gate, output gate, and forget gate. X is the input, h is the weight of the neuron, \tanh is the activation function, and σ is the sigmoid activation function. On the basis of this kind of chain, LSTM improves the interior of the module, using 3 sigmoid neural network layers and a gate composed of point-by-point multiplication to strengthen the control ability of information [11]. The \tanh activation function mainly processes data for state and output functions [12]. It indicates the input gate, f_t represents the forget gate, C_t indicates internal memory, o_t represents the output gate, and h_t represents the output of the LSTM unit at time t . The input gate controls the input of the output information of the upper unit to the unit information of this layer and retains the previous information of the sequence. The calculation equation for each threshold layer is given as follows:

$$f_t = \sigma(W_f \cdot [h_{t-1}, x_t] + b_f), \quad (1)$$

$$i_t = \sigma(W_i \cdot [h_{t-1}, x_t] + b_i), \quad (2)$$

$$o_t = \sigma(W_o \cdot [h_{t-1}, x_t] + b_o), \quad (3)$$

where W is the weight of the threshold layer and b is the offset of the threshold layer. After each threshold layer is updated, the internal memory C_t is updated with the following equation:

$$C_t = f_t * C_{t-1} + i_t * \tanh(W_c \cdot [h_{t-1}, x_t] + b_c), \quad (4)$$

where " W_c " and " b_c " are the weights and offsets, respectively. The neural network output weight h_t of the internal memory is controlled by the output gate, and the activated unit state is output to the next layer of neural network and chain unit, which is specialized as shown in the following equation:

$$h_t = o_t * \tanh(C_t), \quad (5)$$

where σ is the sigmoid activation function. The sigmoid activation function takes the memory state of the network as the output value. When traffic flow data are input to the sigmoid activation function, the sigmoid activation function will compress it to $[0, 1]$: 0 means no amount is allowed to pass and 1 means any amount can pass. If the output value is within the specified range, the output value is matrix multiplied with the calculation result of the current layer, and then the result is input into the lower layer to map the

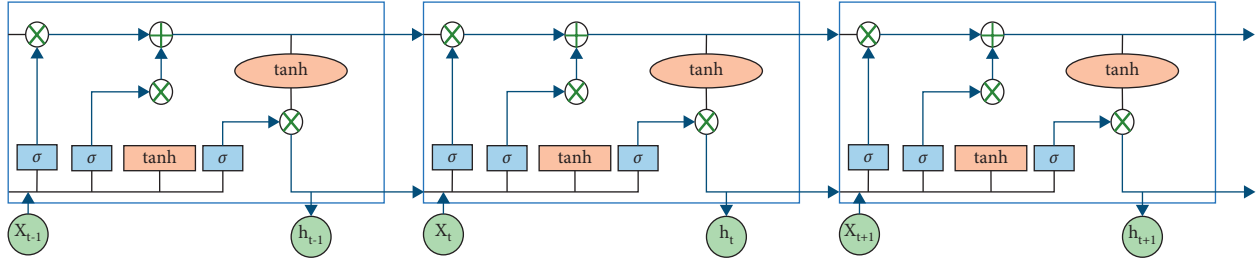


FIGURE 1: The internal structure of LSTM.

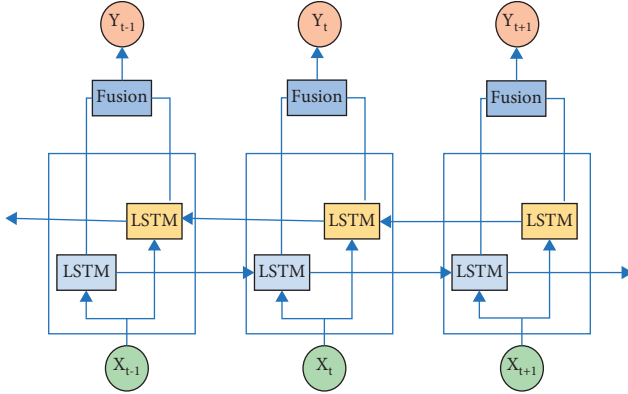


FIGURE 2: Structure of BiLSTM.

real number domain to the range of $[0,1]$. The function value represents the probability of belonging to the positive class [13–15]. Its expression is shown in the following equation:

$$f(z) = \frac{1}{1 + e^{-z}}. \quad (6)$$

The tanh activation function is different from the sigmoid activation function. It can map the real number domain to the range of $[-1,1]$. When the input is 0, the output is also 0. The expression is shown as follows:

$$f(x)_{\tanh} = \frac{e^x - e^{-x}}{e^x + e^{-x}}. \quad (7)$$

In the neural network training stage, LSTM learns the weights and offsets of each threshold layer from the past information. In the real-time prediction stage, the trained model is used to calculate the input data to obtain the predicted value of the time series, thereby improving the efficiency of mining past information and shortening the training time [16].

BiLSTM is an improved version of LSTM, composed of forward standard LSTM and reverse standard LSTM. By adding a layer of reverse LSTM to the LSTM structure, the effect of extracting global data features is achieved [17]. BiLSTM uses the memory unit of the standard LSTM to calculate the input data in order and in reverse order to obtain two different hidden layer features. Although it is carried out simultaneously, the structures in the two directions do not share the hidden state. The hidden state data of the forward LSTM are transmitted to the forward LSTM, the hidden state data of the reverse LSTM are transmitted to

the reverse LSTM, and there is no connection between the two directions. Finally, the two hidden layer features are linearly fused, and the final hidden layer feature result is obtained. In BiLSTM, the output value at each moment is jointly determined by the LSTM in the two directions. Therefore, the obtained model takes into account the parameter factors of the past and future directions, and the accuracy of the algorithm's prediction has been greatly improved [18–20]. Its specific structure is shown in Figure 2.

The BiLSTM structure is divided into two parts: one part is the forward standard LSTM, which is calculated in the forward direction over time and outputs h . The other part is the reverse standard LSTM, which performs reverse operation over time. The essence of the reverse operation is to reverse the input traffic flow data, then output to the reverse LSTM, and finally output H . After the forward and reverse output results are fused, the final output result [21] is obtained. In this process, the state of the hidden layer at time t in the forward LSTM calculation is related to the state at time $t-1$ and the state of the hidden layer at time t in the reverse LSTM calculation is related to the state at time $t+1$. The training is realized using a loss function [22]. The specific BiLSTM derivation principle is shown in Figure 3.

In BiLSTM, the calculation equations for the thresholds of the forward standard LSTM are consistent with those for the thresholds of the standard LSTM, and the calculation equations for the thresholds of the reverse standard LSTM are shown as follows:

$$\begin{aligned} i_t &= \sigma(W_i \cdot [H_{t+1}, X_t] + b_i), \\ f_t &= \sigma(W_f \cdot [H_{t+1}, X_t] + b_f), \\ o_t &= \sigma(W_o \cdot [H_{t-1}, x_t] + b_o), \\ C_t &= f_t * C_{t+1} + i_t * \tanh(W_C \cdot [H_{t+1}, x_t] + b_C). \end{aligned} \quad (8)$$

The output results of the bidirectional LSTM are linearly fused, and the fusion equation is shown as follows:

$$\begin{aligned} Y_t &= g(Uh_t + b) \\ &= g(U[h_t; H_t] + b). \end{aligned} \quad (9)$$

The forward direction extracts past information features from time 1 to t , and the reverse direction extracts future information features from time t to 1. The combined training of forward and reverse will reconsider the factors considered or discarded. Therefore, BiLSTM is more comprehensive than LSTM training and the prediction will be more accurate

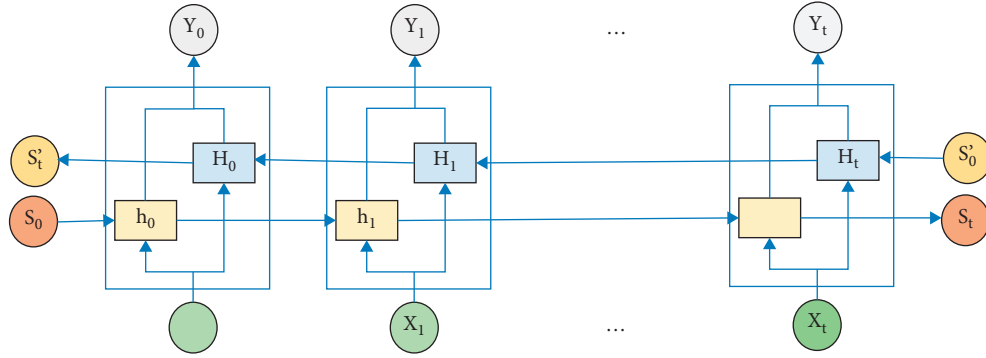


FIGURE 3: Specific derivation principle of BiLSTM.

[23, 24]. The final calculation results are obtained through training in BiLSTM, and the calculation steps are as follows.

Step 1. Defining the initial value. When $t = 1$ is set, the weight derivative value is calculated as shown in the following equations:

$$\varepsilon_C^t = \frac{\partial l}{\partial I_j^t}, \tag{10}$$

$$\varepsilon_C^t = \frac{\partial l}{\partial S_C^t}, \tag{11}$$

where l represents the loss function used for training, S_C^t means that neuron C is at time t , and I_j^t represents the data value input to neuron j at time t .

Step 2. Calculating the weight of the output gate. Since the output gate does not involve the time dimension, the weight of the output gate is shown in equation (12). In the equation, “ O_o^t ” represents the data value output from the output gate at time t and h represents the output activation function of the internal memory c :

$$W_o = W_o - \eta f'(O_o^t) \sum_{c=1}^C h(S_C^t) \varepsilon_C^t. \tag{12}$$

Step 3. Calculating the weight of the forget gate. The weight of the forget gate is shown in the following equation:

$$W_f = W_f - \eta f'(F_f^t) \sum_{c=1}^C S_C^t \varepsilon_S^t, \tag{13}$$

where “ F_f^t ” represents the output data value of the forget gate at time t and “ ε_S^t ” represents the state of the output gate at time t .

Step 4. Calculating the weight of the input gate. The weight of the input gate is shown in the following equation:

$$W_i = W_i - \eta f'(F_i^t) \sum_{c=1}^C g(I_C^t) \varepsilon_S^t, \tag{14}$$

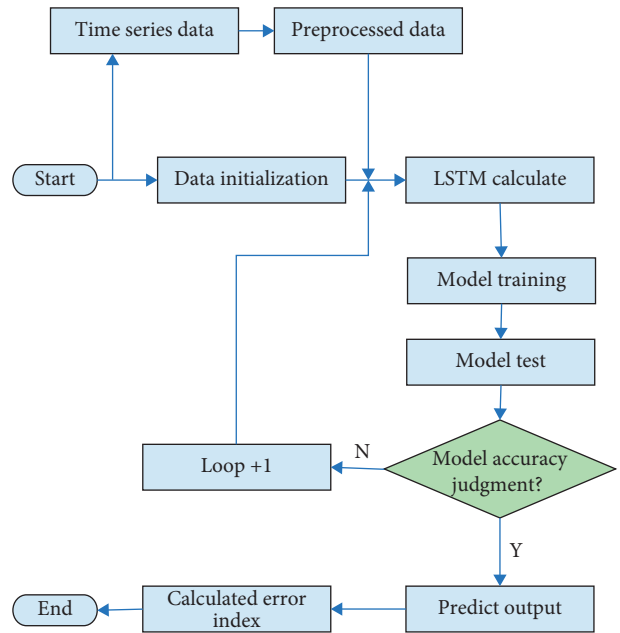


FIGURE 4: Flow of LSTM.

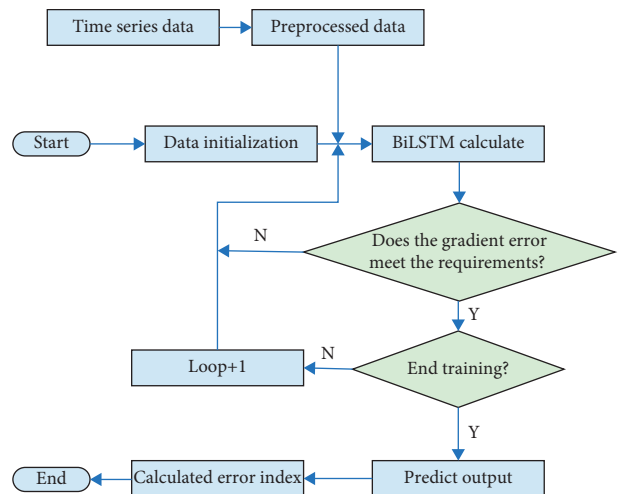


FIGURE 5: Flow of BiLSTM.

TABLE 1: Experimental procedure and experimental steps.

Experimental procedure	Experimental steps
Input	Traffic flow raw data, including time, direction, lanes, and numbers
Firstly, the traffic flow data are preprocessed	Step 1: the original traffic flow data is cleaned and filtered
	Step 2: a direction is determined as the research data
	Step 3: the traffic flows of all lanes in the selected direction are collected and summarized
	Step 4: the generated data set is outputted
Secondly, the training set is trained based on the BiLSTM algorithm	Step 1: the BiLSTM algorithm is initialized
	Step 2: the training data is inputted
	Step 3: the data enter the forward LSTM and are processed
	Step 4: the data enter the reverse LSTM and are processed
	Step 5: linear fusion is performed for the forward processing result and the reverse processing result
Thirdly, 20% of traffic flow data is selected to make predictions	Step 1: the forward and reverse BiLSTM algorithms are loaded
	Step 2: the predicted result values are loaded
	Step 3: the final result is obtained through linear fusion processing
Output	Prediction results and prediction performance evaluation values

where “ F_i^t ” represents the output data value of the input gate at time t and “ I_C^t ” represents the state of the unit at time t .

It has to calculate the weight of LSTM twice in the calculation process, and finally, 8 parameter values are obtained.

2.2. Count Affects. The data set is divided into a training set and a prediction set, which is allocated according to the ratio of 8:2 between the training set and the prediction set. By learning the training set, the algorithm finds the most suitable weights and confirms the values of related factors. The specific LSTM algorithm and BiLSTM algorithm execution flow are shown in Figures 4 and 5, respectively.

As shown in Figure 5, the standard LSTM algorithm can only perform single-item training of data, which means that it can perform feature extraction on existing data, but cannot perform data prediction. The use of BiLSTM for two-way training can process both past data and future data, so that the overall accuracy of the model will be higher [25]. In BiLSTM, the most important step is to train the data. The main purpose of training is to find suitable weights and related factor values through the training set [26].

Features with larger data levels have a greater impact on predictions, and it will cause the algorithm to converge slowly, so the data need to be preprocessed. If the degree of fitting in the linear form is too low (i.e., underfitting), it will not be fully suitable for the training set; if the degree of fitting is overfitted in the high power form, it will affect the prediction results although it is very suitable as a training set. Therefore, when the fitting is not suitable, some unimportant features can be directly discarded or normalization can be performed to reduce the number of parameters [27]. Firstly, the data are cleaned and filtered to find and correct the wrong and invalid values in the data. In this data processing, vehicles in multiple directions are firstly screened, in which vehicles in one direction are screened out and the vehicles in the other directions are discarded. Then, the traffic flows of multiple lanes are summed as data for one direction. Next, the

traffic flow data is serialized and mapped to $[0, 1]$. The original data $X = \{x_1, x_2, \dots, x_n\}$ are converted, and the conversion function is shown in the following equation:

$$y_i = \frac{x_i - \min\{x_j\}}{\max\{x_j\} - \min\{x_j\}}, \quad (1 \leq j \leq n). \quad (15)$$

In the above equation, max is the maximum value of the data and min is the minimum value of the data. The new traffic sequence obtained by conversion is $Y = \{y_1, y_2, \dots, y_n\}$. Finally, 80% of the data is selected as the training set and 20% as the prediction set.

This experiment is mainly divided into three steps as follows: Step 1: the traffic flow data are preprocessed, filtered, cleaned, and standardized to obtain the time series of traffic flow data. Step 2: the training set is trained based on the BiLSTM algorithm to get a suitable model. Step 3: about 20% of the traffic flow data is adopted to make predictions. The specific steps are listed in Table 1.

In traffic flow data prediction, root mean square error (RMSE), mean absolute error (MAE), mean absolute percentage error (MAPE), mean square error (MSE), and coefficient of determination R^2 (R-square) are adopted to evaluate the algorithm in order to reflect the degree of fitting of the algorithm and the accuracy of prediction. The MAPE value reflects the degree of deviation between the predicted result and the actual result. It is suitable for different algorithms of the same set of data. The smaller the MAPE value, the smaller the degree of deviation, indicating the better the prediction effect. MSE reflects a measure of the degree of difference between the predicted result and the actual result. Its value can reflect the degree of change and the distribution of errors. The smaller the MSE, the more concentrated the error distribution and the better the prediction effect. RMSE is used to evaluate the applicability of prediction algorithms to actual data. MAE reflects the average value of the absolute value of the deviation between the prediction result and the arithmetic average and can accurately reflect the magnitude of the prediction error. R^2

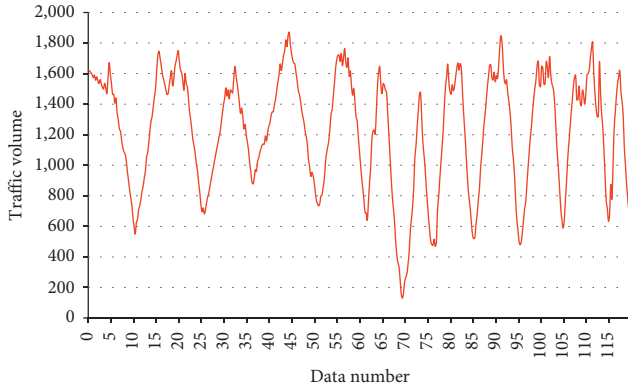


FIGURE 6: Test results of actual traffic flow.

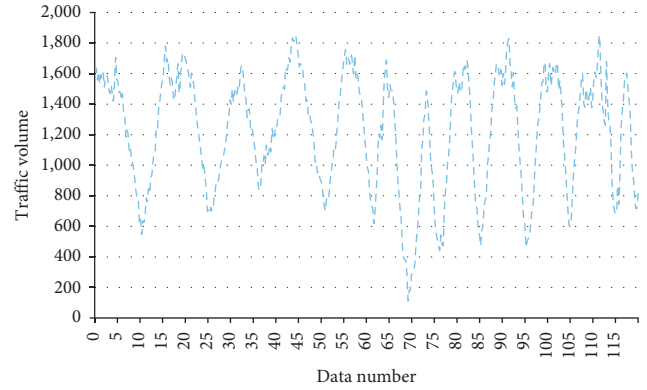


FIGURE 8: Predicted results of BiLSTM.

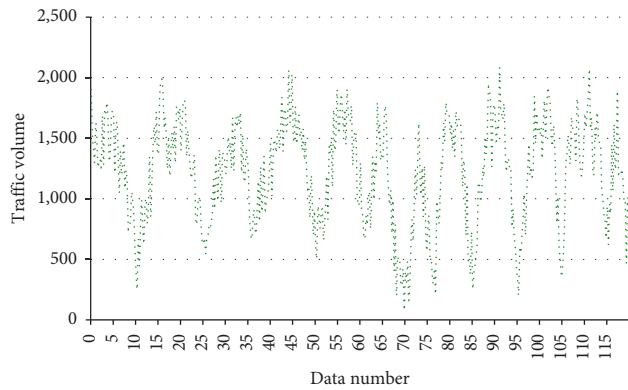


FIGURE 7: Predicted results of LSTM.

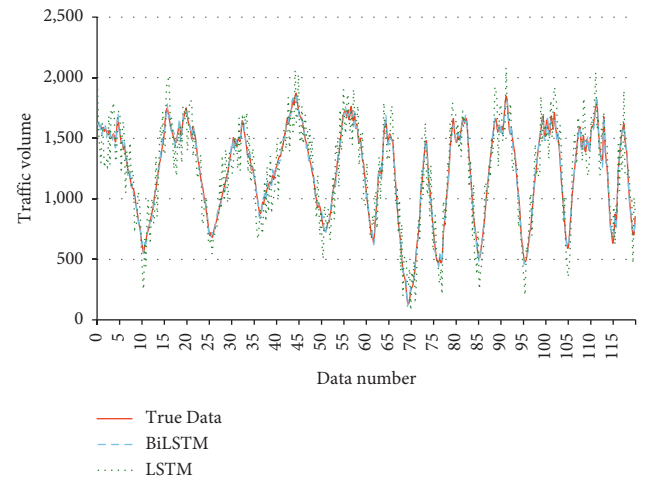


FIGURE 9: Comparison on prediction results of BiLSTM and LSTM.

reflects the degree of fitting between the predicted value and the actual result. The value range is [0, 1]. The closer to 1, the higher the degree of fitting, and the closer to 0, the lower the degree of fitting. These evaluation indicators can evaluate not only the forecast data and actual data but also the suitability of the forecast algorithm. Comprehensive consideration of trend graphs and evaluation indicators can further reflect the applicability of the algorithm in the field of traffic flow prediction. Their expressions are shown in the following equations:

$$MAE = \frac{1}{N} \sum_{i=1}^N |y_i - \hat{y}_i|, \quad (16)$$

$$MAPE = \frac{1}{N} \sum_{i=1}^N \frac{|y_i - \hat{y}_i|}{y_i}, \quad (17)$$

$$MSE = \frac{1}{N} \sum_{i=1}^N (|y_i - \hat{y}_i|)^2, \quad (18)$$

$$RMSE = \sqrt{\frac{1}{N} \sum_{i=1}^N (|y_i - \hat{y}_i|)^2}, \quad (19)$$

TABLE 2: Indicators for prediction performance of BiLSTM.

Item	LSTM	BiLSTM
MAE	106.156847	105.087415
MAPE	9.722147%	9.718624%
MSE	31354.984156	32846.946157
RMSE	176.184617	180.145275
R ²	0.778742	0.795746

$$R^2 = 1 - \frac{\sum_i (y_i - \hat{y}_i)^2}{\sum_i (y_i - \bar{y}_i)^2}. \quad (20)$$

Here, y represents the actual traffic flow observed, \hat{y} represents the corresponding time prediction value, \bar{y} represents the average value, i refers to the amount of change in the traffic flow, and N represents the data volume of the traffic flow prediction experiment.

3. Results and Discussion

3.1. Effect of BiLSTM. In this study, the traffic flow measured by a vehicle detector at an intersection in Beilin District, Xi'an is selected. The duration lasts 10 days from November

1 to 10, 2021, and the traffic flow statistics interval is 2 hours. A total of 120 sets of data are measured. The actual trend, the BiLSTM result trend, and the LSTM trend predicted by the construction training and prediction are shown in Figures 6–8.

As illustrated in Figures 6 to 8, both the LSTM algorithm and the BiLSTM algorithm could roughly predict the real traffic flow data, but the fitting degree of the LSTM algorithm at peak and low peaks was a little bit worse, and the calculation results were more chaotic after simulation. The above three figures are fused, and it can show the difference between the prediction result and the prediction result, as shown in Figure 9.

In the figure, the abscissa is the data number and the interval is 2 hours. A total of 120 sets of data are measured. The ordinate is the traffic flow on the road, and the interval is 500. The figure reveals that the prediction results of LSTM and BiLSTM are consistent with the actual traffic flow trend overall, but the data of LSTM deviate greatly from the real situation, and the error is more serious during peak periods. BiLSTM is in good agreement with the real situation in the stationary period and low peak period and is slightly different from the real situation in the peak period but still has a better deviation than LSTM. In general, the prediction accuracy of the BiLSTM algorithm for the traffic flow is higher than that of the LSTM algorithm, which is in good agreement with the real situation, so it is feasible in the actual traffic flow prediction.

3.2. Algorithm Evaluation. The MAE, MAPE, MSE, RMSE, and R^2 values of the prediction results were calculated, as listed in Table 2.

As presented in Table 2, the R^2 value of BiLSTM is larger than that of LSTM, indicating that BiLSTM shows a higher degree of fitting than LSTM algorithm, and BiLSTM predicts more accurately and is more suitable for predicting traffic flow than LSTM. The MAPE value of BiLSTM is smaller than that of LSTM, indicating that the trend of BiLSTM's prediction results is more consistent than that of LSTM. The MAE value of BiLSTM is smaller than that of LSTM, indicating that the actual prediction error of BiLSTM is smaller than that of LSTM, and the deviation of each data compared with the real data is smaller. The MSE and RMSE values of the BiLSTM algorithm are larger than those of the LSTM, indicating that the LSTM is more concentrated and the effect is better than the BiLSTM. Generally speaking, the BiLSTM algorithm shows more advantages in traffic flow prediction than the LSTM algorithm.

4. Conclusions

This study mainly applies the traffic flow algorithm based on the BiLSTM model. By predicting the traffic flow, the traffic congestion can be managed and optimized. A BiLSTM-based urban road short-term traffic state algorithm network is established based on the collected traffic flow data, and then its internal memory unit structure is optimized. In addition, it is trained to be a high-quality prediction model,

and experimental simulation verification and predictive performance evaluation are performed. Experiments show that BiLSTM is in good agreement with the real situation in the traffic stationary period and low peak period, and there is a slight gap between the peak period and the real situation, but it can still be used as a reference. In general, the prediction accuracy of the BiLSTM algorithm for traffic flow is relatively high, so it is feasible in actual traffic flow prediction. Due to the limited capabilities, a slight flaw can be found in the design of the fusion function of the BiLSTM algorithm, which leads to a decrease in the accuracy of the prediction result. In future, it will conduct in-depth exploration in this aspect to find a more suitable fusion function to reduce the influence of human factors. All in all, this study can play a certain reference role in the dynamic control, monitoring, and guidance of urban traffic, and congestion management.

Data Availability

The datasets used and analyzed during the current study are available from the corresponding author on reasonable request.

Conflicts of Interest

The authors declare that they have no conflicts of interest.

Acknowledgments

This paper was supported by Macau University of Science and Technology Foundation (FRG-21-016-FA).

References

- [1] A. Khanna, R. Goyal, M. Verma, and D. Joshi, "Intelligent traffic management system for smart cities," *Communications in Computer and Information Science*, vol. 958, pp. 152–164, 2019.
- [2] P. Yuan and X. Lin, "How long will the traffic flow time series keep efficacious to forecast the future?" *Physica A: Statistical Mechanics and Its Applications*, vol. 467, pp. 419–431, 2017.
- [3] T. Li, A. Ni, C. Zhang, G. Xiao, and L. Gao, "Short-term traffic congestion prediction with Conv-BiLSTM considering spatio-temporal features," *IET Intelligent Transport Systems*, vol. 14, no. 14, pp. 1978–1986, 2020.
- [4] S. V. Kumar and L. Vanajakshi, "Short-term traffic flow prediction using seasonal ARIMA model with limited input data," *European Transport Research Review*, vol. 7, no. 3, p. 21, 2015.
- [5] W. Huang, G. Song, H. Hong, and K. Xie, "Deep architecture for traffic flow prediction: deep belief networks with multitask learning," *IEEE Transactions on Intelligent Transportation Systems*, vol. 15, no. 5, pp. 2191–2201, 2014.
- [6] Y. Zhang, M. Lu, and H. Li, "Urban traffic flow forecast based on FastGCRNN," *Journal of Advanced Transportation*, vol. 2020, Article ID 8859538, 9 pages, 2020.
- [7] D. Xia, M. Zhang, X. Yan et al., "A distributed WND-LSTM model on MapReduce for short-term traffic flow prediction," *Neural Computing & Applications*, vol. 33, no. 7, pp. 2393–2410, 2021.

- [8] H. Hansika, B. Christoph, and B. Kasun, "Recurrent neural networks for time series forecasting: current status and future directions," *International Journal of Forecasting*, vol. 37, no. 1, pp. 388–427, 2021.
- [9] M. Abdel-Nasser and K. Mahmoud, "Accurate photovoltaic power forecasting models using deep LSTM-RNN," *Neural Computing & Applications*, vol. 31, no. 7, pp. 2727–2740, 2019.
- [10] B. B. Sahoo, R. Jha, A. Singh, and D. Kumar, "Long Short-term Memory (LSTM) recurrent neural network for low-flow hydrological time series forecasting," *Acta Geophysica*, vol. 67, no. 5, pp. 1471–1481, 2019.
- [11] F. Affonso, T. M. R. Dias, and A. L. Pinto, "Financial times series forecasting of clustered stocks," *Mobile Networks and Applications*, vol. 26, no. 1, pp. 256–265, 2021.
- [12] M. Rhif, A. B. Abbes, B. Martinez, and I. R. Farah, "A deep learning approach for forecasting non-stationary big remote sensing time series," *Arabian Journal of Geosciences*, vol. 13, no. 22, pp. 1–11, 2020.
- [13] J. Kumar, R. Goomer, and A. K. Singh, "Long short term memory recurrent neural network (lstm-rnn) based workload forecasting model for cloud datacenters," *Procedia Computer Science*, vol. 125, pp. 676–682, 2018.
- [14] S. Bouktif, A. Fiaz, A. Ouni, and M. ASerhani, "Multi-sequence LSTM-RNN deep learning and metaheuristics for electric load forecasting," *Energies*, vol. 13, no. 2, pp. 1–21, 2020.
- [15] S. V. Belavadi, S. Rajagopal, R. R, and R. Mohan, "Air quality forecasting using LSTM RNN and wireless sensor networks," *Procedia Computer Science*, vol. 170, pp. 241–248, 2020.
- [16] V. Athira, P. Geetha, R. Vinayakumar, and K. P. Soman, "Deep air net: applying recurrent networks for air quality prediction," *Procedia Computer Science*, vol. 132, pp. 1394–1403, 2018.
- [17] T. Chen, R. Xu, Y. He, and X. Wang, "Improving sentiment analysis via sentence type classification using BiLSTM-CRF and CNN," *Expert Systems with Applications*, vol. 72, pp. 221–230, 2017.
- [18] L. Luo, Z. Yang, P. Yang et al., "An attention-based BiLSTM-CRF approach to document-level chemical named entity recognition," *Bioinformatics*, vol. 34, no. 8, pp. 1381–1388, 2018.
- [19] M. Liu, Y. H. Lu, S. Long, J. Bai, and W. Lian, "An attention-based CNN-BiLSTM hybrid neural network enhanced with features of discrete wavelet transformation for fetal acidosis classification," *Expert Systems with Applications*, vol. 186, 2021.
- [20] J. Zheng, L. Zhang, J. Chen et al., "Multiple-load forecasting for integrated energy system based on Copula-DBiLSTM," *Energies*, vol. 14, pp. 1–14, 2021.
- [21] X. Y. Yan, T. Guan, K. X. Fan, and Q. Sun, "Novel double layer BiLSTM minor soft fault detection for sensors in air-conditioning system with KPCA reducing dimensions," *Journal of Building Engineering*, vol. 44, Article ID 102950, 2021.
- [22] C. Gan, Q. Feng, and Z. Zhang, "Scalable multi-channel dilated CNN-BiLSTM model with attention mechanism for Chinese textual sentiment analysis," *Future Generation Computer Systems*, vol. 118, pp. 1–2, 2021.
- [23] J. Deng, L. Cheng, and Z. Wang, "Attention-based BiLSTM fused cnn with gating mechanism model for Chinese long text classification," *Computer Speech & Language*, vol. 68, no. 6, 2021.
- [24] L. Wang, X. Bai, R. Xue, and F. Zhou, "Few-shot SAR automatic target recognition based on Conv-BiLSTM prototypical network," *Neurocomputing*, vol. 443, no. 12, pp. 235–246, 2021.
- [25] T. Hu, K. Li, H. Ma, H. Sun, and K. Liu, "Quantile forecast of renewable energy generation based on indicator gradient descent and deep residual BiLSTM," *Control Engineering Practice*, vol. 114, no. 99, Article ID 104863, 2021.
- [26] H. Wei, A. Zhou, Y. Zhang, F. Chen, W. Qu, and M. Lu, "Biomedical event trigger extraction based on multi-layer residual BiLSTM and contextualized word representations," *International Journal of Machine Learning and Cybernetics*, vol. 18, pp. 1–13, 2021.
- [27] R. Janning, T. Horváth, A. Busche, and L. Schmidt-Thieme, "GamRec: a clustering method using geometrical background knowledge for GPR data preprocessing," *IFIP Advances in Information and Communication Technology*, vol. 381, pp. 347–356, 2017.

Research Article

Identification of Working Trucks and Critical Path Nodes for Construction Waste Transportation Based on Electric Waybills: A Case Study of Shenzhen, China

Jun Bi ^{1,2}, Qiuyue Sai ², Fujun Wang,² and Yakun Chen²

¹Key Laboratory of Transport Industry of Big Data Application Technologies for Comprehensive Transport, Beijing Jiaotong University, Beijing 100044, China

²School of Traffic and Transportation, Beijing Jiaotong University, Beijing 100044, China

Correspondence should be addressed to Qiuyue Sai; 19114026@bjtu.edu.cn

Received 5 January 2022; Accepted 25 February 2022; Published 22 March 2022

Academic Editor: Sang-Bing Tsai

Copyright © 2022 Jun Bi et al. This is an open access article distributed under the Creative Commons Attribution License, which permits unrestricted use, distribution, and reproduction in any medium, provided the original work is properly cited.

Due to the large amount of waste generated by urban construction, the transportation of construction waste has a significant impact on urban traffic. Understanding the transportation trajectory of garbage trucks can improve the management of transportation routes and reduce traffic accidents. This study analyzes electric waybill and state data of garbage trucks to identify hot nodes of construction waste transportation, where the volume of garbage trucks is relatively high. Management should strengthen the hot nodes to reduce traffic accidents. First, several machine learning methods are used to improve the prediction accuracy of electric waybill generation, where the garbage truck recorded on the electric waybill is regarded as a working truck. Second, the transportation trajectory of working trucks is extracted, and its spatiotemporal characteristics are further analyzed. Hot nodes are found based on density clustering. Finally, a case study is conducted based on the Shenzhen construction waste transportation system. The results show that the XGBoost model can improve the accuracy of the generation of waybill to 90.5% compared with the decision tree model, random forest, and GBDT. Moreover, the density clustering model can discover the hot nodes of construction waste transportation. Considering the minimum number of samples and the neighborhood radius, the clustering number is determined as 100. The ratio of noise points is determined as 0.79. The results can provide decision support for the management of electronic waybill and garbage truck transportation.

1. Introduction

Along with urbanization, the renovation and expansion of construction have produced a large amount of construction waste, which has put pressure on the urban environment and traffic [1]. Construction and demolition waste (CDW) is one of the largest waste streams and needs to be transported by cities [2]. Serious traffic accidents can easily occur because of working garbage trucks. Working garbage truck is a garbage truck that is carrying out the transportation task, which has a large weight and size. Working garbage truck has large inertia and large blind spot and is difficult to control. The road it passes is often the key safety management object. Therefore, it is important to analyze the transport trajectory of working garbage trucks to strengthen transportation management [3].

Identifying working garbage trucks is important. Whether the trucks carry out the transportation task is judged according to the waybill information. If a truck is carrying out a task, it is recorded by a waybill. Historically, a paper waybill was used to record the transporting process. However, it requires considerable manpower to record information, which causes the problem of incomplete supervision. To manage the process of construction waste transportation efficiently, electronic waybills have been used in waste transportation based on technologies such as communication technology and the Internet of Vehicles. Electronic waybills are able to store transportation information in the system in the form of electronic data. Applying an electronic waybill can save manpower and record the transportation process online. The state data of garbage

trucks on the construction sites are used to judge the waybill generation. Only the garbage truck carrying out a waybill can be defined as a working garbage truck that is carrying out the transportation task. However, an electronic waybill is automatically generated based on the GPS of vehicles. Because the state of garbage trucks is not considered, a waybill is generated by mistake if the garbage truck passes the construction site without a transport mission, which results in the low prediction accuracy of waybill generation in general and thus contributes to the low identification accuracy of working trucks. Therefore, an accurate prediction model for electronic waybill generation is urgently needed.

After the working trucks are identified, their transport trajectory can be analyzed. Due to the long transportation path from construction sites to suburbs, vehicle management cannot be comprehensive. In general, the transportation of construction waste has a higher risk for traffic accidents because the volume of garbage trucks is high, which may cause heavy losses to transport contractors and society. An effective method for avoiding traffic accidents during construction waste transportation is to analyze the nodes on the road where the accident may occur [4]. Specifically, the transport trajectory can be explored to find the important nodes.

Due to the acceleration of urbanization and the emergence of new technologies, the management of construction waste transportation routes is a new problem. The urban construction waste production of China has increased. Construction waste transportation has put enormous pressure on urban traffic, so the management of construction waste transportation is very urgent. We reviewed a lot of literature on construction waste research. Several studies have discussed construction waste transportation from different aspects. For instance, some studies have focused on the impact of the recycling of construction waste on the environment. Lachat et al. [5] presented a life cycle inventory compilation and life cycle assessment in France. Souza et al. [6] analyzed the impact of recycling proposals for construction waste on the environment. Maués et al. [7] evaluated the environmental impact generated by transportation construction waste. The results showed that transportation waste management needs to be strengthened to improve the sustainability of cities. In addition, studies have focused on construction waste management. Tao and Xiao [2] analyzed the quantification and composition of construction waste in Shanghai, China, and recycling management in this region was discussed and introduced. Franco et al. [8] applied a model to optimize the location of landfills, and it considered the cost of transporting waste and the cost of building the landfill. Spišáková et al. [9] confirmed the economic potential of CDW audit processing, and disposal costs and transport costs of the recommended CDW management were considered.

Moreover, studies have also concentrated on developing construction waste management system design. You et al. [10] proposed an informatization scheme integrating multiple technologies, which was used to monitor illegal behaviors in the waste disposal process. Wang et al. [11] combined building information modeling technology (BIM)

and vehicle positioning technology (GIS) to develop a monitoring and intelligent management information management platform for construction waste, which improved the precision and intelligence of construction waste management. Wang et al. [12] developed a BIM and cost-optimization-based decision-making system for construction waste transportation that suggested a cost-effective transportation plan. Zhang [13] took underground engineering construction as the research object and analyzed the source characteristics of construction waste. To resolve the disadvantages of construction waste management, construction waste construction site management strategies have been proposed to improve the resource utilization of construction waste. In [14], an intelligent urban construction site muck monitoring system was developed and the system was deployed to the cloud server combined with vehicle GPS positioning and video remote monitoring. It improved construction waste transportation management under the data integration and network integration environment. Previous studies on construction waste management mainly focused on the environmental impact, resource utilization, and system design. However, few studies have focused on the characteristics of construction waste transportation trajectories.

Among the researches on transportation problems, some studies focus on the use of electronic waybills in transportation systems. Bakhtyar et al. [15] analyzed information synergy between e-Waybill solutions and intelligent transport system services. Cane et al. [16] designed an electronic multimodal waybill and a solution for implementation using the e-Freight e-Delivery Infrastructure. However, there are few studies on how to apply electronic waybills in construction waste transportation.

In addition, with regard to the study on transportation routes, some studies focused on traffic problems [17, 18]. Machine learning methods can be used to learn from large volumes of data [19, 20]. Some studies found traffic hotspots using clustering methods. Ran et al. [21] introduced a novel K-means clustering algorithm based on a noise algorithm to capture urban hotspots. Jia et al. [22] analyzed traffic crash with point-of-interest spatial clustering. Le et al. [23] found traffic accident hotspot based on kernel density estimation. DBN clustering method is used for key node identification of construction waste transportation path. The use of electronic waybill data and route trajectory data to analyze important nodes in the transportation route of construction waste fills the research gap.

The study aims at solving the problem of frequent traffic accidents in construction waste transportation. The innovative idea is to transform the transport routing problem into a node management problem. These nodes need to be managed centrally. First, it is important to find the trajectory of the trucks at work. The working status of the truck is recorded in the electronic waybill [24]. Based on these data, it is predicted whether the trucks are under working states. XGBoost is designed to judge the working state of the trucks. XGBoost used boosting method to improve the prediction efficiency and accuracy, which is widely adapted to build a prediction model. Second, for trucks in the working state,

the density clustering method is used to find the concentration of trucks at a certain time. The clustering method is to classify based on the density of spatial distribution. Areas where the working truck congregate will be classified into one category [25]. This is the area in the transportation route that should be concentrated.

The contribution of this study is shown as follows. The study aims at solving the problem of frequent traffic accidents in construction waste transportation. We proposed an innovative idea that transforms the transport routing problem into a node management problem. We have found the nodes that need to be managed centrally. Strengthening the management of important nodes can improve management efficiency and reduce the probability of traffic accidents. Moreover, we obtained a model with better accuracy through case studies among several methods. Potential applications of the proposed method are shown as follows. First, based on the emerging electronic waybill and electronic fence technology, machine learning technology is used to design the identification method of working trucks and key nodes in this study. The key node is the area with frequent traffic accidents, which can make the loss of life and property. Therefore, it is helpful to find important path nodes in transportation routes and strengthen management to ensure a healthy transportation environment. Second, electronic fences and electronic waybills are new types of applications. Replacing paper waybills with electronic waybills can save 65%–99% of time [15]. However, the application of electronic waybill technology in the construction waste transportation process is rarely applied. This study can expand the application of electronic waybill technology. The proposed methods may be used by transport contractors and related stakeholders to manage construction waste transport roads.

The remainder of this article is arranged as follows. Section 1 introduces the problem background and main contributions in this study. Section 2 introduces data and data preparation and addresses the problem. Section 3 explains the methodology used to solve the problem. Section 4 presents a case study on Shenzhen and provides managerial insights. Finally, Section 5 provides the conclusions and suggestions for future research.

2. Data Preparation and Definition

2.1. Area and Data Introduction

2.1.1. Study Area Introduction. Construction waste transportation in Shenzhen, China, is explored in this study. Based on the GPS system [26], an electronic waybill is used to manage the whole process of construction waste, including generation, transportation, and disposal. Shenzhen has more than 9084 garbage trucks and 4000 construction sites. The distribution of construction sites in Shenzhen is shown in Figure 1, where the red points represent the locations of construction sites.

2.1.2. Data Introduction. The trajectory data of the garbage truck are obtained by a GPS positioning device. Trajectory data comprise on-road and waybill node information. A

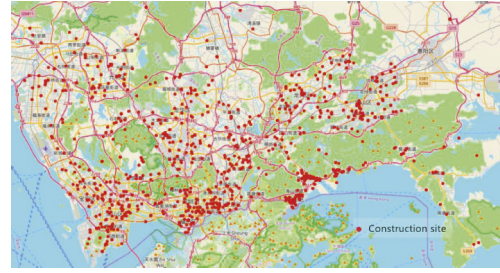


FIGURE 1: Distribution of construction sites in Shenzhen.

total of 128.7 million GPS trajectory data points from 9084 garbage trucks are obtained. Track data fields include track ID (Track_ID), speed, vehicle number (Vehicle_ID), longitude of truck (LNG), latitude of truck (LAT), mileage (Mil), and track GPS data time (GPS_Time). The sample data are shown in Table 1.

A total of 13,947 pieces of state data of vehicles in the waybill nodes are obtained. The data are used for the prediction model of waybill generation. The aim is to identify whether to generate an electronic waybill. The sample data are shown in Table 2.

2.2. Construction Waste Transportation and Node Definition.

A waybill is used to record the complete construction waste transportation process. The process is shown in Figure 2. When the garbage truck enters the electronic fence of the first construction site, a new waybill is generated. Then, when it passes through a construction site, a waybill node corresponding to the construction site is generated. A waybill can have several waybill nodes if the garbage truck needs to carry out transportation missions at several construction sites. After the truck drives into the electronic fence of the disposal site, the end node is generated and the waybill is finished. Some definitions are as follows:

- (1) Electronic fences indicate areas for construction. The truck enters and exits the area for related processing procedures. Electronic fences include construction sites and disposal sites, and they are marked with the red square in Figure 2.
- (2) Electronic waybills records transportation process, including transportation from the source of the construction site to disposal at the end of the disposal site. A disposal site and more than one construction site are included in one complete waybill. If the system identifies that the garbage truck enters a waybill node to work, it will push the electronic waybill to the staff to confirm.
- (3) A waybill node in the waybill is generated at a construction site. If the garbage truck carries out a task in the electronic fence, a waybill node will be recorded on the electronic waybill.
- (4) The path node is the hot node on the transportation path, which is the blue circle marked in Figure 2. The volume of garbage truck at hot node is large.

TABLE 1: Trajectory data of the garbage trucks.

Track_ID	Vehicle_ID	Speed	LNG	LAT	Mil	GPS_Time
23112633404	2453798	15	114.124215	22.629716	147852.3	2019/12/16 0:06:45

TABLE 2: State data of garbage trucks recorded in electronic waybills.

Variables	Data sample	Value introduction
Duration of stay	30	Numeric type
Declaration and discharge states	1	0 is not the specified garbage truck 1 is the specified garbage truck
Load states in and out of the electronic fence	1	0 is no change 1 is empty becomes heavy 2 is heavy becomes empty
Waybill generation	1	1 is generate waybill 0 is no waybill generate
Carrying	1	0 is no-load state 1 is heavy-load state
Carriage open	0	0 is door closed 1 is door opened
Lift	0	0 is unlifted state 1 is lifted state

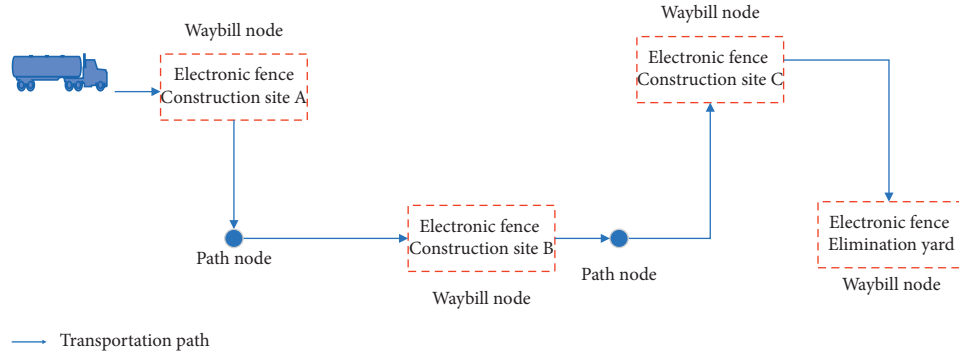


FIGURE 2: Whole process of construction waste transportation.

3. Methodology

3.1. Waybill Node Generation Prediction Based on XGBoost. Previous waybill generation prediction methods were judged using trajectory data, which usually led to misjudgment and low prediction accuracy. To improve the waybill generation prediction accuracy, state data of garbage trucks are considered here to identify waybill generation. The relationship between waybill generation and vehicle state data is complicated. Therefore, a decision tree model can be constructed to improve the waybill generation prediction accuracy based on the simultaneous use of trajectory data and state data of garbage trucks.

Improved decision tree models, such as random forest, GBDT, and XGBoost, in which multiple basic trees are combined, have been constructed [27–30]. Improved decision tree models can enhance computational efficiency and adaptability for prediction operations with large-scale datasets compared to basic decision tree models. In this study, four decision tree models are constructed to fit the

prediction model of an electronic waybill. XGBoost is one of the most efficient decision tree models [31]. The calculation process of XGBoost is as follows [32].

First, the iteration of the objective function and Taylor expansion is shown in equation (1). The loss function is shown as equation (2).

$$\hat{y}_i = \sum_{k=1}^K f_k(x_i), f_k \in F, \quad (1)$$

$$\text{Obj} = \sum_{i=1}^n l(y_i, \hat{y}_i) + \sum_{k=1}^K \Omega(f_k), \quad (2)$$

where k is the number of basic decision tree models; $f_k(x_i)$ is the k -th decision tree model; \hat{y}_i is the prediction result of garbage truck data x_i , obtained by integrating K decision tree models; $l(y_i, \hat{y}_i)$ is the training error; $\Omega(f_k)$ is the regularization of the k -th tree; $\Omega(f_k) = \gamma T + 1/2\lambda \|w\|^2$; T is the number of leaf nodes; w is the value of leaf nodes; γ is the

regularization coefficient of L1; λ is the regularization coefficient of L2. The optimal parameters and optimal model $f^*(x)$ are obtained to minimize $\Omega(f_k)$.

However, it is difficult to calculate the optimal model. Therefore, the problem is transformed to find the weight w and the structure of trees [33, 34]. The initialization model has no tree model. The prediction result is 0. Add the t -th tree to the model as shown in the following:

$$\hat{y}_i^{(t)} = \sum_{k=1}^t f_k(x_i) = \hat{y}_i^{(t-1)} + f_t(x_i). \quad (3)$$

The Taylor expansion is used to approximate the objective function, as shown in the following equation:

$$\text{obj}^t(\theta) = \sum_{j=1}^y \left\{ g_j f_t(x_j) + \frac{1}{2} h_j f_t(x_j) \right\} + \gamma T + \frac{1}{2} \lambda \sum_{j=1}^T w_j^2. \quad (4)$$

Take the derivative and obtain the optimal result, as shown in the following equations:

$$w_j^* = -\frac{\sum g_i}{\sum h_i + \lambda}, \quad (5)$$

$$\text{obj}^* = -\frac{1}{2} \sum_{j=1}^T \frac{(\sum g_i)^2}{\sum h_i + \lambda} + \gamma T. \quad (6)$$

3.2. Hot Nodes Identification Based on DBSCAN. Hot nodes are areas where the volume of garbage trucks is high. Serious traffic accidents often occur in areas with a high volume of garbage trucks. Thus, identifying hot spots and strengthening management can help alleviate traffic problems. In this study, the number of clusters for hot node recognition is not known in advance. The number of clusters is determined according to the hot node aggregation density. Therefore, DBSCAN is used to study the hot node recognition of construction waste transportation [35].

Two important parameters are used to describe the sample distribution, the radius of neighborhood ϵ , and core point threshold MinPts. $X = \{x_1, x_2, \dots, x_n\}$ is the trajectory data of garbage trucks. For $x_j \in X$, its neighborhood ϵ includes data defined as $N_\epsilon(x_j) = \{x_i \in X | \text{dist}(x_i, x_j) \leq \epsilon\}$. For $x_j \in X$, its density is $\rho(x) = |N_\epsilon(x_j)|$. For $x_j \in X$, if $N_\epsilon(x_j) \geq \text{MinPts}$, then x_j is a core point. The collection of the core point is X_c [36].

The trajectory data of 200 garbage trucks during the evening peak of 20:00–21:00 are selected as an example. The sample size is 33,000 trips with latitude and longitude. This is a spherical surface; therefore, the latitude and longitude data should be converted to the actual distance in the rectangular coordinate system. Assume that the latitude and longitude of the two points are (x_1, y_1) and (x_2, y_2) . The radius of the Earth is 6371 kilometers. The actual distance between the two points is shown in the following equation [37]:

$$\text{dist} = R \arccos[\cos(x_1 - x_2) \cos y_1 \cos y_2 + \sin y_1 \sin y_2]. \quad (7)$$

The calculation process is shown in Table 3 [37].

4. Case Study

4.1. Case Study on Waybill Node Generation Prediction. The scenario of the case study is introduced in Section 2.1, where construction waste transportation is explored in Shenzhen, China. The waybill is identified and generated in the waybill node based on GPS. To solve the problem of poor accuracy of the current electronic waybill identification, the characteristics of the garbage truck state data in the waybill node are analyzed. The generation prediction model of the electronic waybill at the construction site is constructed based on improved decision tree methods. The aim is to provide a high-accuracy prediction model to improve the quality and efficiency of construction waste transportation. First, the correlation of the influencing factors is analyzed. Then, the decision tree, random forest, GBDT, and XGBoost methods are used to fit the prediction model. Finally, the prediction results are compared and analyzed.

4.1.1. Variable Independence Test. The types of influencing variables and the objective (whether to generate an electronic waybill) are categorical data. Analyzing whether there is a dependency between two categorical variables is called an independence test. χ^2 is used to perform statistical analysis on the correlation between each influencing variable and the objective to determine the input variables of the waybill generation prediction model. The main process is as follows:

- (1) The original hypothesis is H_0 : there is no dependency between the two categorical variables. H_1 : there is a dependency between the two categorical variables.
- (2) Calculate the expected frequency value, as shown in the following equation:

$$f_{ij}^e = \frac{\sum_{i=1}^R f_{ij}}{n} \times \frac{\sum_{j=1}^C f_{ij}}{n} \times n = \frac{\sum_{i=1}^R f_{ij} \times \sum_{j=1}^C f_{ij}}{n}, \quad (8)$$

where f_{ij} is the actual frequency of variables i and j ; f_{ij}^e is the expected value of the frequency; $\sum_{i=1}^R f_{ij}$ is the frequency of variable j ; $\sum_{j=1}^C f_{ij}$ is the frequency of variable i ; n is the sample size; R is the number of variable i ; C is the number of variable j .

- (3) Calculate the statistics χ^2 and degrees of freedom df as shown in the following equations:

$$\chi^2 = \sum_{i=1}^R \sum_{j=1}^C \frac{(f_{ij} - f_{ij}^e)^2}{f_{ij}^e}, \quad (9)$$

$$df = (R - 1)(C - 1). \quad (10)$$

- (4) Given the significance level $\alpha = 0.5$, according to the calculated statistics χ^2 and degrees of freedom df , find the Chi-square distribution to obtain the value P . If $P > \alpha$, then H_0 cannot be rejected; that is, the two classification variables are independent of each other. Otherwise, reject H_0 and accept that there is a dependency between the two classification variables.

TABLE 3: Description of the DBSCAN algorithm.

Input: garbage truck data set $X = \{x_1, x_2, \dots, x_n\}$; radius of a neighborhood ϵ ; and minimum sample size MinPts

Process:

Initialize data set $\Omega = \emptyset$

for $i = 1, 2, \dots, n$:

Search for $N_\epsilon(x_i)$, if $N_\epsilon(x_i) \geq \text{MinPts}$:

place x_i in set Ω , then $\Omega = \Omega \cup \{x_i\}$

end if

end for

Initialize the number of clustering $k = 0$

Initialize the collection of unclustered samples M , $M = X$

while $\Omega \neq \emptyset$:

save set $M_o = M$

obtain data p from M . Initialize $Q = \{p\}$

$M = M \setminus \{p\}$

while $Q \neq \emptyset$: obtain data q from Q

if $|N_\epsilon(q)| \geq \text{MinPts}$:

$\Lambda = N_\epsilon(q) \cap M$

place Λ in Q

$M = M \setminus \Lambda$

end if

end while

$k = k + 1$, generate $C_k = M_o \setminus M$

$\Omega = \Omega \cup C_k$

end while

Output: $C = \{C_1, C_2, \dots, C_k\}$

The correlation coefficient describes the degree of correlation between two variables. This study uses the correlation coefficient V , with the same symbol used in the independence test, and the calculation is shown as the following equation:

$$V = \sqrt{\frac{\chi^2}{n \times \min[(R-1), (C-1)]}} \quad (11)$$

Correlation analysis between the influencing factors and the generation of electronic waybills was conducted. The results are obtained as shown in Table 4.

This analysis shows whether an electronic waybill that is generated has a certain correlation with some influencing factors. The greatest correlation is observed with the declaration and discharge states, duration of stay, and speed. A relatively large correlation is observed with the load states in and out of the electronic fence, carrying, and carriage open. Therefore, the above six influencing variables are chosen as input variables.

4.1.2. Waybill Prediction Result Based on XGBoost. XGBoost is constructed to predict waybill generation. The method is shown in Section 3.1. Six influencing variables are input variables, and whether generation of a waybill is output variable. Several parameters need to be determined in XGBoost. The number of basic learners is the number of decision trees, which is represented by $n_estimators$; max_depth is the maximum depth of each tree; $min_samples_split$ is the minimum number of samples required for internal node subdivision; $colsample_bytree$ is the percentage of all features used in training each tree.

$scale_pos_weight$ is the weight of positive samples; min_leaf_weight is the sum of the minimum sample weights of the leaf nodes. $gamma$ is the penalty coefficient, namely, the minimum loss function decline value required by node partitioning; $subsample$ is the percentage of subsamples used to train each tree to the total sample; reg_alpha is the regularization coefficient of L1; reg_lambda is the regularization coefficient of L2. In the binary classification task, when the proportion of positive and negative samples is unbalanced, the weight of positive samples is set to achieve a better model effect.

Initialization parameters: $n_estimators$ equals 100; max_depth equals 1; $learning_rate$ equals 0.3; $subsample$ equals 0.7; $colsample_bytree$ is set to 0.7; min_leaf_weight equals 1; $gamma$ equals 1; reg_alpha equals 1; and reg_lambda equals 1. The sample size of the training set is set to 9762, and the sample size of the test set is set to 4184. The model is fitted, and the model accuracy rate is 0.8936. To obtain better results, the parameter tuning process for XGBoost is as follows.

- (1) Parameter max_depth is set from 3 to 10; the step size is set 1; min_child_weight is set from 1 to 6; and the step size is set 1. The result of parameter tuning is shown in Table 5. The optimal max_depth is set to 4, and min_child_weight is set to 1.
- (2) Parameter $gamma$ is set from 0 to 0.5, and the step size is 0.1. The results are shown in Table 6. The best value of $gamma$ is 0.
- (3) The values of the $subsample$ and $colsample_bytree$ are set from 0.7 to 1.0. The step size is 0.1. The results are shown in Table 7. The best value of $subsample$ is 0.9. The best value of $colsample_bytree$ is 0.9.

TABLE 4: Results of the correlation analysis.

Test	Declaration and discharge states	Duration of stay	Load states in and out of the electronic fence	Carrying	Carriage open	Speed
χ^2	5535.128	6640.536	1546.306	2758.526	2575.341	5889.093
Significance	0.000	0.000	0.000	0.000	0.000	0.000
Correlation coefficient V	0.630	0.690	0.333	0.445	0.430	0.650

TABLE 5: Results of parameter tuning with variations in *max_depth* and *min_child_weight*.

Number	Parameters	Mean_validation_score	Cv_validation_scores
0	{'max_depth':3, 'min_child_weight': 1}	0.90196681	[0.90126997 0.90266393]
1	{'max_depth': 3, 'min_child_weight': 2}	0.901761934	[0.90147481 0.90204918]
2	{'max_depth': 3, 'min_child_weight': 3}	0.90196681	[0.90106514 0.90286885]
3	{'max_depth': 4, 'min_child_weight': 1}	0.904118009	[0.90434248 0.90389344]
4	{'max_depth': 4, 'min_child_weight': 2}	0.903605818	[0.90311348 0.90409836]
5	{'max_depth': 4, 'min_child_weight': 3}	0.902581438	[0.90208931 0.90307377]
6	{'max_depth': 5, 'min_child_weight': 1}	0.903708257	[0.90434248 0.90307377]
7	{'max_depth': 5, 'min_child_weight': 2}	0.903196066	[0.90372798 0.90266393]
8	{'max_depth': 5, 'min_child_weight': 3}	0.902376562	[0.90229414 0.90245902]
9	{'max_depth': 6, 'min_child_weight': 1}	0.90299119	[0.90331831 0.90266393]
10	{'max_depth': 6, 'min_child_weight': 2}	0.902888752	[0.90290864 0.90286885]
11	{'max_depth': 6, 'min_child_weight': 3}	0.903093628	[0.90270381 0.90348361]

TABLE 6: Results of parameter tuning with variations in *gamma*.

Number	Parameters	Mean_validation_score	Cv_validation_scores
0	{'gamma': 0}	0.904118009	[0.90434248 0.90389344]
1	{'gamma': 0.1}	0.904118009	[0.90434248 0.90389344]
2	{'gamma': 0.2}	0.903810695	[0.90393281 0.90368852]
3	{'gamma': 0.3}	0.903605818	[0.90372798 0.90348361]
4	{'gamma': 0.4}	0.90350338	[0.90352315 0.90348361]
5	{'gamma': 0.5}	0.90350338	[0.90352315 0.90348361]

TABLE 7: Results of parameter tuning with variations in *subsample* and *colsample_bytree*.

Number	Parameters	Mean_validation_score	Cv_validation_scores
0	{'colsample_bytree': 0.7, 'subsample': 0.7}	0.904322885	[0.90311348 0.90553279]
1	{'colsample_bytree': 0.7, 'subsample': 0.8}	0.903913133	[0.90249898 0.90532787]
2	{'colsample_bytree': 0.7, 'subsample': 0.9}	0.904322885	[0.90393281 0.90471311]
3	{'colsample_bytree': 0.7, 'subsample': 1}	0.903913133	[0.90352315 0.90430328]
4	{'colsample_bytree': 0.8, 'subsample': 0.7}	0.904322885	[0.90311348 0.90553279]
5	{'colsample_bytree': 0.8, 'subsample': 0.8}	0.903913133	[0.90249898 0.90532787]
6	{'colsample_bytree': 0.8, 'subsample': 0.9}	0.904322885	[0.90393281 0.90471311]
7	{'colsample_bytree': 0.8, 'subsample': 1}	0.903913133	[0.90352315 0.90430328]
8	{'colsample_bytree': 0.9, 'subsample': 0.7}	0.903810695	[0.90290864 0.90471311]
9	{'colsample_bytree': 0.9, 'subsample': 0.8}	0.903913133	[0.90372798 0.90409836]
10	{'colsample_bytree': 0.9, 'subsample': 0.9}	0.904732637	[0.90393281 0.90553279]
11	{'colsample_bytree': 0.9, 'subsample': 1}	0.90299119	[0.90311348 0.90286885]
12	{'colsample_bytree': 1, 'subsample': 0.7}	0.903810695	[0.90290864 0.90471311]
13	{'colsample_bytree': 1, 'subsample': 0.8}	0.904118009	[0.90434248 0.90389344]
14	{'colsample_bytree': 1, 'subsample': 0.9}	0.904732637	[0.90413765 0.90532787]
15	{'colsample_bytree': 1, 'subsample': 1}	0.903298504	[0.90393281 0.90266393]

(4) Apply regularization to reduce overfitting and adjust the *reg_alpha* value. Set *reg_alpha* to 0.001, 0.01, 0.1, 1, and 10. The results are shown in Table 8. The best value of *reg_alpha* is 0.001.

4.1.3. *Model Comparison and Analysis.* The optimal results of each model are shown in Table 9. The prediction accuracy of XGBoost is better than that of the decision tree, random forest, and GBDT. Therefore, XGBoost is used to fit the

TABLE 8: Results of parameter tuning with variations in *reg_alpha*.

	Parameters	Mean_validation_score	Cv_validation_scores
0	{'reg_alpha': 0.001}	0.903913133	[0.90311348 0.90471311]
1	{'reg_alpha': 0.01}	0.904015571	[0.90311348 0.90491803]
2	{'reg_alpha': 0.1}	0.904015571	[0.90311348 0.90491803]
3	{'reg_alpha': 1}	0.904732637	[0.90393281 0.90553279]
4	{'reg_alpha': 10}	0.896332719	[0.89430561 0.89836066]

TABLE 9: Model comparison.

Model	Decision tree	Random forest	GDBT	XGBoost
Accuracy	0.8421	0.8769	0.8892	0.9057

prediction model of electronic waybill generation on waybill nodes.

The following is the analysis of the model results constructed by XGBoost. For dichotomy problems, the resulting sample can be divided into true-positive (TP), false-positive (FP), true-negative (TN), and false-negative (FN) examples according to the combination of its true category and model prediction category. The confusion matrix of the classification results is shown in Table 10.

The XGBoost model is used to predict the test dataset. The confusion matrix is shown in Table 11. The accuracy is 90.057%; thus, the model fitting accuracy is good.

The ROC curve is drawn by using the vertical axis as the true-positive rate (TPR) shown in equation (12) and the horizontal axis as the false-positive rate (FPR) shown in equation (13). The area under the ROC curve is the value of AUC. The closer the AUC value to 1, the better the performance and generalization ability of the model. The ROC curve is obtained as shown in Figure 3. The AUC value is 0.91, which is close to 1, indicating that the prediction model is well constructed.

$$TPR = \frac{TP}{TP + FN}, \quad (12)$$

$$FPR = \frac{FP}{TN + FP}. \quad (13)$$

A feature importance analysis can enhance the interpretability of the model, which helps establish model trust and make realistic decisions. The feature importance is obtained based on XGBoost, as shown in Figure 4. The variable f_0 is the declaration and discharge state; f_1 is the load state in and out of the electronic fence; f_2 is acceleration; f_3 is carrying; f_4 is speed; f_5 is carriage open. The declaration and discharge state and load state in and out of the electronic fence variables are the most important. Carriage open and speed are the least important.

4.2. Case Study on Hot Nodes Identification. After the electric waybill is generated, the transport trajectory of working trucks, which is recorded in the waybill, is obtained. With the bottleneck of urban roads, the path node has a complicated traffic environment. To control the important supervision positions on the construction waste transportation path, the time and space characteristics of the transport trajectory are

TABLE 10: Confusion matrix.

Actual	Prediction result	
	True	False
True	TP	FN
False	FP	TN

TABLE 11: Confusion matrix of prediction results.

True	Prediction result	
	Waybill generation	No waybill generation
Waybill generation	2368	333
No waybill generation	83	1400

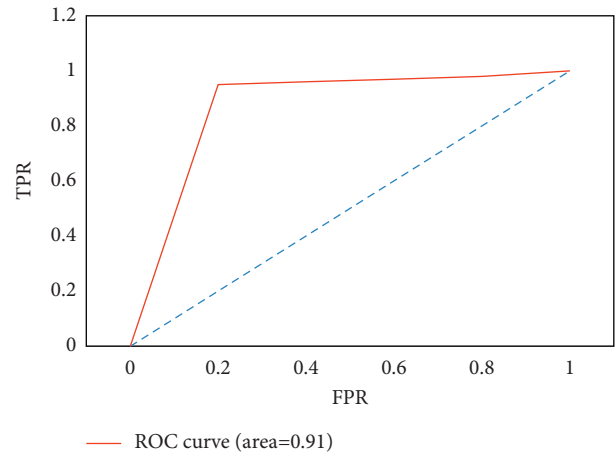


FIGURE 3: ROC curve.

analyzed. The hot nodes of the transport trajectory are developed based on the DBSCAN model. The management of important path nodes in construction waste transportation can not only improve the efficiency of construction waste transportation management but also provide a reference for the selection of construction waste transportation roads.

The thermal map [38] of the operation trajectory of the garbage trucks is shown in Figure 5. For the peak period from 13:00 to 16:00, the spatial distribution of the trajectory of the garbage truck in each period is relatively even. For the trajectory during the period from 20:00 to 21:00, the color of the spatial distribution heatmap is the darkest; therefore, the number of trajectories is obviously greater than that in other periods. Therefore, it can be concluded that the construction waste transportation task is the heaviest in this period.

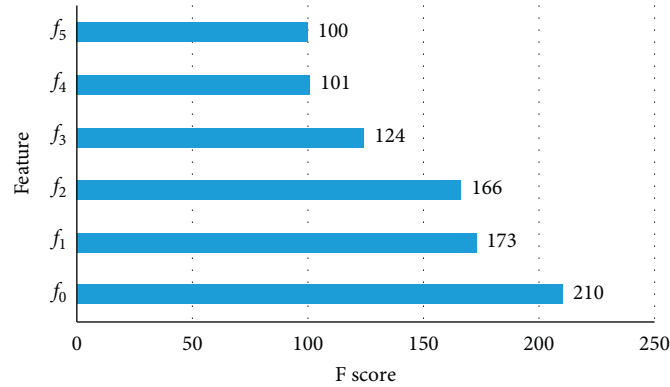


FIGURE 4: Feature importance.

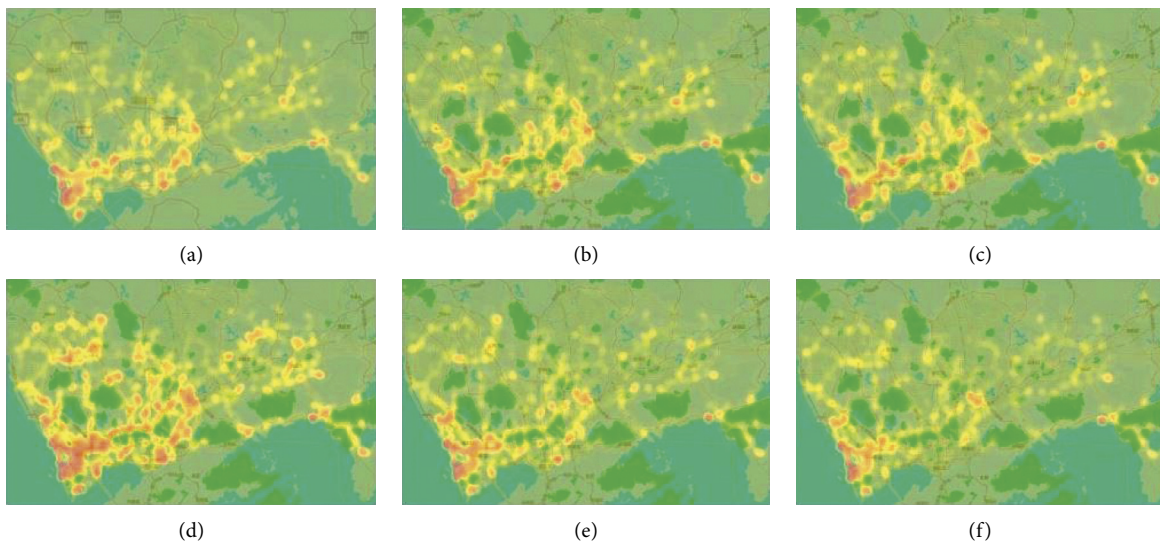


FIGURE 5: Thermal map of the spatial distribution of the operation trajectory of the garbage trucks in each period. (a) 13:00-14:00. (b) 14:00-15:00. (c) 15:00-16:00. (d) 20:00-21:00. (e) 21:00-22:00. (f) 22:00-23:00.

The clustering result of DBSCAN is related to the setting of the neighborhood radius ϵ and the minimum number of samples $MinPts$. The repeated test method is used to find the best clustering effect. According to experience, fix the minimum number of samples $MinPts$ to 100, and set different neighborhood radii ϵ to 50 meters, 100 meters, 150 meters, and 200 meters. The clustering results are shown in Table 12. The clustering results are visualized based on a scatter plot [39], as shown in Figure 6. It shows that as the radius of the neighborhood increases, the clustering number increases, and the clustering radius becomes wider. When ϵ is 50 meters, the clusters are concentrated in two districts of Shenzhen. There are only a few clusters in other districts. When ϵ is 100 meters, the number of clusters has reached 43 types, with noise accounting for 70.61%. When ϵ is 150 meters and 200 meters, there are more clusters, the proportion of noise is less than 65%, and the clustering results are broad. The number of clusters is low, which is not in line with delicacy management. Therefore, when ϵ is selected as 100 meters, the result is more reasonable.

TABLE 12: Clustering results with a minimum number of samples of 100.

$(\epsilon, MinPts)$	Clustering number	Ratio of noise points
(50, 100)	30	0.8057
(100, 100)	43	0.7061
(150, 100)	51	0.6365
(200, 100)	60	0.5336

Then, ϵ is fixed to 100 meters, and the minimum number of samples $MinPts$ is set to 50, 100, 150, and 200. The clustering results are shown in Table 13 and Figure 7. It shows that as the parameter $MinPts$ increases, the number of clusters decreases. When the minimum number of samples $MinPts$ is 50, there are too many clusters, reaching 109. When $MinPts$ is greater than 100, the number of clusters is less than 30, which means that the noise ratio is large. Therefore, considering the minimum number of samples $MinPts$ and the neighborhood radius ϵ , the parameter values selected in this study are $MinPts$ equal to 100 and ϵ equal to 100 meters.

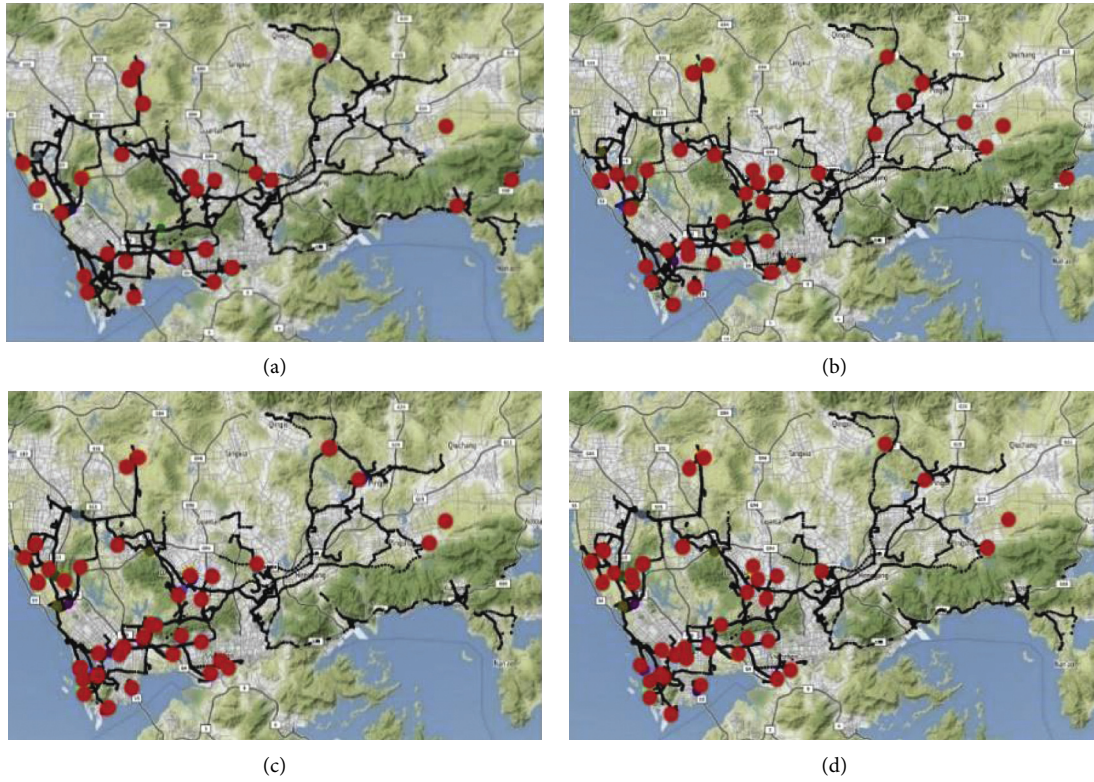


FIGURE 6: DBSCAN clustering result with a minimum number of samples of 100. (a) $\epsilon = 50$, $MinPts = 100$. (b) $\epsilon = 100$, $MinPts = 100$. (c) $\epsilon = 150$, $MinPts = 100$. (d) $\epsilon = 200$, $MinPts = 100$.

TABLE 13: Clustering results with a minimum number of samples of 100.

$(\epsilon, MinPts)$	Clustering number	Ratio of noise points
(100, 50)	109	0.5196
(100, 100)	43	0.7061
(100, 150)	25	0.7964
(100, 200)	12	0.8695

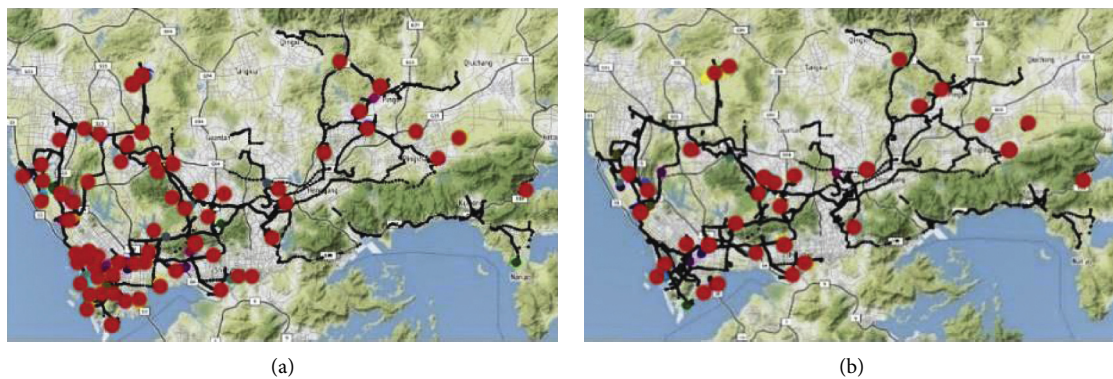


FIGURE 7: Continued.

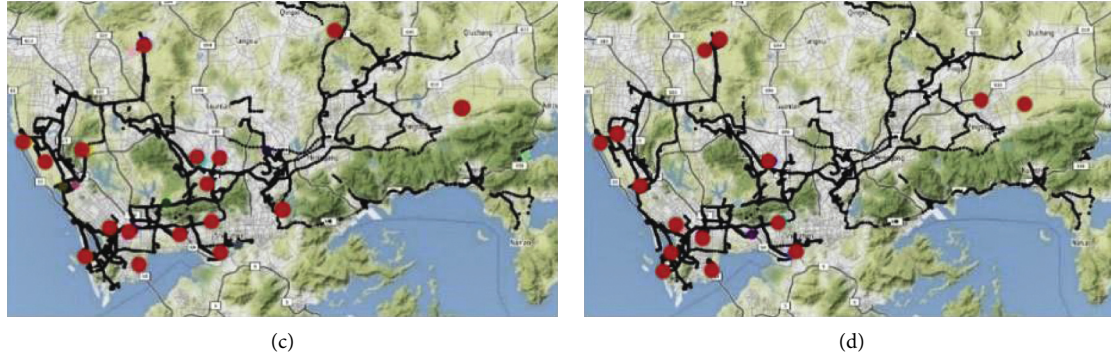


FIGURE 7: DBSCAN clustering results with ε equal to 100 meters. (a) $\varepsilon = 100$, MinPts = 50. (b) $\varepsilon = 100$, MinPts = 100. (c) $\varepsilon = 100$, MinPts = 150. (d) $\varepsilon = 100$, MinPts = 200.

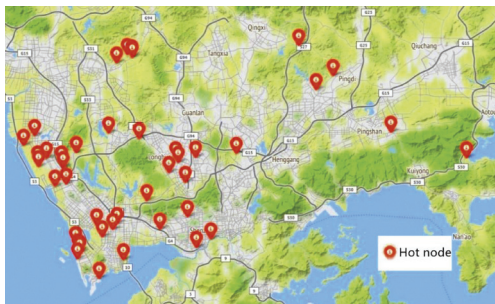


FIGURE 8: Locations of hot nodes.

Due to the density-based clustering analysis, the shape of the clustering results is often irregular. To better represent the location of the hot node, the center position of the cluster is used to represent the location of the hot node. The calculation for the construction waste transportation hot node is shown in the following equation:

$$(x', y') = \left(\frac{\sum_{i=1}^n x_i}{n}, \frac{\sum_{i=1}^n y_i}{n} \right), \quad (14)$$

where (x_i, y_i) is the position of the i -th garbage truck. n is the data number of the cluster, and (x', y') is the central location of the cluster, which is the hot node.

According to the clustering results, calculate the latitude and longitude of the center point of each cluster and mark it on the map, as shown in Figure 8. For hot nodes, managers should carry out key management to prevent irregularities in garbage trucks to reduce the impact of construction waste transportation on urban traffic.

5. Conclusion

A large amount of construction waste is generated in urban construction. Electronic waybill technology is used to manage the process of the generation, transportation, and disposal of construction waste to improve the efficiency of management. Transport trajectories, as important control roads in traffic management, occupy an important position in construction waste transportation management. To this end, the transport trajectory of working trucks is analyzed in this study. Working trucks are obtained from electronic

waybills. Improving the prediction accuracy of electronic waybill generation can improve the identification accuracy of working trucks. Therefore, the generation of electronic waybills is predicted. After obtaining the transport trajectory of working trucks, the spatial-temporal characteristics of the transport trajectory are analyzed and hot nodes are identified. Research on trajectory analyses can improve the quality of construction waste transportation management.

A case study of Shenzhen is introduced. First, a correlation analysis on the influencing factors of electronic waybill generation is conducted, and six influencing factors are found. To predict the generation of waybill, the decision tree, random forest, GBDT, and XGBoost methods are used. According to the model comparison, XGBoost is better at fitting the prediction model, and the accuracy can reach 90.06%. Then, the trajectory data during the peak period of construction waste transportation are clustered based on the DBSCAN model. The results show that the important path nodes can be found and visualized. It is helpful to identify important control positions on the transportation path of construction waste, which will improve the efficiency of transportation management. The method proposed in this study can meet the requirements of engineering practice.

Certain shortcomings were observed in this study. Hot nodes are found based on the trajectory of garbage trucks. However, path nodes that have high traffic accidents due to narrow roads and crowded people may not be considered. In future studies, road environmental factors will be added to the node analysis. Moreover, the other prediction models are tested to improve the accuracy of waybill generation. Electronic waybill technology will be improved to manage the transportation process automatically.

Data Availability

Some or all data, models, or code generated or used during the study are proprietary or confidential in nature and may only be provided with restrictions.

Conflicts of Interest

The authors declare that they have no conflicts of interest.

Acknowledgments

This article was sponsored by National Key R&D Program of China (2018YFC0706005).

References

- [1] M. S. Jain, "A mini review on generation, handling, and initiatives to tackle construction and demolition waste in India," *Environmental Technology & Innovation*, vol. 22, no. 2, Article ID 101490, 2021.
- [2] D. Tao and J. Xiao, "Estimation of building-related construction and demolition waste in Shanghai," *Waste Management*, vol. 34, no. 11, pp. 2327–2334, 2014.
- [3] J. W. Levis, "A life-cycle Analysis of alternatives for the management of waste hot-mix asphalt, commercial food waste, and construction and demolition waste," MS Thesis, Transportation Science & Technology, Raleigh, NC, USA, 2009.
- [4] J. Rogalsky, "The working poor and what GIS reveals about the possibilities of public transit," *Journal of Transport Geography*, vol. 18, no. 2, pp. 226–237, 2010.
- [5] A. Lachat, K. Mantalovas, T. Desbois et al., "From buildings' end of life to Aggregate recycling under a circular economic perspective: A comparative life cycle Assessment case study," *Sustainability*, vol. 13, no. 17, p. 9625, 2021.
- [6] F. Souza, J. Castro Mendes, L. J. B. Morais, J. S. Silva, and R. A. F. Peixoto, "Mapping and Recycling Proposal for the Construction and Demolition Waste Generated in the Brazilian Amazon," *Resources, Conservation and Recycling*, vol. 176.
- [7] L. M. Maués, N. Beltro, and I. Silva, "GHG emissions Assessment of civil construction waste disposal and transportation process in the eastern amazon," *Sustainability*, vol. 13, 2021.
- [8] D. Franco, M. Striner, and F. Assef, "Optimization in waste landfilling partitioning in Paraná State, Brazil," *Journal of Cleaner Production*, vol. 283, Article ID 125353, 2020.
- [9] M. Spišáková, P. Mésáro, and T. Mandiák, "Construction Waste Audit in the Framework of Sustainable Waste Management in Construction Projects - Case Study," *Bulidings*, vol. 11, 2020.
- [10] Z. You, C. Wu, L. Zheng, and L. Feng, "An informatization scheme for construction and demolition waste supervision and management in China," *Sustainability*, vol. 12, no. 4, p. 1672, 2020.
- [11] N. Wang, D. Lou, and D. Chen, "Preliminary study on the information management platform for precise management and control of construction waste based on "BIM+GIS" technology," *Environmental Engineering*, vol. 38, no. 3, pp. 46–50, 2020.
- [12] T. K. Wang, Z. Wu, and C. Luo, "Multi-participant construction waste demolition and transportation decision-making system," *Resources, Conservation and Recycling*, vol. 170, no. 7, Article ID 105575, 2021.
- [13] G. Zhang, *Research on the Source Characteristics and Management Strategies of Construction Waste in Underground Engineering*, Beijing Jiaotong University, Beijing, China, 2019.
- [14] T. Jiang, *Design and Implementation of Urban Construction Site Waste Supervision System Based on GIS Platform*, Huazhong University of Science and Technology, Hubei, China, 2017.
- [15] S. Bakhtyar, J. Holmgren, and J. A. Persson, "Analysis of information synergy between e-Waybill solutions and intelligent transport system services," *World Review of Intermodal Transportation Research*, vol. 4, no. 2-3, pp. 123–139, 2013.
- [16] T. Cane, S. Mattheis, G. Tsoukos, C. Focas, and I. Koliouris, "The E-Freight Multimodal E-Waybill," in *Proceedings of the Conference: efreight Conference, Munich, Transport and Logistics 2012*, Munich, DE, USA, May 2012.
- [17] W. Deng, X. Zhang, Y. Zhou et al., "An enhanced fast non-dominated solution sorting genetic algorithm for multi-objective problems," *Information Sciences*, vol. 585, pp. 441–453, 2022.
- [18] E. Q. Wu, M. C. Zhou, D. Hu et al., "Self-Paced Dynamic Infinite Mixture Model for Fatigue Evaluation of Pilots' Brains," *IEEE Transactions on Cybernetics*, 2020.
- [19] H. Cui, Y. Guan, H. Chen, and W. Deng, "A novel advancing signal processing method based on coupled multi-stable stochastic resonance for fault detection," *Applied Sciences*, vol. 11, no. 12, p. 5385, 2021.
- [20] Z. H. Zhang, F. Min, G. S. Chen, S.-P. Shen, Z.-C. Wen, and X.-B. Zhou, "Tri-partition state alphabet-based sequential pattern for multivariate time series," *Cognitive Computation*, pp. 1–19, 2021.
- [21] X. Ran, X. Zhou, M. Lei, W. Tepsan, and W. Deng, "A novel k-means clustering algorithm with a noise algorithm for capturing urban hotspots," *Applied Sciences*, vol. 11, no. 23, Article ID 11202, 2021.
- [22] R. Jia, A. Khadka, and I. Kim, "Traffic crash analysis with point-of-interest spatial clustering," *Accident Analysis & Prevention*, vol. 121, pp. 223–230, 2018.
- [23] K. G. Le, P. Liu, and L. T. Lin, "Traffic accident hotspot identification by integrating kernel density estimation and spatial autocorrelation analysis: a case study," *International Journal of Crashworthiness*, pp. 1–11, 2020.
- [24] L. Kang, G. Hu, H. Huang, W. Lu, and L. Liu, "Urban traffic travel time short-term prediction model based on spatio-temporal feature extraction," *Journal of Advanced Transportation*, vol. 2020, no. 332, 16 pages, Article ID 3247847, 2020.
- [25] E. Kidando, A. E. Kitali, B. Kutela et al., "Prediction of vehicle occupants injury at signalized intersections using real-time traffic and signal data," *Accident Analysis & Prevention*, vol. 149, Article ID 105869, 2021.
- [26] F. Cai, N. Ding, and X. Qu, "Construction of Urban Traffic Information Service System Based on WebGIS," *Applied Mechanics and Materials*, vol. 353-356, p. 2545, 2013.
- [27] K. Sai, P. Kumar, and C. Mala, "Analysis and prediction of city-scale transportation system using XGBOOST technique," *Advances in Intelligent Systems and Computing*, no. 740, pp. 341–348, 2019.
- [28] Z. Liao, H. Yong, X. Yue, H. Lu, P. Xuan, and Y. Ju, "Silico prediction of gamma-aminobutyric acid type-A receptors using novel machine-learning-based SVM and GBDT approaches," *BioMed Research International*, vol. 2016, no. 6, 12 pages, Article ID 2375268, 2016.
- [29] X. L. Ma, C. Ding, L. Sen, Y. Wang, and Y. Wang, "Prioritizing influential factors for freeway incident clearance time prediction using the gradient boosting decision trees method," *IEEE Transactions on Intelligent Transportation Systems*, vol. 18, no. 9, pp. 2303–2310, 2017.
- [30] Z. Mei, W. Ding, C. Feng, and S. Liting, "Identifying commuters based on random forest of smartcard data," *IET Intelligent Transport Systems*, vol. 14, no. 4, pp. 207–212, 2019.
- [31] M. Chikaraishi, P. Garg, V. Varghese et al., "On the Possibility of Short-Term Traffic Prediction during Disaster with

- Machine Learning Approaches: An Exploratory Analysis,” *Transport Policy*, vol. 98, 2020.
- [32] Q. Jin, X. Fan, J. Liu, Z. Xue, and H. Jian, “Estimating tropical cyclone intensity in the south China sea using the XGBoost model and FengYun satellite images,” *Atmosphere*, vol. 11, no. 4, p. 423, 2020.
- [33] H. Chen, H. Chen, Z. Liu, X. Sun, and R. Zhou, “Analysis of factors affecting the severity of Automated vehicle crashes using XGBoost model combining POI data,” *Journal of Advanced Transportation*, vol. 2020, no. 8, Article ID 8881545, 2 pages, 2020.
- [34] B. Sun, T. Sun, and P. Jiao, “Spatio-temporal segmented traffic flow prediction with ANPRS data based on improved XGBoost,” *Journal of Advanced Transportation*, vol. 2021, no. 1, Article ID 5559562, 24 pages, 2021.
- [35] Q. Zhu, X. Tang, and A. Elahi, “Application of the novel harmony search optimization algorithm for DBSCAN clustering,” *Expert Systems with Applications*, vol. 178, no. 11, Article ID 115054, 2021.
- [36] M. H. Rad and M. Abdolrazzagh-Nezhad, “Data cube clustering with improved DBSCAN based on fuzzy logic and genetic Algorithm,” *Information Technology and Control*, vol. 49, no. 1, pp. 127–143, 2020.
- [37] A. A. Dokuz, M. Celik, and A. Ececi, “Anomaly detection in bitcoin prices using DBSCAN Algorithm,” *European Journal of Science and Technology*, pp. 436–443, 2020.
- [38] X. Chen, T. A. Warner, and D. J. Campagna, “Integrating visible, near-infrared and short-wave infrared hyperspectral and multispectral thermal imagery for geological mapping at Cuprite, Nevada,” *Remote Sensing of Environment*, vol. 110, no. 3, pp. 344–356, 2010.
- [39] I. Benenson, K. Martens, Y. Rofé, and A. Kwartler, “Public transport versus private car GIS-based estimation of accessibility applied to the Tel Aviv metropolitan area,” *The Annals of Regional Science*, vol. 47, no. 3, pp. 499–515, 2011.

Research Article

Rural Road Network Planning Based on 5G and Traffic Big Data

Minqing Zhu,¹ Zi Wang ,¹ Hongjun Cui ,² and Sheng Yao¹

¹School of Architecture and Art Design, Hebei University of Technology, Tianjin 300130, Tianjin, China

²School of Civil and Transportation Engineering, Hebei University of Technology, Tianjin 300401, Tianjin, China

Correspondence should be addressed to Zi Wang; 202022302008@stu.hebut.edu.cn

Received 10 January 2022; Revised 25 January 2022; Accepted 9 February 2022; Published 12 March 2022

Academic Editor: Sang-Bing Tsai

Copyright © 2022 Minqing Zhu et al. This is an open access article distributed under the Creative Commons Attribution License, which permits unrestricted use, distribution, and reproduction in any medium, provided the original work is properly cited.

In order to adapt to the healthy development of China's road network and the prosperity of the rural economy, rural roads are facing the need to continue to promote the construction of roads that reach deeper nodes. It is urgent to conduct in-depth and systematic research on the planning methods of China's rural networked roads. A road network model oriented to rural road network planning is proposed. First, the traffic demand is predicted, and then remote sensing technology and computer technology are used to evaluate the technical performance of the rural road network. The experimental results show that the comprehensive evaluation index value is 0.8 by combining the weight of each index, and the planning scheme is comprehensively evaluated. The evaluation results show that the program better supports the local social and economic development.

1. Introduction

Rural roads are an important part of the road network. Rural roads are like capillaries, spreading all over the province [1]. Realizing that road transportation finally reaches the most terminal road, it forms the entire road transportation network together with national and provincial highways and other arterial roads, thus ensuring the supply of raw materials and the circulation of commodities. It provides conditions for farmers to approach the market, reach the market, and improve their own development capabilities, as shown in Figure 1 [2]. How to build a new rural road? The first task is to plan the new rural roads. Planning is the focus of the preliminary work of all construction projects. Without systematic and comprehensive planning, there can be no good construction results [3]. On the one hand, China has formally proposed a major strategic adjustment of the working ideas and investment structure of rural road construction. It is the first large-scale rural road construction in the history of transportation development. Objectively, it is necessary to formulate a comprehensive and long-term development plan for rural roads; on the other hand, active and effective exploration in the development planning of rural roads and continuous improvement of the overall

functions of the road transportation network are also an important link in realizing the leap-forward development of transportation [4].

2. Literature Review

After the new century, we have ushered in a new era of geospatial data acquisition [5]. Liu et al. found that compared with low resolution and medium resolution remote sensing images, high-resolution images have more abundant feature information, spatial structure, and geometric texture features, which can assist us in more effective feature recognition and real-time data update [6]. Mavromoustakis et al. found that high-resolution image data have gradually become the main data source for GIS data update, target extraction, target recognition, digital mapping, and other technologies [7]. Therefore, an important research direction in the field of remote sensing discovery is how to extract objects of interest quickly and accurately from high resolution remote sensing images. Among many information that people pay attention to, the road as the basic geographic data and the important feature target is an important part of the GIS database. For a long time, the extraction of road feature information has been a hot research topic, and its

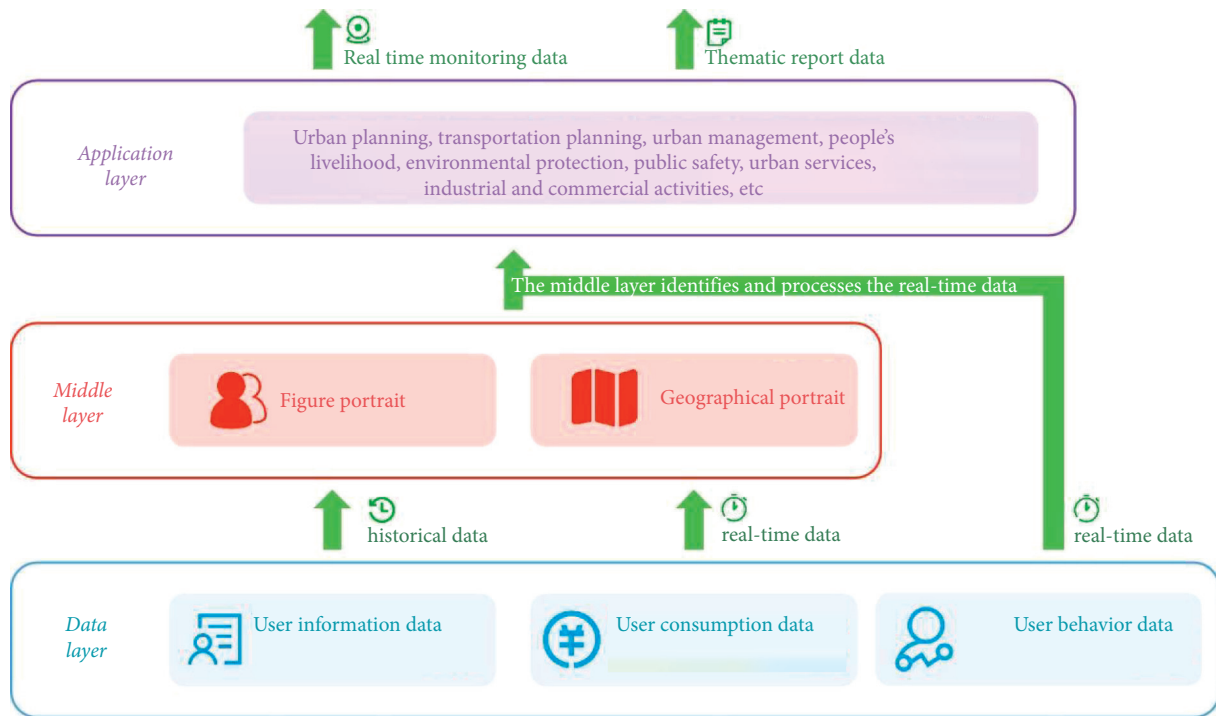


FIGURE 1: Flowchart of data operation.

importance to urban planning and construction, urban navigation, traffic management, database update, etc., is particularly prominent [8]. Park et al. found that high-resolution remote sensing images contain a large amount of extremely rich feature information, and road targets are becoming more and more clear. It breaks the limitations of incomplete details and unclear boundaries caused by low- and medium-resolution images, and basically meets the requirements of GIS data for information accuracy [9]. However, Xu et al. found that due to the increase in resolution, the detailed features of the ground objects in the image are particularly prominent, and the road presents a more complex form of expression [10]. The main characteristics of roads in high-resolution images are as follows: different materials between road segments and different spectral characteristics presented, resulting in the phenomenon of "same objects with different spectrums;" in the urban background with complex target backgrounds, many nonroad area objects show spectral features very similar to roads, with the phenomenon of "same-spectrum foreign objects;" and the different widths of main and secondary roads; all of these have made road extraction more difficult. In addition, Tang et al. found that the occlusion of vehicles, trees, and building shadows also caused interference to the extraction of roads. Extracting road information from high-resolution remote sensing images is a hot and difficult point of current research, and many research results have been achieved. In rural areas where the target background is relatively simple, because the road has a single form of expression and the spectral difference with the background is large, it is less difficult to extract [11]. Chen found that various road extraction algorithms have more or less

problems in the suburbs and urban areas with complex target backgrounds [12]. At present, Hou and Li found that the methods of extracting roads from high-resolution remote sensing images are mainly classified into classification-based methods and template matching-based methods. In the classification-based method, the main technologies involved are object-based image analysis (OBIA) and deep learning technology [13]. Meng et al. found that based on the OBIA classification for road extraction effect is largely dependent on the quality of the image segmentation results. As a preprocessing step, segmentation is also the most critical step. So far, there is no optimal segmentation algorithm to solve this problem [14]. Deep learning technology has been widely used in computer vision due to its powerful feature learning ability. Among them, a convolutional neural network (CNN) has been widely used in image classification and target detection since 2012. The use of CNN's image classification technology for road extraction has become a hot spot, and CNN can automatically perform feature learning from raw data. Liu et al. approached complex classification problems by learning a multilayer nonlinear network structure, searching for and discovering the internal structure and relationship of road targets from massive amounts of big data, which demonstrates the powerful ability to learn the essential characteristics of the dataset from the sample set. Although CNN has achieved some results in ground feature extraction, data input dimensions, network model optimization, and model parameter settings are relatively complicated, and there is no unified reference standard [15]. Because the results of road extraction by various methods are not satisfactory, the design of a new method for extracting roads quickly and

accurately from high-resolution remote sensing images still has important scientific significance and practical value. Combining the advantages of OBIA-based CNN classification and template matching technology, a new template matching method that automatically generates templates is proposed to refine the road based on OBIA-based CNN classification rough extraction. The method strives to reduce the number of manual advances as much as possible, improves the degree of automation and extraction accuracy, and meets the needs of drawing output, as shown in Figure 2.

3. Method

Road networks at all levels are not isolated. They are an organic whole. If the road network is compared to the human body circulatory system, the national road network is the active vein, and the provincial network is the main blood vessel, and blood is transported to all parts of the body through the local road network as the capillaries. Only the coordinated development of the three can work together to complete the blood circulation of the human body and protect the health of life [16], as shown in Figure 3.

According to the analysis of the actual problems faced by rural road network planning, the theory required for rural road network planning should be planned based on the social and economic development in the background and based on the existing social traffic data. The framework diagram of the rural road network planning system is shown in Figure 4.

The scope of rural road network planning is very large. However, for a certain project in a certain area, the scope of influence is small, the amount of work is small, and the construction time is short. Therefore, the exponential smoothing method suitable for medium and short-term forecasts should be used when selecting the method. The quadratic exponential smoothing method is usually used in traffic planning, and the calculation formula is as follows:

$$\begin{cases} S_0 - S_0 - X_1 \\ S_1 - aX_t + (1-a)S_{t-1} \\ S_t^n = aX_t^1 + (1-a)S_t^n - 1 \\ a = \frac{1}{N} \end{cases}, \quad (1)$$

In the above formula, X_t denotes the observation value at time t ; X_1 denotes the observation value at the first time point; N denotes the number of samples; S_t^1 denotes the linear exponential smoothing value at time t ; S_t^2 denotes the second exponential smoothing value of time t ; S_0^1 denotes the initial linear exponential smoothing value; S_0^2 denotes the initial quadratic exponential smoothing value; A denotes the smoothing factor, generally given by experience. Most of the values are between 0.01 and 0.3. Using the smoothed value to predict, the calculation formula is as follows:

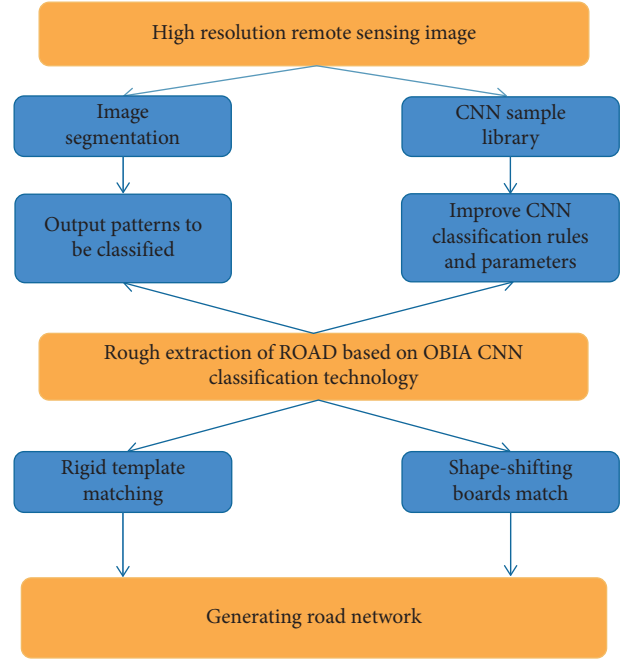


FIGURE 2: Flowchart of road extraction technology.

$$\begin{cases} Y_{t+T} = a_t + b_t T \\ a_t = 2S_t - S_t^n \\ b_t = \frac{a}{1-a} (S_t - S_t^n) \end{cases}. \quad (2)$$

In the above formula, T denotes the time t after time t ; Y_{t+T} denotes the predicted value at time T after time t ; a_t, b_t denotes the calculation factor.

Elastic coefficient method is a comprehensive analysis method which combines qualitative and quantitative methods. The traffic growth rate is predicted according to the future growth of the national economy so as to predict future traffic generation. Therefore, by analyzing the change law of economic development in the planned area and the relationship between them and transportation, we can grasp the change law of transportation demand. When determining the elasticity coefficient, the traffic volume and traffic turnover volume in the planning area are generally used as traffic indicators to analyze with the GDP of the planning area [17]. The elasticity coefficient is defined as follows:

$$E = \frac{i_y}{i_x}. \quad (3)$$

In the above formula, E denotes the elasticity coefficient; i_y denotes the annual traffic index change rate; i_x denotes the annual change rate of social and economic indicators.

The traffic index prediction formula is as follows:

$$Q_N = Q_0 (1 + E \cdot i_x)^N. \quad (4)$$

In the above formula, Q_N denotes the planning annual traffic index value; Q_0 denotes the base year traffic index

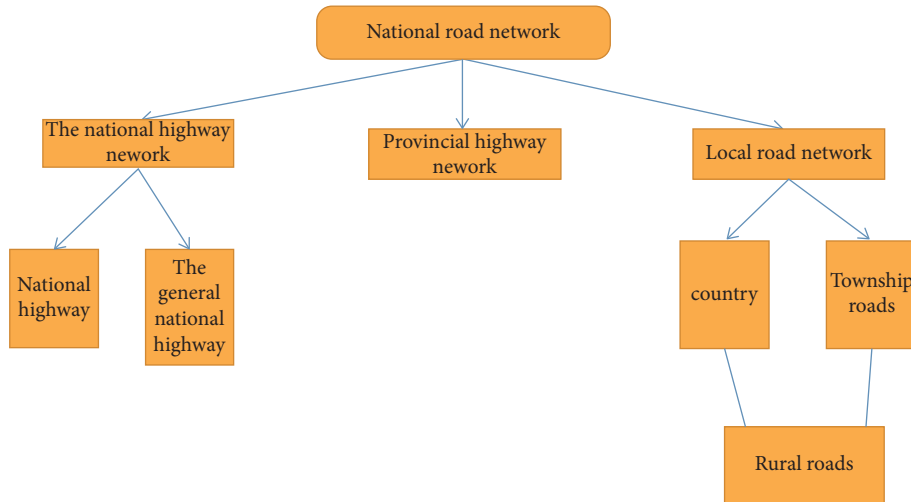


FIGURE 3: Classification of the national highway network according to administrative levels.

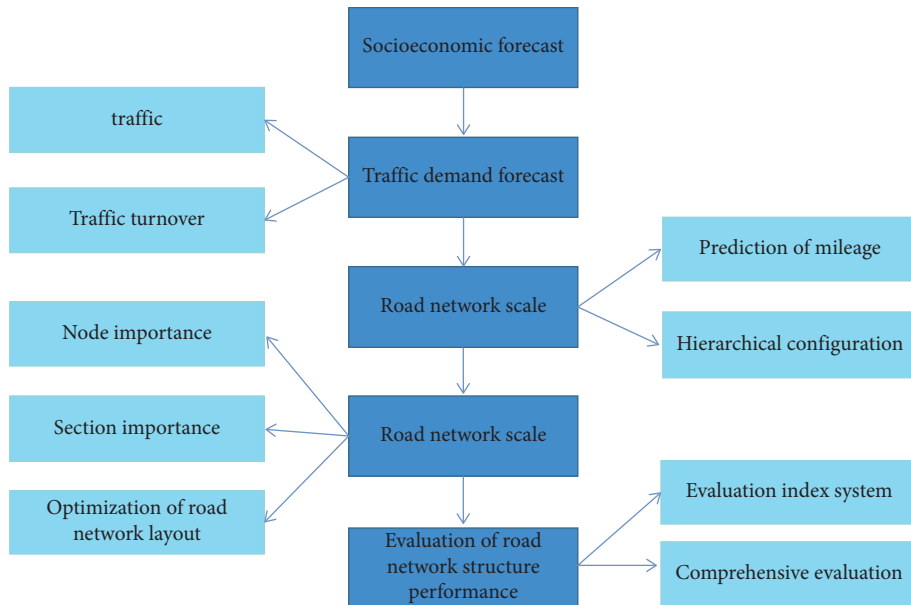


FIGURE 4: Framework diagram of rural road network planning system.

value; i'_x denotes the planning annual change rate of social and economic indicators.

The theoretical basis of the node connectivity method is network geometry, which mainly reflects the degree of connection between the road network and the nodes in the social economic network. This method considers the relationship between the area of the planned area, population, urban distribution, and other factors and the scale of the road network, and uses the connectivity value to reflect the impact of society, economy, and traffic on the scale of the road network. This method can reflect whether the road network is well connected to the nodes of the network and fully meet the requirements of the rural road network planning for the connectivity of the nodes in the road network. For the study of network geometry, the following models are established:

$$L = C \cdot \omega \cdot \sqrt{A \cdot N}. \tag{5}$$

In the above formula, L denotes the total highway mileage, kilometers; C denotes the road network connectivity; N denotes the number of nodes in the planning area; A denotes the planning area, square kilometers; ω denotes the road network deformation coefficient.

In the case of a certain planned area and node administrative division, the scale of the road network is mainly affected by the road network connectivity and the road network deformation coefficient. Each node in the planning area depends on the strength of the road interconnection, which is called the connectivity of the road network. The value of connectivity has a great influence on the total mileage. Therefore, starting from the natural geographical conditions of the planned area, it is necessary to select

appropriate road network planning parameters and not blindly pursue the improvement of node connectivity. The following figure shows the layout of the road network and nodes when different specific values of connectivity are selected [18].

According to Table 1, it is concluded that when determining the value of connectivity, the strategic planning and positioning of the entire road network must be fully considered. When the requirements of the road network are high, the value of connectivity must be large, and vice versa. Therefore, the choice of connectivity should be specifically determined according to different planning areas and different planning goals. Table 2 shows the different connectivity values of different planned target road networks.

The road network deformation coefficient is also called the nonlinear coefficient, which is the ratio of the total mileage of the actual line between the nodes to the total mileage of the straight line. It is usually the road network deformation coefficient selected qualitatively according to the actual situation and planning objectives of the planning area. Generally speaking, for areas with more complex terrain conditions, the value of the road network deformation coefficient is roughly 1.30~1.65; for areas with better terrain conditions, the value is generally 1.10~1.30.

At present, the land coefficient method is the most commonly used method to predict the reasonable scale of the road network. The model believes that the reasonable length of the regional road network is related to the level of regional economic development, population, and land area. The calculation formula is as follows:

$$L = K \cdot \sqrt{A \cdot P}. \quad (6)$$

In the above formula, L denotes the total highway mileage, kilometers; P denotes the number of people in the planning area, ten thousand; A denotes the -planning area, square kilometers; K is the economic development level coefficient.

The coefficient K of the economic development level of the highway network is determined by the statistical regression analysis of the survey data of per capita GDP. After the reasonable scale of the highway network is determined, in accordance with the socioeconomic and highway development strategy, according to specifically related factors, the multiobjective planning theory is applied to optimize various hierarchical structure schemes to determine the highway network hierarchical structure as the basis for the highway planning layout. Under normal circumstances, the determination of the highway network hierarchy mainly considers three main aspects, namely, “the least funds for the construction of the road network,” “the least travel time of the road network,” and “the greatest traffic capacity of the road network.” For other influencing factors, it can also be added or deleted to the influencing factor system based on actual conditions [19]. The optimization model of the highway network hierarchical structure is as follows:

$$f = \min[(n_1^+ + n_1^-)(n_2^+ + n_2^-)(n_3^+ + n_3^-)]. \quad (7)$$

Restrictions are as follows:

$$\sum_{j=3}^4 A_j L_j - n_1^+ + n_1^- = I + I_n, \quad (8)$$

$$\sum_{j=3}^4 C_j L_j - n_3^+ + n_3^- = Q_{NTF} | S_{NF}, \quad (9)$$

$$r_j \sum_{j=3}^4 L_j < L_j < R_j \sum_{j=3}^4 L_j, \quad (10)$$

$$\sum_{j=3}^4 L_j = L_N. \quad (11)$$

Among them, n_j^+, n_j^- denote the deviation variable; L_j denotes the J -level highway planned mileage, kilometers; A_j denotes the J -level highway construction funds, ten thousand yuan/km; I, I_N denote the available funds for road construction and conversion costs of existing roads during the planning period, 10,000 yuan; Q_{NTF} denotes the planned annual road network traffic turnover, vehicle kilometers/year; C_j denotes the J -level highway capacity, vehicles/year; S_{NF} denotes the highway network planning service level, that is, the saturation of the planned road network; r_j, R_j denote the upper and lower limits of the change in the proportion of roads of level j ($j = 3, 4$).

The model starts from three aspects: the least funds for the construction of the road network, the least travel time of the road network, and the largest traffic capacity of the road network, taking increase or decrease in the proportion of each grade of the road in the road network as a variable. The economic parameters, traffic parameters, and road parameters are used to reflect the effects of different hierarchical structures so as to complete the determination of the road network hierarchical structure and optimize the plan [20].

After node importance calculation and adjustment, the nodes are sorted according to the importance of the nodes, the functional status of different nodes in the planning area is determined, and the nodes are divided into different levels to determine the main control points of the route layout of different levels.

Identification of adjacent nodes between different levels is as follows:

$$a = \frac{\sum_{i=1}^N X}{N}. \quad (12)$$

Step 1. Merge the nodes of the adjacent level into this level and recalculate the mean value of the importance of the M nodes in the level after merging

$$b = \frac{\sum_{i=1}^M X}{M}. \quad (13)$$

Step 2. Construct a statistic:

$$t = \frac{a - b}{S(a - b)}. \quad (14)$$

TABLE 1: The layout of the road network and nodes when the connectivity takes different values.

Connectivity value	1.0	2.0	3.15	3.21
Node connectivity	Two-way connection	Four-way connection	Six-way connection	Six-way connection
Road network layout	Tree structure	Lattice structure	Lattice plus diagonal structure	Equilateral triangle structure

TABLE 2: Different connectivity values of different planned target road networks.

Road network connectivity	Low	General	High	Higher
Connectivity value	$C < 1.0$	$1.0 < C < 2.0$	$2.0 < C < 3.14$	$C > 3.14$

This quantity obeys the t distribution with $N + M - 2$ degrees of freedom, where $S(a - b)$ is

$$S(a - b) = \sqrt{\frac{(N - 1)S_1^2 + (M - 1)S_2^2}{N + M - 2}} \cdot \sqrt{\frac{1}{N} + \frac{1}{M}} \quad (15)$$

In the above formula, S_1, S_2 are the standard deviations of the importance of each node before and after the level merging.

Expressed by the weighted average of the technical grades of the various road sections in the area, the level of the road will directly affect the traffic operation of the road, as shown in Figure 5.

4. Results and Analysis

The evaluation index system of rural road network planning is composed of several indexes. The meaning of each index is different, due to the same degree of influence on the evaluation results, and the importance of the evaluation object is different. Therefore, after the evaluation index is determined, the relative importance of each index is expressed by assigning different weight values to them [21]. The determination of index weights uses the analytic hierarchy process, which integrates the qualitative and quantitative mixed problems into a unified whole for analysis and divides the entire system into a target layer, a criterion layer, and a decision-making layer. By establishing a comparison matrix to compare each element layer by layer, the weights of indicators at the criterion level and the evaluation values of each plan at the decision-making level are obtained. The calculation steps are as follows:

4.1. Building a Hierarchical Structure. The evaluation index system of rural road network planning based on the above mentioned is the hierarchical structure of evaluation, as shown in Figure 6.

4.2. Constructing a Judgment Matrix. The judgment matrix represents the relative importance between two elements. The judgment matrix $B = (b_{ij})$ is determined, where b_{ij} is the importance of B_j relative to B_i , as shown in Table 3.

The value of b_{ij} is determined by comparing the relative importance of each element. The value of b_{ij} is shown in Table 4.

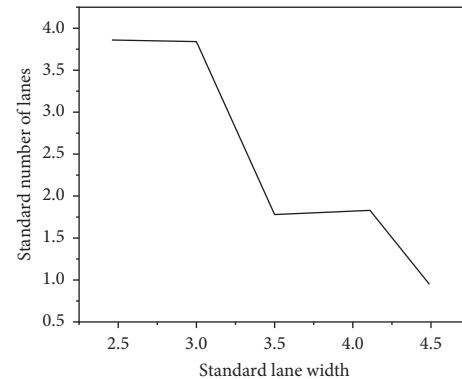


FIGURE 5: The number of standard lanes and lane widths for each class of highway.

If the weight value of each index is directly derived from the eigenvector corresponding to the maximum eigenvalue of the judgment matrix, the maximum eigenvalue of the established judgment matrix is required to be completely consistent. The steps of the consistency check method are shown in Figure 7.

Statistical analysis of social and economic indicators over the years, the use of the quadratic exponential smoothing method to predict the forecasting model, and indicator values of various indicators in the planning year are shown in Table 5:

The forecast of traffic demand mainly uses the relationship between traffic demand indicators and socioeconomic indicators, and the elastic coefficient method is used for forecasting. The traffic indicators over the years are shown in Figure 8, and the predicted models and predicted results are shown in Table 6 [22].

Comprehensive evaluation utilizes two methods: value analysis method and fuzzy comprehensive evaluation. Since only one planning plan was made for the planning area in this case, there is no selection and comparison of multiple plans. The value analysis method is directly used for comprehensive evaluation. The index values of the evaluation indexes of the scheme are processed into dimensionless processing. The dimensionless evaluation indexes are obtained after processing each evaluation index, as shown in Table 7.

Combining the weight of each index, the comprehensive evaluation index value is 0.8. It can be seen that the rural

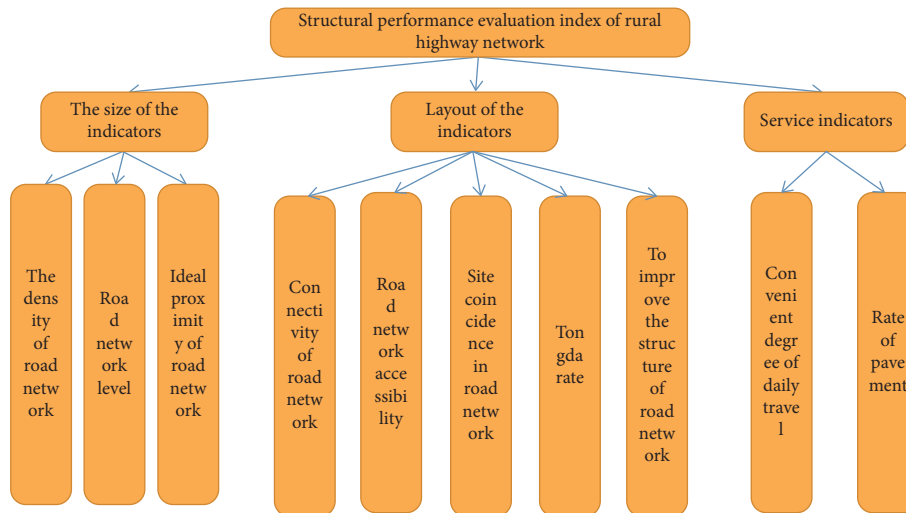


FIGURE 6: Evaluation index system diagram of rural network planning layout.

TABLE 3: NXN order judgment matrix.

A	B1	B2	...	BM
B1	B11	B12	...	B1M
B2	B21	B22	...	B2M
...
BM	BM1	BM2	...	BMM

TABLE 4: Comparison and judgment value of each element.

Scaling	Definition	Instruction
1	Equally important	By contrast, they are equally important
3	The important ones are obvious	In contrast, one of these two elements is more important than the other
5	It is very important	Of these two elements, one is clearly more important than the other
7	Extremely important	In contrast, one of these two elements is much more important than the other
9	It is very important	Comparing two elements, one is definitely more important than the other
2 4 6 8	The compromise between the above two adjacent judgments	Quantitative scale when the above two adjacent standards are compromised
The reciprocal of the above numbers	Inverse comparison	The reciprocal indicates how unimportant the two elements are when compared

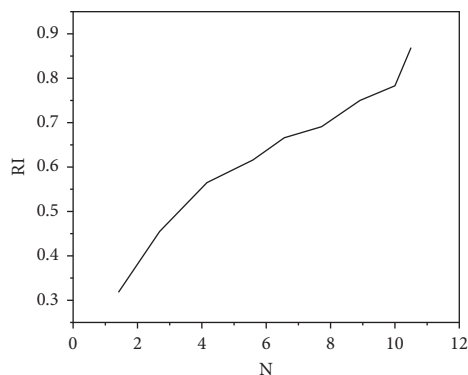


FIGURE 7: RI value selection.

TABLE 5: Socioeconomic index prediction models and index values.

Index	Predictive model	Predictor value
Population (10,000 people)	$Y = 24.01 - 0.07X$	23.65
Gross domestic product (ten thousand yuan)	$Y = 24.01 - 0.07X$	130370

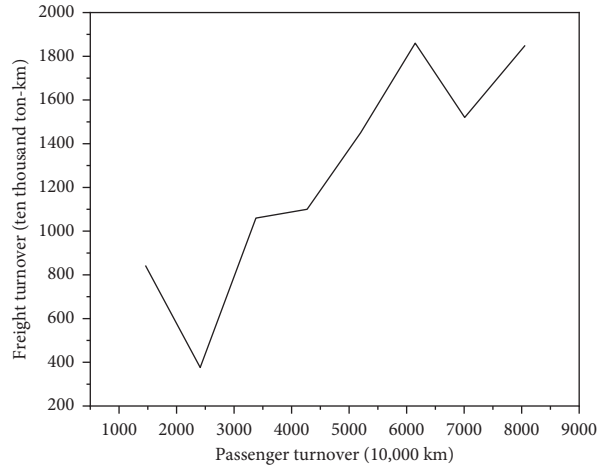


FIGURE 8: Highway passenger and freight turnover in Yuanba district over the years.

TABLE 6: Forecast models and index values of highway passenger turnover and freight turnover over the years.

Index	Predictive model	Correlation coefficient	Predictor value
Passenger turnover (10,000 people/km)	$\text{Ln}(Y) = 2.8231\text{Ln}(X) - 23.413$	0.9050	10578
Freight turnover (10,000 tons/km)	$\text{Ln}(Y) = 0.8169\text{Ln}(X) - 1.4328$	0.9414	3290

TABLE 7: Evaluation of nondimensional index value table.

Primary indicator name	Secondary indicator name	Dimensionless index evaluation value of secondary index	
Evaluation system	Road network density	0.64	
	Scale index	Road network grade level	0.81
		Road network scale	0.77
		Ideal proximity	0.73
	Layout index	Connectivity	1
		Township rate	0.8
	Service index	Completeness	1
		Pavement rate	0.6

road network planning scheme is more reasonable and can adapt to the development of social economy.

5. Conclusion

Transportation is the prerequisite for the development of rural society. As one of the infrastructures of rural society, the planning and development of rural roads are paid more attention to. The transport efficiency of road traffic is directly affected by the development of the rural road network and also directly affects the pace of rural social and economic development. This paper analyzes the characteristics of rural roads and road planning through a series of in-depth studies on the layout of rural road network planning in China, by

using remote sensing technology and computer technology. Combining with the social and economic status of my country's rural areas, the researched theory is applied to rural road planning, and the correctness of the theory in practical applications is verified. Combining the calculation of the weight of each index, the comprehensive evaluation index value is 0.8, and the planning scheme is comprehensively evaluated. The evaluation results show that the program better supports the local social and economic development.

Data Availability

No data were used to support this study.

Conflicts of Interest

The authors declare that there are no conflicts of interest with any financial organizations regarding the material reported in this manuscript.

Acknowledgments

This work was supported by Hebei Provincial High-level Talents Funding Project (project no. A201905003).

References

- [1] K. Long, V. Leung, H. Zhang, Z. Feng, Y. Li, and Z. Zhang, "5G for future wireless networks, lecture notes of the institute for computer sciences, social informatics and telecommunications engineering," in *Proceedings of the First International Conference, 5GWN 2017*, pp. 99–109, Beijing, China, April 21–23, 2017.
- [2] M. M. Rathore, A. Ahmad, A. Paul, and S. Rho, "Urban planning and building smart cities based on the internet of things using big data analytics," *Computer Networks*, vol. 101, no. C, pp. 63–80, 2016.
- [3] J. Moysen and M. García-Lozano, "Learning-based tracking area list management in 4g and 5g networks," *IEEE Transactions on Mobile Computing*, vol. 19, no. 8, pp. 1862–1878, 2020.
- [4] X. Su, L. Meng, and J. Huang, "Intelligent maritime networking with edge services and computing capability," *IEEE Transactions on Vehicular Technology*, vol. 69, no. 99, p. 1, 2020.
- [5] Y. Li, Y. Zhang, K. Luo, T. Jiang, Z. Li, and W. Peng, "Ultra-dense hetnets meet big data: green frameworks, techniques, and approaches," *IEEE Communications Magazine*, vol. 56, no. 6, pp. 56–63, 2018.
- [6] X. Liu, Q. Sun, W. Lu, C. Wu, and H. Ding, "Big-data-based intelligent spectrum sensing for heterogeneous spectrum communications in 5g," *IEEE Wireless Communications*, vol. 27, no. 5, pp. 67–73, 2020.
- [7] C. X. Mavromoustakis, G. Mastorakis, and C. Dobre, "Advances in mobile cloud computing and big data in the 5G era," *Studies in Big Data*, vol. 22, pp. 229–268, 2017.
- [8] E. Baccarelli, N. Cordeschi, A. Mei, M. Panella, and J. Stefa, "Energy-efficient dynamic traffic offloading and reconfiguration of networked data centers for big data stream mobile computing: review, challenges, and a case study," *Computers & Chemical Engineering*, vol. 91, no. 2, pp. 182–194, 2016.
- [9] S.-h. Park, S.-m. Kim, and Y.-g. Ha, "Erratum to: Highway traffic accident prediction using VDS big data analysis," *The Journal of Supercomputing*, vol. 72, no. 7, p. 2832, 2016.
- [10] F. Xu, Y. Lin, J. Huang et al., "Big data driven mobile traffic understanding and forecasting: a time series approach," *IEEE Transactions on Services Computing*, vol. 9, no. 5, pp. 796–805, 2016.
- [11] M. Tang and D. A. Niemeier, "Using big data techniques to better understand high-resolution cumulative exposure assessment of traffic-related air pollution," *ACS ESandT Engineering*, vol. 1, no. 3, pp. 436–445, 2021.
- [12] D. Chen, "Research on traffic flow prediction in the big data environment based on the improved rbf neural network," *IEEE Transactions on Industrial Informatics*, vol. 13, no. 4, p. 1, 2017.
- [13] Z. Hou and X. Li, "Repeatability and similarity of freeway traffic flow and long-term prediction under big data," *IEEE Transactions on Intelligent Transportation Systems*, vol. 17, no. 6, pp. 1–11, 2016.
- [14] W. Meng, W. Li, C. Su, J. Zhou, and R. Lu, "Enhancing trust management for wireless intrusion detection via traffic sampling in the era of big data," *IEEE Access*, vol. 6, no. 99, pp. 7234–7243, 2017.
- [15] Y. Liu, C. Yang, and Q. Sun, "Thresholds based image extraction schemes in big data environment in intelligent traffic management," *IEEE Transactions on Intelligent Transportation Systems*, vol. 22, no. 99, pp. 1–9, 2020.
- [16] G. Gui, Z. Zhou, J. Wang, F. Liu, and J. Sun, "Machine learning aided air traffic flow analysis based on aviation big data," *IEEE Transactions on Vehicular Technology*, vol. 69, no. 5, pp. 4817–4826, 2020.
- [17] E. Alomari, I. Katib, and R. Mehmood, "Iktishaf: a big data road-traffic event detection tool using twitter and spark machine learning," *Mobile Networks and Applications*, vol. 14, no. 6, pp. 1–16, 2020.
- [18] Z. Tian and S. Zhang, "Application of big data optimized clustering algorithm in cloud computing environment in traffic accident forecast," *Peer-to-Peer Networking and Applications*, vol. 14, pp. 2511–2523, 2020.
- [19] W. Queiroz, M. Capretz, and M. Dantas, "An approach for sdn traffic monitoring based on big data techniques," *Journal of Network and Computer Applications*, vol. 131, no. APR, pp. 28–39, 2019.
- [20] A. D'Alconzo, I. Drago, A. Morichetta, M. Mellia, and P. Casas, "A survey on big data for network traffic monitoring and analysis," *IEEE Transactions on Network and Service Management*, vol. 16, no. 3, p. 1, 2019.
- [21] S. Mu, Z. Xiong, and Y. Tian, "Intelligent traffic control system based on cloud computing and big data mining," *IEEE Transactions on Industrial Informatics*, vol. 15, pp. 6583–6592, 2019.
- [22] X. Zhang and Z. Yuan, "The gps trajectory data research based on the intelligent traffic big data analysis platform," *Journal of Computational Methods in Sciences and Engineering*, vol. 17, no. 3, pp. 423–430, 2017.

Research Article

Rotary Kiln Thermal Simulation Model and Smart Supply Chain Logistics Transportation Monitoring Management

Zesheng Liu 

Department of Aerospace and Mechanical Engineering, University of Southern California, Los Angeles 90001, CA, USA

Correspondence should be addressed to Zesheng Liu; zeshengl@usc.edu

Received 20 December 2021; Revised 17 January 2022; Accepted 26 January 2022; Published 16 February 2022

Academic Editor: Sang-Bing Tsai

Copyright © 2022 Zesheng Liu. This is an open access article distributed under the Creative Commons Attribution License, which permits unrestricted use, distribution, and reproduction in any medium, provided the original work is properly cited.

Rotary kiln is a large-scale instrument for industrial firing of cement. Due to its thermal insulation characteristics, this article studies the application of rotary kiln in supply chain logistics transportation. The main research focus of this paper is the thermal simulation model of rotary kiln and intelligent supply chain logistics transportation monitoring management. This paper analyzes the rotary kiln and its parameters and then designs a thermal simulation model of the rotary kiln. Then this article also combines the relationship between logistics and supply chain, studies the characteristics of supply chain, summarizes and designs a new type of smart supply chain logistics transportation method, and then applies the rotary kiln thermal simulation model to this new type of transportation method. In order to optimize its transportation efficiency and thermal insulation degree, this paper designs the supply chain optimization experiment and the rotary kiln simulation thermal numerical optimization experiment. This article also carries out the overall efficiency analysis of logistics based on DEA and analyzes the results of the experiment and applies it to the intelligent supply chain logistics transportation method of the thermal simulation model of the rotary kiln and compares this new type of transportation method with the traditional transportation method. The experimental results show that the intelligent supply chain transportation method based on the thermal simulation model of the rotary kiln improves the insulation effect by 5%–9% compared with the traditional transportation method. Compared with the traditional transportation method, the transportation efficiency of the smart supply chain transportation method based on the thermal simulation model of the rotary kiln has increased by 4%–8%.

1. Introduction

With the rapid development of economic globalization and e-commerce, global competition is becoming increasingly fierce. Enterprises must effectively optimize the supply chain to meet the current severe market demand at the lowest cost. In the modern economic environment, enterprises have realized the reasonable distribution of high logistics efficiency and production factors, ensuring low cost, low consumption, safety, strict timeliness, and complete production. This article will actively solve a series of problems in logistics management through engineering and technical methods.

This article is based on the analysis of third-party logistics application related theories and supply chain logistics application models, using advanced application models of

foreign companies. This paper theoretically puts forward the 3PL-based supply chain logistics operation mode information sharing and coordination control used in the logistics application, as well as the analysis of other aspects of the model. This article combines the research of logistics application elements and information functions to build a supply chain logistics integration framework system that supports this model. The intelligent supply chain logistics transportation based on the thermal simulation model of the rotary kiln has the characteristics of waste heat insulation and efficient transportation, which can accelerate the development of the logistics transportation industry.

In order to study the heat transfer effect of the rotary kiln, Agrawal A. proposed a calculation heat transfer model for the rotary kiln used to produce rutile titanium dioxide by calcining hydrated titanium dioxide in paste form [1]. The research is

carried out in a rotary kiln for producing rutile titanium dioxide by hydrated titanium dioxide. This article can refer to its heat transfer model for simulation experiments. Supply Chain Integration (SCI) is a management concept centered on coordination and collaboration within and between companies. The purpose of Yuen K. F. is to identify and discuss potential barriers to inhibit SCI in the maritime logistics industry [2]. Yuen K. F. studies the integration of the supply chain but does not involve much in logistics and transportation. In order to reduce transportation costs, Sarkar B. designed an integrated inventory model with a make-to-order production policy from buyer to supplier. The variable transportation cost is used as a power function of the delivered quantity, which is used to gradually reduce or consider the proportional rate data [3]. The model designed can reduce the cost of transportation, which has certain reference value for this article. Advances in mobile technology capabilities and affordability have given many Departments of Transportation (DOT) the opportunity to use these technologies to improve the time-consuming collection, recording, and distribution of project inspection information. The mobile technology system designed by Yamaura J. for project inspection is called HeadLight. The work efficiency of project inspectors using mobile technology systems has increased by 25%, the observations collected and shared have tripled, and the timeliness of daily reports and overall data availability have been improved [4]. The mobile technology designed can improve the effect of transportation inspection, but the demand for the supply chain in transportation is not perfect. The development of the COVID-19 vaccine has received great attention from countries all over the world. However, it is difficult to efficiently and safely deliver the COVID-19 vaccine to areas affected by the epidemic. Dai D. discusses vaccine transportation in a supply chain model consisting of a distributor and a retailer (clinic or hospital), where the distributor purchases the COVID-19 vaccine from the manufacturer and then resells it to the retailer [5]. Although it studies the supply chain model of vaccine transportation, it still has certain reference value for this article. Scott provides a reasonable priority method that allows a phased approach to complete the arduous task of collecting a list of previously unmanaged features and evaluating conditions [6]. Scott's method of reasonably determining priorities also has certain reference value in supply chain transportation, although it is not very useful. For research, he chooses the best quality, whose quality assurance (QA) process has a significant impact on the long-term durability and life cycle cost of the transportation project. Oechler E. aims to discuss the influencing factors of project-specific factors that are not documented in the method used by the State Department of Transportation (DOT) to optimize QA [7]. What he studied is the best quality assurance in transportation projects. This research has certain reference value in the supply chain transportation of this article and can guarantee the quality of products during transportation. The New Jersey Department of Transportation (NJDOT) developed and implemented the Integrated Drainage Information, Analysis and Management System (DIAMS). The purpose of Meegoda J.N. was to provide useful tools for managers to evaluate drainage infrastructure, to facilitate the determination of the current cost of maintaining these infrastructures, and to

make decisions on the best use of infrastructure budgets [8]. To improve the quality assurance of drainage facilities, the thermal simulation model of the rotary kiln can have a very good thermal transfer effect. From the literature cited in this article, transportation accounted for the vast majority, the thermal simulation model of the rotary kiln was not very relevant, and the supply chain level was not involved enough. Therefore, the focus of this article is on the construction of the supply chain and the application of the thermal simulation model of the rotary kiln.

The innovation of this paper is to design a thermal simulation model of the rotary kiln by using the numerical parameters of the rotary kiln and combining the characteristics of the rotary kiln. Then this article analyzes the relationship between logistics and supply chain and designs a smart supply chain logistics transportation method based on the characteristics of the supply chain. Finally, this article applies the thermal simulation model of the rotary kiln to the smart supply chain logistics transportation mode. It can not only enhance the thermal insulation effect but also enhance the efficiency of logistics and transportation. The innovation in the experiment of this paper is to design the optimization experiment of supply chain line and the numerical optimization experiment of rotary kiln simulation thermal engineering, and this article analyzes the DEA transportation efficiency and optimizes the supply chain logistics transportation of the rotary kiln simulation model based on the data obtained from the experiment.

2. Intelligent Supply Chain Logistics Transportation Monitoring Management Method

2.1. Smart Supply Chain. Due to the fierce competition among global companies, companies must effectively manage the transportation scheduling process of the supply chain to respond to the current severe market demand with the lowest cost. Properly optimizing the method of supply chain is one of the important problems that enterprises need to solve in emergency situations. Broadly speaking, the supply chain includes all activities of raw material procurement, final product manufacturing and distribution, final product manufacturing and distribution, and reverse logistics [9, 10]. Supply chain optimization scheduling [11] is the process of coordinating and controlling internal and external resources of an enterprise to meet customer needs according to market demand. Its work includes the coordination of storage and distribution of raw materials, storage and processing in the manufacturing process, and every link between the finished product from inventory to distribution center and the final customer. Figure 1 shows the structure of the supply chain.

In the traditional supply chain optimization scheduling, the decision-making of production, manufacturing, and distribution scheduling are independent of each other. The supplier stores and provides the corresponding raw materials to the manufacturer for processing and storage and finally distributes the finished product to the next level of



FIGURE 1: The structure of the supply chain.

distribution center or final customer on demand. However, the coordination between them is often ignored, which also leads to multiple conflicting or infeasible decisions in the production, manufacturing, and distribution processes in supply chain scheduling. Today, when customer requirements are constantly increasing and the transportation resources of the supply chain system are limited, traditional supply chain optimization scheduling can no longer meet the current market requirements, especially for some companies that supply perishable goods or are time-dependent.

In order to achieve a high-performance overall supply chain system under the premise of meeting customer needs [12], it is necessary to coordinate scheduling in different links of the supply chain. The effect of saving the total cost of goods through the coordinated scheduling of the supply chain links is far better than the effect of saving the cost of each link independently. Therefore, coordinated supply chain scheduling can effectively save resources and improve efficiency. Compared with the uncoordinated supply chain, the supply chain after coordinated scheduling can increase the efficiency by 5% to 20% on average. Therefore, it is necessary to make correct scheduling decisions for supply chain logistics transportation. In addition, besides the cost-saving advantages of supply chain logistics scheduling, it can also speed up the delivery time of goods and increase customer satisfaction, which is extremely conducive to increasing the company's market share. Figure 2 shows the areas involved in the supply chain.

2.1.1. Logistics. The essence of logistics [13–15] is the flow of goods and accompanying various services. Its production is not the result of theoretical research but comes from the needs of social economy and business management and has academic characteristics. Therefore, from the perspective of trade, they conducted research on theories and methods

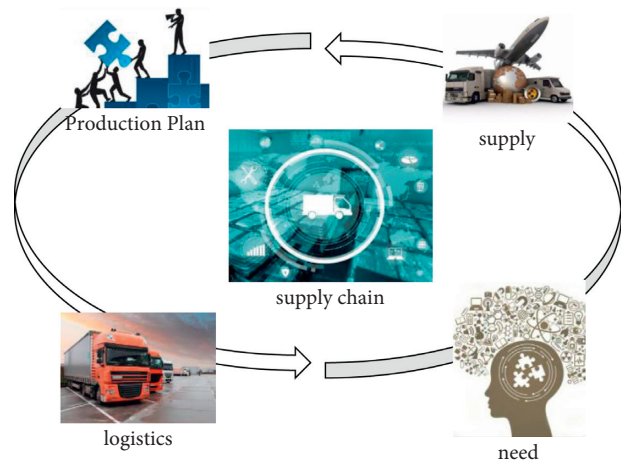


FIGURE 2: Fields involved in the supply chain.

with academic characteristics of experts and scholars involved in various logistics fields. These fields include systems engineering, circular economics, business management, transportation economics, transportation industry, information science, industrial organization, psychology, urban engineering, and accounting.

Because they have explained the concept of logistics from their respective research fields [16], there is no completely correct and widely accepted definition in the world. The definition of logistics adapts to the needs of different economic activities at various stages of economic development and is constantly evolving, adjusting, and improving. This is different even at the same stage of economic development in the same historical period. There are various definitions of logistics from different angles and viewpoints in schools, various academic groups, various institutions, and different countries. The evolution process of logistics definition also reflects the progress of logistics theory, logistics management, and logistics technology in different periods.

2.1.2. Supply Chain Management. Most manufacturing enterprises obtain the lowest possible material prices by purchasing production materials in large quantities. This method of bulk procurement can indeed reduce corporate procurement costs in the short term and obtain lower operating costs. At the same time, it will also face other corresponding increases in costs and increased management risks. The most direct is the increase in management costs caused by high inventory and the occupation of a large amount of corporate liquidity, which will directly reduce the enterprise's ability to resist risks and at the same time will have some adverse effects on the transformation and innovation of the enterprise. The supply chain management theory of manufacturing enterprises also conforms to the logistics management process of manufacturing enterprises. Enterprises can obtain the lowest possible logistics and warehousing prices by concentrating their logistics cargo resources. Compared with the supply chain management of manufacturing enterprises, this method can integrate logistics resources and effectively reduce the logistics and

warehousing costs of enterprises. At the same time, the difficulty and risk of logistics management will increase. Next, this article introduces three management theories:

(1) *Supply Chain Management Theory*. Supply chain has various meanings in various periods of enterprise development, and various scholars have various definitions. Scholars in related fields at home and abroad have defined the supply chain from various angles. The development of logistics supply chain management has gone through three stages: logistics management, value chain management, and network management. The core of operation has gradually shifted from focusing on the advantages of the enterprise itself to focusing on improving the overall value.

(2) *Logistics Outsourcing Theory*. Foreign research on logistics outsourcing [17] mainly focuses on the concept of logistics outsourcing, outsourcing motivation, outsourcing business, and improving enterprise capabilities through outsourcing. The research on the definition and concept of logistics outsourcing is implemented from the understanding of various contracts. The external provision of logistics is usually called third-party logistics, which is the outsourcing trend of logistics and is adopted by many companies. Logistics outsourcing is usually the same as contract logistics, third-party logistics, and third-party logistics providers.

Domestic research on logistics outsourcing mainly focuses on the issue of whether industrial and commercial enterprises are self-employed or outside the store. The establishment of domestic logistics research is mostly based on practice, combined with foreign supply chain management theories.

(3) *Third-Party Logistics Theory*. The concept of third-party logistics [18] (3PL or TPL) originated from business outsourcing in management. Due to traditional outsourcing, the company's logistics business has been subdivided. Logistics companies are mutually independent and difficult to adjust. The key to strategic cooperation is the information platform and the realization of information sharing, but it is difficult to achieve without a large logistics company. Under the integrated logistics operation model, logistics activities include a wide range of industries and geographic areas. It is difficult to realize the secrets of career success including reasonable logistics networks and the lack of first-class logistics companies. The logistics model is a special logistics model for core enterprises, and the ability to integrate social resources is relatively weak. The secret of successful virtual use lies in the existence of major logistics service providers.

2.1.3. Characteristics of Supply Chain Management. The characteristics of supply chain management are also very obvious. As a network system with multiagent participation, there are some of the following characteristics:

- (1) Cross-connectivity [19]: there are different nodes in the supply chain. These nodes are not only an important part of the enterprise but also an important participant in the supply chain. A cross-connected relationship is formed between different subjects;

then, it is dynamic. If it needs to continuously adapt to the ever-changing external market and meet the needs of enterprises to verify the development strategy, supply chain management has significant dynamics.

- (2) The complexity of supply chain management [20]: most of the subjects involved in supply chain construction are composed of multiple node-type enterprises of different nature, type, and scale. This also makes the structure of the supply chain present a complex side, and finally it needs to face the needs of the end users. The reason for the emergence and development of supply chain management is that, after having certain market demand, the information flow, logistics, and capital flow in the supply chain are coordinated and mobilized to meet the final needs of customers.

Simple supply chain management can be applied to all aspects of the enterprise from the emergence of the concept to the development and expansion of production-oriented enterprises. The improvement and promotion of the logistics and warehousing part cannot be studied separately from the supply chain. First of all, it is necessary to analyze the position of the logistics warehousing in the supply chain link and the functional role of the logistics warehousing in the current supply chain link. The value of logistics and warehousing in the supply chain can be exerted by adjusting the functions of logistics and warehousing, or the value of logistics and warehousing can be further improved through the adjustment and optimization of upstream and downstream supply chain links.

2.2. Thermal Simulation Model of Rotary Kiln. The rotary kiln [21] is an inclined rotary cylinder, and its structure is shown in Figure 3.

The raw material enters from the furnace end, but the cylinder has a certain inclination. In order to continuously rotate, it rolls from the furnace end to the furnace head while moving toward the axis. Therefore, the first is the material handling device. The fuel of cycloalkyl [22] is mainly coal, which is smashed and burned fiercely from the alkyl head. The high-temperature flue gas generated after combustion undergoes flow heat exchange with the material and is discharged from the alkyl group. Under the action of the induction draft fan at the tail, the raw materials transported [23] will produce a series of physical and chemical reactions. The clinker will be discharged from the quilting. The air used to burn micropowdered charcoal consists of two parts. The air heated after high-temperature heat exchange is called secondary air, which is generally about 1150°C. Figure 4 shows the rotary kiln.

So far, rotary kilns have had two main disadvantages. The first is that the heat exchange in the alkyl group is greatly affected by the ratio of wind and coal, and the heat exchange efficiency between the hot air and the materials in the alkyl group is low. The second is that the fuel burns under the conditions of high temperature and high oxygen in the firing

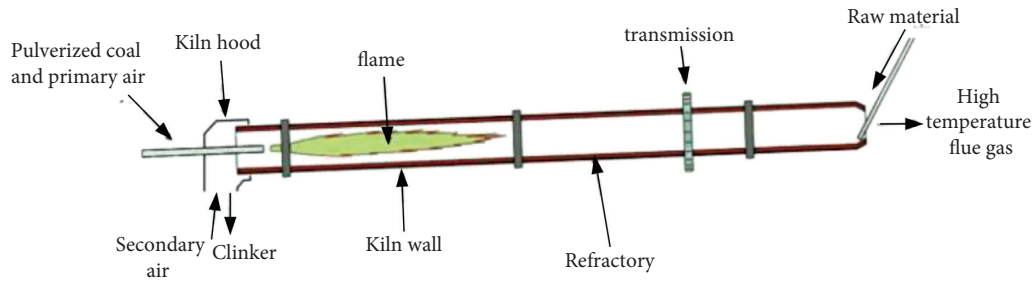


FIGURE 3: Structure diagram of rotary kiln.

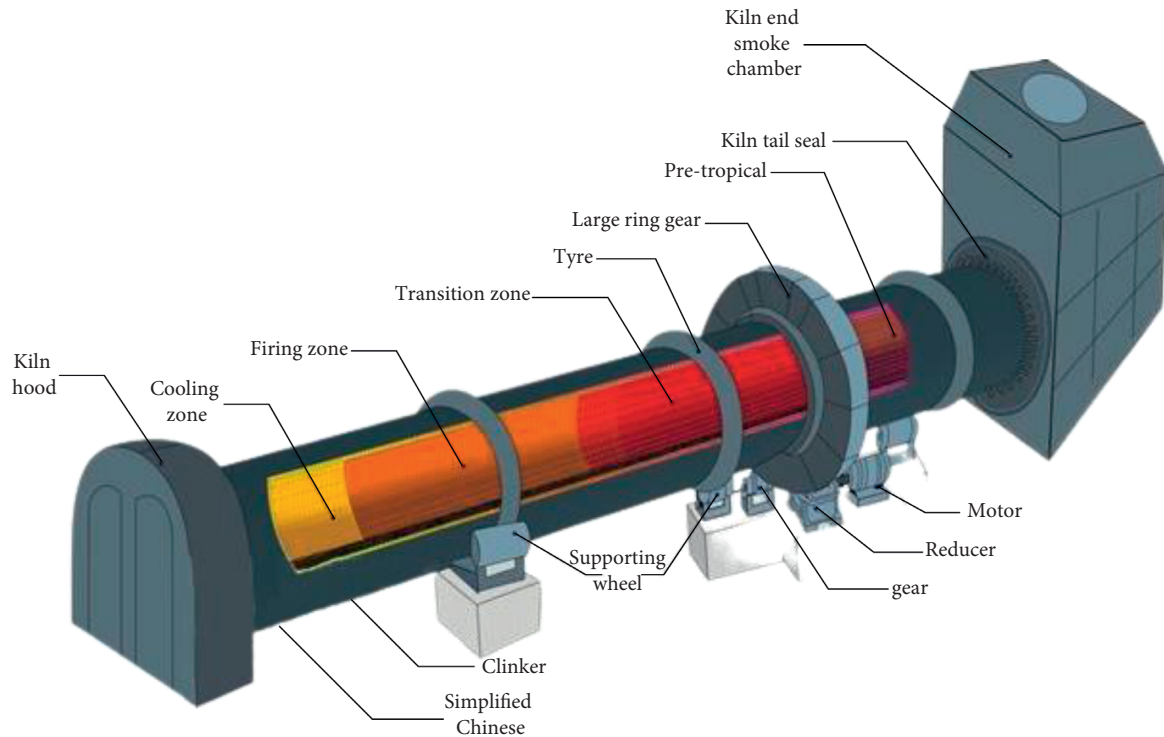


FIGURE 4: Rotary kiln.

zone of the furnace, which produces a large amount of harmful components such as NOX, which causes air pollution.

2.2.1. Analysis of Control Parameters of Rotary Kiln. Cyclic groups have many variable parameters, complicated working conditions, and combinations of various parameters. The control variables and control quantities are determined by analyzing the control parameters of the rotary kiln. The quality manufacturing process directly affects the control of the main process parameters of the rotating base.

(1) *Firing Zone Temperature.* The main control target of rotary alkanes [24] is the temperature of the material in the firing zone. There are many factors that affect the temperature of the material combustion zone, such as the amount of supply, the amount of coal injected, the amount of air, and the temperature of the kiln tail flue chamber.

(2) *Kiln End Temperature (Fume Chamber Temperature).* The temperature of the kiln end [25] (also called the temperature of the flue chamber) is one of the important characteristics of the external performance of the temperature of the firing zone.

(3) *Main Motor Current of Kiln.* The current of the main motor of the kiln can indirectly reflect the temperature of the combustion zone in the furnace and the state of the outer plate of the furnace. Since the liquid phase reaction occurs in the firing zone, the higher the temperature, the higher the liquid phase ratio of the material. The thicker the outer plate of the group, the greater the energy consumption required for the rotation of the rotating group and the higher the current of the main motor.

(4) *Secondary Air Temperature.* Secondary air [26] is the main source of air for ring groups. The stability of the secondary air temperature plays an important role in the stability of the working conditions of the ring group. The high temperature of the secondary air can heat the

pulverized charcoal to promote the combustion of the pulverized charcoal, and the secondary air supplies the oxygen required for the combustion of the pulverized charcoal.

(5) *The Amount of Coal Fed to the Kiln Head.* The amount of coal supplied is one of the most important operating variables in a rotary kiln system. The heat released by the burning of crushed coal directly affects the amount of coal supplied to alkanes.

(6) *Negative Pressure at Kiln Head.* In the circular chain system, the negative pressure of the kiln head is an important parameter. If the negative pressure of the kiln head is too large, the oxygen content in the kiln is insufficient, and the crushed coal cannot be burnt completely. The furnace head pressure is too low, and it may even be damaged by positive pressure.

(7) *Kiln Speed and Raw Meal Feed Rate.* In a normal operating rotary kiln, the speed of the radicals is usually not changed, and the supply of raw coal can be manually adjusted as needed. If an abnormality occurs, the kiln system must adjust the speed of the furnace within time to maintain the stability of the thermal system. In addition, the speed of the kiln must be proportional to the amount of raw food.

2.2.2. Waste Heat Utilization Method. According to different heat sources, waste heat recovery and converter utilization are divided into grate heat recovery, cylinder surface heat recovery, furnace cooler exhaust heat recovery, and waste heat recovery according to the purpose of reuse [27].

The temperature of the low-temperature exhaust gas discharged from the circular chain is generally between 200 and 300°C. As shown in Figure 5, this part of the low-grade heat can be recycled and reused in the exhaust hot water system. The recovered heat can be used as heating in winter. On the other hand, it can also be used to heat household bath water and heat exhaust boiler water supply.

During production, the high-temperature exhaust gas in the rotating tail is mainly reused as a heat source for preheating the raw material powder, or it is mixed with the high-temperature air of the tail air conditioner and reused in the decomposition furnace. Either way, it is a method of applying exhaust gas to the preheating of the current process. In addition, the exhaust gas can also be used as the heat source of the evaporator after dust removal, and it can be added to the heat rejection power generation system to heat the water supply. After heat collection, the temperature of the exhaust gas drops from 600°C to about 400°C. It is released into the atmosphere by smoking. After the steam recovery is stored in the exhaust heat, it enters the steam turbine to generate electricity.

During operation, if the surface temperature of the rotating group may reach 300–500°C, then forced cooling by a fan or natural air cooling to cool the body

will form the heat island effect of the group body. It not only reduces the temperature drastically but also deteriorates the working environment. The collector-type body surface waste heat recovery system can not only reduce the problem of high temperature pollution but also realize the recovery and reuse of energy. Hot water or hot air is transported through pipes for production and life. In this way, not only the fuel and electricity costs of the machine are saved, but also the emissions of CO₂ and dust are reduced. Economic and environmental efficiencies are both very important.

The heat rejection power generation system alleviates the contradiction of power shortage to a certain extent, with relatively low cost and high efficiency. Compared with this, the cogeneration method is more suitable for the waste heat recovery system of complete equipment. As shown in Figure 6, it combines the high-temperature and high-pressure main steam supplied from the kiln-side boiler to be put into the steam turbine. In addition, the low-pressure auxiliary steam of the steam turbine is supplied by the boiler, and they generate electricity together. By adjusting the vacuum degree of the capacitor, it can adapt to the heating season and nonheating season. By reducing the vacuum degree of the condenser, the temperature of the circulating cooling water is raised to the heating standard, and the valve is opened to deliver the warm water to the heat users. In addition, the original vacuum of the condenser is restored, the valve sent to high-temperature users is closed, and the circulating cooling water flows into the cooling tower for cooling.

2.3. Establishment of Logistics Mathematical Model. In order to reasonably select logistics distribution centers that can meet the production of branch products in the existing regions, it has reached a reasonable match between more complex supply and demand, and, in order to form the optimal path, the basic location strategy is determined [28]. Among them, Wx is the fixed cost of the logistics center x ; Fx is the distribution center; y is the fixed cost; Q is the material flow processed by the logistics center x ; inside Ry is the material flow processed by the distribution center y . Cx is the cost from logistics center x to distribution center y ; Cyn is the cost from distribution center y to sales store; S is the number of logistics $a1$ centers to be built; T is the number of distribution centers to be built. $v \max x$ is the maximum logistics processing capacity of logistics center x ; $y \max x$ is the maximum logistics processing capacity of distribution center y ; $P1, P2$ are the correlation factors between the processing costs of the logistics center and the distribution center and the total logistics flow, and $P1, P2 \in (0, 1/2)$ is generally taken as $1/2$. $\theta(1)$ and $\theta(2)$ are the unit processing costs of the logistics center and the distribution center, respectively.

According to the fuzzy programming problem [29], the following mathematical model is established:

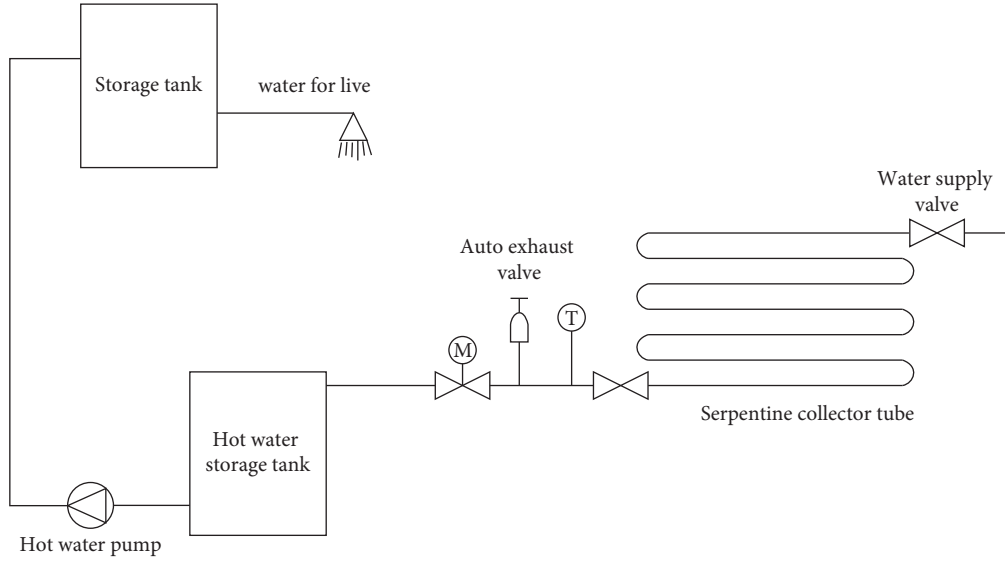


FIGURE 5: Schematic diagram of waste heat hot water system.

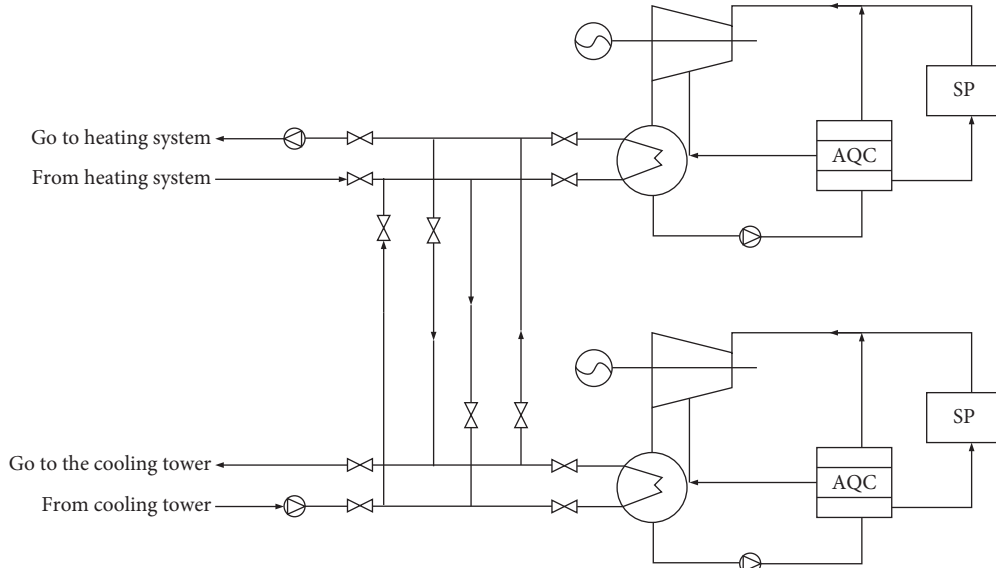


FIGURE 6: Schematic diagram of operating thermal system of waste heat power generation system.

$$\min = \sum_{x=1}^b N_x W_x + \sum_{y=1}^a M_y F_y + \sum_{x=1}^b N_x \theta(1)(Q_i)^{P1} \quad (1) \quad \sum_{x=1}^b f_{xy} \leq M_y V(2), \quad \forall_y \in Y, \quad (4)$$

$$+ \sum_{y=1}^a M_y \theta(2)(R_y)^{P2}. \quad \sum_{y=1}^a f_{xy} \leq q_x, \quad \forall_x \in X, \quad (5)$$

The constraints are

$$\sum_{x=1}^b q_x \leq \tilde{K}, \quad (2) \quad \sum_{p=1}^P f_{xy} \leq \sum_{y=1}^b f_{xy}, \quad \forall_x \in Y, \quad (6)$$

$$q_x \leq N_x V(1), \quad \forall_x \in X, \quad (3) \quad q_x + \sum_{y=1}^a f_{xy} = Q_i, \quad \forall_y \in X, \quad (7)$$

$$\sum_{x=1}^b f_{xy} + \sum_{p=1}^p f_{xy} = R_y, \quad \forall y \in Y, \quad (8)$$

$$\sum_{p=1}^p f_{xy} = \bar{D}_p, \quad \forall p \in P, \quad (9)$$

$$\sum_{x=1}^b N_x = S, \quad (10)$$

$$\sum_{y=1}^a M_y = T,$$

$$q_x, f_{xy}, f_{yp} \geq 0; N_x, M_y = \{0, 1\}. \quad (11)$$

Formula (2) indicates that the total amount of logistics flowing out of the factory must meet the constraints of the factory's production capacity. Formulas (3) and (4), respectively, indicate that the inflow of each logistics center and distribution center cannot exceed the maximum capacity. Formulas (5) and (6) indicate that the material flow of the logistics center and distribution center cannot exceed the inflow. Formulas (7) and (8) are the total workload of each logistics center and distribution center. Formula (9) indicates that the process from the distribution center to each point of sale needs to meet the needs of customers. Formulas (10) and (11), respectively, represent the numbers of planned logistics centers and distribution centers.

The fuzzy programming problem can be transformed into the following fuzzy chance constraint problem (model 2):

$$\min \tilde{f}, \quad (12)$$

$$\text{Pos} \left\{ \left[F_o(\cdot) + \sum_{y=1}^a \sum_{p=1}^p \tilde{f}_{yp} C_{yp} \right] \leq \tilde{f} \right\} \geq \alpha, \quad (13)$$

$$\text{Pos} \left\{ \sum_{x=1}^b q_x \leq \tilde{p} \right\} \geq \beta, \quad (14)$$

$$\text{Pos} \left\{ \sum_{y=1}^a f_{xy} = \bar{D}_p \right\} \geq \gamma, \quad (15)$$

$$F_o(\cdot) = \sum_{x=1}^b N_x W_x + \sum_{y=1}^a M_y F_y + \sum_{x=1}^b N_x \theta(1)(Q_i)^{P1} + \sum_{y=1}^a M_y \theta(2)(R_y)^{P2} + \sum_{x=1}^b \sum_{y=1}^a C_{xy} f_{xy}. \quad (16)$$

Other constraints are the same as formulas (3)~(8) and formulas (10)~(11) in model 1. Pos{·} is the probability of the event in {·} being established.

Since the demand of each point of sale is a triangular fuzzy number, it can be seen from the addition and multiplication of fuzzy numbers that the flow of goods from the circulation center must also be a triangular fuzzy number, denoted as $(f\dot{y}p, f\ddot{y}p, f\check{y}p)$.

The target opportunity constraint (13) is transformed into the following clear equivalence class:

$$F_o(\cdot) + \sum_{y=1}^a \sum_{p=1}^p C_{yp} \times (f\dot{y}p(1-\alpha) + \alpha f\check{y}p) \leq \tilde{f}. \quad (17)$$

Constraint (14) is converted into the following clear equivalence class:

$$\sum_{x=1}^b q_x \leq (1-\beta)P_3 + \beta P_2. \quad (18)$$

Constraint (15) is converted into the following clear equivalence class:

$$\begin{aligned} \sum_{y=1}^a \sum_{p=1}^p f_{yp} &\geq \sum_{y=1}^a \sum_{p=1}^p [(1-\gamma)f\dot{y}p + r f\check{y}p], \\ \sum_{y=1}^a \sum_{p=1}^p f_{yp} &\leq \sum_{y=1}^a \sum_{p=1}^p [(1-\gamma)f\ddot{y}p + r f\check{y}p]. \end{aligned} \quad (19)$$

3. Experiments on Smart Supply Chain Logistics and Transportation Methods That Optimize Thermal Simulation Models of Rotary Kilns

3.1. Optimizing the Circuit Experiment. In order to study the route optimization of the intelligent supply chain logistics transportation based on the thermal simulation model of the rotary kiln, this paper designs a comparative experiment of three transportation schemes. One is all straight hair, another is actual operation, and the last is the optimized scheme designed in this article. The comparison results of the three schemes at different flow rates are shown in Figure 7.

It can be seen from this figure that the average flow of each flow segment in the optimization plan is lower than the average flow of all direct distribution and actual transportation plans. The production line processes of all direct distribution plans are mainly concentrated in the $0 < P < 1T$ and $1 < P < 4T$ stages, and the actual transportation plan is concentrated in the $4 < P < 10T$ and $P > 10T$ stages; the optimized plan is concentrated in the $1 < P < 4T$ and $4 < P < 10T$ stages.

The models and algorithms proposed in this paper are suitable for logistics networks. The logistics network determines the amount of product provided to each demand point from each supply point, and the unit goods of each line are a certain piecewise function. If it knows the relationship between supply and demand and the unit of goods, it can get a better transportation plan. But, in actual use, if supply and demand change between any two locations, the entire network will change. Therefore, it is necessary to regularly update the selection of locations and transportation channels in the logistics network.

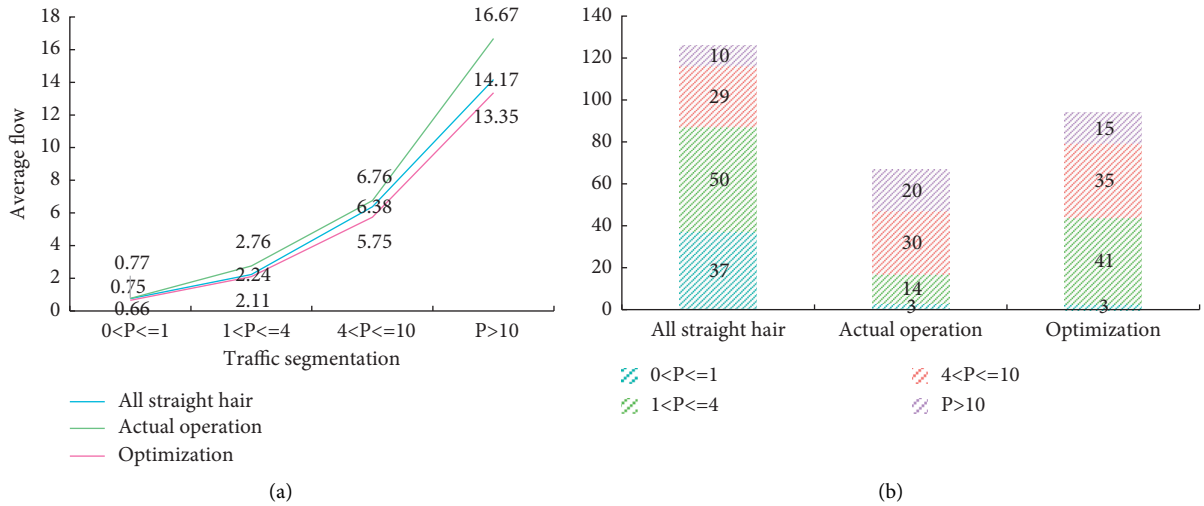


FIGURE 7: Results of the three schemes for different flow segments. (a) Comparison chart of average flow rates on different flow sections of the three plans. (b) Comparison chart of the number of lines in different traffic sections of the three schemes.

3.2. *Rotary Kiln Simulation Model Experiment.* It stores the input data in a matrix and the output data in a column vector. Then, it initializes the regularization parameters and the total width and takes 700 and 14.5 according to the test regularization parameters, and the number of samples used for modeling is 80. Every time a sample is added to the sample set, the recursive algorithm of sample increase will be used for modeling, but the first 80 sets of data will only be trained. When the number of samples in the sample set reaches 80, the temperature will be predicted and the density value corresponding to the modeled sample will be calculated. It uses a sample deletion algorithm to delete the sample with the smallest density and then deletes the new sample. It adds data to the algorithm by adding samples. In the sample collection, for the next prediction, the model will be remodeled after the sample is updated. It repeats this process and compares the 0th to 700th prediction results with the actual values, as shown in Figure 8, and draws the temperature online prediction curve.

It can be seen from the figure that the changing trends of the predicted value and the actual value are consistent and similar. In order to quantitatively obtain the deviation between the predicted value and the true value, the absolute error and the relative error of the predicted value and the true value are calculated. This is shown in Figure 9.

4. Logistics and Transportation Analysis of Smart Supply Chain Based on Thermal Simulation Model of Rotary Kiln

4.1. *The Overall Efficiency of Logistics Based on DEA.* This paper analyzes the overall efficiency of PC component input and output in three prefabricated construction projects of a component factory from 2018 to 2020 from two aspects of efficiency and projection analysis. The original data is shown in Table 1.

Starting from the comprehensive efficiency, samples 1, 2, and 3 can be seen from the table, the comprehensive efficiency is all 1, and the input redundancy and output redundancy are both 0. This shows that the sample values of 1, 2, and 3 are fully effective, and the scale efficiency DEA is effective. The return to scale shows a flat trend, the overall project operation control is effective, and no additional adjustments are needed. But, from the overall data, the output profit value is low, the growth trend is flat, the products are mostly completed within the plan, and the market operation is small. Samples 4, 5, and 6 are shown in Tables 2–4.

Samples 4, 5, and 6 show that the overall efficiency is increasing from the table. The scale efficiency DEA of samples 4 and 5 is invalid, and the scale efficiency DEA of sample 6 is valid. The sample input-output efficiency values are shown in Table 5.

From the perspective of scale efficiency, the scale efficiencies of samples 1, 2, and 3 are all 1, indicating that the PC component factory has a reasonable industrial structure planning for project A. Its effect on the output unit by optimizing various configurations is in line with actual production needs. From the informatization update of the component factory, the optimization of the production route, and the layout of the storage space in the field, the supply chain of the component factory is perfect, and the scale effect shows the improvement of scale efficiency. However, the return to scale has not actually increased under the same input. The scale efficiencies of samples 4, 5, and 6 have shown an increasing trend in three years, while the scale efficiencies in 2018 and 2019 are not DEA effective. Through the improvement of management, personnel training, and technical optimization, it continues to show positive trends in data, and the return to scale is also increasing. The scale efficiencies of samples 7, 8, and 9 are increasing year by year, and the scale efficiencies in 2018 and 2019 are not DEA valid. In the PC component factory supply chain, there are certain problems in the logistics

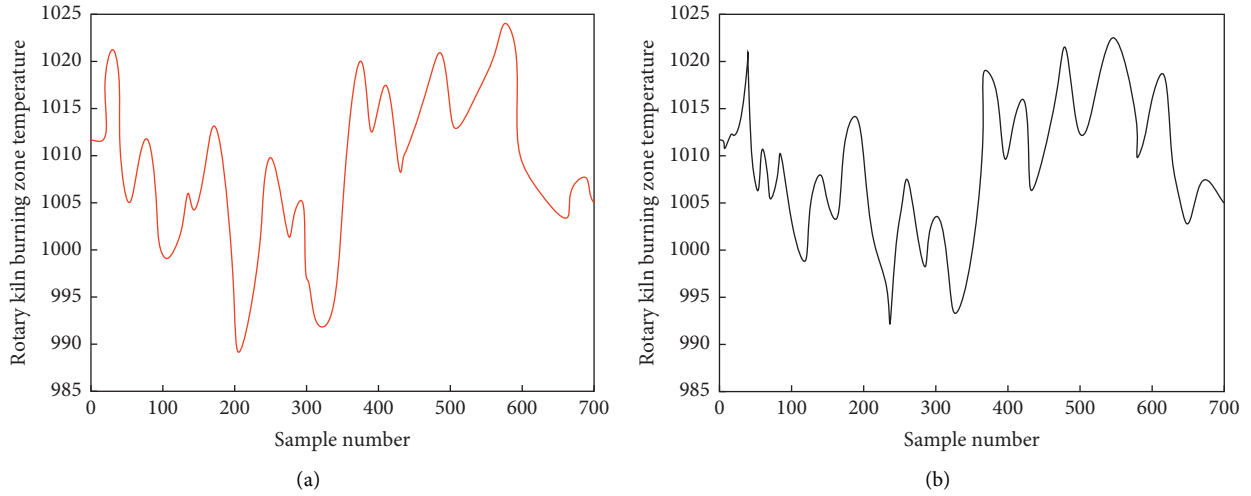


FIGURE 8: Online temperature prediction results. (a) True value. (b) Online LSSVM predicted value.

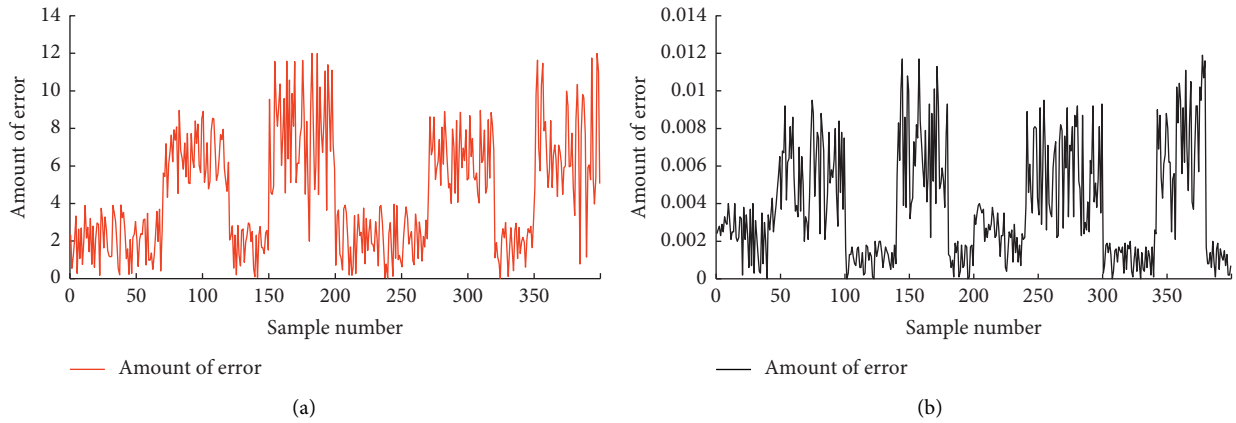


FIGURE 9: Error results between predicted and true values. (a) Absolute temperature error. (b) Relative temperature error.

TABLE 1: Project index data.

Index		P1	P2	P3	P4
Project A	2018	-1025316	13.71	1234	2316.4
	2019	-3254164	26.44	7612	5910.1
	2020	5712611	30	8344	6494.5
Project B	2018	-2238413	19.54	1354	1103
	2019	3157163	22.94	1549	1614.4
	2020	-13518474	43.61	14336	14611.0
Project C	2018	0	0	0	0
	2019	10264452	12.6	1788	619.0
	2020	15138971	17.9	1674	814.3

TABLE 2: Projection summary results of sample 4.

Variable	Original value	Slack variable	Output indicator slack variable	Target value
P1	-2246518	-751161.1	0.000	-2946311.0
P2	18.99	6.54	0.000	26.71
P3	1325	428.91	4221.91	5999.16
P4	1141	369.41	4812.64	6288.16

TABLE 3: Projection summary results of sample 5.

Variable	Original value	Slack variable	Output indicator slack variable	Target value
P1	3172111	1133185.44	0.00	4216943.44
P2	22.145	8.169	0.00	31.554
P3	1534	513.19	5316.14	8134.6
P4	1566.61	526.49	5491.34	6494.2

TABLE 4: Projection summary results of sample 6.

Variable	Original value	Slack variable	Output indicator slack variable	Target value
P1	0.000	0.000	0.000	0.000
P2	0.000	0.000	0.000	0.000
P3	0.000	0.000	0.000	0.000
P4	0.000	0.000	0.000	0.000

TABLE 5: Analysis of input-output efficiency value.

Sample	Overall efficiency	Pure technical efficiency	Scale efficiency	Return to scale
1	1	1	1	—
2	1	1	1	—
3	1	1	1	—
4	0.728	0.749	0.941	irs

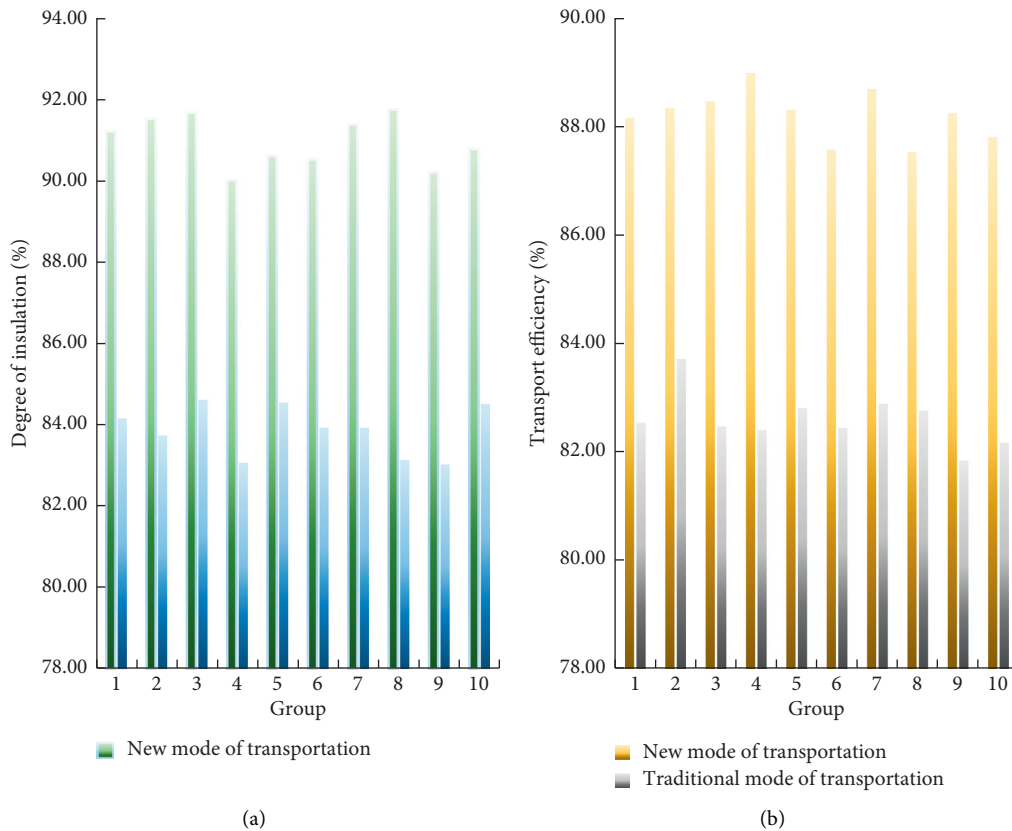


FIGURE 10: Comparison of experimental results. (a) Insulation degree comparison. (b) Transportation efficiency comparison.

transportation process such as route planning and vehicle configuration.

4.2. Comparative Experimental Analysis of Smart Supply Chain Logistics Transportation Based on the Thermal Simulation Model of Rotary Kiln. In this paper, by designing a thermal simulation model of the rotary kiln, it can be used in the logistics and transportation of the supply chain to improve the effect of goods insulation. In order to explore its thermal insulation degree and transportation efficiency, this paper designs a set of control experiments. The experiment is divided into a control group and an experimental group. The control group uses the traditional transportation method, while the experimental group uses the intelligent supply chain logistics transportation method of the rotary kiln thermal simulation model. The two groups were compared through 10 transports. The experimental results are shown in Figure 10.

It can be seen from the figure that the heat preservation degree of the smart supply chain transportation method based on the thermal simulation model of the rotary kiln can reach 90%–92%. However, the thermal insulation effect of the traditional supply chain transportation method is only 83%–85%, which shows that the thermal simulation model based on the rotary kiln improves the thermal insulation effect by 5%–9% compared with the traditional transportation method; the transportation efficiency of the smart supply chain transportation method based on the thermal simulation model of the rotary kiln can reach 87%–89%. The transportation efficiency of the traditional supply chain transportation method is only 81%–83%, which shows that the transportation efficiency based on the thermal simulation model of the rotary kiln has increased by 4%–8% compared with the traditional transportation method. Experiments show that the intelligent transportation method based on the thermal simulation model of the rotary kiln can significantly improve the thermal insulation effect and transportation efficiency during transportation.

5. Conclusions

This paper mainly studies the application of the thermal simulation model of rotary kiln and the logistics and transportation inspection management of smart supply chain. Therefore, this paper designs a thermal simulation model of the rotary kiln based on the analysis of the control parameters of the rotary kiln and the utilization of waste heat. Then this article analyzes the relationship between logistics and supply chain and designs a new intelligent supply chain logistics transportation method based on the characteristics of the supply chain. Therefore, this paper applies the designed thermal simulation model of the rotary kiln to the intelligent supply chain logistics transportation mode. In order to optimize the transportation route and the calorific value parameters of the thermal simulation model of the rotary kiln, this paper also designed the optimization experiment of the intelligent supply chain logistics transportation

mode optimization route and the calorific value parameter optimization experiment of the thermal simulation model of the rotary kiln. It then optimized the results of the experiment. Finally, the smart supply chain logistics transportation mode of the thermal simulation model of the rotary kiln was designed and compared with the traditional logistics transportation mode to verify its insulation degree and transportation efficiency.

Data Availability

No data were used to support this study.

Conflicts of Interest

The author declares that there are no conflicts of interest.

References

- [1] A. Agrawal and P. S. Ghoshdastidar, "Numerical simulation of heat transfer during production of rutile titanium dioxide in a rotary kiln," *International Journal of Heat and Mass Transfer*, vol. 106, pp. 263–279, 2017.
- [2] K. F. Yuen and V. Thai, "Barriers to supply chain integration in the maritime logistics industry," *Maritime Economics & Logistics*, vol. 19, no. 3, pp. 551–572, 2017.
- [3] B. Sarkar, B. K. Shaw, B. Kumar Shaw, T. Kim, M. Sarkar, and D. Shin, "An integrated inventory model with variable transportation cost, two-stage inspection, and defective items," *Journal of Industrial and Management Optimization*, vol. 13, no. 4, pp. 1975–1990, 2017.
- [4] J. Yamaura and S. T. Muench, "Assessing the impacts of mobile technology on public transportation project inspection," *Automation in Construction*, vol. 96, pp. 55–64, 2018.
- [5] D. Dai, X. Wu, and F. Si, "Complexity analysis of cold chain transportation in a vaccine supply chain considering activity inspection and time-delay," *Advances in Difference Equations*, vol. 2021, no. 1, pp. 39–18, 2021.
- [6] A. Scott and S. Rivers, "Corridor management: a means to elevate understanding of geotechnical impacts on system performance," *Transportation Research Record*, vol. 2349, no. 1, pp. 9–15, 2018.
- [7] E. Oechler, K. R. Molenaar, M. Hallowell, and S. Scott, "State-of-practice for risk-based quality assurance in state departments of transportation," *Engineering Construction and Architectural Management*, vol. 25, no. 7, pp. 958–970, 2018.
- [8] J. N. Meegoda, T. M. Juliano, L. Potts, C. Tang, and T. Marhaba, "Implementation of a drainage information, analysis and management system," *Journal of Traffic and Transportation Engineering*, vol. 4, no. 2, pp. 165–177, 2017.
- [9] X. Li, H. Jianmin, B. Hou, and P. Zhang, "Exploring the innovation modes and evolution of the cloud-based service using the activity theory on the basis of big data," *Cluster Computing*, vol. 21, no. 1, pp. 907–922, 2018.
- [10] S.-B. Tsai, Y.-M. Wei, and K.-Y. Chen, "Evaluating green suppliers from a green environmental perspective," *Environment and Planning B: Planning and Design*, vol. 43, no. 5, pp. 941–959, 2016.
- [11] J. Liu, H. Zhang, Z. Yao, X. Li, and J. Tang, "Thermal desorption of PCBs contaminated soil with calcium hydroxide in a rotary kiln," *Chemosphere*, vol. 220, pp. 1041–1046, 2019.
- [12] L. Qi, C. Qza, and D. Bl, "Cold chain transportation decision in the vaccine supply chain," *European Journal of Operational Research*, vol. 283, no. 1, pp. 182–195, 2020.

- [13] W. Liu, S. Wang, D. L. Zhu, W. Di, and S. Xinran, "Order allocation of logistics service supply chain with fairness concern and demand updating: model analysis and empirical examination," *Annals of Operations Research*, vol. 268, no. 2, pp. 1–37, 2018.
- [14] L. Yin, W. Pan, J. Kuang, and M. Zhuang, "Application of bootstrap-dea with fuzzy computing in performance evaluation of forklift leasing supplier," *IEEE Access*, vol. 8, 2019.
- [15] C. Yanyu, Z. Wenzhe, L. Wenbo, and H. Yimiao, "The robustness and sustainability of port logistics systems for emergency supplies from overseas," *Journal of Advanced Transportation*, 2020.
- [16] N. Hackius and M. Petersen, "Translating high hopes into tangible benefits: how incumbents in supply chain and logistics approach blockchain," *IEEE Access*, vol. 8, no. 1, pp. 34993–35003, 2020.
- [17] T. Ko, J. H. Lee, H. Cho, S. Cho, W. Lee, and M. Lee, "Machine learning-based anomaly detection via integration of manufacturing, inspection and after-sales service data," *Industrial Management & Data Systems*, vol. 117, no. 5, pp. 927–945, 2017.
- [18] J. Dobroszek, "Supply chain and logistics controller - two promising professions for supporting transparency in supply chain management," *Supply Chain Management: International Journal*, vol. 25, no. 5, pp. 505–519, 2020.
- [19] Y. Chai, Q. Li, and H. Liu, "Research on the optimisation of supply chain logistics ecosystem under short-cycle product Internet+," *Journal of Environmental Protection and Ecology*, vol. 20, no. 4, pp. 2037–2046, 2019.
- [20] Z. Chuan, F. W. Ling, and U. X. Tian, "Optimal operational strategies of capital-constrained supply chain with logistics service and price dependent demand under 3PL financing service," *Soft Computing*, vol. 24, no. 4, pp. 2793–2806, 2020.
- [21] C. Basve, "Evaluation of: a track substructure management system," *Railway Track and Structures*, vol. 113, no. 2, pp. 13–15, 2017.
- [22] U. Leopoldwildburger, "Multistep quantile forecasts for supply chain and logistics operations: bootstrapping, the GARCH model and quantile regression based approaches," *Central European Journal of Operations Research*, vol. 28, no. 1, pp. 309–336, 2020.
- [23] C. Zhang, L.-W. Fan, and Y.-X. Tian, "Correction to: optimal operational strategies of capital-constrained supply chain with logistics service and price dependent demand under 3PL financing service," *Soft Computing*, vol. 24, no. 4, p. 2807, 2020.
- [24] S. Hemapriya and R. Uthayakumar, "An inventory model with uncertain demand and lost sales reduction under service level constraint," *International Journal of Systems Assurance Engineering and Management*, vol. 8, no. 6, pp. 1–20, 2017.
- [25] M. Altun and S. Kum, "Safety indications of navigation audit for tankers to develop a bridge inspection method," *Journal of Computer and Communications*, vol. 7, no. 1, pp. 18–33, 2019.
- [26] L. Bai, R. Liu, F. Wang, Q. Sun, and F. Wang, "Estimating railway rail service life: a rail-grid-based approach," *Transportation Research Part A: Policy and Practice*, vol. 105, pp. 54–65, 2017.
- [27] I. Durazo-Cardenas, A. Starr, C. J. Turner et al., "An autonomous system for maintenance scheduling data-rich complex infrastructure: fusing the railways' condition, planning and cost," *Transportation Research Part C: Emerging Technologies*, vol. 89, pp. 234–253, 2018.
- [28] Y. Jidong, J. L. Jian, G. Manjiriker, and D. Bruce, "Modeling crack deterioration of flexible pavements: comparison of recurrent Markov chains and artificial neural networks," *Transportation Research Record*, vol. 1974, no. 1, pp. 18–25, 2018.
- [29] D.-W. Kwak, V. S. Rodrigues, R. Mason, S. Pettit, and A. Beresford, "Risk interaction identification in international supply chain logistics," *International Journal of Operations & Production Management*, vol. 38, no. 2, pp. 372–389, 2018.

Research Article

Power Allocation for 5G Mobile Multiuser Cooperative Networks

Fagen Yin ¹ and Wencai Du ²

¹College of Physical Science and Engineering, Yichun University, Yichun 336000, Jiangxi, China

²The Institute of Data Engineering and Sciences, University of Saint Joseph, Macao 999078, China

Correspondence should be addressed to Fagen Yin; ynx522@163.com and Wencai Du; george.du@usj.edu.mo

Received 15 November 2021; Revised 6 December 2021; Accepted 15 December 2021; Published 28 December 2021

Academic Editor: Sang-Bing Tsai

Copyright © 2021 Fagen Yin and Wencai Du. This is an open access article distributed under the Creative Commons Attribution License, which permits unrestricted use, distribution, and reproduction in any medium, provided the original work is properly cited.

With the fifth generation (5G) communication technology, the mobile multiuser networks have developed rapidly. In this paper, the performance analysis of mobile multiuser networks which utilize decode-and-forward (DF) relaying is considered. We derive novel outage probability (OP) expressions. To improve the OP performance, we study the power allocation optimization problem. To solve the optimization problem, we propose an intelligent power allocation optimization algorithm based on grey wolf optimization (GWO). We compare the proposed GWO approach with three existing algorithms. The experimental results reveal that the proposed GWO algorithm can achieve a smaller OP, thus improving system efficiency. Also, compared with other channel models, the OP values of the 2-Rayleigh model are increased by 81.2% and 66.6%, respectively.

1. Introduction

Recently, the increasing provision of multiuser services, the ever-increasing number of devices, and the continuous growth of data pose significant challenges to massive mobile multiuser connectivity. Fifth generation (5G) mobile communication networks are very important in achieving massive mobile multiuser connectivity [1, 2]. To meet this requirement, the boom of 5G mobile communications has resulted in the emergence of many new technologies [3–5]. Nonorthogonal multiple access and millimeter-wave communications are key aspects of 5G technology [6]. However, the complex multiuser communication environment makes the 5G mobile communication challenging.

As an alternative way to ensure reliable multiuser communication, cooperative communication has sparked a great deal of research [7]. Secrecy performance of multiple-relay cooperative communication was investigated in [8]. In [9], cooperative cognitive relaying was employed to provide secure communications. Xu et al. [10] studied the incremental decode-and-forward (DF) cooperative relay network.

To improve the multiuser cooperative communication, power allocation plays a key role [11]. Xu et al. employed the

passive beamforming to improve energy efficiency optimization in [12]. In [13], with multicarrier division, Li et al. investigated resource allocation problem. Filomeno et al. proposed two power allocation algorithms in [14].

To further improve the power allocation performance, various swarm intelligence optimization methods have been used to optimize the parameters [15]. To solve the multi-UAV task allocation problem, an improved genetic algorithm (GA) was proposed in [16]. An adaptive firefly algorithm (FA) algorithm was proposed to enhance data security in [17]. By using the golden section (GS) algorithm, Cuevas et al. optimized the evolutionary computation in [18].

However, research on power allocation optimization of mobile multiuser communications is very rare. Therefore, we investigate power allocation optimization over the 2-Rayleigh model. The main contributions are as follows:

- (1) With transmit antenna selection (TAS), we analyze the OP performance of mobile multiuser networks. New OP expressions are derived. These results are more complex than those in the Rayleigh model.
- (2) To improve the OP performance, we propose an intelligent power allocation optimization method

based on grey wolf optimization (GWO), which reduces computational complexity.

- (3) Compared with Nakagami and Rayleigh channel models, the 2-Rayleigh model has an increase of 81.2% and 66.6% in OP values, respectively. We also test the firefly algorithm (FA), the genetic algorithm (GA), and the golden section (GS) algorithm. Compared with these algorithms, our proposed GWO method achieves a smaller OP.

Table 1 shows the notations in our paper.

2. System Model

In Figure 1, N_t and N_r antennas are installed at mobile source (MS) and mobile relay (MR), respectively. There are L mobile users (MUs). The channel coefficient h follows 2-Rayleigh distribution [19]. The energy E is allocated by K . $W_{\{SUil, RUjl\}}$ are the position gains of $MS_i \rightarrow MU_l$ and $MR_j \rightarrow MU_l$, respectively.

Firstly, MU_l and MR_j receive the signals as

$$r_{SUil} = \sqrt{W_{SUil}KE}h_{SUil}\mathbf{x} + N_{SUil}, \quad (1)$$

$$r_{SRij} = \sqrt{KE}h_{SRij}\mathbf{x} + N_{SRij}, \quad (2)$$

where N_{SRij} and N_{SUil} are Gaussian noises.

Then, MR_j employs DF scheme and transmits signal to MU_l as

$$r_{RUjl} = \beta\sqrt{W_{RUjl}(1-K)E}h_{RUjl}\mathbf{x} + N_{RUjl}. \quad (3)$$

The SNR γ_{SRij} at MR_j is given as

$$\begin{aligned} \gamma_{SRij} &= \frac{K|h_{SRij}|^2 E}{N_0} \\ &= K|h_{SRij}|^2 \bar{\gamma}. \end{aligned} \quad (4)$$

If $\gamma_{Sri} < \gamma_{th}$, MU_l cannot receive the signal from MR. γ_{Sri} is given as

TABLE 1: Notations.

Notations	Designation
K	Power allocation coefficient
W	The position gain
SNR	Signal-to-noise ratio
N_t	The transmit antennas
N_r	The receive antennas

$$\gamma_{Sri} = \max_{1 \leq j \leq N_r} (\gamma_{SRij}). \quad (5)$$

MU_l receives the SNR γ_{il} as where

$$\begin{aligned} \gamma_{SUil} &= KW_{SUil}|h_{SUil}|^2 \bar{\gamma}, \\ \gamma_{RUil} &= (1-K)W_{RUil}|h_{RUil}|^2 \bar{\gamma}, \end{aligned} \quad (6)$$

where $\bar{\gamma}$ is the average SNR.

The best user is chosen from L mobile users:

$$\gamma_i = \max_{1 \leq l \leq L} (\gamma_{il}). \quad (7)$$

The TAS is employed to select w as

$$\begin{aligned} w &= \max_{1 \leq i \leq N_t} (\gamma_i) \\ &= \begin{cases} \max_{1 \leq i \leq N_t, 1 \leq l \leq L} (\gamma_{SUil}), & \text{if } |C| = 0, \\ \max_{1 \leq i \leq N_t, 1 \leq l \leq L, j \in C} (\gamma_{SUil}, \gamma_{RUjl}), & \text{if } |C| \neq 0, \end{cases} \end{aligned} \quad (8)$$

where C is given as

$$C = \{1 \leq i \leq N_t | \gamma_{Sri} \geq \gamma_{th}\}. \quad (9)$$

3. OP Performance with TAS

We obtain the OP as

$$F = Q_1 + Q_2, \quad (10)$$

where

$$\begin{aligned} Q_1 &= \left(G_{1,3}^{2,1} \left[\frac{\gamma_{th}}{K\bar{\gamma}} \Big|_{1,1,0} \right] \right)^{N_t \times N_r} \times \left(G_{1,3}^{2,1} \left[\frac{R_{th}}{KW_{SU}\bar{\gamma}} \Big|_{1,1,0} \right] \right)^{N_t \times L}, \\ Q_2 &= \sum_{n=1}^{N_t} \binom{N_t}{n} \left(G_{1,3}^{2,1} \left[\frac{\gamma_{th}}{K\bar{\gamma}} \Big|_{1,1,0} \right] \right)^{(N_t-n) \times N_r} \left(1 - \left(G_{1,3}^{2,1} \left[\frac{\gamma_{th}}{K\bar{\gamma}} \Big|_{1,1,0} \right] \right)^{N_r} \right)^n \\ &\quad \times \left(G_{1,3}^{2,1} \left[\frac{R_{th}}{KW_{SU}\bar{\gamma}} \Big|_{1,1,0} \right] \right)^{N_t \times L} \left(G_{1,3}^{2,1} \left[\frac{R_{th}}{(1-K)W_{RU}\bar{\gamma}} \Big|_{1,1,0} \right] \right)^{n \times L}, \end{aligned} \quad (11)$$

where R_{th} is a given threshold.

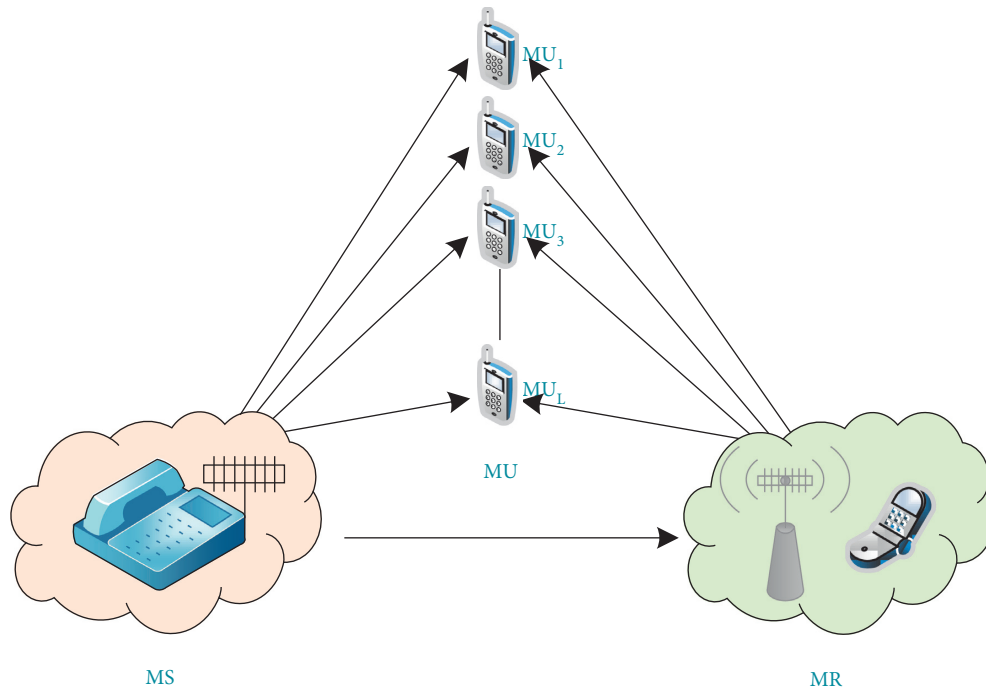


FIGURE 1: The system model.

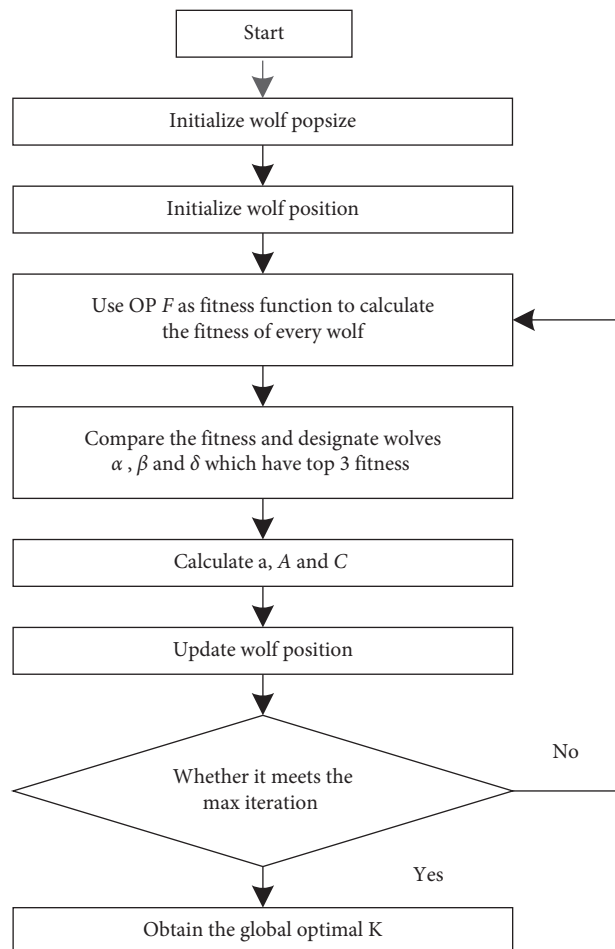


FIGURE 2: GWO algorithm.

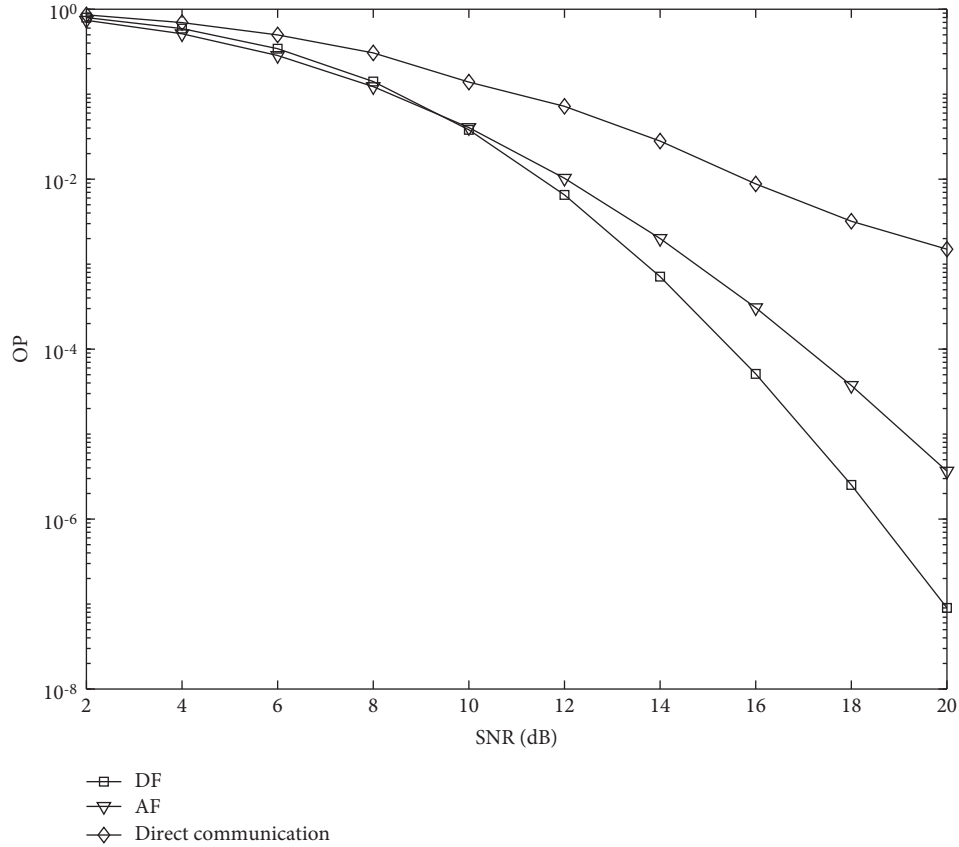


FIGURE 3: OP comparison with different schemes.

4. Power Allocation Intelligent Optimization

According to [20–22], the GWO algorithm is divided into the following parts.

4.1. *Encircling.* The encircling process is expressed as

$$\begin{aligned}
 DD &= |C \cdot XX_p(t) - XX(t)|, \\
 XX(t+1) &= XX_p(t) - A \cdot DD, \\
 A &= 2a \cdot r_1 - r_2, \\
 C &= 2 \cdot r_2,
 \end{aligned} \tag{12}$$

where $r_1, r_2 \in [0, 1]$ and $a \in [0, 2]$.

4.2. *Hunting.* The wolves renew their positions as

$$XX(t+1) = \frac{XX_1 + XX_2 + XX_3}{3}, \tag{13}$$

where

$$\begin{aligned}
 XX_1 &= XX_\alpha(t) - A_\alpha \cdot DD_\alpha, \\
 XX_2 &= XX_\beta(t) - A_\beta \cdot DD_\beta, \\
 XX_3 &= XX_\delta(t) - A_\delta \cdot DD_\delta, \\
 DD_\alpha &= |C_\alpha \cdot XX_\alpha(t) - XX(t)|, \\
 DD_\beta &= |C_\beta \cdot XX_\beta(t) - XX(t)|, \\
 DD_\delta &= |C_\delta \cdot XX_\delta(t) - XX(t)|.
 \end{aligned} \tag{14}$$

4.3. *Attacking.* The wolves attack the prey. The maximum iteration is ter . a is given as

$$a = 2 - \frac{2t}{ter}. \tag{15}$$

Figure 2 shows the GWO algorithm.

5. Performance Results

Figure 3 illustrates the comparison of amplify-and-forward (AF), DF, and direct communication schemes. Table 2 shows

TABLE 2: Parameters of Figure 3.

μ	0 dB
K	0.5
γ_{th}	5 dB
R_{th}	5 dB
N_t	2
N_r	2
L	2

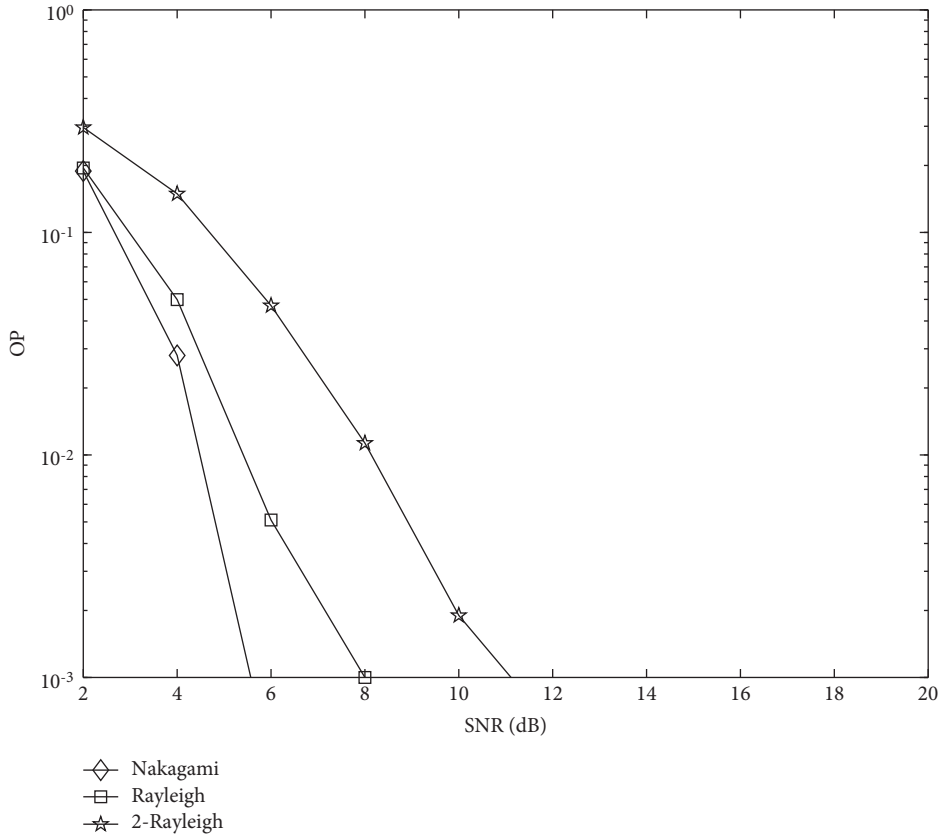


FIGURE 4: OP comparison with different channel models.

the corresponding parameters. The DF scheme is superior to AF and direct communication schemes. This means that with the increase of SNR, the cooperative communication condition becomes good, which reduces the OP. Compared with direct transmission, it also shows that cooperative transmission always reduces the OP.

Figure 4 presents the OP performance comparison under Nakagami, Rayleigh, and 2-Rayleigh models. The parameters are given in Table 3. We can see that the OP performance of the Nakagami model is better than that of Rayleigh and 2-Rayleigh models. When SNR = 4 dB, the OP values are 0.0280, 0.0499, and 0.1492, respectively. Compared with Nakagami and Rayleigh channel models, the 2-Rayleigh model has an increase of 81.2% and 66.6% in OP values, respectively.

TABLE 3: Parameters of Figure 4.

μ	0 dB
K	0.6
γ_{th}	5 dB
R_{th}	5 dB
N_t	2
N_r	2
L	2

In Figures 5–8, we obtain the optimum K for the GWO, GS, GA, and FA methods. The parameters are given in Table 4. Compared with GS, GA, and FA, GWO achieves a smaller OP (0.0005). This is due to the fact that GWO has a simple structure and a strong convergence performance, which is easy to implement.

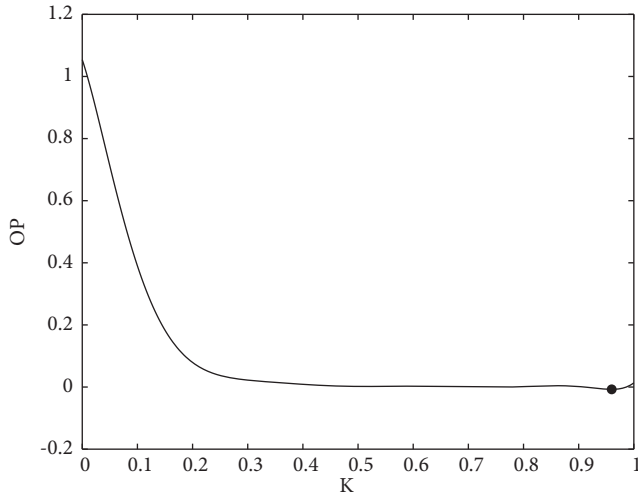
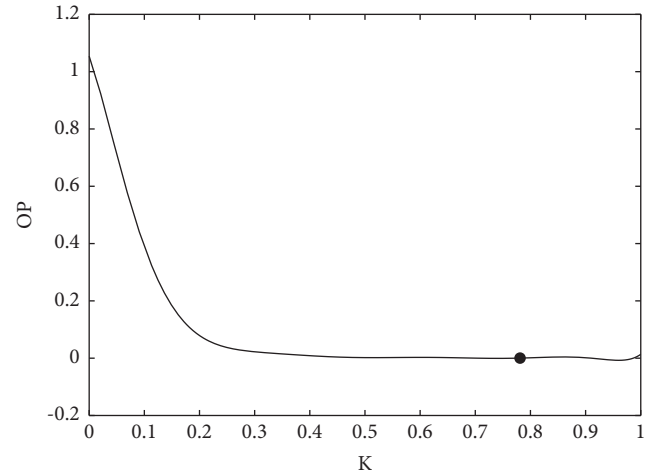
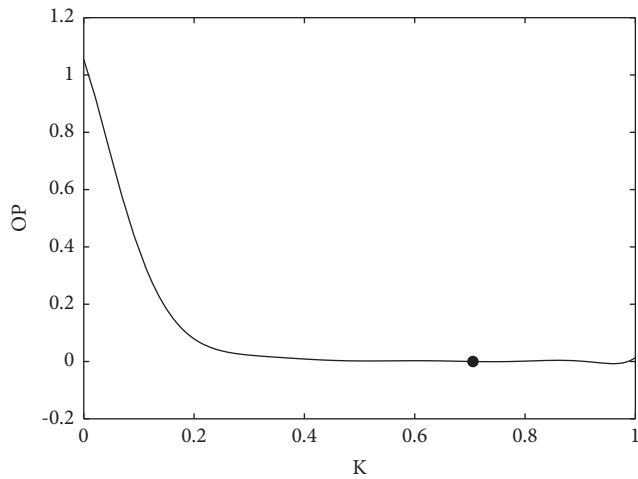
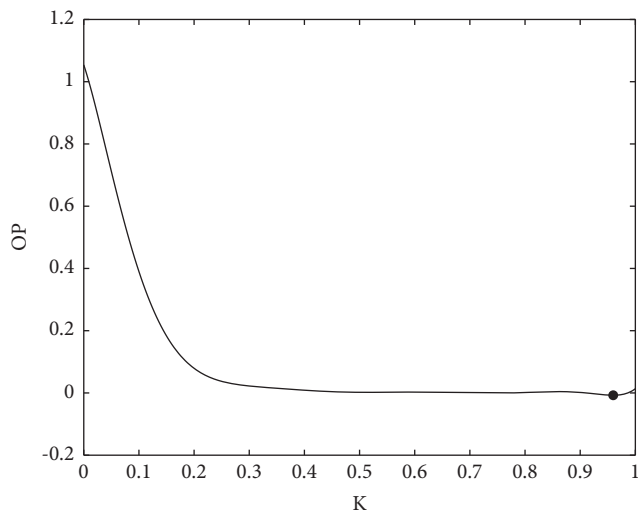
FIGURE 5: Optimum K of GWO.FIGURE 8: Optimum K of GS.FIGURE 6: Optimum K of GA.FIGURE 7: Optimum K of FA.

TABLE 4: Simulation parameters for the 4 methods.

Algorithm	Simulation parameters
GWO	$psize = 50, ter = 1000$
GS	$a = 0, b = 1, \epsilon = 0.2$
GA	$psize = 50, ter = 1000$
FA	$psize = 50, \alpha = 0.5, \beta = 0.2, \gamma = 1, ter = 1000$

6. Conclusions

In this paper, the power allocation optimization of mobile multiuser networks was investigated. Based on the GWO method, we proposed a power allocation optimization algorithm. The simulation results showed that compared with GS, GA, and FA algorithms, GWO algorithm can obtain better OP performance results. Compared with Nakagami and Rayleigh channel models, the 2-Rayleigh model has an increase of 81.2% and 66.6% in OP values, respectively.

In future studies, we will consider using artificial intelligence to obtain the optimal K value.

Data Availability

The data used to support the findings of this study are available from the corresponding authors upon reasonable request and with permission of funders.

Conflicts of Interest

The authors declare that they have no conflicts of interest.

Acknowledgments

This study was supported by the Research Project of Teaching Reform in Higher Education Institutions in Jiangxi Province, China (JXJG-20-15-9).

References

- [1] S. Mumtaz, A. Al-Dulaimi, H. Gacanin, and A. Bo, "Block chain and big data-enabled intelligent vehicular communication," *IEEE Transactions on Intelligent Transportation Systems*, vol. 22, no. 7, pp. 3904–3906, Jul. 2021.
- [2] H. Wang, X. Li, R. H. Jhaveri et al., "Sparse Bayesian Learning based channel estimation in FBMC/OQAM industrial IoT networks," *Computer Communications*, vol. 176, no. 8, pp. 40–45, Aug. 2021.
- [3] L. W. Xu, X. P. Zhou, M. A. Khan, X. W. Li, V. G. Menon, and X. Yu, "Communication quality prediction for internet of vehicle (IoV) networks: an elman approach," *IEEE Transactions on Intelligent Transportation Systems*, 2021.
- [4] F. Q. Wen, J. P. Shi, and Z. Zhang, "Generalized spatial smoothing in bistatic EMVS-MIMO radar," *Signal Processing*, vol. 193, Article ID 108406, 2022.
- [5] J. Shi, Z. Yang, and Y. Liu, "On parameter identifiability of diversity-smoothing-based MIMO radar," *IEEE Transactions on Aerospace and Electronic Systems*, 2021.
- [6] D. Kong, X. Zheng, Y. Zhang, and T. Jiang, "Frame repetition: a solution to imaginary interference cancellation in FBMC/OQAM systems," *IEEE Transactions on Signal Processing*, vol. 68, no. 2, pp. 1259–1273, 2020.
- [7] S. Wang and X. Jiang, "Three-dimensional cooperative positioning in vehicular ad-hoc networks," *IEEE Transactions on Intelligent Transportation Systems*, vol. 22, no. 2, pp. 937–950, 2021.
- [8] H. Lei, Z. Yang, K.-H. Park et al., "Secrecy outage analysis for cooperative NOMA systems with relay selection schemes," *IEEE Transactions on Communications*, vol. 67, no. 9, pp. 6282–6298, 2019.
- [9] A. H. A. El-Malek, A. M. Salhab, and S. A. Zummo, "New bandwidth efficient relaying schemes in cooperative cognitive two-way relay networks with physical layer security," *IEEE Transactions on Vehicular Technology*, vol. 66, no. 6, pp. 5372–5386, 2017.
- [10] L. Xu, H. Wang, and T. A. Gulliver, "Outage probability performance analysis and prediction for mobile IoV networks based on ICS-BP neural network," *IEEE Internet of Things Journal*, vol. 8, no. 5, pp. 3524–3533, 2021.
- [11] P. He and M. Dong, "Energy-efficient power allocation maximization with mixed group sum power bound and QoS constraints," *IEEE Transactions on Communications*, vol. 67, no. 10, pp. 7139–7151, 2019.
- [12] Y. Xu, Z. Gao, Z. Wang, C. Huang, Z. Yang, and C. Yuen, "RIS-enhanced WPCNs: joint radio resource allocation and passive beamforming optimization," *IEEE Transactions on Vehicular Technology*, vol. 70, no. 8, pp. 7980–7991, 2021.
- [13] B. Li, L.-L. Yang, R. G. Maunder, and S. Sun, "Resource allocation in millimeter-wave multicarrier-division duplex systems with hybrid beamforming," *IEEE Transactions on Vehicular Technology*, vol. 70, no. 8, pp. 7921–7935, 2021.
- [14] M. D. L. Filomeno, M. L. R. de Campos, H. V. Poor, and M. V. Ribeiro, "Hybrid power line/wireless systems: an optimal power allocation perspective," *IEEE Transactions on Wireless Communications*, vol. 19, no. 10, pp. 6289–6300, 2020.
- [15] M. Y. Arafat and S. Moh, "Localization and clustering based on swarm intelligence in UAV networks for emergency communications," *IEEE Internet of Things Journal*, vol. 6, no. 5, pp. 8958–8976, 2019.
- [16] X. Wu, Y. Yin, L. Xu, X. Wu, F. Meng, and R. Zhen, "Multi-UAV task allocation based on improved genetic algorithm," *IEEE Access*, vol. 9, Article ID 100369, 2021.
- [17] Q. T. Vien, T. A. Le, X. S. Yang, and T. Q. Duong, "Enhancing security of MME handover via fractional programming and firefly algorithm," *IEEE Transactions on Communications*, vol. 67, no. 3, pp. 6206–6220, 2019.
- [18] E. Cuevas, L. Enríquez, D. Zaldívar, and M. Pérez-Cisneros, "A selection method for evolutionary algorithms based on the golden section," *Expert Systems with Applications*, vol. 106, no. 9, pp. 183–196, 2018.
- [19] G. K. Karagiannidis, N. C. Sagias, and P. T. Mathiopoulos, "\$N\{\text{vast}\}\$Nakagami: a novel stochastic model for cascaded fading channels," *IEEE Transactions on Communications*, vol. 55, no. 8, pp. 1453–1458, 2007.
- [20] L. Xu, X. Yu, and T. A. Gulliver, "Intelligent outage probability prediction for mobile IoT networks based on an IGWO-Elman neural network," *IEEE Transactions on Vehicular Technology*, vol. 70, no. 2, pp. 1365–1375, 2021.
- [21] E. Emary, H. M. Zawbaa, and C. Grosan, "Experienced gray wolf optimization through reinforcement learning and neural networks," *IEEE Transactions on Neural Networks and Learning Systems*, vol. 29, no. 3, pp. 681–694, 2018.
- [22] X. Zhang, Q. Kang, J. Cheng, and X. Wang, "A novel hybrid algorithm based on biogeography-based optimization and grey wolf optimizer," *Applied Soft Computing*, vol. 67, no. 6, pp. 197–214, 2018.